BEILSTEIN JOURNAL OF ORGANIC CHEMISTRY

Earth-abundant 3d metal catalysis

Edited by Lutz Ackermann

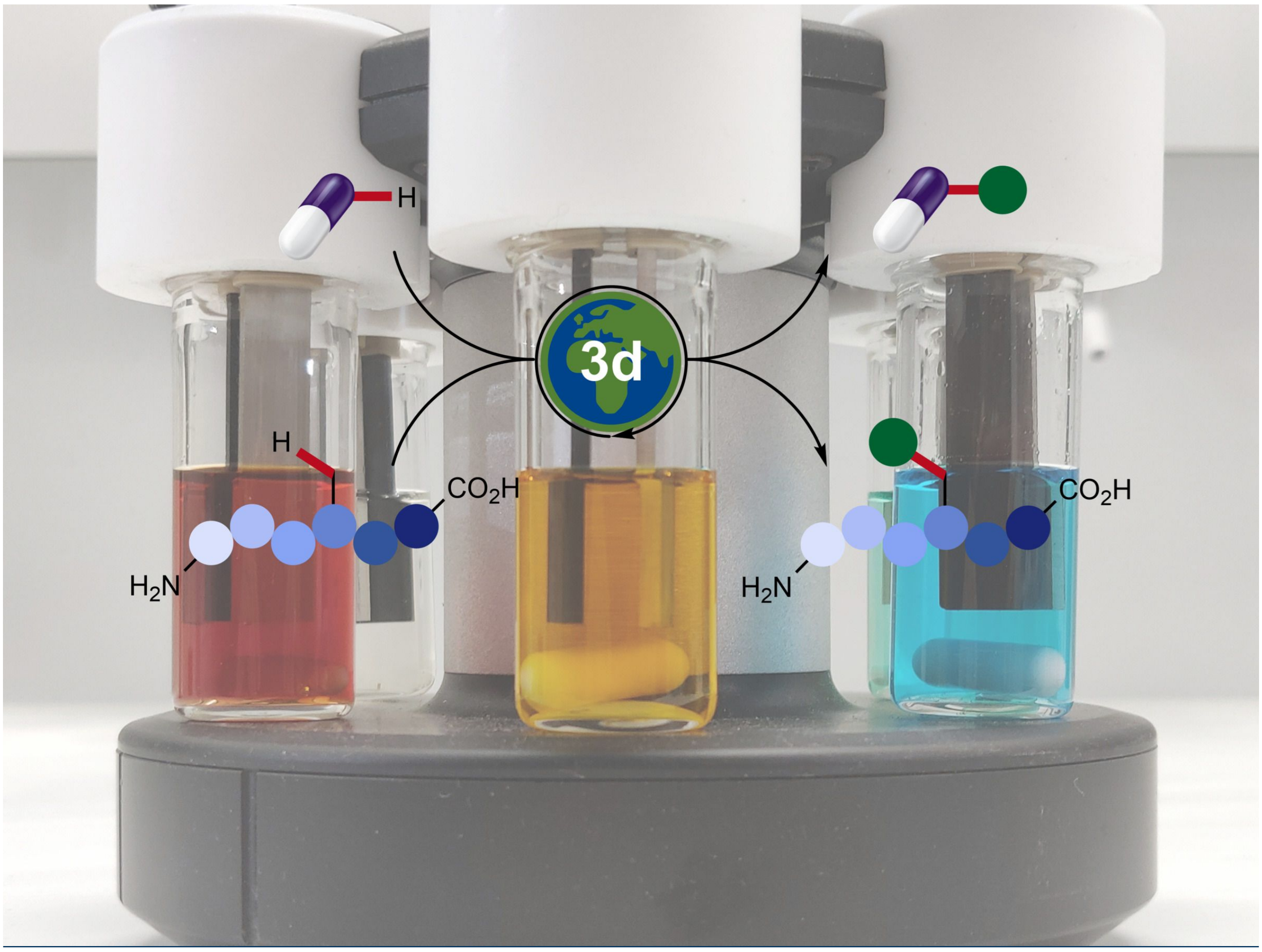
H
3d
H
CO_2H
H_2N
CO_2H
H_2N

Generated on 06 June 2026, 14:28

Imprint

Beilstein Journal of Organic Chemistry
www.bjoc.org
ISSN 1860-5397
Email: journals-support@beilstein-institut.de

The *Beilstein Journal of Organic Chemistry* is published by the Beilstein-Institut zur Förderung der Chemischen Wissenschaften.

Beilstein-Institut zur Förderung der
Chemischen Wissenschaften
Trakehner Straße 7–9
60487 Frankfurt am Main
Germany
www.beilstein-institut.de

The copyright to this document as a whole, which is published in the *Beilstein Journal of Organic Chemistry*, is held by the Beilstein-Institut zur Förderung der Chemischen Wissenschaften. The copyright to the individual articles in this document is held by the respective authors, subject to a Creative Commons Attribution license.

The cover image, copyright 2021 Lutz Ackermann, is licensed under the Creative Commons Attribution 4.0 license (https://creativecommons.org/licenses/by/4.0). The reuse, redistribution or reproduction requires that the author, source and license are credited.
The cover image showcases electrosynthesis by Earth-abundant 3d transition metals for late-stage diversification.

BEILSTEIN JOURNAL OF ORGANIC CHEMISTRY

Earth-abundant 3d transition metals on the rise in catalysis

Nikolaos Kaplaneris[1] and Lutz Ackermann*[1,2]

Editorial

Open Access

Address:
[1]Institut für Organische und Biomolekulare Chemie, Georg-August-Universität Göttingen, Tammannstraße 2, 37077 Göttingen, Germany and [2]Wöhler Research Institute for Sustainable Chemistry (WISCh), Georg-August-Universität Göttingen, Tammannstraße 2, 37077 Göttingen, Germany

Email:
Lutz Ackermann* - Lutz.Ackermann@chemie.uni-goettingen.de

* Corresponding author

Keywords:
C–H activation; 3d transition metals; green chemistry; late-stage functionalization; sustainability

Beilstein J. Org. Chem. **2022,** *18,* 86–88.
https://doi.org/10.3762/bjoc.18.8

Received: 13 December 2021
Accepted: 29 December 2021
Published: 07 January 2022

This article is part of the thematic issue "Earth-abundant 3d metal catalysis".

Associate Editor: L. Ackermann

© 2022 Kaplaneris and Ackermann; licensee Beilstein-Institut.
License and terms: see end of document.

Transition metal catalysis has emerged as a transformative platform for the assembly of increasingly complex compounds, with enabling applications to natural product syntheses, crop protection or medicinal chemistry. Particularly, cross-coupling reactions [1], as well as alkene and alkyne metathesis [2,3], have considerably changed the art of molecular synthesis, with a major impact on neighboring disciplines, such as molecular biology or materials sciences. Despite of these indisputable advances, this approach has, thus far, predominantly relied on precious, often toxic, 4d and 5d transition metals, most prominently palladium, rhodium and iridium. In sharp contrast, the use of less expensive and less toxic Earth-abundant 3d transition metals continues to be underdeveloped. This lack of viable catalysis strategies involving 3d transition metals is largely due to a limited knowledge on the working mode of these metal catalysts, which often involve single-electron-transfer-based redox events. As a consequence, there is a strong demand for efficient and reliable transformations to form C–C and C–heteroatom bonds, thereby providing a more sustainable future for, among others, drug development in generations to come. Particularly, Nobel prize-winning palladium-catalyzed cross-coupling reactions have been recognized by the practitioners in agrochemical and pharmaceutical industries as one of the most powerful methods for molecular assembly. With regard to the cost of goods and the allowance of trace metal impurities in medicinally relevant compounds, 3d transition metal complexes, such as those of iron, copper, cobalt or nickel, represent exciting, more sustainable alternatives. Furthermore, metal-catalyzed cross-couplings do require prefunctionalizations on both substrates and generate stoichiometric quantities of undesired chemical waste, thus reducing the sustainability of these catalytic transformations. To address these major limitations, the past decades have witnessed major momentum in metal-catalyzed C–H activation [4,5] as a more resource-economical strategy. This approach involves the efficient and selective cleavage of otherwise inert, yet omnipresent C–H bonds. This strategy avoids a variety of steps and reduces the amount of chemical waste. Very recently, notable advances have been accomplished with environmentally benign, Earth-abundant 3d transition metals [6,7]. The articles in this thematic issue dedicated to advances in Earth-abundant 3d metal catalysis highlight the unique power of 3d transition metals with a topical focus on homogeneous catalysis. Applications of this strategy range from late-stage functionalization to modern photocatalysis and electrocatalysis, with contributions from around the globe, including Brazil, China, Japan, Germany, India, and South Korea, among others.

The increasing use of C–H activations in academic and industrial laboratories calls for a critical analysis of these methods to enable an efficient transition of these methods. Hence, manganese-catalyzed C–H functionalization for late-stage functionalizations of biomolecules and drug-like scaffolds are summarized [8]. Likewise, 3d transition metal-catalyzed C–H functionalization enabled the de novo assembly of bioactive molecules [9]. The full potential of the mild nature of C–H functionalization is unlocked by the merger with modern photochemistry and electrocatalysis manifolds. In this context, recent advances were realized by the combination of photoredox catalysis and nickel-catalyzed C–H functionalization [10]. Iron complexes are typically cost-effective and nontoxic, and therefore, their use in domino processes represents an outstanding prospect for sustainable organic syntheses [11]. Directed C–H activations have been developed as increasingly amenable tools for proximity-induced C–H functionalizations. In this thematic issue, strategies are presented that guarantee position-selectivity in copper-mediated isoindolin-1-one synthesis [12] as well as in copper-catalyzed aminations of ferrocenes [13]. The exploitation of the innate reactivity of organic molecules can allow for indirected C–H transformations and herein, homolytic C–H cleavages are described for transformative manganese-catalyzed brominations of tertiary C–H bonds [14]. Finally, electrooxidation enabled the site-selective alkynylation of tetrahydroisoquinolines within a TEMPO/copper regime [15].

As the editor of this issue on Earth-abundant 3d metal catalysis, it was a wonderful experience to experience the diversity of 3d transition metal catalysis, which continues to address key challenges of sustainable modern molecular syntheses. The senior author owe a great debt of gratitude to all of the authors for their dedication and time in contributing to this effort. Finally, the senior author thank the staff at the *Beilstein Journal of Organic Chemistry* for their assistance.

Nikolaos Kaplaneris and Lutz Ackermann

Göttingen, December 2021

Funding

Generous support from the ERC Advanced Grant no. 101021358 (LA) is gratefully acknowledged.

ORCID® iDs

Lutz Ackermann - https://orcid.org/0000-0001-7034-8772

References

1. Johansson Seechurn, C. C. C.; Kitching, M. O.; Colacot, T. J.; Snieckus, V. *Angew. Chem., Int. Ed.* **2012,** *51,* 5062–5085. doi:10.1002/anie.201107017
2. Fürstner, A. *J. Am. Chem. Soc.* **2021,** *143,* 15538–15555. doi:10.1021/jacs.1c08040
3. Trnka, T. M.; Grubbs, R. H. *Acc. Chem. Res.* **2001,** *34,* 18–29. doi:10.1021/ar000114f
4. Rogge, T.; Kaplaneris, N.; Chatani, N.; Kim, J.; Chang, S.; Punji, B.; Schafer, L. L.; Musaev, D. G.; Wencel-Delord, J.; Roberts, C. A.; Sarpong, R.; Wilson, Z. E.; Brimble, M. A.; Johansson, M. J.; Ackermann, L. *Nat. Rev. Methods Primers* **2021,** *1,* 43. doi:10.1038/s43586-021-00041-2
5. Guillemard, L.; Kaplaneris, N.; Ackermann, L.; Johansson, M. J. *Nat. Rev. Chem.* **2021,** *5,* 522–545. doi:10.1038/s41570-021-00300-6
6. Gandeepan, P.; Müller, T.; Zell, D.; Cera, G.; Warratz, S.; Ackermann, L. *Chem. Rev.* **2019,** *119,* 2192–2452. doi:10.1021/acs.chemrev.8b00507
7. Loup, J.; Dhawa, U.; Pesciaioli, F.; Wencel-Delord, J.; Ackermann, L. *Angew. Chem., Int. Ed.* **2019,** *58,* 12803–12818. doi:10.1002/anie.201904214
8. Son, J. *Beilstein J. Org. Chem.* **2021,** *17,* 1733–1751. doi:10.3762/bjoc.17.122
9. Carvalho, R. L.; de Miranda, A. S.; Nunes, M. P.; Gomes, R. S.; Jardim, G. A. M.; Júnior, E. N. d. S. *Beilstein J. Org. Chem.* **2021,** *17,* 1849–1938. doi:10.3762/bjoc.17.126
10. Mantry, L.; Maayuri, R.; Kumar, V.; Gandeepan, P. *Beilstein J. Org. Chem.* **2021,** *17,* 2209–2259. doi:10.3762/bjoc.17.143
11. Pounder, A.; Tam, W. *Beilstein J. Org. Chem.* **2021,** *17,* 2848–2893. doi:10.3762/bjoc.17.196
12. Xiong, F.; Li, B.; Yang, C.; Zou, L.; Ma, W.; Gu, L.; Mei, R.; Ackermann, L. *Beilstein J. Org. Chem.* **2021,** *17,* 1591–1599. doi:10.3762/bjoc.17.113
13. Jia, Z.-S.; Yue, Q.; Li, Y.; Xu, X.-T.; Zhang, K.; Shi, B.-F. *Beilstein J. Org. Chem.* **2021,** *17,* 2488–2495. doi:10.3762/bjoc.17.165
14. Sneh, K.; Torigoe, T.; Kuninobu, Y. *Beilstein J. Org. Chem.* **2021,** *17,* 885–890. doi:10.3762/bjoc.17.74
15. Guo, B.; Xu, H.-C. *Beilstein J. Org. Chem.* **2021,** *17,* 2650–2656. doi:10.3762/bjoc.17.178

License and Terms

This is an open access article licensed under the terms of the Beilstein-Institut Open Access License Agreement (https://www.beilstein-journals.org/bjoc/terms), which is identical to the Creative Commons Attribution 4.0 International License (https://creativecommons.org/licenses/by/4.0). The reuse of material under this license requires that the author(s), source and license are credited. Third-party material in this article could be subject to other licenses (typically indicated in the credit line), and in this case, users are required to obtain permission from the license holder to reuse the material.

The definitive version of this article is the electronic one which can be found at:
https://doi.org/10.3762/bjoc.18.8

BEILSTEIN JOURNAL OF ORGANIC CHEMISTRY

Manganese/bipyridine-catalyzed non-directed C(sp^3)–H bromination using NBS and $TMSN_3$

Kumar Sneh[1], Takeru Torigoe[1,2] and Yoichiro Kuninobu*[1,2]

Letter

Open Access

Address:
[1]Department of Molecular and Material Sciences, Interdisciplinary Graduate School of Engineering Sciences, Kyushu University, 6-1 Kasugakoen, Kasuga-shi, Fukuoka 816-8580, Japan and [2]Institute for Materials Chemistry and Engineering, Kyushu University, 6-1 Kasugakoen, Kasuga-shi, Fukuoka 816-8580, Japan

Email:
Yoichiro Kuninobu* - kuninobu@cm.kyushu-u.ac.jp

* Corresponding author

Keywords:
bromination; C–H transformation; hydrogen abstraction; manganese; radical

Beilstein J. Org. Chem. **2021,** *17,* 885–890.
https://doi.org/10.3762/bjoc.17.74

Received: 27 February 2021
Accepted: 12 April 2021
Published: 22 April 2021

This article is part of the thematic issue "Earth-abundant 3d metal catalysis".

Associate Editor: L. Ackermann

© 2021 Sneh et al.; licensee Beilstein-Institut.
License and terms: see end of document.

Abstract

A Mn(II)/bipyridine-catalyzed bromination reaction of unactivated aliphatic C(sp^3)−H bonds has been developed using *N*-bromosuccinimide (NBS) as the brominating reagent. The reaction proceeded in moderate-to-good yield, even on a gram scale. The introduced bromine atom can be converted into fluorine and allyl groups.

Introduction

Organic halides are versatile precursors for various synthetic protocols and are frequently used to introduce a variety of functionalities, such as boron-, silicon-, nitrogen-, and oxygen-based functional groups, and in C−C bond forming reactions, such as cross-coupling reactions [1-6]. The traditional method used for the preparation of alkyl bromides is the reaction of their corresponding alkyl alcohols with HBr, PBr_3, or other brominating reagents [7-13].

Direct C–H halogenation is one of the most efficient methods used for the synthesis of halogenated organic molecules. This direct method involves the reaction of an alkane with Br_2, CBr_4, or H_2O_2–HBr under photolysis or at high temperatures in the absence of a catalyst (Scheme 1a) [14-16]. However, these reactions do not exhibit any selectivity due to the indiscriminate attack of bromine radicals on the C–H bonds in the substrate, which leads to the formation of a mixture of halogenated products. Electrophilic and radical C(sp^3)−H halogenation at the benzylic and allylic position using *N*-halosuccinimide with azobisisobutyronitrile or benzoyl peroxide as a radical initiator is known as the Wohl–Ziegler bromination reaction, which requires heating, acidic/basic conditions, and/or UV irradiation (Scheme 1a) [17-20].

There are several types of transition-metal-catalyzed C(sp^3)−H halogenation reactions reported in the literature (Scheme 1b–d).

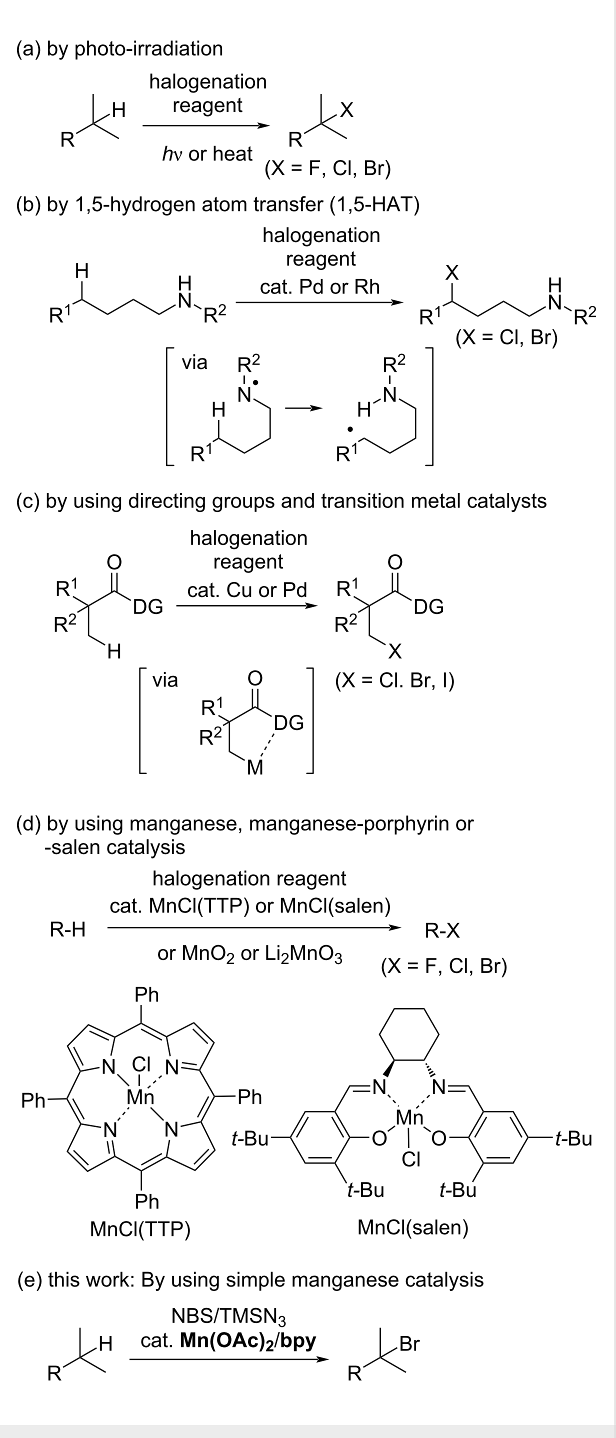
(a) by photo-irradiation
halogenation reagent
hν or heat
(X = F, Cl, Br)
(b) by 1,5-hydrogen atom transfer (1,5-HAT)
halogenation reagent
cat. Pd or Rh
(X = Cl, Br)
via
(c) by using directing groups and transition metal catalysts
halogenation reagent
cat. Cu or Pd
(X = Cl. Br, I)
via
(d) by using manganese, manganese-porphyrin or -salen catalysis
halogenation reagent
cat. MnCl(TTP) or MnCl(salen)
or MnO2 or Li2MnO3
R-H
R-X
(X = F, Cl, Br)
MnCl(TTP)
MnCl(salen)
(e) this work: By using simple manganese catalysis
NBS/TMSN3
cat. Mn(OAc)2/bpy

Scheme 1: Several examples of C(sp^3)–H halogenation.

Transition-metal-catalyzed 1,5-hydrogen atom transfer (1,5-HAT) is effective for promoting regioselective C(sp^3)−H halogenation reactions (Scheme 1b) [21-23]. The regioselectivity is controlled by the formation of a six-membered cyclic intermediate. Directing-group-assisted C(sp^3)−H halogenation reactions are efficient for promoting regioselective C(sp^3)−H halogenations (Scheme 1c) [24-28]. In these reactions, the C(sp^3)−H bond at the β-position of an oxazoline or amide is selectively activated using a copper or palladium catalyst.

Manganese is one of the most abundant and nontoxic transition metals found in the earth's crust and its corresponding complexes and salts are useful in synthetic organic reactions [29-43]. Highly reactive and selective bromination reactions have been achieved using a stoichiometric amount of MnO_2 [44] or a catalytic amount of Li_2MnO_3 [45] under fluorescent light irradiation in the presence of Br_2 (Scheme 1d). Hill [46] and Groves [47-49] have reported the manganese-porphyrin-catalyzed chlorination and bromination of C(sp^3)−H bonds, respectively (Scheme 1d). Groves et al. also reported the manganese-salen-catalyzed fluorination of benzylic C(sp^3)−H bonds [49]. Although these methods are efficient, they have a limited substrate scope (cycloalkanes and substrates bearing a benzylic C–H group). Therefore, there remains room for the development of a simple manganese catalytic system to achieve C(sp^3)−H halogenation using commercially available reagents.

Herein, we report a manganese-catalyzed C(sp^3)–H bromination reaction at the methine and benzylic positions of a wide range of substrates. The manganese catalyst, brominating agent, and additives are commercially available, and the reaction can be achieved by simply mixing these reagents with the substrate.

Results and Discussion

The reaction of isoamyl alcohol derivative **1a** with *N*-bromosuccinimide (NBS) and $TMSN_3$ in the presence of a catalytic amount of $Mn(OAc)_2$ and bipyridine (bpy) in 1,2-dichloroethane (DCE) at 60 °C for 18 h gave C(sp^3)–H brominated product **2a** in 10% yield (Table 1, entry 1). Although the yield of **2a** did not increase when performing the reaction in acetonitrile (Table 1, entry 2), the yield of **2a** was dramatically improved to 62% using $PhCF_3$ as the solvent (Table 1, entry 3). Other manganese salts, such as $MnBr_2$ and $Mn(acac)_2$, were also effective in the reaction, giving similar yields (Table 1, entries 4 and 5). Other first-row transition metal salts, such as $Fe(OAc)_2$ and $Co(OAc)_2$, did not improve the yield of **2a** (Table 1, entries 6 and 7). Product **2a** was formed in 21 and 49% yields, respectively when the reaction was conducted in the absence of the transition metal salt and bpy ligand (Table 1, entries 8 and 9). $TMSN_3$ was indispensable in this reaction because the C(sp^3)–H bromination reaction did not occur in its absence (Table 1, entry 10). We then investigated the following experiments using the conditions described in entry 3.

Under the optimized reaction conditions, we investigated the C(sp^3)–H bromination reaction of several substrates (Scheme 2). The reaction proceeded regioselectively at the methine C(sp^3)–H bond of isoamyl benzoate (**1b**) to give **2b** in

Table 1: Optimization of reaction conditions[a].

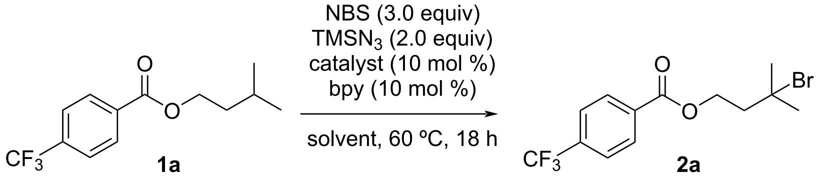
NBS (3.0 equiv)
TMSN3 (2.0 equiv)
catalyst (10 mol %)
bpy (10 mol %)
solvent, 60 ºC, 18 h
CF3
1a
CF3
Br
2a

entry	catalyst	solvent	yield (%)[b]
1	$Mn(OAc)_2$	DCE	10
2	$Mn(OAc)_2$	MeCN	10
3	$Mn(OAc)_2$	$PhCF_3$	62 (53)[c]
4	$MnBr_2$	$PhCF_3$	55
5	$Mn(acac)_2$	$PhCF_3$	54
6	$Fe(OAc)_2$	$PhCF_3$	42
7	$Co(OAc)_2$	$PhCF_3$	30
8	–	$PhCF_3$	21
9[d]	$Mn(OAc)_2$	$PhCF_3$	49
10[e]	$Mn(OAc)_2$	$PhCF_3$	<1

[a]Conditions: **1a** (0.100 mmol, 1.0 equiv), NBS (0.300 mmol, 3.0 equiv), $TMSN_3$ (0.200 mmol, 2.0 equiv), catalyst (10 mol %), bpy (10 mol %), solvent (0.50 mL). [b]The ^1H NMR yields were determined using 1,1,2,2-tetrachloroethane as an internal standard. [c]Isolated yield. [d]Without bpy. [e]Without $TMSN_3$.

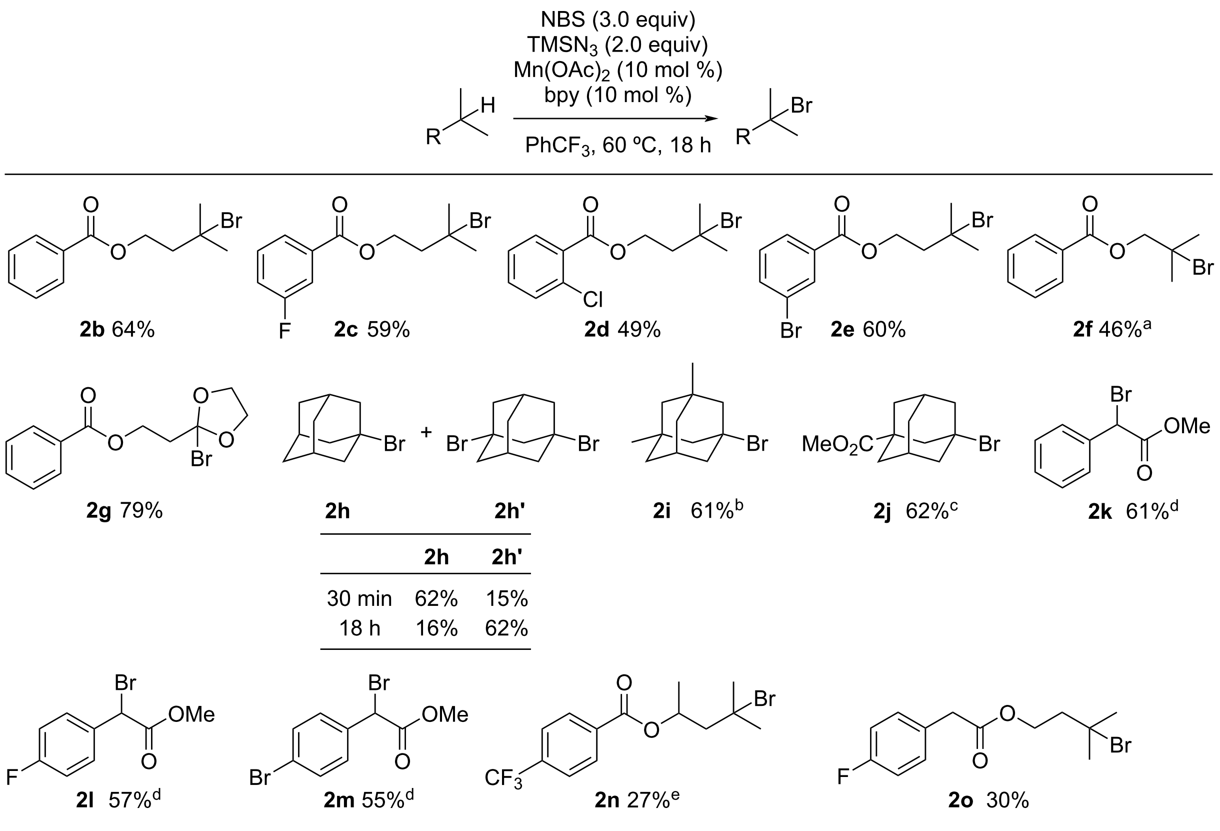
NBS (3.0 equiv)
TMSN3 (2.0 equiv)
Mn(OAc)2 (10 mol %)
bpy (10 mol %)
PhCF3, 60 ºC, 18 h
R
H
R
Br
2b 64%
2c 59%
2d 49%
2e 60%
2f 46%a
2g 79%
2h
2h'
2i 61%b
2j 62%c
2k 61%d
2l 57%d
2m 55%d
2n 27%e
2o 30%
F
Cl
Br
OMe
MeO2C
CF3

	2h	2h'
30 min	62%	15%
18 h	16%	62%

Scheme 2: Substrate scope. [a]80 °C. [b]45 min. [c]4 h. [d]90 °C, [e]GC yield of mono-brominated product **2n** using mesitylene as internal standard.

64% yield. Isoamyl benzoates bearing halogen atoms, such as fluorine, chlorine, or bromine, on the phenyl ring were also suitable substrates and gave C(sp^3)–H brominated products **2c**–**e** in 49–60% yields, without any loss of the halogen substituents. Although the C(sp^3)–H bromination of isobutyl benzoate **1f** did not proceed at 60 °C, the corresponding C(sp^3)–H brominated compound **2f** was produced at higher temperature (80 °C). The C(sp^3)–H bond in acetal **1g** was efficiently brominated to give **2g** in 79% yield. The reaction of adamantane (**1h**) proceeded selectively at the tertiary C(sp^3)–H bond to give a mixture of mono- and dibrominated products (**2h** and **2h′**). The selectivity of **2h** and **2h′** can be controlled by varying the reaction time; mono-brominated **2h** was obtained in 62% yield as the major product after 30 min of reaction and dibrominated **2h′** was afforded as the major product after 18 h. Similarly, 1,3-dimethyladamantane (**1i**) and methyl adamantane-1-carboxylate (**1j**) were successfully converted to brominated products **2i** and **2j**, respectively. For benzeneacetic acid methyl esters **1k**, **1l** and **1m**, the C(sp^3)–H bromination reaction proceeded selectively at the benzylic position and their corresponding brominated products (**2k**, **2l** and **2m**) were obtained in 61, 57 and 55% yield, respectively.

We next investigated the regioselectivity of the reaction using substrates with two possible reaction sites. The reaction of substrate **1n** bearing two methine C(sp^3)–H bonds occurred selectively at the terminal position giving product **2n** in 27% yield. The C(sp^3)–H bromination reaction took place selectively at the methine C(sp^3)–H bond when using substrate **1o**, which has both methine and benzylic C(sp^3)–H bonds, which gave product **2o** in 30% yield.

The manganese-catalyzed C(sp^3)–H bromination reaction proceeded in good yield, even on a gram scale. The reaction was performed using 2.61 g of **1a** with NBS and $TMSN_3$ in the presence of a catalytic amount of $Mn(OAc)_2$ and bpy to give 1.98 g of **2a** in 58% yield (Scheme 3).

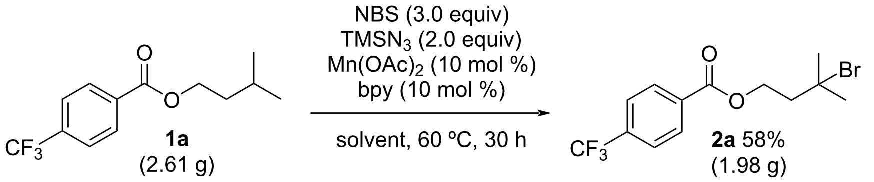

Scheme 3: Gram-scale synthesis of **2a**.

The introduced bromine atom can be converted into other functional groups. The reaction of **2a** with selectfluor in MeCN at 25 °C for 12 h gave fluorinated product **3** in 86% yield (Scheme 4, top) [50]. Allylated product **4** was obtained in 64% yield upon treating **2a** with allyltributylstannane in the presence of a catalytic amount of AIBN (Scheme 4, bottom) [51].

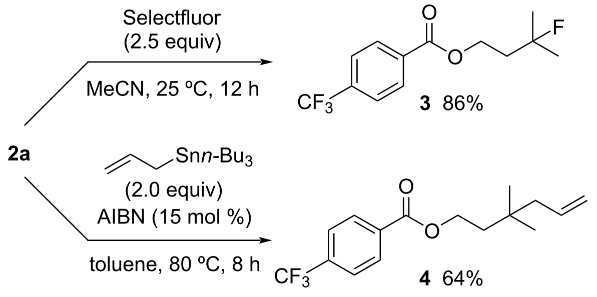

Scheme 4: Conversion of the C(sp^3)–Br bond.

Table 1 shows that the C(sp^3)–H bromination reaction proceeds in the absence of a transition metal salt or bpy ligand, and was accelerated by transition metal salts, especially $Mn(OAc)_2$. In addition, the results also suggest that $TMSN_3$ is required for the C(sp^3)–H bromination reaction. The proposed reaction mechanism is shown in Scheme 5, which involves the following steps. (1) The reaction between NBS and $TMSN_3$ generates bromine azide via the elimination of *N*-(trimethylsilyl)succinimide [52,53]; (2) bromine and azide radicals are then formed via homolytic cleavage of the weak Br–N_3 bond in bromine azide [54,55]; (3) the bromine radical can also be generated from NBS with the formation of a succinimide radical; (4) alkyl radical intermediate **A** is then formed via hydrogen abstraction by the succinimidyl radical and/or azidyl radical [56,57]; (5) the Br–Mn(III) species is then formed from the Mn(II) catalyst and bromine radical; and (6) brominated product **2** formed by the reaction of intermediate **A** with the Br–Mn(III) species with the regeneration of the Mn(II) catalyst.

Conclusion

In summary, we have successfully developed a manganese-catalyzed bromination of unactivated aliphatic C(sp^3)–H bonds. The reaction proceeded selectively at the methine and benzylic positions using simple and commercially available compounds, such as NBS, $TMSN_3$, $Mn(OAc)_2$, and bpy, even on a gram scale. Furthermore, the brominated products can be easily functionalized upon the introduction of other functional groups,

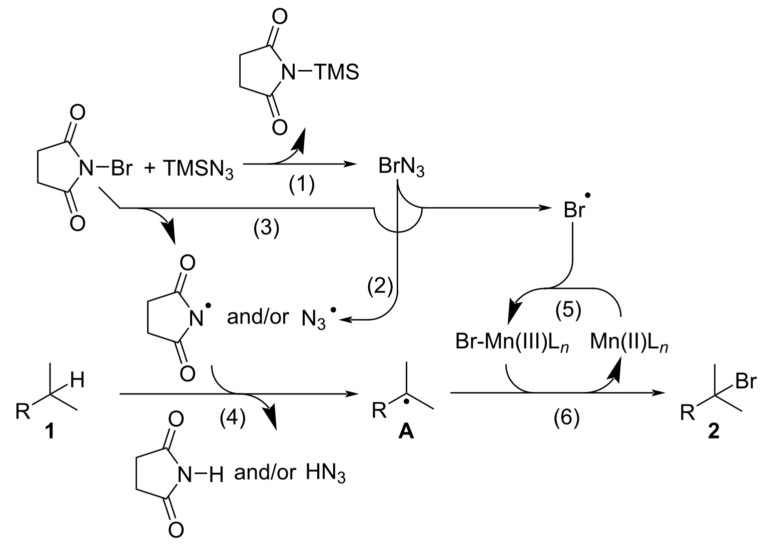

Scheme 5: Proposed mechanism of manganese-catalyzed C(sp^3)–H bromination.

such as fluorine and allyl groups. We hope that this C(sp^3)–H bromination reaction will become a useful method to synthesize organic compounds with bromine atom(s).

Supporting Information

Supporting Information File 1

Experimental procedures, compound characterization data, and copies of ^{1}H and ^{13}C NMR spectra.
[https://www.beilstein-journals.org/bjoc/content/supplementary/1860-5397-17-74-S1.pdf]

Funding

This work was supported in part by JSPS KAKENHI Grant Numbers JP 17H03016, 18H04656, and 20H04824, Takeda Science Foundation, The Mitsubishi Foundation, and Yamada Science Foundation.

ORCID® iDs

Takeru Torigoe - https://orcid.org/0000-0002-4902-1596
Yoichiro Kuninobu - https://orcid.org/0000-0002-8679-9487

References

1. Rosseels, G.; Houben, C.; Kerckx, P. Synthesis of a metabolite of fantofarone. In *Advances in Organobromine Chemistry II;* Desmurs, J. R.; Gérard, B.; Goldstein, M. J., Eds.; Elsevier: Amsterdam, Netherlands, 1995; pp 152–159. doi:10.1016/s0926-9614(05)80016-4
2. Cristau, H.-J.; Desmurs, J.-R. Arylation of hard heteroatomic nucleophiles using bromoarenes substrates and Cu, Ni, Pd-catalysts. In *Advances in Organobromine Chemistry II;* Desmurs, J. R.; Gérard, B.; Goldstein, M. J., Eds.; Elsevier: Amsterdam, Netherlands, 1995; pp 240–263. doi:10.1016/s0926-9614(05)80024-3
3. *Handbook of Grignard Reagents;* Silverman, G. S.; Rakita, P. E., Eds.; CRC Press: Boca Raton, FL, USA, 1996. doi:10.1201/b16932
4. Echavarren, A. M.; Cárdenas, D. J. Mechanistic Aspects of Metal-Catalyzed C, C- and C, X-Bond-Forming Reactions. In *Metal-Catalyzed Cross-Coupling Reactions,* 2nd ed.; de Meijere, A.; Diederich, F., Eds.; Wiley-VCH: Weinheim, Germany, 2004. doi:10.1002/9783527619535
5. Knochel, P.; Dohle, W.; Gommermann, N.; Kneisel, F. F.; Kopp, F.; Korn, T.; Sapountzis, I.; Vu, V. A. *Angew. Chem., Int. Ed.* **2003,** *42,* 4302–4320. doi:10.1002/anie.200300579
6. Gribble, G. W. *Chem. Soc. Rev.* **1999,** *28,* 335–346. doi:10.1039/a900201d
7. Kamm, O.; Marvel, C. S. *Org. Synth.* **1921,** *1,* 3–14. doi:10.15227/orgsyn.001.0003
8. Wiley, G. A.; Hershkowitz, R. L.; Rein, B. M.; Chung, B. C. *J. Am. Chem. Soc.* **1964,** *86,* 964–965. doi:10.1021/ja01059a073
9. Pelletier, J. D.; Poirier, D. *Tetrahedron Lett.* **1994,** *35,* 1051–1054. doi:10.1016/s0040-4039(00)79963-1
10. Ferreri, C.; Costantino, C.; Chatgilialoglu, C.; Boukherroub, R.; Manuel, G. *J. Organomet. Chem.* **1998,** *554,* 135–137. doi:10.1016/s0022-328x(97)00667-0
11. Iranpoor, N.; Firouzabadi, H.; Jamalian, A.; Kazemi, F. *Tetrahedron* **2005,** *61,* 5699–5704. doi:10.1016/j.tet.2005.01.115
12. Dai, C.; Narayanam, J. M. R.; Stephenson, C. R. J. *Nat. Chem.* **2011,** *3,* 140–145. doi:10.1038/nchem.949
13. Wang, G.-Z.; Shang, R.; Cheng, W.-M.; Fu, Y. *J. Am. Chem. Soc.* **2017,** *139,* 18307–18312. doi:10.1021/jacs.7b10009
14. Shaw, H.; Perlmutter, H. D.; Gu, C.; Arco, S. D.; Quibuyen, T. O. *J. Org. Chem.* **1997,** *62,* 236–237. doi:10.1021/jo950371b
15. Podgoršek, A.; Stavber, S.; Zupan, M.; Iskra, J. *Tetrahedron Lett.* **2006,** *47,* 7245–7247. doi:10.1016/j.tetlet.2006.07.109

16. Nishina, Y.; Ohtani, B.; Kikushima, K. *Beilstein J. Org. Chem.* **2013,** *9,* 1663–1667. doi:10.3762/bjoc.9.190
17. Wohl, A. *Ber. Dtsch. Chem. Ges. B* **1919,** *52,* 51–63. doi:10.1002/cber.19190520109
18. Ziegler, K.; Schenck, G.; Krockow, E. W.; Siebert, A.; Wenz, A.; Weber, H. *Justus Liebigs Ann. Chem.* **1942,** *551,* 1–79. doi:10.1002/jlac.19425510102
19. Djerassi, C. *Chem. Rev.* **1948,** *43,* 271–317. doi:10.1021/cr60135a004
20. Wang, Y.; Li, G.-X.; Yang, G.; He, G.; Chen, G. *Chem. Sci.* **2016,** *7,* 2679–2683. doi:10.1039/c5sc04169d
21. Liu, T.; Mei, T.-S.; Yu, J.-Q. *J. Am. Chem. Soc.* **2015,** *137,* 5871–5874. doi:10.1021/jacs.5b02065
22. Liu, T.; Myers, M. C.; Yu, J.-Q. *Angew. Chem., Int. Ed.* **2017,** *56,* 306–309. doi:10.1002/anie.201608210
23. Sathyamoorthi, S.; Banerjee, S.; Du Bois, J.; Burns, N. Z.; Zare, R. N. *Chem. Sci.* **2018,** *9,* 100–104. doi:10.1039/c7sc04611a
24. Giri, R.; Chen, X.; Yu, J.-Q. *Angew. Chem., Int. Ed.* **2005,** *44,* 2112–2115. doi:10.1002/anie.200462884
25. Giri, R.; Wasa, M.; Breazzano, S. P.; Yu, J.-Q. *Org. Lett.* **2006,** *8,* 5685–5688. doi:10.1021/ol0618858
26. Rit, R. K.; Yadav, M. R.; Ghosh, K.; Shankar, M.; Sahoo, A. K. *Org. Lett.* **2014,** *16,* 5258–5261. doi:10.1021/ol502337b
27. Yang, X.; Sun, Y.; Sun, T.-y.; Rao, Y. *Chem. Commun.* **2016,** *52,* 6423–6426. doi:10.1039/c6cc00234j
28. Zhu, R.-Y.; Saint-Denis, T. G.; Shao, Y.; He, J.; Sieber, J. D.; Senanayake, C. H.; Yu, J.-Q. *J. Am. Chem. Soc.* **2017,** *139,* 5724–5727. doi:10.1021/jacs.7b02196
29. Kuninobu, Y.; Takai, K. *Bull. Chem. Soc. Jpn.* **2012,** *85,* 656–671. doi:10.1246/bcsj.20120015
30. Kuninobu, Y.; Sueki, S.; Kaplaneris, N.; Ackermann, L. Manganese Catalysis. In *Catalysis with Earth-abundant Elements;* Schneider, U.; Thomas, S., Eds.; The Royal Society of Chemistry: Cambridge. UK, 2020; pp 139–230. doi:10.1039/9781788012775-00139
31. Rohit, K. R.; Radhika, S.; Saranya, S.; Anilkumar, G. *Adv. Synth. Catal.* **2020,** *362,* 1602–1650. doi:10.1002/adsc.201901389
32. Wang, Y.; Liu, Q. *Synlett* **2020,** *31,* 1464–1473. doi:10.1055/s-0040-1707126
33. Chandra, P.; Ghosh, T.; Choudhary, N.; Mohammad, A.; Mobin, S. M. *Coord. Chem. Rev.* **2020,** *411,* 213241. doi:10.1016/j.ccr.2020.213241
34. Waiba, S.; Maji, B. *ChemCatChem* **2020,** *12,* 1891–1902. doi:10.1002/cctc.201902180
35. Kuninobu, Y.; Nishina, Y.; Takeuchi, T.; Takai, K. *Angew. Chem., Int. Ed.* **2007,** *46,* 6518–6520. doi:10.1002/anie.200702256
36. Kuninobu, Y.; Kikuchi, K.; Takai, K. *Chem. Lett.* **2008,** *37,* 740–741. doi:10.1246/cl.2008.740
37. Kuninobu, Y.; Nishi, M.; Yudha S., S.; Takai, K. *Org. Lett.* **2008,** *10,* 3009–3011. doi:10.1021/ol800969h
38. Kuninobu, Y.; Kawata, A.; Nishi, M.; Takata, H.; Takai, K. *Chem. Commun.* **2008,** 6360–6362. doi:10.1039/b814694b
39. Kuninobu, Y.; Kawata, A.; Nishi, M.; Yudha S., S.; Chen, J.; Takai, K. *Chem. – Asian J.* **2009,** *4,* 1424–1433. doi:10.1002/asia.200900137
40. Kuninobu, Y.; Nishi, M.; Kawata, A.; Takata, H.; Hanatani, Y.; Yudha S., S.; Iwai, A.; Takai, K. *J. Org. Chem.* **2010,** *75,* 334–341. doi:10.1021/jo902072q
41. Kuninobu, Y.; Kawata, A.; Yudha, S. S.; Takata, H.; Nishi, M.; Takai, K. *Pure Appl. Chem.* **2010,** *82,* 1491–1501. doi:10.1351/pac-con-09-09-21
42. Kuninobu, Y.; Uesugi, T.; Kawata, A.; Takai, K. *Angew. Chem., Int. Ed.* **2011,** *50,* 10406–10408. doi:10.1002/anie.201104704
43. Sueki, S.; Wang, Z.; Kuninobu, Y. *Org. Lett.* **2016,** *18,* 304–307. doi:10.1021/acs.orglett.5b03474
44. Jiang, X.; Shen, M.; Tang, Y.; Li, C. *Tetrahedron Lett.* **2005,** *46,* 487–489. doi:10.1016/j.tetlet.2004.11.113
45. Nishina, Y.; Morita, J.; Ohtani, B. *RSC Adv.* **2013,** *3,* 2158–2162. doi:10.1039/c2ra22197g
46. Hill, C. L.; Smegal, J. A.; Henly, T. J. *J. Org. Chem.* **1983,** *48,* 3277–3281. doi:10.1021/jo00167a023
47. Liu, W.; Groves, J. T. *J. Am. Chem. Soc.* **2010,** *132,* 12847–12849. doi:10.1021/ja105548x
48. Liu, W.; Groves, J. T. *Acc. Chem. Res.* **2015,** *48,* 1727–1735. doi:10.1021/acs.accounts.5b00062
49. Liu, W.; Groves, J. T. *Angew. Chem., Int. Ed.* **2013,** *52,* 6024–6027. doi:10.1002/anie.201301097
50. Chen, H.; Liu, Z.; Lv, Y.; Tan, X.; Shen, H.; Yu, H.-Z.; Li, C. *Angew. Chem., Int. Ed.* **2017,** *56,* 15411–15415. doi:10.1002/anie.201708197
51. Keck, G. E.; Yates, J. B. *J. Am. Chem. Soc.* **1982,** *104,* 5829–5831. doi:10.1021/ja00385a066
52. Van Ende, D.; Krief, A. *Angew. Chem., Int. Ed. Engl.* **1974,** *13,* 279–280. doi:10.1002/anie.197402792
53. Saikia, I.; Phukan, P. *C. R. Chim.* **2012,** *15,* 688–692. doi:10.1016/j.crci.2012.05.001
54. Hassner, A.; Boerwinkle, F.; Lavy, A. B. *J. Am. Chem. Soc.* **1970,** *92,* 4879–4883. doi:10.1021/ja00719a021
55. Hassner, A. *Acc. Chem. Res.* **1971,** *4,* 9–16. doi:10.1021/ar50037a002
56. Chalfont, G. R.; Perkins, M. J.; Horsfield, A. *J. Chem. Soc. B* **1970,** 401–404. doi:10.1039/j29700000401
57. Workentin, M. S.; Wagner, B. D.; Lusztyk, J.; Wayner, D. D. M. *J. Am. Chem. Soc.* **1995,** *117,* 119–126. doi:10.1021/ja00106a015

License and Terms

This is an Open Access article under the terms of the Creative Commons Attribution License (https://creativecommons.org/licenses/by/4.0). Please note that the reuse, redistribution and reproduction in particular requires that the author(s) and source are credited and that individual graphics may be subject to special legal provisions.

The license is subject to the *Beilstein Journal of Organic Chemistry* terms and conditions: (https://www.beilstein-journals.org/bjoc/terms)

The definitive version of this article is the electronic one which can be found at: https://doi.org/10.3762/bjoc.17.74

BEILSTEIN JOURNAL OF ORGANIC CHEMISTRY

Copper-mediated oxidative C–H/N–H activations with alkynes by removable hydrazides

Feng Xiong[1], Bo Li[2], Chenrui Yang[1], Liang Zou[1], Wenbo Ma[2], Linghui Gu[*2], Ruhuai Mei[*1,2] and Lutz Ackermann[*3]

Full Research Paper

Open Access

Address:
[1]Key Laboratory of Coarse Cereal Processing, Ministry of Agriculture and Rural Affairs, College of Food and Biological Engineering, Chengdu University, Chengdu 610106, P.R. China, [2]Antibiotics Research and Re-evaluation Key Laboratory of Sichuan Province, Sichuan Industrial Institute of Antibiotics, School of Pharmacy, Chengdu University, Chengdu 610052, P.R. China and [3]Institut für Organische und Biomolekulare Chemie, Georg-August-Universität Göttingen, Tammannstraße 2, 37077 Göttingen, Germany and 4Wöhler Research Institute for Sustainable Chemistry (WISCh), Georg-August-Universität Göttingen, Tammannstraße 2, 37077 Göttingen, Germany

Email:
Linghui Gu[*] - cdglh017@163.com; Ruhuai Mei[*] - rmei@cdu.edu.cn; Lutz Ackermann[*] - lutz.ackermann@chemie.uni-goettingen.de

[*] Corresponding author

Keywords:
benzhydrazides; copper; 3-methyleneisoindolin-1-one; removable directing group

Beilstein J. Org. Chem. **2021,** *17,* 1591–1599.
https://doi.org/10.3762/bjoc.17.113

Received: 19 May 2021
Accepted: 02 July 2021
Published: 08 July 2021

This article is part of the thematic issue "Earth-abundant 3d metal catalysis".

Associate Editor: K. Itami

© 2021 Xiong et al.; licensee Beilstein-Institut.
License and terms: see end of document.

Abstract

The efficient copper-mediated oxidative C–H alkynylation of benzhydrazides was accomplished with terminal alkynes. Thus, a heteroaromatic removable *N*-2-pyridylhydrazide allowed for domino C–H/N–H functionalization. The approach featured remarkable functional group compatibility and ample substrate scope. Thereby, highly functionalized aromatic and heteroaromatic isoindolin-1-ones were accessed with high efficacy with rate-limiting C–H cleavage.

Introduction

Inexpensive copper-promoted oxidative C−H activations [1-11] have been recognized as competent tools for the efficient assembly and late-stage functionalization of organic molecules due to the natural abundance and versatile reactivity. Early examples of copper-promoted C−H activation of 2-arylpyridines were disclosed by Yu et al. [12] and Chatami et al. [13] independently. Inspired by these studies, various copper-induced C−H functionalizations, such as arylations, alkynylations, cyanations, aminations, nitrations, oxygenations, thiolations, halogenations, and phosphorylations, among others, were accomplished [14-19].

The 3-methyleneisoindolin-1-one moiety represents a key structure motif in natural products [20-23] or important pharmacophores [24]. In this context, You [25], Huang [26], Liu [27], Li [28], and co-workers elegantly disclosed copper-mediated/catalyzed cascade C−H alkynylation and annulation with terminal alkynes to afford 3-methyleneisoindolinone derivatives, through the assistance of 8-aminoquinoline [29] or 2-aminophenyl-1*H*-pyrazole [30] auxiliaries (Figure 1a). Besides, the cobalt(II)- [31] or nickel(II)-catalyzed [32,33], pyridine oxide (PyO)-directed tandem alkynylation/annulation was realized by Niu and Song et al., which also provided the 3-methyleneisoindolin-1-one scaffolds (Figure 1b). Notably, a sustainable cupraelectro-catalyzed alkyne annulation was very recently achieved by Ackermann et al., which gave rapid access to synthetically meaningful isoindolones (Figure 1c) [34]. In spite of these indisputable advances, the successful removal of the directing groups to deliver the free-NH 3-methyleneisoindolin-1-one has thus far unfortunately proven elusive [35].

2-(1-Methylhydrazinyl)pyridine (MHP) [36] was identified as a powerful removable bidentate directing group, which found widespread application in various cobalt-catalyzed C−H activations [37-40]. Thus, our group also accomplished a set of electrochemical cobalt-catalyzed C−H activations with the MHP auxiliary [41-44]. In continuation of studies on sustainable 3d transition metal-catalyzed C−H activation [41-49], we have now discovered a robust copper-promoted oxidative C−H/N−H functionalization with terminal alkynes (Figure 1d). Notable advantages of our protocol include: 1) removable MHP auxiliary used for copper-mediated oxidative C–H activations, 2) excellent functional group tolerance and compatibility with valuable heterocycles, and 3) mechanistic studies toward copper-mediated oxidative C−H alkynylations.

Results and Discussion

We initiated our investigation by utilizing benzhydrazide **1a** and ethynylbenzene (**2a**) as the standard substrates (Table 1). After preliminary solvent optimization, we discovered that the desired *ortho*-selective C−H activation occurred efficiently by the treatment of hydrazide **1a** with terminal alkyne **2a** and a stoichiometric amount of $Cu(OAc)_2$ in DMSO (Table 1, entries 1–3). Reaction optimization revealed that the most appropriate temperature was 90 °C (Table 1, entries 3–6). An evaluation of bases showed that Na_2CO_3 was optimal (Table 1, entries 7–11). The best result was obtained when $Cu(OAc)_2$ (1.3 equiv) was utilized in DMSO (6.0 mL, Table 1, entries 12–14). A similar result was obtained when $Cu(OAc)_2 \cdot H_2O$ was used instead of $Cu(OAc)_2$ (Table 1, entry 15). Only a trace amount of product **3aa** was observed in the absence of either $Cu(OAc)_2$ or Na_2CO_3 (Table 1, entries 16 and 17). When the reaction was performed under a nitrogen atmosphere, the efficacy was significantly decreased (Table 1, entry 18).

We next examined the versatility of the copper-promoted ethynylbenzene (**2a**) annulation with various benzhydrazides **1** under the optimized reaction conditions (Scheme 1). To our

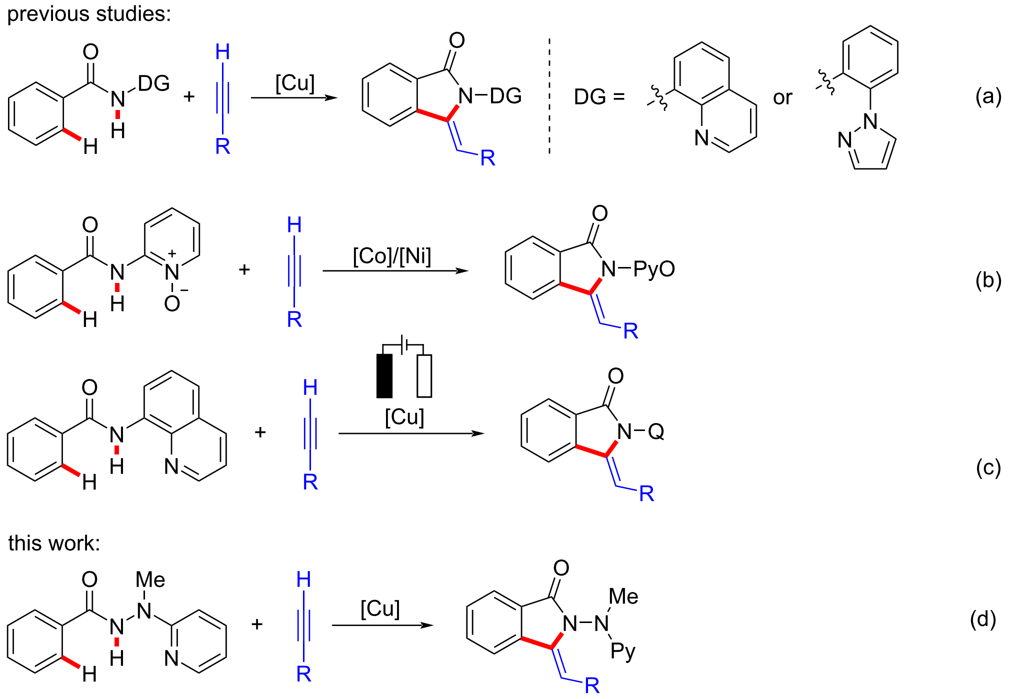

Figure 1: Assembly of 3-methyleneisoindolin-1-one via 3d transition metal-mediated/catalyzed oxidative C−H/N−H activation.

Table 1: Optimization of the copper-mediated C–H/N–H functionalization with terminal alkyne **2a**.[a]

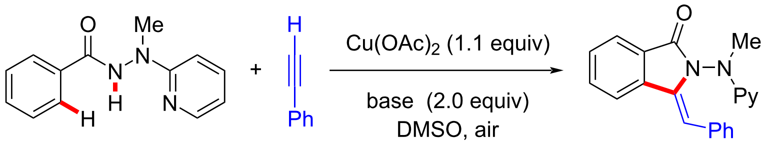

1a **2a** **3aa**

entry	solvent	base	T (°C)	Z/E	yield (%)
1	DMF	Na_2CO_3	90	—	trace
2	NMP	Na_2CO_3	90	—	trace
3	DMSO	Na_2CO_3	90	12:1	67
4	DMSO	Na_2CO_3	110	8:1	57
5	DMSO	Na_2CO_3	80	15:1	41
6	DMSO	Na_2CO_3	60	—	27
7	DMSO	NaOAc	90	—	25
8	DMSO	NaOPiv	90	—	30
9	DMSO	K_2CO_3	90	18:1	58
10	DMSO	Cs_2CO_3	90	20:1	44
11	DMSO	DBU	90	—	13
12[b]	DMSO	Na_2CO_3	90	12:1	42
13[c]	DMSO	Na_2CO_3	90	9:1	83
14[c,d]	DMSO	Na_2CO_3	90	13:1	89
15[d,e]	DMSO	Na_2CO_3	90	12:1	86
16	DMSO	—	90	—	trace
17[f]	DMSO	Na_2CO_3	90	—	trace
18[g]	DMSO	Na_2CO_3	90	—	37

[a]Reaction conditions: **1a** (0.30 mmol), **2a** (0.90 mmol), Cu(OAc)$_2$ (1.1 equiv), base (2.0 equiv), solvent (3.0 mL), 15 h, under air. [b]Cu(OAc)$_2$ (0.8 equiv). [c]Cu(OAc)$_2$ (1.3 equiv). [d]DMSO (6.0 mL). [e]Cu(OAc)$_2$·H$_2$O (1.3 equiv). [f]Without Cu(OAc)$_2$. [g]Under N$_2$.

delight, hydrazides **1** with electron-donating or electron-withdrawing substituents were efficiently converted in the C–H/N–H activation annulation process. Notably, a wide range of valuable electrophilic functional groups, such as halogen, methylthio, cyano, amino, and ester groups, were well compatible, which should prove instrumental for the further diversification of the thus obtained 3-methyleneisoindolin-1-ones **3da**–**ka**. For substrates bearing two potential reactive sites, the annulation selectively took place at the less congested *ortho*-C−H bond (see **3la** and **3ma**). Moreover, the challenging isonicotinic acid hydrazide **1n** was also amenable to this protocol and delivered the desired product **3na** with high regioselectivity.

We further investigated the viable scope of differently substituted terminal alkynes **2** as the general coupling partners for this transformation. As shown in Scheme 2, a variety of valuable electrophilic substitutes were well tolerated. Moreover, substrates with a highly reactive unprotected amino group also delivered the corresponding product **3cn** with good yield. The robustness of this protocol was further highlighted by the excellent reactivity of heterocyclic acetylenes (see **2p**–**r**). However, a complex mixture was observed when an aliphatic terminal alkyne was used, and no annulation product was detected for internal alkynes.

Our copper-promoted C−H annulation protocol was not restricted to terminal alkynes. Under identical reaction conditions, commercially available alkynylcarboxylic acid **4** also proved to be a viable substrate. Thus, the corresponding isoindolone **3aa** was assembled via a tandem decarboxylative C–H/C−C sequence (Scheme 3a). The practical relevance of our approach was reflected by the cleavage of the *N*-2-pyridylhydrazide group, yielding **S-3aa** (Scheme 3b).

Inspired by the remarkable robustness of the copper-promoted C−H activations with alkynes, we became interested to explore the working mode by a set of experiments. To this end, electron-poor arenes inherently reacted preferentially in intermolecular competition experiments (Scheme 4a). This observation

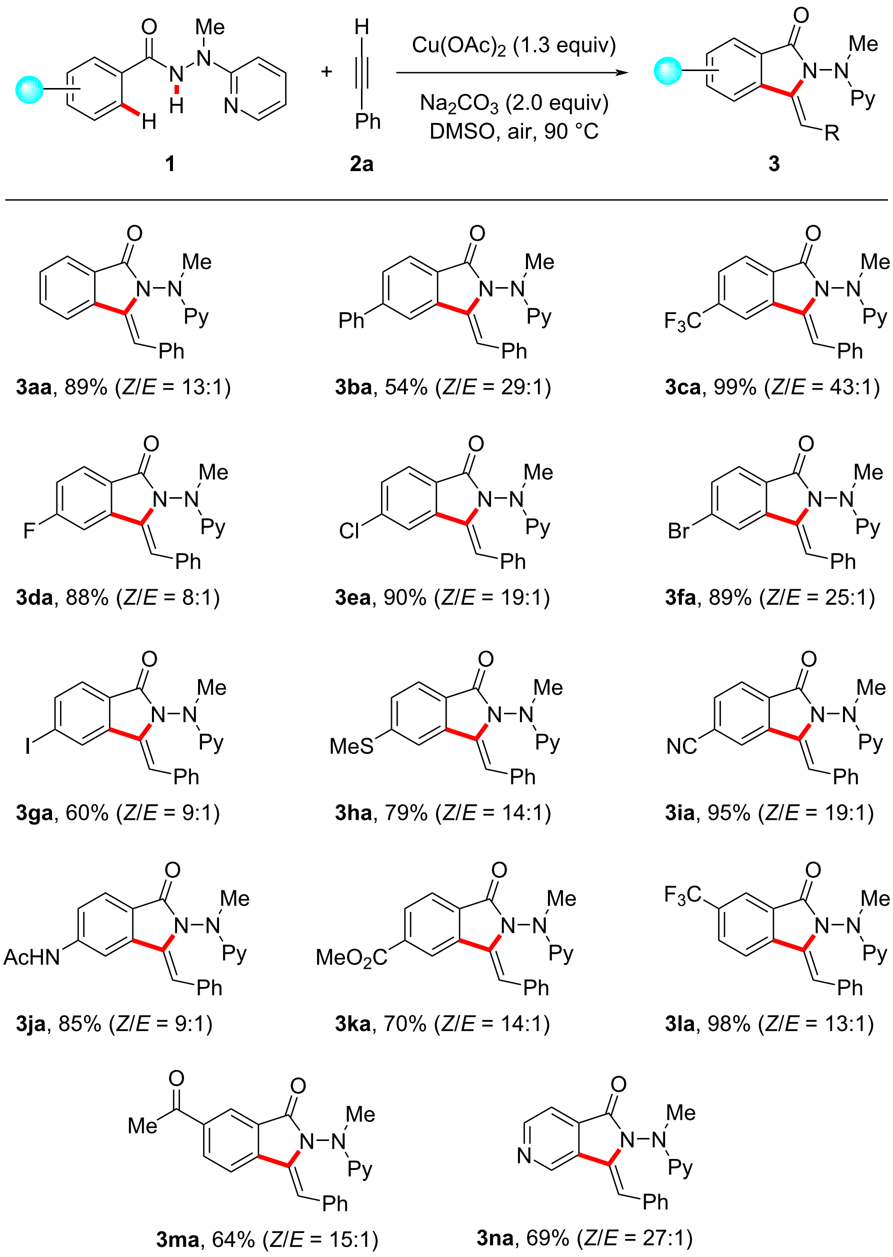
Cu(OAc)$_2$ (1.3 equiv)
Na$_2$CO$_3$ (2.0 equiv)
DMSO, air, 90 °C
1
2a
3
3aa, 89% (Z/E = 13:1)
3ba, 54% (Z/E = 29:1)
3ca, 99% (Z/E = 43:1)
3da, 88% (Z/E = 8:1)
3ea, 90% (Z/E = 19:1)
3fa, 89% (Z/E = 25:1)
3ga, 60% (Z/E = 9:1)
3ha, 79% (Z/E = 14:1)
3ia, 95% (Z/E = 19:1)
3ja, 85% (Z/E = 9:1)
3ka, 70% (Z/E = 14:1)
3la, 98% (Z/E = 13:1)
3ma, 64% (Z/E = 15:1)
3na, 69% (Z/E = 27:1)

Scheme 1: Copper-mediated oxidative C–H/N–H functionalization of hydrazides **1** with ethynylbenzene (**2a**).

could be explained in terms of a concerted metalation deprotonation (CMD) mechanism [50]. Interestingly, electron-rich alkyne **2f** displayed a higher reactivity in the copper-promoted C−H activations as compared to the electron-poor analog **2h** (Scheme 4b). A significant H/D scrambling was not detected in the *ortho*-position of the reisolated benzhydrazide **1c** and product **3ca** when the reaction was conducted with the isotopically labeled D_2O as cosolvent (Scheme 4c). This observation indicated that the C−H cleavage is irreversible. In accordance with this finding, a kinetic isotope effect (KIE) of $k_H/k_D \approx 6.1$ was observed by parallel experiments, again suggesting that the C–H activation is kinetically relevant (Scheme 4d).

Based on our mechanistic findings and previous studies, we propose a tentative plausible reaction pathway in Scheme 5. The transformation commences with substrate coordination and subsequent carboxylate-assisted C−H cleavage to deliver copper(II) intermediate **A**. Next, the copper(III) carboxylate species **B** is generated. Thereafter, a facile base-assisted ligand exchange is followed by reductive elimination to afford the

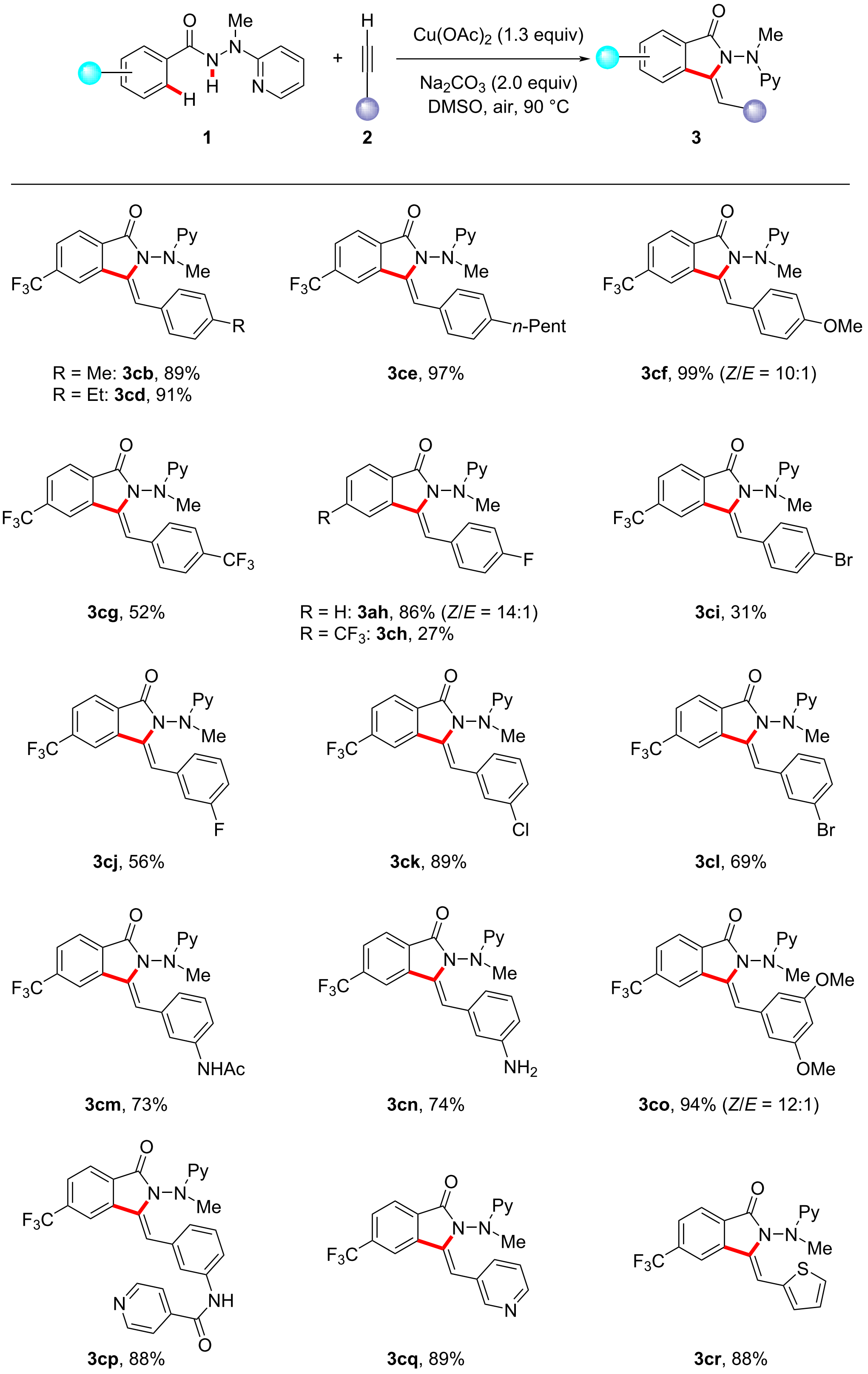
1
2
3
Cu(OAc)2 (1.3 equiv)
Na2CO3 (2.0 equiv)
DMSO, air, 90 °C
R = Me: 3cb, 89%
R = Et: 3cd, 91%
3ce, 97%
3cf, 99% (Z/E = 10:1)
3cg, 52%
R = H: 3ah, 86% (Z/E = 14:1)
R = CF3: 3ch, 27%
3ci, 31%
3cj, 56%
3ck, 89%
3cl, 69%
3cm, 73%
3cn, 74%
3co, 94% (Z/E = 12:1)
3cp, 88%
3cq, 89%
3cr, 88%

Scheme 2: Copper-mediated oxidative C–H/N–H functionalization of **1** with alkynes **2**.

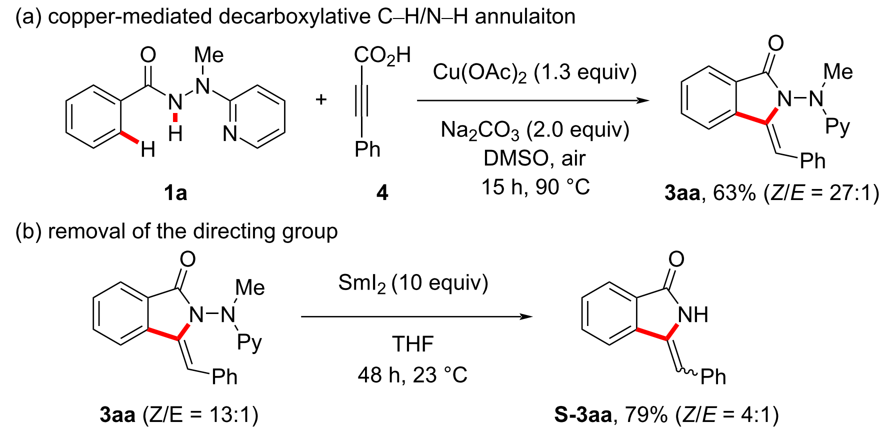
(a) copper-mediated decarboxylative C–H/N–H annulaiton
Cu(OAc)2 (1.3 equiv)
Na2CO3 (2.0 equiv)
DMSO, air
15 h, 90 °C
1a
4
3aa, 63% (Z/E = 27:1)
(b) removal of the directing group
SmI2 (10 equiv)
THF
48 h, 23 °C
3aa (Z/E = 13:1)
S-3aa, 79% (Z/E = 4:1)

Scheme 3: Decaboxylative C–H/N–H activation and cleavage of the directing group.

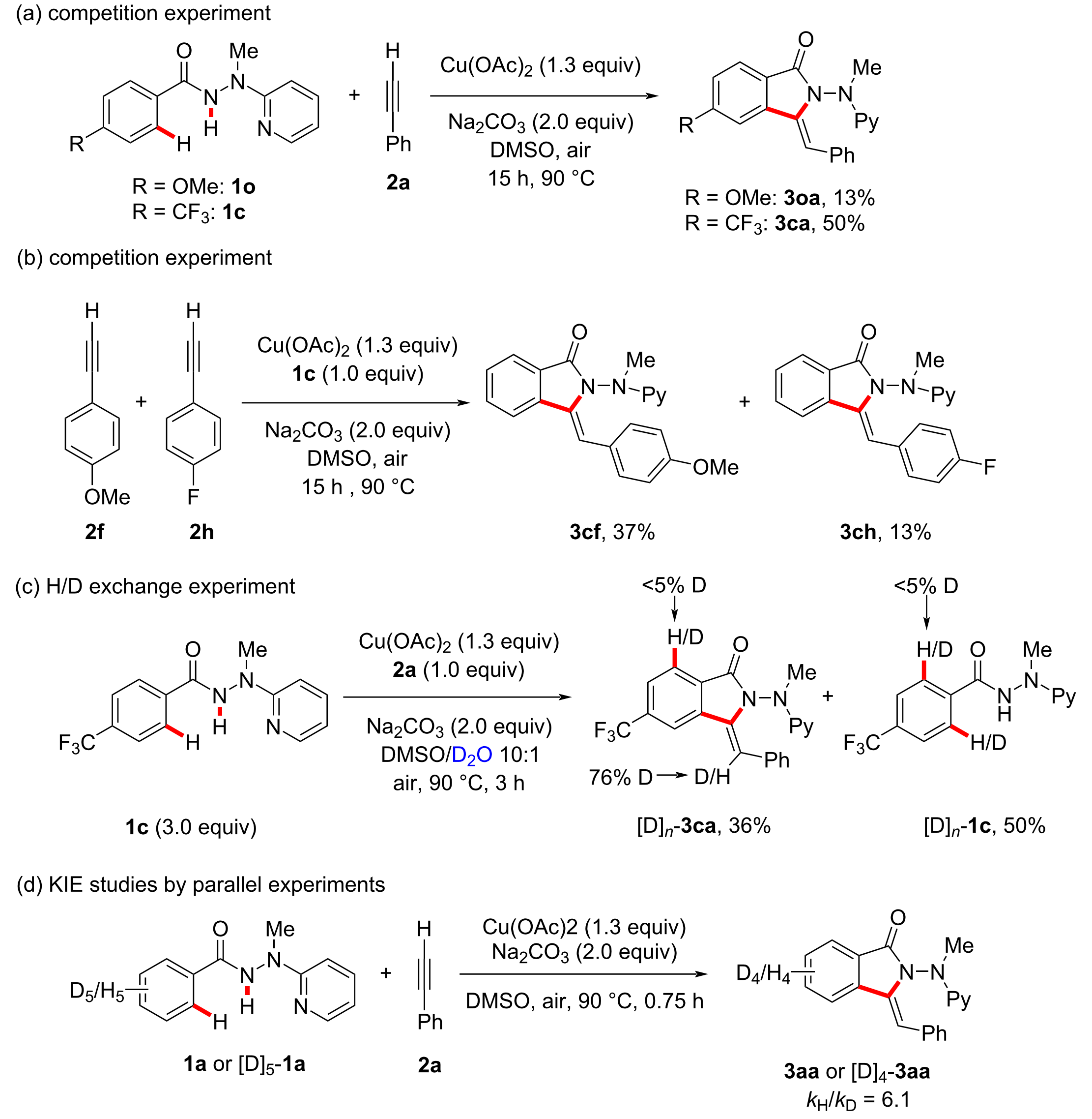
(a) competition experiment
Cu(OAc)2 (1.3 equiv)
Na2CO3 (2.0 equiv)
DMSO, air
15 h, 90 °C
R = OMe: 1o
R = CF3: 1c
2a
R = OMe: 3oa, 13%
R = CF3: 3ca, 50%
(b) competition experiment
Cu(OAc)2 (1.3 equiv)
1c (1.0 equiv)
Na2CO3 (2.0 equiv)
DMSO, air
15 h , 90 °C
2f
2h
3cf, 37%
3ch, 13%
(c) H/D exchange experiment
Cu(OAc)2 (1.3 equiv)
2a (1.0 equiv)
Na2CO3 (2.0 equiv)
DMSO/D2O 10:1
air, 90 °C, 3 h
1c (3.0 equiv)
<5% D
76% D
[D]n-3ca, 36%
<5% D
[D]n-1c, 50%
(d) KIE studies by parallel experiments
Cu(OAc)2 (1.3 equiv)
Na2CO3 (2.0 equiv)
DMSO, air, 90 °C, 0.75 h
1a or [D]5-1a
2a
3aa or [D]4-3aa
kH/kD = 6.1

Scheme 4: Summary of key mechanistic findings.

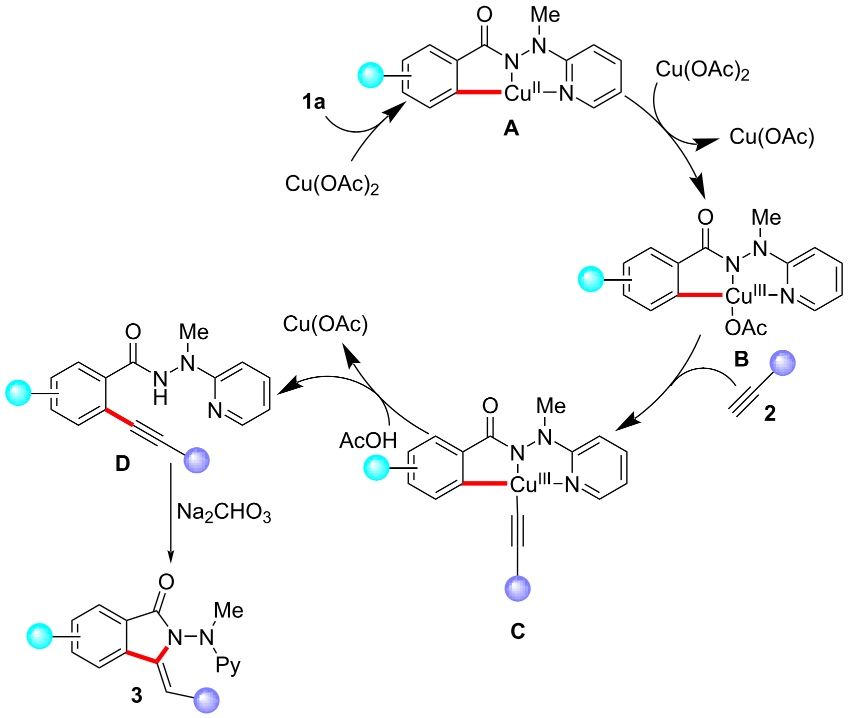

Scheme 5: Proposed reaction pathway.

alkynylated benzamide **D**. Finally, the desired isoindolone **3** is formed via an intramolecular hydroamination in the presence of base.

Conclusion

In conclusion, we have reported on the chelation-assisted oxidative copper-promoted cascade C−H alkynylation and intramolecular annulation. The removable *N*-2-pyridylhydrazide was utilized to facilitate copper(II)-promoted C−H activations. Thus, the robust copper-mediated C−H activation featured remarkable compatibility of synthetically meaningful functional groups, giving facile access to valuable 3-methyleneisoindolin-1-one scaffolds.

Experimental

General information

Yields refer to isolated compounds, estimated to be >95% pure as determined by ^{1}H NMR spectroscopy. Chromatographic separation was carried out on silica gel 60H (200–300 mesh) manufactured by Qingdao Haiyang Chemical Group Co. (China). High-resolution mass spectrometry (HRMS) was measured on a Thermo-DFS mass spectrometer. NMR spectra were recorded on a JEOL 600 NMR device (^{1}H: 600 MHz; ^{13}C: 150 MHz; ^{19}F: 565 MHz) in $CDCl_3$. If not otherwise specified, the chemical shift (δ) is given in ppm.

Materials

Reactions were carried out under an argon atmosphere using predried glassware, if not noted otherwise. Benzhydrazides **1** were synthesized according to a previously described method [36,44]. Other chemicals were obtained from commercial sources and were used without further purification.

General procedure for the copper-promoted oxidative C−H/N−H activation with alkynes

To a 25 mL Schlenk tube were added benzhydrazide **1** (0.30 mmol, 1.00 equiv), the alkyne (0.90 mmol, 3.0 equiv), $Cu(OAc)_2$ (71 mg, 0.39 mmol, 1.30 equiv), and Na_2CO_3 (64 mg, 0.60 mmol, 2.00 equiv) under an air atmosphere. The mixture was stirred at 90 °C for 15 h. At ambient temperature, H_2O (15 mL) and Et_3N (0.5 mL) were added, and a suspension was formed immediately. After filtrated through a Celite® pad, the reaction mixture was extracted with EtOAc (3 × 20 mL). The combined organic phase was washed with brine (20 mL) and dried over Na_2SO_4. Then, Et_3N (0.5 mL) and silica gel (0.8 g) were added, and the combined solvent was removed under reduced pressure. The residue solid sample was purified by column chromatography on silica gel (petroleum/EtOAc 5:1 to 2:1, with 1% Et_3N), yielding the desired product **3**.

(*Z*)-3-Benzylidene-2-(methyl[pyridin-2-yl]amino)isoindolin-1-one (**3aa**)

The general procedure was followed using hydrazide **1a** (68.2 mg, 0.30 mmol) and alkyne **2a** (91.9 mg, 0.90 mmol). Purification by column chromatography on silica gel (petroleum/EtOAc 20:1, with 1% Et_3N) yielded **3aa** (87.4 mg, 89%, *Z*/*E* = 13:1) as a light yellow solid. mp 67–68 °C; ^1H NMR ($CDCl_3$, 600 MHz) δ 8.13 (ddd, *J* = 5.0; 1.9; 0.9 Hz, 1H), 7.90 (dd, *J* = 7.6; 1.0 Hz, 1H), 7.85–7.82 (m, 1H), 7.70 (d, *J* = 1.2 Hz, 1H), 7.56 (dd, *J* = 7.6; 0.9 Hz, 1H), 7.44 (ddd, *J* = 8.8; 7.1; 1.9 Hz, 1H), 7.17–7.05 (m, 5H), 6.85 (d, *J* = 0.9 Hz, 1H), 6.67 (ddd, *J* = 7.2; 5.0; 0.9 Hz, 1H), 6.44–6.41 (m, 1H), 3.01 (s, 3H); $^{13}C\{^1H\}$ NMR ($CDCl_3$, 150 MHz) δ 165.7 (C_q), 157.6 (C_q), 147.7 (CH), 137.4 (CH), 136.2 (C_q), 133.2 (C_q), 132.8 (CH), 132.1 (C_q), 129.3 (CH), 128.7 (CH), 127.3 (CH), 127.3 (CH), 126.5 (C_q), 123.8 (CH), 119.8 (CH), 114.3 (CH), 107.8 (CH), 106.4 (CH), 36.7 (CH_3); HRESIMS (*m/z*): $[M + H]^+$ calcd for $C_{21}H_{18}N_3O$, 328.1444; found, 328.1439.

Supporting Information

Supporting Information File 1

Characterization data for **3** and copies of ^1H, ^{13}C, and ^{19}F NMR spectra.
[https://www.beilstein-journals.org/bjoc/content/supplementary/1860-5397-17-113-S1.pdf]

Funding

Generous support by National Natural Science Foundation of China (Grant No. 21901023), “Thousand Talents Program” of Sichuan Province (R. M.) and the DFG (Gottfried-Wilhelm-Leibniz award to L. A.) is gratefully acknowledged.

ORCID® iDs

Wenbo Ma - https://orcid.org/0000-0002-9690-3639
Linghui Gu - https://orcid.org/0000-0001-6786-5947
Ruhuai Mei - https://orcid.org/0000-0001-7866-231X
Lutz Ackermann - https://orcid.org/0000-0001-7034-8772

Preprint

A non-peer-reviewed version of this article has been previously published as a preprint: https://doi.org/10.3762/bxiv.2021.39.v1

References

1. Gandeepan, P.; Finger, L. H.; Meyer, T. H.; Ackermann, L. *Chem. Soc. Rev.* **2020,** *49,* 4254–4272. doi:10.1039/d0cs00149j
2. Ellman, J. A.; Ackermann, L.; Shi, B.-F. *J. Org. Chem.* **2019,** *84,* 12701–12704. doi:10.1021/acs.joc.9b02663
3. Yi, H.; Zhang, G.; Wang, H.; Huang, Z.; Wang, J.; Singh, A. K.; Lei, A. *Chem. Rev.* **2017,** *117,* 9016–9085. doi:10.1021/acs.chemrev.6b00620
4. Wei, Y.; Hu, P.; Zhang, M.; Su, W. *Chem. Rev.* **2017,** *117,* 8864–8907. doi:10.1021/acs.chemrev.6b00516
5. Rao, W.-H.; Shi, B.-F. *Org. Chem. Front.* **2016,** *3,* 1028–1047. doi:10.1039/c6qo00156d
6. Zheng, Q.-Z.; Jiao, N. *Chem. Soc. Rev.* **2016,** *45,* 4590–4627. doi:10.1039/c6cs00107f
7. Wencel-Delord, J.; Glorius, F. *Nat. Chem.* **2013,** *5,* 369–375. doi:10.1038/nchem.1607
8. Rouquet, G.; Chatani, N. *Angew. Chem., Int. Ed.* **2013,** *52,* 11726–11743. doi:10.1002/anie.201301451
9. Engle, K. M.; Mei, T.-S.; Wasa, M.; Yu, J.-Q. *Acc. Chem. Res.* **2012,** *45,* 788–802. doi:10.1021/ar200185g
10. Yamaguchi, J.; Yamaguchi, A. D.; Itami, K. *Angew. Chem., Int. Ed.* **2012,** *51,* 8960–9009. doi:10.1002/anie.201201666
11. Li, C.-J. *Acc. Chem. Res.* **2009,** *42,* 335–344. doi:10.1021/ar800164n
12. Chen, X.; Hao, X.-S.; Goodhue, C. E.; Yu, J.-Q. *J. Am. Chem. Soc.* **2006,** *128,* 6790–6791. doi:10.1021/ja061715q
13. Uemura, T.; Imoto, S.; Chatani, N. *Chem. Lett.* **2006,** *35,* 842–843. doi:10.1246/cl.2006.842
14. Kim, H.; Heo, J.; Kim, J.; Baik, M.-H.; Chang, S. *J. Am. Chem. Soc.* **2018,** *140,* 14350–14356. doi:10.1021/jacs.8b08826
15. Takamatsu, K.; Hirano, K.; Miura, M. *Angew. Chem., Int. Ed.* **2017,** *56,* 5353–5357. doi:10.1002/anie.201701918
16. Wang, S.; Guo, R.; Wang, G.; Chen, S.-Y.; Yu, X.-Q. *Chem. Commun.* **2014,** *50,* 12718–12721. doi:10.1039/c4cc06246a
17. Nishino, M.; Hirano, K.; Satoh, T.; Miura, M. *Angew. Chem., Int. Ed.* **2013,** *52,* 4457–4461. doi:10.1002/anie.201300587
18. Kim, J.; Kim, H.; Chang, S. *Org. Lett.* **2012,** *14,* 3924–3927. doi:10.1021/ol301674m
19. Zhang, L.; Liu, Z.; Li, H.; Fang, G.; Barry, B.-D.; Belay, T. A.; Bi, X.; Liu, Q. *Org. Lett.* **2011,** *13,* 6536–6539. doi:10.1021/ol2028288
20. Lamblin, M.; Couture, A.; Deniau, E.; Grandclaudon, P. *Org. Biomol. Chem.* **2007,** *5,* 1466–1471. doi:10.1039/b701661a
21. Rys, V.; Couture, A.; Deniau, E.; Grandclaudon, P. *Tetrahedron* **2003,** *59,* 6615–6619. doi:10.1016/s0040-4020(03)01067-6
22. Chia, Y.-C.; Chang, F.-R.; Teng, C.-M.; Wu, Y.-C. *J. Nat. Prod.* **2000,** *63,* 1160–1163. doi:10.1021/np000063v
23. Blaskó, G.; Gula, D. J.; Shamma, M. *J. Nat. Prod.* **1982,** *45,* 105–122. doi:10.1021/np50020a001
24. Botero Cid, H. M.; Tränkle, C.; Baumann, K.; Pick, R.; Mies-Klomfass, E.; Kostenis, E.; Mohr, K.; Holzgrabe, U. *J. Med. Chem.* **2000,** *43,* 2155–2164. doi:10.1021/jm991136e
25. Dong, J.; Wang, F.; You, J. *Org. Lett.* **2014,** *16,* 2884–2887. doi:10.1021/ol501023n
26. Zhang, Y.; Wang, Q.; Yu, H.; Huang, Y. *Org. Biomol. Chem.* **2014,** *12,* 8844–8850. doi:10.1039/c4ob01312c
27. Zhu, W.; Wang, B.; Zhou, S.; Liu, H. *Beilstein J. Org. Chem.* **2015,** *11,* 1624–1631. doi:10.3762/bjoc.11.177
28. Lee, W.-C. C.; Wang, W.; Li, J. J. *J. Org. Chem.* **2018,** *83,* 2382–2388. doi:10.1021/acs.joc.7b02893
29. Zaitsev, V. G.; Shabashov, D.; Daugulis, O. *J. Am. Chem. Soc.* **2005,** *127,* 13154–13155. doi:10.1021/ja054549f
30. Lee, W.-C. C.; Shen, Y.; Gutierrez, D. A.; Li, J. J. *Org. Lett.* **2016,** *18,* 2660–2663. doi:10.1021/acs.orglett.6b01105
31. Zhang, L.-B.; Hao, X.-Q.; Liu, Z.-J.; Zheng, X.-X.; Zhang, S.-K.; Niu, J.-L.; Song, M.-P. *Angew. Chem., Int. Ed.* **2015,** *54,* 10012–10015. doi:10.1002/anie.201504962

32. Zheng, X.-X.; Du, C.; Zhao, X.-M.; Zhu, X.; Suo, J.-F.; Hao, X.-Q.; Niu, J.-L.; Song, M.-P. *J. Org. Chem.* **2016,** *81,* 4002–4011. doi:10.1021/acs.joc.6b00129
33. Hao, X.-Q.; Du, C.; Zhu, X.; Li, P.-X.; Zhang, J.-H.; Niu, J.-L.; Song, M.-P. *Org. Lett.* **2016,** *18,* 3610–3613. doi:10.1021/acs.orglett.6b01632
34. Tian, C.; Dhawa, U.; Scheremetjew, A.; Ackermann, L. *ACS Catal.* **2019,** *9,* 7690–7696. doi:10.1021/acscatal.9b02348
35. Fitzgerald, L. S.; O'Duill, M. L. *Chem. – Eur. J.* **2021,** *27,* 8411–8436. doi:10.1002/chem.202100093
36. Zhai, S.; Qiu, S.; Chen, X.; Wu, J.; Zhao, H.; Tao, C.; Li, Y.; Cheng, B.; Wang, H.; Zhai, H. *Chem. Commun.* **2018,** *54,* 98–101. doi:10.1039/c7cc08533h
37. Zhao, H.; Wang, T.; Qing, Z.; Zhai, H. *Chem. Commun.* **2020,** *56,* 5524–5527. doi:10.1039/d0cc01582b
38. Zhao, H.; Shao, X.; Wang, T.; Zhai, S.; Qiu, S.; Tao, C.; Wang, H.; Zhai, H. *Chem. Commun.* **2018,** *54,* 4927–4930. doi:10.1039/c8cc01774c
39. Zhai, S.; Qiu, S.; Chen, X.; Tao, C.; Li, Y.; Cheng, B.; Wang, H.; Zhai, H. *ACS Catal.* **2018,** *8,* 6645–6649. doi:10.1021/acscatal.8b01720
40. Qiu, S.; Zhai, S.; Wang, H.; Tao, C.; Zhao, H.; Zhai, H. *Adv. Synth. Catal.* **2018,** *360,* 3271–3276. doi:10.1002/adsc.201800388
41. Mei, R.; Fang, X.; He, L.; Sun, J.; Zou, L.; Ma, W.; Ackermann, L. *Chem. Commun.* **2020,** *56,* 1393–1396. doi:10.1039/c9cc09076b
42. Sau, S. C.; Mei, R.; Struwe, J.; Ackermann, L. *ChemSusChem* **2019,** *12,* 3023–3027. doi:10.1002/cssc.201900378
43. Mei, R.; Ma, W.; Zhang, Y.; Guo, X.; Ackermann, L. *Org. Lett.* **2019,** *21,* 6534–6538. doi:10.1021/acs.orglett.9b02463
44. Mei, R.; Sauermann, N.; Oliveira, J. C. A.; Ackermann, L. *J. Am. Chem. Soc.* **2018,** *140,* 7913–7921. doi:10.1021/jacs.8b03521
45. Mei, R.; Dhawa, U.; Samanta, R. C.; Ma, W.; Wencel-Delord, J.; Ackermann, L. *ChemSusChem* **2020,** *13,* 3306–3356. doi:10.1002/cssc.202000024
46. Sauermann, N.; Mei, R.; Ackermann, L. *Angew. Chem., Int. Ed.* **2018,** *57,* 5090–5094. doi:10.1002/anie.201802206
47. Mei, R.; Wang, H.; Warratz, S.; Macgregor, S. A.; Ackermann, L. *Chem. – Eur. J.* **2016,** *22,* 6759–6763. doi:10.1002/chem.201601101
48. Mei, R.; Loup, J.; Ackermann, L. *ACS Catal.* **2016,** *6,* 793–797. doi:10.1021/acscatal.5b02661
49. Mei, R.; Ackermann, L. *Adv. Synth. Catal.* **2016,** *358,* 2443–2448. doi:10.1002/adsc.201600384
50. Ackermann, L. *Chem. Rev.* **2011,** *111,* 1315–1345. doi:10.1021/cr100412j

License and Terms

This is an Open Access article under the terms of the Creative Commons Attribution License (https://creativecommons.org/licenses/by/4.0). Please note that the reuse, redistribution and reproduction in particular requires that the author(s) and source are credited and that individual graphics may be subject to special legal provisions.

The license is subject to the *Beilstein Journal of Organic Chemistry* terms and conditions: (https://www.beilstein-journals.org/bjoc/terms)

The definitive version of this article is the electronic one which can be found at: https://doi.org/10.3762/bjoc.17.113

BEILSTEIN JOURNAL OF ORGANIC CHEMISTRY

Sustainable manganese catalysis for late-stage C–H functionalization of bioactive structural motifs

Jongwoo Son[1,2]

Review

Open Access

Address:
[1]Department of Chemistry, Dong-A University, Busan 49315, South Korea and [2]Department of Chemical Engineering (BK21 FOUR Graduate Program), Dong-A University, Busan 49315, South Korea

Email:
Jongwoo Son - sonorganic@dau.ac.kr

Keywords:
bioactive molecules; 3d transition metals; late-stage functionalization; manganese catalyst; sustainable catalysis

Beilstein J. Org. Chem. **2021,** *17,* 1733–1751.
https://doi.org/10.3762/bjoc.17.122

Received: 27 April 2021
Accepted: 15 July 2021
Published: 26 July 2021

This article is part of the thematic issue "Earth-abundant 3d metal catalysis".

Associate Editor: I. Marek

© 2021 Son; licensee Beilstein-Institut.
License and terms: see end of document.

Abstract

The late-stage C–H functionalization of bioactive structural motifs is a powerful synthetic strategy for accessing advanced agrochemicals, bioimaging materials, and drug candidates, among other complex molecules. While traditional late-stage diversification relies on the use of precious transition metals, the utilization of 3d transition metals is an emerging approach in organic synthesis. Among the 3d metals, manganese catalysts have gained increasing attention for late-stage diversification due to the sustainability, cost-effectiveness, ease of operation, and reduced toxicity. Herein, we summarize recent manganese-catalyzed late-stage C–H functionalization reactions of biologically active small molecules and complex peptides.

Introduction

Manganese, a 3d transition metal, allows for a potentially ideal sustainable catalytic system because of the natural abundance, cost-effectiveness, and low toxicity. In addition, it presents variable oxidation states (−3 to +7), which enable diverse catalytically active manganese complexes, providing characteristic reaction profiles. Since the first pioneering manganese-mediated reaction for accessing azobenzenes was unveiled [1], manganese catalysts have exhibited a significant capacity for powerful C–H functionalization, and they have therefore been actively utilized in the area of sustainable organic syntheses [2-6].

Catalytic late-stage C–H functionalization, a highly efficient synthetic strategy, is regarded as a crucial tactic in the area of natural products, drug discovery, and medicinal chemistry [7-12] as it confers an invaluable synthetic opportunity for the facile diversification of biologically active complex molecules at the late stage. In recent years, much effort has been devoted to developing sustainable catalytic late-stage C–H functionalization methods that utilize naturally abundant 3d metal catalysts.

This review will provide an overview on recent studies on Mn-catalyzed late-stage C–H functionalization of challenging substrates, such as biologically active molecules and complex peptides, which are of great importance to medicinal chemists and are categorized according to the transformations involved.

Review

Manganese-catalyzed late-stage C–H fluorination

The fluorination of organic molecules [13-16], a highly valuable synthetic transformation, has been widely investigated in medicinal chemistry and in the pharmaceutical industry as it generally imparts the targeted fluorinated molecules with dramatically improved physical, biological, and/or chemical properties [17-21]. Among the catalytic C–F forming processes, aliphatic late-stage fluorination (C_{sp3}–F) is relatively challenging due to the omnipresent unactivated C–H bonds of the substrate molecules. In 2012, Groves et al. revealed a manganese porphyrin-catalyzed late-stage C_{sp3}–H fluorination method (Scheme 1) [22]. In the authors' approach, a direct late-stage process facilitated the fluorination of sclareolide (**1**) and complex steroid **3**. Sclareolide (**1**) is a naturally available terpenoid with antifungal and anticancer activities [23]. Under the optimized reaction conditions, sclareolide (**1**) is fluorinated at the C2 and C3 positions in 42% (see **2a**) and 16% yield (see **2b**), respectively. Therein, C2 fluorination was favored, and **2a** was observed as the major product due to the sterically congested environment at C3 created by the adjacent *gem*-dimethyl groups. The regioselectivity at the C2 position was observed similarly in a study on Mn-catalyzed chlorination [24]. This manganese porphyrin catalytic system was also effective in the direct site-selective fluorination of complex steroid scaffold **3**, containing 28 unactivated C–H bonds. Based on the authors' analysis of steric and electronic factors, it was suggested that the methylene units at C2 and C3 of the A-ring system were the most reactive sites for hydrogen abstraction, yielding fluorinated steroids **4a** and **4b** in 32% and 23% yield, respectively. For both products, α-fluorination was dominant over β-fluorination, likely because α-fluorination occurred on the less sterically hindered face. Additionally, difluorination was observed with negligible amounts because the monofluorinated product is rendered more electronically deficient by the first fluorine atom.

Based on an analysis by DFT calculations, the postulated reaction pathway of manganese-catalyzed C–H fluorination is described in Figure 1. Initially, resting Mn(TMP)F undergoes oxidation, generating oxomanganese(V) complex O=Mn(TMP)F (**5A**), followed by H-abstraction of the substrate **1** or **3**, providing HO–Mn(TMP)F (**5B**) and a C-centered radical. The *trans*-

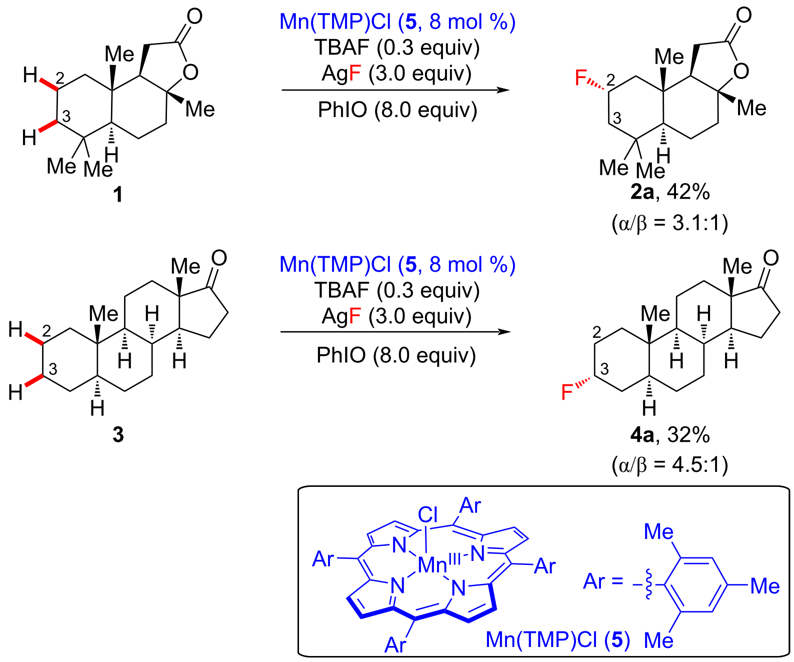

Scheme 1: Mn-catalyzed late-stage fluorination of sclareolide (**1**) and complex steroid **3**.

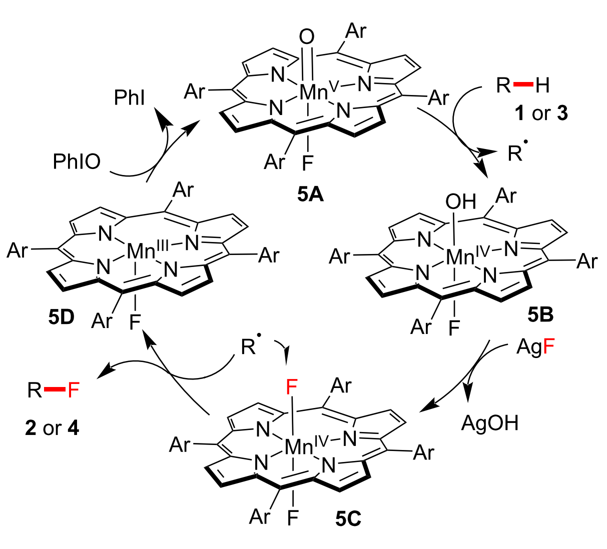
O
Ar
Mn^{V}
N
Ar
Ar
F
5A
R–H
1 or 3
R•
PhI
PhIO
Ar
Mn^{III}
5D
F
OH
Mn^{IV}
5B
AgF
AgOH
R•
R–F
2 or 4
F
Mn^{IV}
5C

Figure 1: Proposed reaction mechanism of C–H fluorination by a manganese porphyrin catalyst.

difluoro-substituted Mn(TMP) intermediate **5C**, generated by an excess of the fluoride source, traps the C-centered radical, finally delivering the fluorinated product **2** or **4**.

Thereafter, the same group successively reported the first manganese-catalyzed late-stage ^{18}F-fluorination of a wide range of biologically active compounds (Scheme 2) [25]. It is well known that the most utilized radioisotope for positron emission tomography (PET) in clinical and preclinical research is ^{18}F. Radiopharmaceuticals should be prepared at the late stage of the entire synthetic protocol because of the short half-lives of radioisotopes [26-29]. In their study, the authors used an aqueous ^{18}F-fluoride solution obtained by the nuclear reaction using a cyclotron, and manganese–salen complex **7** was used as a fluoride transfer catalyst, which facilitated late-stage C–H radiofluorination, affording the corresponding radiofluorinated bioactive molecules **8a**–**h**. In general, the regioselectivity of fluorination was observed at the less sterically hindered benzylic position.

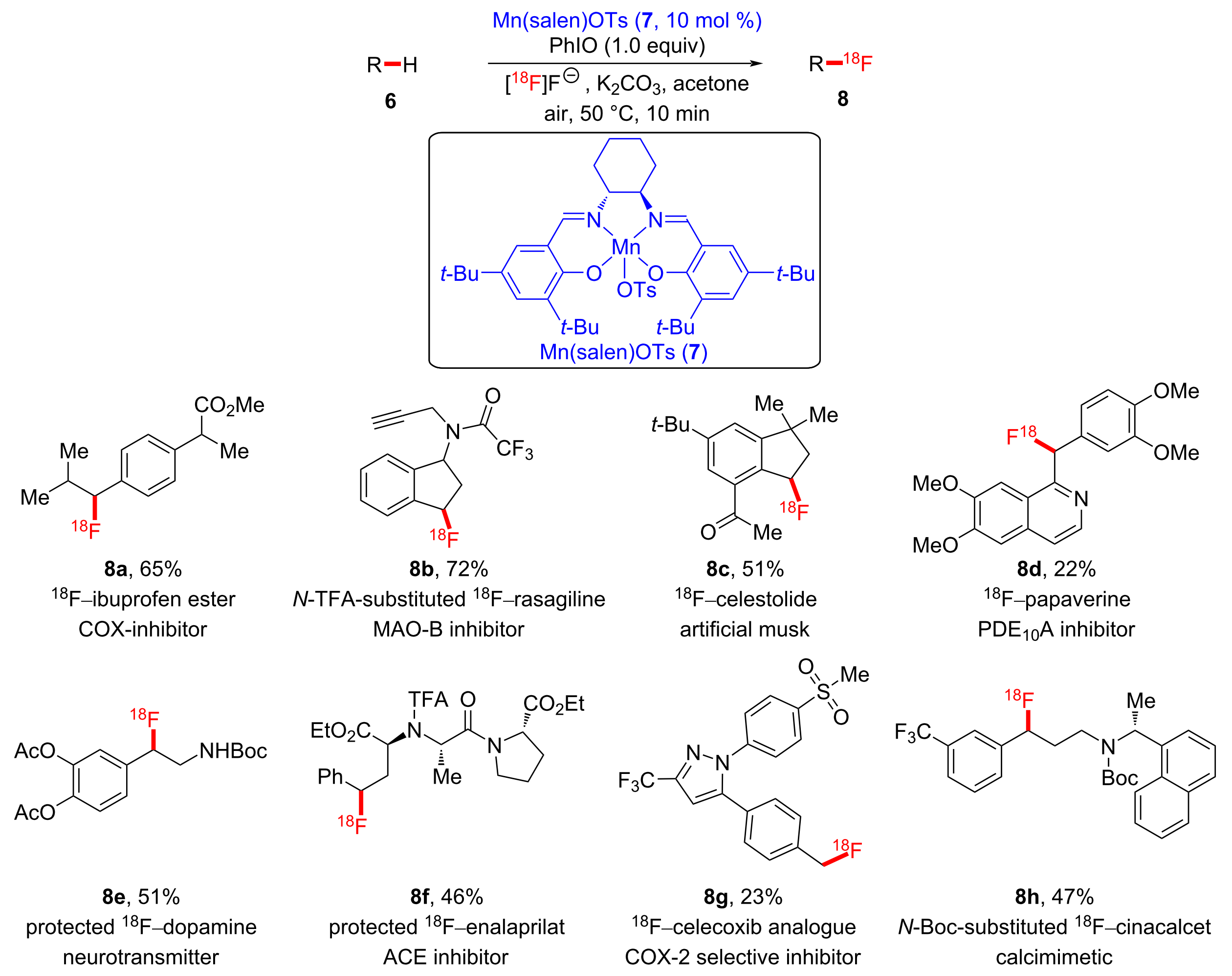
R–H
6
Mn(salen)OTs (7, 10 mol %)
PhIO (1.0 equiv)
[^{18}F]F$^{\ominus}$, K$_2$CO$_3$, acetone
air, 50 °C, 10 min
R–^{18}F
8
t-Bu
Mn
OTs
Mn(salen)OTs (7)
8a, 65%
^{18}F–ibuprofen ester
COX-inhibitor
8b, 72%
N-TFA-substituted ^{18}F–rasagiline
MAO-B inhibitor
8c, 51%
^{18}F–celestolide
artificial musk
8d, 22%
^{18}F–papaverine
PDE$_{10}$A inhibitor
8e, 51%
protected ^{18}F–dopamine
neurotransmitter
8f, 46%
protected ^{18}F–enalaprilat
ACE inhibitor
8g, 23%
^{18}F–celecoxib analogue
COX-2 selective inhibitor
8h, 47%
N-Boc-substituted ^{18}F–cinacalcet
calcimimetic

Scheme 2: Late-stage radiofluorination of biologically active complex molecules.

The proposed reaction mechanism for radiofluorination is depicted in Figure 2. Although the *trans*-difluoro-substituted Mn(IV) complex is the reactive F-transfer intermediate in ^{19}F chemistry, the formation of a *trans*-^{18}F-difluoro-substituted Mn(IV) complex is not reasonable because of the limiting amount of the ^{18}F source. Therefore, it was suggested that ^{18}F-fluorination is more likely to occur through an intermediate HO–Mn–^{18}F motif as in **7C**. These manganese-catalyzed late-stage C–H fluorinations showcase a convenient and operationally simple fluorination strategy suitable for bioactive structural motifs.

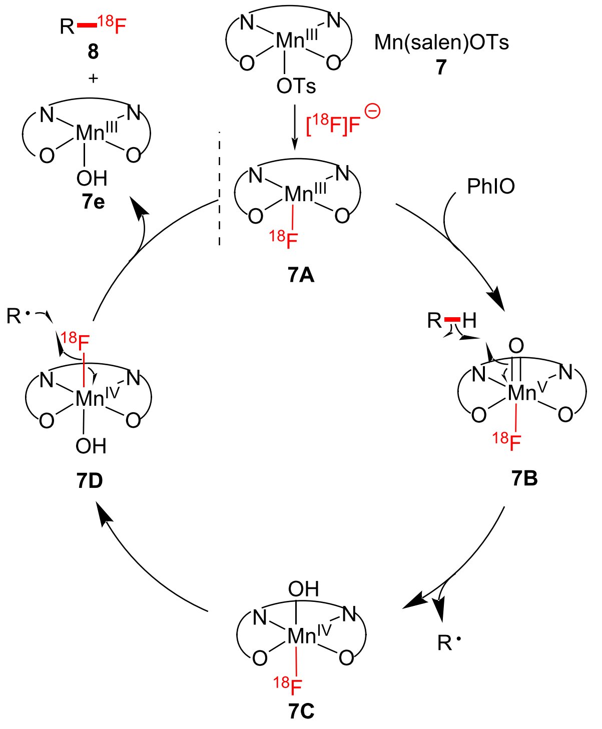

Figure 2: Proposed mechanism of C–H radiofluorination.

Manganese-catalyzed late-stage C–H azidation

In organic synthesis, organic azides are of considerable significance in the fields of medicinal chemistry, chemical biology, and nanotechnology as they can participate in elegant conjugative transformations, such as azide–alkyne [3 + 2]-cycloaddition [30-37].

Based on their previous late-stage fluorination studies [22,25], Groves et al. further showcased a manganese(III)–salen-catalyzed azidation process using an aqueous azide solution as a convenient azide source to execute facile C–H azidation of pharmaceutical-like complex molecules (Scheme 3) [38]. In this study, the regioselectivity is governed not only by electronic and steric effects of the manganese catalysts **5** and **10** but also by the electronic properties of the substrates. Pregabalin is an anticonvulsant drug used to treat epilepsy and anxiety disorders [39], and an analogue of pregabalin was transformed to azidated derivative **11a**. It is noteworthy that positional selectivity was observed for the α-position of the carbamate functional group due to the stabilization of the carbon radical by the adjacent carbamate group. The naturally available substrate **9b** was shown to undergo the azidation process at the less sterically hindered position. An analogue of rasagiline (Azilect®), a Parkinson's disease drug, successfully underwent benzylic azidation, providing product **11c**. Other complex molecules bearing aromatic groups were also successfully azidated, predominantly at the benzylic position (see **11e** and **11f**). Notably, diazidation of **9e** was observed as the major side reaction (18%). Interestingly, OBz-substituted artemisinin **9g** was converted to OBz-substituted N_3–artemisinin **11g** via azidation at the tertiary position using the manganese–salen catalyst. Furthermore, this Mn-catalyzed azidation protocol is highly robust in air, highlighting the practical simplicity of late-stage C–H azidation of bioactive molecules.

A plausible reaction pathway was proposed, as illustrated in Figure 3. Similar to manganese-catalyzed C–H fluorination [22], the resting Mn(III) catalyst is oxidized to O=Mn(V)–N_3 complex **10B**. Subsequently, an alkyl radical is generated upon H-abstraction by forming Mn(VI) intermediate **10C**. The resulting alkyl radical is then trapped by Mn(IV)–N_3 intermediate **10D**, affording azidation product **11**. Upon regeneration, the catalyst participates in the next catalytic cycle. In this Mn-catalyzed azidation study, the azide/oxygenated product ratio was 2:1–4:1. Therefore, a chemoselective manner is of dire need to avoid unwanted C–H oxygenation.

In 2020, the Lei group disclosed the combination of a manganese catalyst and a electrophotocatalyst for the late-stage C_{sp3}–H azidation of biologically active molecules in a selective and sustainable manner (Scheme 4) [40]. Memantine is a drug used to treat neurodegenerative disorders such as Alzheimer's disease [41,42]. In the authors' study, azidated *N*-protected memantine **13a** was successfully generated by employing electricity and visible-light irradiation in the presence of a Mn catalyst. High regioselectivity was observed at tertiary or benzylic positions (see **13a**–**c**). For commercially available drug derivatives, methyl esters of ibuprofen and loxoprofen underwent regioselective azidation at the secondary benzylic sites over tertiary benzylic sites (see **13d** and **13e**).

Additional mechanistic studies support the reaction pathway depicted in Figure 4. The azide anion is oxidized to a radical species on the anodic surface, where Mn(II)/L–N_3 is also

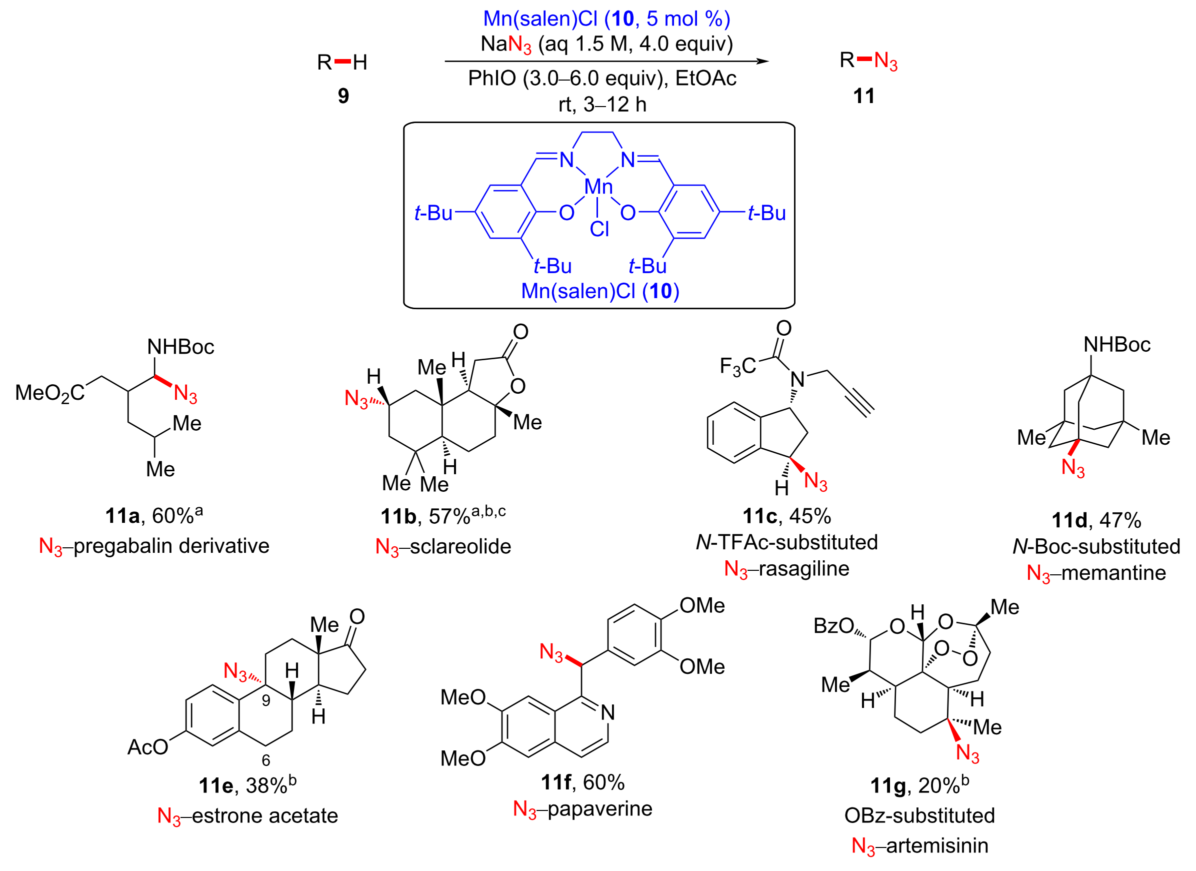
R–H
9
Mn(salen)Cl (10, 5 mol %)
NaN3 (aq 1.5 M, 4.0 equiv)
PhIO (3.0–6.0 equiv), EtOAc
rt, 3–12 h
R–N3
11
Mn(salen)Cl (10)
11a, 60%a
N3–pregabalin derivative
11b, 57%a,b,c
N3–sclareolide
11c, 45%
N-TFAc-substituted
N3–rasagiline
11d, 47%
N-Boc-substituted
N3–memantine
11e, 38%b
N3–estrone acetate
11f, 60%
N3–papaverine
11g, 20%b
OBz-substituted
N3–artemisinin

Scheme 3: Late-stage C–H azidation of bioactive molecules. [a]1.5 mol % of Mn(TMP)Cl (**5**) was used. [b]Methyl acetate was used as a solvent. [c]The ratio of α/β azidation was 7.5:1.

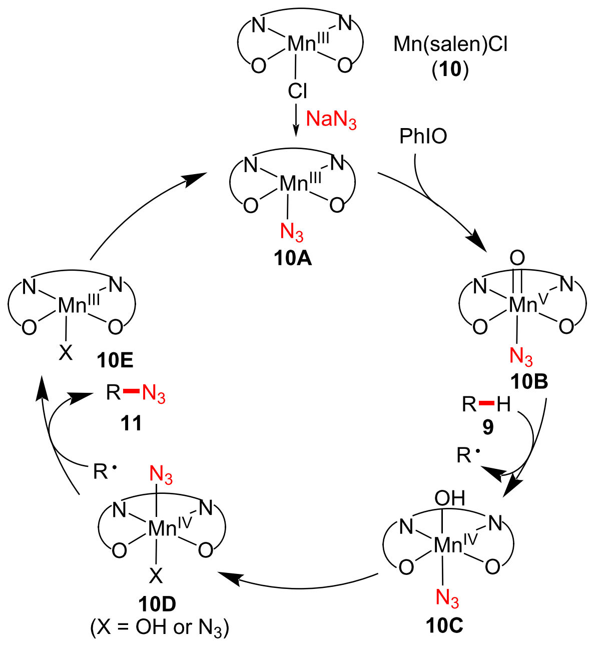
Mn(salen)Cl
(10)
NaN3
PhIO
10A
10B
R–H
9
R•
10C
10D
(X = OH or N3)
10E
R–N3
11

Figure 3: Proposed reaction mechanism of manganese-catalyzed C–H azidation.

oxidized to Mn(III)/L–N_3. Azide radical addition to Mn(II)/L to form Mn(III)/L–N_3 was considered as a possible route. Concurrently, the photocatalyst is irradiated by blue LED light to induce hydrogen atom transfer (HAT) at the C–H bond of substrate **12**, generating alkyl radicals and enabling C–N_3 bond formation to afford **13** via the reaction with Mn(III)/L–N_3. The anodic surface oxidizes the radical adjacent to the hydroxy group of the photocatalyst, thereby regenerating it. At the same time, the hydrogen atom abstraction of radical species of photocatalyst by Mn(III)–N_3 could not be excluded. This late-stage process by Mn catalysis, electrochemistry, and visible-light catalysis exhibits high value as a sustainable tool to investigate problematic synthetic transformations.

Recently, the Ackermann group disclosed a convenient manganese-catalyzed late-stage C–H azidation of bioactive molecules bearing unactivated C_{sp3}–H bonds facilitated by electricity (Scheme 5) [43]. Several pharmaceutically active molecules were committed to the external oxidant-free reaction conditions and were shown to undergo chemoselective azidation. Azidation of ibuprofen methyl ester (**14a**) was selective for the secondary benzylic position over the tertiary. Similar regio-

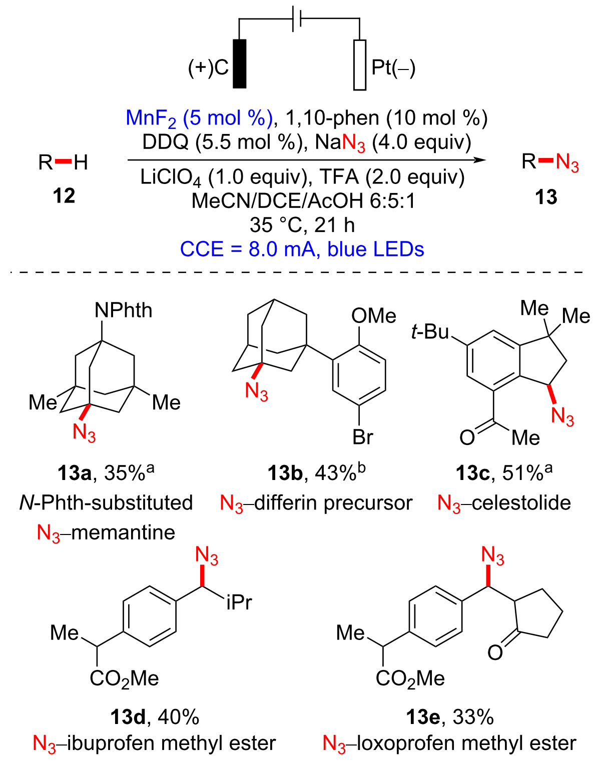
(+)C
Pt(–)
MnF2 (5 mol %), 1,10-phen (10 mol %)
DDQ (5.5 mol %), NaN3 (4.0 equiv)
LiClO4 (1.0 equiv), TFA (2.0 equiv)
MeCN/DCE/AcOH 6:5:1
35 °C, 21 h
CCE = 8.0 mA, blue LEDs
R–H
12
R–N3
13
NPhth
Me
Me
N3
13a, 35%a
N-Phth-substituted N3–memantine
OMe
N3
Br
13b, 43%b
N3–differin precursor
t-Bu
Me
Me
N3
O
Me
13c, 51%a
N3–celestolide
N3
iPr
Me
CO2Me
13d, 40%
N3–ibuprofen methyl ester
N3
Me
CO2Me
O
13e, 33%
N3–loxoprofen methyl ester

Scheme 4: Mn-catalyzed late-stage C–H azidation of bioactive molecules via electrophotocatalysis. [a]2.5 mol % of MnF_2 was used. [b]NaN_3 (5.0 equiv), MnF_2 (10 mol %), 1,10-phenanthroline (20 mol %), TFA (4.0 equiv), and $LiClO_4$ (2.0 equiv) were used with 4.5 mA for 15 h (5.0 mmol scale).

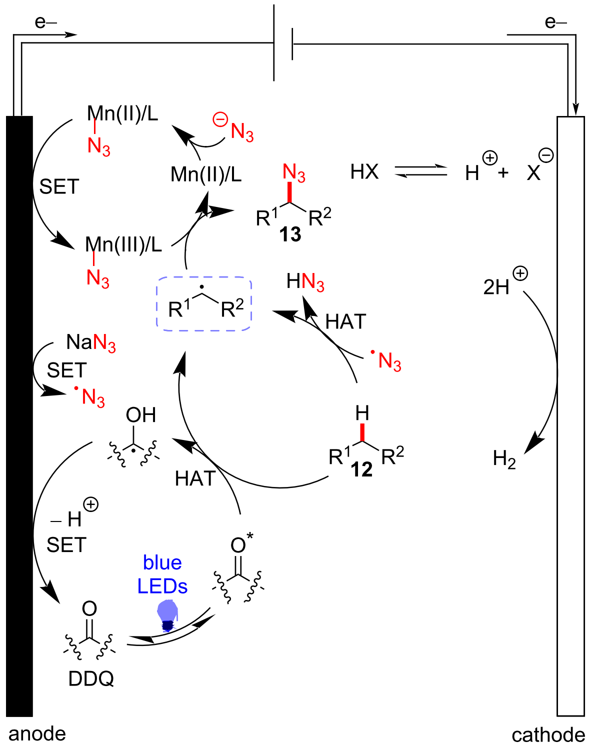
e–
e–
Mn(II)/L
N3
⊖N3
Mn(II)/L
N3
R1
R2
13
HX
H⊕ + X⊖
SET
Mn(III)/L
N3
R1
R2
HN3
HAT
•N3
2H⊕
H2
NaN3
SET
•N3
OH
H
R1
R2
12
HAT
– H⊕
SET
blue LEDs
O*
O
DDQ
anode
cathode

Figure 4: Proposed reaction mechanism of electrophotocatalytic azidation.

selectivity pattern of ibuprofen methyl ester (**14a**) and celestolide (**14b**) was observed in a study on manganese-catalyzed isocyanation [44]. Moreover, (−)-menthol acetate (**14c**) was successfully azidated, indicating that azidation favors tertiary C–H bonds in less sterically congested environments. A mixture of diastereomers (1:1 ratio) resulted from the azidation of estrone acetate (**14e**), strongly supporting a radical reaction pathway.

Based on their additional mechanistic experiments, the authors suggested that the oxidation of the Mn(III) species to Mn(IV) takes place on the anodic surface, resulting in the formation of a *trans*-diazide Mn(IV) intermediate (Figure 5). The high-valent manganese(IV) complex is susceptible to HAT from the substrate **14**, generating an alkyl radical [45,46]. Subsequently, further azide radical transfer from the *trans*-diazide Mn(IV) complex was proposed to furnish the formation of the $C–N_3$ bond.

Manganese-catalyzed late-stage C–H amination

The installation of amine functional groups onto biologically active molecules is regarded as a potentially versatile synthetic transformation for accessing diverse potent candidates with tailored physical and biological properties [47]. For example, ampicillin, an analogue of benzylpenicillin (penicillin G), also used as an antibiotic, contains an amine group at the benzylic position [48]. Likewise, other commercially available small-molecule drugs, such as Plavix® (antiplatelet), Gleevec® (anticancer), and augmentin (antibiotic), also contain the benzylic amine motif. Therefore, C–H amination is synthetically important for the diversification of biologically active molecules. Transition metal catalysis has set the stage for C–H amination processes in organic syntheses [49]. To date, there are several examples of late-stage C–H amination methods that utilize iron and manganese as 3d transition metal catalysts [50-52]. However, intermolecular benzylic C–H amination has rarely been explored due to the challenges associated with selectivity and reactivity.

In 2018, White et al. disclosed the late-stage manganese-catalyzed benzylic C–H amination of sophisticated biologically active molecules (Scheme 6) [53]. Their site-selective late-stage C–H amination strategy is practically scalable and convenient and exhibits excellent functional group tolerance. Several derivatives of complex biologically active compounds and natural products were evaluated in the late-stage benzylic C–H amina-

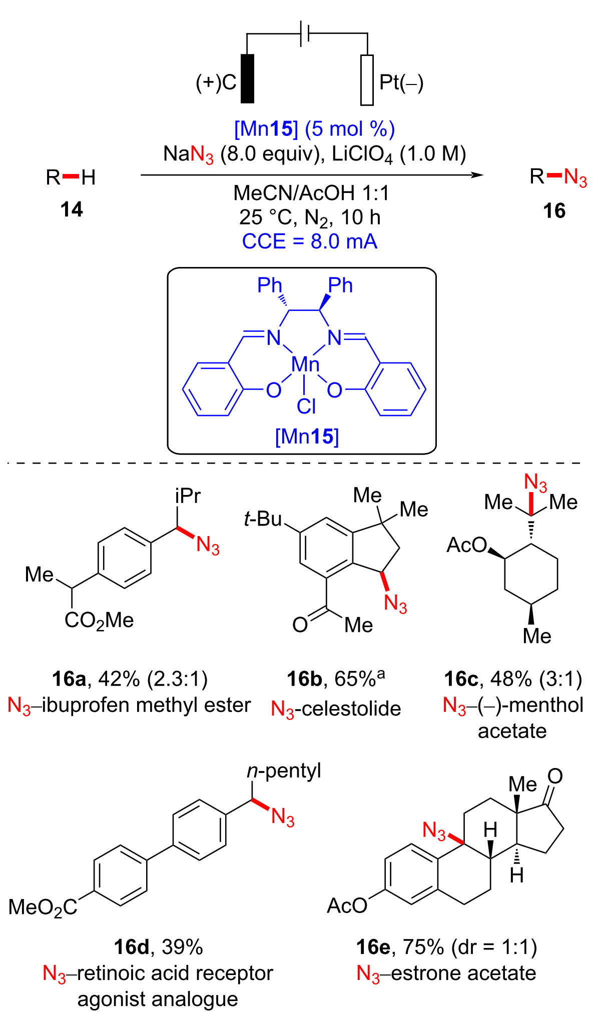
(+)C
Pt(−)
[Mn15] (5 mol %)
NaN3 (8.0 equiv), LiClO4 (1.0 M)
MeCN/AcOH 1:1
25 °C, N2, 10 h
CCE = 8.0 mA
R–H
14
R–N3
16
[Mn15]
16a, 42% (2.3:1)
N3–ibuprofen methyl ester
16b, 65%a
N3-celestolide
16c, 48% (3:1)
N3–(−)-menthol acetate
16d, 39%
N3–retinoic acid receptor agonist analogue
16e, 75% (dr = 1:1)
N3–estrone acetate

Scheme 5: Manganaelectro-catalyzed late-stage azidation of bioactive molecules.

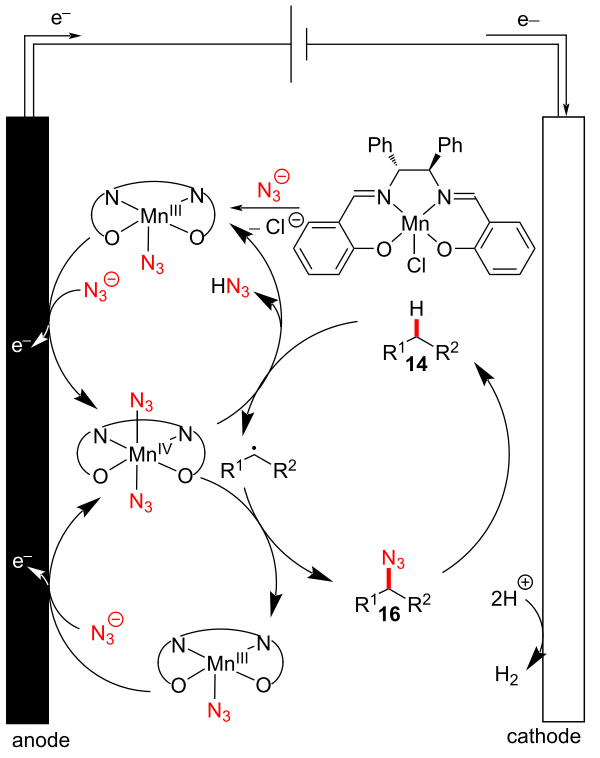
e⁻
e–
anode
cathode
Mn^III
Mn^IV
N3⊖
Cl⊖
HN3
14
16
2H⊕
H2

Figure 5: Proposed reaction pathway of manganaelectro-catalyzed late-stage C–H azidation.

tion process using Mn^{III}(ClPc) (**18**) and iminoiodinane. For example, the amination of FKGK11 (**17a**), a potent inhibitor of iPLA2, proceeded smoothly in a moderate yield. Notably, citalopram (**17b**), an antidepressant, was also reacted under amination conditions involving HBF_4, affording product **19b** in good yield and excellent diastereoselectivity (dr > 20:1). Other multiple benzylic C–H bond-containing molecules, including a dopamine receptor agonist analogue **17c** as well as derivatives of dextromethorphan, oestradiol, sulbactam, and leelamine **17d**–**g**, respectively, were shown to undergo amination at the less sterically congested benzylic position, affording aminated products **19c**–**g**. Further traceless removal of the Tces group was also investigated under Zn/Cu coupling conditions to install the free NH functionality. These findings highlight the convenience of manganese catalysis for the late-stage benzylic C–H amination of sophisticated bioactive molecules and natural products.

The proposed mechanism of the Mn-catalyzed benzylic amination is shown in Figure 6. Initially, metallonitrene intermediate **18A** is formed from the reaction of catalyst **18** with iminoiodinane, which is subsequently transformed to Mn–imido complex **18B** via conversion of substrate **17** into a temporary benzylic radical species, wherein C–H bond cleavage is proposed to be the rate-determining step (inter- and intramolecular KIEs of C–H cleavage are 2.5 and 3.0, respectively). Next, the benzylic radical is trapped by the Mn–imido complex to afford aminated product **19**. Based on additional mechanistic experiments, it was suggested that the Mn^{III}(ClPc) (**18**)-catalyzed C–H amination process is regioselective for the more electron-rich benzylic position, rationalizing the involvement of electrophilic metallonitrene intermediate **18A**.

Manganese-catalyzed late-stage C–H methylation

The incorporation of methyl groups has the potential to manipulate absorption, distribution, metabolism, and excretion (ADME), solubility, and protein–ligand binding properties as well as biological activities of small molecules, potentially leading to dramatic increases in potency, and thus has been widely explored in drug discovery [54-56]. Late-stage C–H methylation has recently been investigated using iron and cobalt catalysts as sustainable 3d metal catalysts [57,58], while

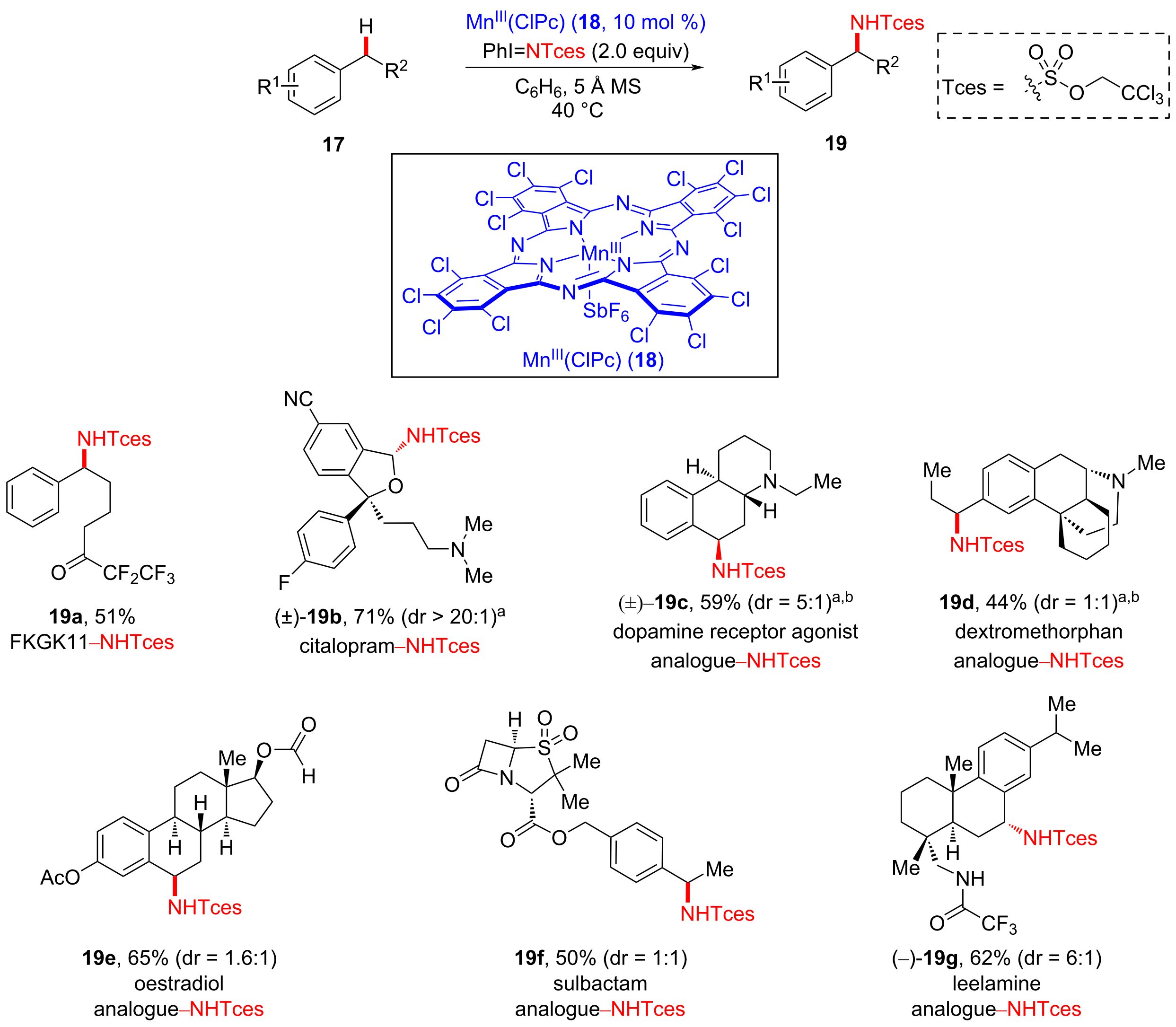
Mn^{III}(ClPc) (18, 10 mol %)
PhI=NTces (2.0 equiv)
C$_6$H$_6$, 5 Å MS
40 °C
17
19
Tces =
Mn^{III}(ClPc) (18)
19a, 51%
FKGK11–NHTces
(±)-19b, 71% (dr > 20:1)^a
citalopram–NHTces
(±)–19c, 59% (dr = 5:1)^{a,b}
dopamine receptor agonist
analogue–NHTces
19d, 44% (dr = 1:1)^{a,b}
dextromethorphan
analogue–NHTces
19e, 65% (dr = 1.6:1)
oestradiol
analogue–NHTces
19f, 50% (dr = 1:1)
sulbactam
analogue–NHTces
(–)-19g, 62% (dr = 6:1)
leelamine
analogue–NHTces

Scheme 6: Mn-catalyzed late-stage amination of bioactive molecules. ^{a}3 Å MS were used. Protonation with HBF$_4$·OEt$_2$ (1.1 equiv) in dichloromethane before amination, then deprotonation with 1 M NaOH in dichloromethane after amination. ^{b}3.0 equiv of PhI=NTces were used.

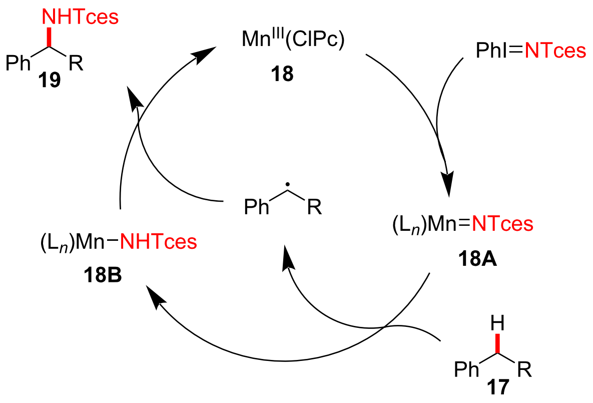
NHTces
Ph
R
19
Mn^{III}(ClPc)
18
PhI=NTces
Ph
R
(L$_n$)Mn=NTces
18A
(L$_n$)Mn–NHTces
18B
H
Ph
R
17

Figure 6: Proposed mechanism of manganese-catalyzed C–H amination.

manganese-catalyzed C–H methylations are scarce [59,60]. This disparity is due to the challenges in functional group tolerance of Mn-mediated late-stage transformations.

The White group reported a late-stage Mn-catalyzed C–H methylation protocol that utilizes an external Lewis acid and trimethylaluminum as a methyl source (Scheme 7) [61]. The late-stage methylation of simple heterocyclic motifs was initially investigated using (*S*,*S*)-Mn(CF$_3$–PDP) (**21**), providing methylated lactams **22a**–**e**. Notably, methylation site selectivity was observed for the carbon atoms adjacent to a heteroatom, such as a nitrogen (see **22a**–**d**) or oxygen (see **22e**).

Moreover, the above described manganese-catalyzed late-stage methylation process was implemented to provide methylated

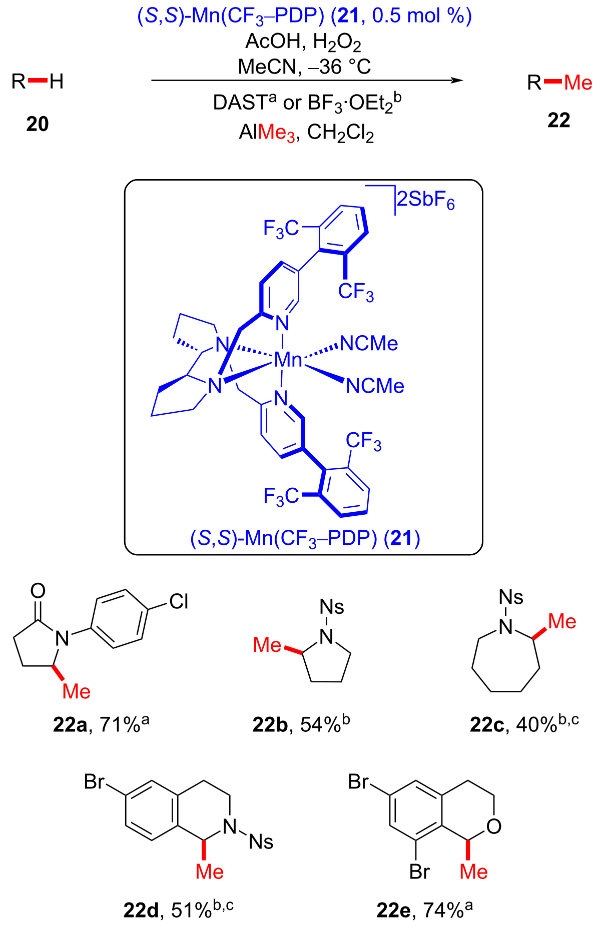
(S,S)-Mn(CF3–PDP) (21, 0.5 mol %)
AcOH, H2O2
MeCN, –36 °C
DASTa or BF3·OEt2b
AlMe3, CH2Cl2
R–H
20
R–Me
22
2SbF6
F3C
CF3
N
Mn
NCMe
NCMe
(S,S)-Mn(CF3–PDP) (21)
22a, 71%a
22b, 54%b
22c, 40%b,c
22d, 51%b,c
22e, 74%a
Me
Ns
Cl
Br
O

Scheme 7: Mn-catalyzed C–H methylation of heterocyclic scaffolds commonly found in small-molecule drugs. [a]DAST activation. [b]BF$_3$·OEt$_2$ activation. [c]1 mol % of (*S*,*S*)-Mn(CF$_3$–PDP) was used.

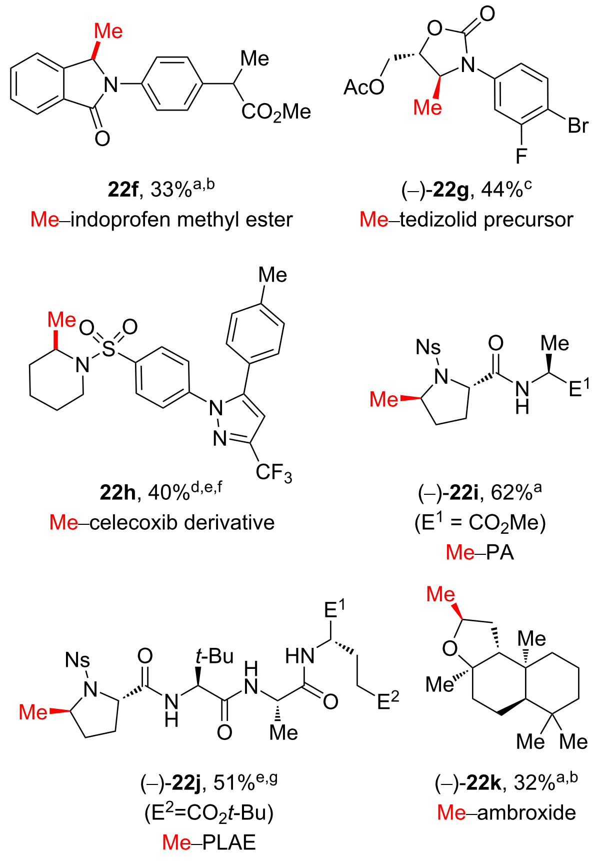
22f, 33%a,b
Me–indoprofen methyl ester
(–)-22g, 44%c
Me–tedizolid precursor
22h, 40%d,e,f
Me–celecoxib derivative
(–)-22i, 62%a
(E1 = CO2Me)
Me–PA
(–)-22j, 51%e,g
(E2=CO2t-Bu)
Me–PLAE
(–)-22k, 32%a,b
Me–ambroxide
Me
CO2Me
AcO
Br
F
CF3
Ns
t-Bu
E1
E2

Scheme 8: Examples of late-stage C–H methylation of bioactive molecules. [a]DAST activation. [b]For insoluble substrates, CH$_2$Cl$_2$ was added and/or the reaction temperature of the oxidation reaction was increased to 0 °C. [c]TMSOTf activation. [d]BF$_3$·OEt$_2$ activation. [e]Oxidation intermediate was isolated before methylation. [f]HBF$_4$ protection was performed. [g]Deoxo-Fluro® activation.

bioactive molecules, effectively avoiding conventionally lengthy de novo synthetic pathways (Scheme 8). The late-stage methylation of complex drug derivatives, such as of indoprofen (anti-inflammatory), tedizolid (antibiotic), and celecoxib (anti-inflammatory), successfully delivered methylated drug candidates **22f**–**h**, respectively. In addition, methylation of proline-containing multipeptides was achieved via fluorine activation (see **22i**–**j**), and the oxygen-containing natural terpenoid ambroxide was methylated at the methylene position next to the O atom on the tetrahydrofuran ring (see **22k**). This manganese-catalyzed late-stage approach enables the direct methylation of unactivated C–H bonds with excellent site selectivity, which is observed at the more electron-rich and the less sterically hindered position.

Manganese-catalyzed late-stage C–H alkynylation

Alkynes are invaluable intermediates in organic synthesis and are conventionally prepared via palladium-catalyzed cross-coupling reactions [62]. Moreover, they constitute an important structural modality in small-molecule drugs, such as levonorgestrel (birth control drug), efavirenz (HIV/AIDS treatment), and erlotinib (anticancer). Although step-economical C–H alkynylations have been investigated with 4d and 5d transition metals, 3d metal-catalyzed late-stage C–H alkynylations of bioactive structural motifs are rare [63].

In 2017, the Ackermann group disclosed a late-stage Mn(I)-catalyzed C–H alkynylation of various complex peptide scaffolds [64]. As shown in Scheme 9, manganese(I) catalysis remarkably resulted in racemization-free alkynylation, representing a step-economical approach to several tryptophan-containing peptides with significant potential for drug discovery and medicinal chemistry. Positional selectivity was observed at the C2 position due to the presence of the pyrimidine directing group. Interestingly, alkynylative conjugation of tryptophan to a steroid motif was successfully achieved (see **25b**). In addition to accessing the monopeptide **25a**, tri-, tetra-, and pentapeptides

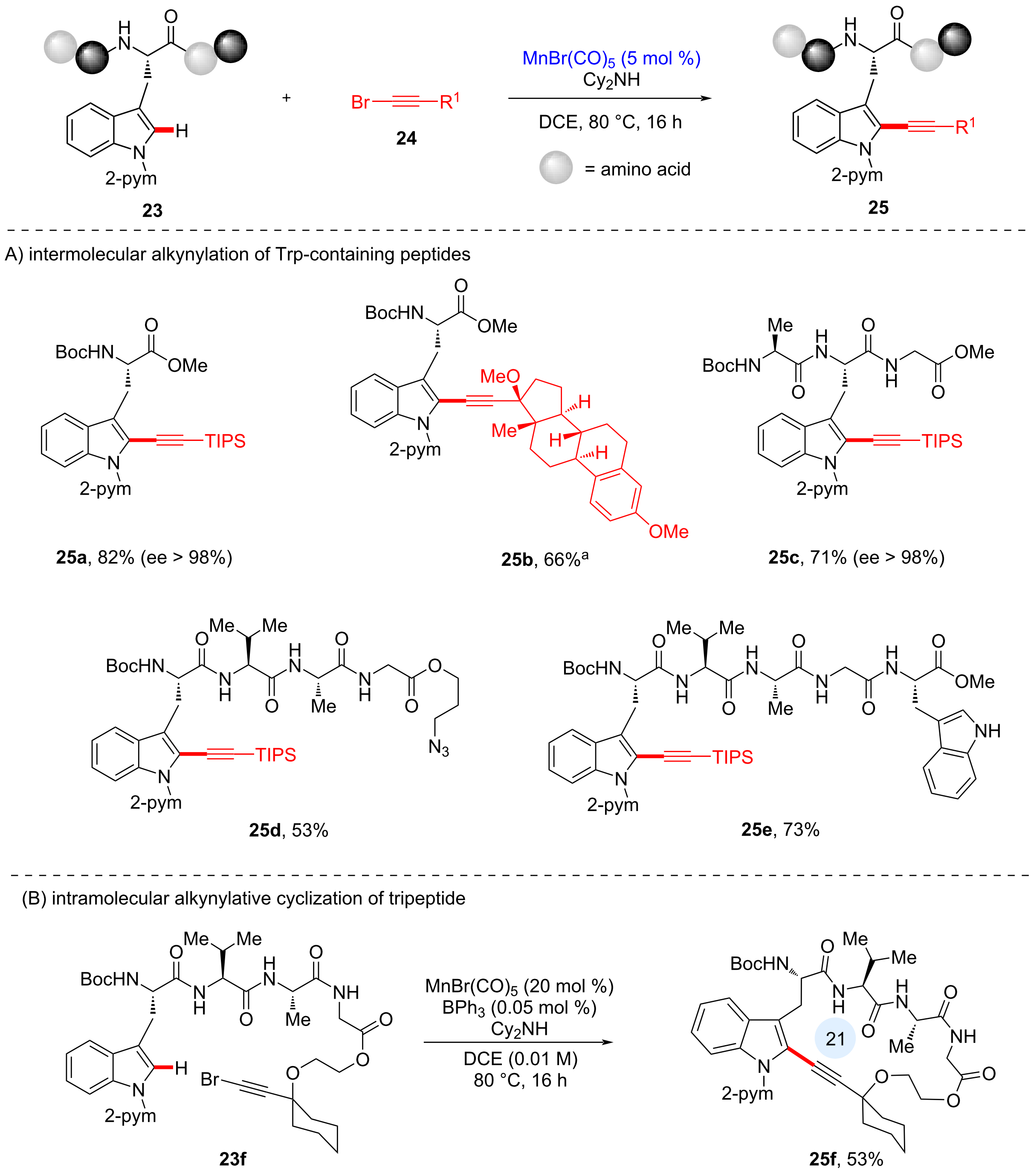
MnBr(CO)5 (5 mol %)
Cy2NH
DCE, 80 °C, 16 h
= amino acid
Br—≡—R1
2-pym
23
24
25
A) intermolecular alkynylation of Trp-containing peptides
BocHN
OMe
TIPS
MeO
Me
25a, 82% (ee > 98%)
25b, 66%a
25c, 71% (ee > 98%)
N3
NH
25d, 53%
25e, 73%
(B) intramolecular alkynylative cyclization of tripeptide
MnBr(CO)5 (20 mol %)
BPh3 (0.05 mol %)
Cy2NH
DCE (0.01 M)
80 °C, 16 h
21
23f
25f, 53%

Scheme 9: A) Mn-catalyzed late-stage C–H alkynylation of peptides. B) Intramolecular late-stage alkynylative cyclic peptide formation. [a]0.05 mol % of BPh_3 was added.

25c–**e**, respectively, were obtained under the developed reaction conditions. It is noteworthy that substrates containing an azido group (see **25d**) or free NH (see **25e**) were tolerated, demonstrating significant bioorthogonality in manganese(I) catalysis. The robustness of the method bears significance for further synthetic applications, such as "Click" chemistry or N-functionalization. Moreover, as shown in Scheme 9B, the manganese(I) catalysis regime enabled peptide macrocyclization (see **25f**).

Based on additional mechanistic investigations, it was proposed that substrate **23** forms five-membered manganacycle complex **23A** under basic conditions, which undergoes alkyne insertion to provide seven-membered manganacycle complex **23B** (Figure 7). Subsequently, intermediate **23B** undergoes β-bromo elimination to produce **23C**, whereby the addition of BPh_3 presumably accelerates this process [65]. Subsequently, the manganese species participate in the catalytic cycle by yielding alkynylated product **25**. However, the mechanism entailing oxidative addition, followed by reductive elimination could not be ruled out.

Manganese-catalyzed late-stage C–H allylation

The late-stage modification of peptides has received increasing attention due to the convenient and efficient modality. However, such protocols generally require substrate prefunctionalization and expensive metal catalysts, such as Pd [66-87], Rh [88-91], and Ru [92,93]. In 2019, the Ackermann group demonstrated that a manganese(I) catalyst enabled the late-stage C–H allylation of structurally complex peptides in a site-selective fashion (Scheme 10) [94]. Based on an initial optimization study, manganese(I) pentacarbonyl bromide was deemed as the optimal catalyst, enabling a robust racemization-free allylation process. In addition to tryptophan-containing peptides, diazepam and nucleoside analogues were found to be viable allylation substrates, affording highly complex peptides.

Cyclic peptides are known to be structurally and chemically stable against enzymatic degradation because the cyclic skeleton restricts the conformation and limits β-turns. In this manganese catalysis, the late-stage C–H allylation manifold was extended to the construction of a cyclic peptide motif (Scheme 11). Dipeptide substrate **26f** decorated with a Morita–Baylis–Hillman carbonate underwent the intramolecular C–H allylation process to yield cyclic peptide **28f** under dilute reaction conditions. This macrocyclization strategy introduces an exocyclic olefin motif onto the cyclic peptide, which can be further utilized as a Michael acceptor for a variety of nucleophiles.

Based on their manganese-catalyzed allylation using Morita–Baylis–Hillman carbonates, the Ackermann group established an applicable late-stage C–H glycosylation of peptides (Scheme 12) [95]. Thus, allylative peptide–carbohydrate conjugation was achieved using tryptophan-containing peptides **29** and sugar-containing allyl carbonates **30** in chemo- and site-selective manners using a pyridyl directing group. The optimized reaction conditions entailed the use of dimanganese decacarbonyl as the catalyst and sodium acetate as the base to deliver the corresponding peptide–sugar conjugates **31** at the late stage. Notably, the chemoselective glycoconjugation strategy was compatible with various sugar scaffolds, affording glycotryptophans bearing either furanose or pyranose motifs. In addition, a brevianamide F analogue, a natural product scaffold, was transformed into glycosylated tryptophan **31f**. It is noteworthy that this manganese(I)-catalyzed glycoconjugation method avoids racemization.

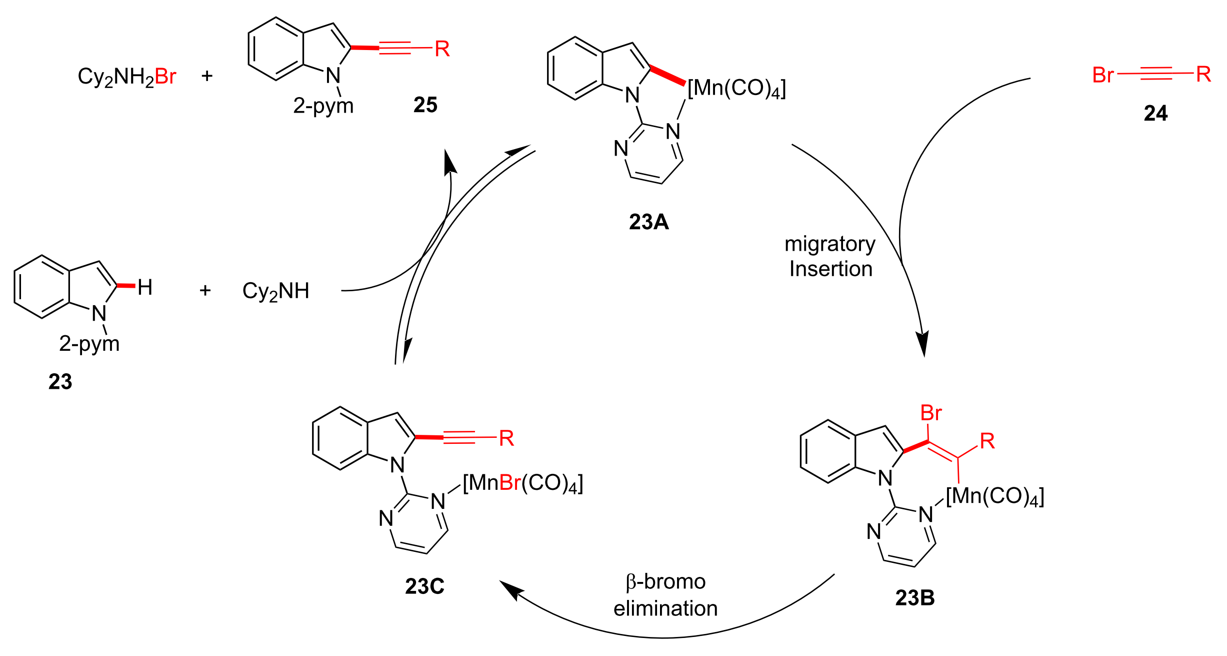

Figure 7: Proposed reaction mechanism of Mn(I)-catalyzed C–H alkynylation.

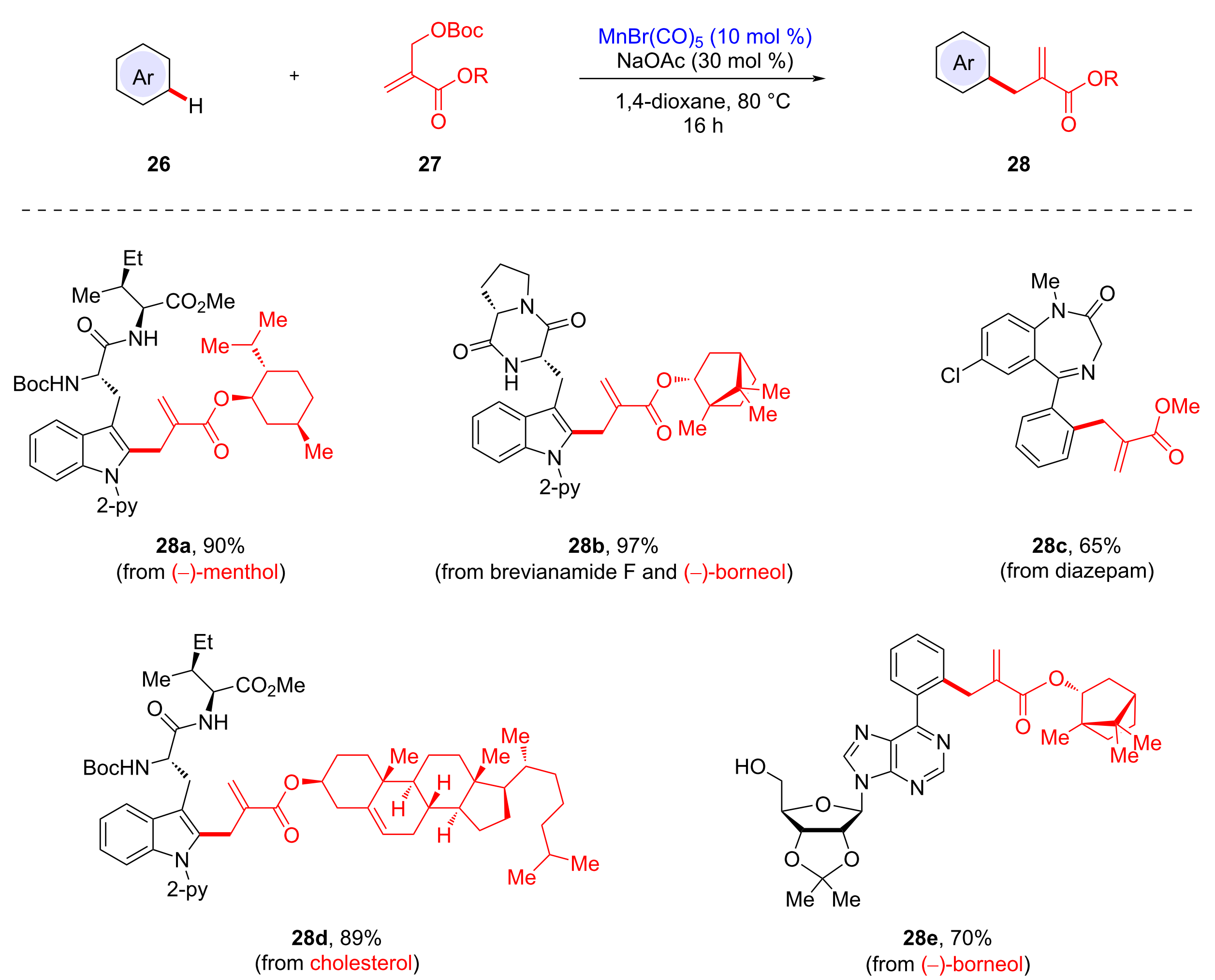
Ar
H
26
+
OBoc
OR
O
27
MnBr(CO)5 (10 mol %)
NaOAc (30 mol %)
1,4-dioxane, 80 °C
16 h
Ar
OR
O
28
28a, 90%
(from (–)-menthol)
28b, 97%
(from brevianamide F and (–)-borneol)
28c, 65%
(from diazepam)
28d, 89%
(from cholesterol)
28e, 70%
(from (–)-borneol)

Scheme 10: Late-stage Mn-catalyzed C–H allylation of peptides and bioactive motifs.

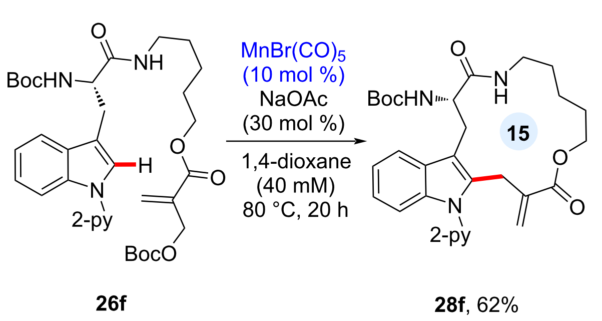
BocHN
NH
O
H
N
2-py
BocO
26f
MnBr(CO)5
(10 mol %)
NaOAc
(30 mol %)
1,4-dioxane
(40 mM)
80 °C, 20 h
15
28f, 62%

Scheme 11: Intramolecular C–H allylative cyclic peptide formation.

Furthermore, manganese-catalyzed allylative linchpin C–H glycosylation was investigated using structurally sophisticated tryptophan-containing peptides (Scheme 13). A wide variety of complex peptides was explored, affording glycosylated conjugates with high stereoselectivity. The free NH functional group was tolerated in the manganese catalysis protocol, suggesting that the chemoselectivity was controlled by chelation of the adjacent directing group (see **31h**). This manganese(I)-catalyzed late-stage glycosylation provides hexaglycopeptide conjugate **31m** without epimerization. Moreover, the late-stage C–H diversification process enabled bioorthogonal access to glycosylated peptides, such as a fluorescent BODIPY-labeled tryptophan **31n**, regarded as a potentially viable peptide-based biosensor.

Manganese-catalyzed inter- and intramolecular C–H alkenylations

Manganese(I)-catalyzed C–H alkenylation of 2-phenylpyridines or *N*-pyridinylindoles with alkynes is characterized by proximity-induced C–H activation through chelation assistance.

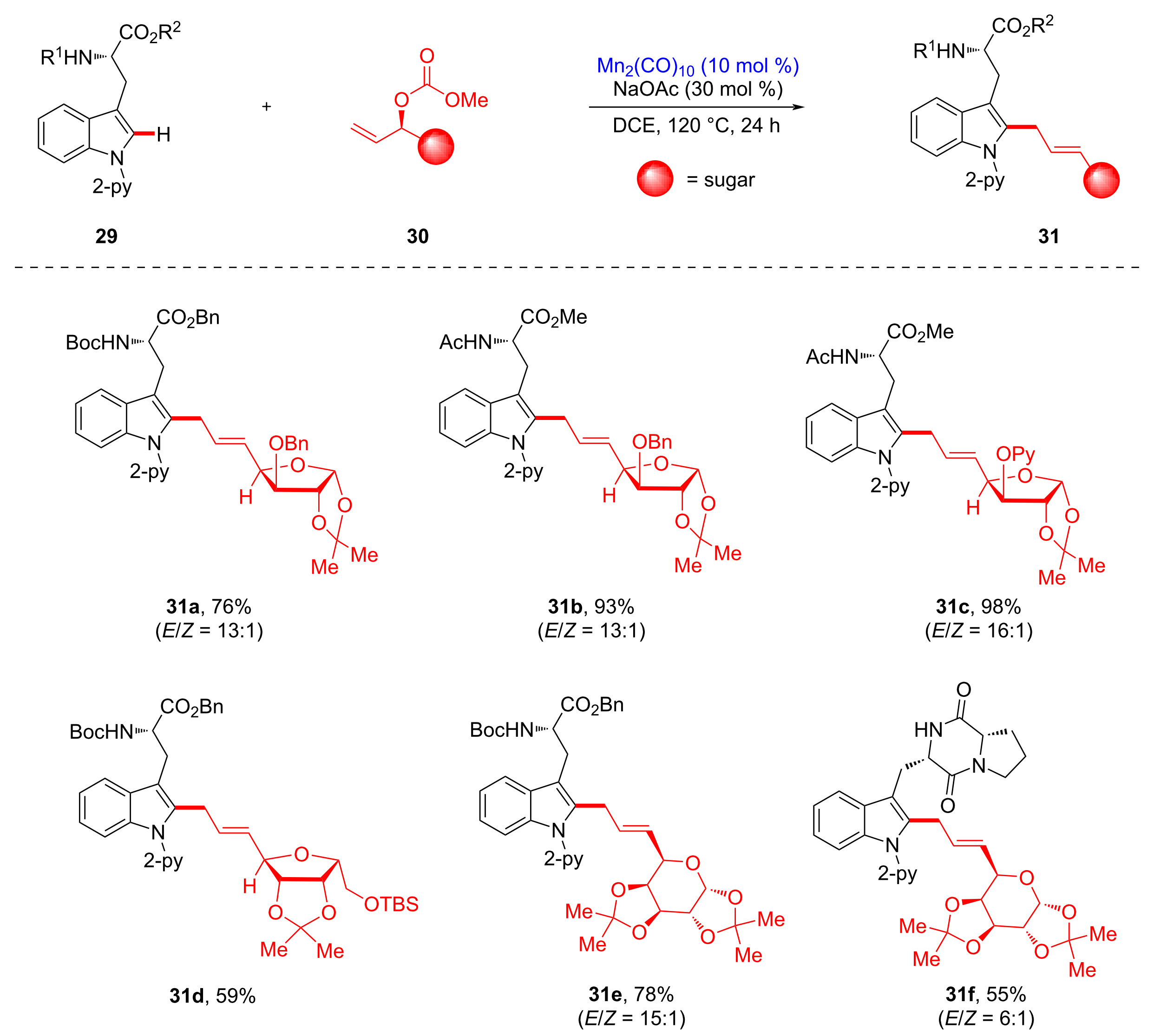

Scheme 12: Late-stage C–H glycosylation of tryptophan analogues.

However, application of this protocol for late-stage functionalization remains challenging [96-103].

In 2021, it was revealed by the Ackermann group that manganese(I) catalysis enabled the bioorthogonal late-stage alkenylation of structurally sophisticated peptides [104]. The manganese(I)-catalyzed intermolecular alkenylation of tryptophan-containing peptides **32** was performed under basic conditions, yielding hybrid peptides **34** without racemization, containing a *trans*-alkene linker bearing biologically active motifs in chemo- and site-selective manners assisted by the pyridyl directing group (Scheme 14). For example, a substrate containing a free OH or NH was successfully alkenylated at the late stage, suggesting a high functional group tolerance (see **34a** and **34b**). In addition, a more complex pentapeptide provided the corresponding product **34c**, bearing a free-NH tryptophan. Notably, alkenylative ligation of tryptophan-containing peptides and alkynes containing biomolecular motifs including sugar, menthol, or coumarin units was successful, delivering unprecedented hybrid complex peptides **34d–f** in good yield.

Based on the developed intermolecular process, late-stage intramolecular C–H macrocyclization was also investigated (Scheme 15). To avoid unwanted intermolecular oligomerization, the reaction was performed at a high dilution, furnishing either C- or N-terminus-alkenylated products with excellent chemoselectivity. In this macrocyclization, cyclic multipeptides of varying ring size were successfully obtained with excellent functional group tolerance. In addition, selective *N*-methylation of the 2-pyridine directing group and successive hydrogenation

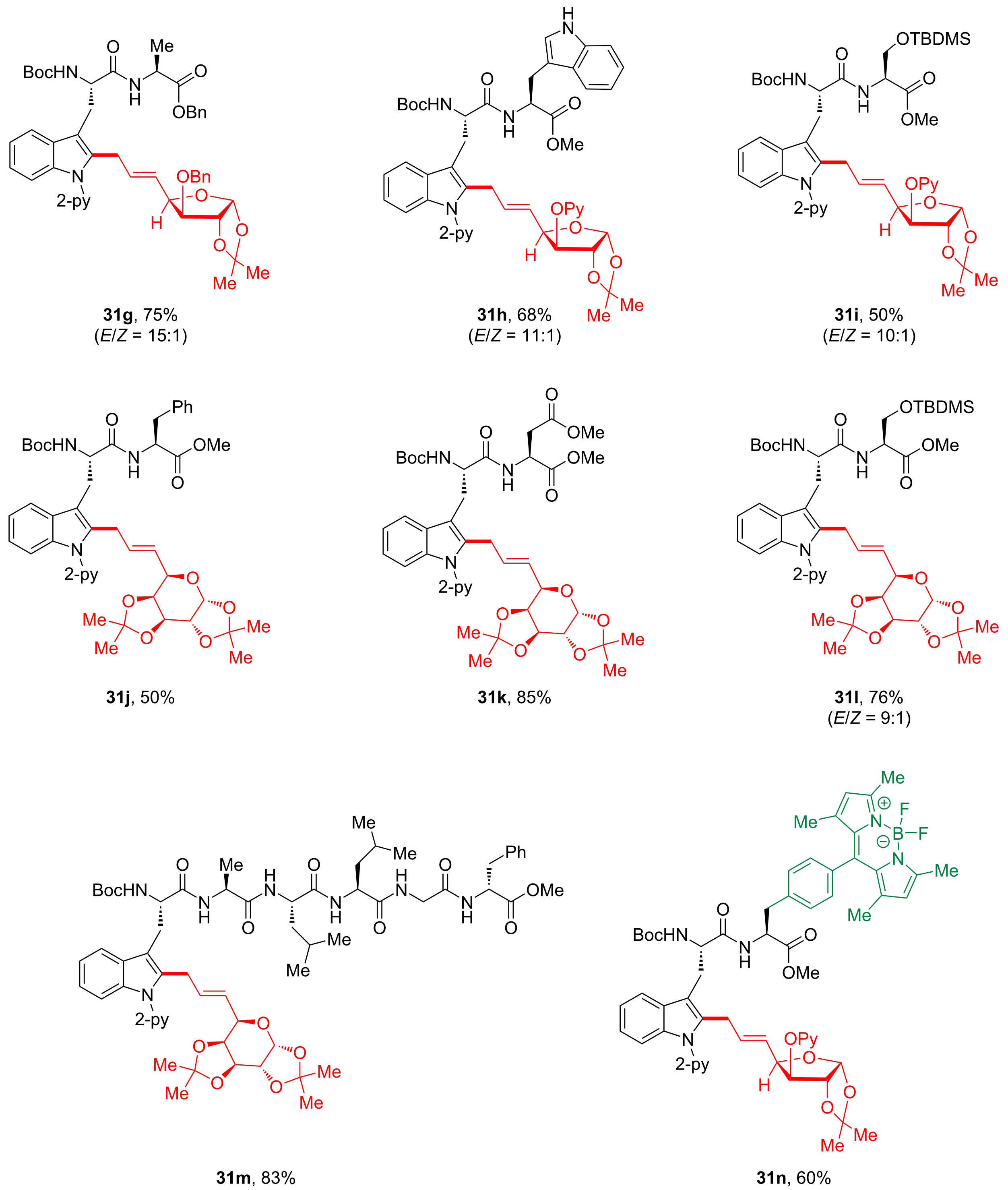
31g, 75%
(*E*/*Z* = 15:1)
31h, 68%
(*E*/*Z* = 11:1)
31i, 50%
(*E*/*Z* = 10:1)
31j, 50%
31k, 85%
31l, 76%
(*E*/*Z* = 9:1)
31m, 83%
31n, 60%
BocHN
2-py
OBn
OPy
OTBDMS
OMe
Ph
Me
F
B

Scheme 13: Late-stage C–H glycosylation of tryptophan-containing peptides.

processes provided an efficient traceless removal of the directing group, affording free-NH tryptophan-containing peptide **37g**.

Conclusion

Metal-catalyzed late-stage functionalization has shown significant potential in the fields of medicinal chemistry, agrochem-

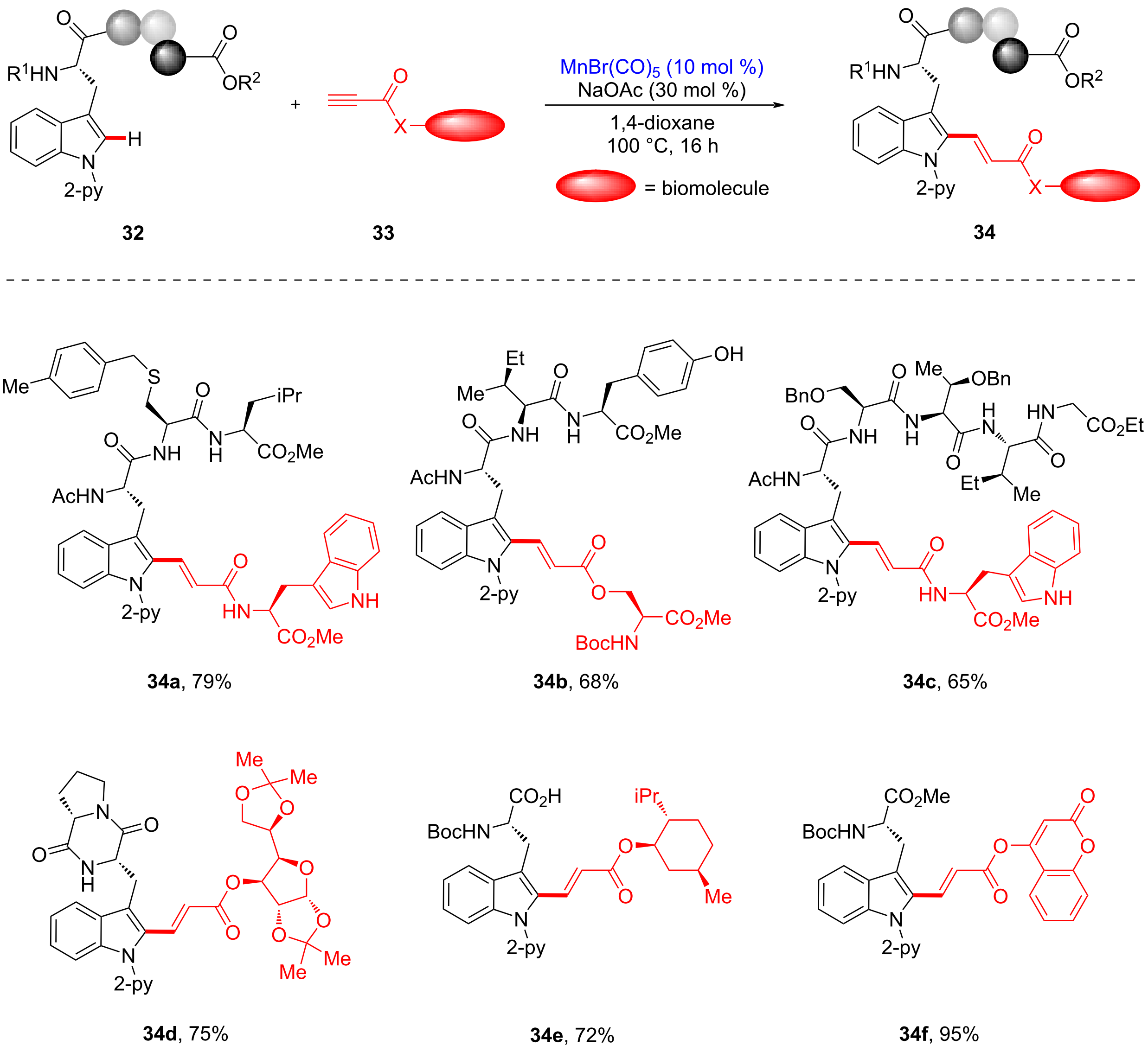

Scheme 14: Late-stage C–H alkenylation of tryptophan-containing peptides.

istry, and chemical biology. While transition metal catalysis has been a reliable and efficient strategy for late-stage functionalization, it suffers several disadvantages, such as the need for additional prefunctionalization and the use of expensive and toxic precious metals. To avoid these issues, 3d-metal-catalyzed C–H functionalization has recently been realized as a sustainable catalytic system and is actively being investigated for various late-state functionalization purposes. Notably, late-stage functionalization with manganese catalysts offers a sustainable catalytic system, and recent advancements have allowed for the construction of diversified bioactive small molecules and peptides through late-stage C–H aminations, azidations, fluorinations, allylations, alkynylations, alkenylations, and fluorescent labeling with BODIPY. Moreover, manganese catalysis exhibits excellent functional group tolerance in late-stage C–H functionalization, indicating a robust and versatile catalytic system. Several challenges still remain since there are multiple steps to prepare suitable high-valent Mn complexes. Furthermore, Mn(I)-catalyzed enantioselective C–H functionalization at the late stage is still underexplored. Given the sustainability and versatility of manganese-catalyzed late-stage functionalization, further advances are expected in the future, such as protecting-group-free methodologies, peptide biosensors, and facile functionalizations within unexplored realms of complex peptides.

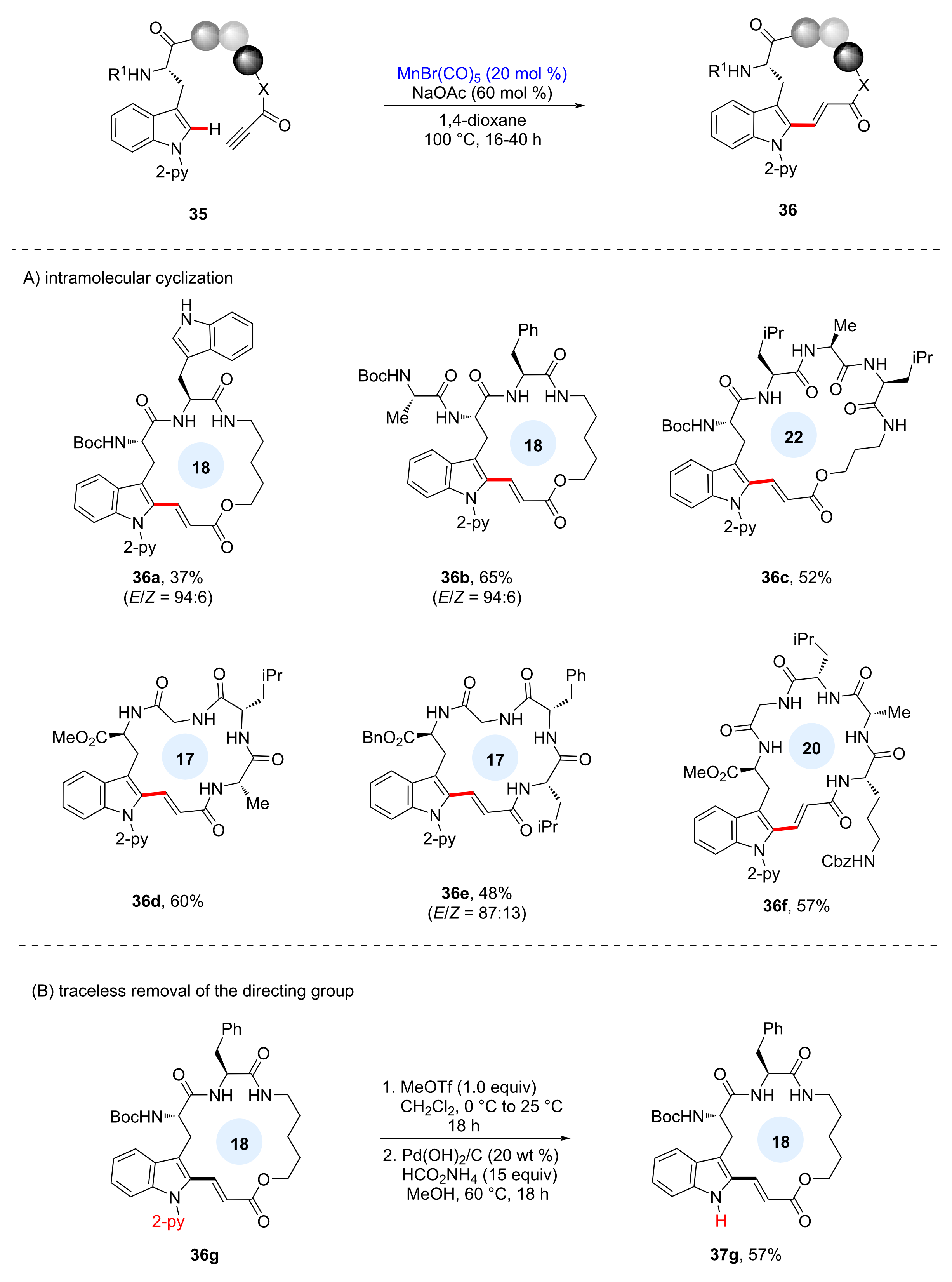
R^{1}HN
O
X
H
N
2-py
O
35
MnBr(CO)$_5$ (20 mol %)
NaOAc (60 mol %)
1,4-dioxane
100 °C, 16-40 h
36
A) intramolecular cyclization
36a, 37%
(E/Z = 94:6)
36b, 65%
(E/Z = 94:6)
36c, 52%
36d, 60%
36e, 48%
(E/Z = 87:13)
36f, 57%
18
22
17
20
BocHN
MeO$_2$C
BnO$_2$C
CbzHN
iPr
Ph
Me
(B) traceless removal of the directing group
1. MeOTf (1.0 equiv)
CH$_2$Cl$_2$, 0 °C to 25 °C
18 h
2. Pd(OH)$_2$/C (20 wt %)
HCO$_2$NH$_4$ (15 equiv)
MeOH, 60 °C, 18 h
36g
37g, 57%

Scheme 15: A) Late-stage C–H macrocyclization of tryptophan-containing peptides and B) traceless removal of pyridyl directing group.

Funding

This work was supported by the Dong-A University Research Fund.

ORCID® iDs

Jongwoo Son - https://orcid.org/0000-0003-0420-5065

References

1. Bruce, M. I.; Iqbal, M. Z.; Stone, F. G. A. *J. Chem. Soc. A* **1970,** 3204–3209. doi:10.1039/j19700003204
2. Carney, J. R.; Dillon, B. R.; Thomas, S. P. *Eur. J. Org. Chem.* **2016,** 3912–3929. doi:10.1002/ejoc.201600018
3. Cano, R.; Mackey, K.; McGlacken, G. P. *Catal. Sci. Technol.* **2018,** *8,* 1251–1266. doi:10.1039/c7cy02514a
4. Hu, Y.; Zhou, B.; Wang, C. *Acc. Chem. Res.* **2018,** *51,* 816–827. doi:10.1021/acs.accounts.8b00028
5. Gandeepan, P.; Müller, T.; Zell, D.; Cera, G.; Warratz, S.; Ackermann, L. *Chem. Rev.* **2019,** *119,* 2192–2452. doi:10.1021/acs.chemrev.8b00507
6. Aneeja, T.; Neetha, M.; Afsina, C. M. A.; Anilkumar, G. *Catal. Sci. Technol.* **2021,** *11,* 444–458. doi:10.1039/d0cy02087g
7. Lu, X.; He, S.-J.; Cheng, W.-M.; Shi, J. *Chin. Chem. Lett.* **2018,** *29,* 1001–1008. doi:10.1016/j.cclet.2018.05.011
8. Wang, W.; Lorion, M. M.; Shah, J.; Kapdi, A. R.; Ackermann, L. *Angew. Chem., Int. Ed.* **2018,** *57,* 14700–14717. doi:10.1002/anie.201806250
9. White, M. C.; Zhao, J. *J. Am. Chem. Soc.* **2018,** *140,* 13988–14009. doi:10.1021/jacs.8b05195
10. Abrams, D. J.; Provencher, P. A.; Sorensen, E. J. *Chem. Soc. Rev.* **2018,** *47,* 8925–8967. doi:10.1039/c8cs00716k
11. Baudoin, O. *Angew. Chem., Int. Ed.* **2020,** *59,* 17798–17809. doi:10.1002/anie.202001224
12. Kelly, C. B.; Padilla-Salinas, R. *Chem. Sci.* **2020,** *11,* 10047–10060. doi:10.1039/d0sc03833d
13. Wu, J. *Tetrahedron Lett.* **2014,** *55,* 4289–4294. doi:10.1016/j.tetlet.2014.06.006
14. Yang, X.; Wu, T.; Phipps, R. J.; Toste, F. D. *Chem. Rev.* **2015,** *115,* 826–870. doi:10.1021/cr500277b
15. Li, X.; Shi, X.; Li, X.; Shi, D. *Beilstein J. Org. Chem.* **2019,** *15,* 2213–2270. doi:10.3762/bjoc.15.218
16. Szpera, R.; Moseley, D. F. J.; Smith, L. B.; Sterling, A. J.; Gouverneur, V. *Angew. Chem., Int. Ed.* **2019,** *58,* 14824–14848. doi:10.1002/anie.201814457
17. Gillis, E. P.; Eastman, K. J.; Hill, M. D.; Donnelly, D. J.; Meanwell, N. A. *J. Med. Chem.* **2015,** *58,* 8315–8359. doi:10.1021/acs.jmedchem.5b00258
18. Wang, J.; Sánchez-Roselló, M.; Aceña, J. L.; del Pozo, C.; Sorochinsky, A. E.; Fustero, S.; Soloshonok, V. A.; Liu, H. *Chem. Rev.* **2014,** *114,* 2432–2506. doi:10.1021/cr4002879
19. Purser, S.; Moore, P. R.; Swallow, S.; Gouverneur, V. *Chem. Soc. Rev.* **2008,** *37,* 320–330. doi:10.1039/b610213c
20. Smart, B. E. *J. Fluorine Chem.* **2001,** *109,* 3–11. doi:10.1016/s0022-1139(01)00375-x
21. Meanwell, N. A. *J. Med. Chem.* **2018,** *61,* 5822–5880. doi:10.1021/acs.jmedchem.7b01788
22. Liu, W.; Huang, X.; Cheng, M.-J.; Nielsen, R. J.; Goddard, W. A.; Groves, J. T. *Science* **2012,** *337,* 1322–1325. doi:10.1126/science.1222327
23. Oh, S.; Jeong, I. H.; Shin, W.-S.; Wang, Q.; Lee, S. *Bioorg. Med. Chem. Lett.* **2006,** *16,* 1656–1659. doi:10.1016/j.bmcl.2005.12.009
24. Liu, W.; Groves, J. T. *J. Am. Chem. Soc.* **2010,** *132,* 12847–12849. doi:10.1021/ja105548x
25. Huang, X.; Liu, W.; Ren, H.; Neelamegam, R.; Hooker, J. M.; Groves, J. T. *J. Am. Chem. Soc.* **2014,** *136,* 6842–6845. doi:10.1021/ja5039819
26. Miller, P. W.; Long, N. J.; Vilar, R.; Gee, A. D. *Angew. Chem., Int. Ed.* **2008,** *47,* 8998–9033. doi:10.1002/anie.200800222
27. Tredwell, M.; Gouverneur, V. *Angew. Chem., Int. Ed.* **2012,** *51,* 11426–11437. doi:10.1002/anie.201204687
28. Jacobson, O.; Kiesewetter, D. O.; Chen, X. *Bioconjugate Chem.* **2015,** *26,* 1–18. doi:10.1021/bc500475e
29. Preshlock, S.; Tredwell, M.; Gouverneur, V. *Chem. Rev.* **2016,** *116,* 719–766. doi:10.1021/acs.chemrev.5b00493
30. Kolb, H. C.; Finn, M. G.; Sharpless, K. B. *Angew. Chem., Int. Ed.* **2001,** *40,* 2004–2021. doi:10.1002/1521-3773(20010601)40:11<2004::aid-anie2004>3.0.co;2-5
31. Moses, J. E.; Moorhouse, A. D. *Chem. Soc. Rev.* **2007,** *36,* 1249–1262. doi:10.1039/b613014n
32. Hein, C. D.; Liu, X.-M.; Wang, D. *Pharm. Res.* **2008,** *25,* 2216–2230. doi:10.1007/s11095-008-9616-1
33. Jewett, J. C.; Bertozzi, C. R. *Chem. Soc. Rev.* **2010,** *39,* 1272–1279. doi:10.1039/b901970g
34. Liang, L.; Astruc, D. *Coord. Chem. Rev.* **2011,** *255,* 2933–2945. doi:10.1016/j.ccr.2011.06.028
35. Thirumurugan, P.; Matosiuk, D.; Jozwiak, K. *Chem. Rev.* **2013,** *113,* 4905–4979. doi:10.1021/cr200409f
36. Tang, W.; Becker, M. L. *Chem. Soc. Rev.* **2014,** *43,* 7013–7039. doi:10.1039/c4cs00139g
37. Poonthiyil, V.; Lindhorst, T. K.; Golovko, V. B.; Fairbanks, A. J. *Beilstein J. Org. Chem.* **2018,** *14,* 11–24. doi:10.3762/bjoc.14.2
38. Huang, X.; Bergsten, T. M.; Groves, J. T. *J. Am. Chem. Soc.* **2015,** *137,* 5300–5303. doi:10.1021/jacs.5b01983
39. Silverman, R. B. *Angew. Chem., Int. Ed.* **2008,** *47,* 3500–3504. doi:10.1002/anie.200704280
40. Niu, L.; Jiang, C.; Liang, Y.; Liu, D.; Bu, F.; Shi, R.; Chen, H.; Chowdhury, A. D.; Lei, A. *J. Am. Chem. Soc.* **2020,** *142,* 17693–17702. doi:10.1021/jacs.0c08437
41. Wenk, G. L.; Danysz, W.; Mobley, S. L. *Eur. J. Pharmacol., Environ. Toxicol. Pharmacol. Sect.* **1995,** *293,* 267–270. doi:10.1016/0926-6917(95)00028-3
42. Gideons, E. S.; Kavalali, E. T.; Monteggia, L. M. *Proc. Natl. Acad. Sci. U. S. A.* **2014,** *111,* 8649–8654. doi:10.1073/pnas.1323920111
43. Meyer, T. H.; Samanta, R. C.; Del Vecchio, A.; Ackermann, L. *Chem. Sci.* **2021,** *12,* 2890–2897. doi:10.1039/d0sc05924b
44. Huang, X.; Zhuang, T.; Kates, P. A.; Gao, H.; Chen, X.; Groves, J. T. *J. Am. Chem. Soc.* **2017,** *139,* 15407–15413. doi:10.1021/jacs.7b07658
45. Mayer, J. M. *Acc. Chem. Res.* **2011,** *44,* 36–46. doi:10.1021/ar100093z
46. Capaldo, L.; Ravelli, D. *Eur. J. Org. Chem.* **2017,** 2056–2071. doi:10.1002/ejoc.201601485
47. Richter, M. F.; Drown, B. S.; Riley, A. P.; Garcia, A.; Shirai, T.; Svec, R. L.; Hergenrother, P. J. *Nature* **2017,** *545,* 299–304. doi:10.1038/nature22308

48. Campoli-Richards, D. M.; Brogden, R. N. *Drugs* **1987,** *33,* 577–609. doi:10.2165/00003495-198733060-00003
49. Park, Y.; Kim, Y.; Chang, S. *Chem. Rev.* **2017,** *117,* 9247–9301. doi:10.1021/acs.chemrev.6b00644
50. Paradine, S. M.; White, M. C. *J. Am. Chem. Soc.* **2012,** *134,* 2036–2039. doi:10.1021/ja211600g
51. Hennessy, E. T.; Betley, T. A. *Science* **2013,** *340,* 591–595. doi:10.1126/science.1233701
52. Paradine, S. M.; Griffin, J. R.; Zhao, J.; Petronico, A. L.; Miller, S. M.; Christina White, M. *Nat. Chem.* **2015,** *7,* 987–994. doi:10.1038/nchem.2366
53. Clark, J. R.; Feng, K.; Sookezian, A.; White, M. C. *Nat. Chem.* **2018,** *10,* 583–591. doi:10.1038/s41557-018-0020-0
54. Barreiro, E. J.; Kümmerle, A. E.; Fraga, C. A. M. *Chem. Rev.* **2011,** *111,* 5215–5246. doi:10.1021/cr200060g
55. Leung, C. S.; Leung, S. S. F.; Tirado-Rives, J.; Jorgensen, W. L. *J. Med. Chem.* **2012,** *55,* 4489–4500. doi:10.1021/jm3003697
56. Schönherr, H.; Cernak, T. *Angew. Chem., Int. Ed.* **2013,** *52,* 12256–12267. doi:10.1002/anie.201303207
57. Zhu, N.; Zhao, J.; Bao, H. *Chem. Sci.* **2017,** *8,* 2081–2085. doi:10.1039/c6sc04274k
58. Friis, S. D.; Johansson, M. J.; Ackermann, L. *Nat. Chem.* **2020,** *12,* 511–519. doi:10.1038/s41557-020-0475-7
59. Sato, T.; Yoshida, T.; Al Mamari, H. H.; Ilies, L.; Nakamura, E. *Org. Lett.* **2017,** *19,* 5458–5461. doi:10.1021/acs.orglett.7b02778
60. Liu, W.; Cera, G.; Oliveira, J. C. A.; Shen, Z.; Ackermann, L. *Chem. – Eur. J.* **2017,** *23,* 11524–11528. doi:10.1002/chem.201703191
61. Feng, K.; Quevedo, R. E.; Kohrt, J. T.; Oderinde, M. S.; Reilly, U.; White, M. C. *Nature* **2020,** *580,* 621–627. doi:10.1038/s41586-020-2137-8
62. Sonogashira, K.; Tohda, Y.; Hagihara, N. *Tetrahedron Lett.* **1975,** *16,* 4467–4470. doi:10.1016/s0040-4039(00)91094-3
63. Caspers, L. D.; Nachtsheim, B. J. *Chem. – Asian J.* **2018,** *13,* 1231–1247. doi:10.1002/asia.201800102
64. Ruan, Z.; Sauermann, N.; Manoni, E.; Ackermann, L. *Angew. Chem., Int. Ed.* **2017,** *56,* 3172–3176. doi:10.1002/anie.201611118
65. Wierschke, S. G.; Chandrasekhar, J.; Jorgensen, W. L. *J. Am. Chem. Soc.* **1985,** *107,* 1496–1500. doi:10.1021/ja00292a008
66. Gong, W.; Zhang, G.; Liu, T.; Giri, R.; Yu, J.-Q. *J. Am. Chem. Soc.* **2014,** *136,* 16940–16946. doi:10.1021/ja510233h
67. Vinogradova, E. V.; Zhang, C.; Spokoyny, A. M.; Pentelute, B. L.; Buchwald, S. L. *Nature* **2015,** *526,* 687–691. doi:10.1038/nature15739
68. Zhu, Y.; Bauer, M.; Ackermann, L. *Chem. – Eur. J.* **2015,** *21,* 9980–9983. doi:10.1002/chem.201501831
69. Mondal, B.; Roy, B.; Kazmaier, U. *J. Org. Chem.* **2016,** *81,* 11646–11655. doi:10.1021/acs.joc.6b01963
70. Lee, H. G.; Lautrette, G.; Pentelute, B. L.; Buchwald, S. L. *Angew. Chem., Int. Ed.* **2017,** *56,* 3177–3181. doi:10.1002/anie.201611202
71. Liu, T.; Qiao, J. X.; Poss, M. A.; Yu, J.-Q. *Angew. Chem., Int. Ed.* **2017,** *56,* 10924–10927. doi:10.1002/anie.201706367
72. Noisier, A. F. M.; García, J.; Ionuț, I. A.; Albericio, F. *Angew. Chem., Int. Ed.* **2017,** *56,* 314–318. doi:10.1002/anie.201608648
73. Rojas, A. J.; Zhang, C.; Vinogradova, E. V.; Buchwald, N. H.; Reilly, J.; Pentelute, B. L.; Buchwald, S. L. *Chem. Sci.* **2017,** *8,* 4257–4263. doi:10.1039/c6sc05454d
74. Tang, J.; He, Y.; Chen, H.; Sheng, W.; Wang, H. *Chem. Sci.* **2017,** *8,* 4565–4570. doi:10.1039/c6sc05530c
75. Bauer, M.; Wang, W.; Lorion, M. M.; Dong, C.; Ackermann, L. *Angew. Chem., Int. Ed.* **2018,** *57,* 203–207. doi:10.1002/anie.201710136
76. Kubota, K.; Dai, P.; Pentelute, B. L.; Buchwald, S. L. *J. Am. Chem. Soc.* **2018,** *140,* 3128–3133. doi:10.1021/jacs.8b00172
77. Wang, W.; Lorion, M. M.; Martinazzoli, O.; Ackermann, L. *Angew. Chem., Int. Ed.* **2018,** *57,* 10554–10558. doi:10.1002/anie.201804654
78. Zhan, B.-B.; Li, Y.; Xu, J.-W.; Nie, X.-L.; Fan, J.; Jin, L.; Shi, B.-F. *Angew. Chem., Int. Ed.* **2018,** *57,* 5858–5862. doi:10.1002/anie.201801445
79. Zhang, X.; Lu, G.; Sun, M.; Mahankali, M.; Ma, Y.; Zhang, M.; Hua, W.; Hu, Y.; Wang, Q.; Chen, J.; He, G.; Qi, X.; Shen, W.; Liu, P.; Chen, G. *Nat. Chem.* **2018,** *10,* 540–548. doi:10.1038/s41557-018-0006-y
80. Bai, Q.; Tang, J.; Wang, H. *Org. Lett.* **2019,** *21,* 5858–5861. doi:10.1021/acs.orglett.9b01953
81. Li, B.; Li, X.; Han, B.; Chen, Z.; Zhang, X.; He, G.; Chen, G. *J. Am. Chem. Soc.* **2019,** *141,* 9401–9407. doi:10.1021/jacs.9b04221
82. Yuan, F.; Hou, Z.-L.; Pramanick, P. K.; Yao, B. *Org. Lett.* **2019,** *21,* 9381–9385. doi:10.1021/acs.orglett.9b03607
83. Zhan, B.-B.; Fan, J.; Jin, L.; Shi, B.-F. *ACS Catal.* **2019,** *9,* 3298–3303. doi:10.1021/acscatal.9b00544
84. Liu, L.; Liu, Y.-H.; Shi, B.-F. *Chem. Sci.* **2020,** *11,* 290–294. doi:10.1039/c9sc04482e
85. Weng, Y.; Ding, X.; Oliveira, J. C. A.; Xu, X.; Kaplaneris, N.; Zhu, M.; Chen, H.; Chen, Z.; Ackermann, L. *Chem. Sci.* **2020,** *11,* 9290–9295. doi:10.1039/d0sc03830j
86. Wu, J.; Kaplaneris, N.; Ni, S.; Kaltenhäuser, F.; Ackermann, L. *Chem. Sci.* **2020,** *11,* 6521–6526. doi:10.1039/d0sc01260b
87. Zhan, B.-B.; Jiang, M.-X.; Shi, B.-F. *Chem. Commun.* **2020,** *56,* 13950–13958. doi:10.1039/d0cc06133f
88. Key, H. M.; Miller, S. J. *J. Am. Chem. Soc.* **2017,** *139,* 15460–15466. doi:10.1021/jacs.7b08775
89. Liu, J.; Liu, X.; Zhang, F.; Qu, J.; Sun, H.; Zhu, Q. *Chem. – Eur. J.* **2020,** *26,* 16122–16128. doi:10.1002/chem.202003548
90. Peng, J.; Li, C.; Khamrakulov, M.; Wang, J.; Liu, H. *Org. Lett.* **2020,** *22,* 1535–1541. doi:10.1021/acs.orglett.0c00086
91. Wang, W.; Wu, J.; Kuniyil, R.; Kopp, A.; Lima, R. N.; Ackermann, L. *Chem* **2020,** *6,* 3428–3439. doi:10.1016/j.chempr.2020.10.026
92. Schischko, A.; Ren, H.; Kaplaneris, N.; Ackermann, L. *Angew. Chem., Int. Ed.* **2017,** *56,* 1576–1580. doi:10.1002/anie.201609631
93. Schischko, A.; Kaplaneris, N.; Rogge, T.; Sirvinskaite, G.; Son, J.; Ackermann, L. *Nat. Commun.* **2019,** *10,* No. 3553. doi:10.1038/s41467-019-11395-3
94. Kaplaneris, N.; Rogge, T.; Yin, R.; Wang, H.; Sirvinskaite, G.; Ackermann, L. *Angew. Chem., Int. Ed.* **2019,** *58,* 3476–3480. doi:10.1002/anie.201812705
95. Wang, W.; Subramanian, P.; Martinazzoli, O.; Wu, J.; Ackermann, L. *Chem. – Eur. J.* **2019,** *25,* 10585–10589. doi:10.1002/chem.201902788
96. Zhou, B.; Chen, H.; Wang, C. *J. Am. Chem. Soc.* **2013,** *135,* 1264–1267. doi:10.1021/ja311689k
97. Shi, L.; Zhong, X.; She, H.; Lei, Z.; Li, F. *Chem. Commun.* **2015,** *51,* 7136–7139. doi:10.1039/c5cc00249d

98. Wang, H.; Pesciaioli, F.; Oliveira, J. C. A.; Warratz, S.; Ackermann, L. *Angew. Chem., Int. Ed.* **2017,** *56,* 15063–15067. doi:10.1002/anie.201708271
99. Zell, D.; Dhawa, U.; Müller, V.; Bursch, M.; Grimme, S.; Ackermann, L. *ACS Catal.* **2017,** *7,* 4209–4213. doi:10.1021/acscatal.7b01208
100. Wang, C.; Rueping, M. *ChemCatChem* **2018,** *10,* 2681–2685. doi:10.1002/cctc.201800553
101. Ma, X.; Dang, Y. *J. Org. Chem.* **2019,** *84,* 1916–1924. doi:10.1021/acs.joc.8b02914
102. Cembellín, S.; Dalton, T.; Pinkert, T.; Schäfers, F.; Glorius, F. *ACS Catal.* **2020,** *10,* 197–202. doi:10.1021/acscatal.9b03965
103. Wan, S.; Luo, Z.; Xu, X.; Yu, H.; Li, J.; Pan, Y.; Zhang, X.; Xu, L.; Cao, R. *Adv. Synth. Catal.* **2021,** *363,* 2586–2593. doi:10.1002/adsc.202100056
104. Kaplaneris, N.; Kaltenhuser, F.; Sirvinskaite, G.; Fan, S.; De Oliveira, T.; Conradi, L.-C.; Ackermann, L. *Sci. Adv.* **2021,** *7,* eabe6202. doi:10.1126/sciadv.abe6202

License and Terms

This is an Open Access article under the terms of the Creative Commons Attribution License (https://creativecommons.org/licenses/by/4.0). Please note that the reuse, redistribution and reproduction in particular requires that the author(s) and source are credited and that individual graphics may be subject to special legal provisions.

The license is subject to the *Beilstein Journal of Organic Chemistry* terms and conditions: (https://www.beilstein-journals.org/bjoc/terms)

The definitive version of this article is the electronic one which can be found at:
https://doi.org/10.3762/bjoc.17.122

BEILSTEIN JOURNAL OF ORGANIC CHEMISTRY

On the application of 3d metals for C–H activation toward bioactive compounds: The key step for the synthesis of silver bullets

Renato L. Carvalho[1], Amanda S. de Miranda[1], Mateus P. Nunes[1], Roberto S. Gomes[2], Guilherme A. M. Jardim[*1,3] and Eufrânio N. da Silva Júnior[*1]

Review

Open Access

Address:
[1]Institute of Exact Sciences, Department of Chemistry, Federal University of Minas Gerais - UFMG, CEP 31270-901, Belo Horizonte, MG, Brazil, [2]Department of Pharmaceutical Sciences, North Dakota State University, Fargo, ND, United States, and [3]Centre for Excellence for Research in Sustainable Chemistry (CERSusChem), Department of Chemistry, Federal University of São Carlos – UFSCar, CEP 13565-905, São Carlos, SP, Brazil

Email:
Guilherme A. M. Jardim* - guilhermeamj@ufmg.br;
Eufrânio N. da Silva Júnior* - eufranio@ufmg.br

* Corresponding author

Keywords:
bioactive compounds; C–H activation; 3d metals; drugs; medicinal chemistry

Beilstein J. Org. Chem. **2021,** *17,* 1849–1938.
https://doi.org/10.3762/bjoc.17.126

Received: 29 April 2021
Accepted: 28 June 2021
Published: 30 July 2021

This article is part of the thematic issue "Earth-abundant 3d metal catalysis".

Associate Editor: K. Itami

© 2021 Carvalho et al.; licensee Beilstein-Institut.
License and terms: see end of document.

Abstract

Several valuable biologically active molecules can be obtained through C–H activation processes. However, the use of expensive and not readily accessible catalysts complicates the process of pharmacological application of these compounds. A plausible way to overcome this issue is developing and using cheaper, more accessible, and equally effective catalysts. First-row transition (3d) metals have shown to be important catalysts in this matter. This review summarizes the use of 3d metal catalysts in C–H activation processes to obtain potentially (or proved) biologically active compounds.

Introduction

The discovery of new biologically active substances represents not only an advance in the chemistry field but also offers innovative chances for pharmacological and biomedical sciences. Every year, several molecules are discovered and studied against different types of diseases, such as cancer [1,2], malaria [3,4], Chagas disease [5,6], HIV [7,8], depression [9,10], amnesia [11], Alzheimer [12], and maybe even in a more recent scenario, COVID-19 [13]. Even though many compounds are found to present activity against these diseases, only a few of them become approved, due to their toxicity or other issues related to their applicability. Therefore, synthetic methodologies that facilitate the successful production of potential biologically active molecules have a relevant role in the organic synthesis research field.

One of the key synthetic methodologies is the C–H bond activation process that enables a straightforward access to several important and innovative compounds [14-18]. In the last few years, metals such as ruthenium [19-21], rhodium [22-24], palladium [25-27], and iridium [28-30] have been widely applied as catalysts for this matter, including in the synthesis of bioactive substances. Although catalysts based on these metals, are known to be efficient in C–H bond activation reactions affording the products in good yields and mild conditions, they are also known to be usually expensive. This fact may negatively affect the industrial application of synthetic procedures relying on such catalysts. The substitution by cheaper and more accessible metals such as any members of the first row of transition metals (Scheme 1) could overcome this drawback. The application of these metals as catalysts for C–H activation processes deserves a better exploration.

This review compiles the application of 3d metals as catalysts for C–H activation processes to obtain biologically active compounds or building blocks applied in the synthesis of molecules with known biological effects.

Review

Scandium-catalyzed C–H activation

Scandium is the first metal of the 3d metals row. It is relatively cheap compared to heavier transition metals, and it is commonly used on catalytic procedures, such as catalyzed polymerization [31,32] and C–C coupling reactions [33,34]. It is also an increasing metal option to develop C–H activation methods, since it can be used as the metallic center of innovative and elaborated complexes [35,36]. Scandium-based catalysts have not been directly applied to the synthesis of known biologically active compounds via C–H activation reactions. Therefore, as challenging as it seems to be, there is still a demand for applying this relevant methodology to obtain new compounds with known pharmacological properties. However, several molecules based on structural scaffolds related to important biological activities have been successfully achieved via scandium-catalyzed C–H activation [37-41]. Hou’s group presented various studies on this theme [42,43], such as a notable work recently published in which they promoted a scandium-catalyzed intramolecular cyclization on benzimidazole substrates, via a C–H activation at the C-2 position (Scheme 2B). In this process, a scandium(III)/Cp* catalyst containing two units of an *o*-*N*,*N*-(dimethylamino)benzyl ligand [**Sc-1**] was applied, and several examples of cyclic benzimidazole compounds were obtained in excellent yields (Scheme 2C) [37]. Benzimidazole compounds bearing substituents in their C-2 position are present in several bioactive molecules. They are also known to present valuable biological activities, such as anti-HBV (**1**) [44], anti-HIV (**2**) [45], antitumor (**3**) [46] and even antiplasmodial activities (**4**) [47] (Scheme 2A). Although these studied bioactive compounds do not directly represent the structural moieties obtained in Hou’s group, this fact still gathers some critical value to the large variety of products obtained in the above-cited work. Incoming research works may lead to the observation of relevant activities and the applicability of this class of molecules.

Lou, Hou and co-workers also used the same catalyst to perform a regioselective scandium-catalyzed alkylation of 2-phenyl-quinoline derivatives (Scheme 3B) [38]. It is important to highlight the biological importance of quinoline derivatives, since several quinolines are known to present valuable biological activities, such as anti-HIV (**5**) [48], antiviral in general (**6**) [49], antituberculotic (**7**), and antimalarial (**8**) [50] (Scheme 3A). Using 2-phenylquinoline derivatives as substrates includes some intrinsic challenges, since there are two sites in the molecule where the C–H activation can take place. The authors were able to selectively obtain the C-8-substituted product (product A) in a proportion higher than 20:1 over the

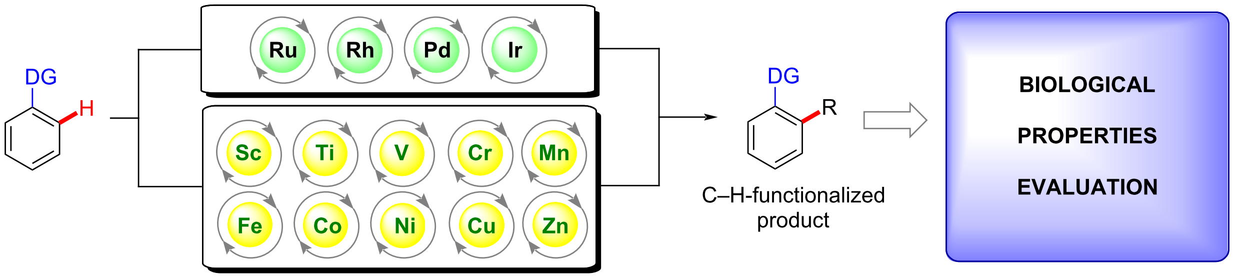

Scheme 1: Schematic overview of transition metals studied in C–H activation processes.

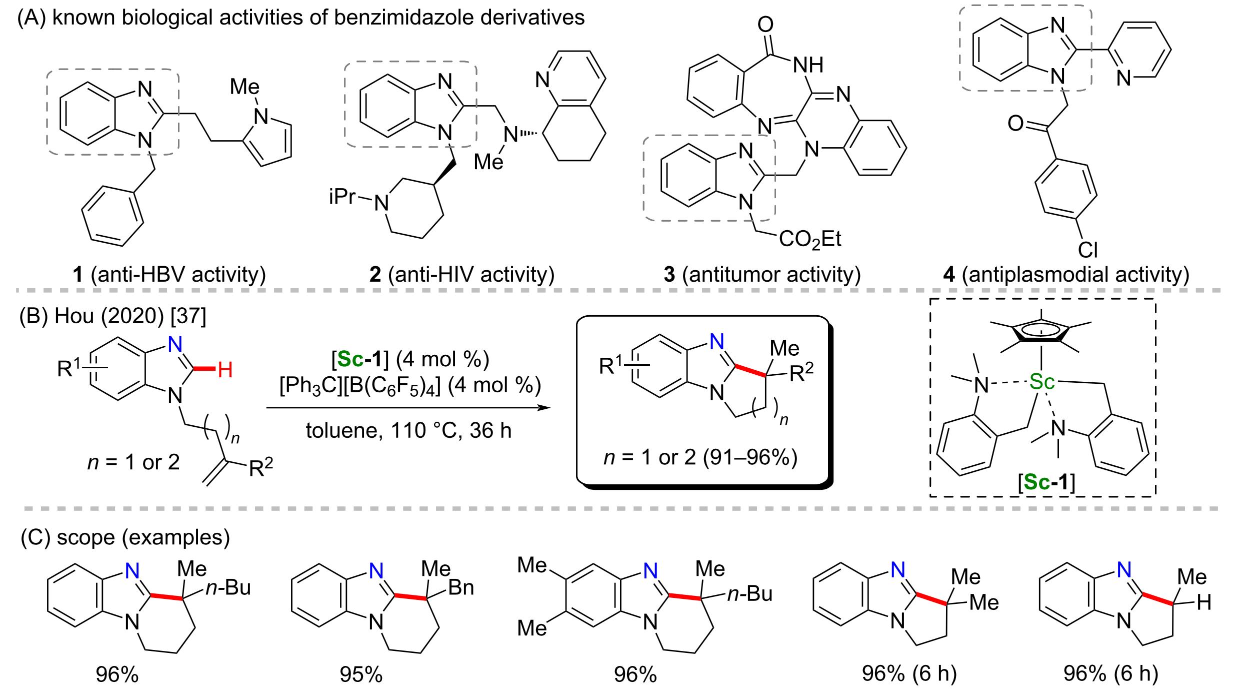
(A) known biological activities of benzimidazole derivatives
1 (anti-HBV activity)
2 (anti-HIV activity)
3 (antitumor activity)
4 (antiplasmodial activity)
(B) Hou (2020) [37]
n = 1 or 2
[Sc-1] (4 mol %)
[Ph3C][B(C6F5)4] (4 mol %)
toluene, 110 °C, 36 h
n = 1 or 2 (91–96%)
[Sc-1]
(C) scope (examples)
96%
95%
96%
96% (6 h)
96% (6 h)

Scheme 2: (A) Known biological activities related to benzimidazole-based compounds; (B and C) an example of a scandium-catalyzed C–H cyclization on benzimidazoles.

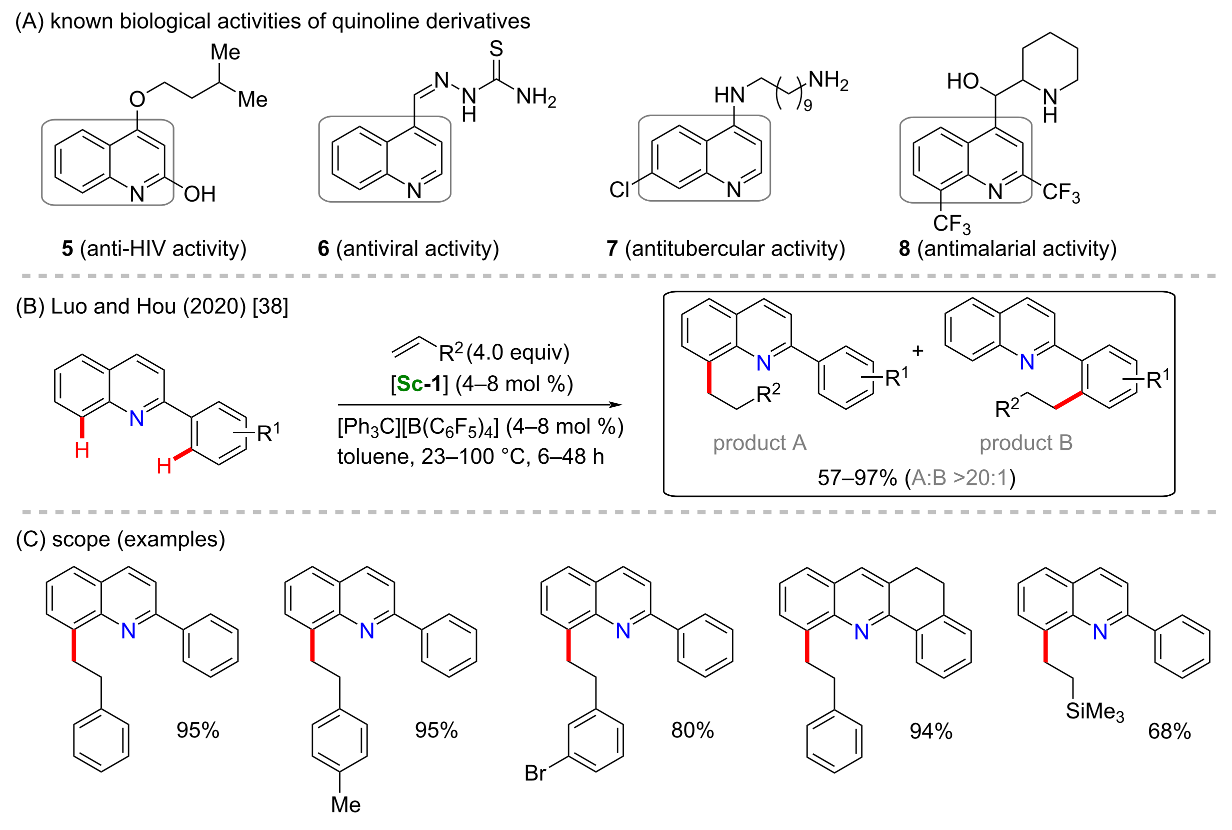
(A) known biological activities of quinoline derivatives
5 (anti-HIV activity)
6 (antiviral activity)
7 (antitubercular activity)
8 (antimalarial activity)
(B) Luo and Hou (2020) [38]
R2 (4.0 equiv)
[Sc-1] (4–8 mol %)
[Ph3C][B(C6F5)4] (4–8 mol %)
toluene, 23–100 °C, 6–48 h
product A
product B
57–97% (A:B >20:1)
(C) scope (examples)
95%
95%
80%
94%
68%

Scheme 3: (A) Known biological activities related to quinoline-based compounds; (B and C) an example of a scandium-catalyzed C–H alkylation of 2-phenylquinoline derivatives.

product resulting from C'-2 activation (product B) in good to excellent yields (Scheme 3C).

Another biologically active structural motif that can be activated by this catalyst are thioethers, as was well described by Hou and co-workers in 2018 [39]. In this work, the presence of [**Sc-1**] and several alkenes resulted in the successful scandium-C(sp^3)–H alkylation of methyl thioethers (Scheme 4B), by which different activated internal thioethers were obtained in good yields (Scheme 4C). The transformation facilitates direct access to several sulfur-containing pharmacological compounds that present valuable biological activities, such as anti-HIV (**9**) [51], inhibition of snake venom enzymes (**10**) [52], or even anti-estrogenic effects (**11**) [53] (Scheme 4A).

Recently, Hou and co-workers also explored the utility of a similar catalyst, [**Sc-2**], which bears a more electron-rich cyclopentadienyl ligand, in a scandium-catalyzed C–H [3 + 2] cyclization (Scheme 5B) [40]. In this transformation, several aminoindane derivatives were obtained from benzylimines in the presence of the catalyst [**Sc-2**], alkenes and $[Ph_3C][B(C_6F_5)_4]$. The desired aminoindane derivatives were obtained with good regio- and enantioselectivity, (product A/ product B was observed in a ratio higher than 19:1, Scheme 5C). It is worth mentioning that aminoindanes are scaffolds also present in biologically active molecules that may present, for example, antipsychotic (**12**) [54], anticonvulsant (**13**) [55], and antiparkinsonian activities (**14**) [56,57] (Scheme 5A).

A few years earlier, Hou and co-workers reported the very first metal-catalyzed C–H hydroaminoalkylation of tertiary amines using norbornene as the coupling partner [41]. For this method, the scandium catalyst that presented the best performance was a homoleptic trialkylscandium, [**Sc-3**] (Scheme 6B), instead of the usual cyclopentadienyl-containing dialkylscandium catalysts described so far in this review. Several substituted norbornene derivatives were obtained in good to excellent yields (Scheme 6C). These bicyclic structures may present unique biological activities including neuroprotective properties (**15**), as it was recently reported by Joubert and co-workers [58], as well as acting as agonists of nicotinic receptors (**16**) [59], representing an alternative option for the treatment of cigarette addiction (Scheme 6A).

The use of scandium as the metallic motif in catalysts applied in C–H activation methodologies leads to the formation of important structures not yet been studied for their biological activities. Therefore, there is more to be achieved and studied, considering what scandium-based catalysts can still offer.

Titanium-catalyzed C–H activation

Titanium is another well-known and considerably cheap 3d metal which is underexplored in the C–H activation field [60],

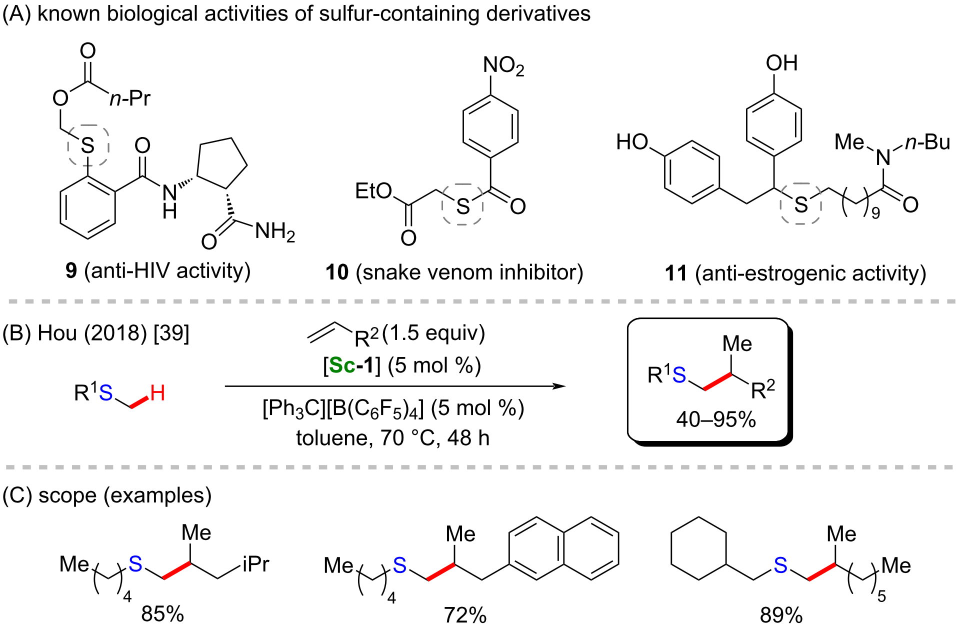

Scheme 4: (A) Known biological activities related to sulfur-containing compounds; (B and C) an example of a scandium-catalyzed C(sp^3)–H alkylation of methyl thioether derivatives.

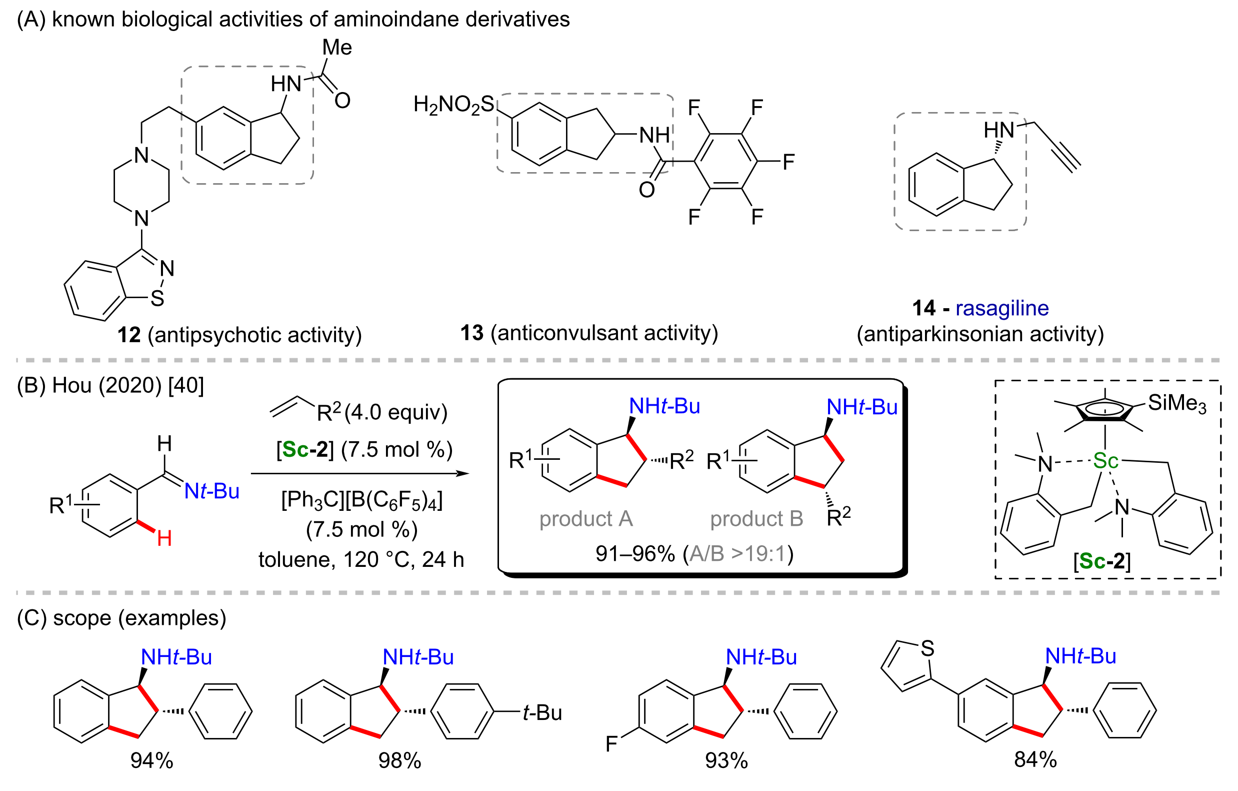
(A) known biological activities of aminoindane derivatives
Me
HN
O
N
N
N
S
12 (antipsychotic activity)
H2NO2S
NH
O
F
F
F
F
F
13 (anticonvulsant activity)
HN
14 - rasagiline
(antiparkinsonian activity)
(B) Hou (2020) [40]
R2 (4.0 equiv)
[Sc-2] (7.5 mol %)
[Ph3C][B(C6F5)4]
(7.5 mol %)
toluene, 120 °C, 24 h
H
Nt-Bu
R1
H
NHt-Bu
R1
R2
product A
NHt-Bu
R1
product B
R2
91–96% (A/B >19:1)
SiMe3
N
Sc
N
[Sc-2]
(C) scope (examples)
NHt-Bu
94%
NHt-Bu
t-Bu
98%
NHt-Bu
F
93%
S
NHt-Bu
84%

Scheme 5: (A) Known biological activities related to aminoindane derivatives; (B and C) an example of a scandium-catalyzed C–H cyclization on aminoindane derivatives.

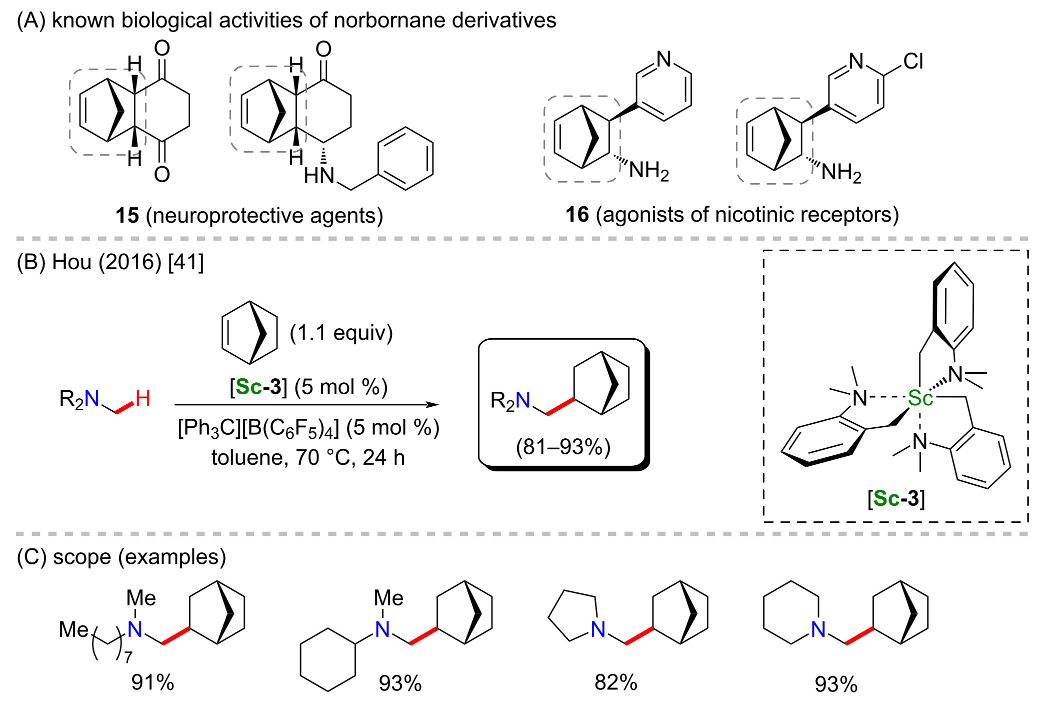
(A) known biological activities of norbornane derivatives
H
O
H
O
H
O
H
HN
15 (neuroprotective agents)
N
NH2
N
Cl
NH2
16 (agonists of nicotinic receptors)
(B) Hou (2016) [41]
(1.1 equiv)
R2N
H
[Sc-3] (5 mol %)
[Ph3C][B(C6F5)4] (5 mol %)
toluene, 70 °C, 24 h
R2N
(81–93%)
N
N
Sc
N
[Sc-3]
(C) scope (examples)
Me
Me
N
7
91%
Me
N
93%
N
82%
N
93%

Scheme 6: (A) Known biological activities related to norbornane derivatives; (B and C) an example of a scandium-catalyzed C–H hydroaminoalkylation of tertiary amines.

especially with regard to the synthesis of biologically active compounds. Therefore, further studies on the applicability of this specific metal are highly desirable. Titanium is well known to be used as titanium dioxide, a powerful photocatalyst present in inks [61,62] and sunscreens [63,64]. As a catalyst, it can be used, for example, in polymerization methods to synthesize polypropylene [65]. With regard to C–H activation reactions, Doye's group has dedicated its research to the development of significant titanium-catalyzed amine-directed C–H activation [66,67]. Recently, a good example was reported, in which C(sp^3)–H hydroaminoalkylation of *N*-alkylaniline derivatives was achieved [68]. For this process, the authors used a bulky titanium catalyst, by which a desirable regioselectivity could be achieved (Scheme 7B and C). The obtained *N*-substituted anilines resemble some important compounds already known for their biological activities, such as antimalarial (**17**) [69] and anticancer (**18**) [70,71] properties (Scheme 7A).

Beckhaus and Doye reported cyclization processes mediated by titanium catalysis, that led to pyridinone derivatives or external cycloamines via an intramolecular titanium-catalyzed C–H hydroaminoalkylation [72-74]. In these works, two titanium catalysts were studied, tetrakis(dimethylamino)titanium [Ti(NMe$_2$)$_4$] and tetrabenzyltitanium [TiBn$_4$], and it was observed that a better stereoselectivity was achieved by using the first catalyst while a better yield was obtained when the second catalyst was applied (Scheme 8B). Although the authors did not explore any possible biological activity of the obtained products, some compounds bearing an *N*-substituted cyclohexylamine moiety are known to present antidepressant and analgesic activities (e.g., compounds **19**, **20**, and **21**, Scheme 8A) [75]. Further studies could reveal other notable biological activities, thus justifying the need to develop new and accessible titanium catalysts.

As it can be observed from the previous cited works, titanium is by far one of the least explored metal in the field. Since it is a widely accessible and considerably cheap metal, it would be highly suitable for the development of methodologies for the synthesis of biologically active molecules. Based on the exam-

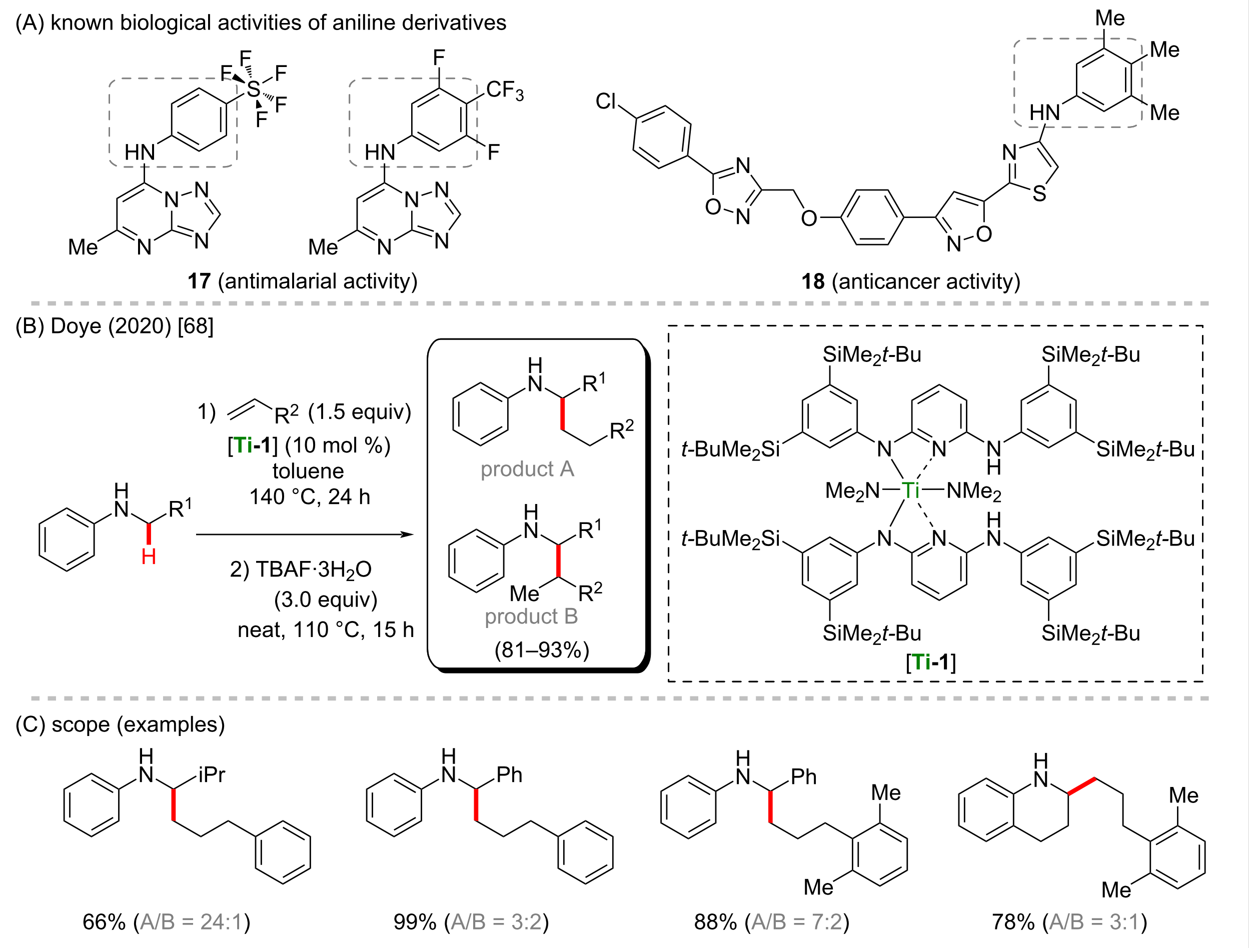

Scheme 7: (A) Known biological activities related to aniline derivatives; (B and C) an example of a titanium-catalyzed C–H hydroaminoalkylation of *N*-alkylanilines.

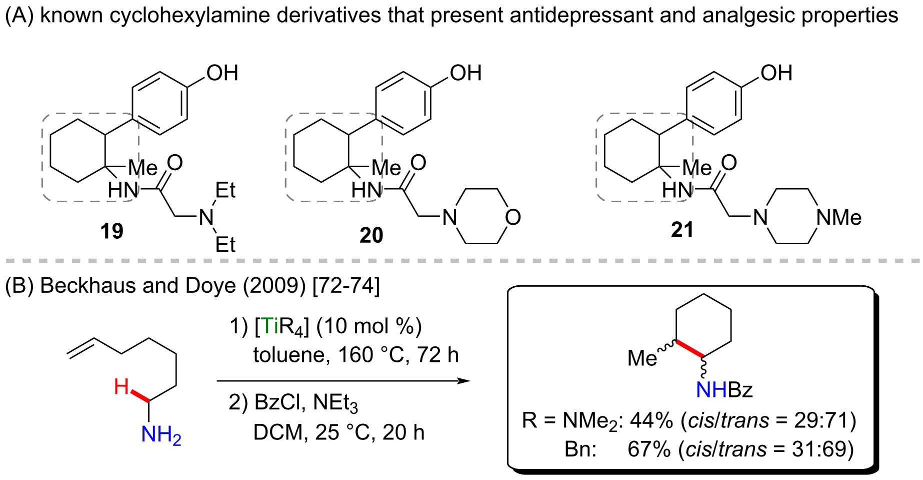
(A) known cyclohexylamine derivatives that present antidepressant and analgesic properties
OH
Me
O
HN
Et
N
Et
19
20
21
O
NMe
(B) Beckhaus and Doye (2009) [72-74]
H
NH2
1) [TiR4] (10 mol %)
toluene, 160 °C, 72 h
2) BzCl, NEt3
DCM, 25 °C, 20 h
NHBz
R = NMe2: 44% (cis/trans = 29:71)
Bn: 67% (cis/trans = 31:69)

Scheme 8: (A) Known biological activities related to cyclohexylamine derivatives; (B) an example of an intramolecular titanium-catalyzed C–H hydroaminoalkylation of alkenes.

ples mentioned above, there is a specific preference for studies of amine derivatives. However, different functional groups that may go well along with titanium catalysis need still to be explored.

Vanadium-catalyzed C–H activation

Vanadium is the twentieth most abundant element and the sixth most abundant transition metal in Earth's crust. Rarely encountered in its metallic form, vanadium exists in oxidation states ranging from +5 to −3, including the four adjacent states +2 to +5 in aqueous solutions, and usually presents 4, 5 or 6 coordination numbers. The V(II) and V(V) species are reducing and oxidizing agents, respectively, whereas V(IV) is often encountered, mainly in the form of dioxovanadium ion VO^{2+} center [76].

Vanadium-based compounds have been reported to mediate the oxidation of alkanes to alcohols and ketones [76]. The reactions are usually mediated by V(V) and V(IV)-oxo-peroxo complexes, which are produced in situ from vanadium-oxo and dioxo precatalysts in the presence of oxidants, such as H_2O_2, O_2, and *tert*-butyl hydroperoxide (TBHP) [76-82]. Inorganic acids and chelating and non-chelating carboxylic acids have been used as additives in these reactions and are suggested to act as ligands, assist proton transfer and promote the formation of oligovanadates by decreasing the pH value of the solution.

The mechanisms of some vanadium-mediated oxidation reactions of alkanes have been studied, most of them providing evidence for the involvement of radical species and a few suggesting non-radical pathways in the presence of a Lewis acid or oligovanadate complexes in solution [77,82-90]. Because most of the reactions are not likely to occur through either a direct metal-mediated C–H activation involving carbon–metal bond or a mechanism involving the usual metal-mediated coupling pathways comprising oxidative addition, transmetalation and reductive elimination steps, they are beyond the scope of this review and will not be extensively covered herein.

Homogeneous and heterogeneous vanadium-based catalysts have been employed to obtain alcohols and carbonyl compounds through oxidation, including $VOSO_4$, $Na(VO_3)$, $VO(acac)_2$, VOX_3, among others. Obtaining ketones and aldehydes from hydrocarbon compounds through vanadium-mediated activation of $C(sp^3)$–H bonds in a benzylic position has been selectively feasible without activating a $C(sp^2)$–H bond in the arene moiety. Verma and co-workers [91] have reported the use of $VO(acac)_2$ immobilized over graphitic carbon nitride ($VO@gC_3N_4$) under visible light irradiation to perform a photocatalytic C–H activation of arene methides and derivatives. Using H_2O_2 as an oxidant agent, ketones and aldehydes were obtained from hydrocarbons with high yields (85–99%, Scheme 9B and 9C). Although the authors did not explore the biological effects of the obtained products, this class of molecules resembles the basic structure of several important biologically active molecules (**22** and **23**) (Scheme 9A) [92].

Interestingly, the same conditions could be used for benzene hydroxylation to obtain phenol but were ineffective with benzene rings bearing either electron-donating or electron-withdrawing substituents. Notably, the catalyst could be reused five times to oxidize ethylbenzene without significant loss of activi-

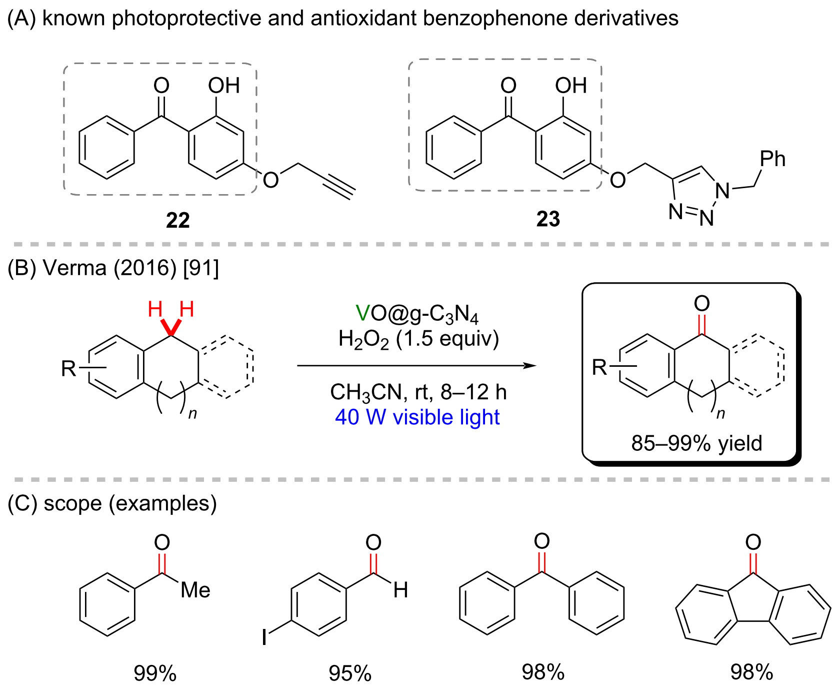

Scheme 9: (A) Known biologically active benzophenone derivatives; (B and C) photocatalytic oxidation of benzylic C–H bonds mediated by supported vanadium.

ty and metal leaching. The authors have suggested a mechanism for the reaction involving radical species bearing a benzylic carbon–vanadium bond.

Fluorine presents unique features and may lead to essential changes in the structural and physicochemical properties of a compound, thus affecting its pharmacodynamic and pharmacokinetic profile. Consequently, fluorination methods are particularly useful in the synthesis of bioactive substances, including marketed drugs (**24** and **25**) (Scheme 10A) [93]. In addition to oxygen insertion, vanadium use has also been reported for the direct C(sp^3)–H fluorination. Chen and co-workers [94] described a fluorination method employing Selectfluor as fluorine source and the commercially available V_2O_3 to give fluorine-containing compounds under mild conditions and with moderate to good yields (Scheme 10B,C). The reaction showed to be chemoselective, maintaining good yields with compounds bearing varied functional groups, whereas low yields were observed for benzylic fluorination. Preliminary mechanistic studies suggested the C–H abstraction to be the rate-determining step and the high oxygen sensitivity of the reaction suggested it goes through a radical pathway.

Similar to the oxidation of alkanes to give alcohols and carbonyl compounds, vanadium complexes have been reported to mediate the hydroxylation of arenes, including the obtaining of phenol from benzene. However, most mechanistic studies provided evidence for radical pathways involving vanadium-peroxo species [76], with a few exceptions [95].

Vanadium-based catalysts have been employed in carbon–carbon bond formation reactions, such as arene couplings, thereby proving especially useful in the synthesis of bioactive compounds, including natural compounds and biaryl chiral auxiliaries. Also, the oxidative coupling of phenolic substrates has been reported to be mediated by vanadium complexes such as VCl_4, $VOCl_3$, and VOF_3, among others. For instance, an intramolecular coupling of phenolic moieties using VOF_3 has been reported as a final step in the synthesis of the bioactive natural macrolactone (±)-decinine (**30**) (Scheme 11B) [96]. These compounds (**26**–**29**) derive from the class of Lythraceae alkaloids (Scheme 11A), extracted from *Heimia salicifolia*, and present valuable pharmacological properties, such as antisyphilitic, sudoritic, antipyretic, laxative, and diuretic activities [97]. Trifluoroacetic acid was used as an additive, being suggested to avoid oxidation of the amine moiety by the formation of the corresponding ammonium salt.

Similar conditions have been reported for an alternative synthesis of both enantiomers of the antitumor phenanthroindolizidine alkaloid boehmeriasin A (**31**) (Scheme 12A) [98], and phenanthroindolizidines through an intramolecular oxidative

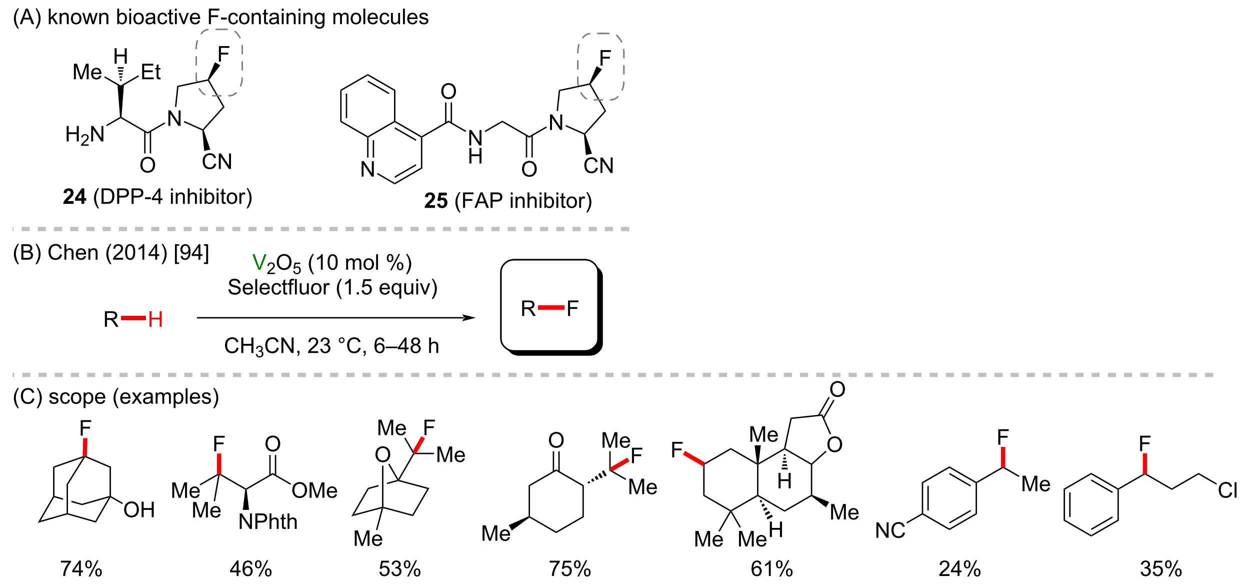
(A) known bioactive F-containing molecules
24 (DPP-4 inhibitor)
25 (FAP inhibitor)
(B) Chen (2014) [94]
V2O5 (10 mol %)
Selectfluor (1.5 equiv)
CH3CN, 23 °C, 6–48 h
R–H
R–F
(C) scope (examples)
74%
46%
53%
75%
61%
24%
35%

Scheme 10: (A) Known bioactive fluorine-containing compounds; (B and C) vanadium-mediated C(sp^3)–H fluorination.

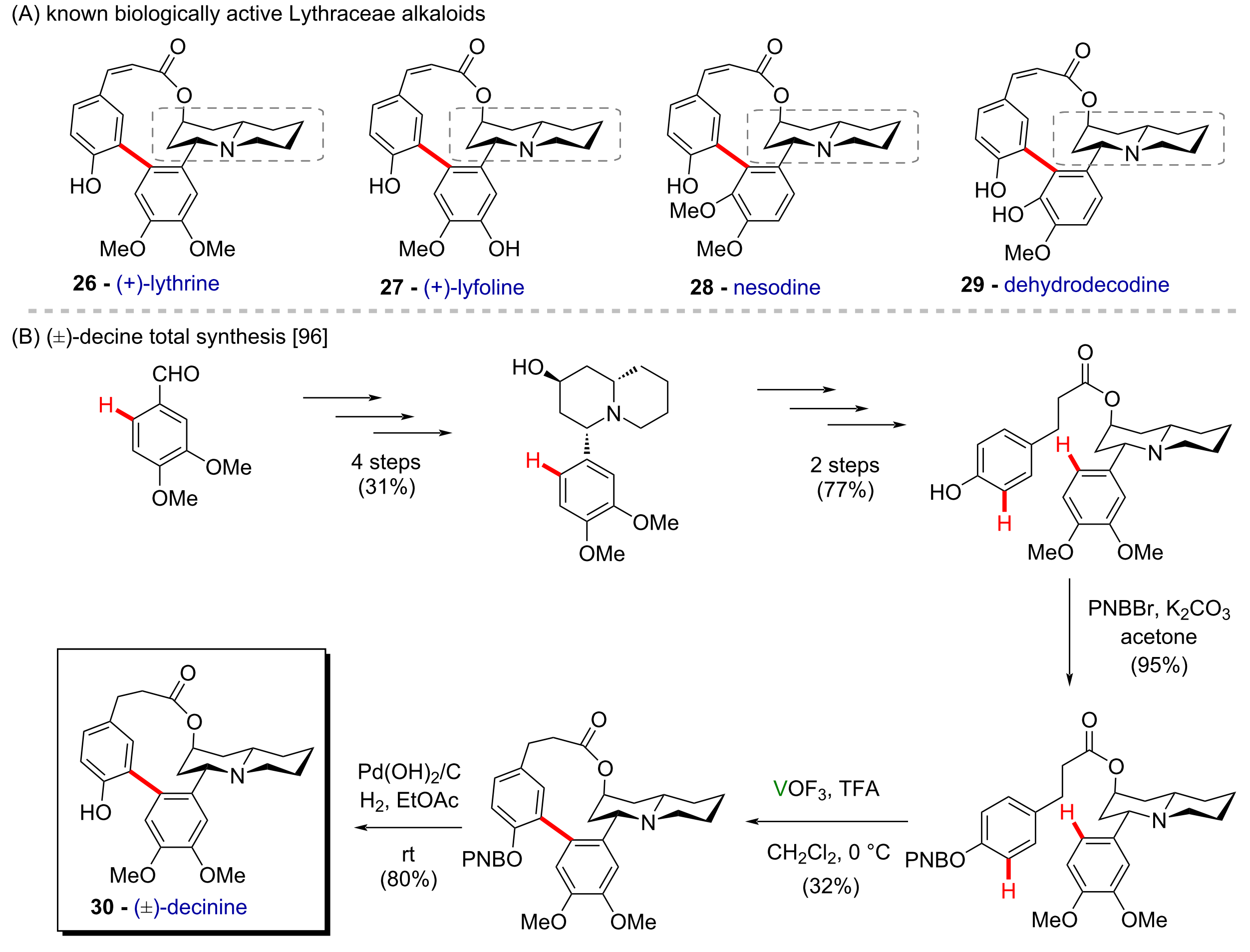
(A) known biologically active Lythraceae alkaloids
26 - (+)-lythrine
27 - (+)-lyfoline
28 - nesodine
29 - dehydrodecodine
(B) (±)-decine total synthesis [96]
4 steps
(31%)
2 steps
(77%)
PNBBr, K2CO3
acetone
(95%)
VOF3, TFA
CH2Cl2, 0 °C
(32%)
Pd(OH)2/C
H2, EtOAc
rt
(80%)
30 - (±)-decinine

Scheme 11: (A) Known biologically active Lythraceae alkaloids; (B) synthesis of (±)-decinine (**30**).

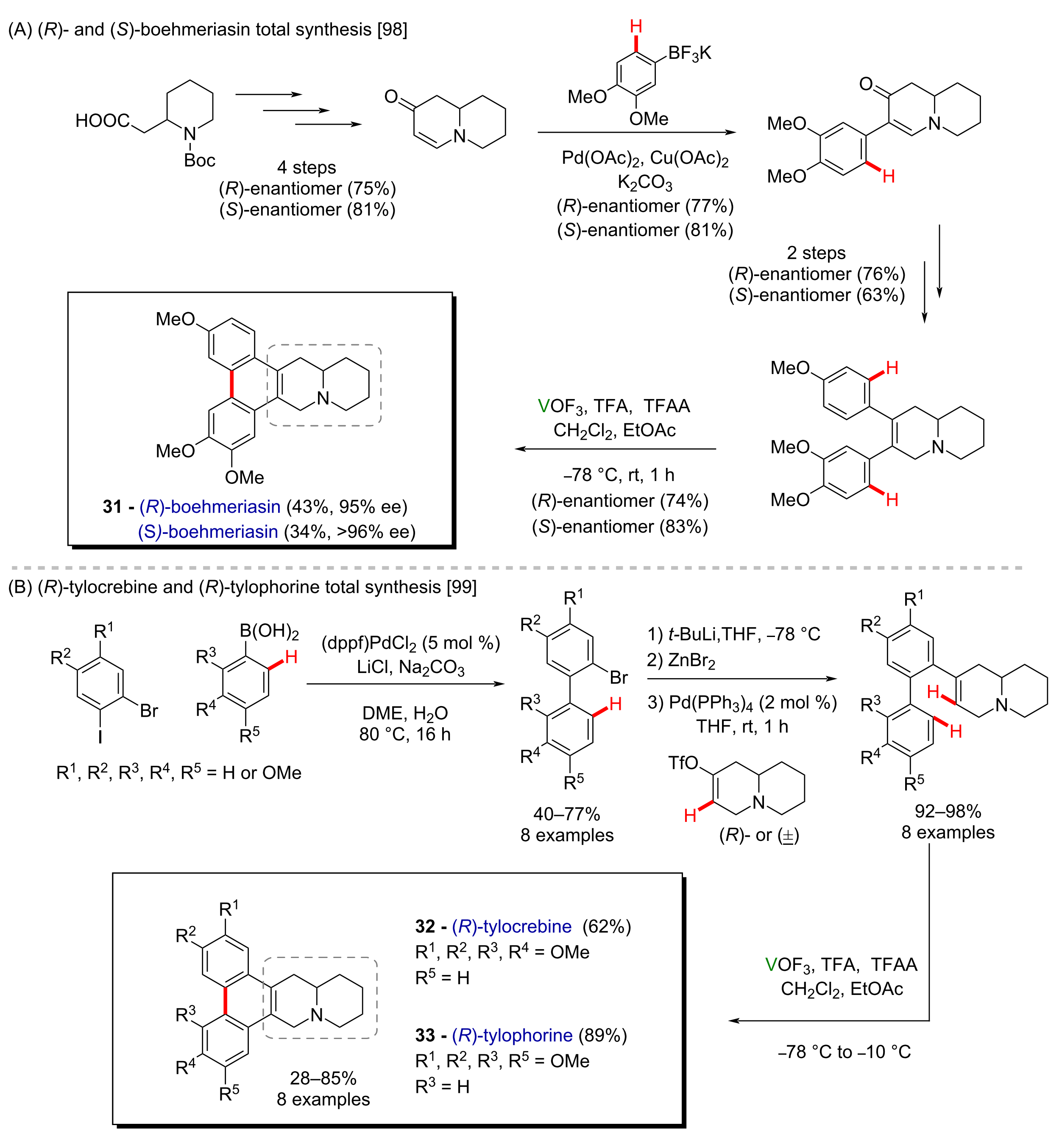
(A) (R)- and (S)-boehmeriasin total synthesis [98]
HOOC
N
Boc
4 steps
(R)-enantiomer (75%)
(S)-enantiomer (81%)
O
N
H
BF3K
MeO
OMe
Pd(OAc)2, Cu(OAc)2
K2CO3
(R)-enantiomer (77%)
(S)-enantiomer (81%)
MeO
MeO
H
2 steps
(R)-enantiomer (76%)
(S)-enantiomer (63%)
VOF3, TFA, TFAA
CH2Cl2, EtOAc
–78 °C, rt, 1 h
(R)-enantiomer (74%)
(S)-enantiomer (83%)
31 - (R)-boehmeriasin (43%, 95% ee)
(S)-boehmeriasin (34%, >96% ee)
(B) (R)-tylocrebine and (R)-tylophorine total synthesis [99]
R1
R2
Br
I
B(OH)2
R3
R4
R5
R1, R2, R3, R4, R5 = H or OMe
(dppf)PdCl2 (5 mol %)
LiCl, Na2CO3
DME, H2O
80 °C, 16 h
40–77%
8 examples
1) t-BuLi,THF, –78 °C
2) ZnBr2
3) Pd(PPh3)4 (2 mol %)
THF, rt, 1 h
TfO
(R)- or (±)
92–98%
8 examples
VOF3, TFA, TFAA
CH2Cl2, EtOAc
–78 °C to –10 °C
28–85%
8 examples
32 - (R)-tylocrebine (62%)
R1, R2, R3, R4 = OMe
R5 = H
33 - (R)-tylophorine (89%)
R1, R2, R3, R5 = OMe
R3 = H

Scheme 12: (A) Synthesis of (*R*)- and (*S*)-boehmeriasin (**31**); (B) synthesis of phenanthroindolizidines by vanadium-mediated aryl–alkene coupling.

aryl–alkene coupling (Scheme 12B) [99], which is a far less common transformation in organic synthesis. This approach was employed to synthesize eight phenanthroindolizidines, including (*R*)-tylocrebrine (**32**) and (*R*)-tylophorine (**33**), which were found to display antiproliferative activity in the nanomolar range against human colorectal carcinoma, human breast carcinoma and drug-resistant human ovarian adenocarcinoma cell lines.

Methods for the oxidative homocoupling of phenolic compounds to produce the corresponding biaryl products with high enantiopurity using vanadium chelated with chiral ligands, such as tridentate asymmetric imine ligands, have been reported. For instance, (*S*)-binol derivatives could be successfully prepared from 2-naphthols using a dimeric vanadium complex (Scheme 13B and C) [100]. Binols have been reported to present bactericidal (**34**) [101] and anticancer activities (**35**)

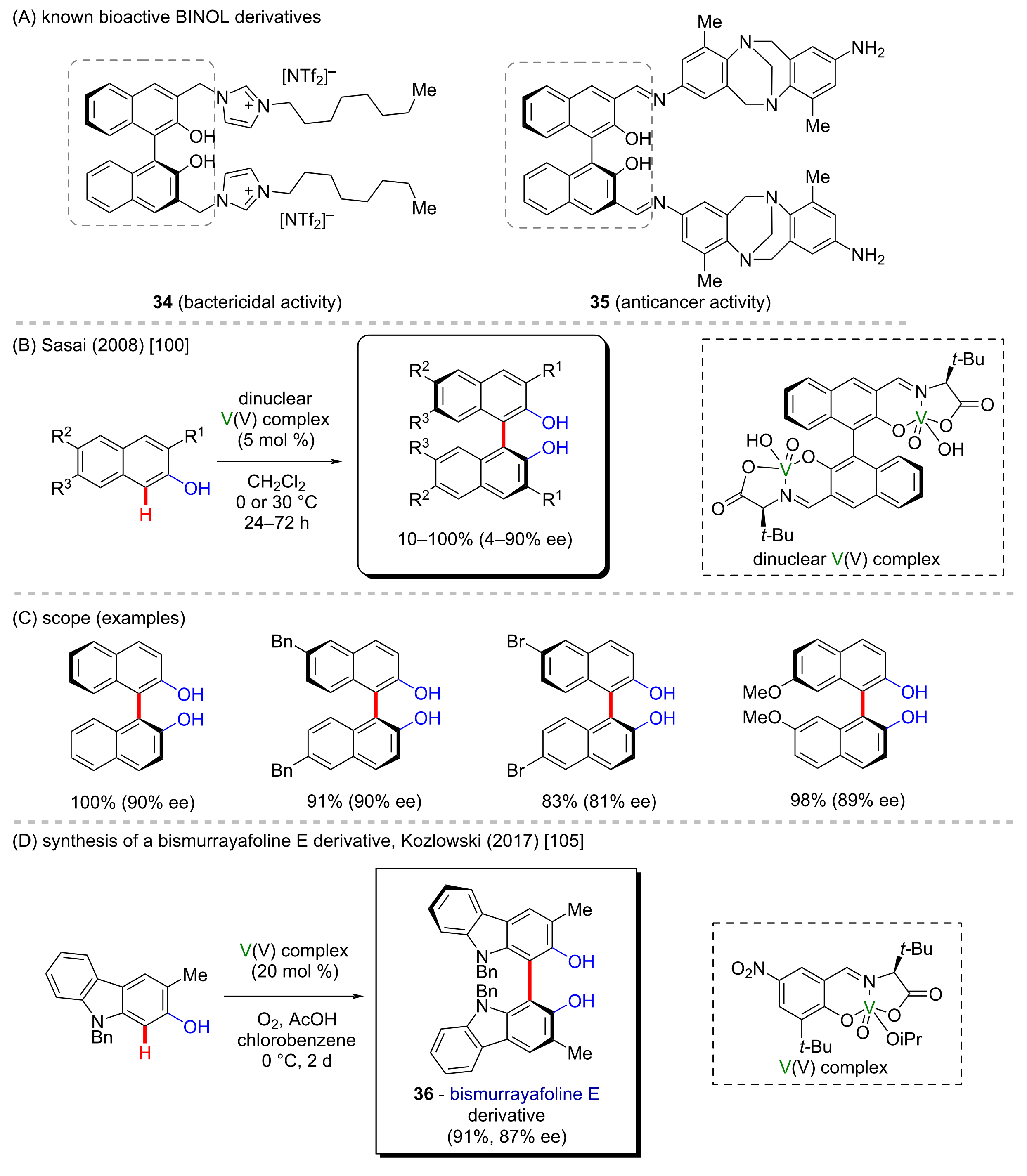
(A) known bioactive BINOL derivatives
[NTf2]⁻
Me
OH
OH
[NTf2]⁻
Me
34 (bactericidal activity)
Me
N
N
NH2
Me
OH
OH
Me
NH2
Me
35 (anticancer activity)
(B) Sasai (2008) [100]
R2
R1
R3
OH
H
dinuclear
V(V) complex
(5 mol %)
CH2Cl2
0 or 30 °C
24–72 h
R2
R1
R3
OH
R3
OH
R2
R1
10–100% (4–90% ee)
t-Bu
O
OH
HO
O
t-Bu
dinuclear V(V) complex
(C) scope (examples)
OH
OH
100% (90% ee)
Bn
OH
OH
Bn
91% (90% ee)
Br
OH
OH
Br
83% (81% ee)
MeO
OH
MeO
OH
98% (89% ee)
(D) synthesis of a bismurrayafoline E derivative, Kozlowski (2017) [105]
Me
N
Bn
OH
H
V(V) complex
(20 mol %)
O2, AcOH
chlorobenzene
0 °C, 2 d
Me
N
Bn
OH
Bn
N
OH
Me
36 - bismurrayafoline E
derivative
(91%, 87% ee)
O2N
t-Bu
O
t-Bu
OiPr
V(V) complex

Scheme 13: (A) Known bioactive BINOL derivatives; (B and C) vanadium-mediated oxidative coupling of 2-naphthols; (D) synthesis of a bismurrayafoline E derivative (**36**).

[102] (Scheme 13A). In this work, the use of a dinuclear catalyst was found to strikingly increase the reaction rate, presumably by reducing entropic costs associated with bringing two molecules of substrate together. In addition, the high enantiopurity was ascribed to a chiral environment that presents three elements of asymmetry. Other examples of vanadium-mediated oxidative homocouplings of phenolic substrates include regioselective and asymmetric homocoupling of phenols and 2-hydroxycarbazoles [103,104].

Notably, Kozlowsky and co-workers were the first who reported a method for the vanadium-based asymmetric coupling of phenols and 2-hydroxycarbazoles [105] that allowed the synthesis of a wide range of chiral biphenols and bicarbazoles. The use of a vanadium complex with less electron-rich ligands along with the addition of Brønsted and Lewis acids, such as acetic acid and LiCl, was suggested to account for the suitability of the method for the coupling of oxidatively resistant substrates. The usefulness of this method was demonstrated in the preparation of the bicarbazole moiety present in the natural product bismurrayafoline E (**36**) [105], an alkaloid found in the leaves of *Murraya koeniggi* (Scheme 13D) [106].

The oxidative formation of carbon–carbon bonds mediated by vanadium has been reported as a method for the aminomethylation of arenes and heteroarenes. The so far described methods include V_2O_5 and $VO(acac)_2$ used for the alkylation of 2-naphthol and nitrogen-containing heteroaromatic moieties containing *N*-methylmorpholine-*N*-oxide, tetrahydroisoquinolines, and *N*,*N*-dimethylacetamide [107-113]. The mechanisms involving oxidation of the amine mediated by vanadium to give iminium ions, followed by a nucleophilic attack of the heteroaromatic ring, have been suggested for most reactions. Evidence comes from the observed regioselectivity and the tolerance of the reactions to radical scavengers, which are in accordance with the occurrence of a heteroaromatic electrophilic substitution and a non-radical pathway. An aminomethylation of the heteroaromatic ring with *N*-methylmorpholine-*N*-oxide catalyzed by $VO(aca)_2$ reported by Mitchell and co-workers [109], however, was found to undergo with a regioselective outcome incompatible to an electrophilic aromatic substitution reaction. The substrate failed to give the same product when subjected to alkylation with the isolated putative iminium ion intermediate. The authors then suggested the reaction took place through a radical mechanism instead. This vanadium-mediated aminoalkylation reaction was found to be a helpful strategy in the synthesis of compound LY2784544 (**41**), a potent inhibitor of Janus kinase 2 that is under clinical trials for the management of myeloproliferative disorders (Scheme 14B) [109,110]. Beyond that, this class of molecules (imidazopyridazines) are known to present a

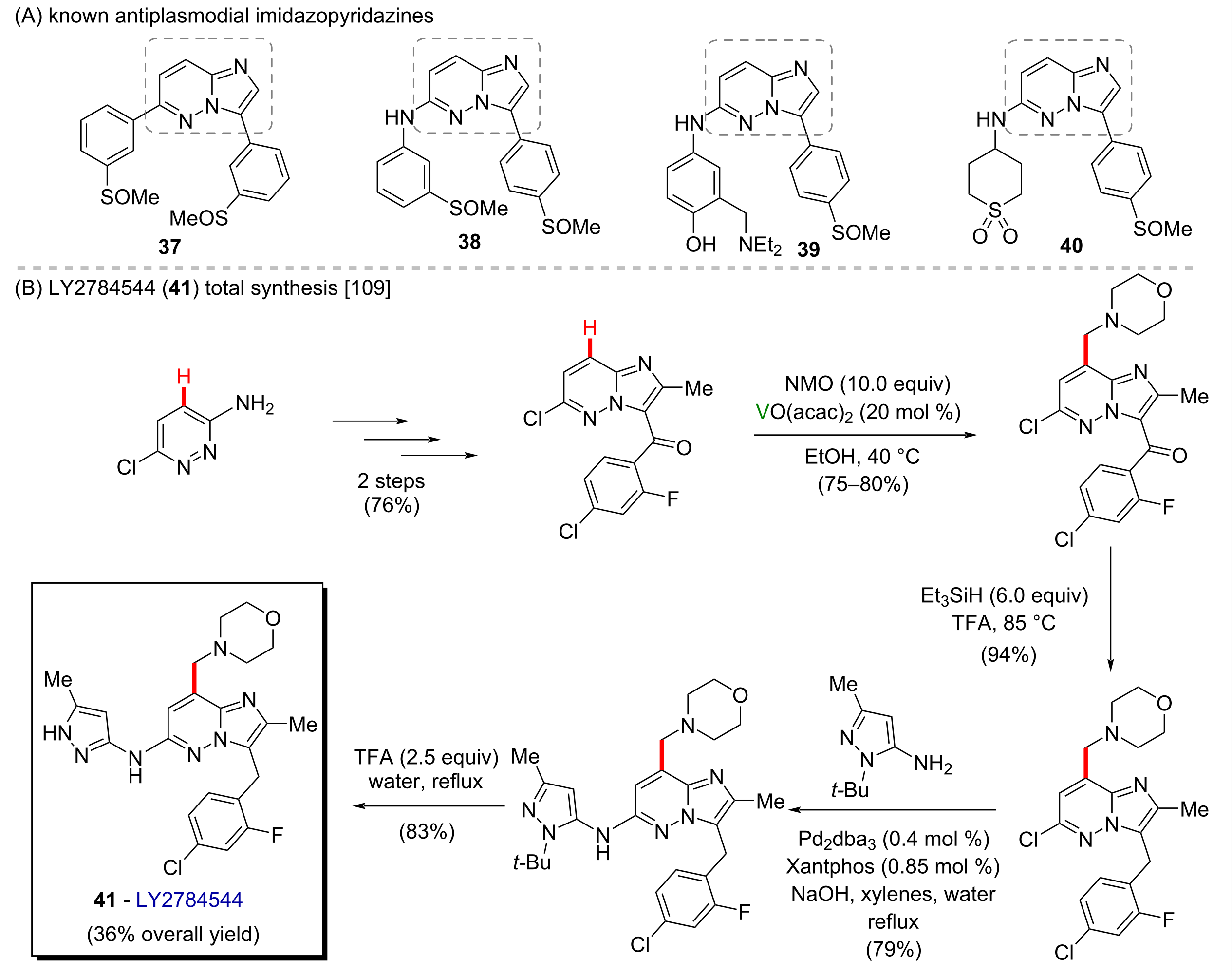
(A) known antiplasmodial imidazopyridazines
SOMe
MeOS
37
HN
SOMe
SOMe
38
HN
OH
NEt2
39
SOMe
HN
S
O O
40
SOMe
(B) LY2784544 (41) total synthesis [109]
H
NH2
Cl
N N
2 steps
(76%)
H
N
Me
Cl
N
N
O
F
Cl
NMO (10.0 equiv)
VO(acac)2 (20 mol %)
EtOH, 40 °C
(75–80%)
O
N
Me
Cl
O
F
Cl
Et3SiH (6.0 equiv)
TFA, 85 °C
(94%)
Me
N
N
t-Bu
NH2
Pd2dba3 (0.4 mol %)
Xantphos (0.85 mol %)
NaOH, xylenes, water
reflux
(79%)
TFA (2.5 equiv)
water, reflux
(83%)
Me
HN
N
H
Me
F
Cl
41 - LY2784544
(36% overall yield)

Scheme 14: (A) Known antiplasmodial imidazopyridazines; (B) practical synthesis of **41**.

potent antiplasmodial activity (**37**–**40**) (Scheme 14A) [114]. The use of vanadium-mediated aminoalkylation led to the introduction of a morpholinomethyl moiety into the heteroaromatic ring in a single step instead of the 5 steps required in the previously used route, thus significantly shortening the synthetic route, and increasing the overall yield. The resulting eight-step synthesis could be scaled to produce more than 100 kg of compound **41** [109].

Based on what was presented so far, vanadium catalysis is mainly applied as one of the steps involved in a total synthesis that usually leads to the formation of a valuable biologically active substance. This fact clarifies the high importance of further studies and evaluations in this field. With this information in mind and the fact that vanadium catalysis is also considerably accessible, it is possible to expect that more complex and currently high-cost drugs may be obtained in a cheaper way leading to an easier access of currently expensive treatments to the general population.

Chromium-catalyzed C–H activation

Chromium is a relatively abundant transition metal that has been used for oxidative reactions, including cross-coupling and carbon–carbon bond formation involving organochromium species generated from alkyl halides [115,116]. Whereas its toxicity has hindered the use of Cr(VI) in organic synthesis, the less toxic Cr(III) and Cr(II) salts have been exploited as plausible catalysts in organic synthesis [117,118]. A good example is a redox-neutral reaction for the allylation of aldehydes promoted by a dual catalytic system comprising $CrCl_3$ and an iridium-based photocatalyst that was recently developed by Schwarz and co-workers [119]. Similar conditions were further employed to synthesize monoprotected 1,2-homoallylic diols from aldehydes and silyl and alkyl enol ethers as the allylic counterpart [120].

In the field of C–H activation studies, not many examples have been described in the literature so far, especially towards the synthesis of biologically active compounds. However, an interesting example of a C(sp^2)–H activation reaction promoted by Cr(III) salts and $AlMe_3$ as a base for the regioselective *ortho* functionalization of aromatic secondary amides has been recently reported [121]. The reaction is performed with 1–2 mol % of $CrCl_3$ or Cr(aca)$_3$, a stoichiometric amount of $AlMe_3$ and bromoalkynes (Scheme 15B), allyl bromide or 1,4-dihydro-1,4-epoxynaphthalene as electrophiles. Several 2-alkynylbenzamide products were achieved in good yields, including a derivate of moclobemide (**42**), a drug used to treat depression and anxiety (Scheme 15C) [122]. It is worth mentioning here that this class of molecules can be used as effective anticancer drug carriers, which via a gold catalysis can be triggered to release the drug on specific sites of the target cell in a controlled manner (Scheme 15A) [123]. A proposed catalytic cycle based on kinetic isotopic effect and kinetics data is illustrated in Scheme 15D. At the beginning of the reaction, intermediate **III** can be formed from **I** and the Cr(III) salt to start the cycle, thereby providing intermediate **VI**. The latter then undergoes a ligand exchange with **I** to give the product and the key intermediate **II**. It is noteworthy that the secondary amide works both as the substrate and the ligand for the metal center, so that no additional ligand is required. The method presents a broad scope regarding the amide substrate. It gives moderate to excellent yields for heteroaromatic and aromatic carboxamides bearing electron-donating and electron-withdrawing substituents, whereas substrates with *ortho*-substituents were found to be unreactive, probably due to steric hindrance.

The one-pot difunctionalization of arenes involving a sequential C–O cleavage and C(sp^2)–H activation mediated by chromium was recently reported by Luo and Zeng [124]. The reaction allows an *ortho*-directed diarylation of *o*-methoxybenzaldehyde imine derivatives with phenyl Grignard reagents as coupling partners. As the catalyst $CrCl_2$ is used and either 2,3-dichlorobutane (DCB) or 1,2-dichloropropane (DCP) are used as oxidant to give 2,5-diarylbenzaldehyde after imine hydrolysis (Scheme 16B). Although benzaldehyde is a basic structure, it is present in compounds that have a significant anti-inflammatory activity (**43** and **44**) (Scheme 16A) [125]. The introduction of two distinct aryl moieties into arenes was also shown to be feasible through the sequential functionalization with two different Grignard reagents. For this purpose, the reaction was kept at room temperature to avoid the difunctionalization, and the oxidant was added only in the second step. Following this route, six examples were obtained with moderate yields (56–70%, Scheme 16C).

Although the use of chromium catalysis is still considered challenging due to the high toxicity of some chromium species, based on the above cited examples, by using this metal valuable biologically active molecules can be safely obtained. The correct, judicious, and optimized application of chromium-based catalysts can lead to the easier access of several drugs. Further studies in this area could help expanding the currently available methods in organic synthesis.

Manganese-catalyzed C–H activation

Manganese is the twelfth most abundant element in the Earth's crust and the third most abundant transition metal after iron and titanium [126]. The valence electron configuration of elemental manganese is $3d^54s^2$ with a high redox potential due to the high number of available oxidation states (−3 to +7), allowing the formation of compounds with a coordination number of up to 7

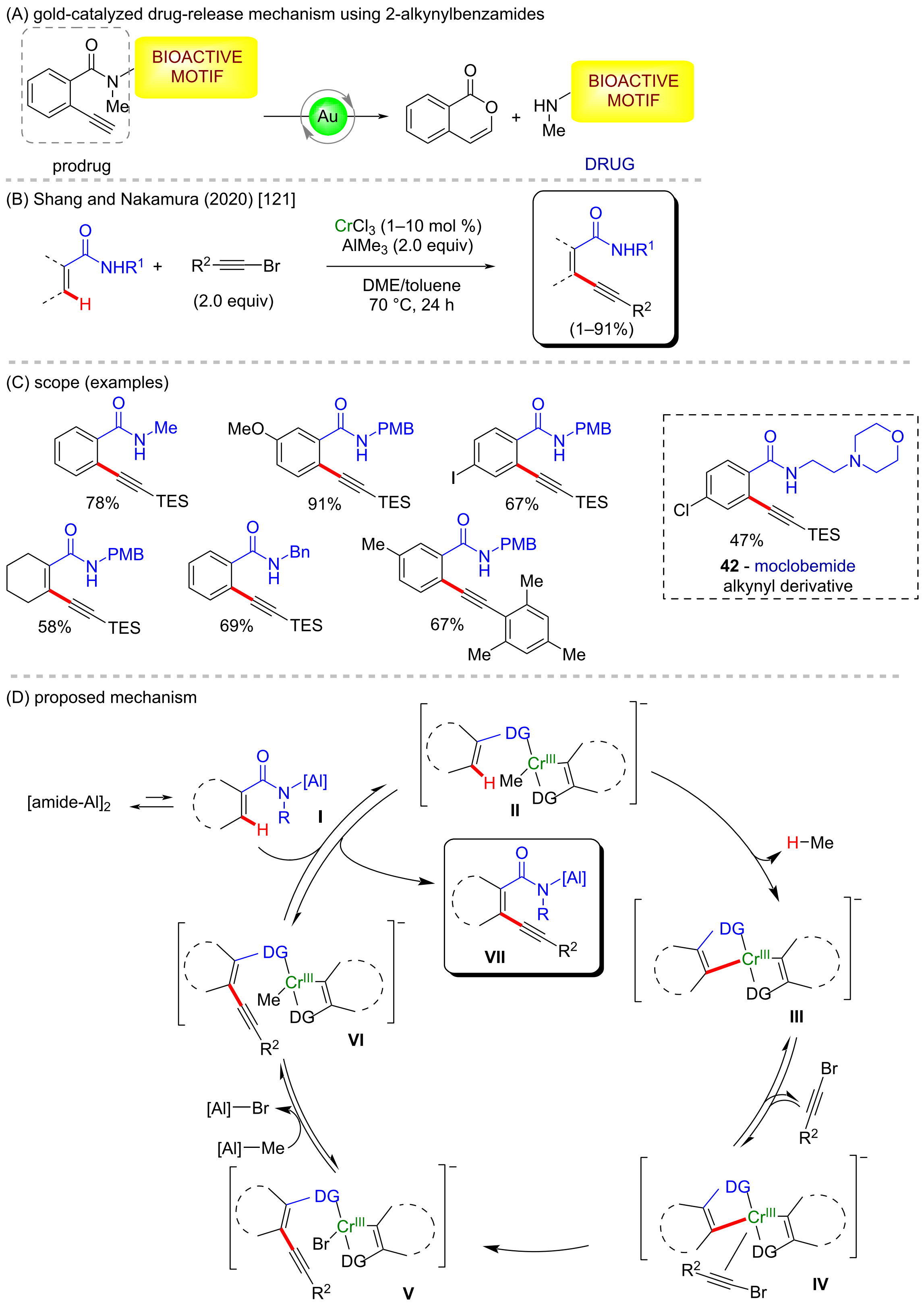
(A) gold-catalyzed drug-release mechanism using 2-alkynylbenzamides
BIOACTIVE MOTIF
prodrug
Au
DRUG
(B) Shang and Nakamura (2020) [121]
NHR1
R2—≡—Br
(2.0 equiv)
CrCl3 (1–10 mol %)
AlMe3 (2.0 equiv)
DME/toluene
70 °C, 24 h
(1–91%)
(C) scope (examples)
78%
91%
67%
47%
42 - moclobemide alkynyl derivative
58%
69%
67%
TES
PMB
Bn
MeO
(D) proposed mechanism
[amide-Al]2
I
II
III
IV
V
VI
VII
H–Me
[Al]—Br
[Al]—Me
DG
CrIII

Scheme 15: (A) Gold-catalyzed drug-release mechanism using 2-alkynylbenzamides; (B and C) chromium-mediated alkynylation of carboxamides; (D) proposed mechanism.

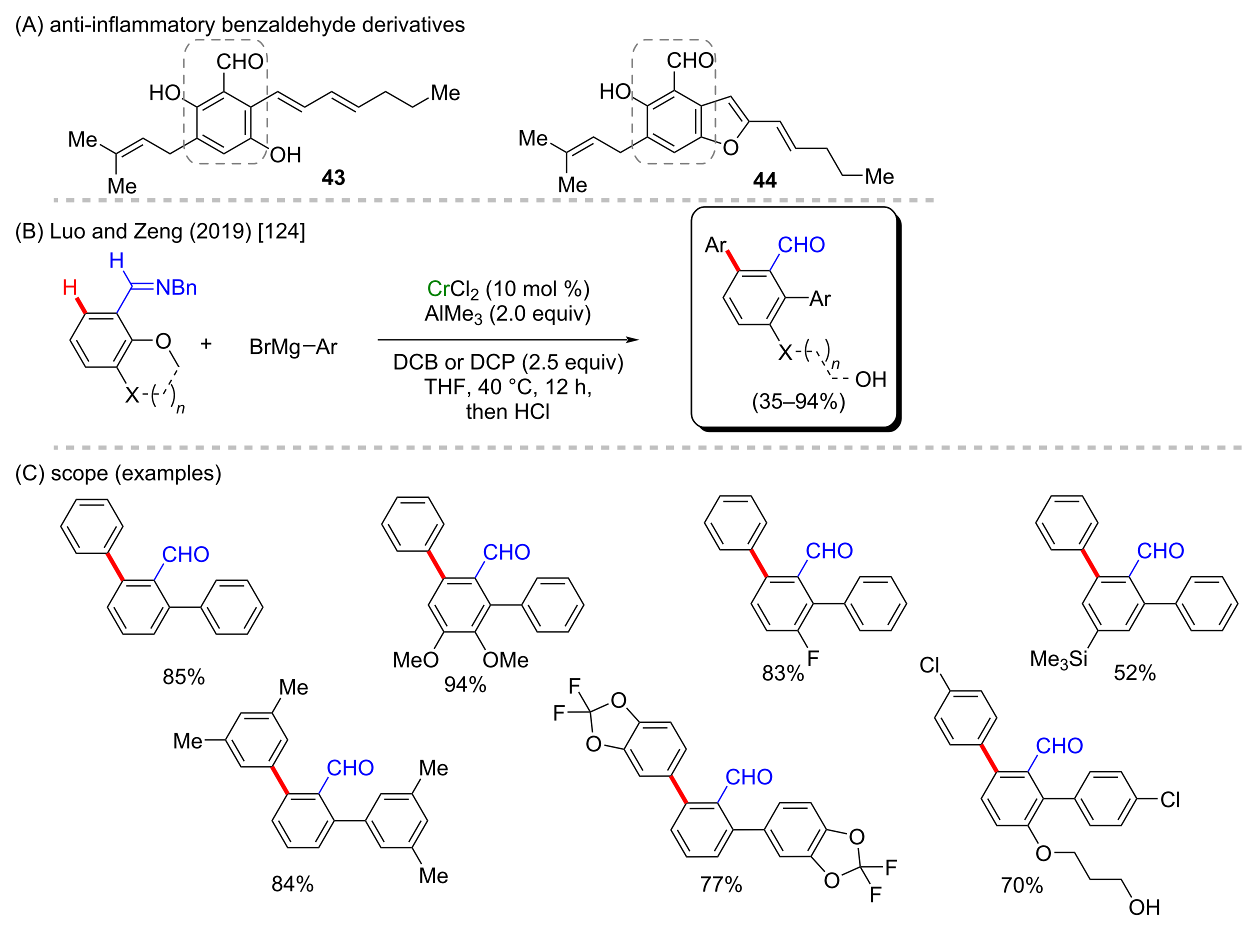
(A) anti-inflammatory benzaldehyde derivatives
CHO
HO
Me
Me
Me
OH
43
CHO
HO
O
Me
Me
Me
44
(B) Luo and Zeng (2019) [124]
H
H
NBn
O
X-( )n
+
BrMg−Ar
CrCl2 (10 mol %)
AlMe3 (2.0 equiv)
DCB or DCP (2.5 equiv)
THF, 40 °C, 12 h,
then HCl
Ar
CHO
Ar
X-( )n
OH
(35–94%)
(C) scope (examples)
CHO
85%
CHO
MeO
OMe
94%
CHO
F
83%
CHO
Me3Si
52%
Me
Me
CHO
Me
Me
84%
F
F
O
O
CHO
O
O
F
F
77%
Cl
CHO
Cl
O
OH
70%

Scheme 16: (A) Examples of anti-inflammatory benzaldehyde derivatives; (B and C) chromium-mediated difunctionalization of arenes.

[127]. These properties associated with a low toxicity and low cost make manganese a metal with great potential in organometallic chemistry and catalysis [128]. The first example of a stoichiometric manganese-mediated C–H activation, reported by Stone, Bruce, and co-workers (1970) [129], was an *ortho*-metalation in azobenzenes. In recent years, with the expansion of the C–H activation field, manganese catalysts have been applied in some very sophisticated protocols including several examples reported by the White group. In 2015, White and co-workers reported a new catalytic method using manganese *tert*-butylphthalocyanine [Mn(*t*-BuPc)Cl] for the chemoselective intramolecular amination of various C(sp^3)–H bond types like benzylic, allylic, 3°, 2°, and 1° aliphatic, using unsubstituted linear sulfamate esters (Scheme 17A and B) [130]. This method is also compatible with substrates containing adjacent substituents like protected amines and tolerates the presence of electron-withdrawing groups as well as α-substituted alkynes. The authors also succesfully applied the method toward a C-substituted indol, which is a particularly useful heteroaromatic motif in medicinal chemistry, being encountered in many bioactive compounds. The corresponding product was obtained with good yield and high diastereoisomeric ratio. Following these results, the late-stage diversification using the [Mn(*t*-BuPc)Cl] catalyst was applied to more complex natural compounds such as the isosteviol derivative **45** and the betulinic acid derivative **47**, which underwent conversion in good and high yields and with high chemoselectivity. The functionalized isosteviol derivate furnished a useful and versatile oxathiazinane (**46**). The betulinic acid-derived sulfamate ester preferentially underwent amination at the γ primary C–H bond of the equatorial C23 methyl group with high site- and diastereoselectivity to furnish the oxathiazinane derivative in 76% yield (Scheme 17C).

The White group also reported a series of manganese-catalyzed intermolecular benzylic C(sp^3)–H amination reactions using 2,2,2-trichloroethyl sulfamate ($TcesNH_2$) and $PhI(OPiv)_2$ as the oxidant (Scheme 18A and 18B) [131]. The manganese perchlorophthalocyanine [Mn^{III}(ClPc)Cl] catalyst enabled a highly site-selective and wide functional-group tolerant reaction. To test this protocol versatility over biologically relevant scaffolds, a $COCF_3$-leelamine analogue **48** with two sterically

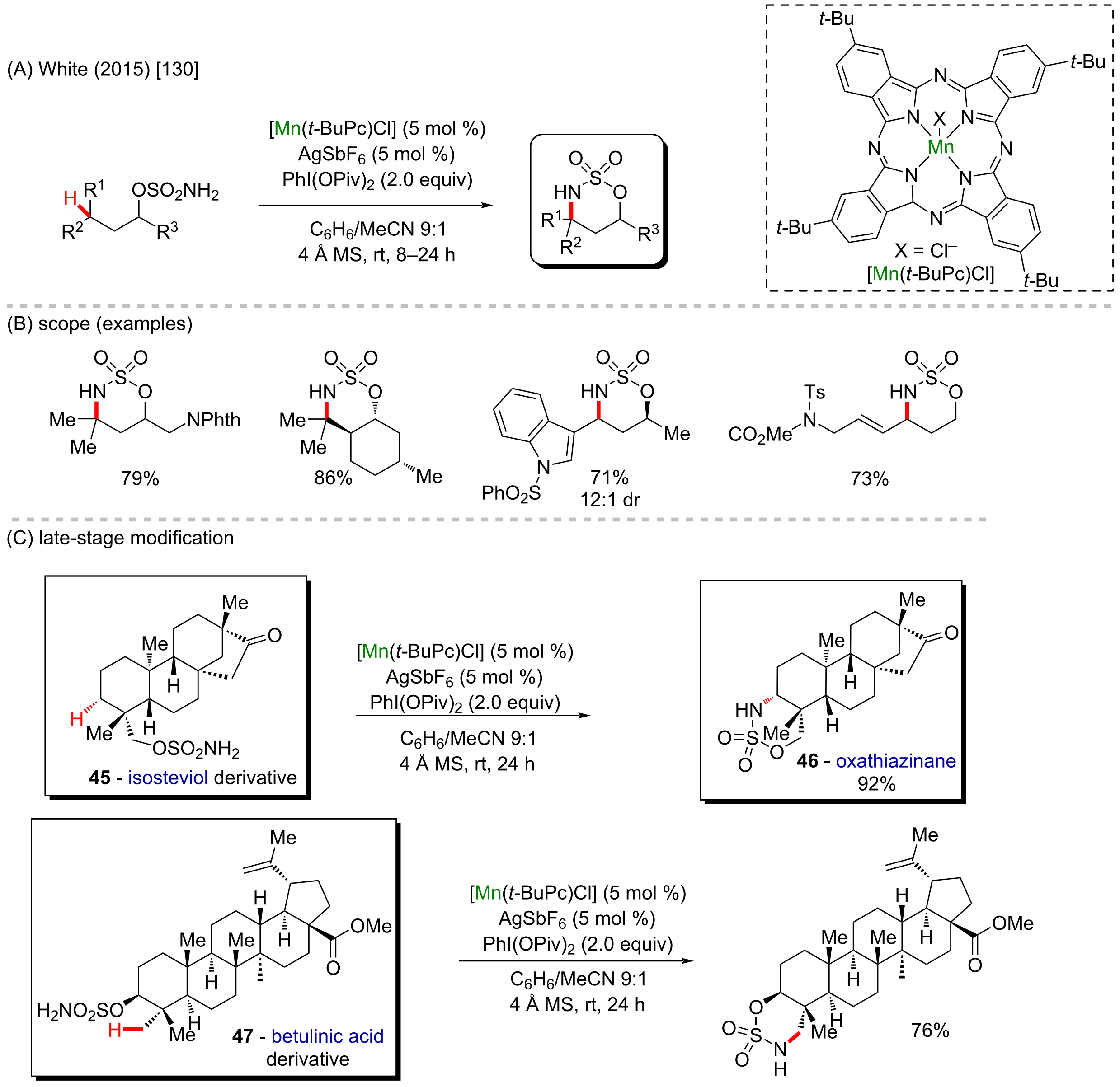
(A) White (2015) [130]
[Mn(t-BuPc)Cl] (5 mol %)
AgSbF6 (5 mol %)
PhI(OPiv)2 (2.0 equiv)
C6H6/MeCN 9:1
4 Å MS, rt, 8–24 h
X = Cl⁻
[Mn(t-BuPc)Cl]
(B) scope (examples)
79%
86%
71%
12:1 dr
73%
(C) late-stage modification
45 - isosteviol derivative
46 - oxathiazinane
92%
[Mn(t-BuPc)Cl] (5 mol %)
AgSbF6 (5 mol %)
PhI(OPiv)2 (2.0 equiv)
C6H6/MeCN 9:1
4 Å MS, rt, 24 h
47 - betulinic acid derivative
76%

Scheme 17: (A and B) Manganese-catalyzed chemoselective intramolecular C(sp^3)–H amination; (C) late-stage modification of an isosteviol derivative (**45**) and a betulinic acid derivative (**47**).

differentiated benzylic sites was selectively aminated at the secondary benzylic site. After Tces deprotection, the free amine derivative was produced in 43% overall yield. The 2,8-dioxabicyclo[3.3.1]nonane skeleton is contained in biflavonoids and was shown to exhibit many medicinal activities like antiviral, anti-inflammatory and antitumor properties. The bicyclic compound **49** was aminated at the benzylic position in 57% yield (1:1 dr, Scheme 18C).

Nitrogen-containing heterocycles are present in several valuable bioactive compounds, such as piracetam (**50**) [132], anisomycin (**51**) [133], and alogliptin (**52**) [134] (Scheme 20A). Sometimes better biological results are observed after simple structural modifications, and the introduction of methyl groups has an attractive effect on the properties of medicinal compounds [135]. However, the selective late-stage methylation has a limited scope due to the lack of suitable methodologies [136]. The insertion of methyl groups at positions adjacent to heteroatoms often has a further effect improvement, however, it is even more challenging. In front of this, White and co-workers (2020) adopted a strategy consisting of an initial hydroxylation of the C(sp^3)–H bonds adjacent to N- or O-heteroatoms followed by a methylation step (Scheme 19B and C) [137]. The hydroxylation of positions next to heteroatoms leads to hemi-

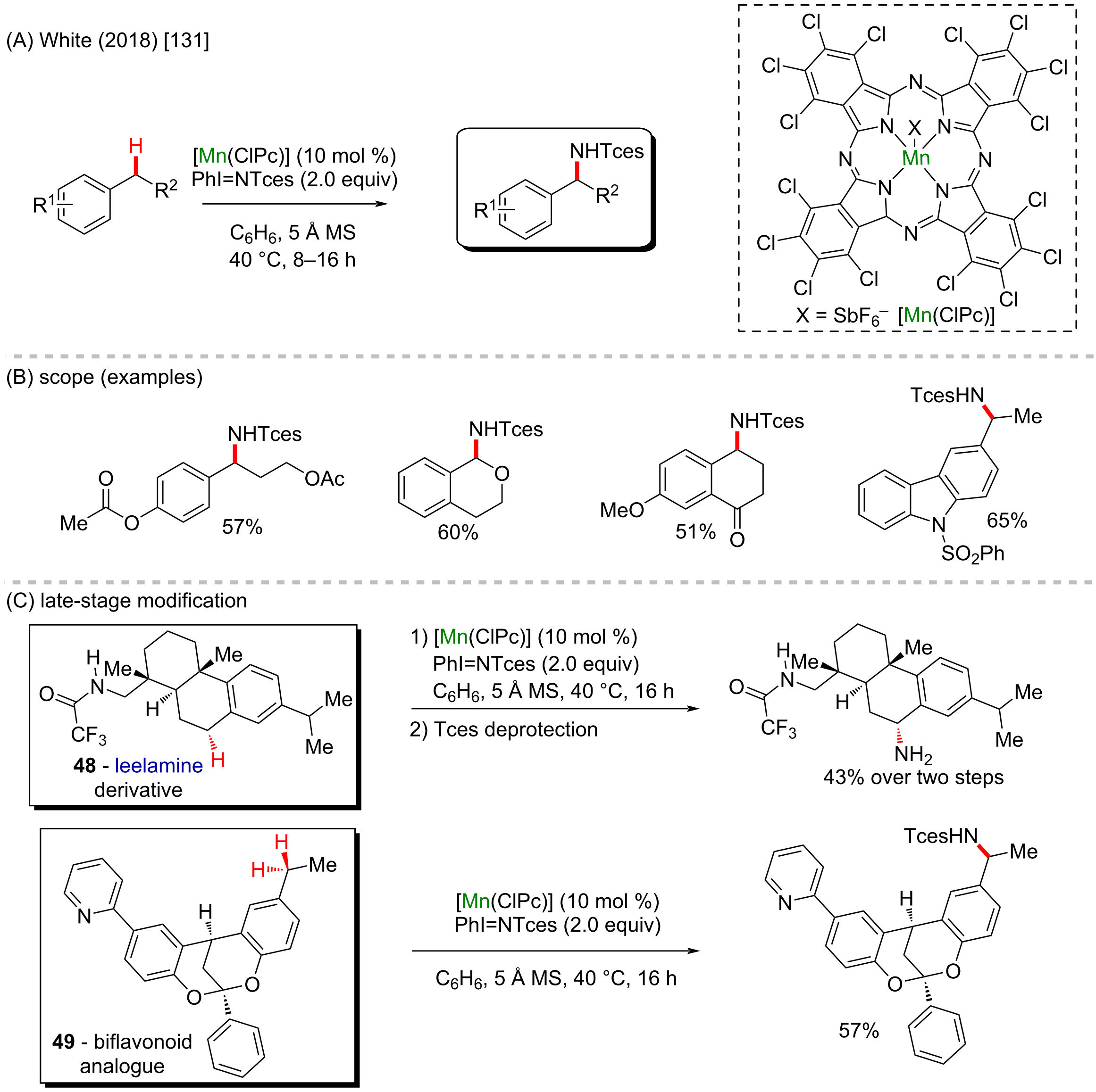
(A) White (2018) [131]
[Mn(ClPc)] (10 mol %)
PhI=NTces (2.0 equiv)
C6H6, 5 Å MS
40 °C, 8–16 h
X = SbF6− [Mn(ClPc)]
(B) scope (examples)
57%
60%
51%
65%
(C) late-stage modification
48 - leelamine derivative
1) [Mn(ClPc)] (10 mol %) PhI=NTces (2.0 equiv) C6H6, 5 Å MS, 40 °C, 16 h
2) Tces deprotection
43% over two steps
49 - biflavonoid analogue
[Mn(ClPc)] (10 mol %) PhI=NTces (2.0 equiv)
C6H6, 5 Å MS, 40 °C, 16 h
57%

Scheme 18: (A and B) Manganese-catalyzed C(sp^3)–H amination; (C) late-stage modification of a leelamine derivative (**48**) and a biflavonoid analogue (**49**).

aminals and hemiacetals which typically promotes an overoxidation to the corresponding carbonyl compound. The sterically hindered catalyst $Mn(CF_3PDP)(MeCN)_2(SbF_6)_2$ (where CF_3PDP is 1,1′-bis((5-(2,6-bis(trifluoromethyl)phenyl)pyridin-2-yl)methyl)-2,2′-bipyrrolidine) controls the site- and chemoselectivity in the hydroxylating step of the methylene C(sp^3)–H bond while milder oxidation conditions help to increase the chemoselectivity. The methylation step is accomplished using a modestly nucleophilic organoaluminium reagent ($AlMe_3$) to activate the hemiaminal/hemiacetal avoiding undesirable elimination to the enamine, or attack at other electrophilic sites in complex substrates. The presence of a fluorine source like diethylaminosulfur trifluoride (DAST) or the Lewis acid boron trifluoride diethyl etherate ($BF_3{\cdot}OEt_2$) result in the formation of reactive iminium or oxonium species in the methylation step. Abiraterone acetate (**53**) is a drug used in cancer treatment [138]. The Mn-catalyzed methylation of an abiraterone analogue was achieved by replacing the fluorination step by mesylation in 15% of overall yield and only a single diastereoisomer was observed (Scheme 19D). In carbocyclic substrates the displacement of a C–F bond or ionization with a Lewis acid is difficult, but mesylates are stable and suitable for $AlMe_3$ activation.

As already mentioned, indoles are an important class of molecules with potential antidiabetic properties since they can act as

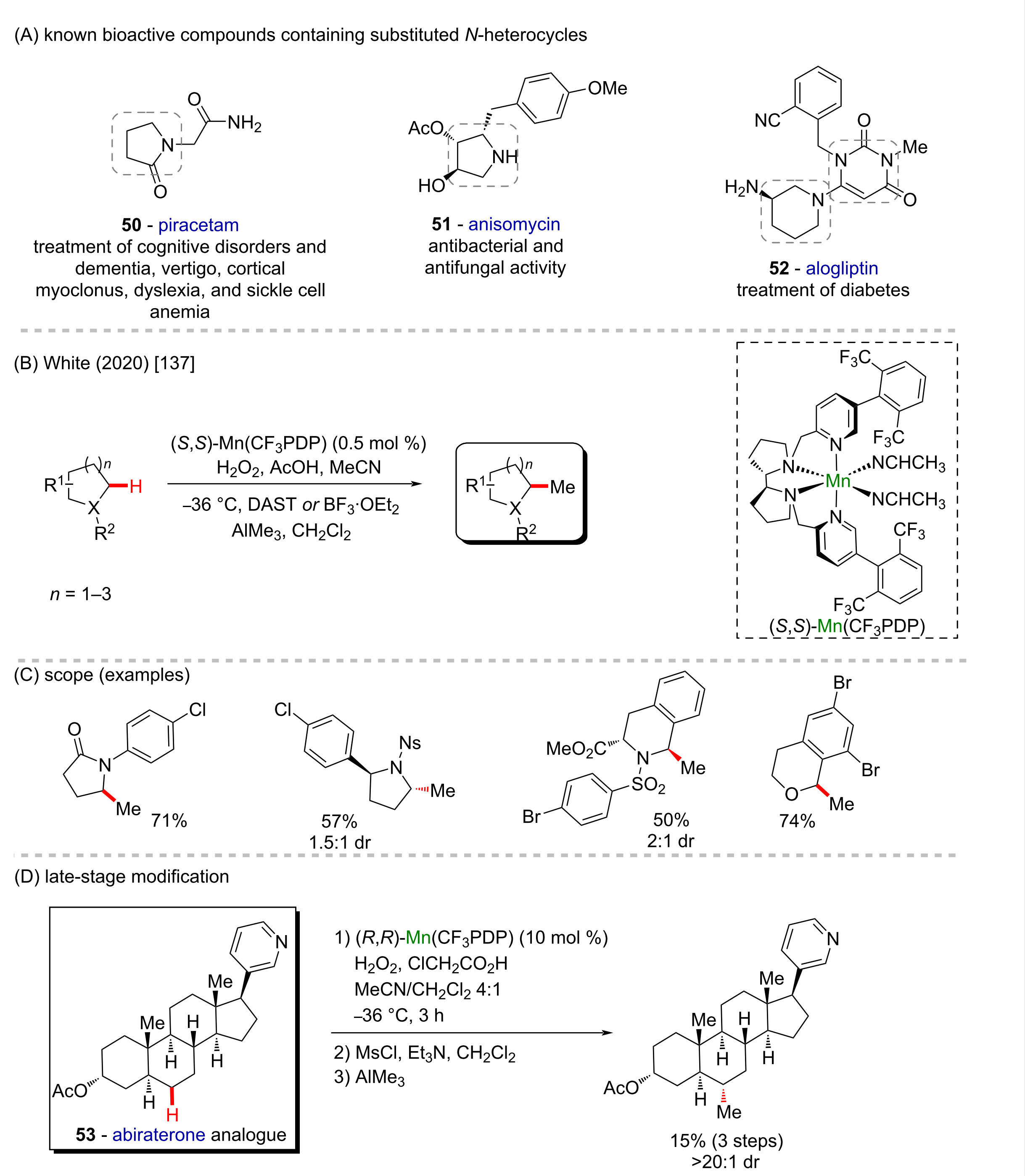
(A) known bioactive compounds containing substituted *N*-heterocycles
50 - piracetam
treatment of cognitive disorders and dementia, vertigo, cortical myoclonus, dyslexia, and sickle cell anemia
51 - anisomycin
antibacterial and antifungal activity
52 - alogliptin
treatment of diabetes
(B) White (2020) [137]
(S,S)-Mn(CF3PDP) (0.5 mol %)
H2O2, AcOH, MeCN
–36 °C, DAST or BF3·OEt2
AlMe3, CH2Cl2
n = 1–3
(S,S)-Mn(CF3PDP)
(C) scope (examples)
71%
57%
1.5:1 dr
50%
2:1 dr
74%
(D) late-stage modification
53 - abiraterone analogue
1) (R,R)-Mn(CF3PDP) (10 mol %)
H2O2, ClCH2CO2H
MeCN/CH2Cl2 4:1
–36 °C, 3 h
2) MsCl, Et3N, CH2Cl2
3) AlMe3
15% (3 steps)
>20:1 dr

Scheme 19: (A) Known bioactive compounds containing substituted *N*-heterocycles; (B and C) manganese-catalyzed oxidative C(sp^3)–H methylation; (D) late-stage modification of an abiraterone analogue **53**.

GPR40 full agonists (**54** and **55**, Scheme 20A) [139]. Ackermann and co-workers presented a manganese(I)-catalyzed C–H allylation, installing α,β-unsaturated esters in peptide analogues bearing indole motifs (Scheme 22B) [140]. Starting with tryptophan, the enantioselective allylation reaction afforded the product (98% yield) (Scheme 20C). More complex structures like dipeptides and substrates containing multiple Lewis-basic functionalities also presented good yields and chemoselectivities with this protocol. The robust allylation reaction was tested in even more complex structures, including steroid-containing substrates, and its high efficiency makes it an excellent methodology for late-stage modifications (Scheme 20D).

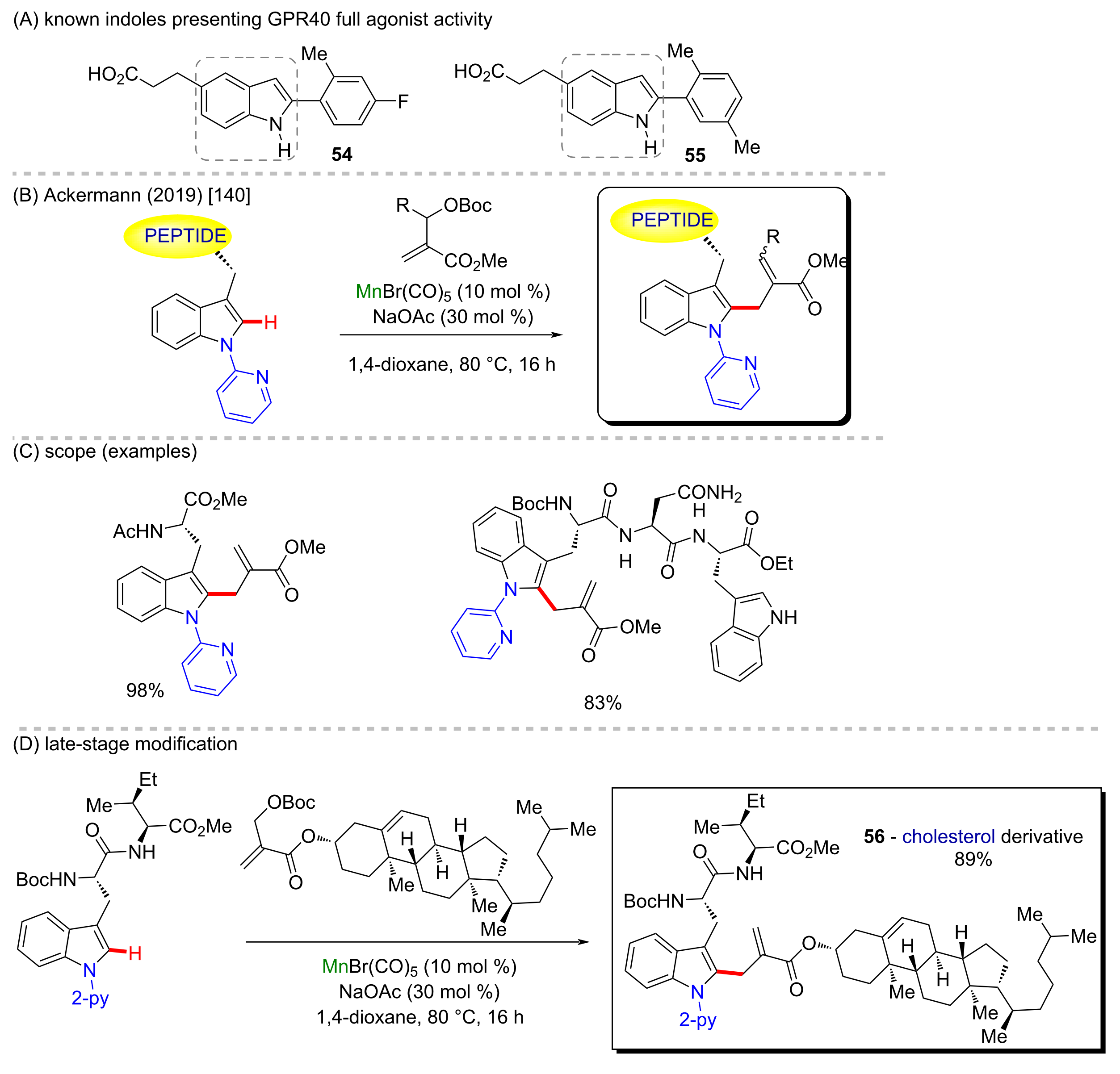
(A) known indoles presenting GPR40 full agonist activity
HO_2C
Me
F
N
H
54
HO_2C
Me
N
H
55
Me
(B) Ackermann (2019) [140]
PEPTIDE
H
N
N
R
OBoc
CO_2Me
MnBr(CO)$_5$ (10 mol %)
NaOAc (30 mol %)
1,4-dioxane, 80 °C, 16 h
PEPTIDE
R
OMe
O
N
N
(C) scope (examples)
CO_2Me
AcHN
OMe
O
N
N
98%
BocHN
O
$CONH_2$
H
O
N
H
N
O
OEt
N
N
OMe
O
NH
83%
(D) late-stage modification
Et
Me
CO_2Me
O
NH
BocHN
H
N
2-py
OBoc
O
O
H
H
H
Me
Me
Me
Me
Me
MnBr(CO)$_5$ (10 mol %)
NaOAc (30 mol %)
1,4-dioxane, 80 °C, 16 h
Et
Me
CO_2Me
O
NH
BocHN
N
2-py
O
O
H
H
H
Me
Me
Me
Me
Me
56 - cholesterol derivative
89%

Scheme 20: (A) Known indoles that present GPR40 full agonist activity; (B and C) manganese-catalyzed C–H alkylation; (D) late-stage modification furnishing **56**, using a cholesterol derivative as coupling partner.

Biaryl structures are present in several important drugs currently commercially available (**57**, **58**, and **59**, Scheme 21A) [141] and synthetic methods to achieve the aryl–aryl connection are crucial. In 2018, Ackermann and co-workers described a novel room temperature C–H arylation by using a continuous visible light photo-flow technique, allied with a manganese photocatalyst CpMn(CO)$_3$ [142]. The new flow protocol enabled the synthesis of several arene- and heterocyclic-based compounds in excellent yields and short reaction times (Scheme 21B and C). The robustness of the manganese-catalyzed photo-flow reaction was demonstrated by a gram-scale preparation of the key intermediate in the synthesis of the pharmaceutical compound dantrolene (**60**) in high yields (Scheme 21D).

The azide group is another powerful organic function present for example in zidovudine, a worldwide known anti-HIV drug, but also in its derivatives (**61** and **62**) (Scheme 22A), which can present 10-times higher activities against HIV replication [143]. In 2020 the same group reported the use of a manganese catalyst in the azidation of inert C(sp^3)–H bonds using organic electrosynthesis in a straightforward procedure, enabling the azidation of a series of primary, secondary and tertiary alkyl moieties

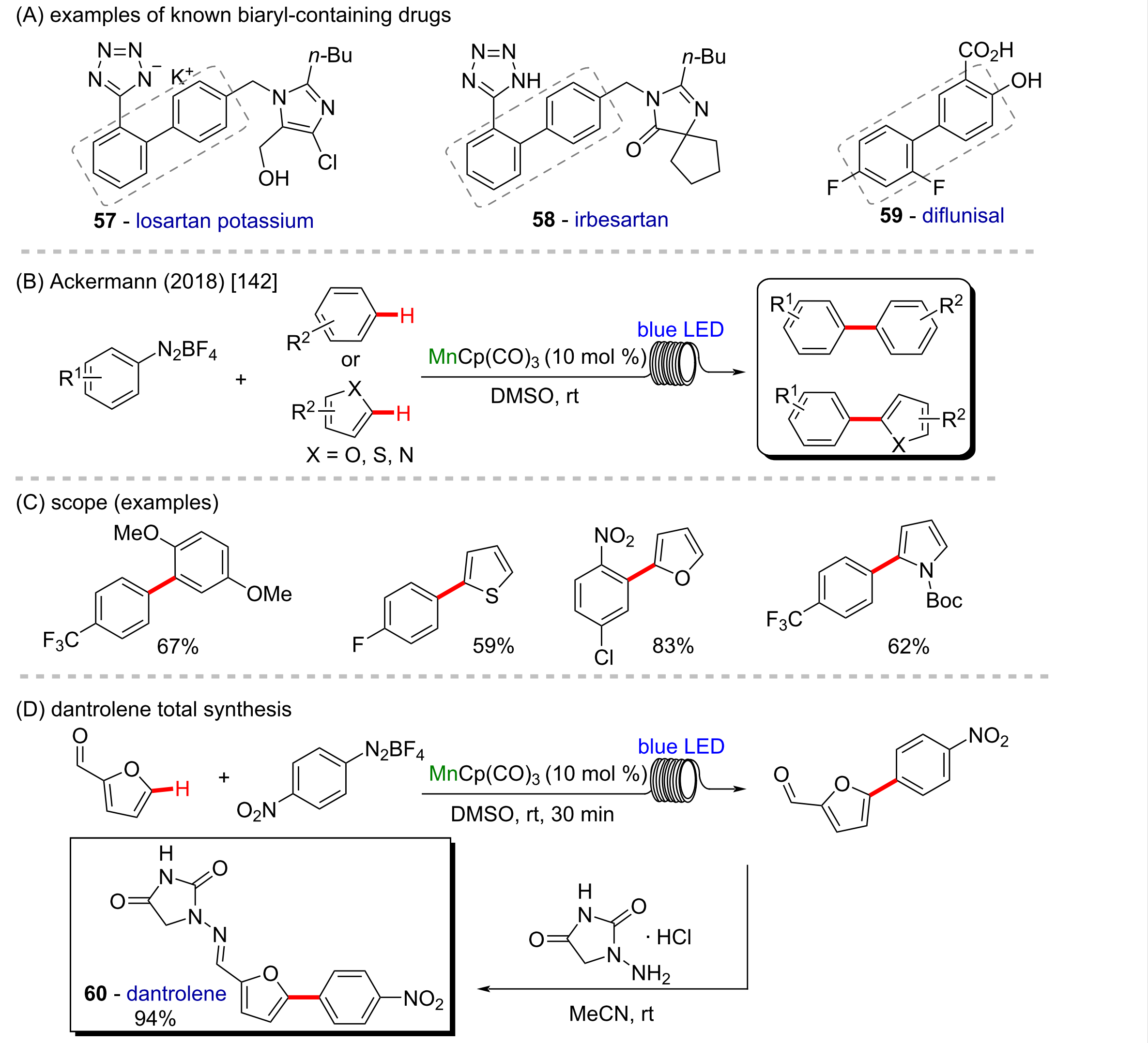
(A) examples of known biaryl-containing drugs
57 - losartan potassium
58 - irbesartan
59 - diflunisal
(B) Ackermann (2018) [142]
blue LED
MnCp(CO)3 (10 mol %)
DMSO, rt
X = O, S, N
(C) scope (examples)
67%
59%
83%
62%
(D) dantrolene total synthesis
blue LED
MnCp(CO)3 (10 mol %)
DMSO, rt, 30 min
MeCN, rt
60 - dantrolene
94%

Scheme 21: (A) Examples of known biaryl-containing drugs; (B and C) manganese-catalyzed C–H arylation through continuous visible light photoflow reaction; (D) dantrolene (**60**) total synthesis.

(Scheme 22B and C) [144]. In general, the new methodology proved to be resource-economic and straightforward, operating under mild conditions without the need of directing groups, using traceless electrons as sole redox reagents, presenting high scope and chemoselectivity. The robustness of the reaction was proved by the late-stage modification of pharmaceutically relevant compounds by promoting the azidation of a retinoic acid receptor agonist analogue **63** and an estrone acetate derivative **64** (Scheme 22D).

A seminal work involving manganese-catalyzed C–H organic electrosynthesis and photoredox catalysis was reported in the same year by Lei and co-workers, also regarding the azidation of alkyl scaffolds (Scheme 23A and B) [145]. The authors successfully applied a manganese salt in catalytic amounts, allied with the use of an electrical current in combination with blue LED lights and an organic photocatalyst (DDQ), affording azidated alkyl moieties in excellent yields and chemoselectivity through alkyl C–H bonds. The photo-electro methodology allowed the late-stage functionalization of valuable bioactive molecules, and the structures of a adapalene precursor (**65**) and ibuprofen derivative (**66**) were successfully azidated in moderate yields (Scheme 23C).

Some silylated compounds like **67** have proven to be efficient antibacterial compounds (Scheme 24A) [146]. In 2021, a divergent silylation of alkenes via a manganese-catalyzed C–H activation was reported by Xie et al. by using a ligand-tuned metalloradical reactivity strategy (Scheme 24B and C) [147]. Using $Mn_2(CO)_{10}$ as a catalyst precursor, the authors described the dehydrosilylation and hydrosilylation of alkenes to afford silylated alkanes and alkenes in excellent yields and stereoselectivi-

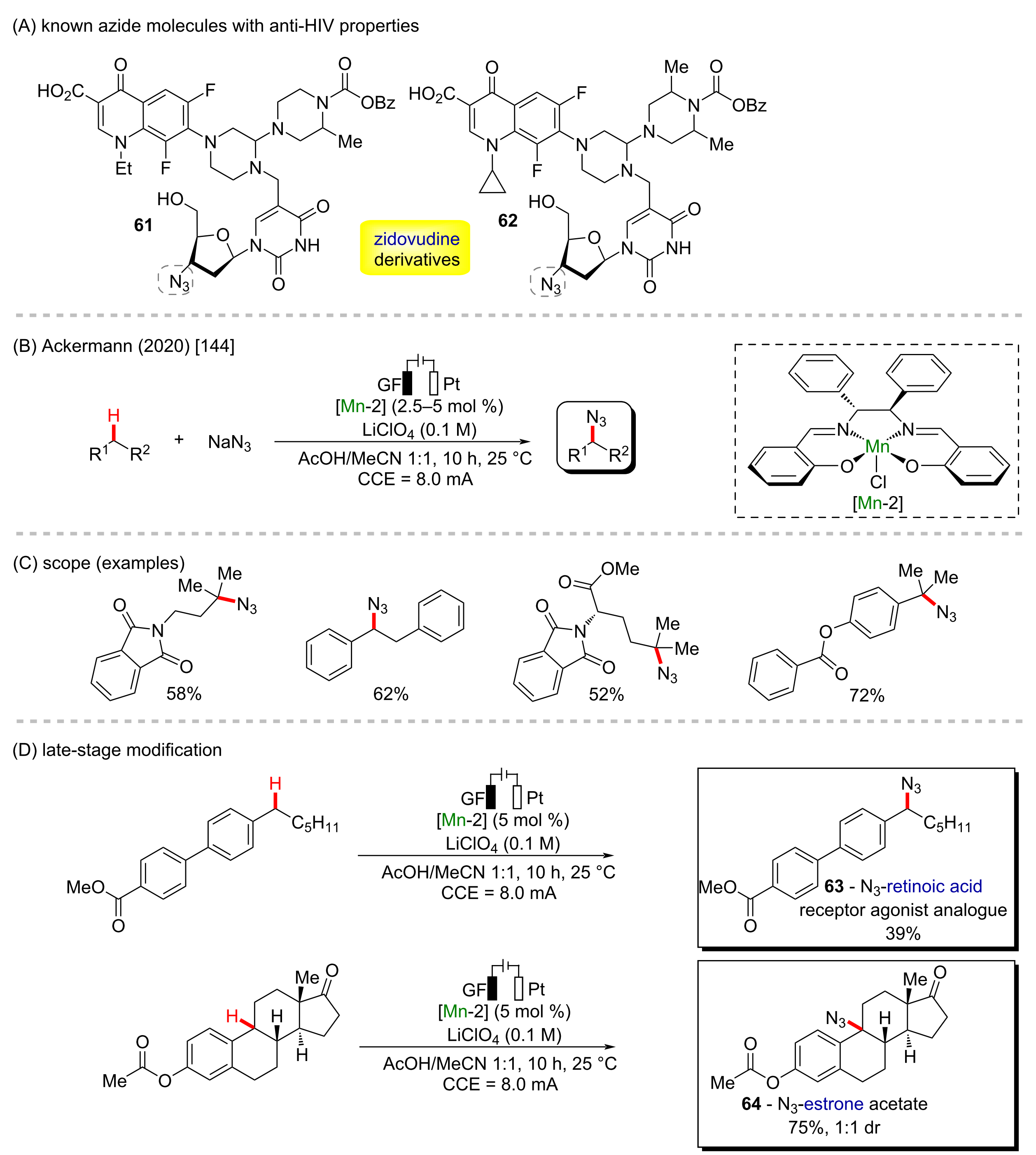
(A) known azide molecules with anti-HIV properties
61
62
zidovudine derivatives
(B) Ackermann (2020) [144]
GF
Pt
[Mn-2] (2.5–5 mol %)
LiClO4 (0.1 M)
AcOH/MeCN 1:1, 10 h, 25 °C
CCE = 8.0 mA
[Mn-2]
(C) scope (examples)
58%
62%
52%
72%
(D) late-stage modification
[Mn-2] (5 mol %)
63 - N3-retinoic acid receptor agonist analogue
39%
64 - N3-estrone acetate
75%, 1:1 dr

Scheme 22: (A) Known zidovudine derivatives with potent anti-HIV properties; (B and C) manganese-catalyzed C–H organic electrosynthesis; (D) late-stage modification.

ty, depending on the phosphine-based ligand employed. The reaction proved to work through a redox-neutral path, being considered an atom-economical process, exhibiting a broad substrate scope and excellent functional group tolerance. It enabled the late-stage diversification of a complex molecule like a pregnenolone derivative (**68**, Scheme 24D).

As it can be seen, using either more complex or more simple manganese catalysis, it is possible to obtain a large variety of functionalized compounds, from arylated compounds to new azide substances. This is an important characteristic in the synthesis and evaluation of biologically active molecules, since using different methods, a large variety of potential compounds

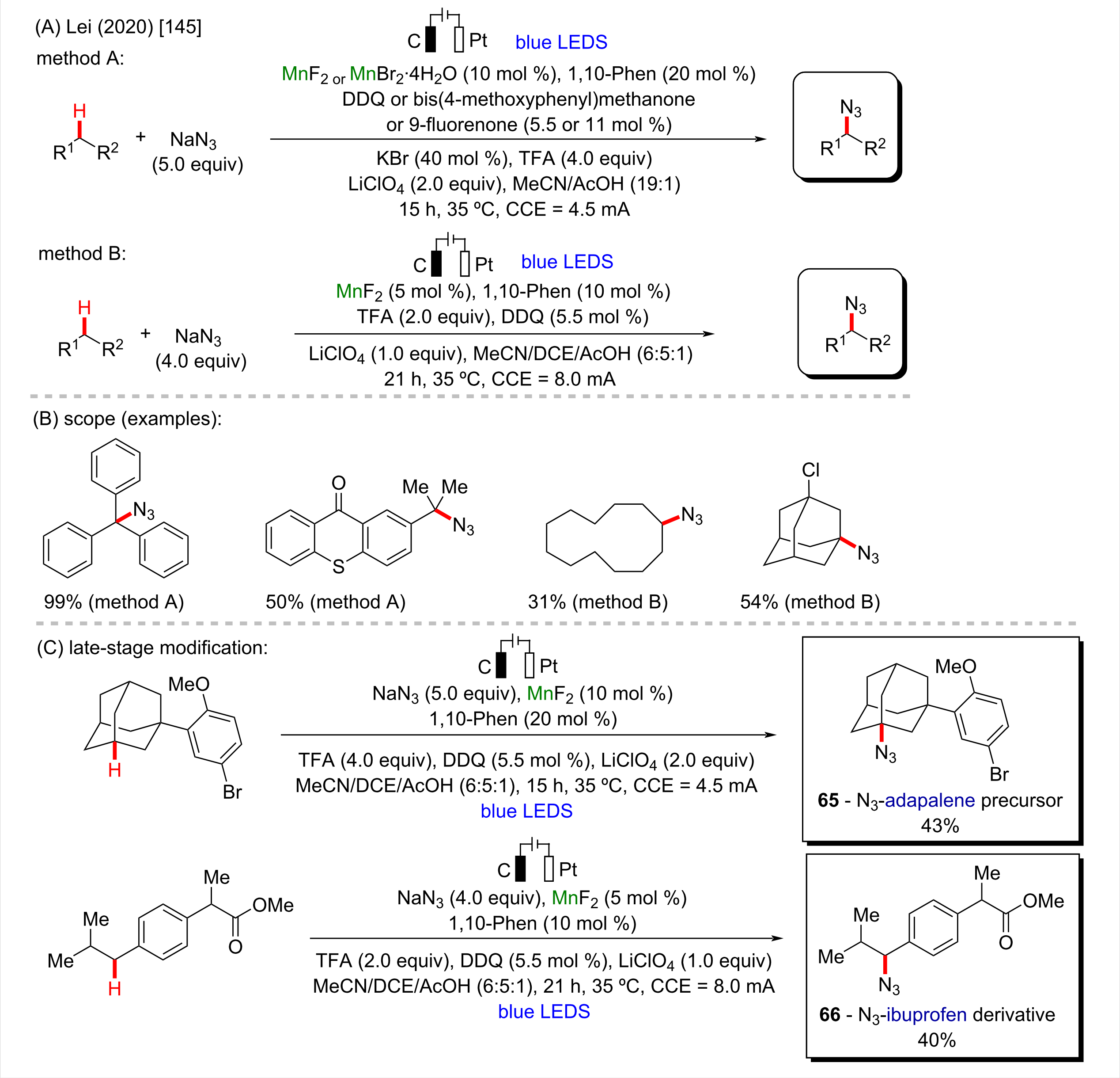
(A) Lei (2020) [145]
method A:
C
Pt
blue LEDS
MnF2 or MnBr2·4H2O (10 mol %), 1,10-Phen (20 mol %)
DDQ or bis(4-methoxyphenyl)methanone
or 9-fluorenone (5.5 or 11 mol %)
KBr (40 mol %), TFA (4.0 equiv)
LiClO4 (2.0 equiv), MeCN/AcOH (19:1)
15 h, 35 °C, CCE = 4.5 mA
H
R1
R2
NaN3
(5.0 equiv)
N3
method B:
MnF2 (5 mol %), 1,10-Phen (10 mol %)
TFA (2.0 equiv), DDQ (5.5 mol %)
LiClO4 (1.0 equiv), MeCN/DCE/AcOH (6:5:1)
21 h, 35 °C, CCE = 8.0 mA
NaN3
(4.0 equiv)
(B) scope (examples):
99% (method A)
50% (method A)
31% (method B)
54% (method B)
O
Me
S
Cl
(C) late-stage modification:
MeO
Br
NaN3 (5.0 equiv), MnF2 (10 mol %)
1,10-Phen (20 mol %)
TFA (4.0 equiv), DDQ (5.5 mol %), LiClO4 (2.0 equiv)
MeCN/DCE/AcOH (6:5:1), 15 h, 35 °C, CCE = 4.5 mA
blue LEDS
65 - N3-adapalene precursor
43%
OMe
NaN3 (4.0 equiv), MnF2 (5 mol %)
1,10-Phen (10 mol %)
TFA (2.0 equiv), DDQ (5.5 mol %), LiClO4 (1.0 equiv)
MeCN/DCE/AcOH (6:5:1), 21 h, 35 °C, CCE = 8.0 mA
66 - N3-ibuprofen derivative
40%

Scheme 23: (A and B) Manganese-catalyzed C–H organic photo-electrosynthesis; (C) late-stage modification.

can be obtained and studied. Larger scopes increase the chance of finding plausible new drugs, with potent activities.

Iron-catalyzed C–H activation

By mass, iron is the most abundant metal on Earth. Therefore, it has been and still is widely used in many fields, from ancient but still applicable appliance as feedstock to construct basic steel tools [148], to the most recent nanotechnology field [149]. Iron presents powerful catalyst properties [150-152], including applications in C–H activation reactions [153-155].

In 2007, White and Chen reported a seminal work regarding predictably selective aliphatic C–H oxidations by using an iron-based small molecule catalyst and hydrogen peroxide as oxidizing agent (Scheme 25A and B) [156]. This pioneering methodology changed the way how complex molecules and pharmaceuticals are synthesized, by using the steric and electronic properties of the substrates to achieve selectivity, without the need for directing groups, presenting a broad scope and satisfactory yields. The late-stage modification of complex molecules like (+)-artemisinin (**69**) and a (+)-tetrahydrogibberellic acid analogue **70** could be rapidly achieved in moderate yields (Scheme 25C).

In 2014, Brown and Rasik employed White's oxidation method as the final step in the first total synthesis of gracilioether F (**75**)

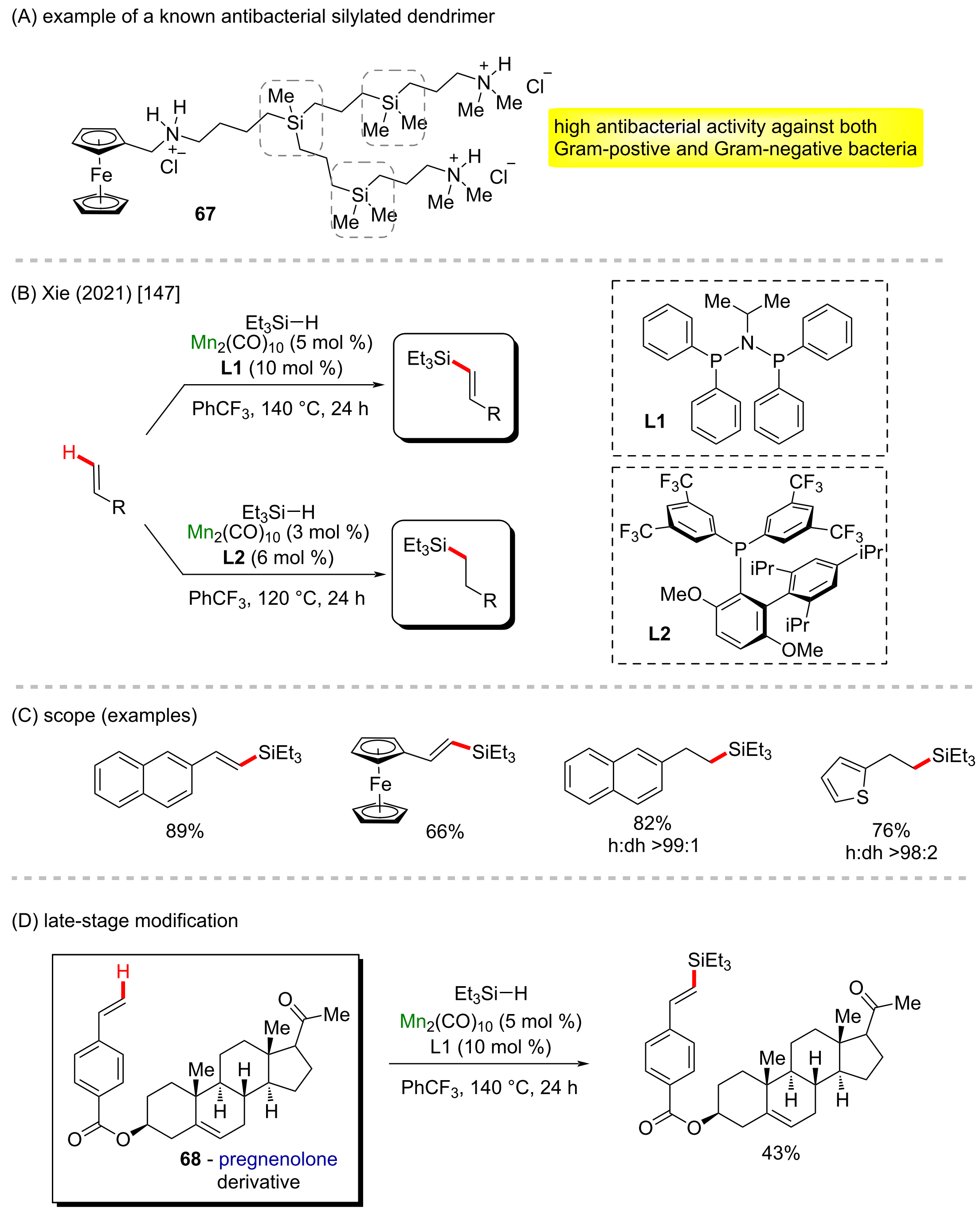
(A) example of a known antibacterial silylated dendrimer
67
high antibacterial activity against both Gram-postive and Gram-negative bacteria
(B) Xie (2021) [147]
Et3Si–H
Mn2(CO)10 (5 mol %)
L1 (10 mol %)
PhCF3, 140 °C, 24 h
Et3Si–H
Mn2(CO)10 (3 mol %)
L2 (6 mol %)
PhCF3, 120 °C, 24 h
L1
L2
(C) scope (examples)
89%
66%
82%
h:dh >99:1
76%
h:dh >98:2
(D) late-stage modification
68 - pregnenolone derivative
Et3Si–H
Mn2(CO)10 (5 mol %)
L1 (10 mol %)
PhCF3, 140 °C, 24 h
43%

Scheme 24: (A) Example of a known antibacterial silylated dendrimer; (B and C) manganese-catalyzed C–H silylation; (D) late-stage modification of the pregnenolone derivative **68**.

[157], a natural polyketide with an unusual tricyclic core and five contiguous stereocenters, part of the family of gracilioethers **71–74** (Scheme 26A) extracted from the marine sponge *Plakinastrella mamillaris* [158]. The synthesis started with a cyclopentene derivative, obtained after two steps from a diol via tosylation/displacement strategy with $Me_2CuLi{\cdot}LiI$. Then, after a Lewis acid-promoted cycloaddition, the alkylation of the α-carbon atom followed by regioselective Baeyer–Villiger oxidation provided the target lactone in 61% yield over two steps. The final steps involved a one-pot ozonolysis with quenching under Pinnick oxidation conditions to afford the carboxylic acid derivative in 83% yield, followed by White's selective C–H oxidation (Scheme 26B).

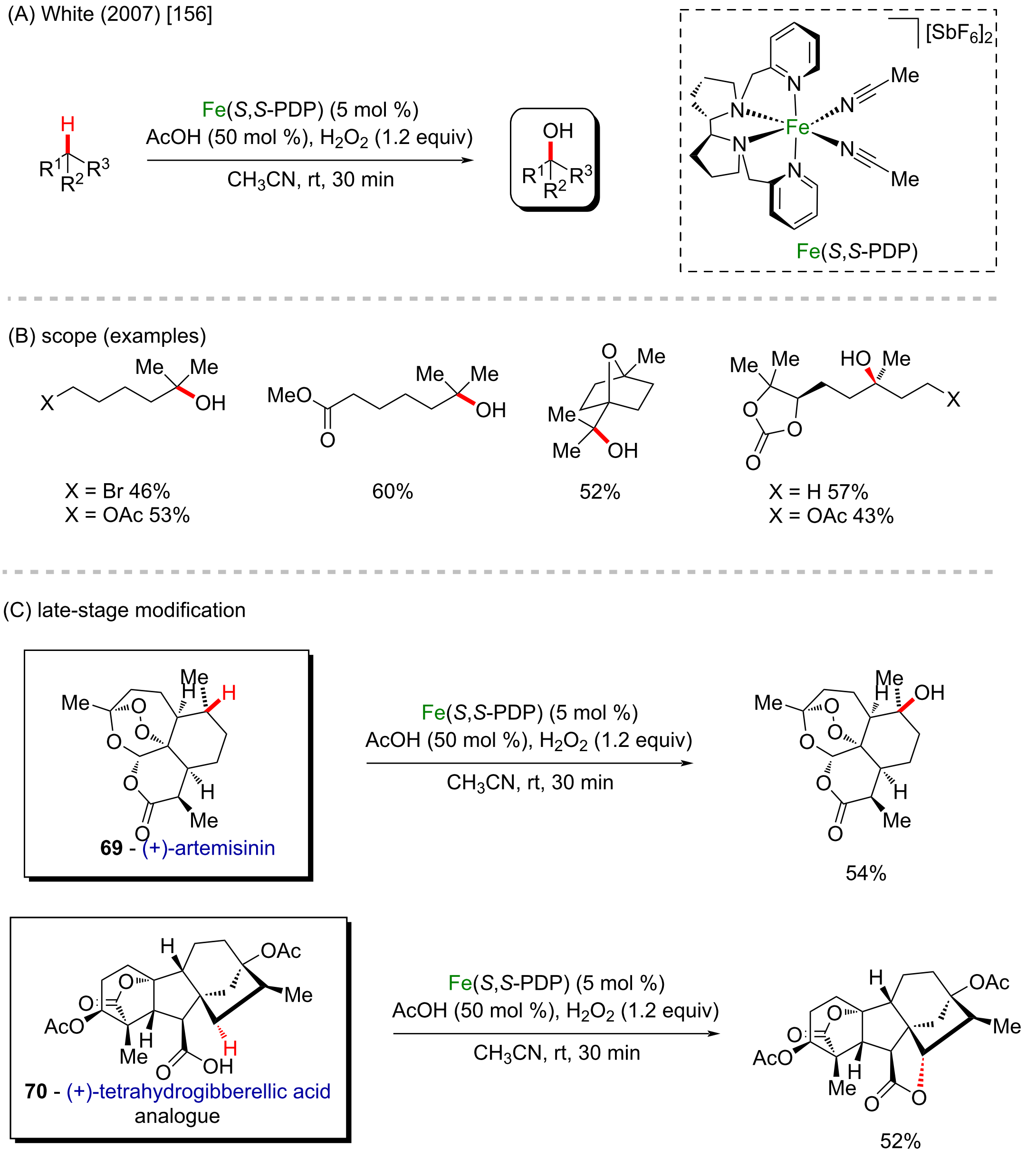
(A) White (2007) [156]
Fe(S,S-PDP) (5 mol %)
AcOH (50 mol %), H2O2 (1.2 equiv)
CH3CN, rt, 30 min
[SbF6]2
Fe(S,S-PDP)
(B) scope (examples)
X = Br 46%
X = OAc 53%
60%
52%
X = H 57%
X = OAc 43%
(C) late-stage modification
69 - (+)-artemisinin
54%
70 - (+)-tetrahydrogibberellic acid analogue
52%

Scheme 25: (A and B) Fe-based small molecule catalyst applied for selective aliphatic C–H oxidations; (C) late-stage modification of (+)-artemisinin (**69**) and a (+)-tetrahydrogibberellic acid analogue **70**.

White's selective C–H oxidation was also applied in the late-stage modification of amino acids and peptides in 2016 (Scheme 27A and B) [159]. The methodology facilitated the targeted C–H oxidative modifications in amino acids and peptides concomitant with the preservation of the α-center chirality in good yields and broad scope regarding the number of amino acids and peptide scaffolds compatible with the transformation. The late-stage oxidation of proline **76** to 5-hydroxyproline furnished interesting intermediates, giving access to relevant motifs in peptide chemistry (Scheme 27C).

Sesquiterpenes are known to present complex polycyclic structures with several chiral centers, and nowadays, several sesquiterpenes have been isolated from plants of the *Illicium* genus (**77**–**79**, Scheme 28A) [160]. (+)-Pseudoanisatin (**80**) is one example, and its first chemical synthesis was achieved in 12 steps by Maimone and collaborators in 2016 utilizing a straightforward site-selective C(sp^3)–H bond functionalization strategy (Scheme 28B) [160]. Starting from the abundant feedstock chemical cedrol, oxidation of the *gem*-dimethyl group was achieved on a gram scale, with the formation of a strained tetra-

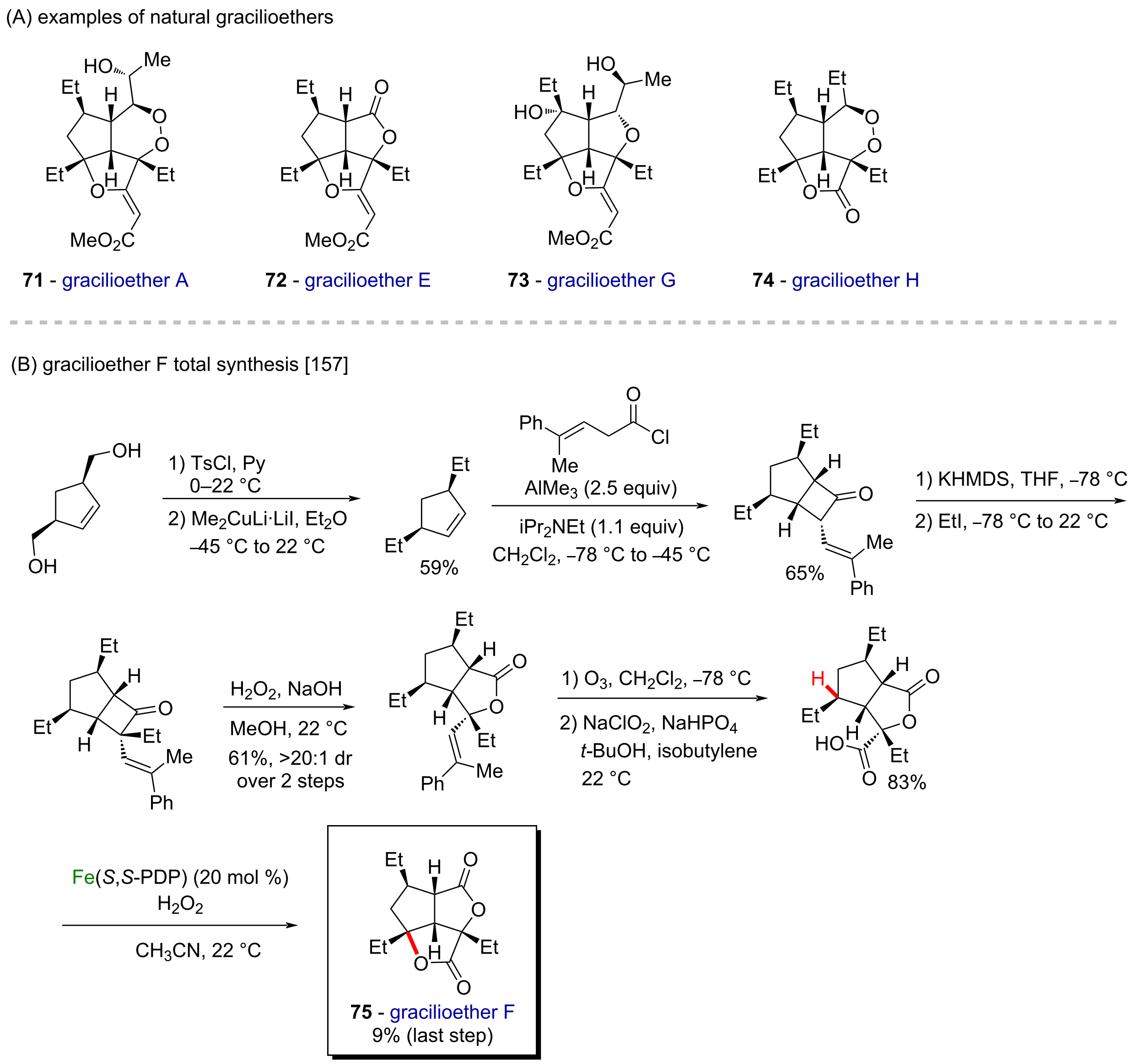
(A) examples of natural gracilioethers
71 - gracilioether A
72 - gracilioether E
73 - gracilioether G
74 - gracilioether H
(B) gracilioether F total synthesis [157]
1) TsCl, Py 0–22 °C
2) Me2CuLi·LiI, Et2O –45 °C to 22 °C
59%
AlMe3 (2.5 equiv)
iPr2NEt (1.1 equiv)
CH2Cl2, –78 °C to –45 °C
65%
1) KHMDS, THF, –78 °C
2) EtI, –78 °C to 22 °C
H2O2, NaOH
MeOH, 22 °C
61%, >20:1 dr over 2 steps
1) O3, CH2Cl2, –78 °C
2) NaClO2, NaHPO4 t-BuOH, isobutylene 22 °C
83%
Fe(S,S-PDP) (20 mol %)
H2O2
CH3CN, 22 °C
75 - gracilioether F
9% (last step)

Scheme 26: (A) Examples of naturally occurring gracilioethers; (B) the first total synthesis of gracilioether F (**75**) utilizing a C–H oxidation in the final step.

hydrofuran ring. The latter was methylated and eliminated via the action of Meerwein's salt (Me_3OBF_4) and a mild base (proton sponge) to afford a methoxy cedrene derivative. Next, oxidative cleavage of the double bond using $NaIO_4$/$RuCl_3 \cdot xH_2O$ enabled a ring opening, followed by lactonization promoted by $CuBr_2$ via an intramolecular acyloxylation. The 5,5-fused ring system was then converted to a 5,6-fused *seco*-prezizaane scaffold through an α-ketol rearrangement promoted by a strong base and after secondary alcohol protection with TBSCl, a Fe-catalyzed C–H activation reaction promoted a second lactonization to afford (+)-pseudoanisatin (Scheme 28B).

In 2016, Chirik and co-workers described the deuteration of several pharmaceuticals via an Fe-catalyzed C–H activation protocol (Scheme 29A and B) [161]. The site selectivity of the bulky iron catalyst was orthogonal to conventional iridium catalysts used in deuterium labelling experiments, allowing the functionalization of complementary positions in several molecules of medicinal importance. Using molecular deuterium gas, the deuterium exchange occurred at different positions in small molecules in different proportions and satisfactory yields. Late-stage site-selective deuteration of pharmaceuticals like paroxetine (**81**), loratadine (**82**), and suvorexant (**83**) was achieved in moderate yields (Scheme 29C).

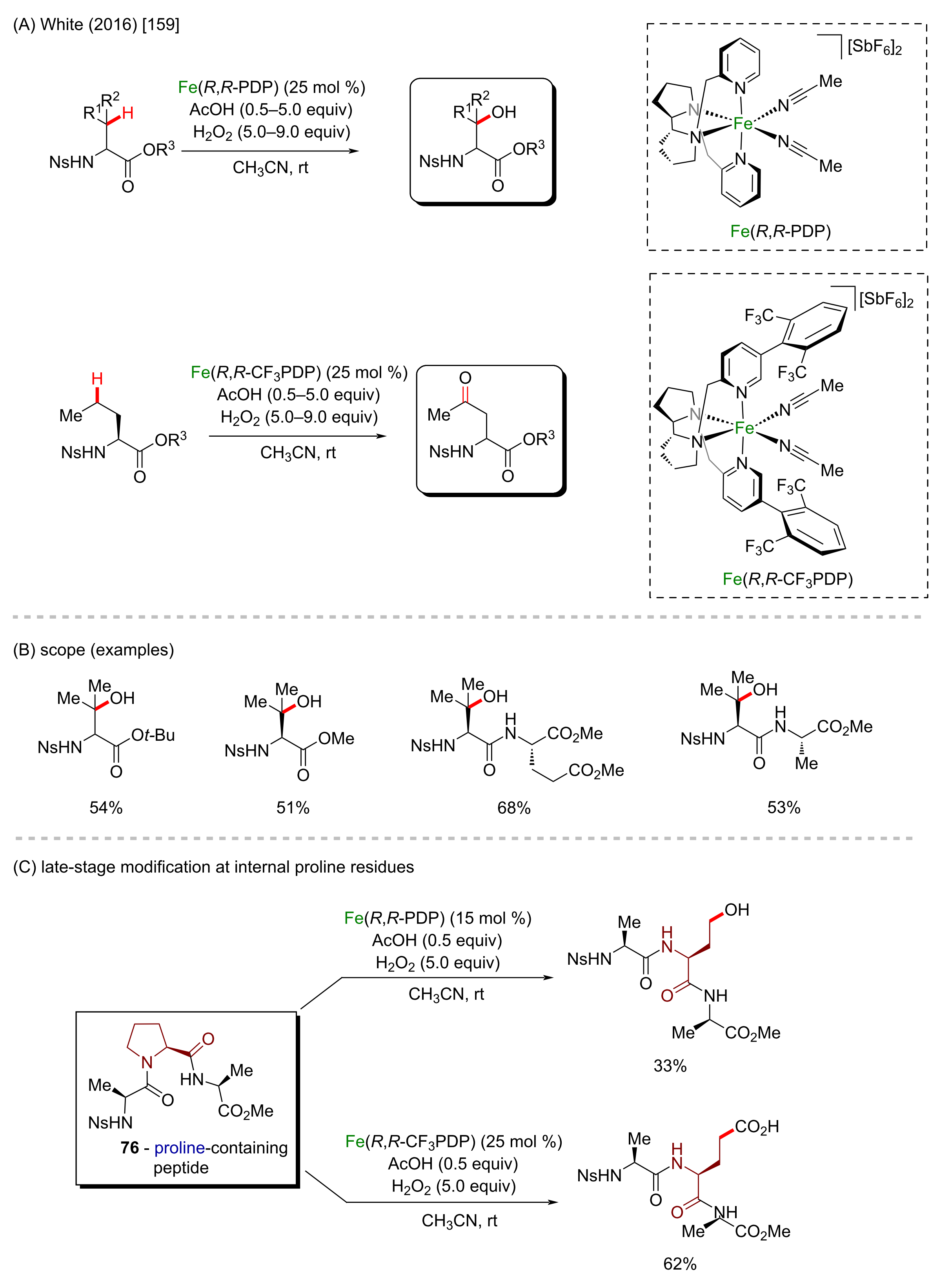
(A) White (2016) [159]
Fe(R,R-PDP) (25 mol %)
AcOH (0.5–5.0 equiv)
H2O2 (5.0–9.0 equiv)
CH3CN, rt
NsHN
OR3
R1
R2
H
OH
O
[SbF6]2
Fe
N
Me
Fe(R,R-PDP)
Fe(R,R-CF3PDP) (25 mol %)
AcOH (0.5–5.0 equiv)
H2O2 (5.0–9.0 equiv)
CH3CN, rt
F3C
Fe(R,R-CF3PDP)
(B) scope (examples)
Ot-Bu
OMe
CO2Me
54%
51%
68%
53%
(C) late-stage modification at internal proline residues
Fe(R,R-PDP) (15 mol %)
AcOH (0.5 equiv)
H2O2 (5.0 equiv)
CH3CN, rt
33%
76 - proline-containing peptide
Fe(R,R-CF3PDP) (25 mol %)
AcOH (0.5 equiv)
H2O2 (5.0 equiv)
CH3CN, rt
CO2H
62%

Scheme 27: (A and B) Selective aliphatic C–H oxidation of amino acids; (C) late-stage modification of proline-containing tripeptide **76**.

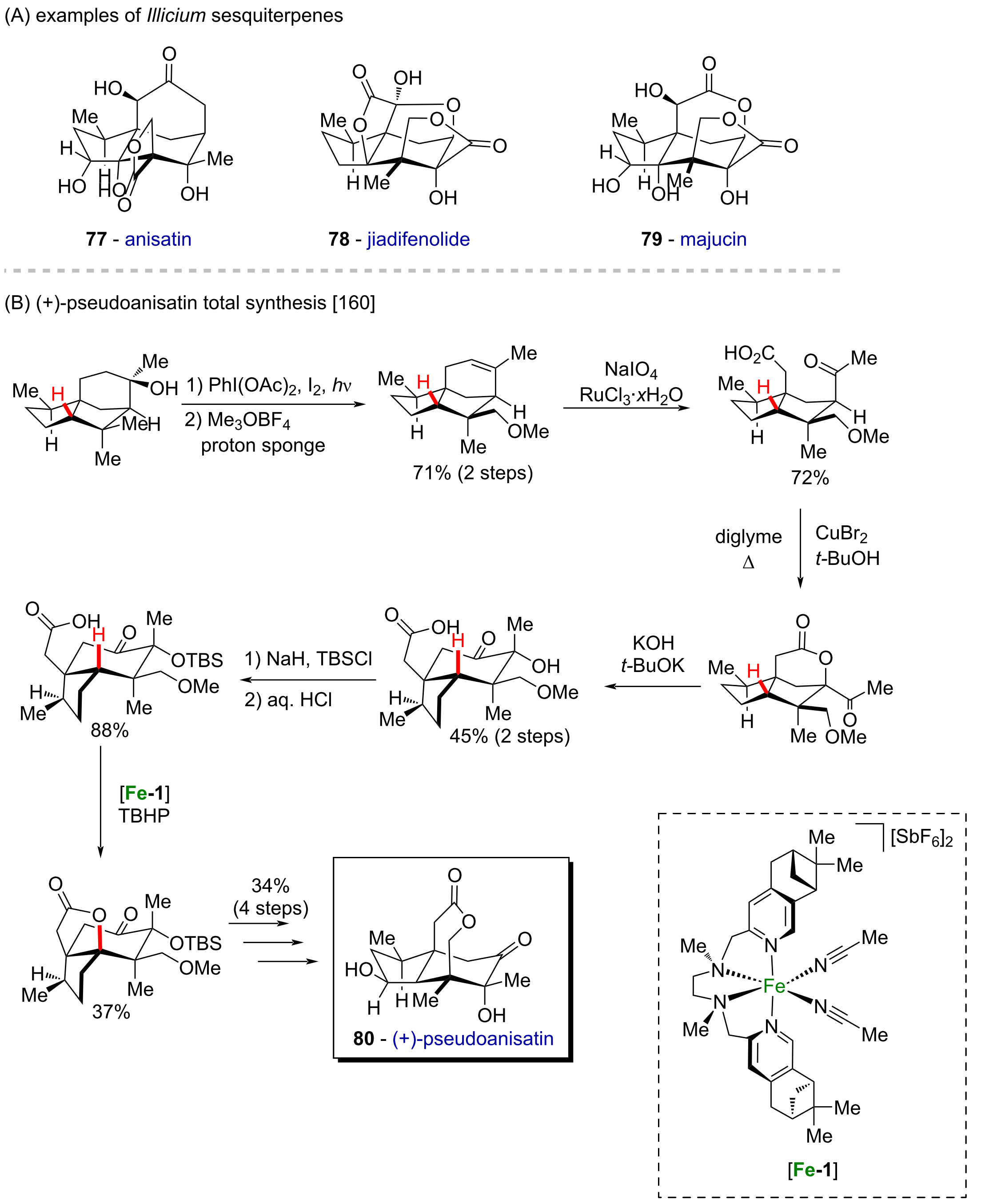
(A) examples of *Illicium* sesquiterpenes
77 - anisatin
78 - jiadifenolide
79 - majucin
(B) (+)-pseudoanisatin total synthesis [160]
1) PhI(OAc)2, I2, hν
2) Me3OBF4
proton sponge
71% (2 steps)
NaIO4
RuCl3·xH2O
72%
diglyme
Δ
CuBr2
t-BuOH
KOH
t-BuOK
45% (2 steps)
1) NaH, TBSCl
2) aq. HCl
88%
[Fe-1]
TBHP
37%
34%
(4 steps)
80 - (+)-pseudoanisatin
[SbF6]2
[Fe-1]

Scheme 28: (A) Examples of *Illicium* sesquiterpenes; (B) first chemical synthesis of (+)-pseudoanisatin (**80**) in 12 steps.

In 2019, Han and collaborators reported a biomimetic Fe-catalyzed aerobic oxidation of methylarenes to benzaldehydes by using inexpensive and nontoxic reactants (Scheme 30A and B) [162]. The method was inspired by the biocatalytic action of the cytochrome P-450 cycle, which is driven by a reductase or bioreductant, and presented high versatility in incorporating both aldehyde and ketone functionalities into unprotected arylboronic acids. The reaction consists of using a porphyrin-based iron catalyst, and several scaffolds were successfully oxidized in good to excellent yields. The methodology also enabled the late-stage oxidation of complex molecules bearing benzylic C–H bonds like tocopherol nicotinate (**84**), which has never been demonstrated for any other catalytic oxidations of alkylaromatics (Scheme 30C).

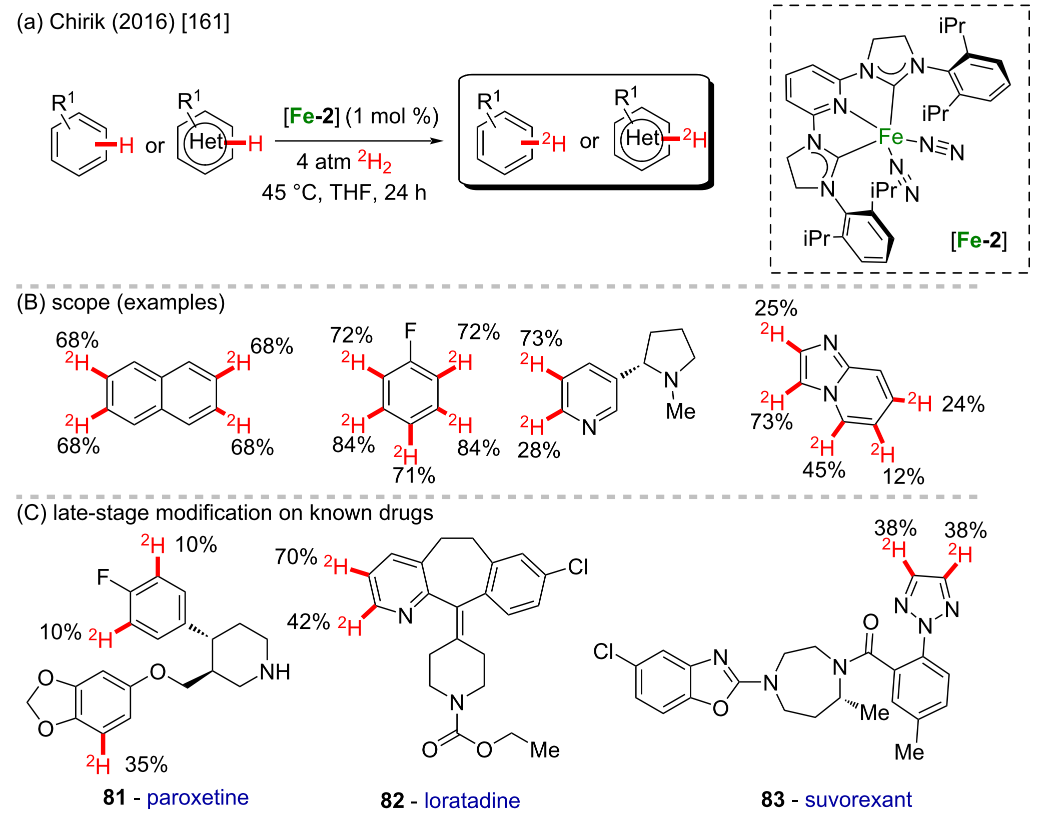
(a) Chirik (2016) [161]
R1
H
or
Het
[Fe-2] (1 mol %)
4 atm 2H2
45 °C, THF, 24 h
2H
iPr
N
Fe
N≡N
[Fe-2]
(B) scope (examples)
68%
72%
F
73%
25%
N
Me
24%
84%
71%
28%
73%
45%
12%
(C) late-stage modification on known drugs
10%
35%
70%
42%
Cl
NH
O
38%
Me
81 - paroxetine
82 - loratadine
83 - suvorexant

Scheme 29: (A and B) Fe-catalyzed deuteration; (C) late-stage modification of pharmaceuticals.

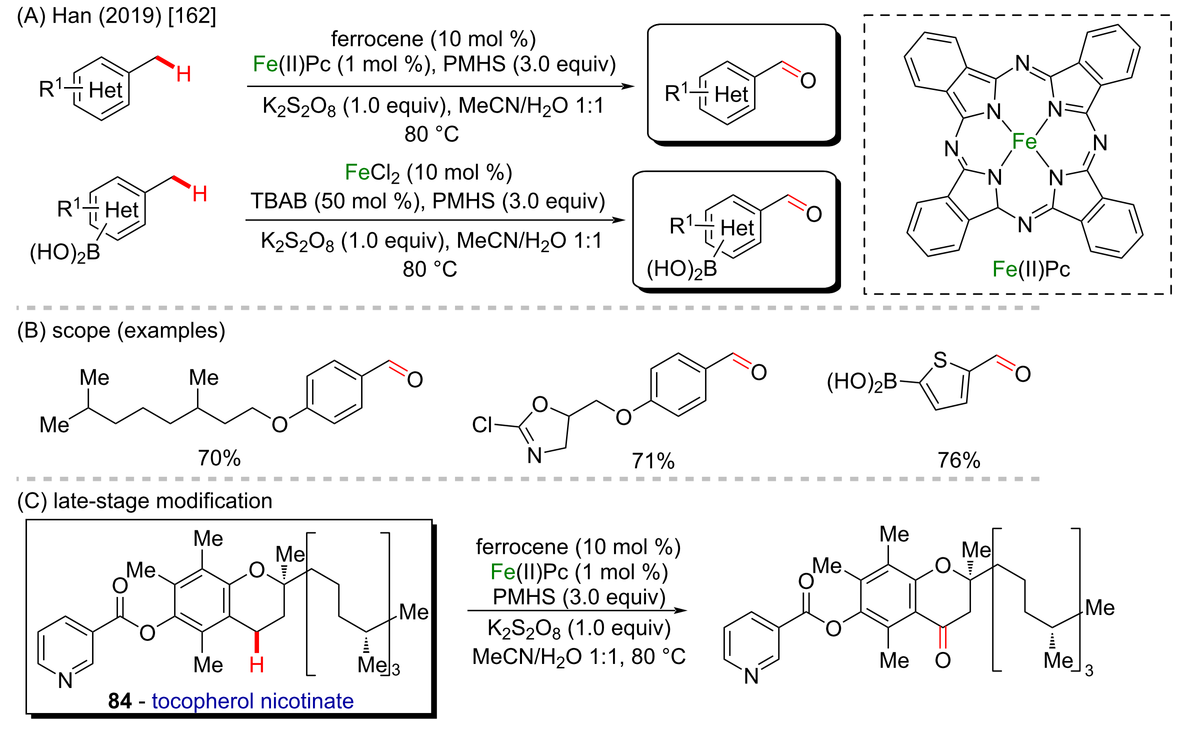
(A) Han (2019) [162]
R1
Het
H
ferrocene (10 mol %)
Fe(II)Pc (1 mol %), PMHS (3.0 equiv)
K2S2O8 (1.0 equiv), MeCN/H2O 1:1
80 °C
O
FeCl2 (10 mol %)
TBAB (50 mol %), PMHS (3.0 equiv)
K2S2O8 (1.0 equiv), MeCN/H2O 1:1
80 °C
(HO)2B
Fe(II)Pc
(B) scope (examples)
Me
70%
Cl
71%
S
76%
(C) late-stage modification
84 - tocopherol nicotinate
ferrocene (10 mol %)
Fe(II)Pc (1 mol %)
PMHS (3.0 equiv)
K2S2O8 (1.0 equiv)
MeCN/H2O 1:1, 80 °C
N
3

Scheme 30: (A and B) Biomimetic Fe-catalyzed aerobic oxidation of methylarenes to benzaldehydes (PMHS, polymethylhydrosiloxane); (C) late-stage modification of tocopherol nicotinate (**84**).

A straightforward method for an α-amino C−H bond functionalization was described by Kang et al. in 2020 to promote the synthesis of tetrahydroquinolines from tertiary anilines (Scheme 31B and C) [163]. Tetrahydroquinolines are a class of compounds already known to present varied biological effects (**85**–**89**, Scheme 31A), such as antioxidant, α-amylase inhibitor, anticancer, and anti-inflammatory activities [164]. The reaction was promoted by non heme-Fe catalyst, behaving similarly to the bioinspired iron catalyst in a redox-selective way. The combination of Fe(phen)$_3$(PF$_6$)$_3$ and tertiary anilines afforded α-aminoalkyl radicals that could be coupled with a wide range of electrophilic partners to afford the products in moderate to good yields. The new reaction was also used in the first step of the total synthesis of a caspase-3 inhibitor (**90**), and mechanistic investigations showed that O$_2$ behaves as a terminal oxidant to form α-aminoalkyl radicals, whereas the formation of an Fe-peroxo species in the catalytic cycle was confirmed using a combination of EPR and ESI mass spectrometry experiments (Scheme 31D).

One-pot processes for the synthesis of benzo[*b*]furans from aryl- or alkylketones using nonprecious Fe and Cu catalysis have been described by Sutherland and co-workers in 2020 (Scheme 32B and C) [165]. Benzofurans are important scaffolds present in several bioactive compounds, such as balsaminone A (**91**, antipruritic activity), xylarianaphthol-1 (**92**, anticancer activity), and amiodarone (**93**, antiarrhythmic activity) (Scheme 32A) [166]. The method consists of a tandem, regioselective Fe(III)-catalyzed C–H halogenation, followed by an Fe or Cu-catalyzed *O*-arylation to access the benzo[*b*]furan derivatives in high yields. Several natural products and pharmacologically active targets bearing the furan ring were synthesized in moderate to good yields. Overall, the new protocol presented a broad scope and excellent functional group toler-

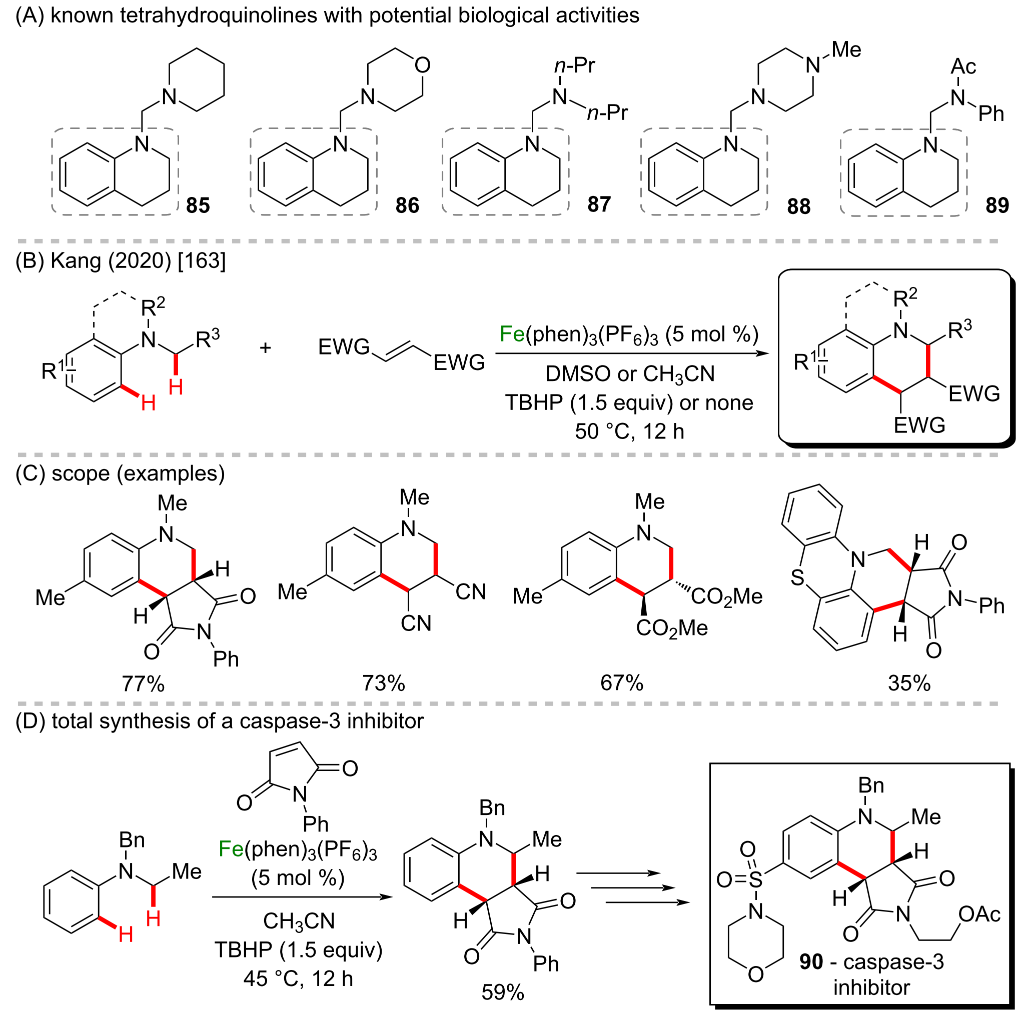
(A) known tetrahydroquinolines with potential biological activities
85
86
87
88
89
n-Pr
Me
Ac
Ph
(B) Kang (2020) [163]
R2
R3
R1
H
EWG
+
Fe(phen)3(PF6)3 (5 mol %)
DMSO or CH3CN
TBHP (1.5 equiv) or none
50 °C, 12 h
(C) scope (examples)
77%
73%
67%
35%
CO2Me
CN
(D) total synthesis of a caspase-3 inhibitor
Bn
Me
Fe(phen)3(PF6)3
(5 mol %)
CH3CN
TBHP (1.5 equiv)
45 °C, 12 h
59%
OAc
90 - caspase-3 inhibitor

Scheme 31: (A) Known tetrahydroquinolines with potential biological activities; (B and C) redox-selective Fe catalysis; (D) total synthesis of a caspase-3 inhibitor **90**.

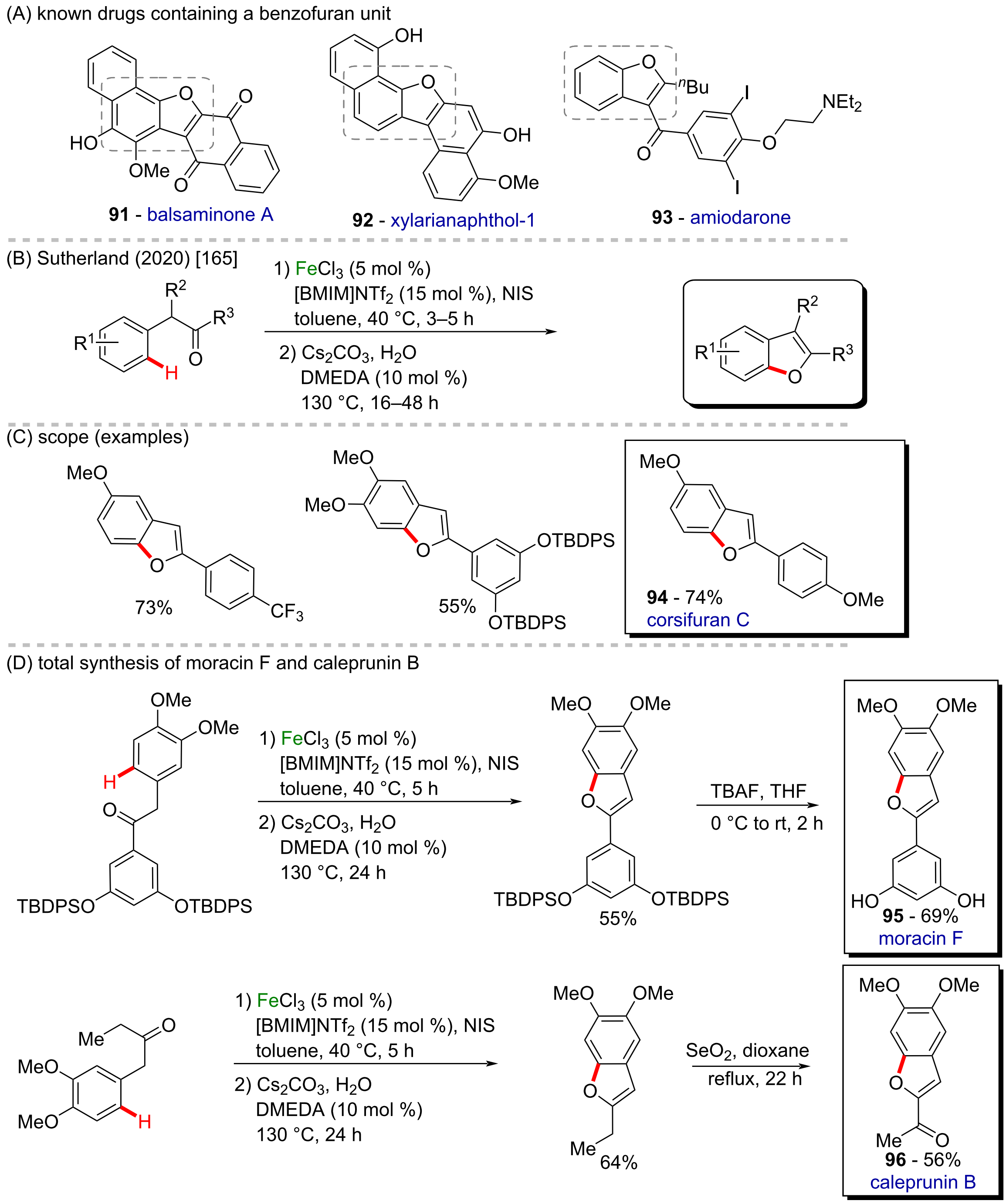
(A) known drugs containing a benzofuran unit
OH
O
O
HO
OMe
O
OH
OMe
O
nBu
I
NEt2
O
I
91 - balsaminone A
92 - xylarianaphthol-1
93 - amiodarone
(B) Sutherland (2020) [165]
R2
R3
R1
H
O
1) FeCl3 (5 mol %)
[BMIM]NTf2 (15 mol %), NIS
toluene, 40 °C, 3–5 h
2) Cs2CO3, H2O
DMEDA (10 mol %)
130 °C, 16–48 h
(C) scope (examples)
MeO
73%
CF3
55%
OTBDPS
94 - 74%
corsifuran C
OMe
(D) total synthesis of moracin F and caleprunin B
TBDPSO
OTBDPS
1) FeCl3 (5 mol %)
[BMIM]NTf2 (15 mol %), NIS
toluene, 40 °C, 5 h
2) Cs2CO3, H2O
DMEDA (10 mol %)
130 °C, 24 h
TBAF, THF
0 °C to rt, 2 h
HO
OH
95 - 69%
moracin F
Me
64%
SeO2, dioxane
reflux, 22 h
96 - 56%
caleprunin B

Scheme 32: (A) Known drugs containing a benzofuran unit; (B and C) Fe/Cu-catalyzed tandem *O*-arylation to access benzo[*b*]furan derivatives; (D) total synthesis of moracin F (**95**) and caleprunin B (**96**).

ance, allowing the synthesis of valuable molecules like corsifuran C (**94**), moracin F (**95**), and caleprunin B (**96**) (Scheme 32D).

In 2020, Chattopadhyay and collaborators reported a new concept involving the intramolecular denitrogenative C(sp^3)–H amination of 1,2,3,4-tetrazoles bearing unactivated primary, secondary, and tertiary C–H bonds via an Fe-catalyzed C–H activation (Scheme 33B and 33C) [167]. The new C(sp^3)–H amination protocol presented high levels of selectivity, reactivity, and functional group tolerance, providing a large number of complex nitrogen heterocycles like azaindolines, pyrrolo-quino-

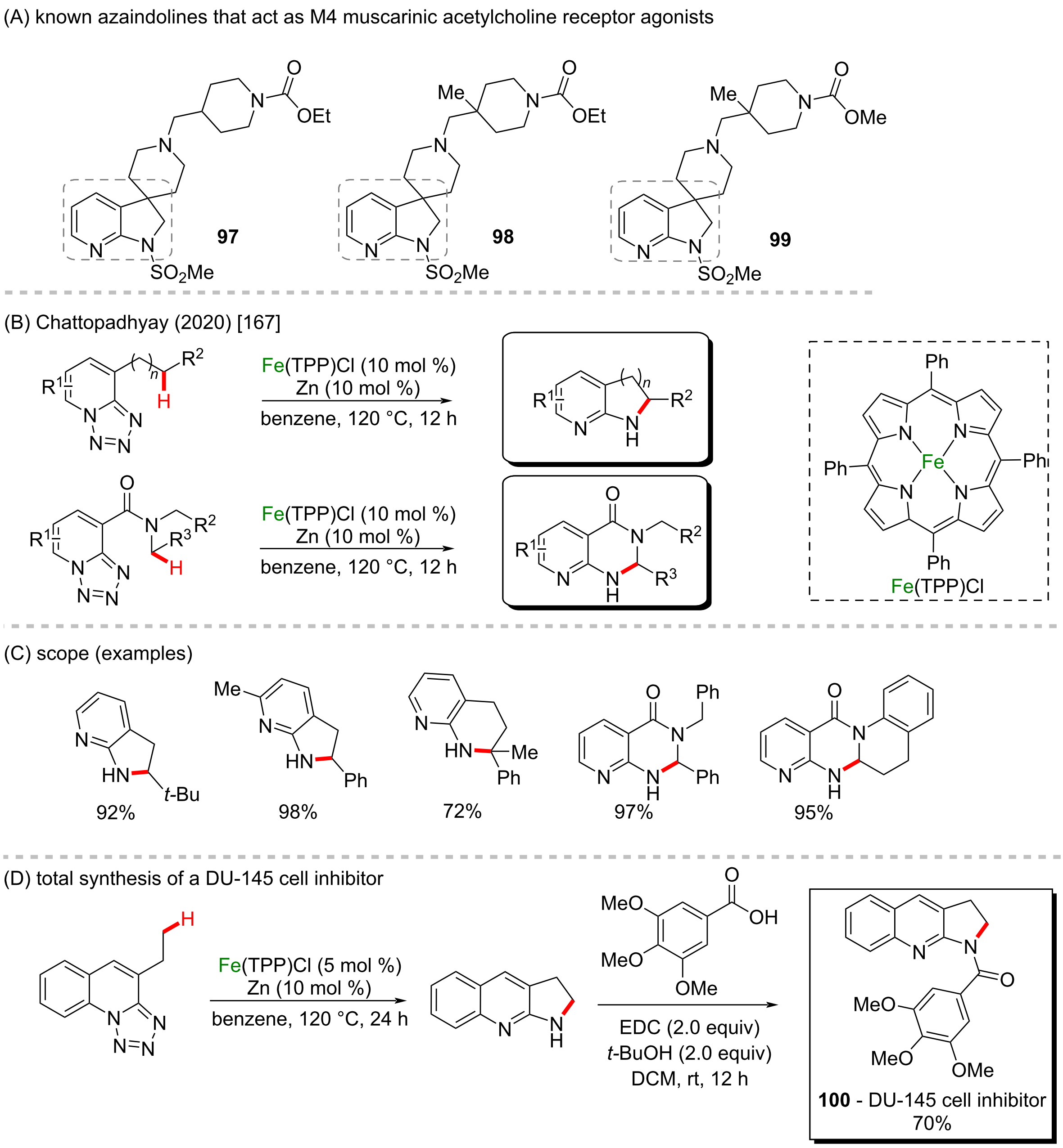
(A) known azaindolines that act as M4 muscarinic acetylcholine receptor agonists
97
98
99
(B) Chattopadhyay (2020) [167]
Fe(TPP)Cl (10 mol %)
Zn (10 mol %)
benzene, 120 °C, 12 h
Fe(TPP)Cl
(C) scope (examples)
92%
98%
72%
97%
95%
(D) total synthesis of a DU-145 cell inhibitor
Fe(TPP)Cl (5 mol %)
Zn (10 mol %)
benzene, 120 °C, 24 h
EDC (2.0 equiv)
t-BuOH (2.0 equiv)
DCM, rt, 12 h
100 - DU-145 cell inhibitor
70%

Scheme 33: (A) Known azaindolines that act as M4 muscarinic acetylcholine receptor agonists; (B and C) intramolecular denitrogenative C(sp^3)–H amination of 1,2,3,4-tetrazoles; (D) total synthesis of the DU-145 cell inhibitor **100**.

lines and -quinolones in excellent yields. Amongst the synthesized scaffolds, especially azaindolines are known to be present in M4 muscarinic acetylcholine receptor agonists (**97**, **98**, and **99**, Scheme 33A) [168]. Asymmetric variations of the porphyrin-based iron catalysts also provided the desired product with 100% conversion and enantiomeric ratios up to 73:27 in some cases. The straightforward Fe catalysis was used as a key step in the synthesis of a DU-145 cell inhibitor (**100**), that was obtained in 70% yield over two steps (Scheme 33D).

Indolones are known to present potent anticholinesterase activity (**101**, **102**, and **103**) (Scheme 34A). Therefore, the use of this class of molecules as substrates in organic functionalization methods is of high importance in the field of Alzheimer's disease studies [169]. In 2020, Xu and co-workers described an unprecedented dual C–H functionalization of indolin-2-ones and benzofuran-2-ones via an oxidative C(sp^3)–H cross-coupling protocol catalyzed by inexpensive $FeCl_3$ and ligand-free conditions (Scheme 34B and 34C) [170]. The new method

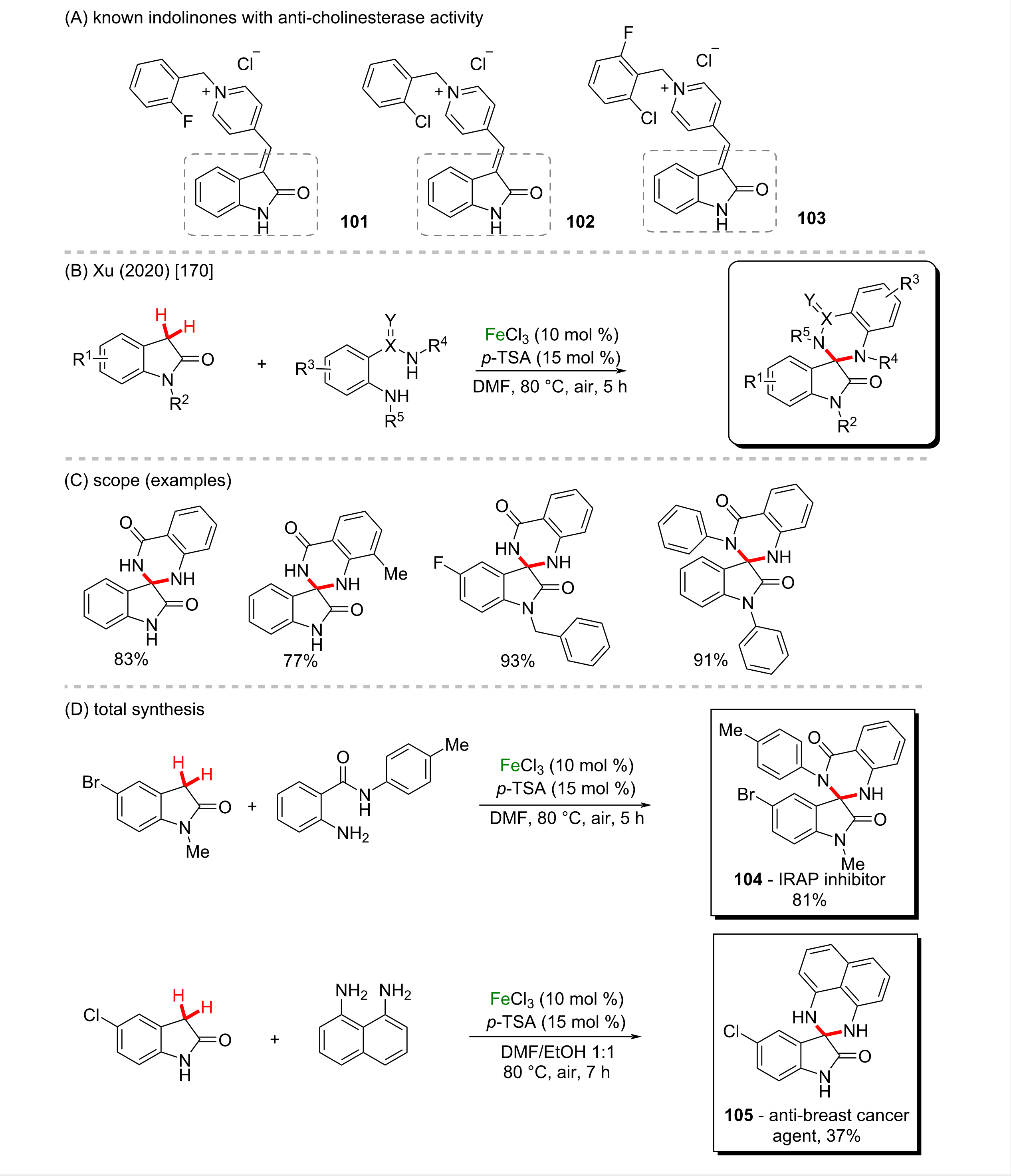
(A) known indolinones with anti-cholinesterase activity
101
102
103
(B) Xu (2020) [170]
FeCl3 (10 mol %)
p-TSA (15 mol %)
DMF, 80 °C, air, 5 h
(C) scope (examples)
83%
77%
93%
91%
(D) total synthesis
FeCl3 (10 mol %)
p-TSA (15 mol %)
DMF, 80 °C, air, 5 h
104 - IRAP inhibitor
81%
FeCl3 (10 mol %)
p-TSA (15 mol %)
DMF/EtOH 1:1
80 °C, air, 7 h
105 - anti-breast cancer agent, 37%

Scheme 34: (A) Known indolinones with anticholinesterase activity; (B and C) oxidative C(sp^3)–H cross coupling protocol; (D) total synthesis of representative bioactive compounds.

presented broad scope in the construction of tetrasubstituted carbon centers from methylenes to access a wide range of spiro *N*-heterocyclic oxindoles in excellent yields, including diamine, benzamide, and spirothiazole scaffolds. The high potential of the reaction was demonstrated by the synthesis of bioactive compounds like an IRAP inhibitor (**104**) and an antibreast cancer agent (**105**) in good yields (Scheme 34D).

Iron is by far the cheapest and most abundant metal to be used from the 3d series, and these facts are reflected by the amount and quality of studies that has been done so far. From the simplest iron salts to the most enantiospecific complex forms, iron catalysis is playing an important role for the development of additional accessible C–H activation methods. From these perspectives it can be assumed that in the near future iron will be one of the most studied metal applied in C–H functionalization methodologies.

Cobalt-catalyzed C–H activation

Cobalt is a cheap metal that presents powerful colors in its ionic forms and therefore, it has been used as a basic element in ink since ancient periods [171,172]. Cobalt alloys are used in blades [173] and batteries [174]. Due to its accessibility, it is well explored in catalysis for many fields, such as cycloaddition reactions [175], polymerization [176], and C–C cross-coupling methods [177]. Several biologically active compounds have been obtained through cobalt catalysis [178-180] including its application in C–H activation reactions [181-185]. The synthesis of biologically important compounds using C–H activation techniques has been described by Ackermann and co-workers in 2019 [186]. In this specific work, a cobalt-Cp* catalyzed C–H alkenylation was performed at the C-2 position of indole derivatives bearing peptide units in the C-3 position (Scheme 35A). This process led to several activated products in good yields, including one whose basic structure is already known to present important biological activities (**106**) [187] (Scheme 35B). Still in this work, several products were submitted to a subsequent metathesis mediated by Grubbs-II catalyst and a further palladium-catalyzed C=C reduction and DG-removal process, from which the desired macrocyclic peptides were obtained in good to excellent yields (Scheme 35C).

Recently, again Ackermann and co-workers [188] described a cobalt-Cp*-catalyzed C–H methylation of several well-known pharmaceuticals, such as diazepam (a commercially available anxiolytic drug [189]), paclitaxel (a commercially available anticancer drug [190]), celecoxib (a commercially available analgesic drug [191]), and rucaparib (a commercially available anticancer drug [192]). They achieved the C–H methylation by following two methods (method A or method B, Scheme 36A) and obtained the methylated analogues **107**–**119** in moderate to very high yields (Scheme 36B and C).

Ellman and co-workers described a powerful and interesting three-component reaction in which a cobalt-Cp*-catalyzed C–H bond addition afforded complex scaffolds in good yields (Scheme 37B and C) [193]. The authors explained the stereoselectivity by means of a mechanism involving a hydride migration suffering influence of steric effects related not only to the catalyst ligands but also to the diene R^5 and R^6 substituents. With this innovative method in hands, the authors explored the synthetic applicability in the preparation of a core unit from lasalocid A (**124**), a known antibiotic drug [194] that, along with its four analogues **120**–**123** (Scheme 37A), were extracted from *Streptomyces lasaliensis* cultures [195]. The synthesis succeeded in five steps, each one of them in good yields, including the cobalt-catalyzed C–H bond addition (Scheme 37D).

One year later, the same group described a unique cobalt-Cp* catalyzed C(sp^2)–H amidation technique [196] applied to thiostrepton (**125**), a known biosynthetic antibiotic drug that presents a highly complex chemical structure [197] (Scheme 38A). The activation exclusively occurs at one of the hydrogen atoms of the dehydroalanine (Dha) portions Dha1 and Dha2, towards the formation of the *Z*-stereoisomer (Scheme 38A). No reaction was observed at the Dha-3 part and, according to the substitution pattern from the coupling partner, a higher preference for the substitution at the Dha-1 (product A) over the Dha-2 (product B) site was also observed (Scheme 38B), characterizing an excellent and valuable regio- and diastereoselectivity.

In the same year, Wu, Li and co-workers described a successful cobalt-Cp*-catalyzed C–H amidation of benzaldehyde derivatives (Scheme 39B), in which the aldehyde portion works as the directing group [198]. After an acid workup using diluted hydrochloric acid, the desired *ortho*-amidated products were obtained in good yields (Scheme 39C). The authors used the same methodology to synthesize two 4*H*-benzo[*d*][1,3]oxazin-4-one derivatives that act as inhibitors of two enzymes (compounds **130** and **131** in Scheme 39D). The first one is the enzyme C1r serine protease, involved in both inflammation and renal scarring [199], and the second one is the enzyme elastase, responsible for consuming elastine, leading to aging processes [200]. Beyond that, 4*H*-benzo[*d*][1,3]oxazin-4-one derivatives **126**–**129** have been studied as potential hypolipidemic drugs (Scheme 39A) [201].

Beyond the above-cited cobalt-Cp* examples, other classes of cobalt catalysts can also be used to affect C–H activation in different substrates. A good example is the use of chelated cobalt(III) catalysts, such as [Co(acac)$_3$], as recently mentioned by Lu, Loh and co-workers [202]. In this work, the catalyst was used to mediate a C–H arylation at the C-2 position of *N*-(2-pyrimidyl)pyrrole derivatives (Scheme 40A). Several activated products were obtained in moderate to good yields (Scheme 40B). The authors extrapolated this methodology, using it to synthesize a derivative of vilazodone (**135**, Scheme 40C), a known antidepressant drug commercialized under the name viibryd which also bears potential activity against Parkinson's disease [203].

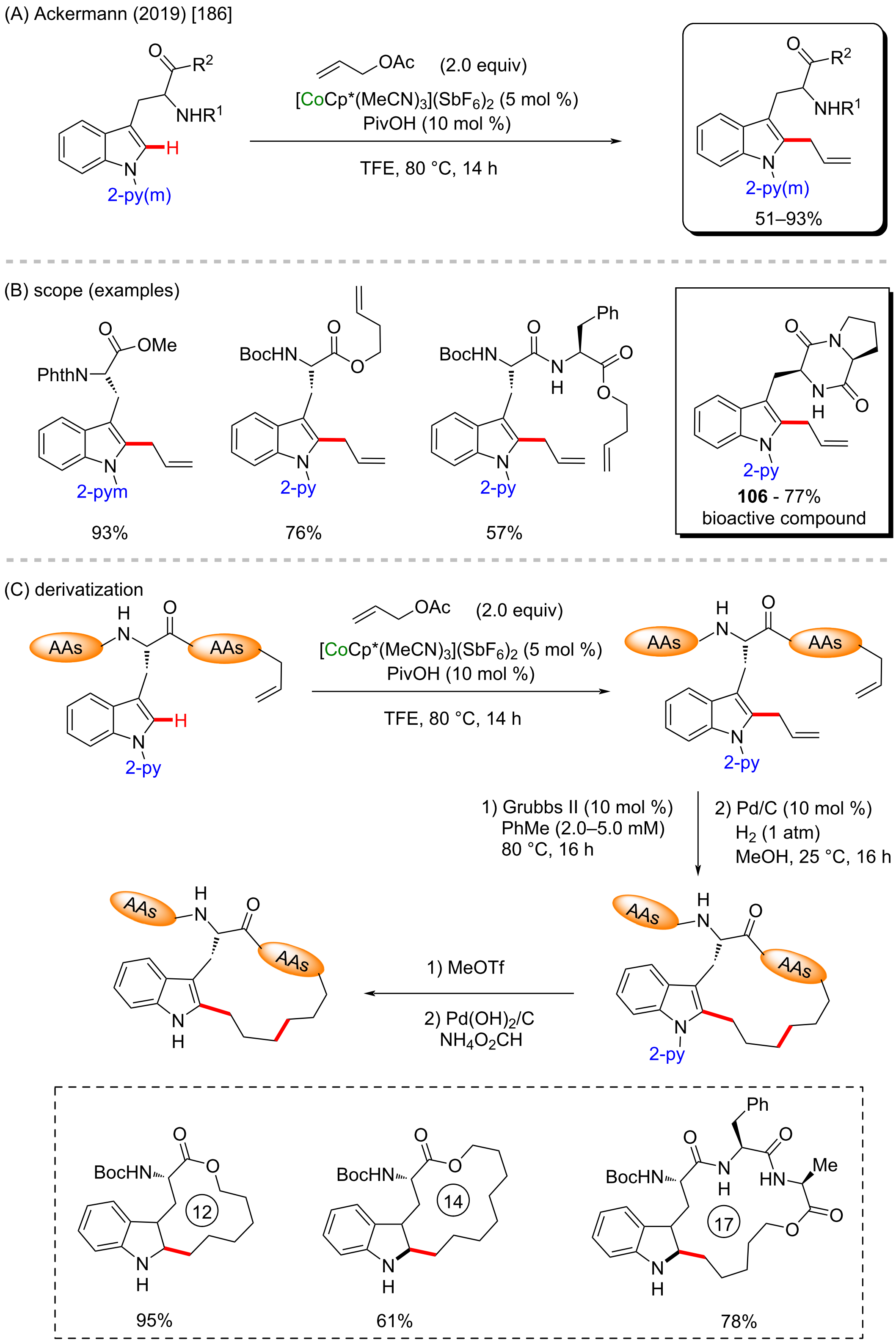
(A) Ackermann (2019) [186]
O
R2
NHR1
H
N
2-py(m)
OAc (2.0 equiv)
[CoCp*(MeCN)3](SbF6)2 (5 mol %)
PivOH (10 mol %)
TFE, 80 °C, 14 h
51–93%
(B) scope (examples)
PhthN
OMe
2-pym
93%
BocHN
2-py
76%
Ph
57%
106 - 77%
bioactive compound
(C) derivatization
AAs
1) Grubbs II (10 mol %)
PhMe (2.0–5.0 mM)
80 °C, 16 h
2) Pd/C (10 mol %)
H2 (1 atm)
MeOH, 25 °C, 16 h
1) MeOTf
2) Pd(OH)2/C
NH4O2CH
12
95%
14
61%
Me
HN
17
78%

Scheme 35: (A and B) Cobalt-catalyzed C–H alkenylation of C-3-peptide-containing indoles; (C) derivatization by Grubbs-II-catalyzed metathesis to macrocyclic peptides.

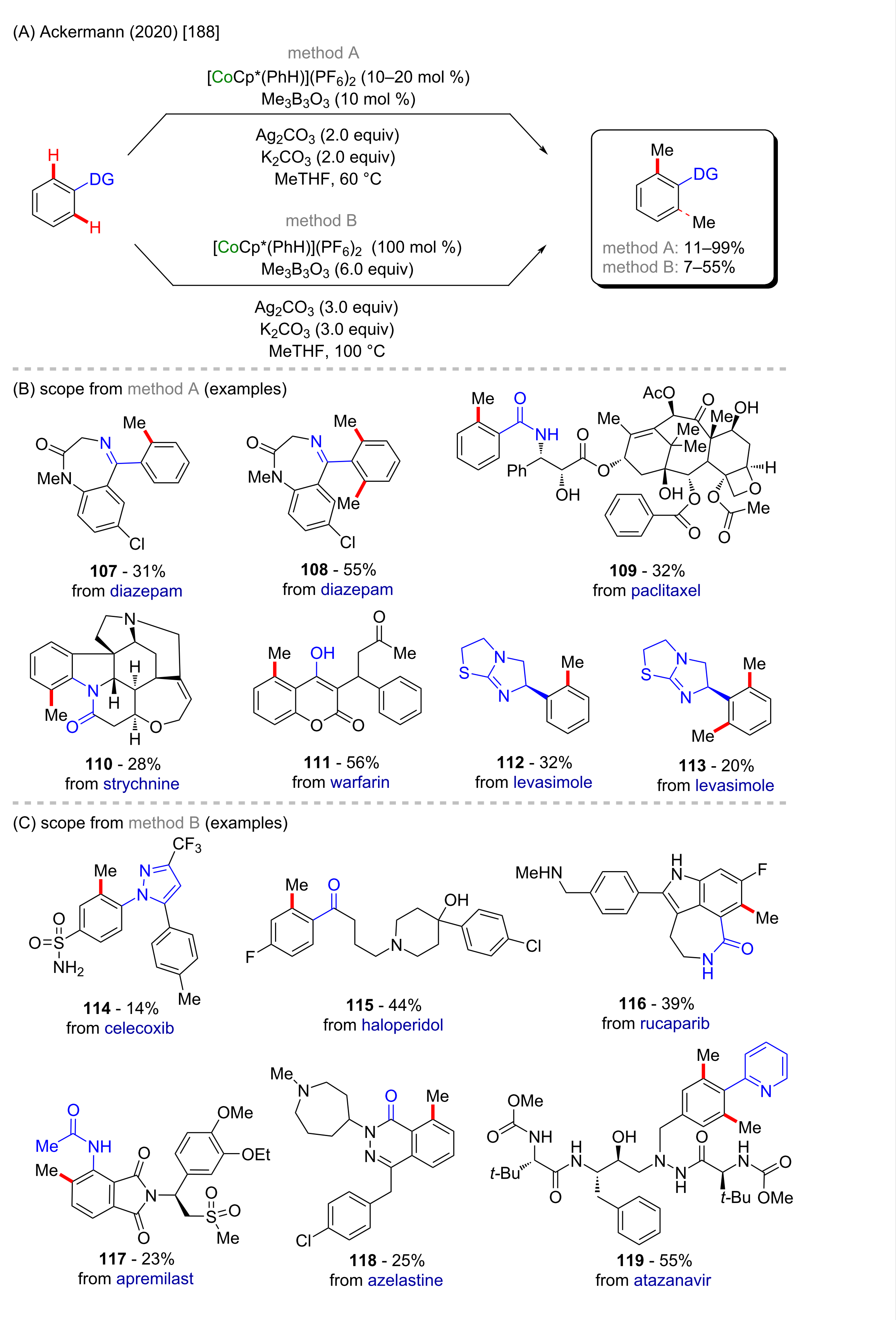
(A) Ackermann (2020) [188]
method A
[CoCp*(PhH)](PF6)2 (10–20 mol %)
Me3B3O3 (10 mol %)
Ag2CO3 (2.0 equiv)
K2CO3 (2.0 equiv)
MeTHF, 60 °C
method B
[CoCp*(PhH)](PF6)2 (100 mol %)
Me3B3O3 (6.0 equiv)
Ag2CO3 (3.0 equiv)
K2CO3 (3.0 equiv)
MeTHF, 100 °C
H
DG
H
Me
DG
Me
method A: 11–99%
method B: 7–55%
(B) scope from method A (examples)
107 - 31%
from diazepam
108 - 55%
from diazepam
109 - 32%
from paclitaxel
110 - 28%
from strychnine
111 - 56%
from warfarin
112 - 32%
from levasimole
113 - 20%
from levasimole
(C) scope from method B (examples)
114 - 14%
from celecoxib
115 - 44%
from haloperidol
116 - 39%
from rucaparib
117 - 23%
from apremilast
118 - 25%
from azelastine
119 - 55%
from atazanavir

Scheme 36: (A) Cobalt-Cp*-catalyzed C–H methylation of known drugs; (B and C) scope of the *o*-methylated derivatives.

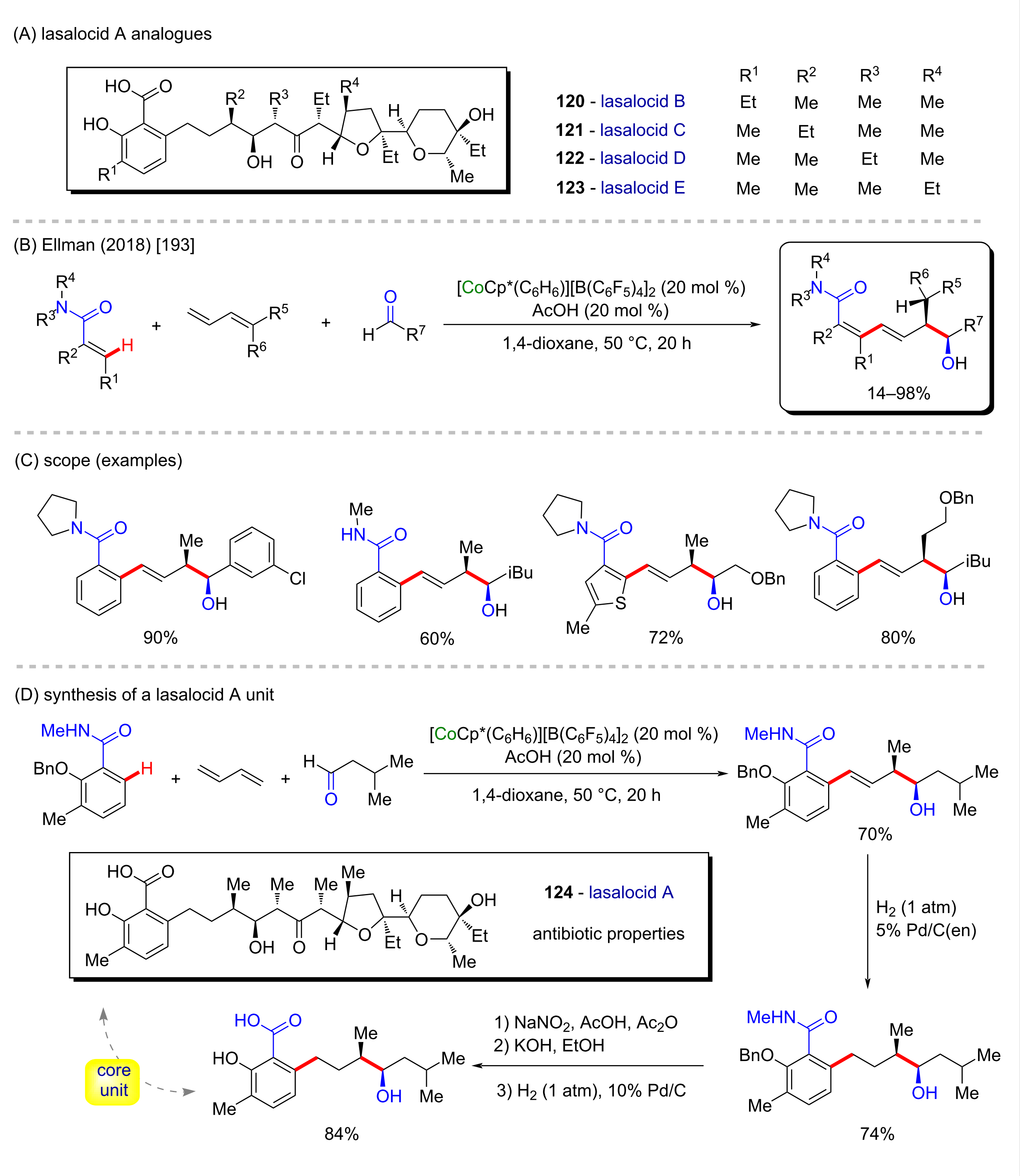
(A) lasalocid A analogues
R1 R2 R3 R4
120 - lasalocid B Et Me Me Me
121 - lasalocid C Me Et Me Me
122 - lasalocid D Me Me Et Me
123 - lasalocid E Me Me Me Et
(B) Ellman (2018) [193]
[CoCp*(C6H6)][B(C6F5)4]2 (20 mol %)
AcOH (20 mol %)
1,4-dioxane, 50 °C, 20 h
14–98%
(C) scope (examples)
90%
60%
72%
80%
(D) synthesis of a lasalocid A unit
70%
124 - lasalocid A
antibiotic properties
H2 (1 atm)
5% Pd/C(en)
74%
1) NaNO2, AcOH, Ac2O
2) KOH, EtOH
3) H2 (1 atm), 10% Pd/C
84%
core unit

Scheme 37: (A) Known lasalocid A analogues; (B and C) three-component cobalt-catalyzed C–H bond addition; (D) lasalocid A core unit synthesis.

In previous studies it has been observed that 2-phenoxypyridines belong to a class of compounds that presents potent herbicidal properties (**136**, **137**, Scheme 41A) [204]. Chelated cobalt(II) catalysts, such as $[Co(acac)_2]$, can also be used in C–H activation methods to modify 2-phenoxypyridines, from which other biological activities can be discovered. Although they present a lower oxidation state, they are also powerful catalysts, as described by Gou, Cao, and co-workers for a C–H acetoxylation of phenol derivatives (Scheme 43B) [205]. In the presence of phenyliodine(III) diacetate (PIDA) the reaction leads to several *ortho*-directed acetoxylated products in moderate to good yields

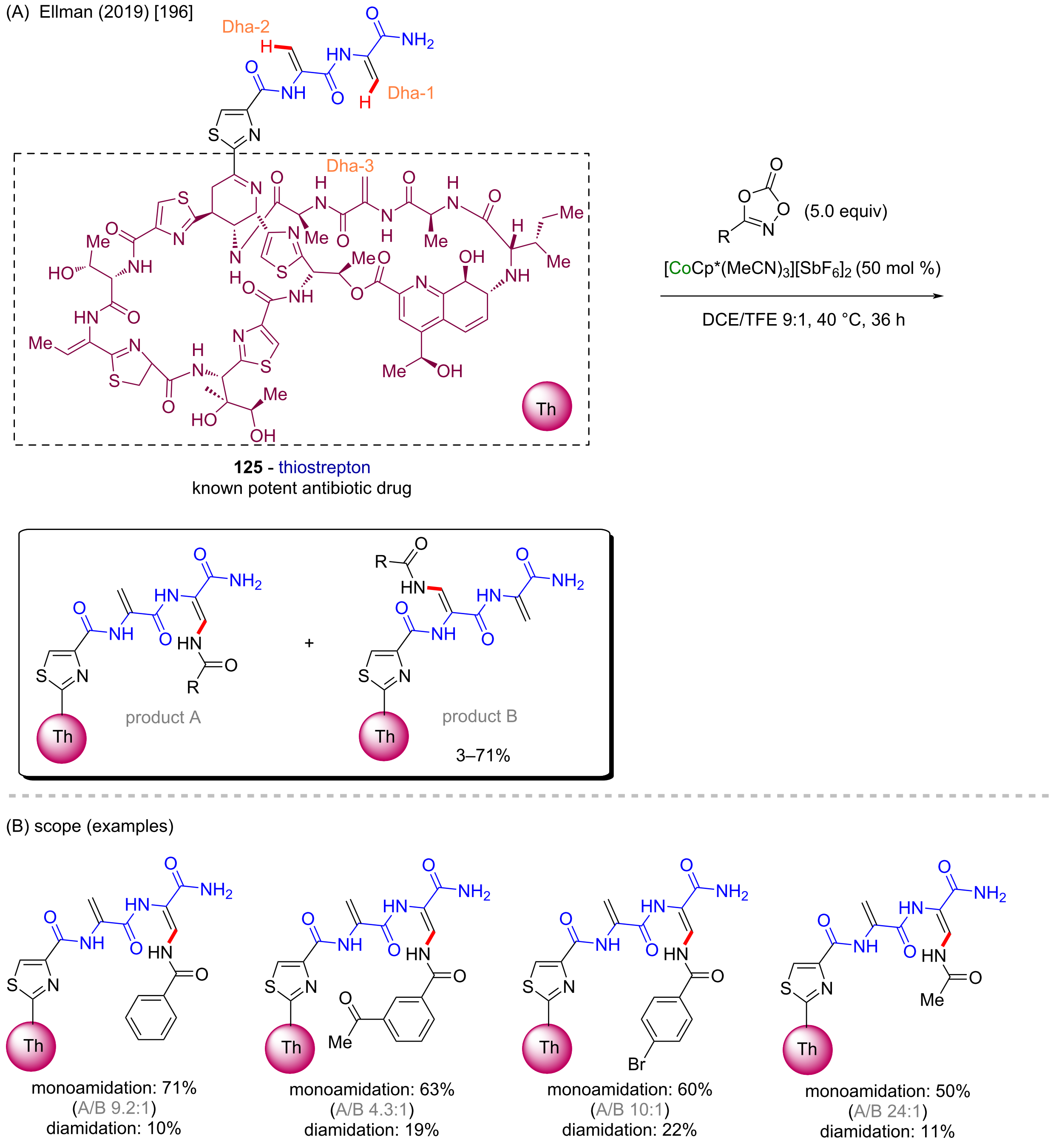
(A) Ellman (2019) [196]
Dha-2
Dha-1
Dha-3
Th
125 - thiostrepton
known potent antibiotic drug
(5.0 equiv)
[CoCp*(MeCN)3][SbF6]2 (50 mol %)
DCE/TFE 9:1, 40 °C, 36 h
product A
product B
3–71%
(B) scope (examples)
monoamidation: 71%
(A/B 9.2:1)
diamidation: 10%
monoamidation: 63%
(A/B 4.3:1)
diamidation: 19%
monoamidation: 60%
(A/B 10:1)
diamidation: 22%
monoamidation: 50%
(A/B 24:1)
diamidation: 11%

Scheme 38: (A and B) Cobalt-catalyzed C(sp^2)–H amidation of thiostrepton.

(Scheme 41C). The authors used the same method in a late-stage functionalization of the *ortho*-position of diflufenican (**138**, Scheme 41D), a known commercial pesticide [206].

Cinnamic acid and its derivatives **139**–**142** are commonly found in food consumed daily, and are known for their antidiabetic properties (Scheme 42A) [207]. In 2017, Mita, Sato, and co-workers published a C(sp^3)–H carboxylation using the same cobalt(acac)$_2$ catalyst mentioned in the previous example for the synthesis of cinnamic acid derivatives and analogues [208]. The authors used CO_2 as a carbonyl source in the presence of a Lewis acid ($AlMe_3$), and a bulky ligand (Xantphos), followed by acid treatment (Scheme 42B), to promote the tautomerization that leads to the formation of the desired terminal

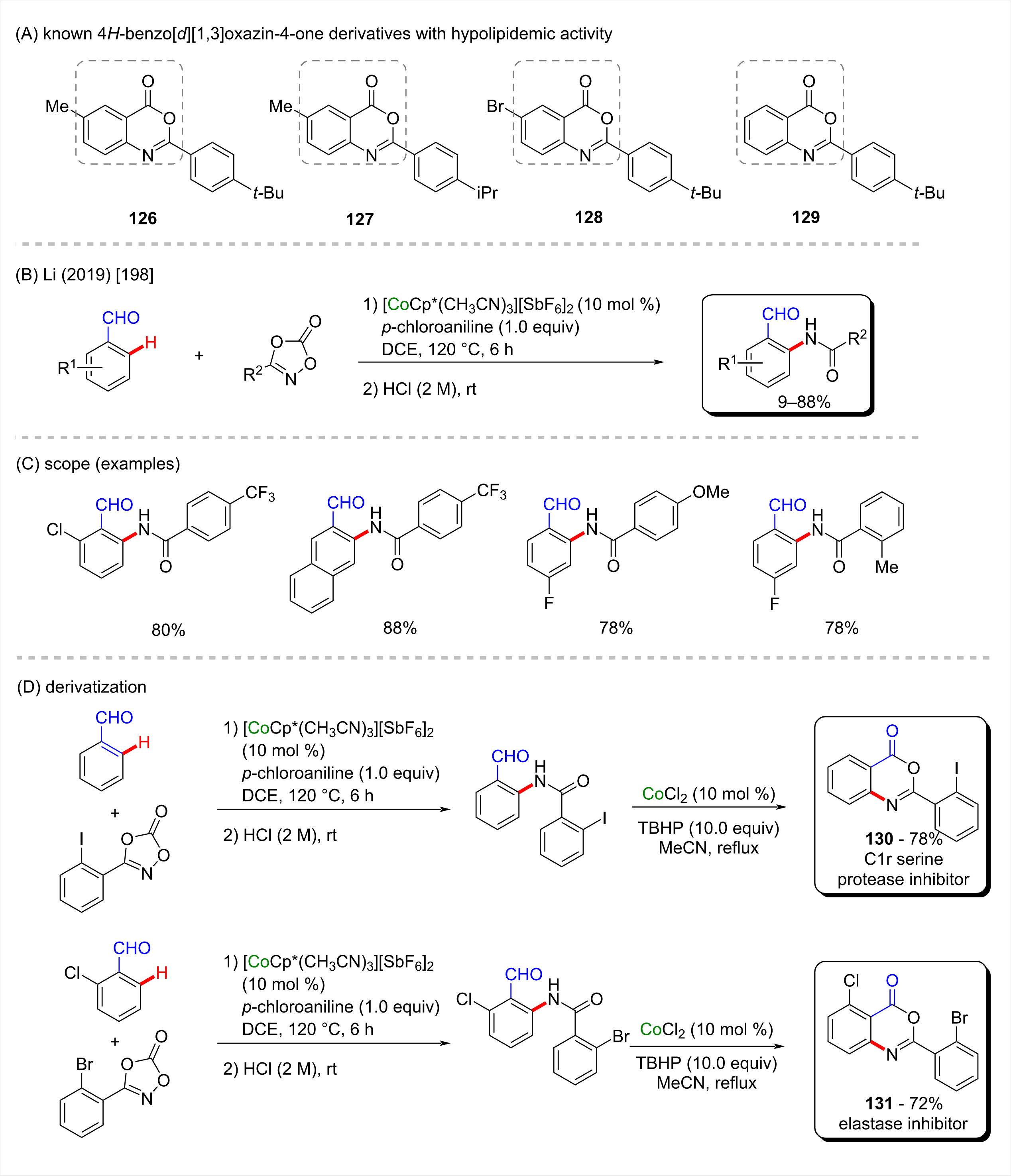
(A) known 4*H*-benzo[*d*][1,3]oxazin-4-one derivatives with hypolipidemic activity
Me
O
O
N
t-Bu
126
Me
iPr
127
Br
t-Bu
128
t-Bu
129
(B) Li (2019) [198]
CHO
H
R1
+
R2
N
O
1) [CoCp*(CH3CN)3][SbF6]2 (10 mol %)
p-chloroaniline (1.0 equiv)
DCE, 120 °C, 6 h
2) HCl (2 M), rt
9–88%
(C) scope (examples)
Cl
CF3
80%
88%
OMe
F
78%
Me
78%
(D) derivatization
1) [CoCp*(CH3CN)3][SbF6]2
(10 mol %)
p-chloroaniline (1.0 equiv)
DCE, 120 °C, 6 h
2) HCl (2 M), rt
I
CoCl2 (10 mol %)
TBHP (10.0 equiv)
MeCN, reflux
130 - 78%
C1r serine
protease inhibitor
Br
131 - 72%
elastase inhibitor

Scheme 39: (A) Known 4*H*-benzo[*d*][1,3]oxazin-4-one derivatives with hypolipidemic activity; (B and C) cobalt-catalyzed *ortho*-directed C–H amidation of benzaldehyde derivatives; (D) application of the synthesis to important enzyme inhibitors.

carboxylic acids in good yields (Scheme 42C). The chemo- and regioselective method was applied, along with other cyclization/oxidation methods for the preparation of a tricyclic quinoidal compound, resembling the structure of (+)-frenolicin B (**143**, Scheme 42D), a known natural product extracted from the ferment supernatant residue from *Streptomyces sp.* that presents fungicidal activity [209].

A cobalt(III)-catalyzed C–H borylation was described by Chirik and co-workers in 2017 where they used a unique chelated

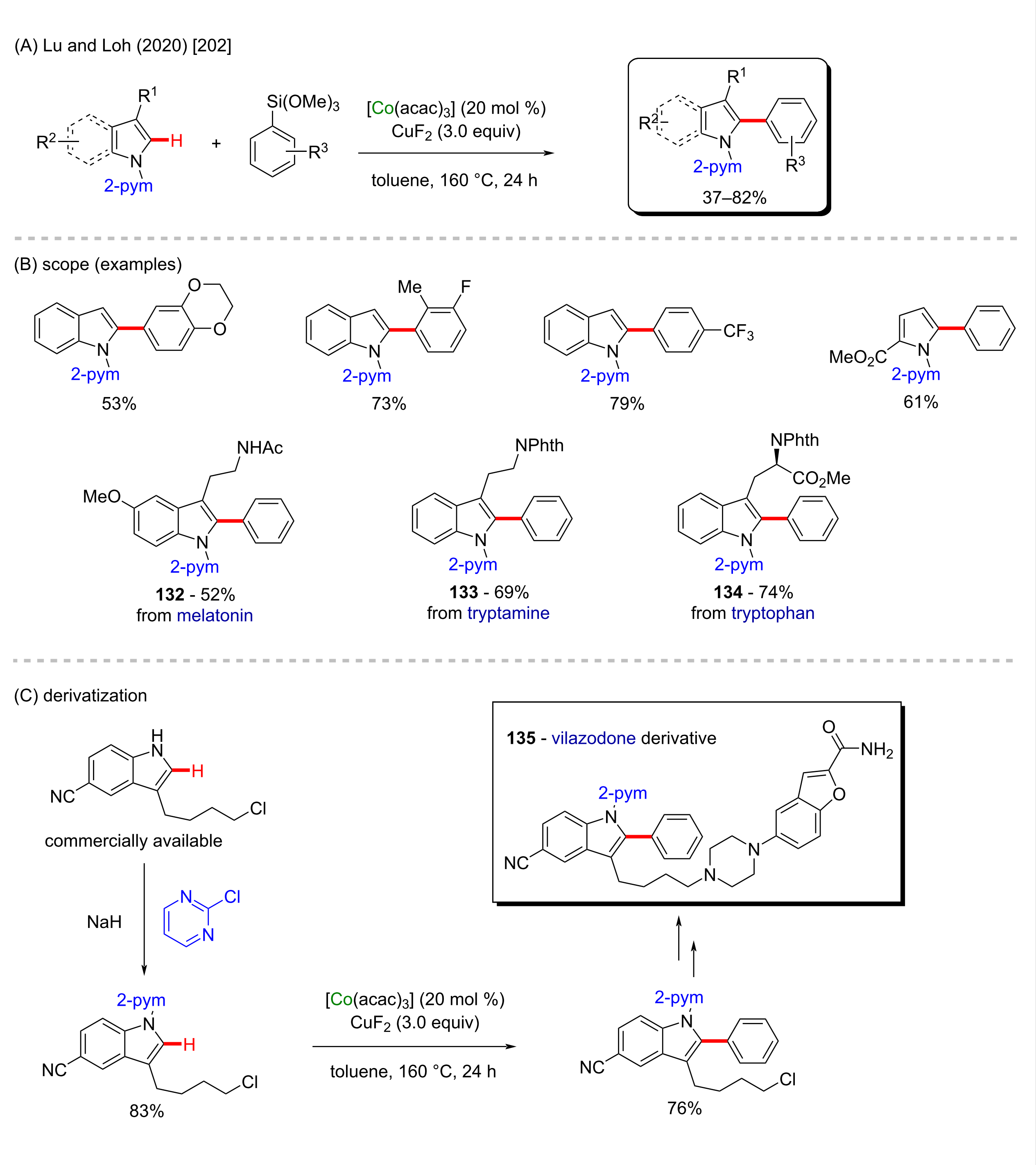
(A) Lu and Loh (2020) [202]
[Co(acac)3] (20 mol %)
CuF2 (3.0 equiv)
toluene, 160 °C, 24 h
37–82%
(B) scope (examples)
53%
73%
79%
61%
132 - 52%
from melatonin
133 - 69%
from tryptamine
134 - 74%
from tryptophan
(C) derivatization
commercially available
NaH
83%
76%
135 - vilazodone derivative
2-pym

Scheme 40: (A and B) Cobalt-catalyzed C–H arylation of pyrrole derivatives; (C) application for the synthesis of a vilazodone derivative.

cobalt catalyst (Scheme 43A) [210]. In this case, the electronic intrinsic effects of fluorinated arenes were responsible for the innate *ortho*-direction of this reaction, from which several borylated compounds were achieved in excellent yields. However, some of them were obtained as an *ortho/meta* mixture, with higher selectivity towards the *ortho*-isomers (Scheme 43B). Using the same method, the authors also described the successful synthesis of flurbiprofen (**144**), a potent anti-inflammatory drug [211], that was obtained in a four-step procedure, starting from the commercially available 3-iodofluorobenzene (Scheme 43C).

An interesting cobalt/ruthenium cross-coupling cyclization was described by Wu and Lei in 2015 [212]. In this work, the

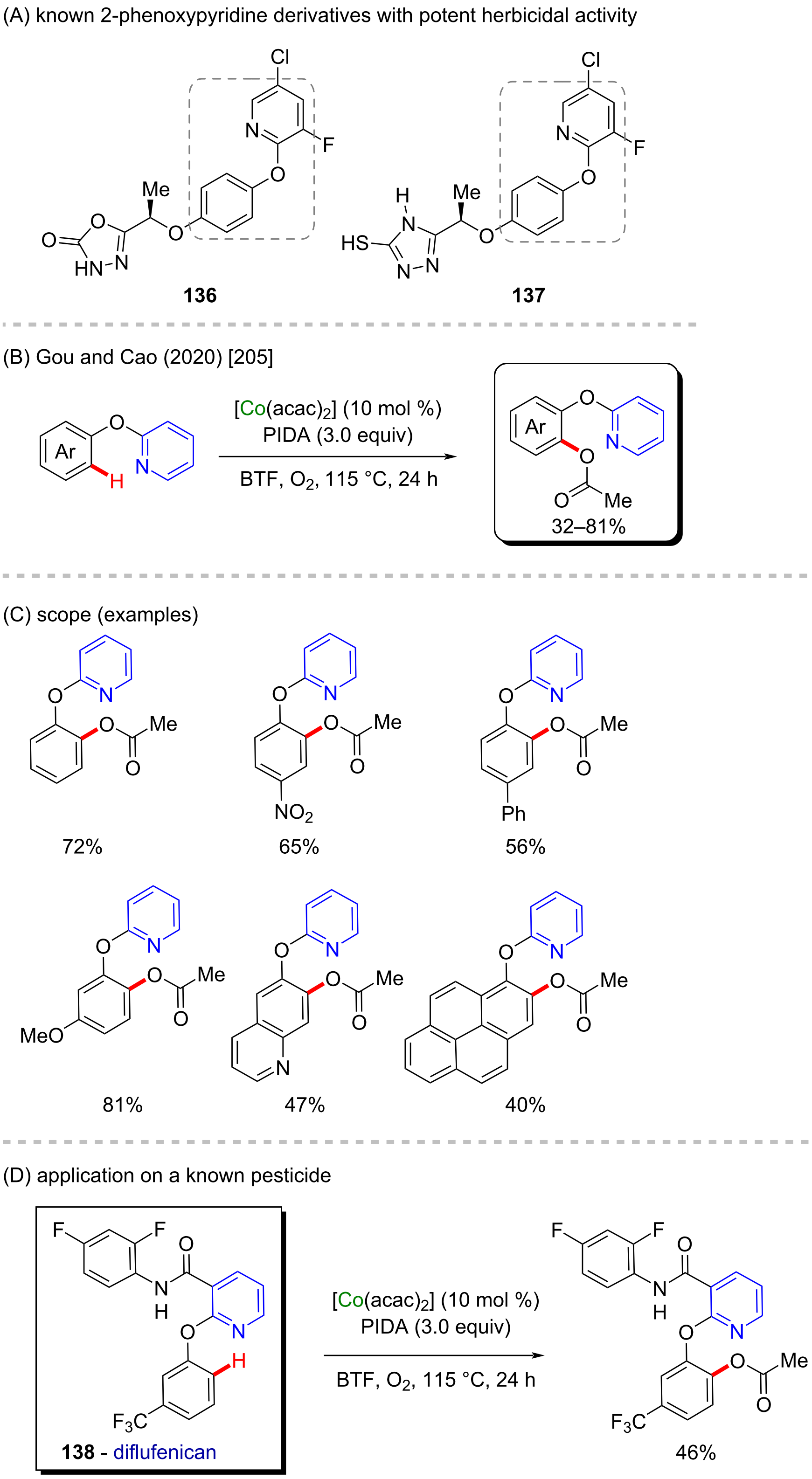
(A) known 2-phenoxypyridine derivatives with potent herbicidal activity
Cl
N
F
O
Me
O
O
HN
N
136
Cl
N
F
O
H
N
Me
HS
N
N
O
137
(B) Gou and Cao (2020) [205]
Ar
O
H
N
[Co(acac)2] (10 mol %)
PIDA (3.0 equiv)
BTF, O2, 115 °C, 24 h
Ar
O
N
O
O
Me
32–81%
(C) scope (examples)
72%
NO2
65%
Ph
56%
MeO
81%
N
47%
40%
(D) application on a known pesticide
F
F
O
N
H
N
O
H
F3C
138 - diflufenican
[Co(acac)2] (10 mol %)
PIDA (3.0 equiv)
BTF, O2, 115 °C, 24 h
F
F
O
N
H
N
O
O
Me
O
F3C
46%

Scheme 41: (A) Known 2-phenoxypyridine derivatives with potent herbicidal activity; (B and C) cobalt-catalyzed C–H acetoxylation of 2-(aryloxy)pyridine derivatives; (D) application to the functionalization of diflufenican (**138**).

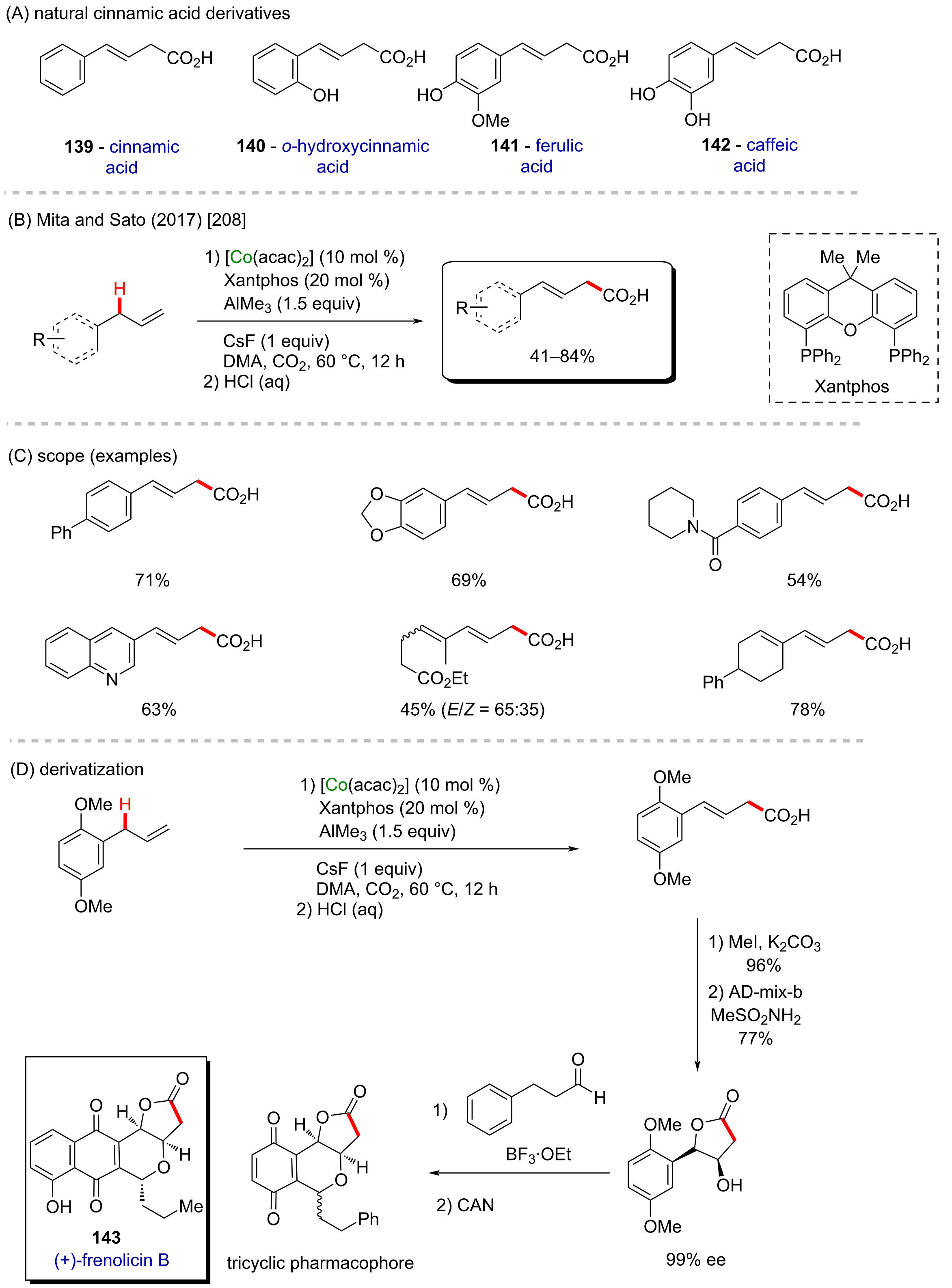
(A) natural cinnamic acid derivatives
CO2H
OH
HO
OMe
OH
139 - cinnamic acid
140 - o-hydroxycinnamic acid
141 - ferulic acid
142 - caffeic acid
(B) Mita and Sato (2017) [208]
H
R
1) [Co(acac)2] (10 mol %)
Xantphos (20 mol %)
AlMe3 (1.5 equiv)
CsF (1 equiv)
DMA, CO2, 60 °C, 12 h
2) HCl (aq)
41–84%
Me Me
O
PPh2
PPh2
Xantphos
(C) scope (examples)
Ph
71%
69%
N
O
54%
N
63%
CO2Et
45% (E/Z = 65:35)
Ph
78%
(D) derivatization
OMe
OMe
1) MeI, K2CO3
96%
2) AD-mix-b
MeSO2NH2
77%
99% ee
1) H
BF3·OEt
2) CAN
tricyclic pharmacophore
Me
143
(+)-frenolicin B

Scheme 42: (A) Natural cinnamic acid derivatives; (B and C) cobalt-catalyzed C–H carboxylation of terminal alkenes; (D) application of the method to the synthesis of a (+)-frenolicin B derivative (**143**).

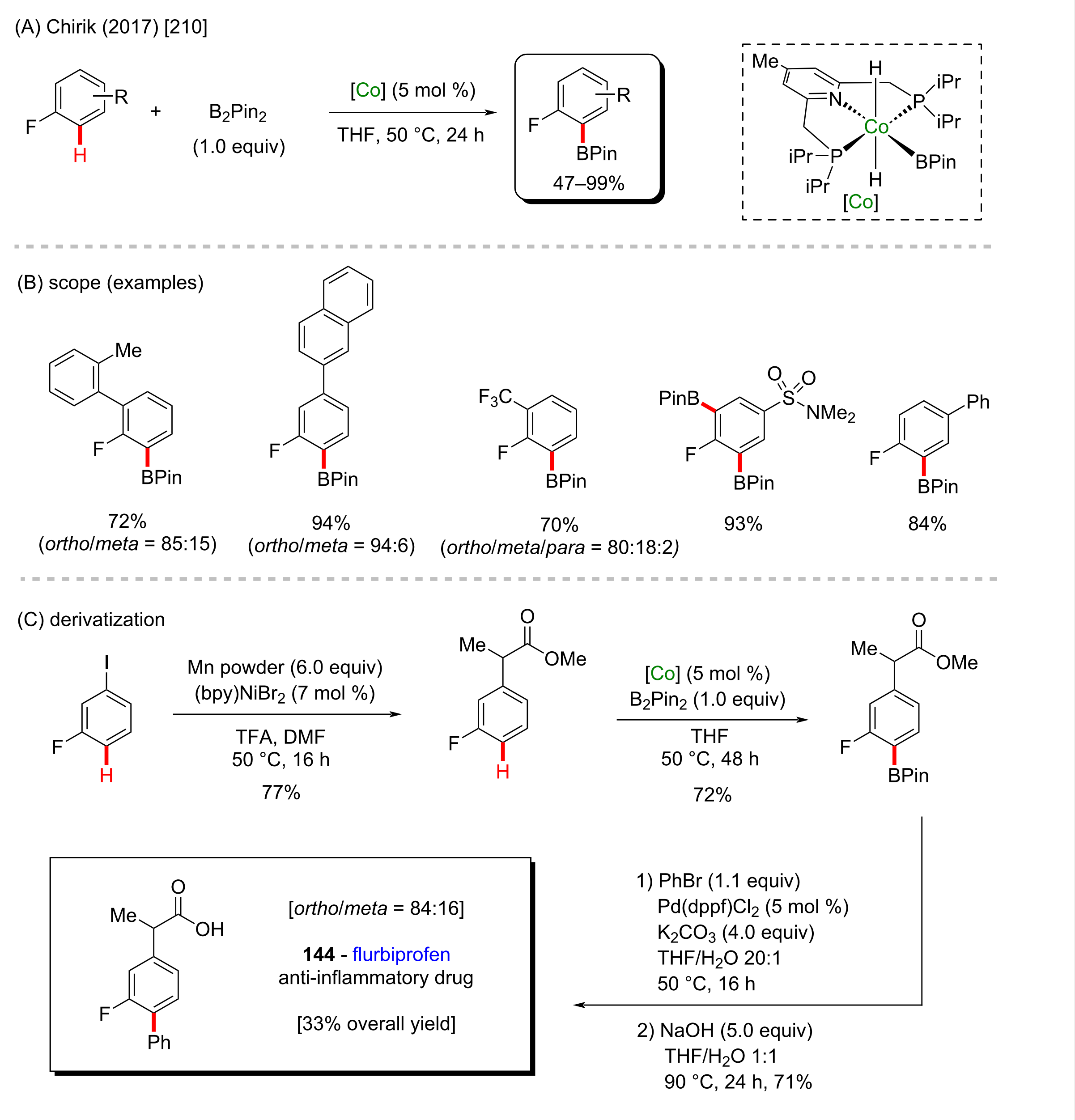
(A) Chirik (2017) [210]
F
H
R
+
B2Pin2
(1.0 equiv)
[Co] (5 mol %)
THF, 50 °C, 24 h
BPin
47–99%
Me
N
H
iPr
P
Co
iPr
iPr–P
iPr
H
BPin
[Co]
(B) scope (examples)
Me
BPin
72%
(ortho/meta = 85:15)
94%
(ortho/meta = 94:6)
F3C
70%
(ortho/meta/para = 80:18:2)
PinB
O
O
S
NMe2
93%
Ph
84%
(C) derivatization
I
Mn powder (6.0 equiv)
(bpy)NiBr2 (7 mol %)
TFA, DMF
50 °C, 16 h
77%
OMe
[Co] (5 mol %)
B2Pin2 (1.0 equiv)
THF
50 °C, 48 h
72%
1) PhBr (1.1 equiv)
Pd(dppf)Cl2 (5 mol %)
K2CO3 (4.0 equiv)
THF/H2O 20:1
50 °C, 16 h
2) NaOH (5.0 equiv)
THF/H2O 1:1
90 °C, 24 h, 71%
OH
Ph
[ortho/meta = 84:16]
144 - flurbiprofen
anti-inflammatory drug
[33% overall yield]

Scheme 43: (A and B) Cobalt-catalyzed C–H borylation; (C) application to the synthesis of flurbiprofen.

authors described an intramolecular photoredox cobalt-catalyzed C–H thiolation of thioamide substrates using two different methods (Scheme 44B). Using both methods, several benzothiazoles were obtained in excellent yields, most of them higher than 90% (Scheme 44C). Amongst the obtained products, one of them (**148**) is already known for its important antitumor activity [213]. Beyond that, benzothiazoles **145**–**147** present anticonvulsant activity (Scheme 44A) [214].

More simple cobalt(II) catalysts can also mediate valuable C–H activation processes, as exemplified by Stahl and co-workers in 2017 [215]. In this work, a cobalt-catalyzed aerobic oxidation leads to the formation of several ketones in good to excellent yields (Scheme 45A and B). One of the obtained products is a precursor of AMG 579 (**149**), an important phosphodiesterase 10A inhibitor (Scheme 45C) [216], being a potentially useful drug to treat schizophrenia.

Wang and co-workers described a C–H difluoroalkylation method using only cobalt(II) bromide as catalyst (Scheme 46B) [217]. This fact represents a simple and highly accessible method for the synthesis of important compounds in good to excellent yields (Scheme 46C), mostly tetralones, an organic

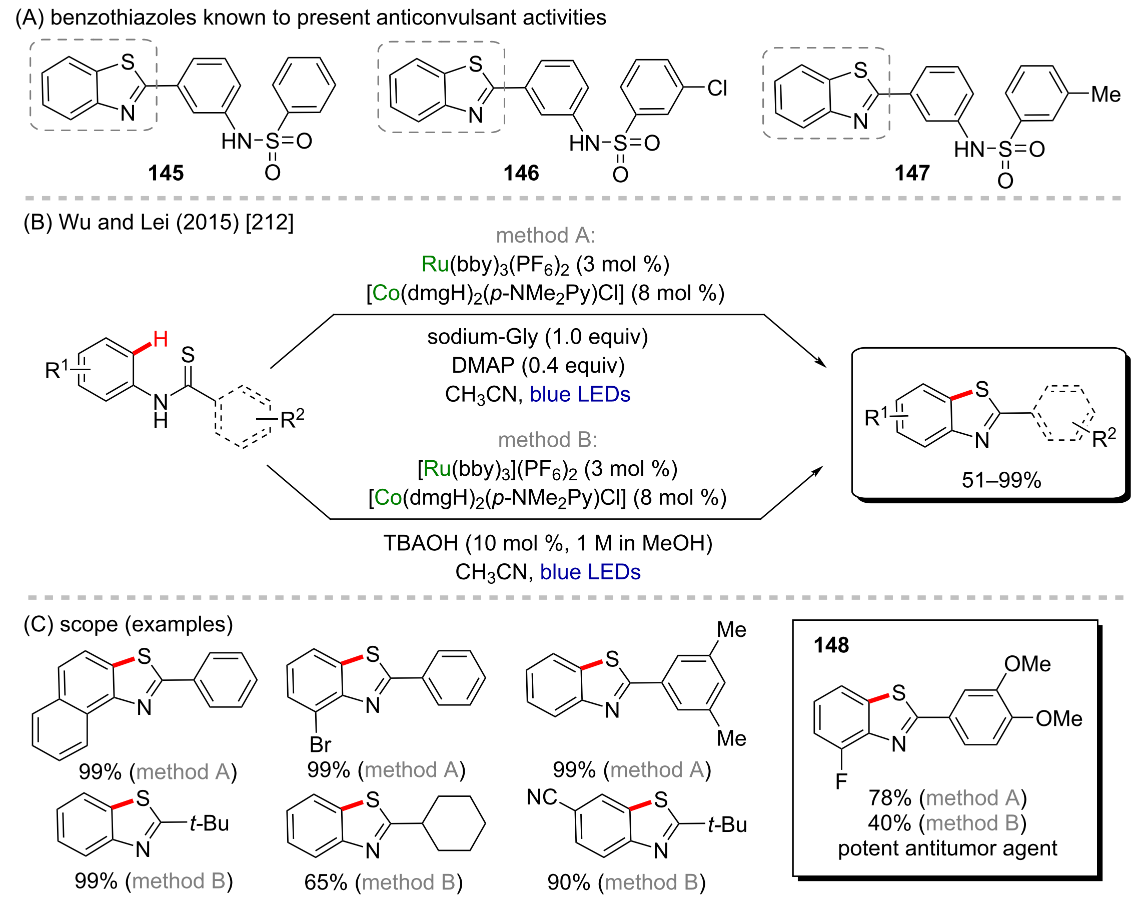
(A) benzothiazoles known to present anticonvulsant activities
145
146
147
Cl
Me
HN-S=O
(B) Wu and Lei (2015) [212]
method A:
Ru(bby)$_3$(PF$_6$)$_2$ (3 mol %)
[Co(dmgH)$_2$(*p*-NMe$_2$Py)Cl] (8 mol %)
sodium-Gly (1.0 equiv)
DMAP (0.4 equiv)
CH$_3$CN, blue LEDs
method B:
[Ru(bby)$_3$](PF$_6$)$_2$ (3 mol %)
[Co(dmgH)$_2$(*p*-NMe$_2$Py)Cl] (8 mol %)
TBAOH (10 mol %, 1 M in MeOH)
CH$_3$CN, blue LEDs
R^1
R^2
51–99%
(C) scope (examples)
99% (method A)
Br
99% (method A)
Me
Me
99% (method A)
t-Bu
99% (method B)
65% (method B)
NC
t-Bu
90% (method B)
148
OMe
OMe
F
78% (method A)
40% (method B)
potent antitumor agent

Scheme 44: (A) Benzothiazoles known to present anticonvulsant activities; (B and C) cobalt/ruthenium-catalyzed cross-coupling reaction towards an intramolecular cyclization via the C–H thiolation of thioamides.

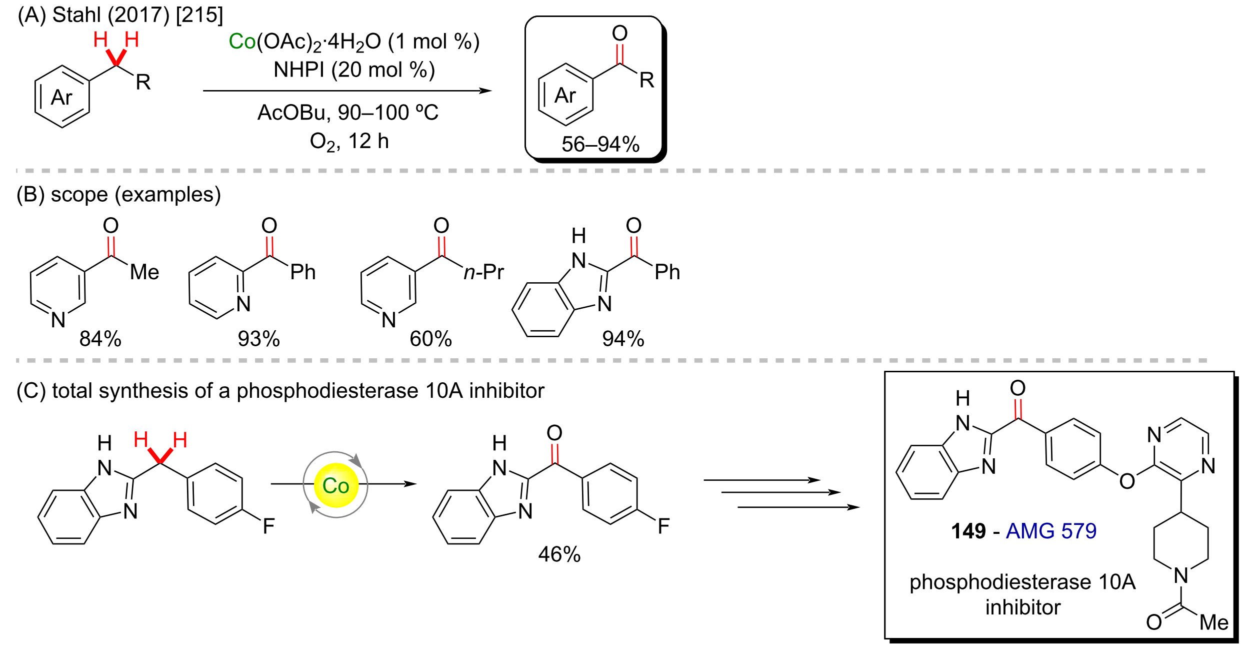
(A) Stahl (2017) [215]
Ar
R
Co(OAc)$_2$·4H$_2$O (1 mol %)
NHPI (20 mol %)
AcOBu, 90–100 ºC
O$_2$, 12 h
56–94%
(B) scope (examples)
Me
84%
Ph
93%
n-Pr
60%
Ph
94%
(C) total synthesis of a phosphodiesterase 10A inhibitor
Co
F
46%
149 - AMG 579
phosphodiesterase 10A inhibitor
Me

Scheme 45: (A and B) Cobalt-catalyzed oxygenation of methylene groups towards ketone synthesis; (C) synthesis of the AMG 579 precursor **149**.

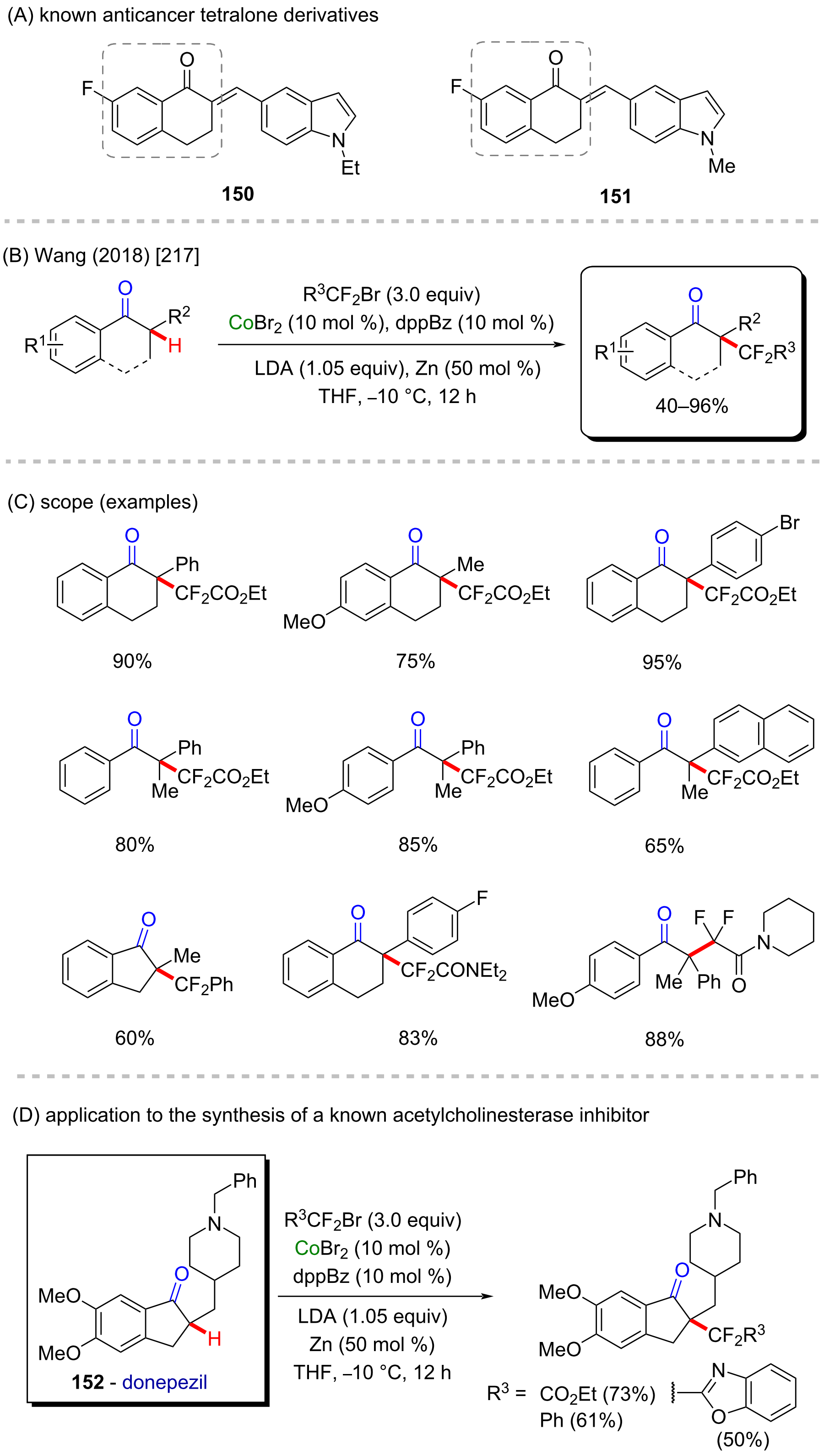
(A) known anticancer tetralone derivatives
150
151
(B) Wang (2018) [217]
R3CF2Br (3.0 equiv)
CoBr2 (10 mol %), dppBz (10 mol %)
LDA (1.05 equiv), Zn (50 mol %)
THF, –10 °C, 12 h
40–96%
(C) scope (examples)
90%
75%
95%
80%
85%
65%
60%
83%
88%
(D) application to the synthesis of a known acetylcholinesterase inhibitor
152 - donepezil
R3CF2Br (3.0 equiv)
CoBr2 (10 mol %)
dppBz (10 mol %)
LDA (1.05 equiv)
Zn (50 mol %)
THF, –10 °C, 12 h
R3 = CO2Et (73%)
Ph (61%)
(50%)

Scheme 46: (A) Known anticancer tetralone derivatives; (B and C) cobalt-catalyzed C–H difluoroalkylation of aryl ketones; (D) application of the method using donepezil (**152**) as the substrate.

function present in anticancer substances (compounds **150** and **151**, Scheme 46A) [218]. The authors described a late-stage application of this new method using donepezil (**152**) as substrate (Scheme 46D), a well-known acetylcholinesterase inhibitor used to treat Alzheimer's disease [219].

A successful *ortho*-directed cobalt-catalyzed C–H thiolation was described by Wang and co-workers in 2018 [220], also using solely cobalt(II) bromide as the cobalt source (Scheme 47A). Through this process, several *ortho*-activated products were obtained in good yields (Scheme 47B). The authors applied the process as one of the five steps towards the synthesis of quetiapine (**153**, Scheme 47C), a known antipsychotic agent [221].

Benzoxazoles belong to a class of organic compounds known to present several biological activities, such as anticancer, antibacterial, and antifungal effects (compounds **154**, **155**, and **156**, Scheme 48A) [222]. Wang and co-workers described an important cobalt-catalyzed C–H/C–H cross-coupling reaction using cobalt(II) acetate and silver(I) carbonate (Scheme 48B) [223]. This method enabled the formation of 2-(2-arylphenyl)azoles, mostly benzoxazoles, in moderate to good yields (Scheme 48C). The authors also modified the directing-group moiety of two products and one of the substrates and explored the fungicidal activity of the obtained final products (Scheme 48D) against four fungal species: *Fusarium graminearum*, *Physalospora piricola*, *Rhizactonia cerealis*, and *Bipolaris maydis*. A comparison of the observed activities to the activity of bixafen (**157**, a

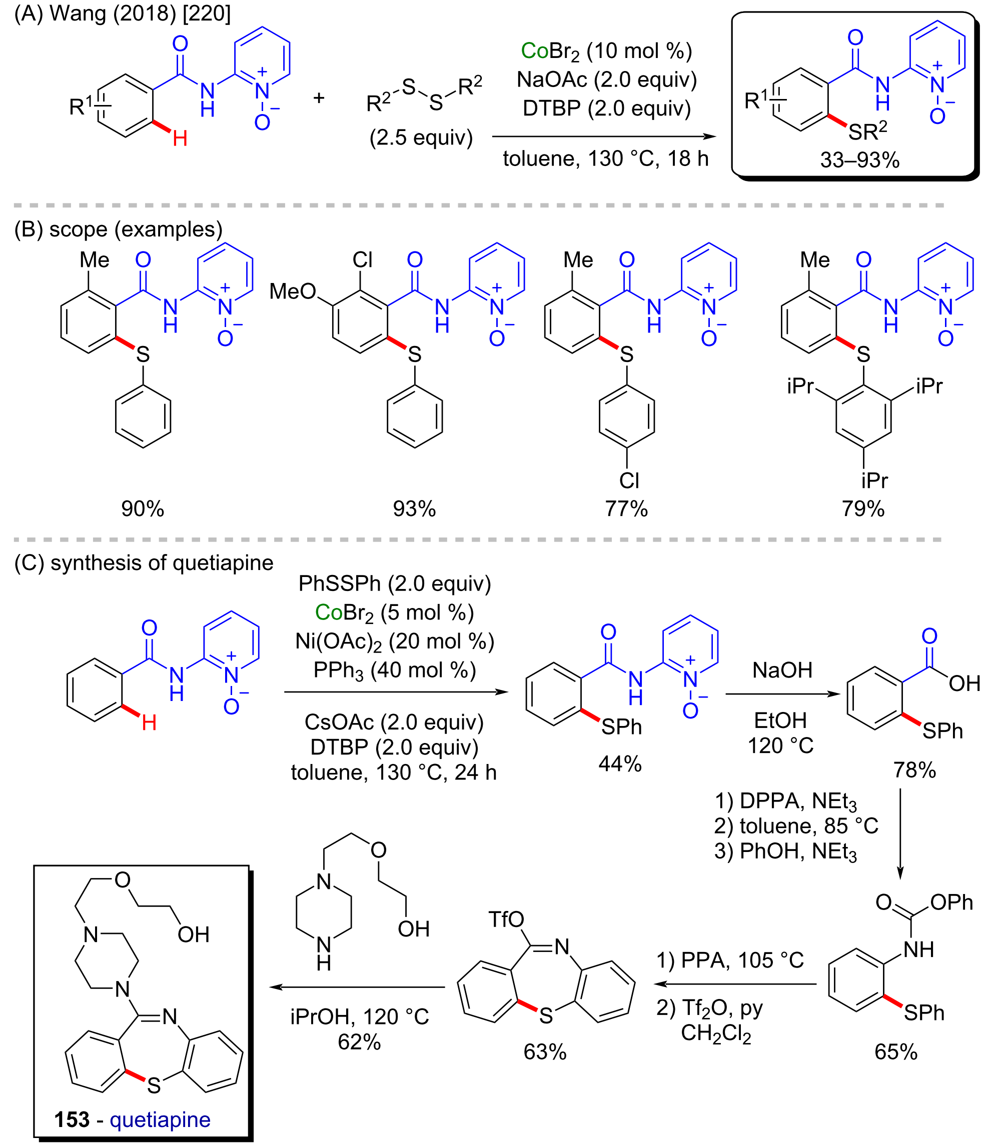

(A) Wang (2018) [220]
(2.5 equiv)
CoBr2 (10 mol %)
NaOAc (2.0 equiv)
DTBP (2.0 equiv)
toluene, 130 °C, 18 h
33–93%
(B) scope (examples)
90%
93%
77%
79%
(C) synthesis of quetiapine
PhSSPh (2.0 equiv)
CoBr2 (5 mol %)
Ni(OAc)2 (20 mol %)
PPh3 (40 mol %)
CsOAc (2.0 equiv)
DTBP (2.0 equiv)
toluene, 130 °C, 24 h
44%
NaOH
EtOH
120 °C
78%
1) DPPA, NEt3
2) toluene, 85 °C
3) PhOH, NEt3
65%
1) PPA, 105 °C
2) Tf2O, py
CH2Cl2
63%
iPrOH, 120 °C
62%
153 - quetiapine

Scheme 47: (A and B) Cobalt-catalyzed C–H thiolation; (C) application in the synthesis of quetiapine (**153**).

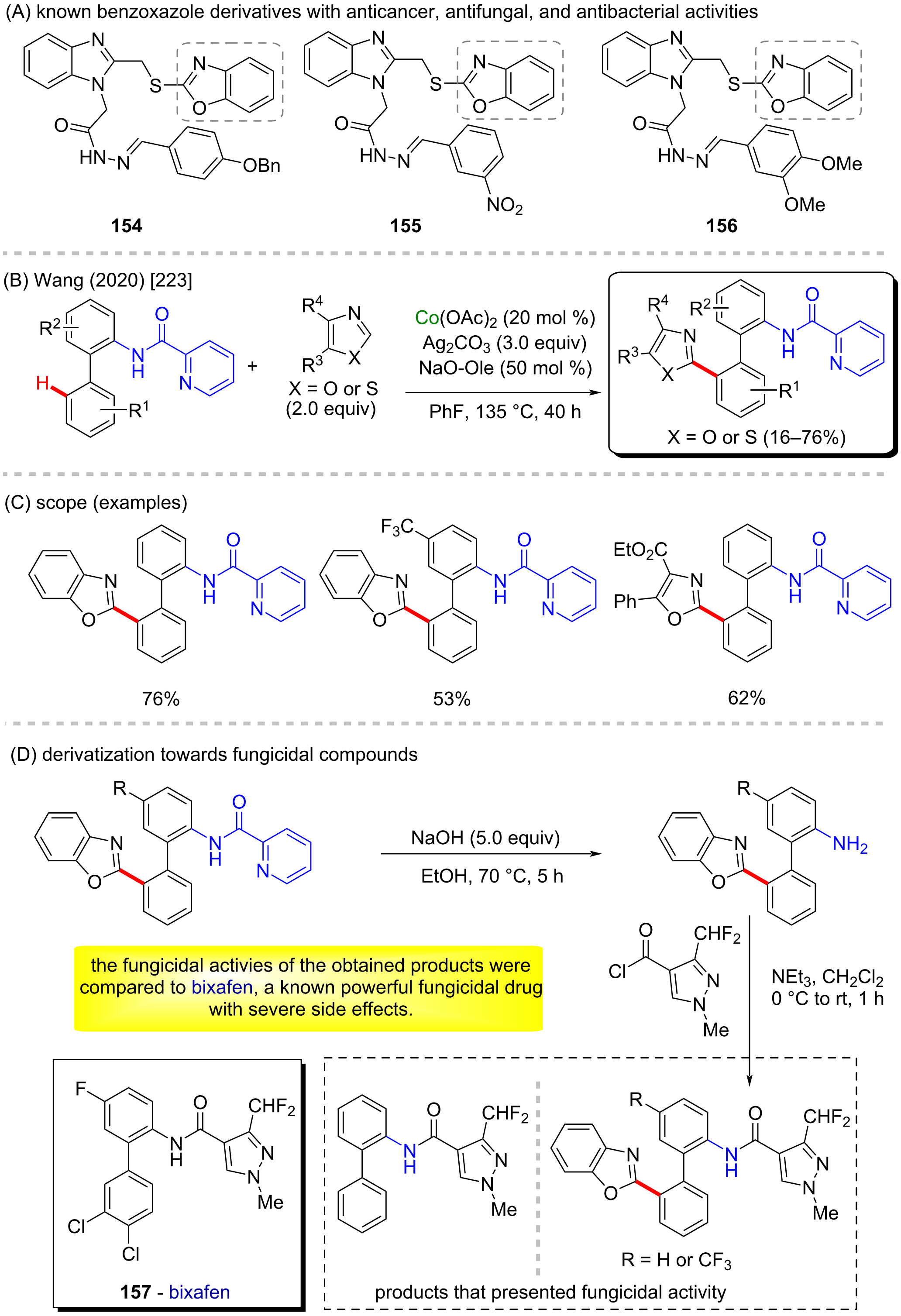
(A) known benzoxazole derivatives with anticancer, antifungal, and antibacterial activities

(B) Wang (2020) [223]

(C) scope (examples)

(D) derivatization towards fungicidal compounds

the fungicidal activies of the obtained products were compared to bixafen, a known powerful fungicidal drug with severe side effects.

products that presented fungicidal activity

154
155
156
OBn
NO2
OMe
OMe
R1
R2
R3
R4
X = O or S
(2.0 equiv)
Co(OAc)2 (20 mol %)
Ag2CO3 (3.0 equiv)
NaO-Ole (50 mol %)
PhF, 135 °C, 40 h
X = O or S (16–76%)
76%
53%
62%
F3C
EtO2C
Ph
NaOH (5.0 equiv)
EtOH, 70 °C, 5 h
NH2
NEt3, CH2Cl2
0 °C to rt, 1 h
CHF2
Me
R = H or CF3
157 - bixafen

Scheme 48: (A) Known benzoxazole derivatives with anticancer, antifungal, and antibacterial activities; (B and C) cobalt-catalyzed C–H/C–H cross-coupling; (D) synthesis of compounds with antifungal activities.

known fungicidal agent with severe side effects [224]) indicated that the new compounds presented valuable biological activity and may represent promising new antifungal drugs.

Wu and co-workers reported a cobalt-catalyzed C–H carbonylation of naphthylamides to afford a series of free *NH*-benzo[*cd*]indol-2-(1*H*)-ones in moderate to high yields

(Scheme 49A and B). This carbonylative methodology uses the practical and helpful solid reagent benzene-1,3,5-triyl triformate (TBFen) as a CO source [225]. The further application of this efficient C–H functionalization protocol demonstrated by the authors consisted in the synthesis of biologically active compounds containing the benzo[*cd*]indol-2-(1*H*)-one core which were shown to act as inhibitors of the Bromodomain and Extra-Terminal (BET) family A and B (compounds **158** and

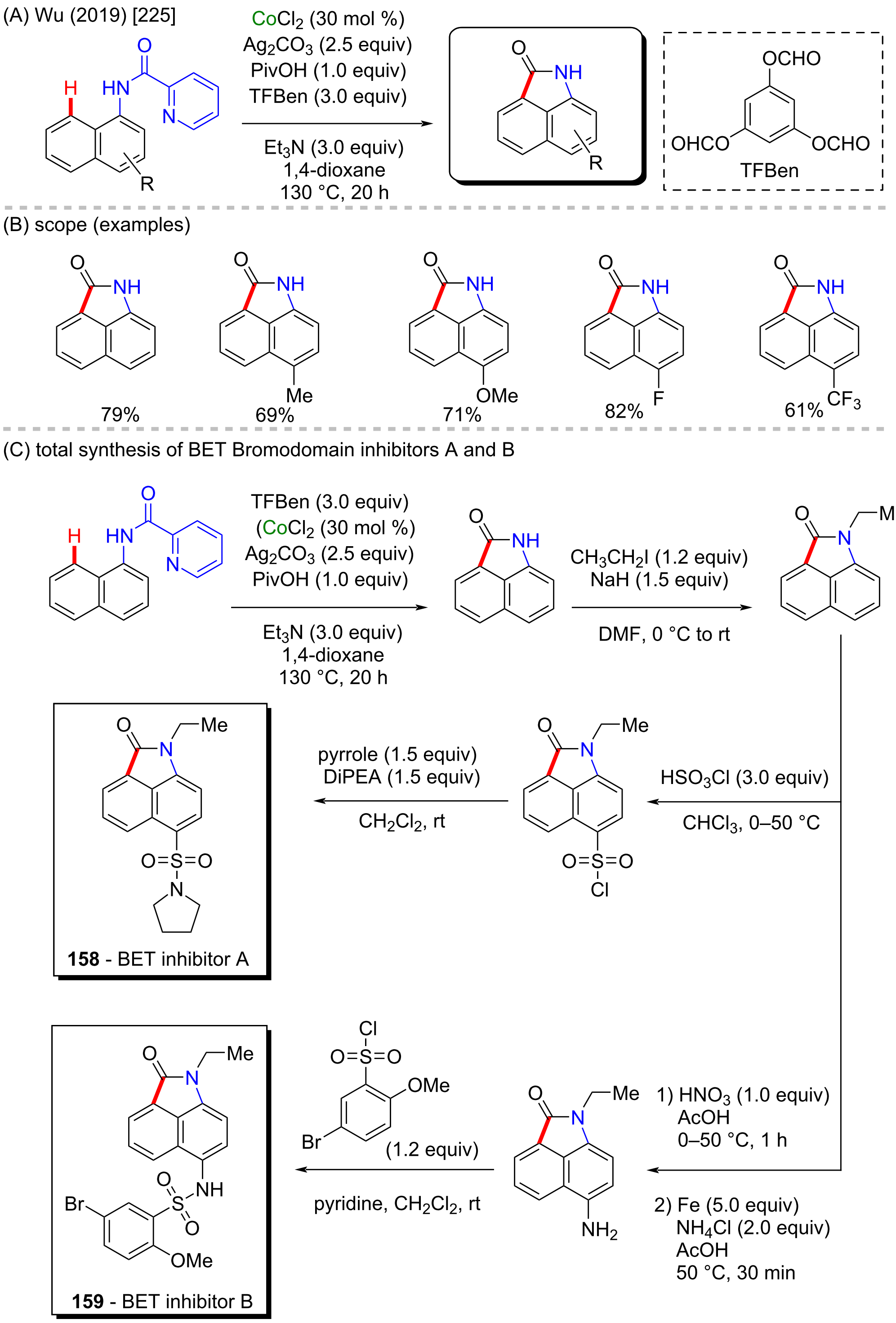
(A) Wu (2019) [225]
H
HN
O
N
R
CoCl2 (30 mol %)
Ag2CO3 (2.5 equiv)
PivOH (1.0 equiv)
TFBen (3.0 equiv)
Et3N (3.0 equiv)
1,4-dioxane
130 °C, 20 h
O
NH
R
OCHO
OHCO
OCHO
TFBen
(B) scope (examples)
O
NH
79%
Me
69%
OMe
71%
F
82%
CF3
61%
(C) total synthesis of BET Bromodomain inhibitors A and B
TFBen (3.0 equiv)
(CoCl2 (30 mol %)
Ag2CO3 (2.5 equiv)
PivOH (1.0 equiv)
Et3N (3.0 equiv)
1,4-dioxane
130 °C, 20 h
CH3CH2I (1.2 equiv)
NaH (1.5 equiv)
DMF, 0 °C to rt
Me
N
HSO3Cl (3.0 equiv)
CHCl3, 0–50 °C
O=S=O
Cl
pyrrole (1.5 equiv)
DiPEA (1.5 equiv)
CH2Cl2, rt
158 - BET inhibitor A
1) HNO3 (1.0 equiv)
AcOH
0–50 °C, 1 h
2) Fe (5.0 equiv)
NH4Cl (2.0 equiv)
AcOH
50 °C, 30 min
NH2
Br
(1.2 equiv)
pyridine, CH2Cl2, rt
S
159 - BET inhibitor B

Scheme 49: (A and B) Cobalt-catalyzed C–H carbonylation of naphthylamides; (C) BET inhibitors **158** and **159** total synthesis.

159, Scheme 49C) [226]. The BET family of proteins plays an important role in gene transcription and epigenetics by binding acetylated lysines and has emerged as a driver of tumorigenesis in diverse human cancers. In this sense, the inhibition of BET proteins is an attractive target for cancer drug discovery [227,228].

In a similar approach, Ying, Wu, and co-workers, reported the synthesis of the (*NH*)-indolo[1,2-*a*]quinoxaline-6(5*H*)-one core through a cobalt-catalyzed direct C–H carbonylative annulation of *N*-arylindoles using picolinamide as the directing group and employing TFBen as the CO source (Scheme 50B and C) [229]. This methodology was applied to a pyrrole derivative affording

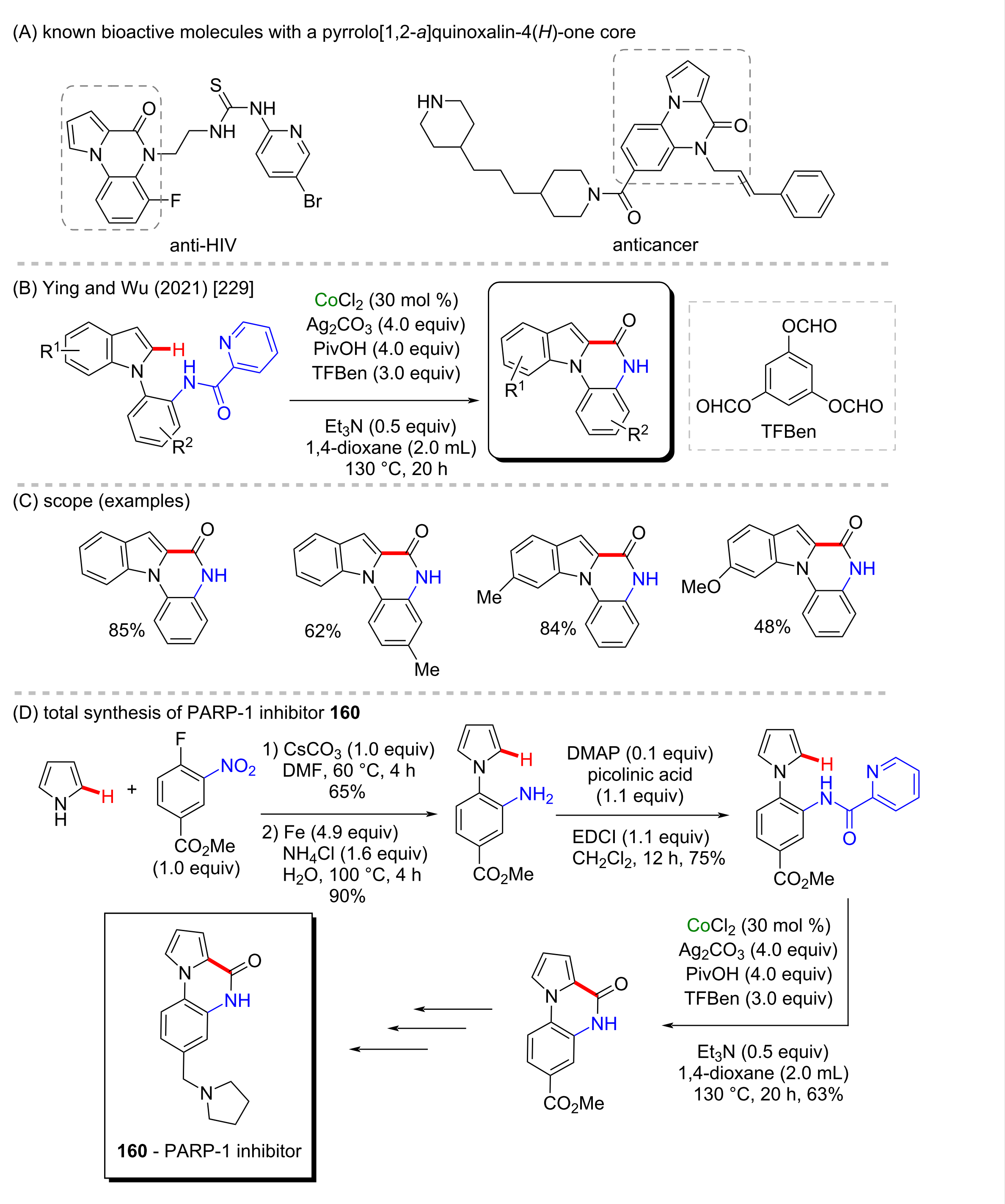
(A) known bioactive molecules with a pyrrolo[1,2-a]quinoxalin-4(H)-one core
anti-HIV
anticancer
(B) Ying and Wu (2021) [229]
CoCl2 (30 mol %)
Ag2CO3 (4.0 equiv)
PivOH (4.0 equiv)
TFBen (3.0 equiv)
Et3N (0.5 equiv)
1,4-dioxane (2.0 mL)
130 °C, 20 h
TFBen
(C) scope (examples)
85%
62%
84%
48%
(D) total synthesis of PARP-1 inhibitor 160
1) CsCO3 (1.0 equiv)
DMF, 60 °C, 4 h
65%
2) Fe (4.9 equiv)
NH4Cl (1.6 equiv)
H2O, 100 °C, 4 h
90%
(1.0 equiv)
DMAP (0.1 equiv)
picolinic acid
(1.1 equiv)
EDCI (1.1 equiv)
CH2Cl2, 12 h, 75%
CoCl2 (30 mol %)
Ag2CO3 (4.0 equiv)
PivOH (4.0 equiv)
TFBen (3.0 equiv)
Et3N (0.5 equiv)
1,4-dioxane (2.0 mL)
130 °C, 20 h, 63%
160 - PARP-1 inhibitor

Scheme 50: (A) Known bioactive pyrrolo[1,2-*a*]quinoxalin-4(5*H*)-one derivatives; (B and C) cobalt-catalyzed C–H carbonylation of *N*-arylindole derivatives; (D) PARP-1 inhibitor **160** total synthesis.

the pyrrolo[1,2-*a*]quinoxaline-(4*H*)-one skeleton, that after reductive amination afforded the poly(ADP-ribose)polymerase-1 (PARP-1) inhibitor **160** (Scheme 50D). PARP-1 is a nuclear enzyme that acts in some crucial cellular processes such as DNA repair and programmed cell death and is seen as a potential auxiliary in cancer treatment [230]. It is important to highlight here that this basic core is present in several known bioactive molecules [231] (Scheme 50A).

Cyclic sulfonamides are encountered in compounds presenting potent antibacterial properties (compounds **161** and **162**, Scheme 51A) [232]. In 2014, Lu and Zhang reported a chemoselective intramolecular amination of propargylic C–H bonds of sulfamoyl azides using a cobalt–porphyrin complex ([Co(P1)]) as the catalyst (Scheme 51B). This cobalt–porphyrin complex exists as a stable metalloradical and was found to effectively activate azides as nitrene sources for the amination of the prob-

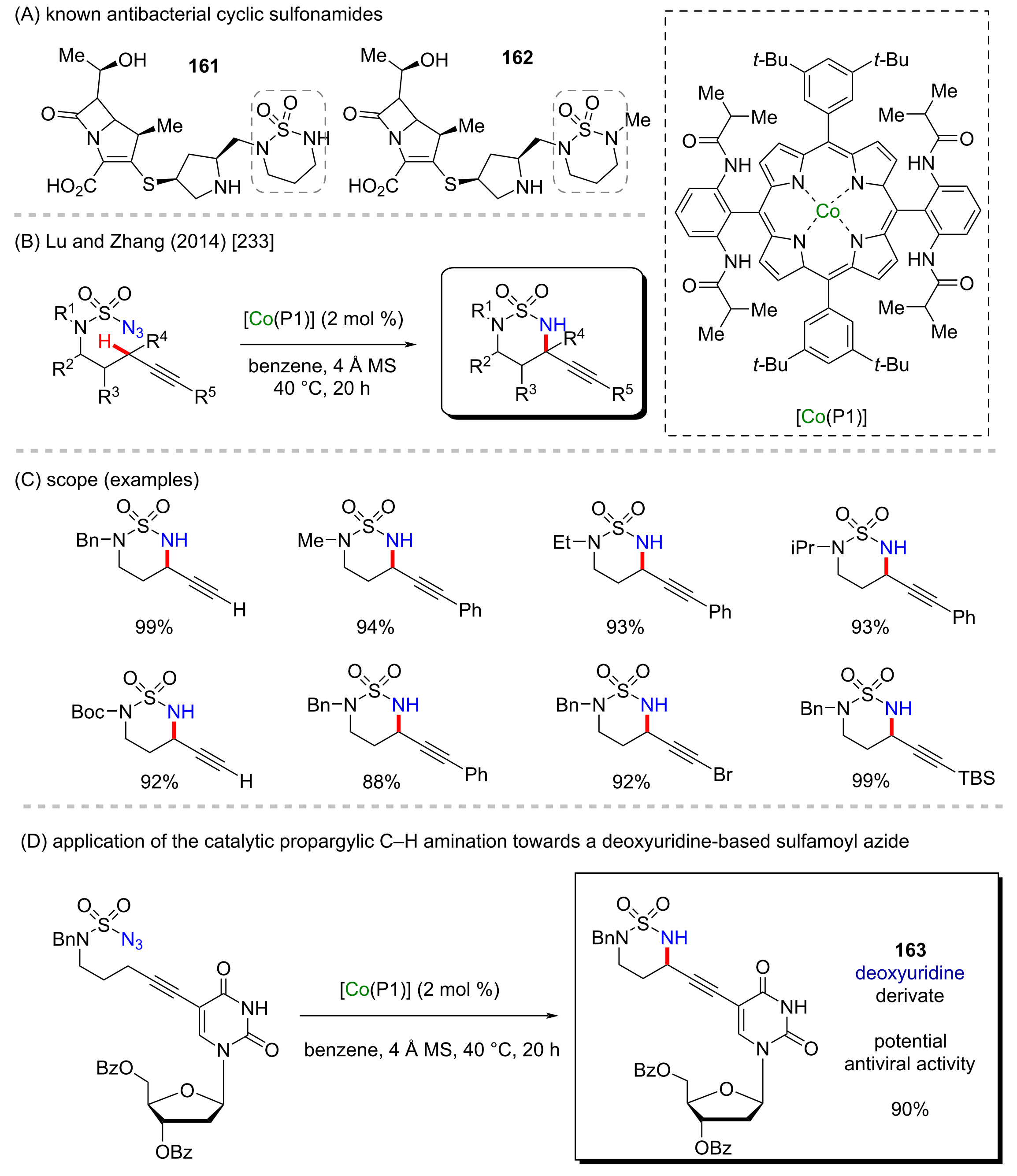
(A) known antibacterial cyclic sulfonamides
161
162
(B) Lu and Zhang (2014) [233]
[Co(P1)] (2 mol %)
benzene, 4 Å MS
40 °C, 20 h
[Co(P1)]
(C) scope (examples)
99%
94%
93%
93%
92%
88%
92%
99%
(D) application of the catalytic propargylic C–H amination towards a deoxyuridine-based sulfamoyl azide
[Co(P1)] (2 mol %)
benzene, 4 Å MS, 40 °C, 20 h
163
deoxyuridine
derivate
potential
antiviral activity
90%

Scheme 51: (A) Known antibacterial cyclic sulfonamides; (B and C) cobalt-catalyzed C–H amination of propargylic C–H bonds; (D) application of the method towards the synthesis of a deoxyuridine-based sulfamoyl azide.

lematic propargylic C–H bonds [233]. Generally, the electrophilic nature of this bond makes the C≡C bonds preferred for amination over the propargylic bonds [234]. However, the reaction conditions allowed the practical access to numerous unsymmetric sulfamide derivatives (Scheme 51C). To prove the potential of the protocol in late-stage functionalizations, the authors synthesized the deoxyuridine derivative **163** (Scheme 51D). Deoxyuridine is similar to drugs like idoxuridine and trifluridine, which have been used as antiviral drugs [235].

In another interesting work, Lu and Zhang demonstrated the application of this protocol to construct new strained 5-membered cyclic sulfamides via a chemoselective intramolecular 1,5-C(sp^3)–H amination. The cobalt(II)-based metalloradical (MRC) catalysis afforded the desired sulfamides in high yields and with nitrogen gas as the only byproduct (Scheme 52A and B) [236]. The application of this methodology in a late-stage functionalization of biologically active compounds was demonstrated by the [Co(P1)]-catalyzed 1,5-C–H amination of the allylic C–H bond of stigmasterol-based azide **164** in a chemo- and stereoselective fashion in 70% yield (Scheme 52C).

Biaryl synthesis often is performed through well-established cross-coupling reactions. However, this type of reaction possesses some drawbacks like the necessity of prefunctionalized starting materials and the production of relatively expensive and stoichiometric amounts of toxic byproducts [237,238]. In 2018, Zhang and co-workers developed a method for biaryl synthesis involving the cobalt-assisted C–H/C–H cross-coupling between benzamides and oximes (Scheme 53A and B) [239]. Further transformations of the resulted biaryl compounds included a Beckmann rearrangement affording 2-amino-2′-carboxybiaryls, which are valuable synthetic precursors of some bioactive compounds [240]. Another example of a suitable post-modification of biaryl compounds was exemplified by the synthesis of benzazepine derivative **165**, as described by the authors (Scheme 53C). Benzazepines are present in some important pharmaceutical compounds, such as the antipsychotic drug clozapine [241,242].

Several isoquinoline derivatives have been studied for their anticancer activity (compounds **166** and **167** in Scheme 54A) [243]. Zhu and co-workers reported a cobalt-catalyzed C(sp^2)–H 2-hydrazinylpyridine-directed C–H annulation with

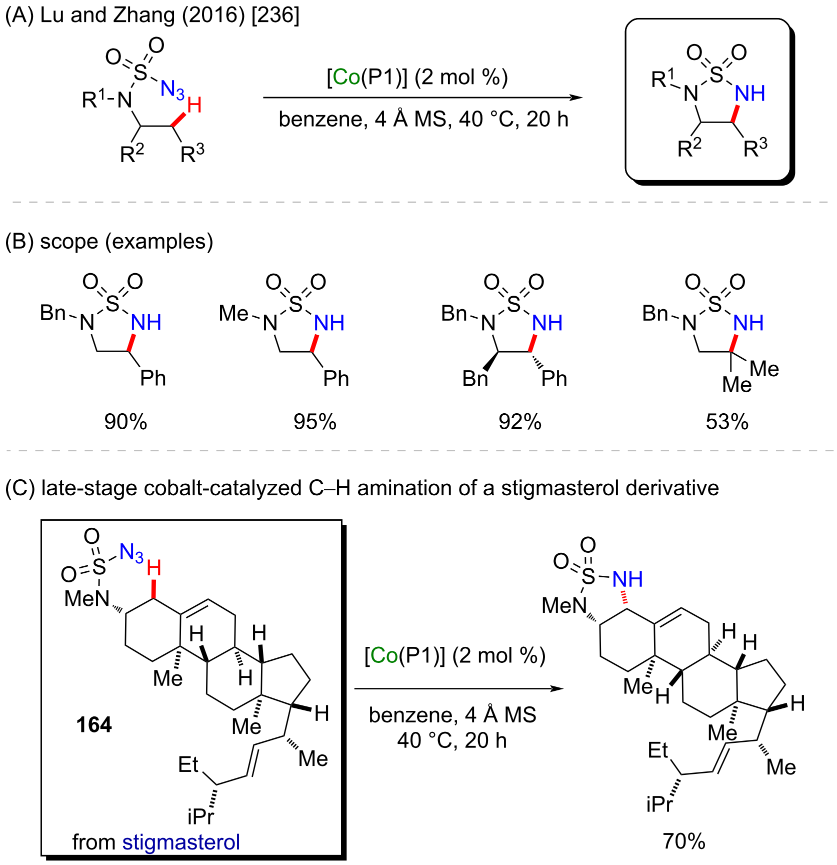
(A) Lu and Zhang (2016) [236]
R1-N
N3
H
R2
R3
[Co(P1)] (2 mol %)
benzene, 4 Å MS, 40 °C, 20 h
NH
(B) scope (examples)
Bn
Me
Ph
Me
90%
95%
92%
53%
(C) late-stage cobalt-catalyzed C–H amination of a stigmasterol derivative
MeN
164
Et
iPr
from stigmasterol
benzene, 4 Å MS
40 °C, 20 h
70%

Scheme 52: (A and B) Cobalt-catalyzed intramolecular 1,5-C(sp^3)–H amination; (C) late-stage functionalization of stigmasterol derivative **164**.

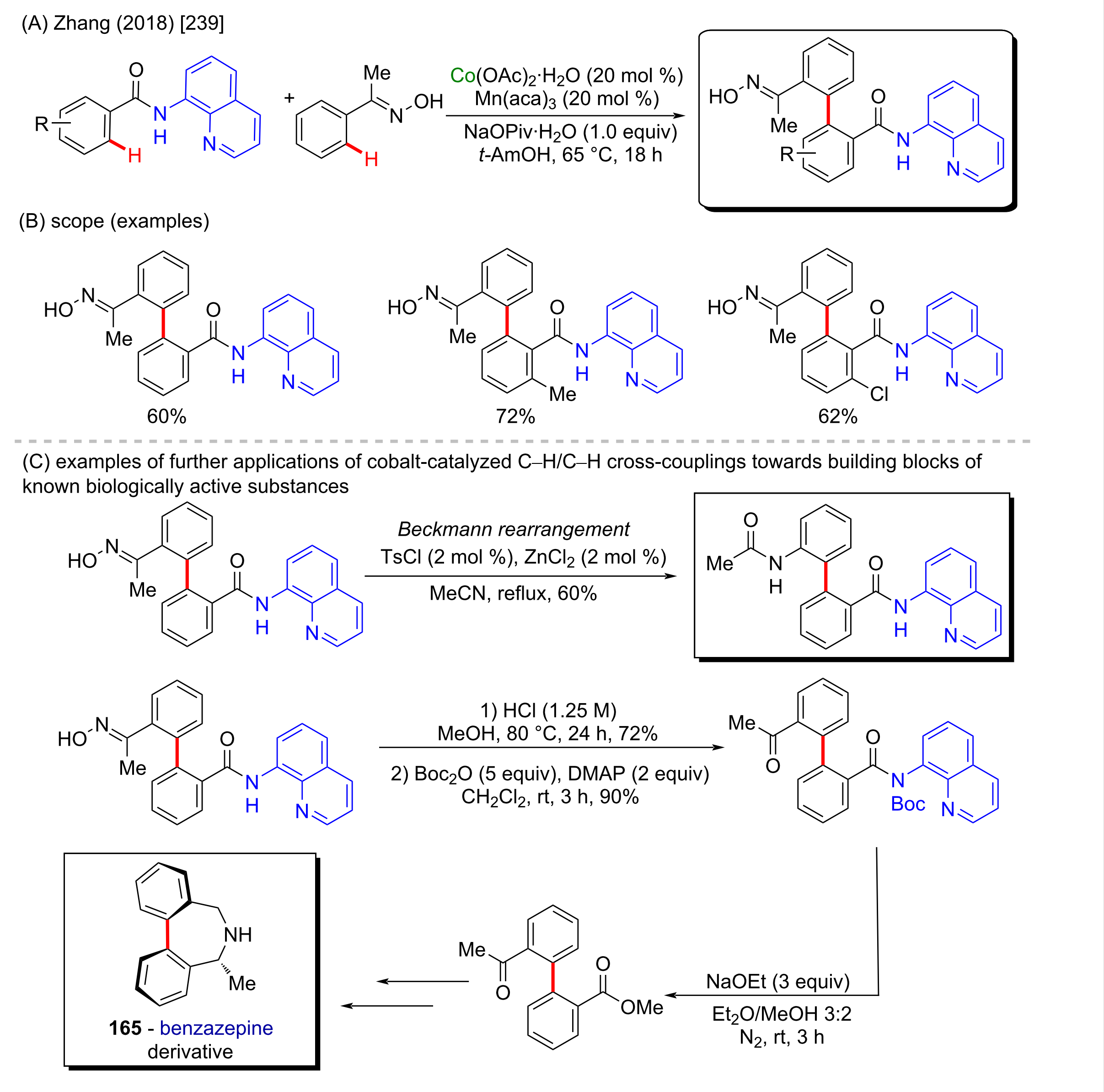
(A) Zhang (2018) [239]
R
O
N
H
N
H
+
Me
N
OH
H
Co(OAc)2·H2O (20 mol %)
Mn(aca)3 (20 mol %)
NaOPiv·H2O (1.0 equiv)
t-AmOH, 65 °C, 18 h
HO
N
Me
R
O
N
H
N
(B) scope (examples)
60%
72%
62%
Me
Cl
(C) examples of further applications of cobalt-catalyzed C–H/C–H cross-couplings towards building blocks of known biologically active substances
Beckmann rearrangement
TsCl (2 mol %), ZnCl2 (2 mol %)
MeCN, reflux, 60%
1) HCl (1.25 M)
MeOH, 80 °C, 24 h, 72%
2) Boc2O (5 equiv), DMAP (2 equiv)
CH2Cl2, rt, 3 h, 90%
Boc
NaOEt (3 equiv)
Et2O/MeOH 3:2
N2, rt, 3 h
OMe
NH
Me
165 - benzazepine derivative

Scheme 53: (A and B) Cobalt-catalyzed C–H/C–H cross-coupling between benzamides and oximes; (C) late-state synthesis of benzazepine derivative **165**.

alkynes providing new isoquinoline derivatives in 2016. The robust reaction performed in open air provides a broad scope of new isoquinolines (Scheme 54B and C) [244]. To demonstrate the applicability of this method, the authors applied of the protocol to iloperidone (**168**), a compound with known antipsychotic effects [245], as substrate for the cobalt-catalyzed annulation (Scheme 54D). The 2-hydrazinylpyridine auxiliary group was introduced in the ketone portion of iloperidone and the sequential C–H annulation afforded the corresponding isoquinoline derivative.

As demonstrated by the examples above, cobalt is another example of a well-established and well-explored metal applicable as a catalyst for C–H activation reactions. Cobalt-catalysis, allows to obtain a huge variety of compounds, including bioactive species, using both complex and simple catalysts. Therefore, this metal represents high potential for future developments in catalysis.

Nickel-catalyzed C–H activation

Nickel is a versatile metal that is used in several products, from simple day-by-day coinage [246] to electrodes used for *Escherichia coli* detection in water [247]. It is one of the metals contained in stainless steel [248], a stable alloy used to construct several industrial products. It is also applied as a powerful catalyst in polymerization [249,250], C–C coupling [251],

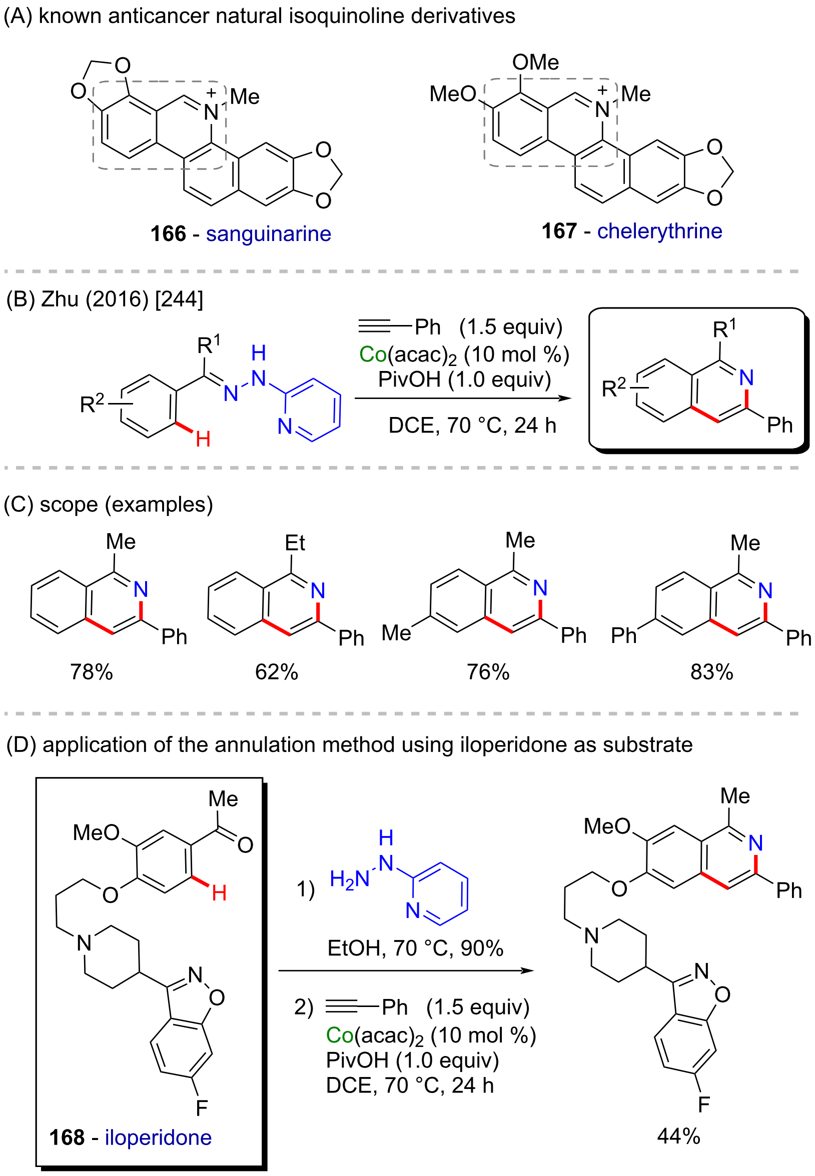
(A) known anticancer natural isoquinoline derivatives
O
O
Me
N
+
O
O
166 - sanguinarine
OMe
MeO
Me
N
+
O
O
167 - chelerythrine
(B) Zhu (2016) [244]
R1
H
N
N
R2
H
N
Ph (1.5 equiv)
Co(acac)2 (10 mol %)
PivOH (1.0 equiv)
DCE, 70 °C, 24 h
R1
R2
N
Ph
(C) scope (examples)
Me
N
Ph
78%
Et
N
Ph
62%
Me
N
Me
Ph
76%
Me
N
Ph
Ph
83%
(D) application of the annulation method using iloperidone as substrate
Me
MeO
O
O
H
N
N
O
F
168 - iloperidone
1) H2N N H
N
EtOH, 70 °C, 90%
2) Ph (1.5 equiv)
Co(acac)2 (10 mol %)
PivOH (1.0 equiv)
DCE, 70 °C, 24 h
Me
MeO
N
Ph
O
N
N
O
F
44%

Scheme 54: (A) Known anticancer natural isoquinoline derivatives; (B and C) cobalt-catalyzed C(sp^2)–H annulation on 2-hydrazinylpyridine derivatives; (D) late-state annulation of iloperidone.

oxygen [252] or hydrogen evolution [253], or even cycloaddition reactions [254]. Its accessibility and high catalytic activity have been well-explored also in C–H activation processes [255-259]. Some of the discoveries led to the formation of important biologically active substances that play a crucial role in pharmaceutical studies, as exemplified by a work published by Ackermann and co-workers in 2019 [260]. In this work, the authors described an enantioselective intramolecular C–H activation of several imidazole derivatives in the presence of an effective chiral ferrocene ligand and nickel-cod as catalyst (Scheme 55A). Through this process, several 6-membered cyclic products were obtained in moderate to excellent yields and excellent enantiomeric ratios (er). Several known bioactive motifs were synthesized, such as theophylline and purine derivatives **169–175** (Scheme 55B) [261-263]. The authors also proposed a plausible mechanism (Scheme 55C). The chiral interaction between the ferrocene ligand, the substrate, and the nickel catalyst, form intermediate **A** that, after a migratory insertion, leads to the formation of the intermediate **B**, which already presents the desired chiral product coordinated to the nickel center. A subsequent coordination to another equivalent of the substrate leads to the formation of intermediate C. Through a C–H activation step, hydrogen is transferred from the second coordinated substrate moiety to the first coordinated substrate

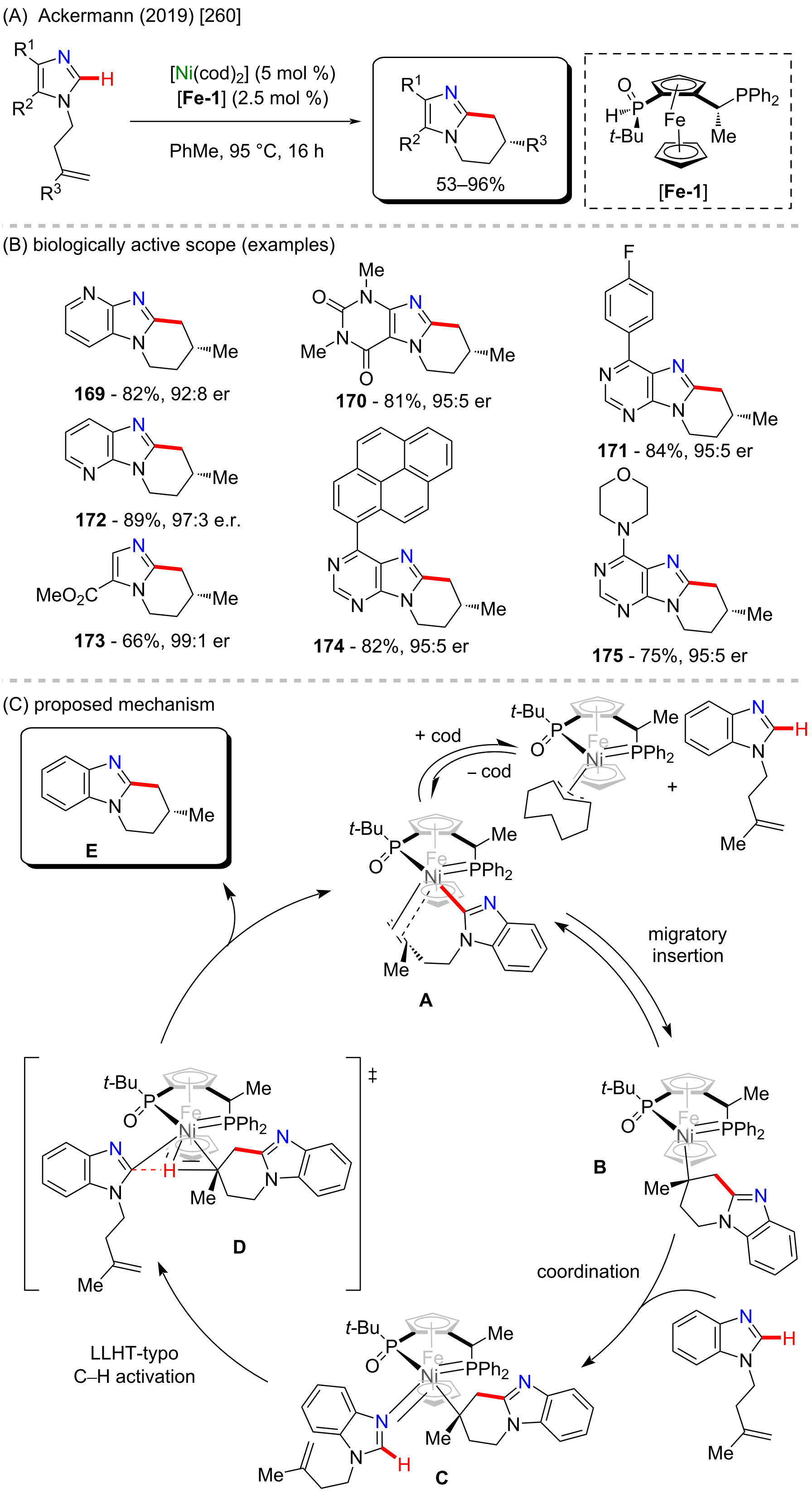
(A) Ackermann (2019) [260]
[Ni(cod)2] (5 mol %)
[Fe-1] (2.5 mol %)
PhMe, 95 °C, 16 h
53–96%
[Fe-1]
(B) biologically active scope (examples)
169 - 82%, 92:8 er
170 - 81%, 95:5 er
171 - 84%, 95:5 er
172 - 89%, 97:3 e.r.
173 - 66%, 99:1 er
174 - 82%, 95:5 er
175 - 75%, 95:5 er
(C) proposed mechanism
E
+ cod
– cod
A
migratory insertion
B
coordination
C
LLHT-typo C–H activation
D

Scheme 55: (A) Enantioselective intramolecular nickel-catalyzed C–H activation; (B) bioactive obtained motifs; (C) proposed mechanism.

already present in the coordination sphere of the catalyst, which is represented by transition state **D**, that leads to the formation of the product **E** and the starting intermediate **A**.

The same catalyst used in the previous example (nickel-cod) was also explored very recently by Amgoune and co-workers in an α-C(sp^3)–H arylation of ketones in the presence of another chiral ferrocene ligand [264]. The desired arylated products were successfully obtained in moderate to good yields (Scheme 56A and B). Amongst the obtained products, two were derived from the commercially available drugs clofibrate (**176**) [265] (trade name Atromid-S®) and fenofibrate (**177**) [266] (marketed under the name TriCor®), used to treat abnormal blood lipid levels (Scheme 56C).

In 2016, Doyle and co-workers described a notable nickel/photoredox-catalyzed C(sp^3)–H acylation of several pyrrolidine derivatives [267]. They used thioesters as coupling-partners in the presence of [Ni(cod)$_2$] and [Ir(ppy)$_2$(dtbbpy)]PF$_6$ (Scheme 57A and B). Valuable acylated products were obtained, including a complex one originating from TBS-lithocholic acid **178**, with a steroidal backbone (Scheme 57C).

One year later, the same group published another notable work describing a nickel/photo-catalyzed C(sp^3)–H arylation of dioxolane in the presence of several aryl chlorides (Scheme 58A) [268]. In this study, the authors built a library using known commercially available drugs as coupling partners, such as procymidone (**181**) (a known potent fungicide used in agriculture [269]), hexythiazox (**183**) (a known pesticide used in agriculture [270]) and zomepirac (**187**) (withdrawn anti-inflammatory drug [271]), from which the arylated products were obtained in moderate to good yields (Scheme 58B).

Beyond the examples cited above, another interesting nickel-cod use was described by Shi and co-workers in 2019 [272]. In this work, an enantioselective intramolecular C–H cycloalkylation proceeded in the presence of robust chiral ligands

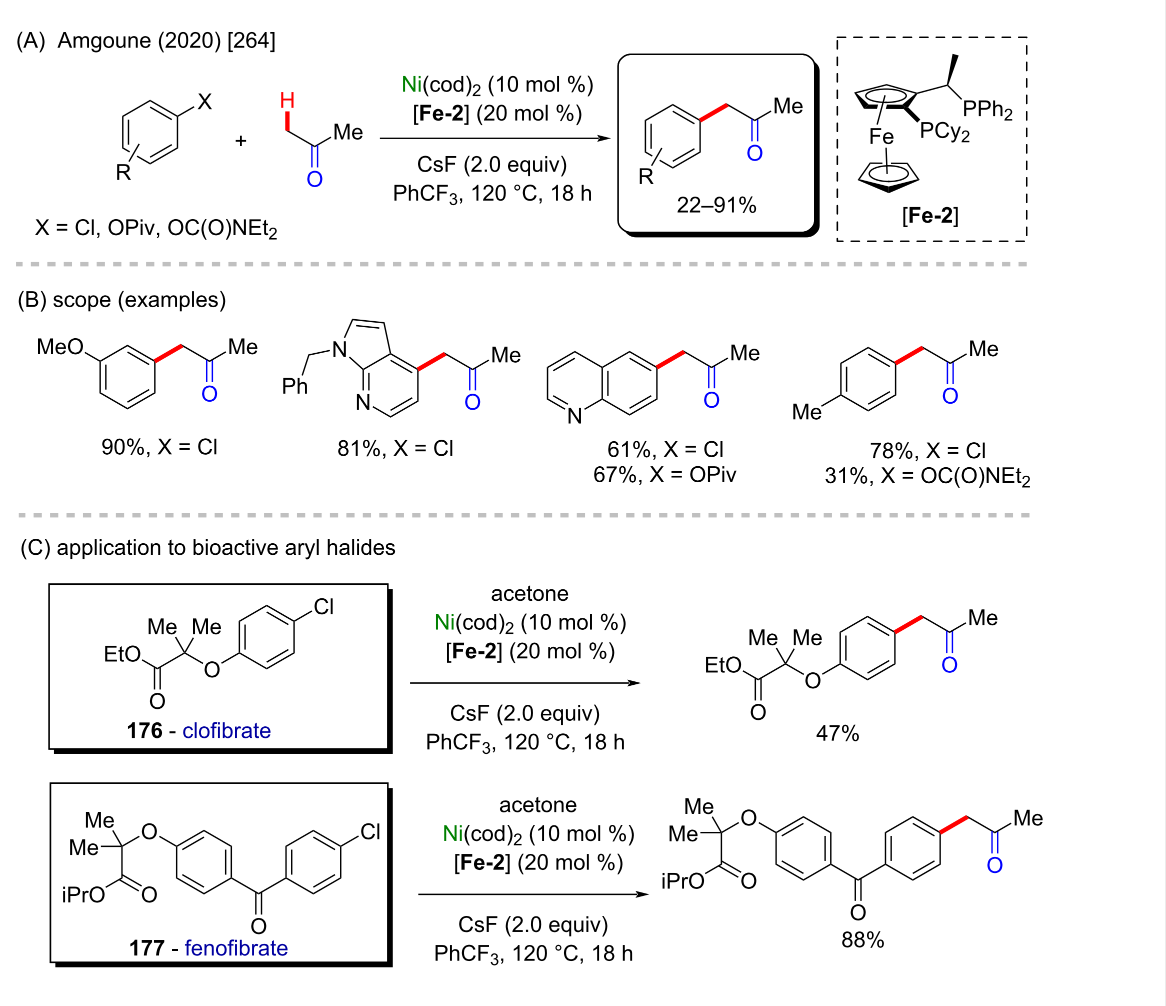

(A) Amgoune (2020) [264]
X
R
+
H
Me
O
X = Cl, OPiv, OC(O)NEt2
Ni(cod)2 (10 mol %)
[Fe-2] (20 mol %)
CsF (2.0 equiv)
PhCF3, 120 °C, 18 h
22–91%
Fe
PPh2
PCy2
[Fe-2]
(B) scope (examples)
MeO
90%, X = Cl
Ph
N
81%, X = Cl
61%, X = Cl
67%, X = OPiv
78%, X = Cl
31%, X = OC(O)NEt2
(C) application to bioactive aryl halides
EtO
Cl
176 - clofibrate
acetone
47%
iPrO
177 - fenofibrate
88%

Scheme 56: (A and B) Nickel-catalyzed α-C(sp^3)–H arylation of ketones; (C) application of the method using known drugs as coupling partners.

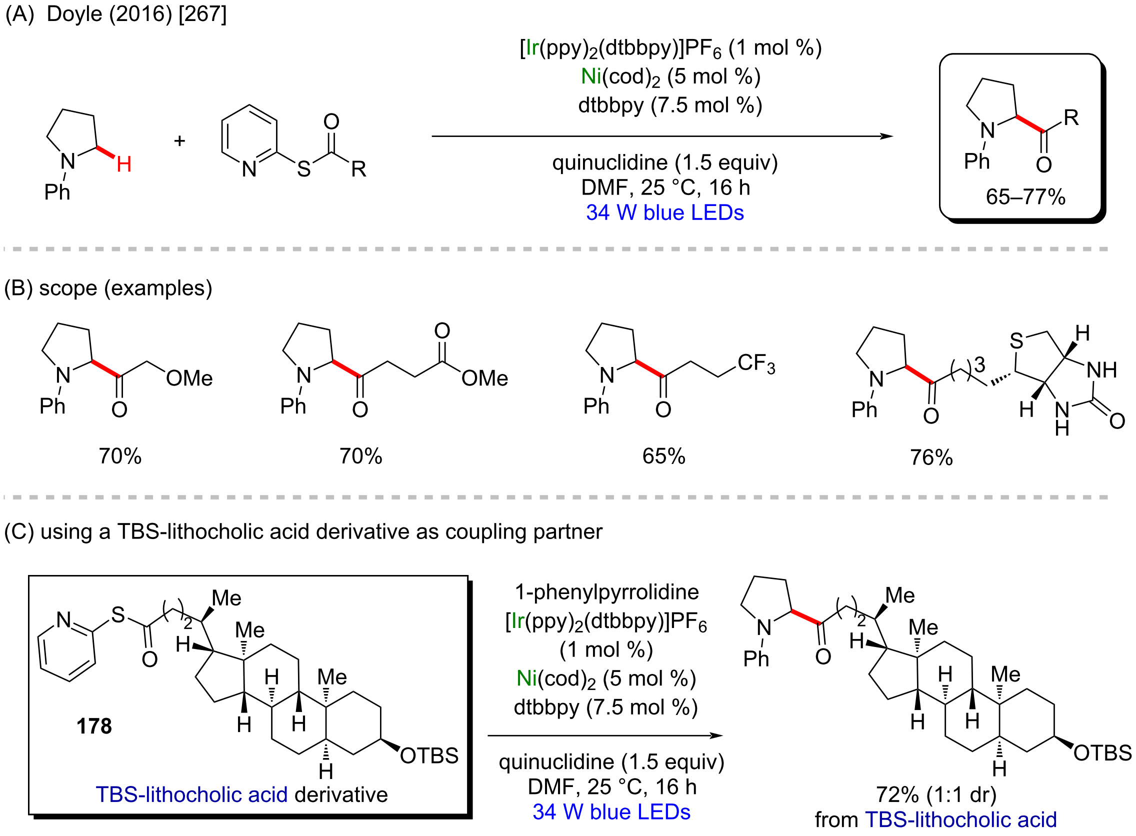
(A) Doyle (2016) [267]
[Ir(ppy)2(dtbbpy)]PF6 (1 mol %)
Ni(cod)2 (5 mol %)
dtbbpy (7.5 mol %)
quinuclidine (1.5 equiv)
DMF, 25 °C, 16 h
34 W blue LEDs
65–77%
(B) scope (examples)
70%
70%
65%
76%
(C) using a TBS-lithocholic acid derivative as coupling partner
178
TBS-lithocholic acid derivative
1-phenylpyrrolidine
[Ir(ppy)2(dtbbpy)]PF6
(1 mol %)
Ni(cod)2 (5 mol %)
dtbbpy (7.5 mol %)
quinuclidine (1.5 equiv)
DMF, 25 °C, 16 h
34 W blue LEDs
72% (1:1 dr)
from TBS-lithocholic acid

Scheme 57: (A and B) Nickel-catalyzed C(sp^3)–H acylation of pyrrolidine derivatives; (C) exploring the use of a steroidal residue as coupling partner.

(Scheme 59A). All cyclic products were obtained in good yields (Scheme 59B), and amongst the products, two derived from the known pharmacological substances, **191** from clofibrate (previously mentioned drug used to clean lipid levels in blood [265]) and **192** from loratadine (known antihistamine drug [273]).

In 2012, another interesting nickel-catalyzed C–H activation method was described by Itami and co-workers (Scheme 60A) [274]. In this work, a deoxy-arylation process of azoles led to the formation of several arylated products in moderate to good yields, including the important alkaloids texamine (**193**) [275] and uguenenazole (**194**) [276] (Scheme 60B). The authors applied the same developed methodology in a late-stage study to modify the derivative of the naturally occurring compounds estrone triflate (**195**) [277] and quinine triflate (**196**) [278] (Scheme 60C).

Yamaguchi, Itami and co-workers explored a similar procedure, in another report the same year [279], in which they described a nickel-cod-catalyzed decarbonylative C–H arylation of azole derivatives (Scheme 61A). This method afforded the desired products in good to excellent yields (Scheme 61B) and it was further applied to the total synthesis of muscoride A (**197**, Scheme 61C), a compound known to present antibacterial activities [280].

Further investigations from these authors of this innovative method led to the observation of a good catalytic activity of another nickel(II) source, as described in another work published in 2015 [281]. This work describes a nickel(II) triflate-catalyzed C–H arylation of azoles, by which several arylated products were successfully obtained in good yields (Scheme 62A and B). Amongst the obtained products, two are worth mentioning here since they derive from two important biologically active substances (Scheme 62C). The first one was obtained in 69% yield derived from pilocarpine (**198**), a known drug used in the treatment of glaucoma [282]. The second one derives from indomethacin (**199**), a known anti-inflammatory drug that, in combination with vitamin D, substantially decreases the frequency of colorectal cancer occurrence [283].

Already in 2011, Itami and co-workers explored the catalytic activity of nickel(II) acetate in a C–H arylation of azole deriva-

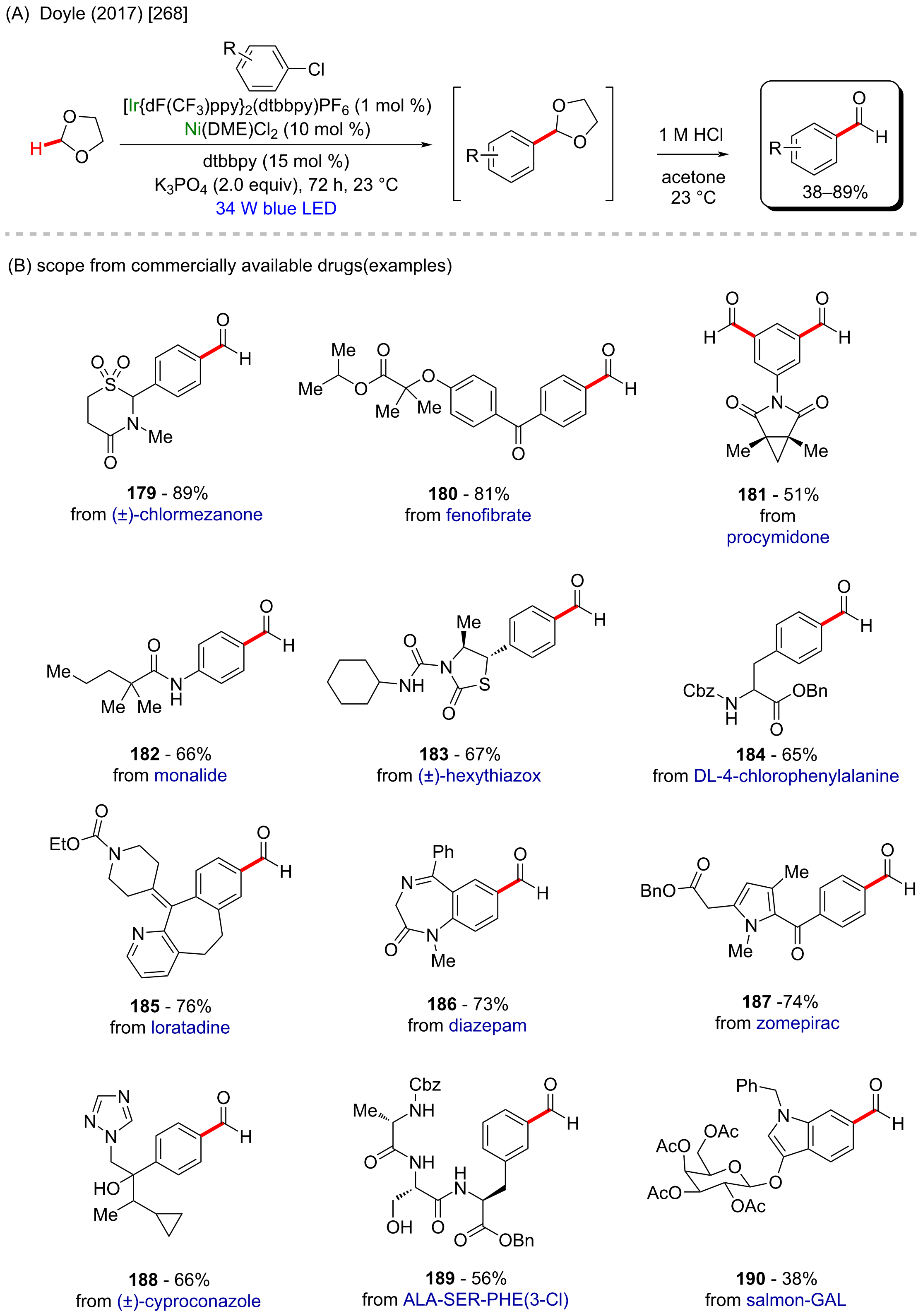
(A) Doyle (2017) [268]
R
Cl
[Ir{dF(CF$_3$)ppy}$_2$(dtbbpy)PF$_6$ (1 mol %)
Ni(DME)Cl$_2$ (10 mol %)
dtbbpy (15 mol %)
K$_3$PO$_4$ (2.0 equiv), 72 h, 23 °C
34 W blue LED
H
O
O
R
1 M HCl
acetone
23 °C
38–89%
(B) scope from commercially available drugs(examples)
179 - 89%
from (±)-chlormezanone
180 - 81%
from fenofibrate
181 - 51%
from
procymidone
182 - 66%
from monalide
183 - 67%
from (±)-hexythiazox
184 - 65%
from DL-4-chlorophenylalanine
185 - 76%
from loratadine
186 - 73%
from diazepam
187 -74%
from zomepirac
188 - 66%
from (±)-cyproconazole
189 - 56%
from ALA-SER-PHE(3-Cl)
190 - 38%
from salmon-GAL

Scheme 58: (A) Nickel-catalyzed C(sp^3)–H arylation of dioxolane; (B) library of products obtained from biologically active aryl chlorides as coupling partners.

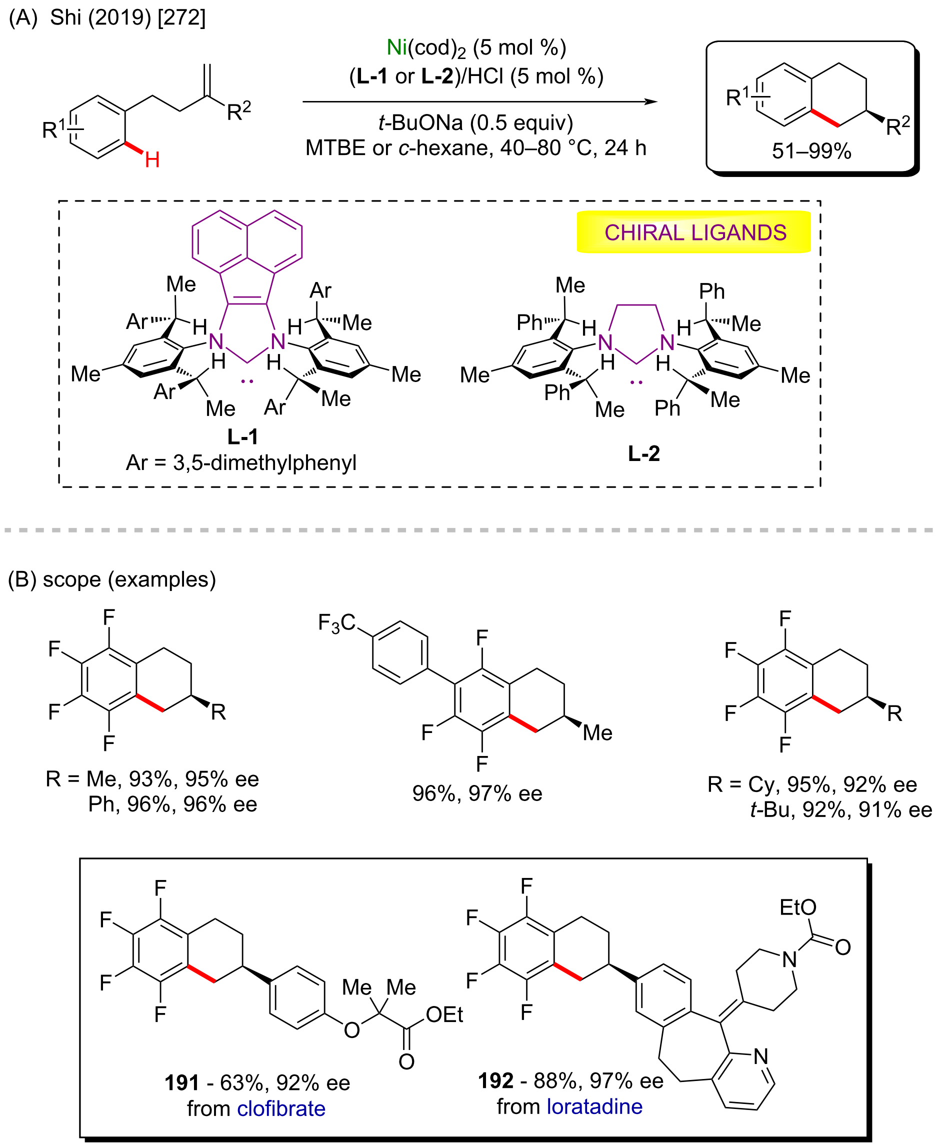
(A) Shi (2019) [272]
Ni(cod)2 (5 mol %)
(L-1 or L-2)/HCl (5 mol %)
t-BuONa (0.5 equiv)
MTBE or c-hexane, 40–80 °C, 24 h
R1
R2
H
51–99%
CHIRAL LIGANDS
L-1
Ar = 3,5-dimethylphenyl
L-2
(B) scope (examples)
R = Me, 93%, 95% ee
Ph, 96%, 96% ee
96%, 97% ee
R = Cy, 95%, 92% ee
t-Bu, 92%, 91% ee
191 - 63%, 92% ee
from clofibrate
192 - 88%, 97% ee
from loratadine

Scheme 59: (A) Intramolecular enantioselective nickel-catalyzed C–H cycloalkylation; (B) product examples, including two drug derivatives.

tives (Scheme 63A) [284]. Since then, this method led to the formation of several arylated products in good yields (Scheme 63B). The same methodology was applied in a late-stage functionalization towards the synthesis of three important drugs (Scheme 63C): tafamidis (**200**) (used to treat amyloidosis [285]), febuxostat (**201**) (used to treat gout [286]), and texaline (**202**) (presents antitubercular activity [287]).

A similar methodology was explored by Truong and co-workers in 2017 [288]. In this work, a nickel-based metalorganic framework (MOF-74-Ni) mediated a C–H arylation process of several azole derivatives (Scheme 64A). The desired arylated products were obtained in good yields, including compounds known to present important biological activities (Scheme 64B and C) such as the caffeine derivative from **203** [289], texamine (**204**) [290], balsoxin (**205**) [290], and the previously mentioned uguenenazole (**194**) [276].

Currently, there are several examples of commercially available drugs containing a benzothiophene unit in their structures (**206**–**208**, Scheme 65A) [291]. Following this idea, it is worthy to mention here an important work published by Canivet and co-workers in 2020 [292], in which the authors described a regioselective C–H arylation of benzothiophene derivatives. Through this method, a large variety of arylated products were successfully obtained in plausible yields (Scheme 65B and C).

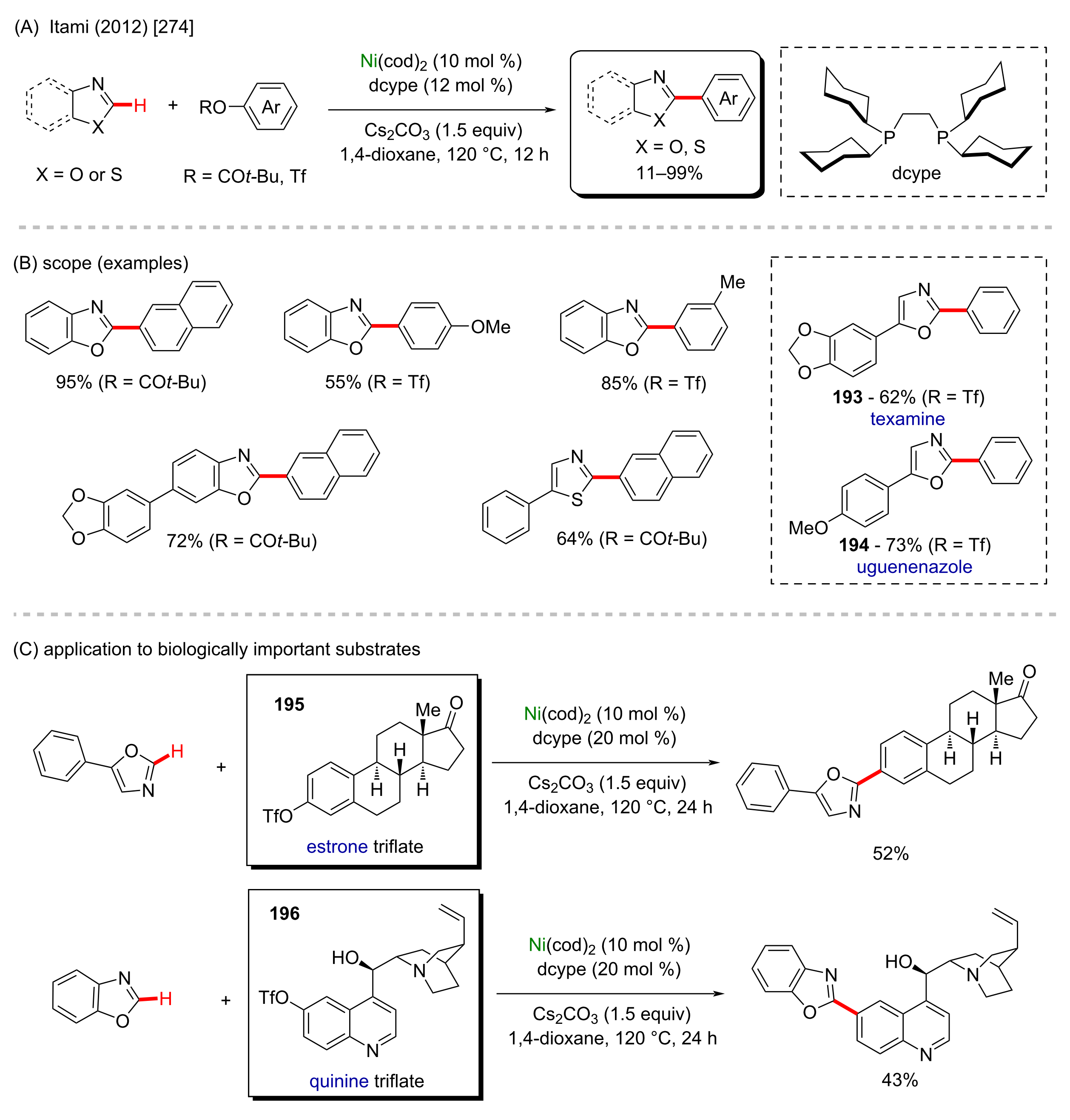
(A) Itami (2012) [274]
Ni(cod)2 (10 mol %)
dcype (12 mol %)
Cs2CO3 (1.5 equiv)
1,4-dioxane, 120 °C, 12 h
X = O or S
R = COt-Bu, Tf
X = O, S
11–99%
dcype
(B) scope (examples)
95% (R = COt-Bu)
55% (R = Tf)
85% (R = Tf)
72% (R = COt-Bu)
64% (R = COt-Bu)
193 - 62% (R = Tf)
texamine
194 - 73% (R = Tf)
uguenenazole
(C) application to biologically important substrates
195
estrone triflate
Ni(cod)2 (10 mol %)
dcype (20 mol %)
Cs2CO3 (1.5 equiv)
1,4-dioxane, 120 °C, 24 h
52%
196
quinine triflate
43%

Scheme 60: (A and B) Nickel-catalyzed C–H deoxy-arylation of azole derivatives; (C) late-stage functionalization on naturally occurring alkaloids.

A further study of this methodology led to the synthesis of an essential building block of raloxifene (**209**) (Scheme 65D), a known anticancer drug [293].

Some important bioactive natural molecules (**210** and **211**) present at least one tetrahydrofuran unit in their structure, so reactions that promote a structural modification of this organic class of molecules are extremely valuable (Scheme 66A) [294]. Hashmi and co-workers published in 2019 a notable work in which they described a nickel-catalyzed photoredox C(sp^3)–H alkylation/arylation process [295]. In this work, NiBr$_2$·glyme was used as a nickel source in the presence of benzaldehyde as a photosensitizer, and 4,4′-di-*tert*-butyl-2,2′-dipyridyl (dtbbpy) as the ligand under UVA light irradiation (Scheme 66B). The desired tetrahydrofuran-based products were obtained in good yields (Scheme 66C). Subsequently, the developed procedure was successfully applied as a late-stage modification of the natural substance (−)-ambroxide (**212**) (Scheme 66D), a com-

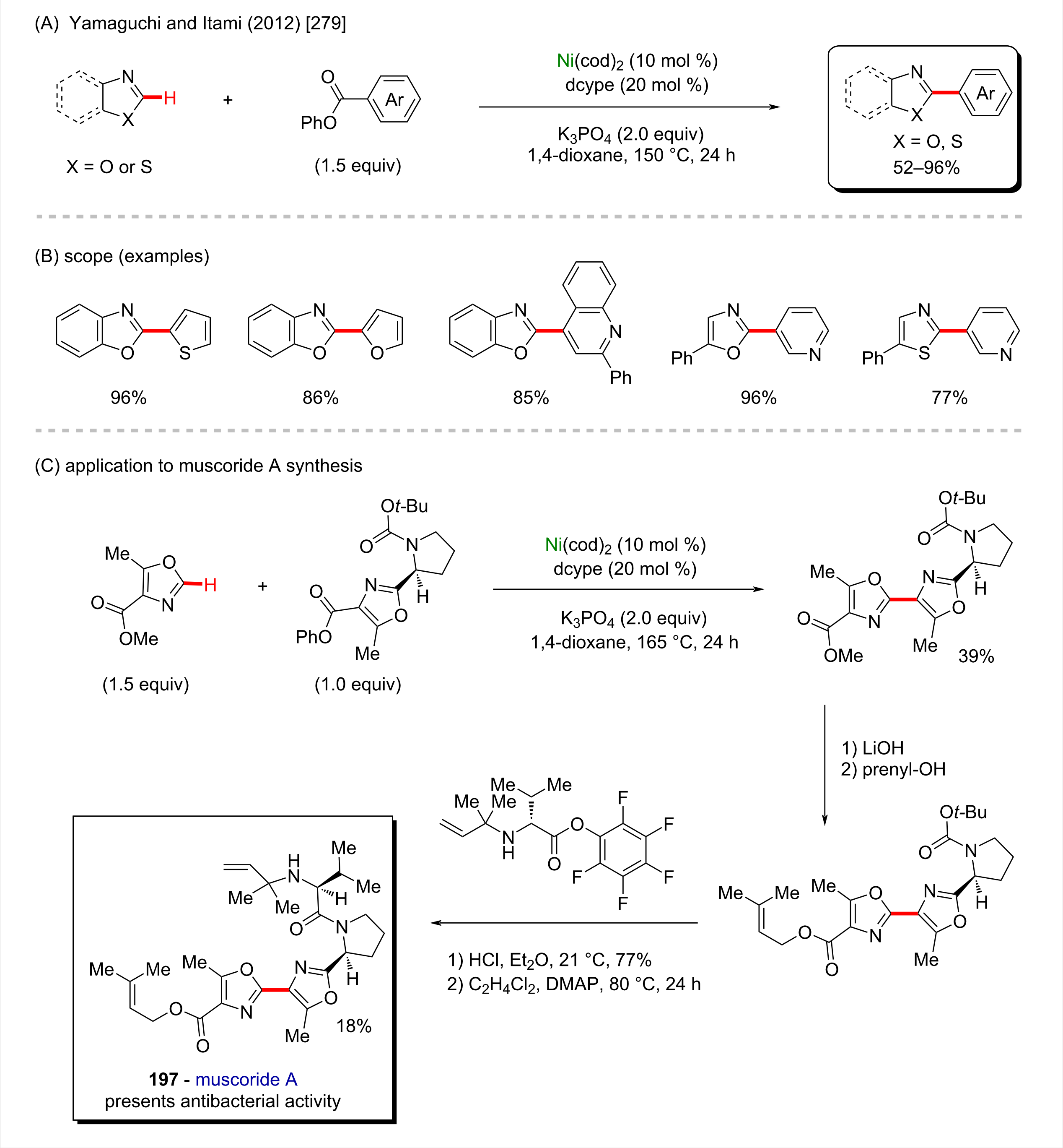
(A) Yamaguchi and Itami (2012) [279]
N
H
X
X = O or S
+
O
PhO
Ar
(1.5 equiv)
Ni(cod)2 (10 mol %)
dcype (20 mol %)
K3PO4 (2.0 equiv)
1,4-dioxane, 150 °C, 24 h
X = O, S
52–96%
(B) scope (examples)
96%
86%
85%
Ph
96%
77%
(C) application to muscoride A synthesis
Me
OMe
(1.5 equiv)
Ot-Bu
(1.0 equiv)
Ni(cod)2 (10 mol %)
dcype (20 mol %)
K3PO4 (2.0 equiv)
1,4-dioxane, 165 °C, 24 h
39%
1) LiOH
2) prenyl-OH
1) HCl, Et2O, 21 °C, 77%
2) C2H4Cl2, DMAP, 80 °C, 24 h
F
18%
197 - muscoride A
presents antibacterial activity

Scheme 61: (A and B) Nickel-catalyzed decarbonylative C–H arylation of azole derivatives; (C) application of this method to the synthesis of muscoride A (**197**).

pound excreted by the sperm whale (*Physeter catodon*) with a direct effect on the odor sensibility of women during the menstrual cycle [296].

Using a similar methodology, Martin and co-workers described in 2018 another nickel/photocatalyzed C–H arylation/alkylation [297] but using Ni(acac)$_2$ as a catalyst, in the presence of an asymmetric benzophenone derivative (**A**) and a bipyridine ligand (**L**) (Scheme 67A). The authors described the successful synthesis of many activated products (**213**–**216**), including examples of bromides derived from bioactive compounds, that afforded the final products in excellent yields (Scheme 67B). Similar to what was discussed in the previous example, the authors also performed a late-stage functionalization of (−)-ambroxide (**212**), that led to three arylated products with potential biological activities (Scheme 67C).

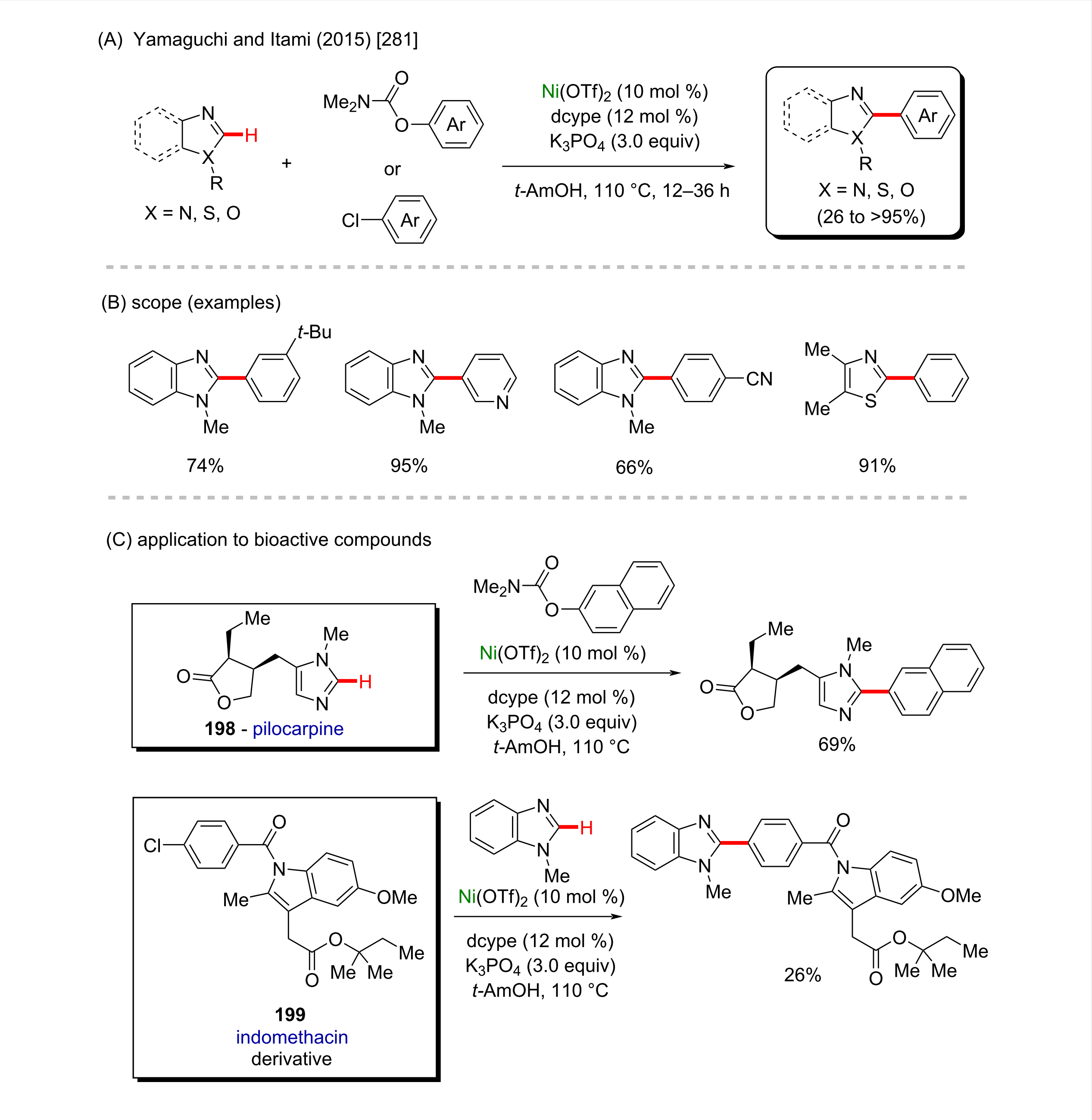
(A) Yamaguchi and Itami (2015) [281]
X = N, S, O
Ni(OTf)2 (10 mol %)
dcype (12 mol %)
K3PO4 (3.0 equiv)
t-AmOH, 110 °C, 12–36 h
X = N, S, O
(26 to >95%)
(B) scope (examples)
74%
95%
66%
91%
(C) application to bioactive compounds
198 - pilocarpine
Ni(OTf)2 (10 mol %)
dcype (12 mol %)
K3PO4 (3.0 equiv)
t-AmOH, 110 °C
69%
199
indomethacin
derivative
Ni(OTf)2 (10 mol %)
dcype (12 mol %)
K3PO4 (3.0 equiv)
t-AmOH, 110 °C
26%

Scheme 62: (A and B) Another important example of nickel-catalyzed C–H arylation of azole derivatives; (C) application of the method to bioactive compounds.

Another nickel-catalyzed C–H activation was described by Ackermann and co-workers in 2020 [298], in which an *ortho*-directed C–H alkoxylation was mediated in an electrochemical environment (Scheme 68A). Using this methodology, the authors achieved several interesting alkoxylated products in moderate to good yields. Amongst the obtained substances, it is worth to mention the successful late-stage functionalization using natural alcohols, such as menthol, cholesterol, and β-estradiol, from which the final products **217**–**219** were obtained in 53%, 61%, and 65% yields, respectively, without compromising the chiral centers already present in the original natural substances (Scheme 68B).

In 2019, Lu and co-workers reported a unique enantioselective photoredox/nickel-catalyzed C(sp^3)–H arylation method in the presence of a chiral ligand (Scheme 69A) [299]. By this method, several chiral 1,1-diarylethane products were obtained in good enantioselectivities. The applicability of this method was defended by the authors by the synthesis of a menthol-derived product **220**, and another compound (**221**) already

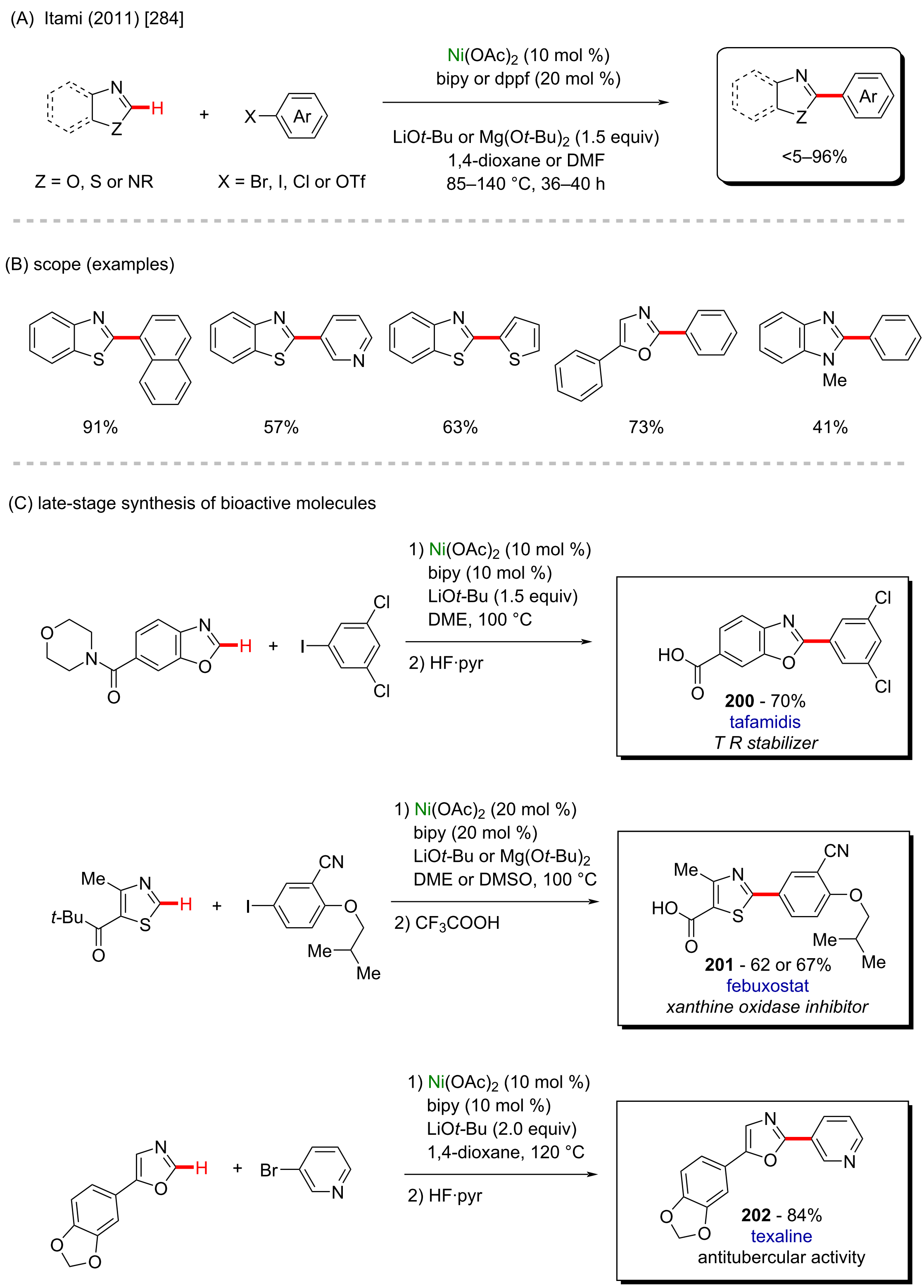

(A) Itami (2011) [284]

(B) scope (examples)

(C) late-stage synthesis of bioactive molecules

N
H
Z
+
X
Ar
Z = O, S or NR
X = Br, I, Cl or OTf
Ni(OAc)2 (10 mol %)
bipy or dppf (20 mol %)
LiOt-Bu or Mg(Ot-Bu)2 (1.5 equiv)
1,4-dioxane or DMF
85–140 °C, 36–40 h
<5–96%
91%
57%
63%
73%
41%
Me
O
N
H
+
I
Cl
Cl
1) Ni(OAc)2 (10 mol %)
bipy (10 mol %)
LiOt-Bu (1.5 equiv)
DME, 100 °C
2) HF·pyr
HO
200 - 70%
tafamidis
T R stabilizer
Me
t-Bu
S
CN
1) Ni(OAc)2 (20 mol %)
bipy (20 mol %)
LiOt-Bu or Mg(Ot-Bu)2
DME or DMSO, 100 °C
2) CF3COOH
201 - 62 or 67%
febuxostat
xanthine oxidase inhibitor
Br
1) Ni(OAc)2 (10 mol %)
bipy (10 mol %)
LiOt-Bu (2.0 equiv)
1,4-dioxane, 120 °C
2) HF·pyr
202 - 84%
texaline
antitubercular activity

Scheme 63: (A and B) Another notable example of a nickel-catalyzed C–H arylation of azole derivatives; (C) late-stage application to the synthesis of potent drugs.

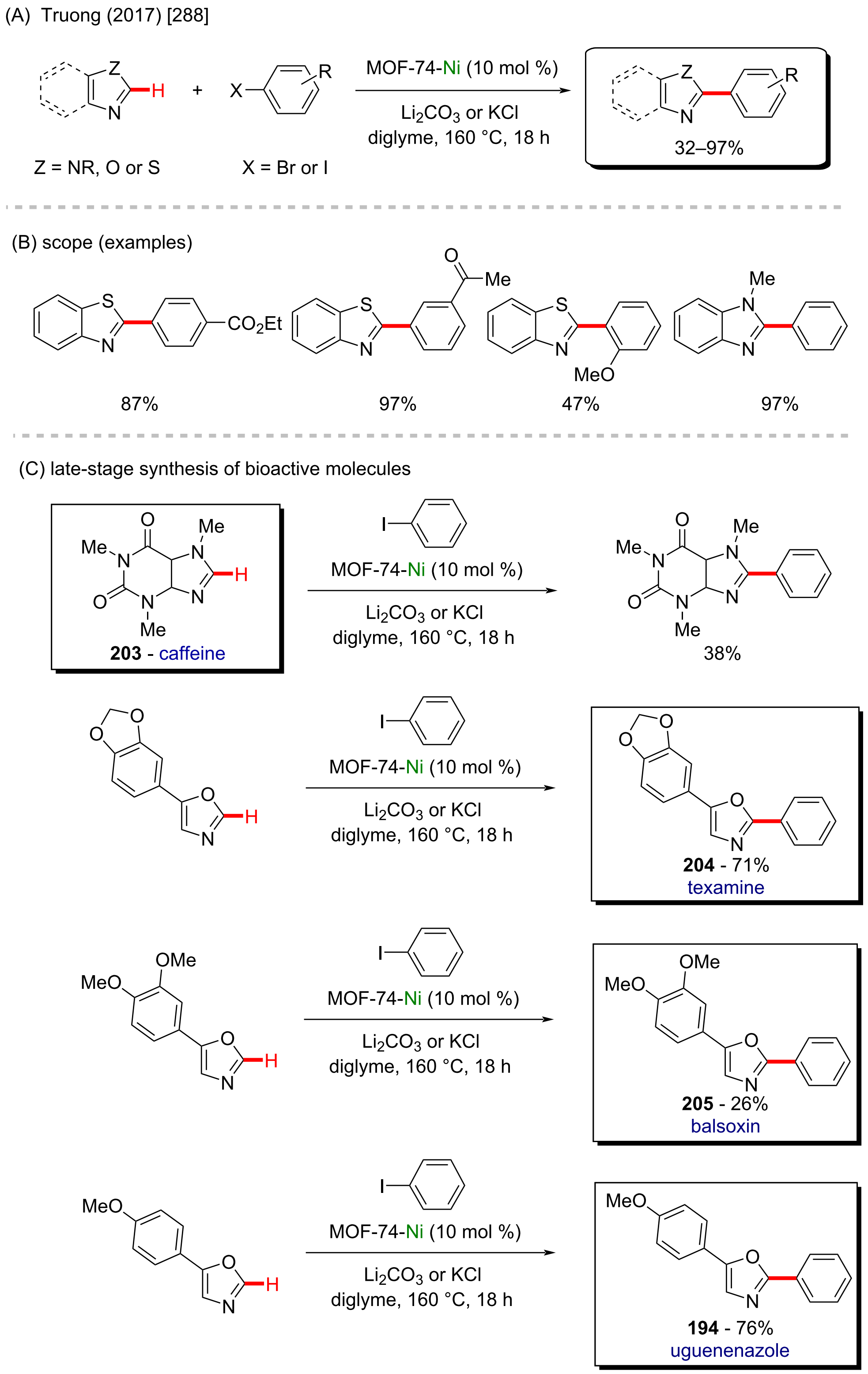
(A) Truong (2017) [288]
Z
H
N
+
X
R
Z = NR, O or S
X = Br or I
MOF-74-Ni (10 mol %)
Li2CO3 or KCl
diglyme, 160 °C, 18 h
32–97%
(B) scope (examples)
CO2Et
87%
O
Me
97%
MeO
47%
Me
97%
(C) late-stage synthesis of bioactive molecules
O
Me
Me
N
H
Me
203 - caffeine
I
MOF-74-Ni (10 mol %)
Li2CO3 or KCl
diglyme, 160 °C, 18 h
38%
204 - 71%
texamine
OMe
MeO
205 - 26%
balsoxin
194 - 76%
uguenenazole

Scheme 64: (A and B) Nickel-based metalorganic framework (MOF-74-Ni)-catalyzed C–H arylation of azole derivatives; (C) application to the synthesis of compounds with biological activity.

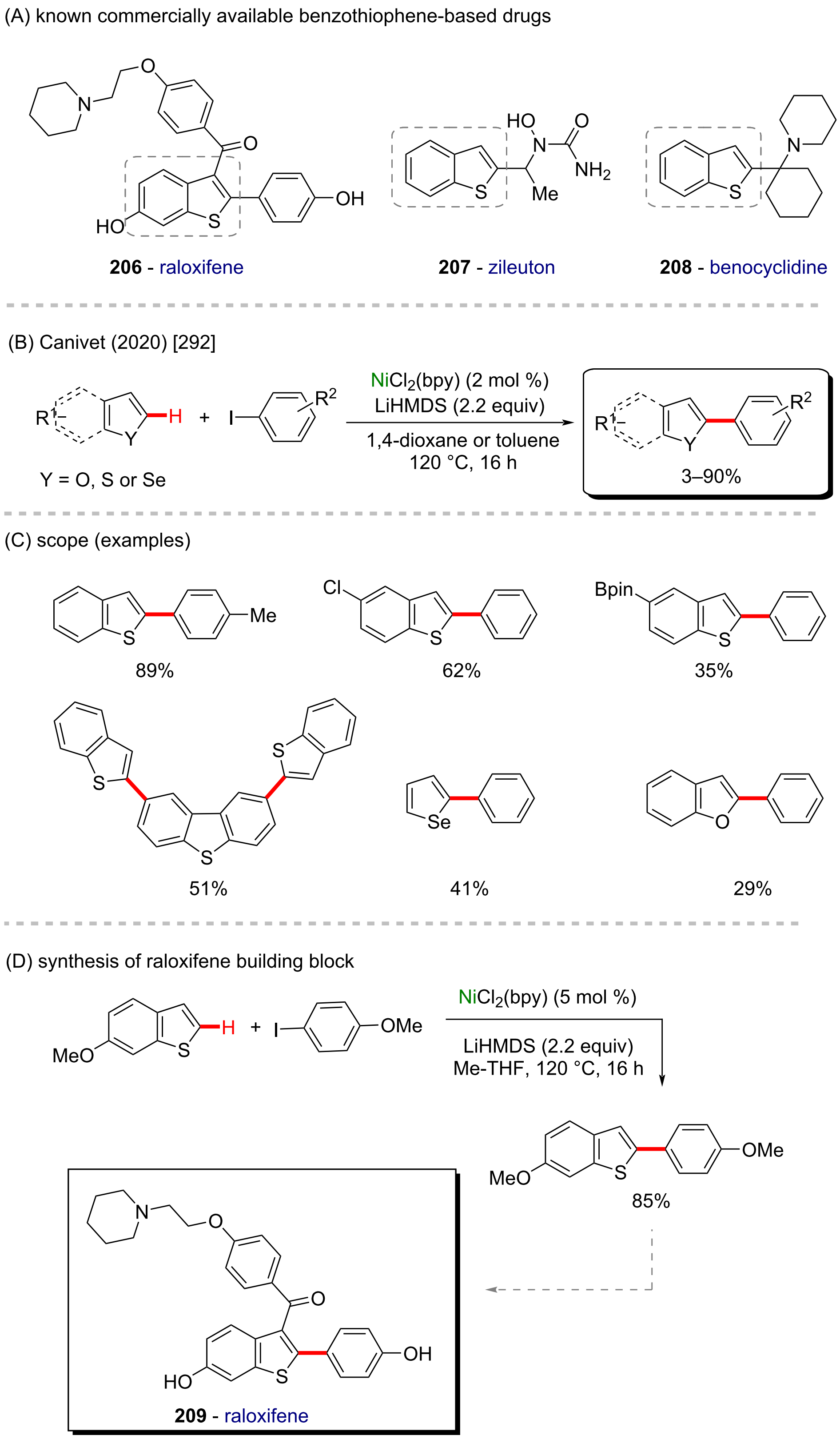
(A) known commercially available benzothiophene-based drugs
N
O
O
HO
S
OH
206 - raloxifene
HO
N
O
NH$_2$
S
Me
207 - zileuton
N
S
208 - benocyclidine
(B) Canivet (2020) [292]
R^1
Y
H
+
I
R^2
NiCl$_2$(bpy) (2 mol %)
LiHMDS (2.2 equiv)
1,4-dioxane or toluene
120 °C, 16 h
R^1
Y
R^2
3–90%
Y = O, S or Se
(C) scope (examples)
S
Me
89%
Cl
S
62%
Bpin
S
35%
S
S
S
51%
Se
41%
O
29%
(D) synthesis of raloxifene building block
MeO
S
H
+
I
OMe
NiCl$_2$(bpy) (5 mol %)
LiHMDS (2.2 equiv)
Me-THF, 120 °C, 16 h
MeO
S
OMe
85%
N
O
O
HO
S
OH
209 - raloxifene

Scheme 65: (A) Known commercially available benzothiophene-based drugs; (B and C) nickel-catalyzed C–H arylation of benzothiophene derivatives; (D) synthesis of a raloxifene building block.

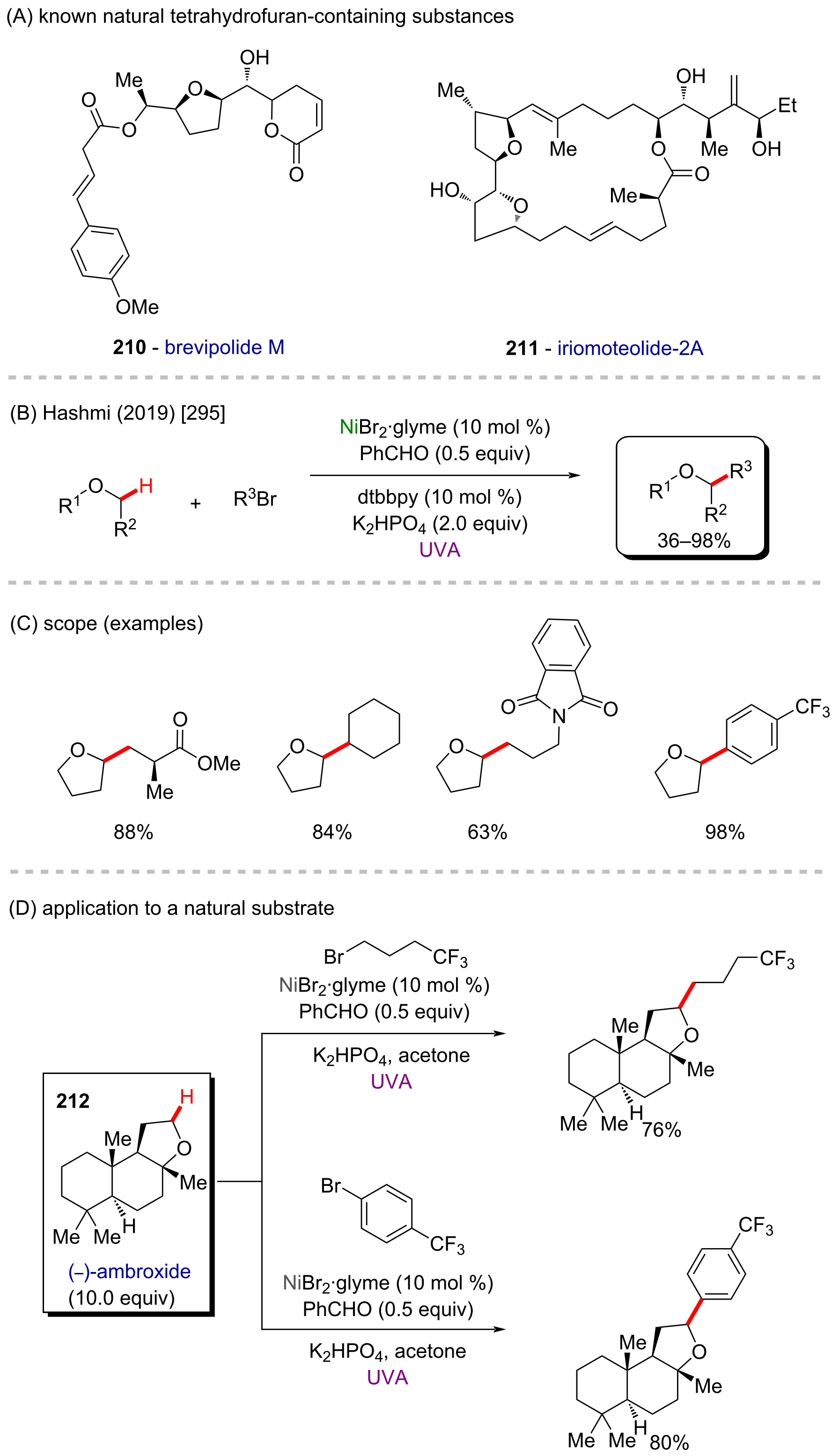
(A) known natural tetrahydrofuran-containing substances
210 - brevipolide M
211 - iriomoteolide-2A
(B) Hashmi (2019) [295]
NiBr2·glyme (10 mol %)
PhCHO (0.5 equiv)
dtbbpy (10 mol %)
K2HPO4 (2.0 equiv)
UVA
R3Br
36–98%
(C) scope (examples)
88%
84%
63%
98%
(D) application to a natural substrate
212
(−)-ambroxide
(10.0 equiv)
NiBr2·glyme (10 mol %)
PhCHO (0.5 equiv)
K2HPO4, acetone
UVA
76%
80%

Scheme 66: (A) Known natural tetrahydrofuran-containing substances; (B and C) nickel-catalyzed photoredox C(sp^3)–H alkylation/arylation; (C) late-stage modification of (−)-ambroxide (**212**).

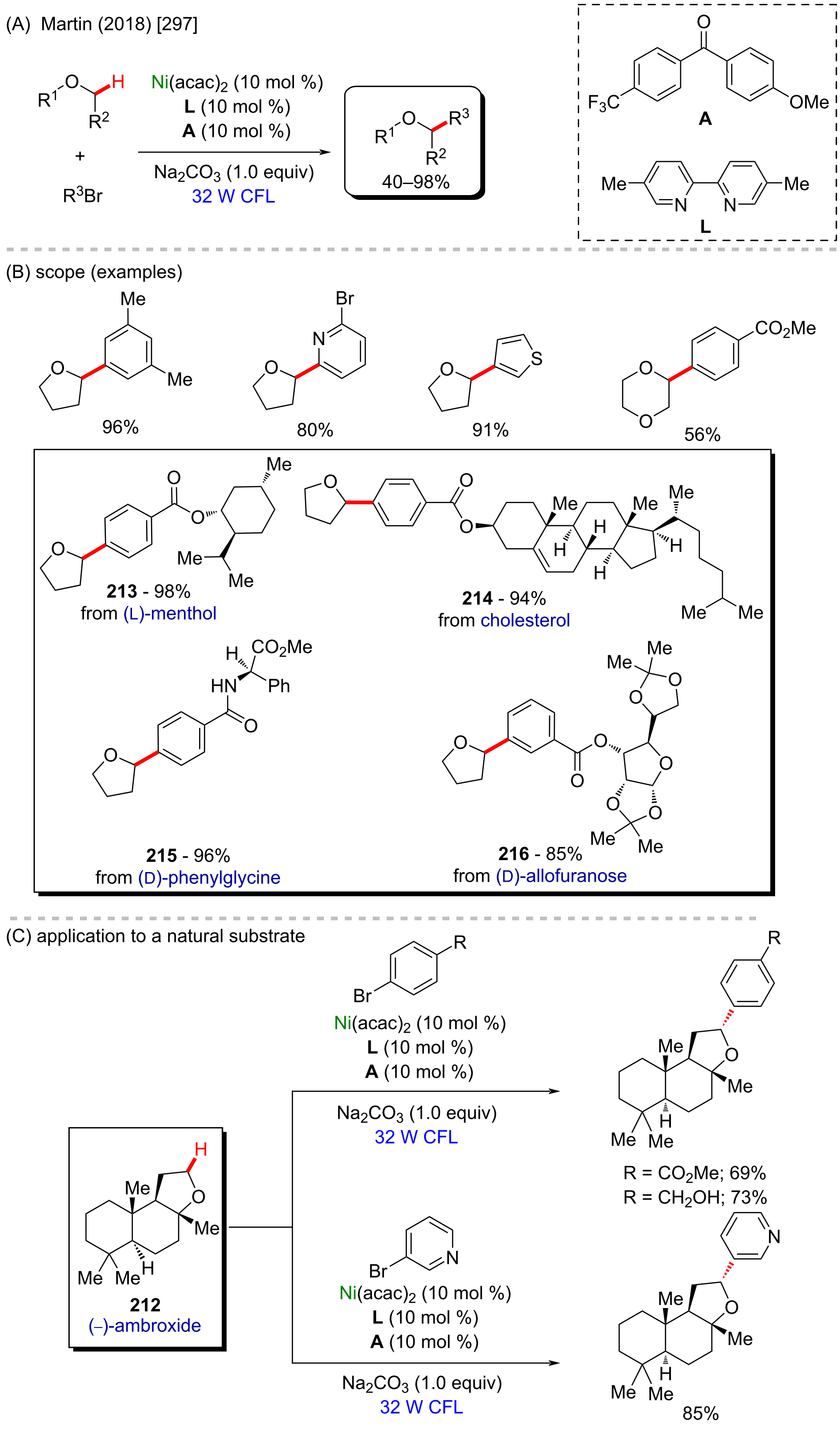
(A) Martin (2018) [297]
Ni(acac)2 (10 mol %)
L (10 mol %)
A (10 mol %)
Na2CO3 (1.0 equiv)
32 W CFL
40–98%
A
L
(B) scope (examples)
96%
80%
91%
56%
213 - 98%
from (L)-menthol
214 - 94%
from cholesterol
215 - 96%
from (D)-phenylglycine
216 - 85%
from (D)-allofuranose
(C) application to a natural substrate
212
(–)-ambroxide
R = CO2Me; 69%
R = CH2OH; 73%
85%

Scheme 67: (A and B) Another notable example of a nickel-catalyzed photoredox C(sp^3)–H alkylation/arylation; (C) late-stage application to (–)-ambroxide (**212**).

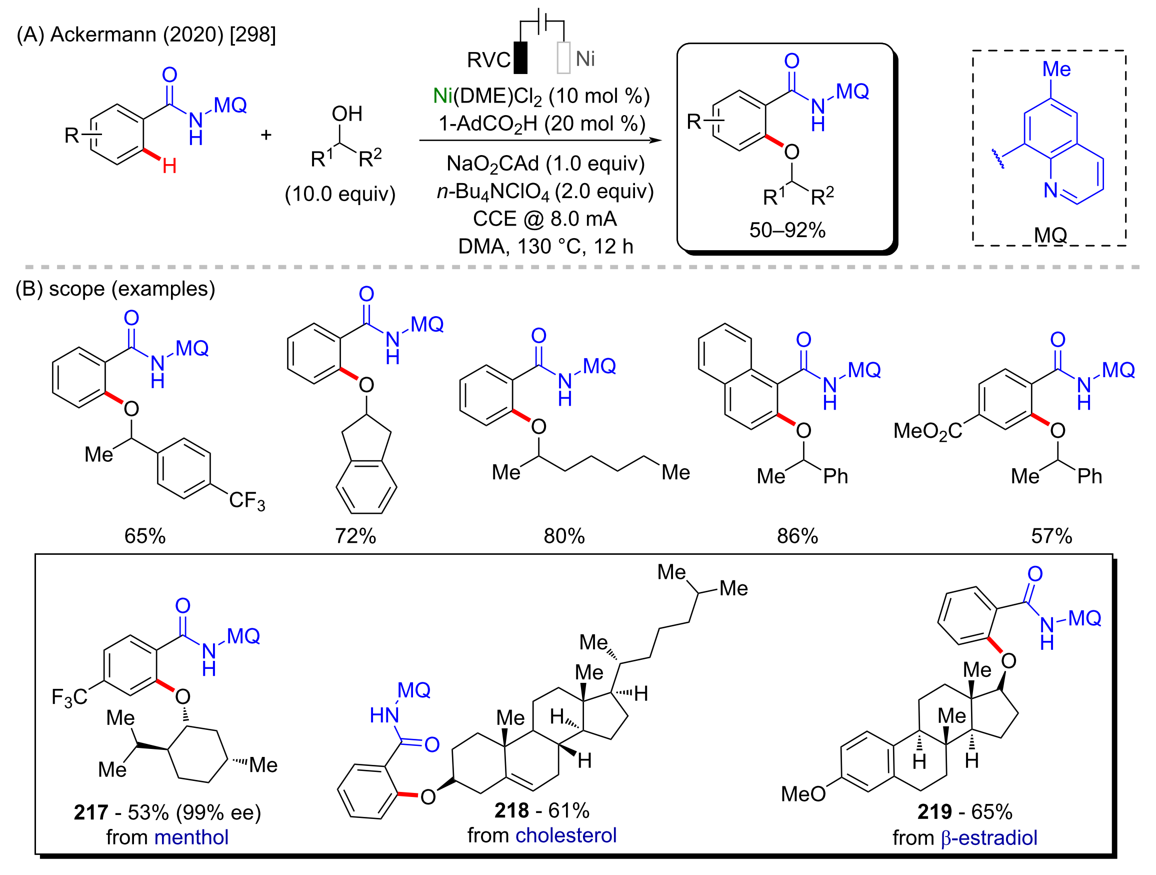
(A) Ackermann (2020) [298]
RVC
Ni
Ni(DME)Cl2 (10 mol %)
1-AdCO2H (20 mol %)
NaO2CAd (1.0 equiv)
n-Bu4NClO4 (2.0 equiv)
CCE @ 8.0 mA
DMA, 130 °C, 12 h
(10.0 equiv)
50–92%
MQ
(B) scope (examples)
65%
72%
80%
86%
57%
217 - 53% (99% ee)
from menthol
218 - 61%
from cholesterol
219 - 65%
from β-estradiol

Scheme 68: (A) Electrochemical/nickel-catalyzed C–H alkoxylation; (B) achieved scope, including three using natural compounds as coupling partners.

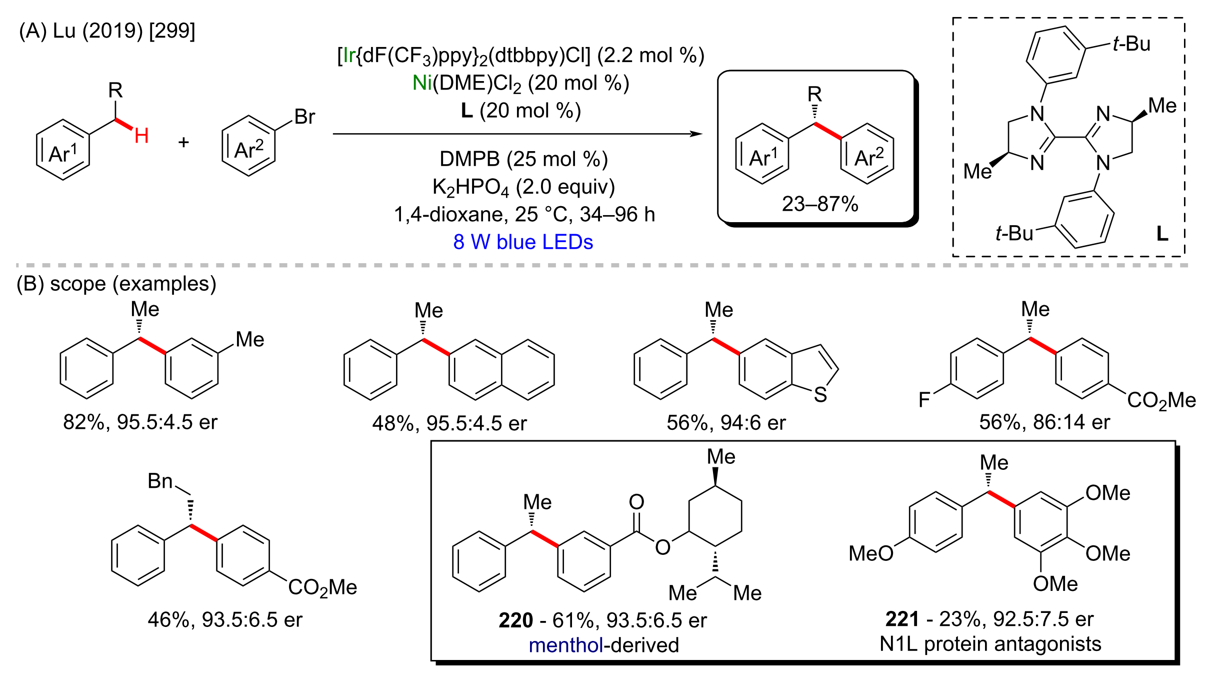
(A) Lu (2019) [299]
[Ir{dF(CF3)ppy}2(dtbbpy)Cl] (2.2 mol %)
Ni(DME)Cl2 (20 mol %)
L (20 mol %)
DMPB (25 mol %)
K2HPO4 (2.0 equiv)
1,4-dioxane, 25 °C, 34–96 h
8 W blue LEDs
23–87%
L
(B) scope (examples)
82%, 95.5:4.5 er
48%, 95.5:4.5 er
56%, 94:6 er
56%, 86:14 er
46%, 93.5:6.5 er
220 - 61%, 93.5:6.5 er
menthol-derived
221 - 23%, 92.5:7.5 er
N1L protein antagonists

Scheme 69: (A) Enantioselective photoredox/nickel catalyzed C(sp^3)–H arylation; (B) achieved scope, including two potential bioactive compounds.

known to present antagonist activity against the N1L protein (Scheme 69B) [300], therefore a potential anti-variola agent.

Some important commercially available drugs have a trifluoromethane unit, such as efavirenz (**222**), sitagliptin (**223**), and cinacalcet (**224**) (Scheme 70A) [301]. Nickel catalysis can also be used to mediate a C–H trifluoromethylation, as was well-exemplified in the work published by Sanford and co-workers in 2019 [302]. In this work, the authors used 2,8-difluoro-5-(trifluoromethyl)-5*H*-dibenzo-[*b*,*d*]thiophen-5-ium trifluoromethanesulfonate as a trifluoromethane source in combination with a robust nickel complex as catalyst (Scheme 70B). In the scope study, the authors not only described the successful synthesis of several activated compounds (**225**–**228**), but they also used known biologically active substances as substrates for this methodology (Scheme 70C).

In the same year, Wang and co-workers published a work describing a stereoselective nickel-catalyzed C–H difluoroalkylation for the formation of both tetrasubstituted alkenes and quaternary difluoroalkylated products [303]. The distinction of which reaction takes place relies not only on the structure of the coupling partner, but also on the structure of the reactant itself since there are two removable hydrogen atoms necessary for the tetrasubstituted alkene to be formed (Scheme 71A and B). The method was also applied in a late-stage functionalization of bioactive molecules such as an estrone derivative (**229**) and donepezil (**152**) [219]. In both cases, the final products were successfully formed in good yields (Scheme 71C).

The versatility of nickel metal has made it also a considerably emerging metal. From the previous examples, it is clear that this metal plays an important role not only in usual C–H processes,

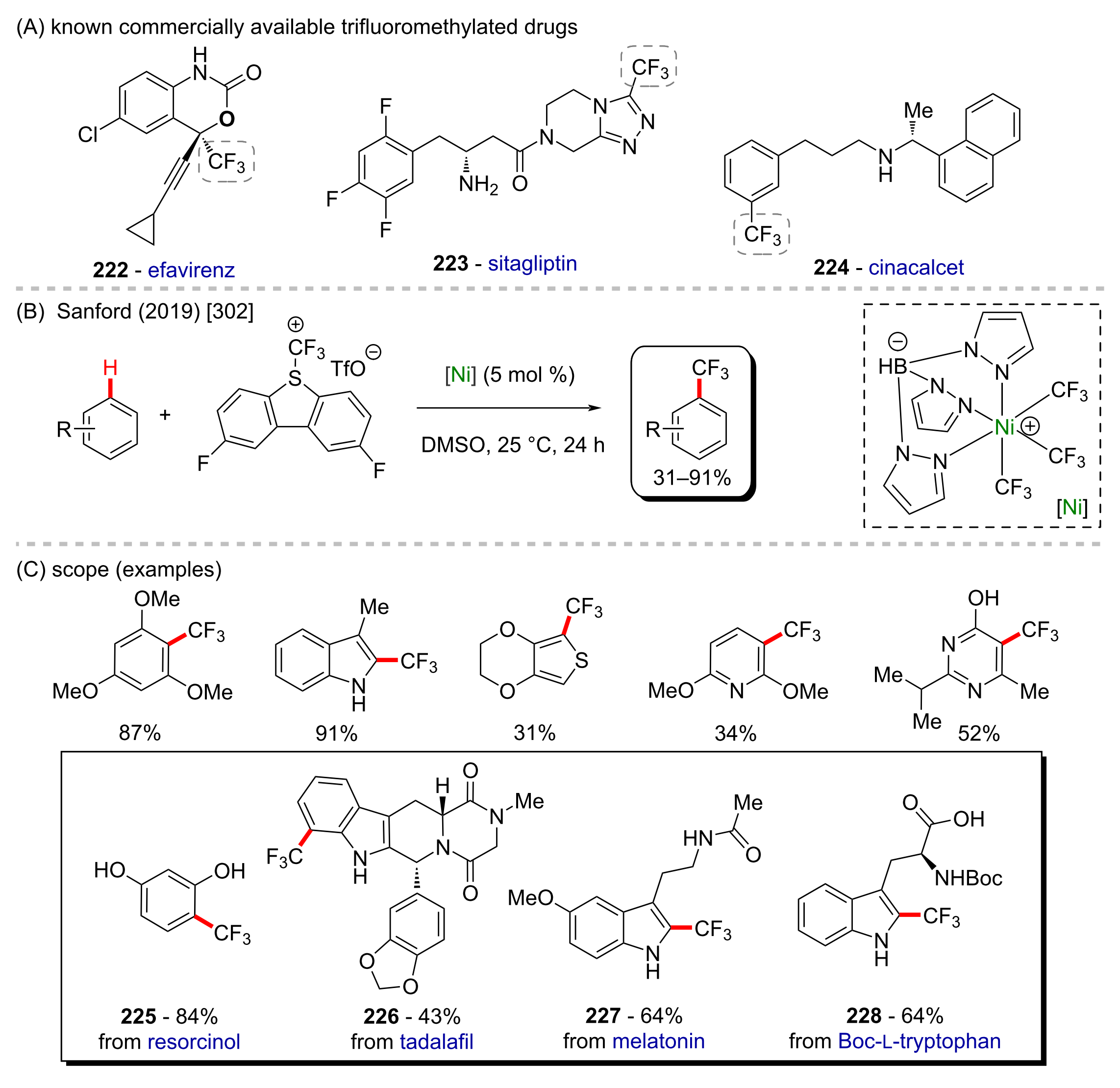
(A) known commercially available trifluoromethylated drugs
222 - efavirenz
223 - sitagliptin
224 - cinacalcet
(B) Sanford (2019) [302]
[Ni] (5 mol %)
DMSO, 25 °C, 24 h
31–91%
[Ni]
(C) scope (examples)
87%
91%
31%
34%
52%
225 - 84%
from resorcinol
226 - 43%
from tadalafil
227 - 64%
from melatonin
228 - 64%
from Boc-L-tryptophan

Scheme 70: (A) Known commercially available trifluoromethylated drugs; (B and C) nickel-catalyzed C–H trifluoromethylation.

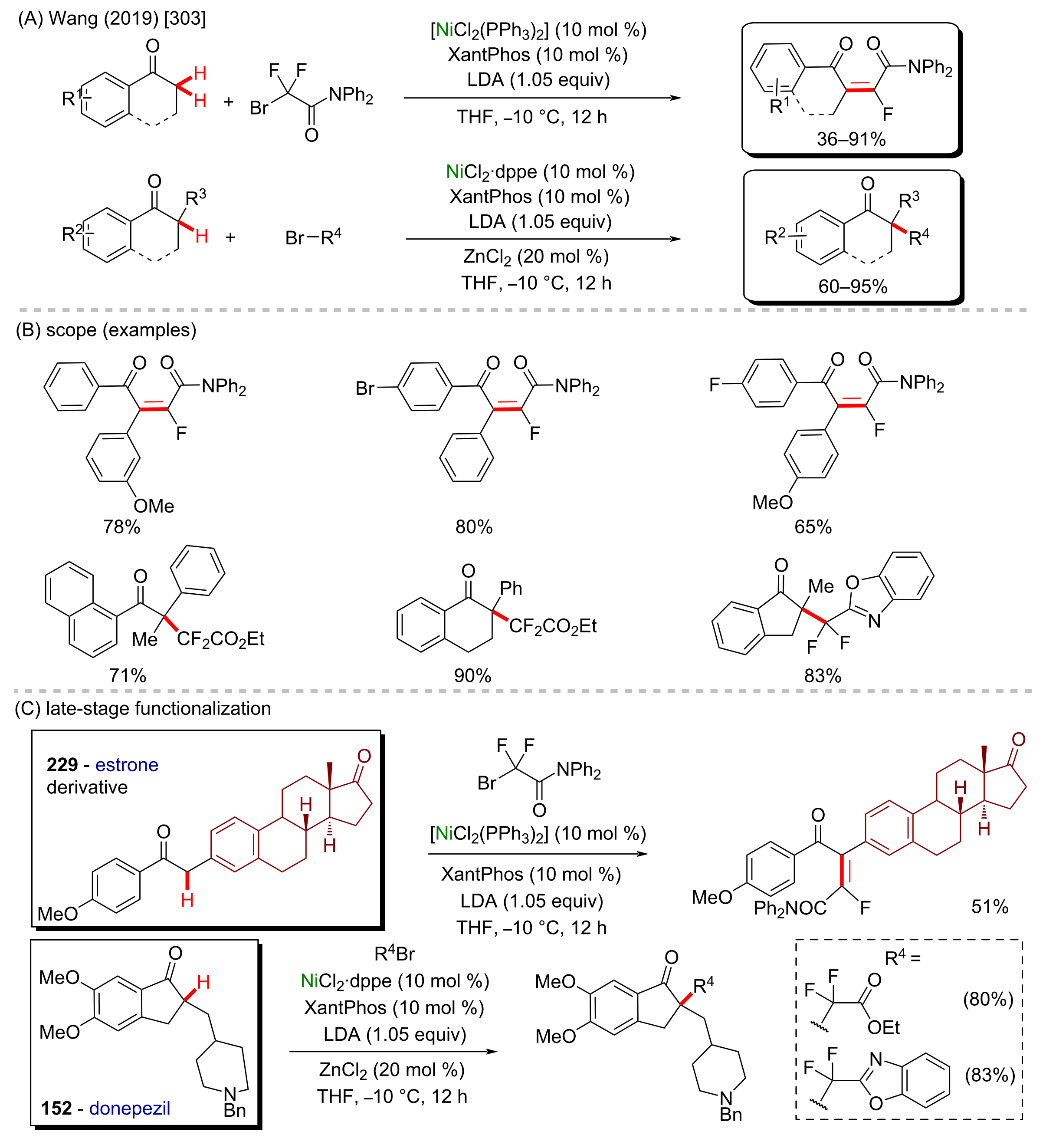
(A) Wang (2019) [303]
[NiCl$_2$(PPh$_3$)$_2$] (10 mol %)
XantPhos (10 mol %)
LDA (1.05 equiv)
THF, –10 °C, 12 h
36–91%
NiCl$_2$·dppe (10 mol %)
XantPhos (10 mol %)
LDA (1.05 equiv)
ZnCl$_2$ (20 mol %)
THF, –10 °C, 12 h
60–95%
(B) scope (examples)
78%
80%
65%
71%
90%
83%
(C) late-stage functionalization
229 - estrone derivative
51%
152 - donepezil
R^{4}Br
R^4 =
(80%)
(83%)

Scheme 71: (A and B) Stereoselective nickel-catalyzed C–H difluoroalkylation; (C) late-stage functionalization of bioactive molecules.

but even further, for the synthesis of bioactive molecules. Various important C–H functionalizations can be performed, including alkoxylations and trifluoromethylations.

Copper-catalyzed C–H activation

Copper is an abundant, non-expensive, and relatively nontoxic transition metal, and therefore copper-mediated reactions for direct functionalization of C–H bonds have emerged as promising tools for development of more sustainable methods for the synthesis of fine chemicals. Reactions involving copper-mediated C–H activations allow for a direct insertion of functional groups in unreactive C–H bonds and the formation of carbon–carbon bonds without the requirement of prefunctionalized substrates, which allow for shorter synthetic routes or late-stage modifications of structurally complex compounds [304-312]. However, the development of efficient methods can be challenging due to the requirement of directing groups and control of selectivity. In the case of reactions for applications in the synthesis of bioactive compounds, an additional challenge is the frequent presence of heterocycles containing metal-coordinating atoms, such as nitrogen and sulfur, that can compete with ligands and directing groups for coordination with the metal, leading to poor selectivity [313]. On the other hand, such heterocyclic moieties present in bioactive compounds, or their synthetic intermediates may eventually play the role of a directing group, thus providing an opportunity for convenient and straightforward transformations based on metal-mediated C–H activation [314]. Many methods potentially useful for the synthesis or modification of bioactive compounds based on copper-promoted activation of C–H bonds in (hetero)arenes have been reported in the last years, including methods for the formation of C–C [304-312], C–X [315-319], C–N [305,320-324], C–O [325-330], and C–S [324,331,332] bonds. Some of these methods are highlighted herein. It is worth mentioning that the covered examples were selected based on evidence for reaction mechanisms involving a metal-mediated C–H activation through the formation of cyclometalated species and applications in medicinal chemistry. The field of copper-mediated functionalization of C–H bonds is much broader and has been covered by excellent reviews [333-336].

Nitrogen-containing motifs, especially heteroaromatic rings, amines, and amides, are usually encountered in bioactive compounds, such as natural products, particularly alkaloids, and marketed drugs. For this reason, convenient methods for C–N bond formation reactions are particularly useful in medicinal chemistry and drug development and cost-effective and sustainable methods are required for industrial applications. Amination reactions involving a copper-mediated C(sp^2)–H bond activation were first achieved in 2006 by Yu and co-workers [315] and have proven useful for the synthesis of a wide range of anilines and heteroanilines, including drug intermediates.

A method for direct *ortho*-coupling of amines with anilines using a removable directing group and molecular oxygen as oxidant was recently reported by Wu and co-workers [337]. In this work, the introduction of cyclic secondary amines in the *ortho*-position through Cu-mediated C–H activation was achieved by using oxalamide as a weakly coordinating directing group (Scheme 72A), which can be removed after the reaction under basic conditions to deliver the corresponding *o*-aminoani-

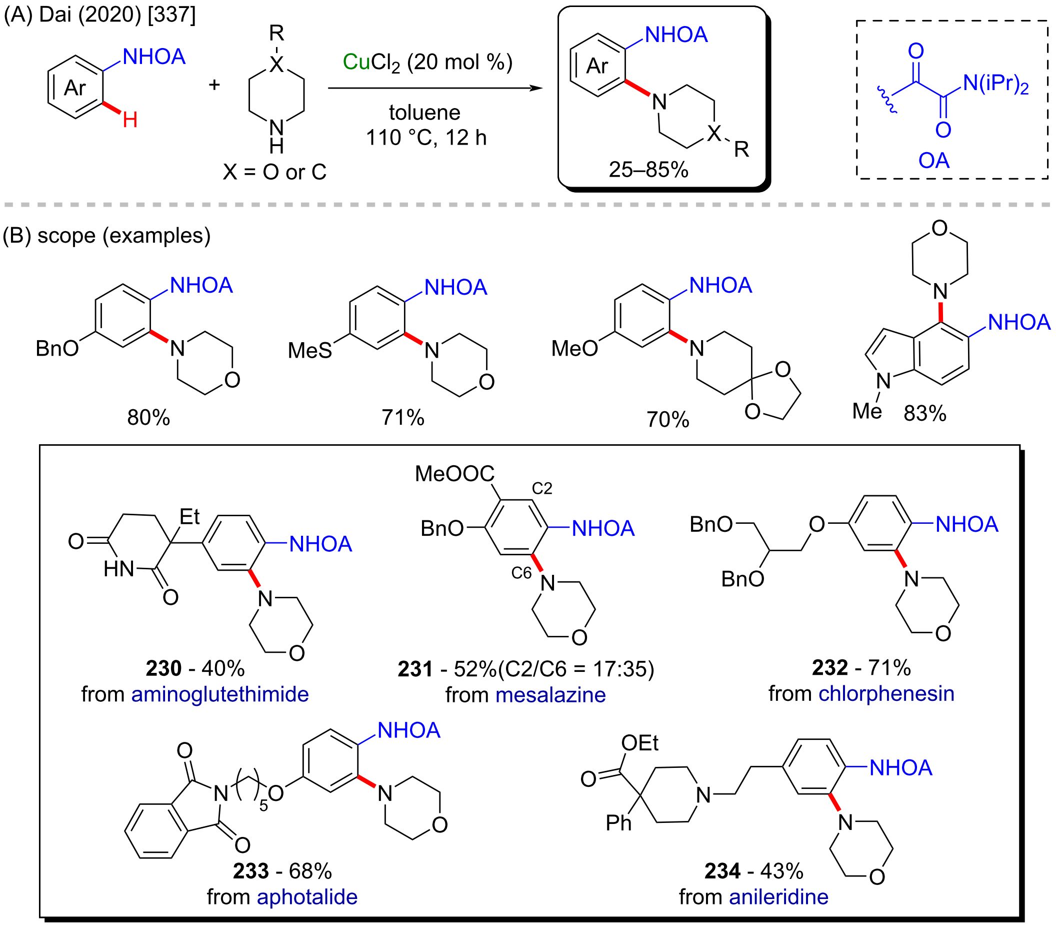
(A) Dai (2020) [337]
Ar
NHOA
H
R
X
N
H
X = O or C
CuCl2 (20 mol %)
toluene
110 °C, 12 h
25–85%
O
N(iPr)2
OA
(B) scope (examples)
BnO
MeS
MeO
O
80%
71%
70%
Me
83%
Et
HN
MeOOC
C2
C6
BnO
230 - 40%
from aminoglutethimide
231 - 52%(C2/C6 = 17:35)
from mesalazine
232 - 71%
from chlorphenesin
5
233 - 68%
from aphotalide
OEt
Ph
234 - 43%
from anileridine

Scheme 72: (A) Cu-mediated *ortho*-amination of oxalamides; (B) achieved scope, including derivatives obtained from bioactive compounds.

lines. The amination reaction is performed with Cu(I), which is oxidized by oxygen to Cu(II). The mechanism was suggested to involve a single-electron transfer step since radical scavengers completely inhibited the reaction. The method was showed to be suitable for a wide range of oxalamides as substrates whereas secondary amines, such as morpholine and piperazine, were used. Notably, the mild reaction conditions were compatible with many functional groups and with substrates bearing various heteroaromatic rings, which are common motifs in bioactive compounds. These features allowed the reaction to be applied for a late diversification of drugs (compounds **230**–**234**) (Scheme 72B).

A method for the C(sp^2)–N bond formation through a copper-mediated C(sp^2)–H bond activation without the requirement of an external oxidant was developed by Kathiravan and Nicholl's group [338]. Using a Pt plate and RVC electrodes and Cu(II) salts, a Cu-mediated electro-oxidative C–H/N–H cross coupling of 8-aminoquinoline-derived aryl amides and secondary amines could be performed (Scheme 73A). The reaction takes place under mild conditions and solely molecular hydrogen is released as a byproduct. This is in contrast to undesired metal products formed in reactions using stoichiometric external oxidants. The method was found feasible with several 8-aminoquinoline-derived amides and several secondary amines and the

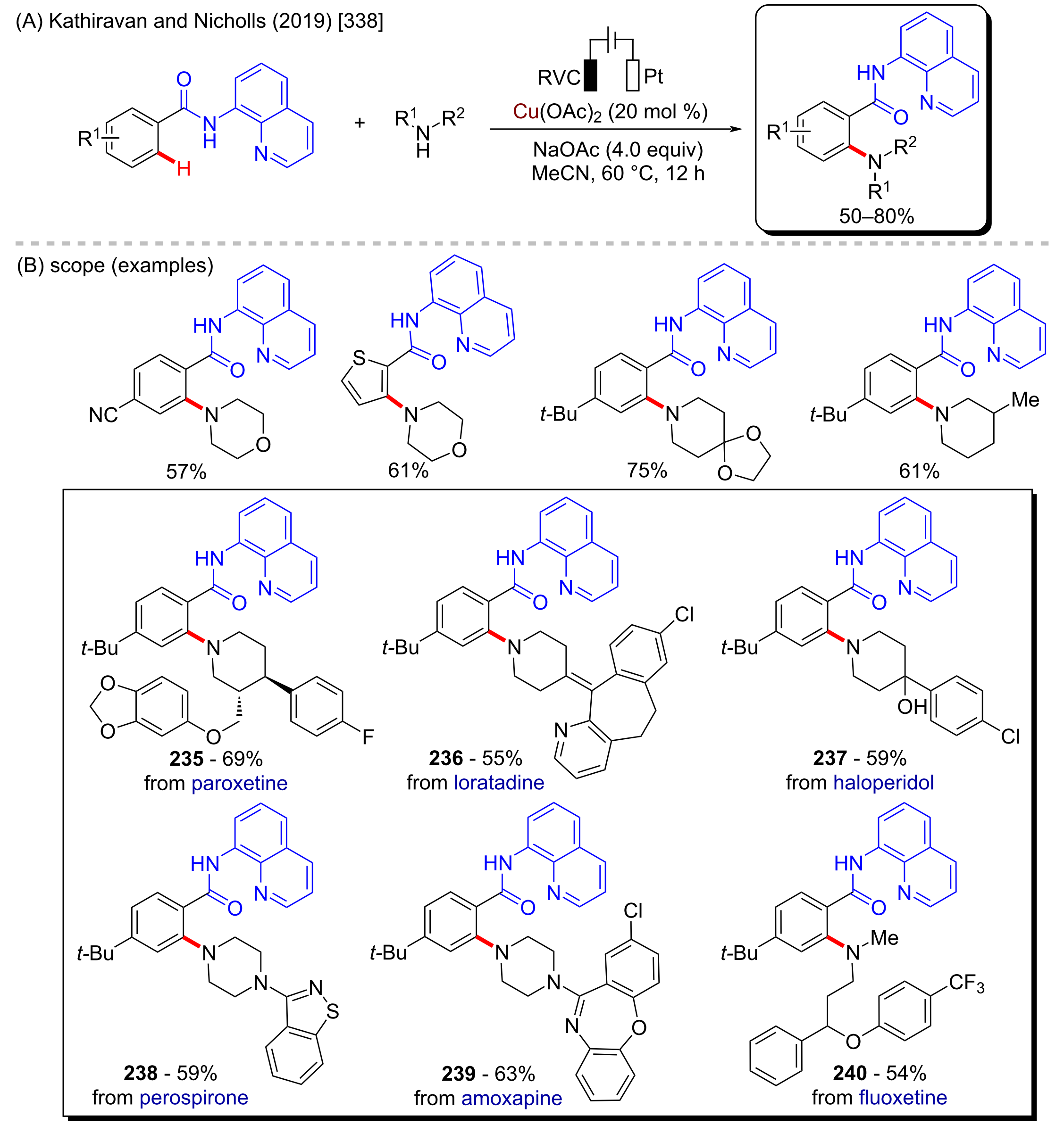
(A) Kathiravan and Nicholls (2019) [338]
R1
H
O
N
H
N
+
R1 N R2
H
RVC
Pt
Cu(OAc)2 (20 mol %)
NaOAc (4.0 equiv)
MeCN, 60 °C, 12 h
HN
O
N
R1
N R2
R1
50–80%
(B) scope (examples)
NC
57%
S
61%
t-Bu
75%
Me
61%
235 - 69%
from paroxetine
F
236 - 55%
from loratadine
Cl
237 - 59%
from haloperidol
OH
Cl
238 - 59%
from perospirone
239 - 63%
from amoxapine
240 - 54%
from fluoxetine
CF3

Scheme 73: (A) Electro-oxidative copper-mediated amination of 8-aminoquinoline-derived amides; (B) achieved scope, including derivatives obtained from bioactive compounds.

broad scope and chemoselectivity were corroborated by applying drugs (compounds **235**–**240**) as the amine counterparts (Scheme 73B).

Primary anilines are useful building blocks in medicinal chemistry since they can be used as intermediates in the synthesis of heterocycles and are often a structural motif in bioactive compounds [69-71]. For this reason, the direct introduction of a free amino group into an arene moiety through C(sp^2)–H amination to give primary anilines is a valuable transformation. However, selectivity issues and the strength of the metal–NH_2 bond make the development of methods for such reactions a challenging task. For this purpose, the use of oximes as amino group sources and Cu(I) salts were reported to promote the *ortho*-amination of amides via metal-mediated C(sp^2)–H activation (Scheme 74A and B) [314]. The reaction was found to work well with an amide oxazoline group as a directing group, CuOAc as Cu(I) salt, and K_2HPO_4 as an additive giving aryl imines, which could then be hydrolyzed in situ under acid conditions to give the corresponding primary anilines. Because oximes also acted as oxidants, no additional external oxidant was required. The method was found to present a broad scope and displayed high chemoselectivity, being feasible for the *ortho*-amination of a wide variety of aryl amides bearing

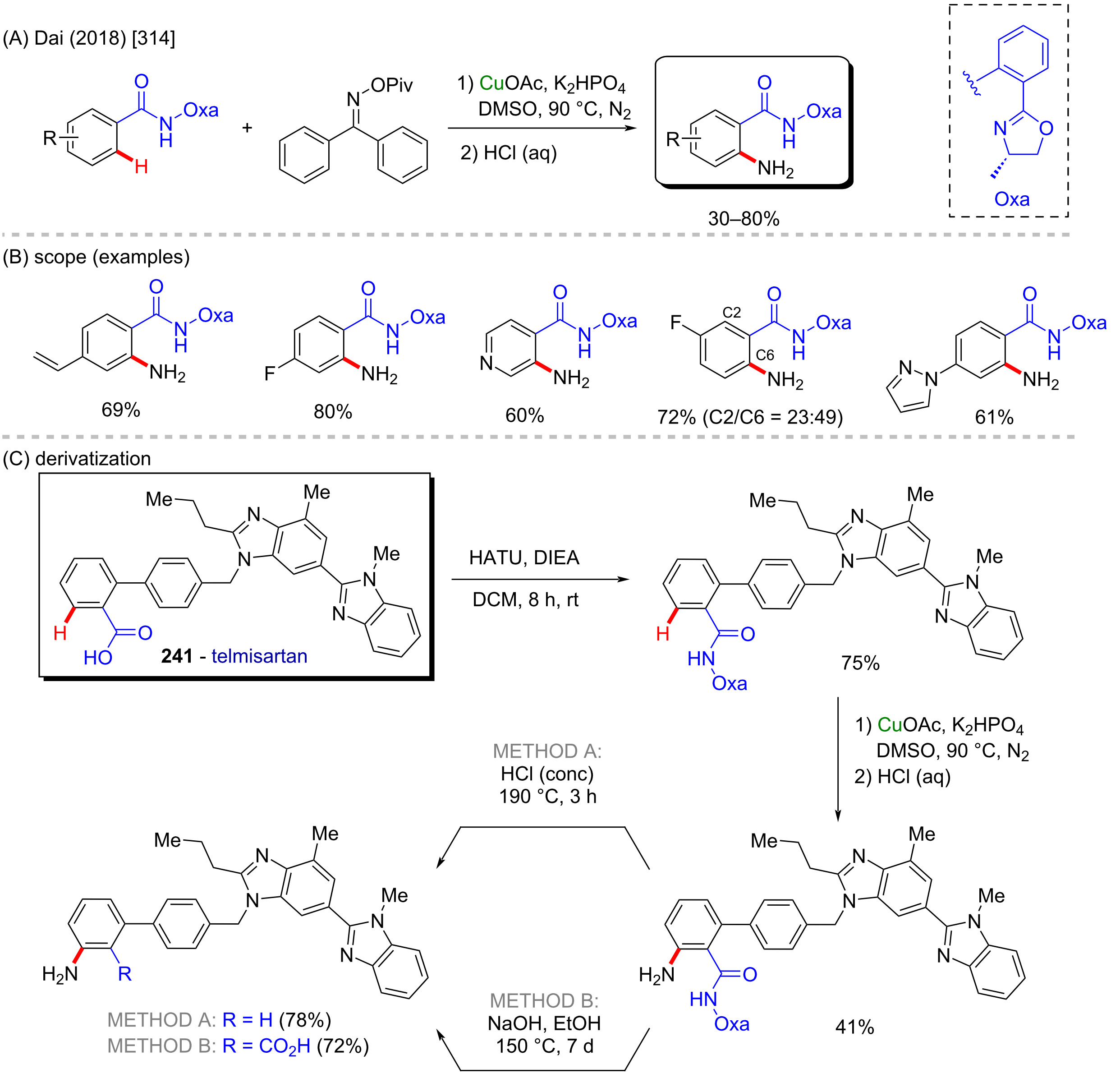
(A) Dai (2018) [314]
O
N-Oxa
H
R
H
+
N-OPiv
1) CuOAc, K2HPO4
DMSO, 90 °C, N2
2) HCl (aq)
NH2
30–80%
N
O
Oxa
(B) scope (examples)
69%
80%
F
60%
N
F
C2
C6
72% (C2/C6 = 23:49)
N-N
61%
(C) derivatization
Me
N
241 - telmisartan
HO
HATU, DIEA
DCM, 8 h, rt
HN
Oxa
75%
1) CuOAc, K2HPO4
DMSO, 90 °C, N2
2) HCl (aq)
41%
METHOD A:
HCl (conc)
190 °C, 3 h
METHOD B:
NaOH, EtOH
150 °C, 7 d
H2N
R
METHOD A: R = H (78%)
METHOD B: R = CO2H (72%)

Scheme 74: (A and B) Cu(I)-mediated C–H amination with oximes; (C) derivatization using telmisartan (**241**) as starting material.

various functional groups. It is noteworthy that the reaction also could be performed with heteroaryl amides featuring *N*-containing heteroaromatic rings to give the products in moderate to good yields, since these are challenging substrates due to the possibility of undesired coordination to the metal. The oxazoline amide group could also be further converted to a carboxyl group by treatment with a base or completely removed through decarboxylation under acid conditions at high temperature. The usefulness of the method was demonstrated by the introduction of an amino group into the drug telmisartan (**241**). Taking advantage of a carboxyl group in the molecule, the directing group could be introduced through an amidation reaction. The Cu(I)-mediated C–H amination was then performed and followed either by amide hydrolysis to give the original carboxyl group or by a complete removal of the directing group (Scheme 74C).

Although ammonia strongly coordinates to metals, leading to catalyst poisoning, the introduction of an amino group into the *ortho*-position of oxazoline-derived aryl amides via C–H activation using aqueous ammonia was accomplished by aid of a soft, low-valent Cu(I) species (Scheme 75A and B) [339]. Preliminary studies suggested that the reaction mechanism involves disproportionation of the Cu(I) species leading to the in situ formation of a Cu(III) species, which results in an increased acidity of a copper–amido intermediate, thus allowing for the deprotonation of copper-bound ammonia and a reductive elimination step to give the product. Noteworthy, attempts to perform the reaction using other transition metals, such as Pd, Pt, Co, Rh, and Ir were unsuccessful. The reaction was optimized with the use of acetate as the base to assist deprotonation and NMO as an oxidant, so that CuOAc could be used as the Cu(I) source in a substoichiometric amount. The method was

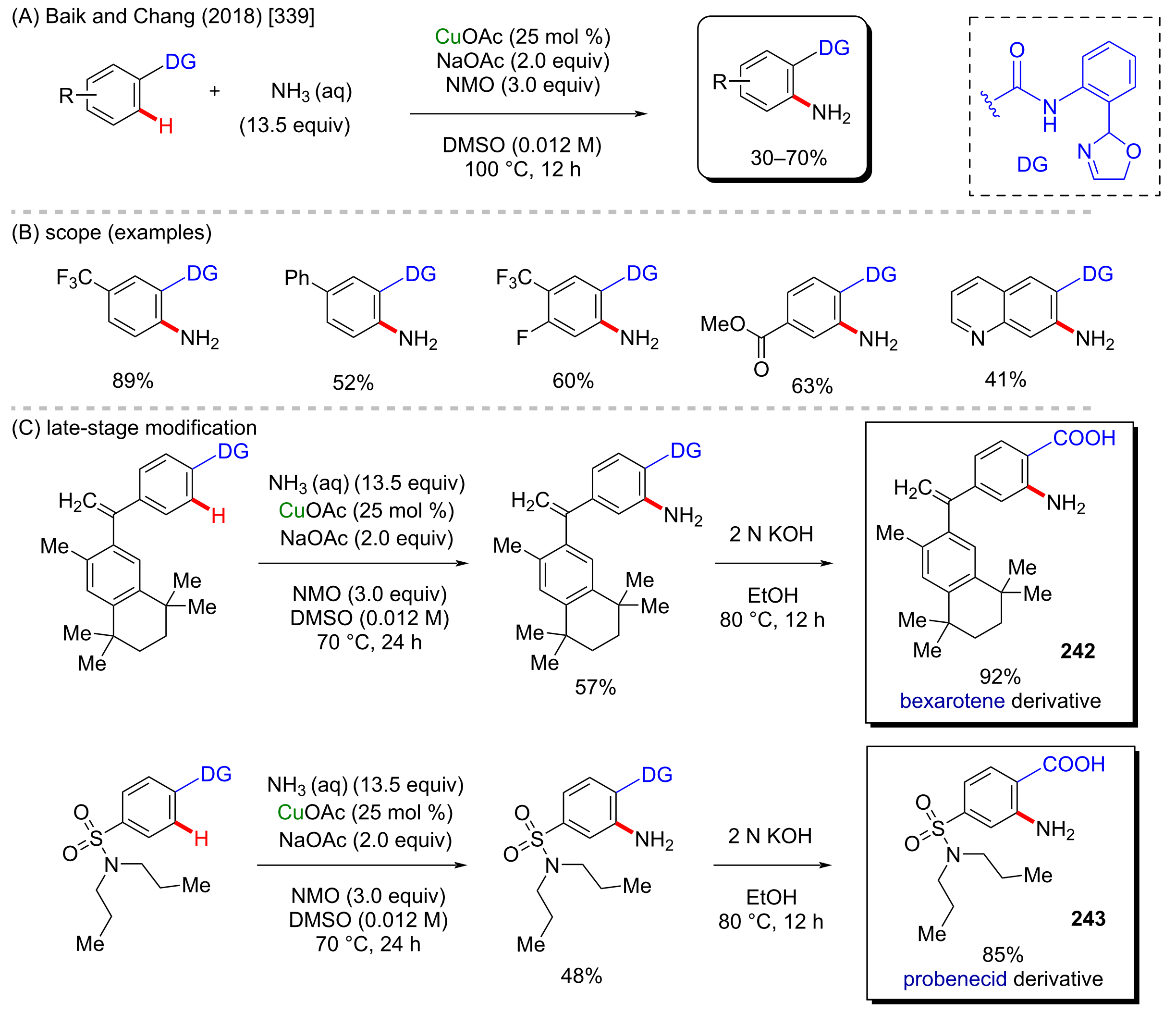
(A) Baik and Chang (2018) [339]
R
DG
H
+
NH_3 (aq)
(13.5 equiv)
CuOAc (25 mol %)
NaOAc (2.0 equiv)
NMO (3.0 equiv)
DMSO (0.012 M)
100 °C, 12 h
NH_2
30–70%
O
N
H
N
O
DG
(B) scope (examples)
F_3C
Ph
F
MeO
N
89%
52%
60%
63%
41%
(C) late-stage modification
H_2C
Me
NH3 (aq) (13.5 equiv)
CuOAc (25 mol %)
NaOAc (2.0 equiv)
NMO (3.0 equiv)
DMSO (0.012 M)
70 °C, 24 h
57%
2 N KOH
EtOH
80 °C, 12 h
COOH
242
92%
bexarotene derivative
O=S=O
48%
243
85%
probenecid derivative

Scheme 75: (A and B) Cu-mediated amination of aryl amides using ammonia; (C) late-stage modification of probenecid (**242**) and bexarotene (**243**).

found to present a broad scope and selectivity and was proven useful for the late-stage modification of drugs, such as probenecid (**242**) and bexarotene (**243**) (Scheme 75C).

The copper-mediated C–H activation for C–N bond formation is useful in the synthesis of *N*-containing heterocycles commonly encountered in bioactive compounds, such as pyrido[1,2-*a*]benzimidazoles [320], 1*H*-indazoles and 1*H*-pyrazoles [322], among others. For instance, a method for the modification of 6-anilinopurine nucleosides through copper-mediated C(sp^2)–H activation and intramolecular amination was reported to synthesize modified nucleosides, which are useful scaffolds in the design of antiviral drugs. The reaction could be performed with 6-anilinopurine nucleosides taking advantage of a purine ring as directing group without cleaving the fragile purine–glycoside bond (Scheme 76) [305].

Another example of the usefulness of a copper-mediated C–H activation reaction was reported by Duan, Zhang and co-workers in the synthesis of polycyclic 2-quinolinones, which are scaffolds present in bioactive alkaloids, such as orixalone D, mertinellic acid and meloscine (Scheme 77A) [321]. By using $Cu(OAc)_2$ in substoichiometric amount, O_2 as oxidant, and Kobayashi aryne precursors, the coupling of acrylamides derived from 8-aminoquinoline and arynes could be achieved with moderate to good yields, including three core skeletons of

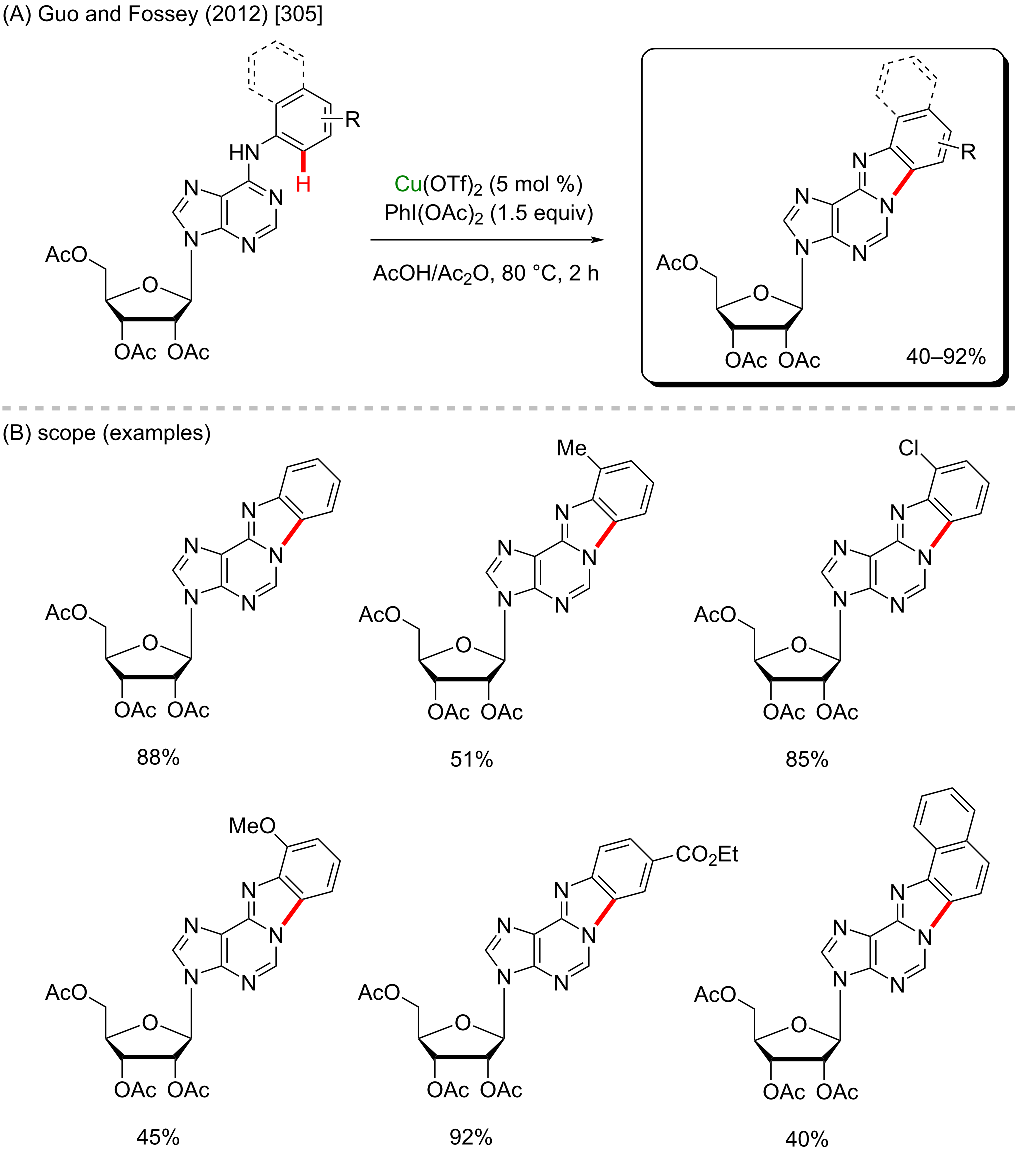

Scheme 76: (A and B) Synthesis of purine nucleoside analogues using copper-mediated C(sp^2)–H activation.

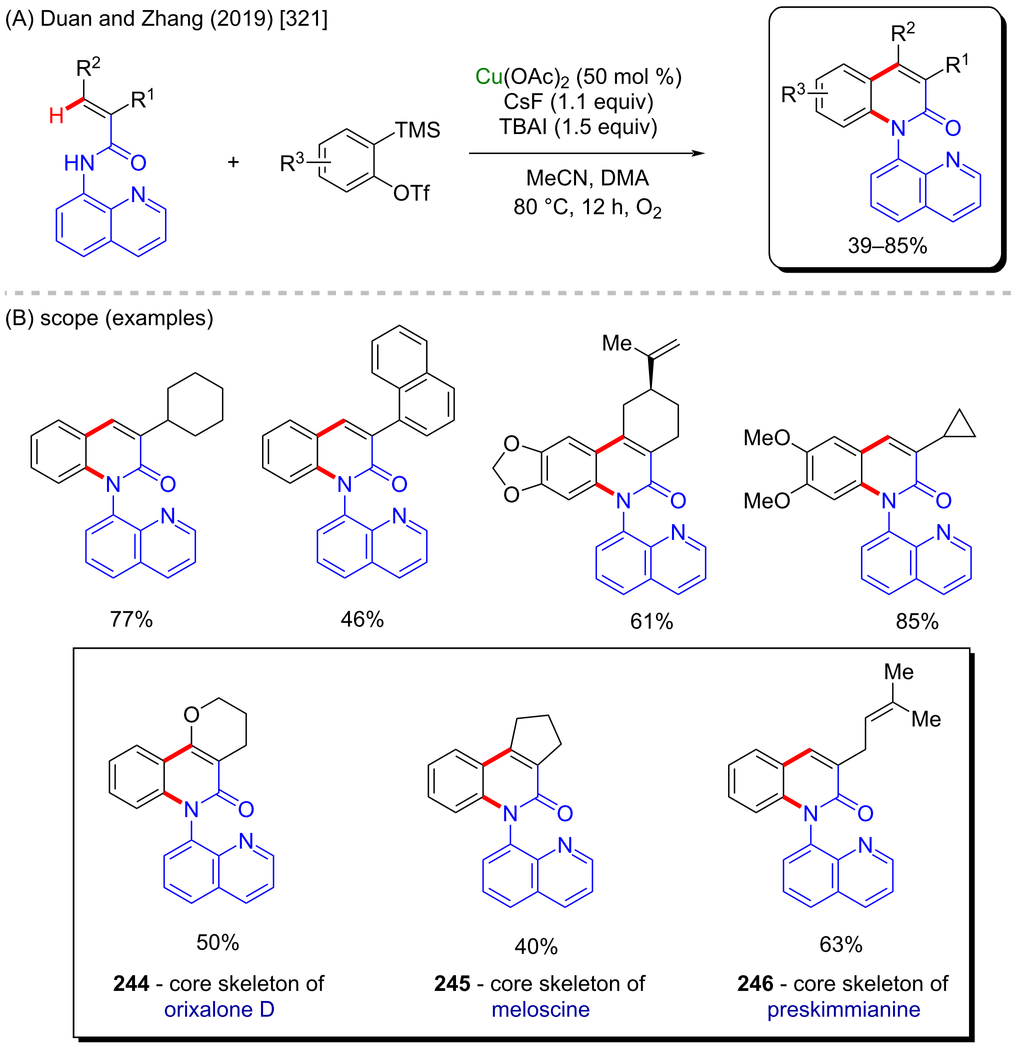
(A) Duan and Zhang (2019) [321]
R2
R1
H
HN
O
N
+
R3
TMS
OTf
Cu(OAc)2 (50 mol %)
CsF (1.1 equiv)
TBAI (1.5 equiv)
MeCN, DMA
80 °C, 12 h, O2
39–85%
(B) scope (examples)
77%
46%
Me
MeO
MeO
61%
85%
50%
244 - core skeleton of orixalone D
40%
245 - core skeleton of meloscine
63%
246 - core skeleton of preskimmianine

Scheme 77: (A) Copper-mediated annulation of acrylamide; (B) achieved scope, including the synthesis of the core skeletons of three bioactive molecules.

three important bioactive molecules (compounds **244–246**, Scheme 77B).

Copper has been reported to be useful in C–O bond-formation reactions involving C(sp^2)–H activation for the introduction of tosyl-, hydroxy-, acyloxy-, alkoxy-, and aryloxy groups into arenes [324-328,330]. A copper-based method was reported by Punniyamurthy and co-workers who applied a copper-based method to the synthesis of naphthyl aryl ethers, which are motifs featured by bioactive compounds, such as the antimalarial drug tafenoquine (**248**) (Scheme 78A) [329]. The naphthyl aryl ethers were obtained from picolinic acid-derived naphthylamides, arylboronic acids, and water as an oxygen source. Picolinamide was found to be a proper directing group, which was ascribed to its ability to act as *N*,*N*-bidentate ligand with copper and the relative acidity of its NH group (Scheme 78B and C). Mechanistic studies confirmed water, which is released into the reaction medium by reaction of the base with acetic acid, as the oxygen source. They suggested the reaction to involve an intramolecular C–H activation through cyclometalation and the formation of a Cu(III) species. The method was shown to present a broad scope and chemo- and regioselectivity. Also, the directing group could be removed by hydrolysis with an ethanolic solution of NaOH under reflux.

Reactions for C–C-bond formation involving copper-mediated C–H bond activation have been reported and some of them have shown to be useful in medicinal chemistry. For instance, Tian, Loh and co-workers reported a method for the direct and *ortho*-selective alkylation of *N*-oxide arenes under mild conditions with a copper-complex as a photocatalyst (Scheme 79A and B) [340]. In this method, several hypervalent iodine carboxylates

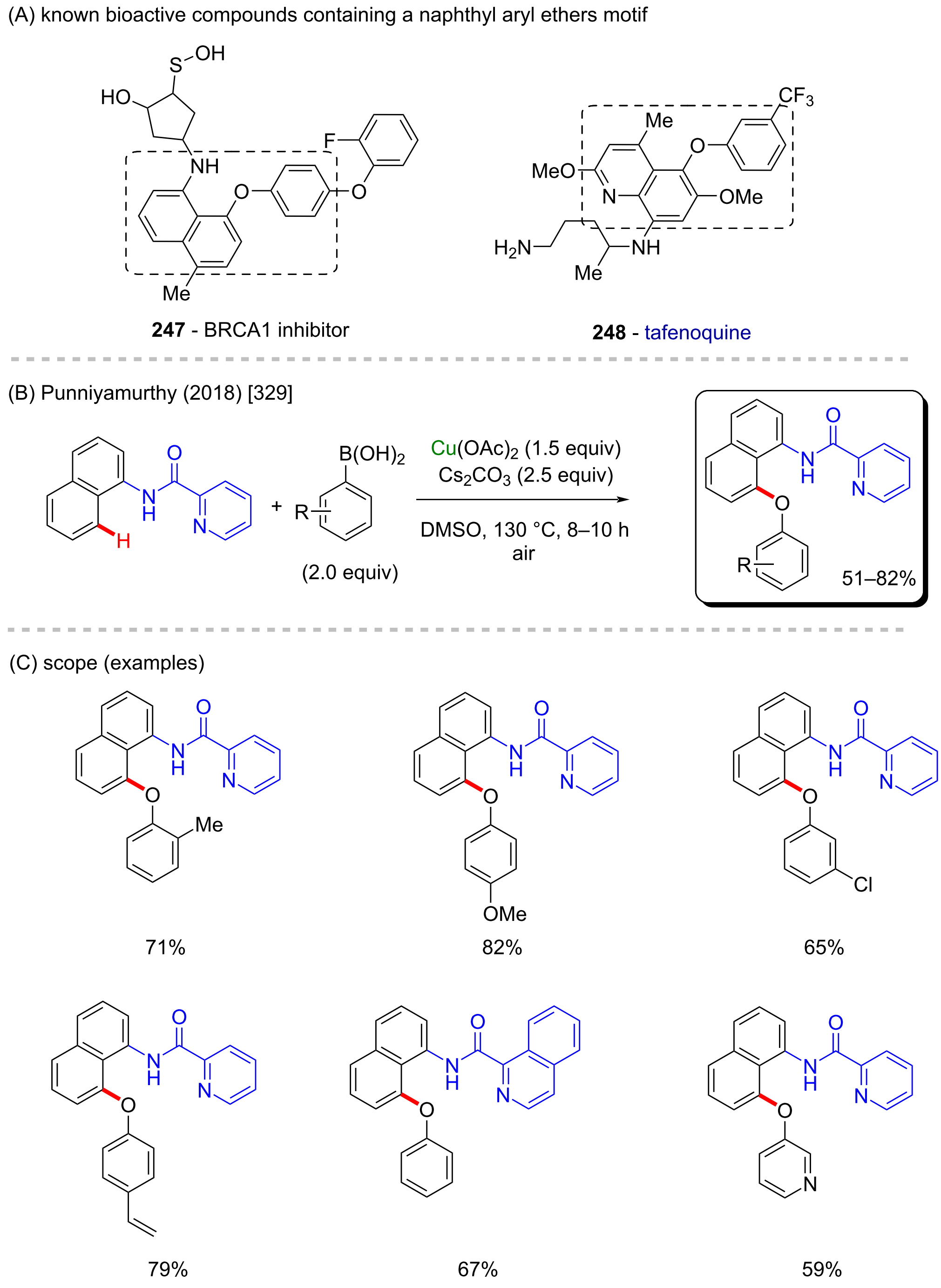
(A) known bioactive compounds containing a naphthyl aryl ethers motif
S
OH
HO
NH
O
F
O
Me
247 - BRCA1 inhibitor
CF3
Me
MeO
N
O
OMe
H2N
NH
Me
248 - tafenoquine
(B) Punniyamurthy (2018) [329]
O
N
H
N
H
+
R
B(OH)2
(2.0 equiv)
Cu(OAc)2 (1.5 equiv)
Cs2CO3 (2.5 equiv)
DMSO, 130 °C, 8–10 h
air
51–82%
(C) scope (examples)
Me
71%
OMe
82%
Cl
65%
79%
67%
59%

Scheme 78: (A) Known bioactive compounds containing a naphthyl aryl ether motif; (B and C) copper-mediated etherification of naphthylamides through C–H bond activation.

prepared from non-expensive raw materials were used as alkylating agents. The reaction took place under visible light irradiation and was proposed to involve the photocatalytic production of an alkyl radical and metallization of position C-2 of the *N*-oxide heteroarene. The reaction could be carried out with diverse *N*-oxide arenes and alkylating agents affording the products in moderate to good yields. The usefulness and chemoselectivity of the method were demonstrated by the coupling of a quinine derivative **249** and dehydrocholic acid (**250**) (Scheme 79C).

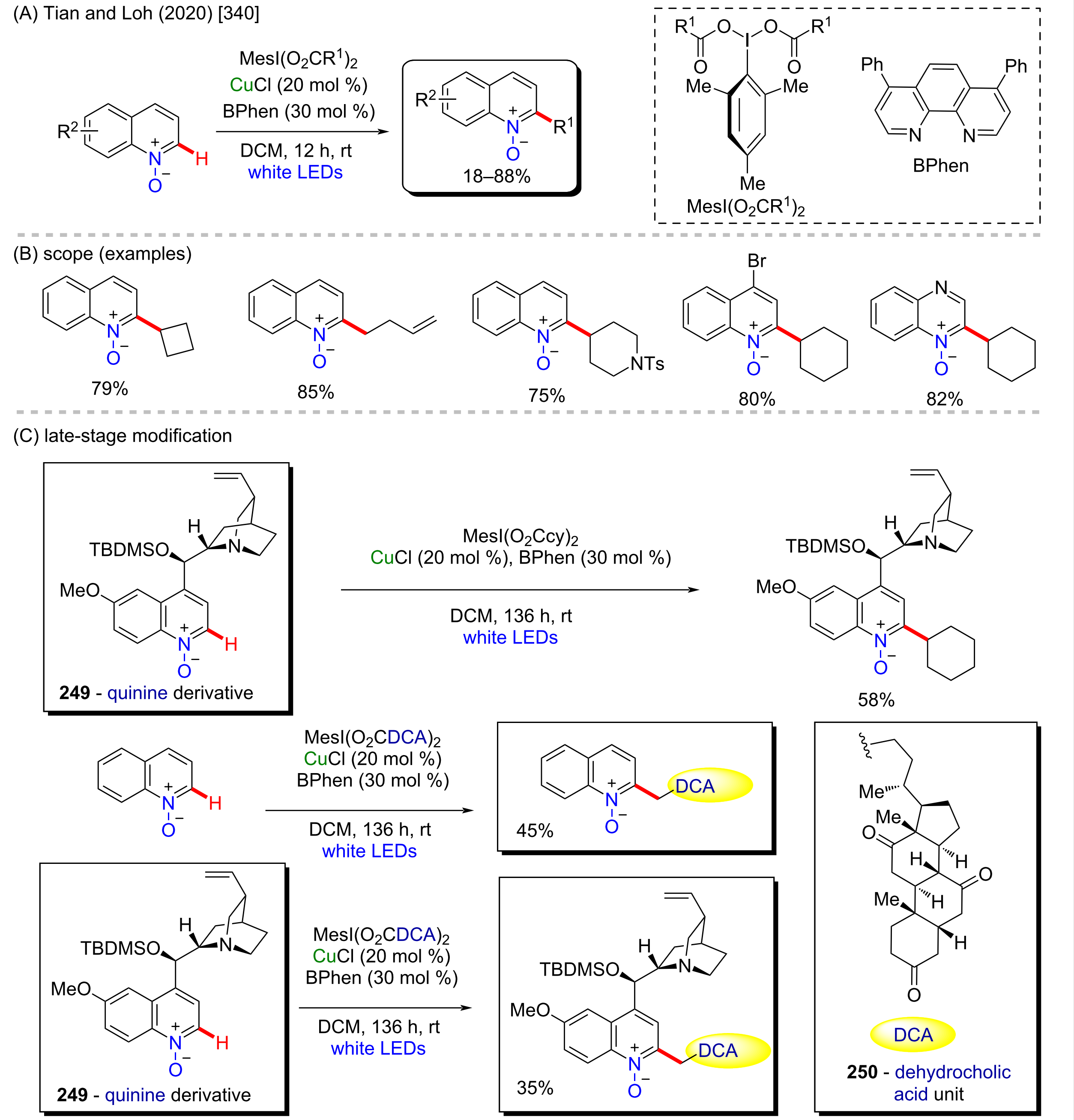
(A) Tian and Loh (2020) [340]
MesI(O2CR1)2
CuCl (20 mol %)
BPhen (30 mol %)
DCM, 12 h, rt
white LEDs
18–88%
MesI(O2CR1)2
BPhen
(B) scope (examples)
79%
85%
75%
80%
82%
(C) late-stage modification
249 - quinine derivative
MesI(O2Ccy)2
CuCl (20 mol %), BPhen (30 mol %)
DCM, 136 h, rt
white LEDs
58%
MesI(O2CDCA)2
CuCl (20 mol %)
BPhen (30 mol %)
DCM, 136 h, rt
white LEDs
45%
35%
250 - dehydrocholic acid unit

Scheme 79: (A and B) Cu-mediated alkylation of *N*-oxide-heteroarenes; (C) late-stage modification.

A method for the direct alkylation of polyfluoroarenes using non-functionalized alkanes was recently reported. The reaction requires the activation of both the C(sp^2)–H bond of the fluoroarene and the C(sp^3)–H bond of the alkane, thus it is challenging due to the possibility of homocoupling and overall alkylation. A cross-dehydrogenative coupling of polyfluoroarenes and alkanes was achieved by the use of a Cu(I) salt and a β-ketimide ligand in the presence of di-*tert*-butyl peroxide as the oxidant (Scheme 80A) [313]. The choice of a proper ligand was suggested to be a crucial issue to achieve selectivity and facilitate the reaction due to interactions with the arene substrates. The reaction was found to present a broad scope regarding the obtained drug derivatives and the synthesis of the fluorinated drug precursors **251**–**256** (Scheme 80B and C). In addition, the method was carried out in a decagram scale to furnish the polyfluorinated biaryl product with 80% yield from the coupling of 2,3,5,6-tetrafluoroanisole and ethylbenzene, which could be further converted to different products through hydrodefluorination by nucleophilic aromatic substitution of fluorine atoms.

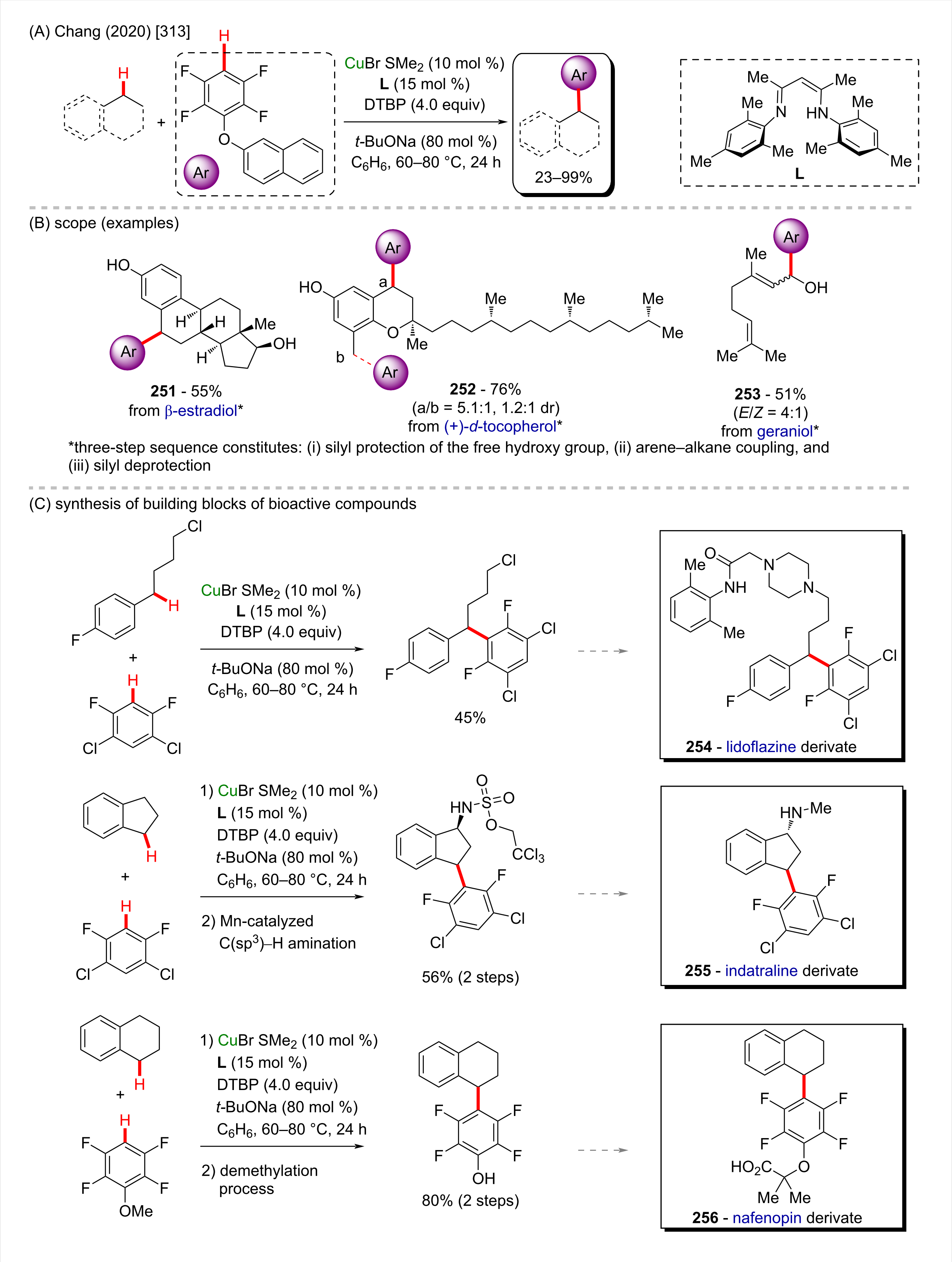
(A) Chang (2020) [313]
H
F
F
F
F
O
Ar
CuBr SMe2 (10 mol %)
L (15 mol %)
DTBP (4.0 equiv)
t-BuONa (80 mol %)
C6H6, 60–80 °C, 24 h
Ar
23–99%
Me
Me
Me
N
HN
Me
Me
Me
Me
Me
L
(B) scope (examples)
HO
H
H
H
Me
OH
Ar
251 - 55%
from β-estradiol*
HO
a
Ar
O
Me
Me
Me
Me
Me
b
Ar
252 - 76%
(a/b = 5.1:1, 1.2:1 dr)
from (+)-d-tocopherol*
Ar
Me
OH
Me
Me
253 - 51%
(E/Z = 4:1)
from geraniol*
(C) synthesis of building blocks of bioactive compounds
Cl
H
F
+
H
F
F
Cl
Cl
CuBr SMe2 (10 mol %)
L (15 mol %)
DTBP (4.0 equiv)
t-BuONa (80 mol %)
C6H6, 60–80 °C, 24 h
Cl
F
Cl
F
F
Cl
45%
Me
O
N
NH
N
Me
F
Cl
F
F
Cl
254 - lidoflazine derivate
H
+
H
F
F
Cl
Cl
1) CuBr SMe2 (10 mol %)
L (15 mol %)
DTBP (4.0 equiv)
t-BuONa (80 mol %)
C6H6, 60–80 °C, 24 h
2) Mn-catalyzed
C(sp3)–H amination
O
HN
S
O
O
CCl3
F
F
Cl
Cl
56% (2 steps)
HN
Me
F
F
Cl
Cl
255 - indatraline derivate
H
+
H
F
F
F
F
OMe
1) CuBr SMe2 (10 mol %)
L (15 mol %)
DTBP (4.0 equiv)
t-BuONa (80 mol %)
C6H6, 60–80 °C, 24 h
2) demethylation
process
F
F
F
F
OH
80% (2 steps)
F
F
F
F
HO2C
O
Me
Me
256 - nafenopin derivate

*three-step sequence constitutes: (i) silyl protection of the free hydroxy group, (ii) arene–alkane coupling, and (iii) silyl deprotection

Scheme 80: (A) Cu-mediated cross-dehydrogenative coupling of polyfluoroarenes and alkanes; (B) scope from known bioactive substrates; (C) synthesis of building blocks for bioactive compounds.

The acrylonitrile products **257** and **258** have shown potential anticancer activity against eight different cell lines (Scheme 81A) [341]. The direct cyanation of alkenes and (hetero)aromatic compounds are useful reactions that have been reported to be accomplished through copper-mediated activation of C(sp^2)–H bonds [342-344]. Such cyanation reactions are attractive for medicinal chemistry purposes, since nitrile groups are present in drugs, such as nivapidine and entacapone, and can also give access to other medicinally relevant functional groups, such as amines, amides, carboxylic acids, and *N*-containing heterocycles. A method for obtaining acrylonitriles through copper-mediated activation of alkene C–H bonds was recently reported for the first time by Zhu and co-workers (Scheme 81B and C) [343]. The reaction could be performed by using iminonitrile as a nitrile source and a pyridine moiety as a directing group to give the cyanated compounds with moderate to good yields.

Methods for introducing halogens into organic compounds are useful in organic synthesis, since halogen atoms can be further replaced by other functional groups, so that halogenated compounds are often required as synthetic intermediates [345-347]. Moreover, many bioactive compounds feature halogen atoms [348]. The halogenation of arenes has been accomplished through the Cu-mediated activation of C(sp^2)–H bonds. An example of the usefulness of this transformation for drug development was provided by Scott and Sanford, who developed a method for radiofluorination of arenes mediated by Cu(I) salts and K^{18}F as a source of nucleophilic radioactive fluorine (Scheme 82A) [349]. The reaction was accomplished using NMM, DBU as the base additive and with 8-aminoquinoline as a directing group, so that an *ortho*-selective radiofluorination of 8-aminoquinoline-derived arylamide could be achieved. The chemoselectivity and broad scope allowed the reactions to be employed for late-stage radiofluorination of the bioactive compounds **259** and **260**, thus furnishing ^{18}F-containing compounds which are useful for positron emission tomography (PET) imaging (Scheme 82B). The method could be adapted for automated synthesis and further amide hydrolysis to remove the directing group. The developed protocol was found to be useful for the ^{18}F-labeling of AC261066 (**261**), an agonist of the retinoic acid receptor β (RAR-β).

The cited examples make is easy to understand why copper is one of the most applicable metals in C–H activation reactions. Its versatility makes it possible to develop not only C–H amina-

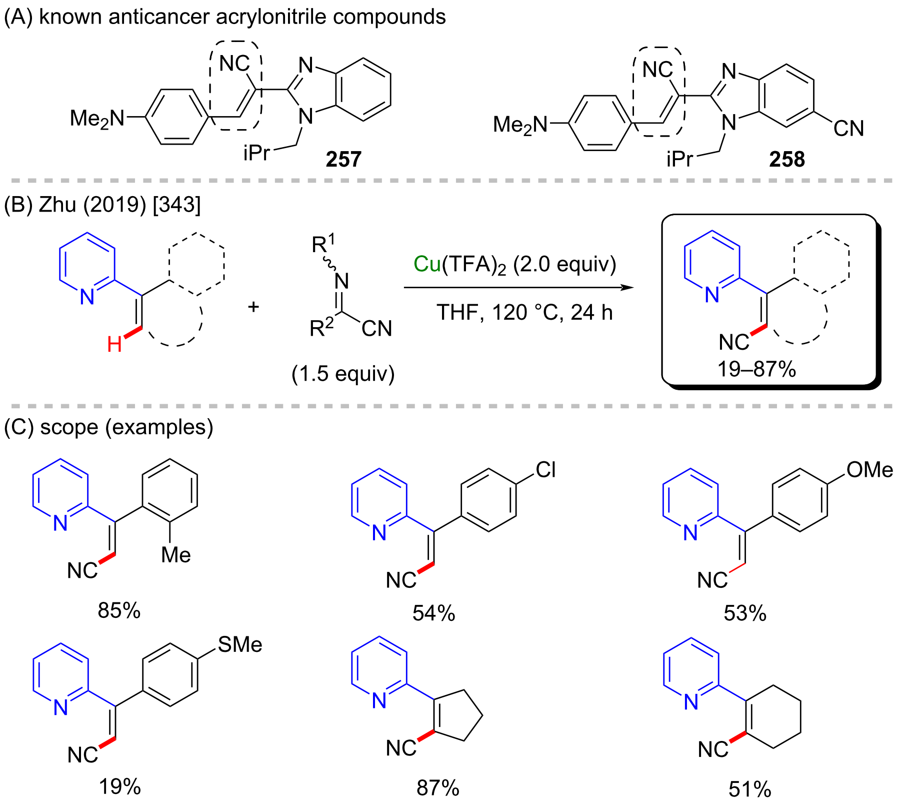

Scheme 81: (A) Known anticancer acrylonitrile compounds; (B and C) Copper-mediated cyanation of unactivated alkenes.

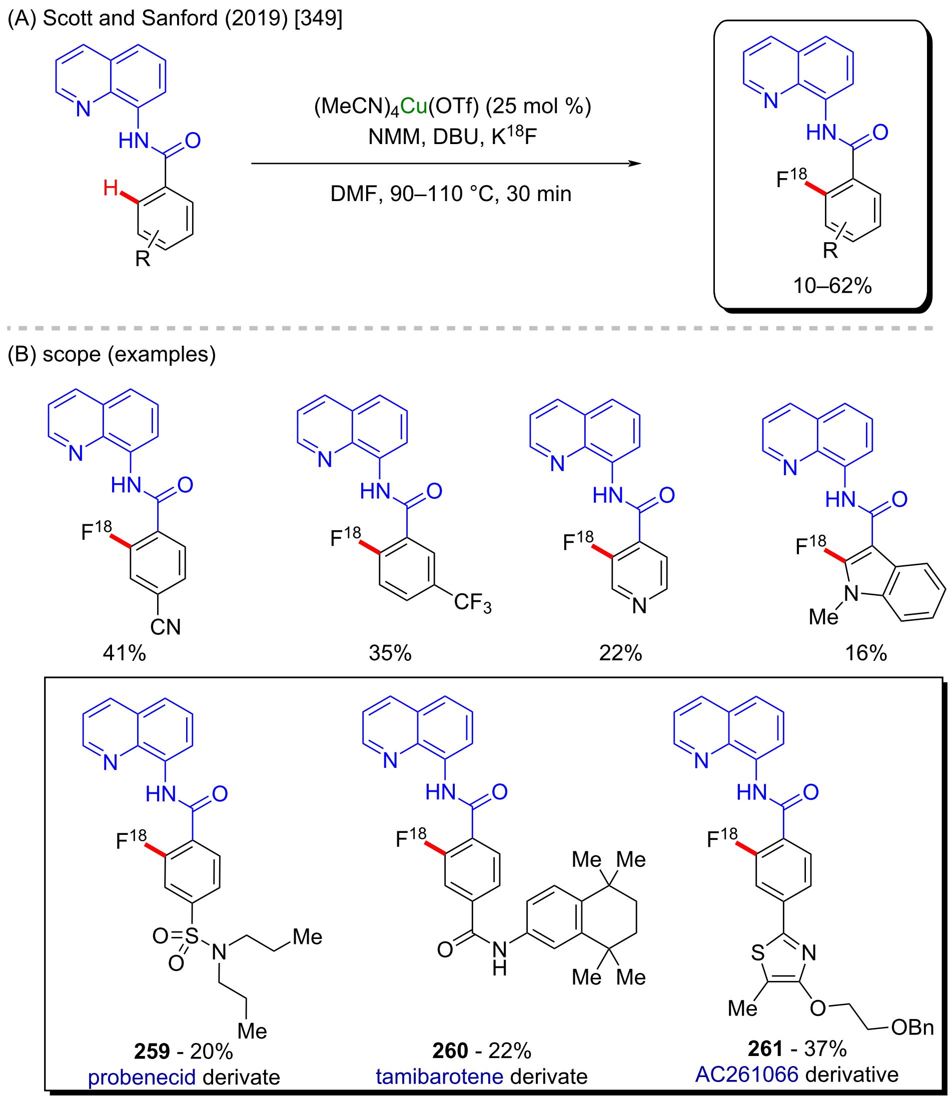

Scheme 82: (A) Cu-mediated radiofluorination of 8-aminoquinoline-derived aryl amides; (B) achieved scope, including three derivatives of bioactive molecules.

tion procedures, but also to achieve C–H arylation, and fluorination, among others. Using these different methodologies, several different bioactive motifs can be directly achieved and evaluated. Amongst with iron, nickel, and cobalt, copper represents one of the most promising metals for future progress in organic synthesis.

Zinc-catalyzed C–H activation

Zinc is the last 3d-metal in the periodic table, and it is extremely useful due to its numerous applications in different fields such as animal [350] and human diets [351], galvanizing solutions [352], cosmetics [353], and potential pharmaceutics [354]. Due to its relatively low costs it has been widely studied as a metallic source of several catalysts, either in its metallic [355], or in its ionic form [356]. Zinc-based catalysts have been successfully applied to the hydroamination of several ynamides [357], in the synthesis of chiral 2-arylpyrrolidines of pharmacological importance such as compounds **262**–**264**) [358], and in C–H-bond activation reactions [359,360]. Its use in the synthesis of biologically active compounds via C–H-bond activation remains a challenge, with only few examples being reported in the literature so far. One good example is presented in a work published by Lu, Ye and co-workers in 2015 [361]. In this work, the authors described an intramolecular zinc-catalyzed C–H functionalization towards the formation of several β-carboline derivatives (Scheme 83B). This scaffold is present in several important natural compounds with valuable biological activities (Scheme 83A) [362]. Using this singular method,

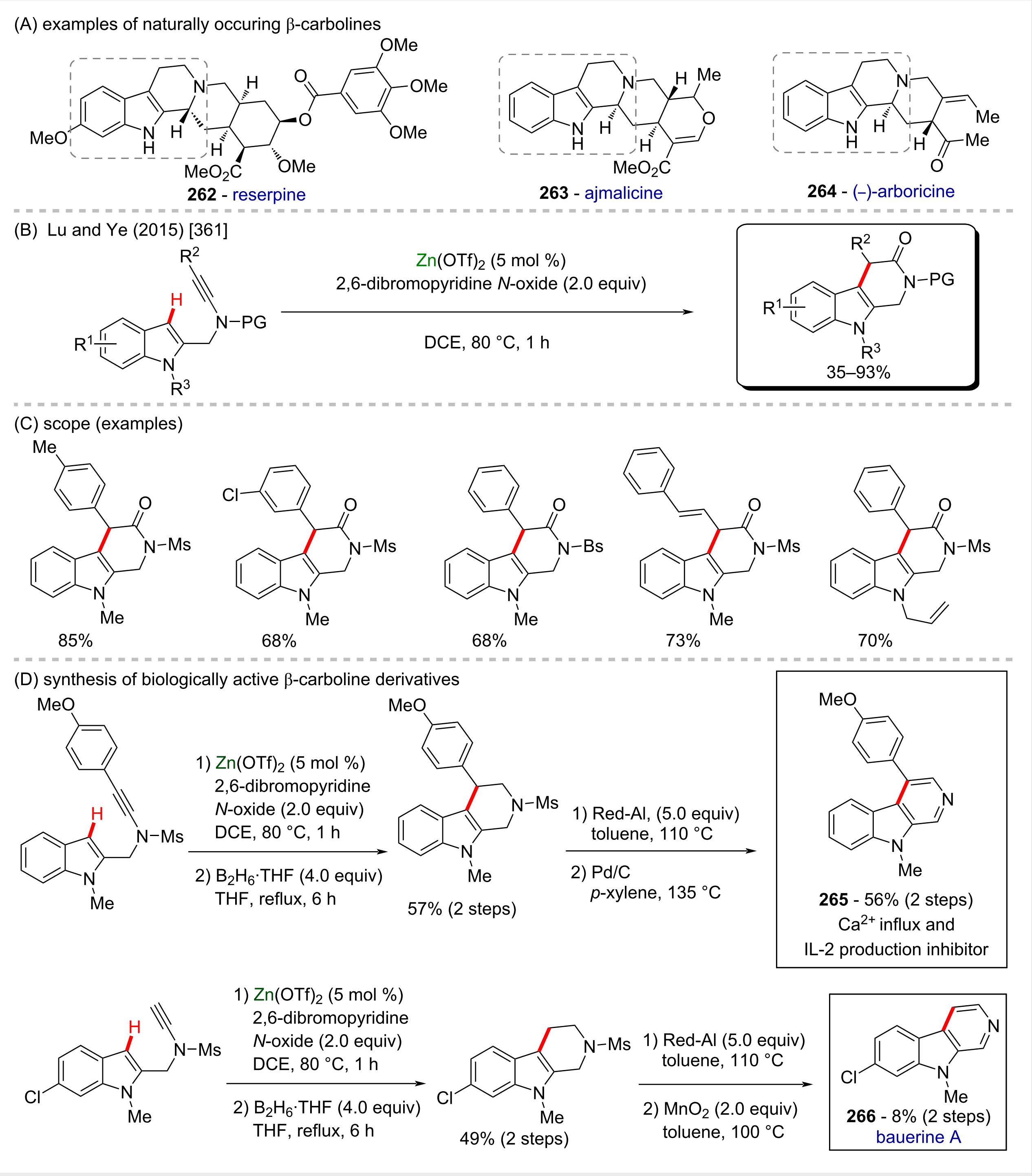
(A) examples of naturally occuring β-carbolines
262 - reserpine
263 - ajmalicine
264 - (–)-arboricine
(B) Lu and Ye (2015) [361]
Zn(OTf)2 (5 mol %)
2,6-dibromopyridine N-oxide (2.0 equiv)
DCE, 80 °C, 1 h
35–93%
(C) scope (examples)
85%
68%
68%
73%
70%
(D) synthesis of biologically active β-carboline derivatives
1) Zn(OTf)2 (5 mol %) 2,6-dibromopyridine N-oxide (2.0 equiv) DCE, 80 °C, 1 h
2) B2H6·THF (4.0 equiv) THF, reflux, 6 h
57% (2 steps)
1) Red-Al, (5.0 equiv) toluene, 110 °C
2) Pd/C p-xylene, 135 °C
265 - 56% (2 steps)
Ca2+ influx and IL-2 production inhibitor
49% (2 steps)
1) Red-Al (5.0 equiv) toluene, 110 °C
2) MnO2 (2.0 equiv) toluene, 100 °C
266 - 8% (2 steps)
bauerine A

Scheme 83: (A) Examples of natural β-carbolines; (B and C) an example of a zinc-catalyzed C–H functionalization; (D) synthesis of biologically active β-carbolines.

it was possible to obtain many cyclic benzyl- and indole-lactams in good to excellent yields (Scheme 83C). Following the same procedure, it was possible to synthesize the β-carboline **265** that acts as Ca^{2+} influx and IL-2 production inhibitor, and the natural β-carboline bauerine A (**266**) (Scheme 83D).

In 2012, Zhang and co-workers described a C–H amination of β-carbonylated compounds and one example of a β-ketophosphonate compound, in the presence of tosylamine and iodosobenzene [363]. The in situ-generated PhI=NTs, along with zinc perchlorate led to the formation of several aminated products in moderate to excellent yields (Scheme 84B and C),

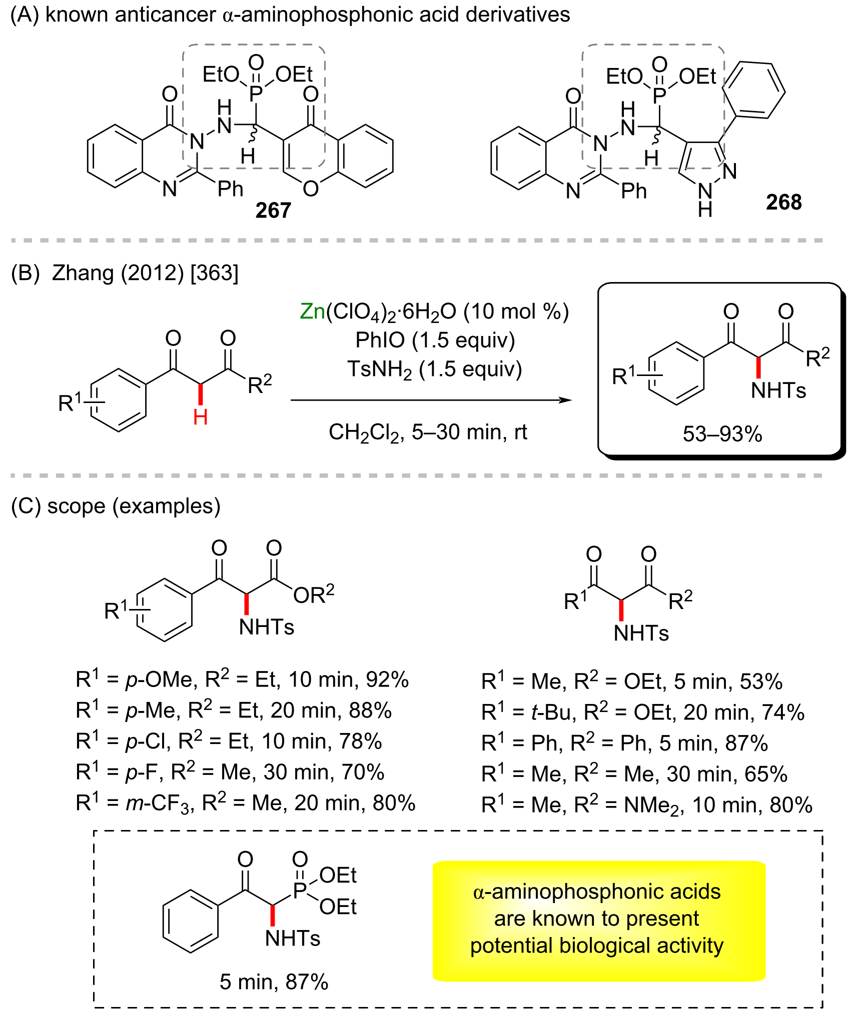
(A) known anticancer α-aminophosphonic acid derivatives
EtO
O
OEt
P
O
H
N
N
H
O
N
Ph
O
267
268
N
N
H
(B) Zhang (2012) [363]
Zn(ClO4)2·6H2O (10 mol %)
PhIO (1.5 equiv)
TsNH2 (1.5 equiv)
CH2Cl2, 5–30 min, rt
R1
R2
H
NHTs
53–93%
(C) scope (examples)
OR2
R1 = p-OMe, R2 = Et, 10 min, 92%
R1 = p-Me, R2 = Et, 20 min, 88%
R1 = p-Cl, R2 = Et, 10 min, 78%
R1 = p-F, R2 = Me, 30 min, 70%
R1 = m-CF3, R2 = Me, 20 min, 80%
R1 = Me, R2 = OEt, 5 min, 53%
R1 = t-Bu, R2 = OEt, 20 min, 74%
R1 = Ph, R2 = Ph, 5 min, 87%
R1 = Me, R2 = Me, 30 min, 65%
R1 = Me, R2 = NMe2, 10 min, 80%
5 min, 87%
α-aminophosphonic acids are known to present potential biological activity

Scheme 84: (A) Examples of anticancer α-aminophosphonic acid derivatives; (B and C) an example of a zinc-catalyzed C–H amination.

including α-aminophosphoric acid derivatives which resemble structures of known previously studied anticancer compounds **267** and **268** (Scheme 84A) [364].

In contrast to the previously discussed metals, zinc is lacking examples of its use as catalyst for the synthesis of bioactive compounds via C–H activation processes. It is also a cheap and low-toxic metal, and therefore it might have more to offer in this particular field. Therefore, deeper studies are worthy to be developed in order to make it easier and cheaper to obtain some complex but valuable potent bioactive substances using zinc catalysis.

Conclusion

This review visualizes not only the versatile applicability of the 3d metals as powerful catalysts in C–H functionalization methods, but in a deeper analysis, it allows to perceive that these accessible catalysts enable an easier formation of important biologically active substances. The access to crucial medicines that save thousands of lives every day can be difficult in several places due to the costs involved in their production and, of course, the subsequent cost to the final consumers. Therefore, it is highly desirable to support and develop innovative and cheaper synthetic methods for the production of already known drugs and to discover new ones. The combination of less expensive 3d metals and C–H activation processes towards the synthesis of biologically active molecules could enable this essential goal to be achieved.

Funding

ENSJ thanks CNPq (PQ 309774/2020-9), CAPES, FAPEMIG (PPM-00635-18), Return Fellowship of the Alexander von Humboldt Foundation (AvH) and the Royal Society of Chemistry for the research fund grant (R19-9781). GAM Jardim thanks CAPES for PNPD fellowship and funding. RSG thanks NDEPSCoR (FAR0034259) and (FAR0033944).

ORCID® iDs

Renato L. Carvalho - https://orcid.org/0000-0002-8515-9306
Amanda S. de Miranda - https://orcid.org/0000-0002-8887-2772
Mateus P. Nunes - https://orcid.org/0000-0003-4796-3448
Roberto S. Gomes - https://orcid.org/0000-0002-8075-9716
Guilherme A. M. Jardim - https://orcid.org/0000-0002-9882-3085
Eufrânio N. da Silva Júnior - https://orcid.org/0000-0003-1281-5453

References

1. Ji, H.; Tan, Y.; Gan, N.; Zhang, J.; Li, S.; Zheng, X.; Wang, Z.; Yi, W. *Bioorg. Med. Chem.* **2021,** *29,* 115870. doi:10.1016/j.bmc.2020.115870
2. Şahin, İ.; Özgeriş, F. B.; Köse, M.; Bakan, E.; Tümer, F. *J. Mol. Struct.* **2021,** *1232,* 130042. doi:10.1016/j.molstruc.2021.130042
3. Jaromin, A.; Czopek, A.; Parapini, S.; Basilico, N.; Misiak, E.; Gubernator, J.; Zagórska, A. *Biomolecules* **2021,** *11,* 33. doi:10.3390/biom11010033
4. Peric, M.; Pešić, D.; Alihodžić, S.; Fajdetić, A.; Herreros, E.; Gamo, F. J.; Angulo-Barturen, I.; Jiménez-Díaz, M. B.; Ferrer-Bazaga, S.; Martínez, M. S.; Gargallo-Viola, D.; Mathis, A.; Kessler, A.; Banjanac, M.; Padovan, J.; Bencetić Mihaljević, V.; Munic Kos, V.; Bukvić, M.; Eraković Haber, V.; Spaventi, R. *Br. J. Pharmacol.* **2021,** *178,* 363–377. doi:10.1111/bph.15292
5. Velásquez, A. M. A.; Francisco, A. I.; Kohatsu, A. A. N.; Silva, F. A. d. J.; Rodrigues, D. F.; Teixeira, R. G. d. S.; Chiari, B. G.; de Almeida, M. G. J.; Isaac, V. L. B.; Vargas, M. D.; Cicarelli, R. M. B. *Bioorg. Med. Chem. Lett.* **2014,** *24,* 1707–1710. doi:10.1016/j.bmcl.2014.02.046
6. Marquissolo, C.; de Fátima, Â.; Kohn, L. K.; Ruiz, A. L. T. G.; de Carvalho, J. E.; Pilli, R. A. *Bioorg. Chem.* **2009,** *37,* 52–56. doi:10.1016/j.bioorg.2008.12.001
7. Xu, Z.; Chen, Q.; Zhang, Y.; Liang, C. *Fitoterapia* **2021,** *150,* 104863. doi:10.1016/j.fitote.2021.104863
8. Zhao, Y.; Chen, C.-H.; Morris-Natschke, S. L.; Lee, K.-H. *Eur. J. Med. Chem.* **2021,** *215,* 113287. doi:10.1016/j.ejmech.2021.113287
9. Mostafa, A.; Kandeil, A.; Elshaier, Y. A. M. M.; Kutkat, O.; Moatasim, Y.; Rashad, A. A.; Shehata, M.; Gomaa, M. R.; Mahrous, N.; Mahmoud, S. H.; GabAllah, M.; Abbas, H.; Taweel, A. E.; Kayed, A. E.; Kamel, M. N.; Sayes, M. E.; Mahmoud, D. B.; El-Shesheny, R.; Kayali, G.; Ali, M. A. *Pharmaceuticals* **2020,** *13,* 443. doi:10.3390/ph13120443
10. da Silva Oliveira, G. L.; da Silva, J. C. C. L.; dos Santos C. L da Silva, A. P.; Feitosa, C. M.; de Castro Almeida, F. R. *Curr. Mol. Pharmacol.* **2021,** *14,* 36–51. doi:10.2174/1874467213666200510004622
11. Sharma, H.; Chawla, P. A.; Bhatia, R. *CNS Neurol. Disord.: Drug Targets* **2020,** *19,* 448–465. doi:10.2174/1871527319999200818182249
12. Cappelli, A.; Anzini, M.; Castriconi, F.; Grisci, G.; Paolino, M.; Braile, C.; Valenti, S.; Giuliani, G.; Vomero, S.; Di Capua, A.; Betti, L.; Giannaccini, G.; Lucacchini, A.; Ghelardini, C.; Di Cesare Mannelli, L.; Frosini, M.; Ricci, L.; Giorgi, G.; Mascia, M. P.; Biggio, G. *J. Med. Chem.* **2016,** *59,* 3353–3372. doi:10.1021/acs.jmedchem.6b00034
13. Saeedi, M.; Maleki, A.; Iraji, A.; Hariri, R.; Akbarzadeh, T.; Edraki, N.; Firuzi, O.; Mirfazli, S. S. *J. Mol. Struct.* **2021,** *1229,* 129828. doi:10.1016/j.molstruc.2020.129828
14. Provencher, P. A.; Bay, K. L.; Hoskin, J. F.; Houk, K. N.; Yu, J.-Q.; Sorensen, E. J. *ACS Catal.* **2021,** *11,* 3115–3127. doi:10.1021/acscatal.0c05081
15. Lasmari, S.; Gürbüz, N.; Boulcina, R.; Özdemir, N.; Özdemir, İ. *Polyhedron* **2021,** *199,* 115091. doi:10.1016/j.poly.2021.115091
16. Zhong, X.; Lin, S.; Gao, H.; Liu, F.-X.; Zhou, Z.; Yi, W. *Org. Lett.* **2021,** *23,* 2285–2291. doi:10.1021/acs.orglett.1c00418
17. Wang, F.; Huang, F.; Yu, Y.; Zhou, S.; Wang, Z.; Zhang, W. *Catal. Commun.* **2021,** *153,* 106296. doi:10.1016/j.catcom.2021.106296
18. Campbell, M. W.; Yuan, M.; Polites, V. C.; Gutierrez, O.; Molander, G. A. *J. Am. Chem. Soc.* **2021,** *143,* 3901–3910. doi:10.1021/jacs.0c13077
19. Xu, H.-B.; Chen, Y.-J.; Chai, X.-Y.; Yang, J.-H.; Xu, Y.-J.; Dong, L. *Org. Lett.* **2021,** *23,* 2052–2056. doi:10.1021/acs.orglett.0c03906
20. Zhou, Z.-X.; Li, J.-W.; Wang, L.-N.; Li, M.; Liu, Y.-J.; Zeng, M.-H. *Org. Lett.* **2021,** *23,* 2057–2062. doi:10.1021/acs.orglett.1c00237
21. Zhu, Z.-F.; Chen, G.-L.; Liu, F. *Chem. Commun.* **2021,** *57,* 3411–3414. doi:10.1039/d1cc00039j
22. Wang, Y.; Oliveira, J. C. A.; Lin, Z.; Ackermann, L. *Angew. Chem., Int. Ed.* **2021,** *60,* 6419–6424. doi:10.1002/anie.202016895
23. Xing, Y.-K.; Chen, X.-R.; Yang, Q.-L.; Zhang, S.-Q.; Guo, H.-M.; Hong, X.; Mei, T.-S. *Nat. Commun.* **2021,** *12,* 930. doi:10.1038/s41467-021-21190-8
24. Huang, T.; Wang, T.; Shi, Y.; Chen, J.; Guo, X.; Lai, R.; Liu, X.; Wu, Z.; Peng, D.; Wang, L.; Li, H.; Hai, L.; Wu, Y. *Org. Lett.* **2021,** *23,* 1548–1553. doi:10.1021/acs.orglett.0c04155
25. Buğday, N.; Khan, S.; Yaşar, S.; Özdemir, İ. *J. Organomet. Chem.* **2021,** *937,* 121730. doi:10.1016/j.jorganchem.2021.121730
26. Wang, D.; Li, M.; Chen, X.; Wang, M.; Liang, Y.; Zhao, Y.; Houk, K. N.; Shi, Z. *Angew. Chem., Int. Ed.* **2021,** *60,* 7066–7071. doi:10.1002/anie.202015117
27. González, J. M.; Cendón, B.; Mascareñas, J. L.; Gulías, M. *J. Am. Chem. Soc.* **2021,** *143,* 3747–3752. doi:10.1021/jacs.1c01929
28. Du, R.; Liu, L.; Xu, S. *Angew. Chem., Int. Ed.* **2021,** *60,* 5843–5847. doi:10.1002/anie.202016009
29. Pan, Z.; Liu, L.; Xu, S.; Shen, Z. *RSC Adv.* **2021,** *11,* 5487–5490. doi:10.1039/d0ra10211c
30. Fukumoto, Y.; Shiratani, M.; Noguchi, H.; Chatani, N. *Synthesis* **2021,** in press. doi:10.1055/a-1375-5283
31. Ren, W.; Liu, H.; You, F.; Mao, P.; So, Y.-M.; Kang, X.; Shi, X. *Dalton Trans.* **2021,** *50,* 1334–1343. doi:10.1039/d0dt04040a
32. Zhong, Y.; Li, M.; Deng, M.; Gong, M.; Xie, H.; Luo, Y. *Dalton Trans.* **2021,** *50,* 346–354. doi:10.1039/d0dt03680c
33. Feng, H.; Zhao, Y.; Liu, P.; Hu, L. *Org. Lett.* **2021,** *23,* 1632–1637. doi:10.1021/acs.orglett.1c00056
34. Chen, M.; Liang, C.; Zhang, F.; Li, H. *ACS Sustainable Chem. Eng.* **2014,** *2,* 486–492. doi:10.1021/sc400391r
35. Navale, B. S.; Laha, D.; Bhat, R. G. *Tetrahedron Lett.* **2019,** *60,* 1899–1903. doi:10.1016/j.tetlet.2019.06.026
36. Su, J.; Cai, Y.; Xu, X. *Org. Lett.* **2019,** *21,* 9055–9059. doi:10.1021/acs.orglett.9b03451
37. Lou, S.-J.; Mo, Z.; Nishiura, M.; Hou, Z. *J. Am. Chem. Soc.* **2020,** *142,* 1200–1205. doi:10.1021/jacs.9b12503
38. Lou, S.-J.; Zhang, L.; Luo, Y.; Nishiura, M.; Luo, G.; Luo, Y.; Hou, Z. *J. Am. Chem. Soc.* **2020,** *142,* 18128–18137. doi:10.1021/jacs.0c08362
39. Luo, Y.; Ma, Y.; Hou, Z. *J. Am. Chem. Soc.* **2018,** *140,* 114–117. doi:10.1021/jacs.7b11245

40. Cong, X.; Zhan, G.; Mo, Z.; Nishiura, M.; Hou, Z. *J. Am. Chem. Soc.* **2020,** *142,* 5531–5537. doi:10.1021/jacs.0c01171
41. Nako, A. E.; Oyamada, J.; Nishiura, M.; Hou, Z. *Chem. Sci.* **2016,** *7,* 6429–6434. doi:10.1039/c6sc02129h
42. Lou, S.-J.; Zhuo, Q.; Nishiura, M.; Luo, G.; Hou, Z. *J. Am. Chem. Soc.* **2021,** *143,* 2470–2476. doi:10.1021/jacs.0c13166
43. Oyamada, J.; Hou, Z. *Angew. Chem., Int. Ed.* **2012,** *51,* 12828–12832. doi:10.1002/anie.201206233
44. Luo, Y.; Yao, J.-P.; Yang, L.; Feng, C.-L.; Tang, W.; Wang, G.-F.; Zuo, J.-P.; Lu, W. *Bioorg. Med. Chem.* **2010,** *18,* 5048–5055. doi:10.1016/j.bmc.2010.05.076
45. Miller, J. F.; Turner, E. M.; Gudmundsson, K. S.; Jenkinson, S.; Spaltenstein, A.; Thomson, M.; Wheelan, P. *Bioorg. Med. Chem. Lett.* **2010,** *20,* 2125–2128. doi:10.1016/j.bmcl.2010.02.053
46. Omar, M. A.; Shaker, Y. M.; Galal, S. A.; Ali, M. M.; Kerwin, S. M.; Li, J.; Tokuda, H.; Ramadan, R. A.; El Diwani, H. I. *Bioorg. Med. Chem.* **2012,** *20,* 6989–7001. doi:10.1016/j.bmc.2012.10.010
47. Saify, Z. S.; Azim, M. K.; Ahmad, W.; Nisa, M.; Goldberg, D. E.; Hussain, S. A.; Akhtar, S.; Akram, A.; Arayne, A.; Oksman, A.; Khan, I. A. *Bioorg. Med. Chem. Lett.* **2012,** *22,* 1282–1286. doi:10.1016/j.bmcl.2011.10.018
48. Ahmed, N.; Brahmbhatt, K. G.; Sabde, S.; Mitra, D.; Singh, I. P.; Bhutani, K. K. *Bioorg. Med. Chem.* **2010,** *18,* 2872–2879. doi:10.1016/j.bmc.2010.03.015
49. Jones, D. H.; Slack, R.; Squires, S.; Wooldridge, K. R. H. *J. Med. Chem.* **1965,** *8,* 676–680. doi:10.1021/jm00329a026
50. de Souza, M. V. N.; Pais, K. C.; Kaiser, C. R.; Peralta, M. A.; de L. Ferreira, M.; Lourenço, M. C. S. *Bioorg. Med. Chem.* **2009,** *17,* 1474–1480. doi:10.1016/j.bmc.2009.01.013
51. Nikolayevskiy, H.; Robello, M.; Scerba, M. T.; Pasternak, E. H.; Saha, M.; Hartman, T. L.; Buchholz, C. A.; Buckheit, R. W., Jr.; Durell, S. R.; Appella, D. H. *Eur. J. Med. Chem.* **2019,** *178,* 818–837. doi:10.1016/j.ejmech.2019.06.020
52. Henao Castañeda, I. C.; Pereañez, J. A.; Preciado, L. M. *Pharmaceuticals* **2019,** *12,* 80. doi:10.3390/ph12020080
53. Poirier, D.; Auger, S.; Mérand, Y.; Simard, J.; Labrie, F. *J. Med. Chem.* **1994,** *37,* 1115–1125. doi:10.1021/jm00034a009
54. Graham, J. M.; Coughenour, L. L.; Barr, B. M.; Rock, D. L.; Nikam, S. S. *Bioorg. Med. Chem. Lett.* **2008,** *18,* 489–493. doi:10.1016/j.bmcl.2007.11.106
55. Chazalette, C.; Masereel, B.; Rolin, S.; Thiry, A.; Scozzafava, A.; Innocenti, A.; Supuran, C. T. *Bioorg. Med. Chem. Lett.* **2004,** *14,* 5781–5786. doi:10.1016/j.bmcl.2004.09.061
56. Finberg, J. P. M.; Lamensdorf, I.; Commissiong, J. W.; Youdim, M. B. H. Pharmacology and neuroprotective properties of rasagiline. In *Deprenyl — Past and Future;* Kuhn, W.; Kraus, P.; Przuntek, H., Eds.; Journal of Neural Transmission (Supplement 48), Vol. 48; Springer: Vienna, Austria, 1996; pp 95–101. doi:10.1007/978-3-7091-7494-4_9
57. Finberg, J. P. M.; Takeshima, T.; Johnston, J. M.; Commissiong, J. W. *NeuroReport* **1998,** *9,* 703–707. doi:10.1097/00001756-199803090-00026
58. Egunlusi, A. O.; Malan, S. F.; Omoruyi, S. I.; Ekpo, O. E.; Palchykov, V. A.; Joubert, J. *Eur. J. Med. Chem.* **2020,** *204,* 112617. doi:10.1016/j.ejmech.2020.112617
59. Manetti, D.; Garifulina, A.; Bartolucci, G.; Bazzicalupi, C.; Bellucci, C.; Chiaramonte, N.; Dei, S.; Di Cesare Mannelli, L.; Ghelardini, C.; Gratteri, P.; Spirova, E.; Shelukhina, I.; Teodori, E.; Varani, K.; Tsetlin, V.; Romanelli, M. N. *J. Med. Chem.* **2019,** *62,* 1887–1901. doi:10.1021/acs.jmedchem.8b01372
60. Chong, E.; Schafer, L. L. *Org. Lett.* **2013,** *15,* 6002–6005. doi:10.1021/ol402890m
61. Wang, C.; Yan, K.; Luo, X.; Jin, S.; Wang, L.; Luo, J.; Zheng, J. *Color. Technol.* **2021,** *137,* 348–350. doi:10.1111/cote.12532
62. Kholghi Eshkalak, S.; Kowsari, E.; Chinnappan, A.; Ramakrishna, S. *J. Mater. Sci.: Mater. Electron.* **2019,** *30,* 11307–11316. doi:10.1007/s10854-019-01478-8
63. Catalano, R.; Labille, J.; Gaglio, D.; Alijagic, A.; Napodano, E.; Slomberg, D.; Campos, A.; Pinsino, A. *Nanomaterials* **2020,** *10,* 2102. doi:10.3390/nano10112102
64. Slomberg, D. L.; Catalano, R.; Bartolomei, V.; Labille, J. *Environ. Pollut.* **2021,** *271,* 116263. doi:10.1016/j.envpol.2020.116263
65. Zhao, X.; Li, H.; Liu, Y.; Ma, Y. *Macromolecules* **2020,** *53,* 10803–10812. doi:10.1021/acs.macromol.0c01981
66. Bielefeld, J.; Doye, S. *Angew. Chem., Int. Ed.* **2020,** *59,* 6138–6143. doi:10.1002/anie.202001111
67. Lühning, L. H.; Brahms, C.; Nimoth, J. P.; Schmidtmann, M.; Doye, S. *Z. Anorg. Allg. Chem.* **2015,** *641,* 2071–2082. doi:10.1002/zaac.201500542
68. Warsitz, M.; Doye, S. *Chem. – Eur. J.* **2020,** *26,* 15121–15125. doi:10.1002/chem.202003223
69. Gujjar, R.; El Mazouni, F.; White, K. L.; White, J.; Creason, S.; Shackleford, D. M.; Deng, X.; Charman, W. N.; Bathurst, I.; Burrows, J.; Floyd, D. M.; Matthews, D.; Buckner, F. S.; Charman, S. A.; Phillips, M. A.; Rathod, P. K. *J. Med. Chem.* **2011,** *54,* 3935–3949. doi:10.1021/jm200265b
70. Yakantham, T.; Sreenivasulu, R.; Raju, R. R. *Russ. J. Gen. Chem.* **2019,** *89,* 1485–1490. doi:10.1134/s1070363219070181
71. Huang, X.-F.; Lu, X.; Zhang, Y.; Song, G.-Q.; He, Q.-L.; Li, Q.-S.; Yang, X.-H.; Wei, Y.; Zhu, H.-L. *Bioorg. Med. Chem.* **2012,** *20,* 4895–4900. doi:10.1016/j.bmc.2012.06.056
72. Prochnow, I.; Kubiak, R.; Frey, O. N.; Beckhaus, R.; Doye, S. *ChemCatChem* **2009,** *1,* 162–172. doi:10.1002/cctc.200900092
73. Müller, C.; Saak, W.; Doye, S. *Eur. J. Org. Chem.* **2008,** 2731–2739. doi:10.1002/ejoc.200701146
74. Kubiak, R.; Prochnow, I.; Doye, S. *Angew. Chem., Int. Ed.* **2009,** *48,* 1153–1156. doi:10.1002/anie.200805169
75. Glushkov, V. A.; P'yankova, O. S.; Anikina, L. V.; Vikharev, Y. B.; Feshina, E. V.; Shklyaev, Y. V.; Tolstikov, A. G. *Pharm. Chem. J.* **2006,** *40,* 298–302. doi:10.1007/s11094-006-0114-7
76. Langeslay, R. R.; Kaphan, D. M.; Marshall, C. L.; Stair, P. C.; Sattelberger, A. P.; Delferro, M. *Chem. Rev.* **2019,** *119,* 2128–2191. doi:10.1021/acs.chemrev.8b00245
77. Kirillov, A. M.; Shul'pin, G. B. *Coord. Chem. Rev.* **2013,** *257,* 732–754. doi:10.1016/j.ccr.2012.09.012
78. Shul'pina, L. S.; Kirillova, M. V.; Pombeiro, A. J. L.; Shul'pin, G. B. *Tetrahedron* **2009,** *65,* 2424–2429. doi:10.1016/j.tet.2009.01.088
79. Kobayashi, H.; Yamanaka, I. *J. Mol. Catal. A: Chem.* **2008,** *294,* 43–50. doi:10.1016/j.molcata.2008.07.019
80. Stepovik, L. P.; Potkina, A. Yu. *Russ. J. Gen. Chem.* **2013,** *83,* 1047–1059. doi:10.1134/s1070363213060078
81. Pokutsa, A.; Kubaj, Y.; Zaborovskyi, A.; Maksym, D.; Muzart, J.; Sobkowiak, A. *Appl. Catal., A* **2010,** *390,* 190–194. doi:10.1016/j.apcata.2010.10.010

82. Kirillova, M. V.; Kuznetsov, M. L.; Kozlov, Y. N.; Shul'pina, L. S.; Kitaygorodskiy, A.; Pombeiro, A. J. L.; Shul'pin, G. B. *ACS Catal.* **2011,** *1,* 1511–1520. doi:10.1021/cs200237m
83. Khaliullin, R. Z.; Bell, A. T.; Head-Gordon, M. *J. Phys. Chem. B* **2005,** *109,* 17984–17992. doi:10.1021/jp058162a
84. Kirillova, M. V.; Kuznetsov, M. L.; Romakh, V. B.; Shul'pina, L. S.; Fraústo da Silva, J. J. R.; Pombeiro, A. J. L.; Shul'pin, G. B. *J. Catal.* **2009,** *267,* 140–157. doi:10.1016/j.jcat.2009.08.006
85. Pokutsa, A.; Kubaj, Y.; Zaborovskyi, A.; Sobkowiak, A.; Muzart, J. *React. Kinet., Mech. Catal.* **2017,** *122,* 757–774. doi:10.1007/s11144-017-1274-z
86. Pokutsa, A.; Kubaj, Y.; Zaborovskyi, A.; Maksym, D.; Paczesniak, T.; Mysliwiec, B.; Bidzinska, E.; Muzart, J.; Sobkowiak, A. *Mol. Catal.* **2017,** *434,* 194–205. doi:10.1016/j.mcat.2017.02.013
87. Xia, J.-B.; Cormier, K. W.; Chen, C. *Chem. Sci.* **2012,** *3,* 2240–2245. doi:10.1039/c2sc20178j
88. Mishra, G. S.; Silva, T. F. S.; Martins, L. M. D. R. S.; Pombeiro, A. J. L. *Pure Appl. Chem.* **2009,** *81,* 1217–1227. doi:10.1351/pac-con-08-10-08
89. Krivosudský, L.; Schwendt, P.; Gyepes, R. *Inorg. Chem.* **2015,** *54,* 6306–6311. doi:10.1021/acs.inorgchem.5b00600
90. Kamata, K.; Yonehara, K.; Nakagawa, Y.; Uehara, K.; Mizuno, N. *Nat. Chem.* **2010,** *2,* 478–483. doi:10.1038/nchem.648
91. Verma, S.; Nasir Baig, R. B.; Nadagouda, M. N.; Varma, R. S. *ACS Sustainable Chem. Eng.* **2016,** *4,* 2333–2336. doi:10.1021/acssuschemeng.6b00006
92. Dias, M. C. F.; de Sousa, B. L.; Ionta, M.; Teixeira, R. R.; Goulart, T. Q.; Ferreira-Silva, G. A.; Pilau, E. J.; dos Santos, M. H. *J. Braz. Chem. Soc.* **2021,** *32,* 572–587. doi:10.21577/0103-5053.20200211
93. Gillis, E. P.; Eastman, K. J.; Hill, M. D.; Donnelly, D. J.; Meanwell, N. A. *J. Med. Chem.* **2015,** *58,* 8315–8359. doi:10.1021/acs.jmedchem.5b00258
94. Xia, J.-B.; Ma, Y.; Chen, C. *Org. Chem. Front.* **2014,** *1,* 468–472. doi:10.1039/c4qo00057a
95. Zhou, Y.; Ma, Z.; Tang, J.; Yan, N.; Du, Y.; Xi, S.; Wang, K.; Zhang, W.; Wen, H.; Wang, J. *Nat. Commun.* **2018,** *9,* 2931. doi:10.1038/s41467-018-05351-w
96. Shan, Z.-H.; Liu, J.; Xu, L.-M.; Tang, Y.-F.; Chen, J.-H.; Yang, Z. *Org. Lett.* **2012,** *14,* 3712–3715. doi:10.1021/ol3015573
97. Malone, M. H.; Rother, A. *J. Ethnopharmacol.* **1994,** *42,* 135–159. doi:10.1016/0378-8741(94)90080-9
98. Leighty, M. W.; Georg, G. I. *ACS Med. Chem. Lett.* **2011,** *2,* 313–315. doi:10.1021/ml1003074
99. Niphakis, M. J.; Georg, G. I. *Org. Lett.* **2011,** *13,* 196–199. doi:10.1021/ol1023954
100. Takizawa, S.; Katayama, T.; Kameyama, C.; Onitsuka, K.; Suzuki, T.; Yanagida, T.; Kawai, T.; Sasai, H. *Chem. Commun.* **2008,** 1810–1812. doi:10.1039/b717068h
101. Vidal, M.; Elie, C.-R.; Campbell, S.; Claing, A.; Schmitzer, A. R. *Med. Chem. Commun.* **2014,** *5,* 436–440. doi:10.1039/c3md00293d
102. Yuan, R.; Li, M.-q.; Ren, X.-x.; Chen, W.; Zhou, H.; Wan, Y.; Zhang, P.; Wu, H. *Res. Chem. Intermed.* **2020,** *46,* 2275–2287. doi:10.1007/s11164-020-04091-1
103. Liu, L.; Carroll, P. J.; Kozlowski, M. C. *Org. Lett.* **2015,** *17,* 508–511. doi:10.1021/ol503521b
104. Sako, M.; Sugizaki, A.; Takizawa, S. *Bioorg. Med. Chem. Lett.* **2018,** *28,* 2751–2753. doi:10.1016/j.bmcl.2018.02.033
105. Kang, H.; Lee, Y. E.; Reddy, P. V. G.; Dey, S.; Allen, S. E.; Niederer, K. A.; Sung, P.; Hewitt, K.; Torruellas, C.; Herling, M. R.; Kozlowski, M. C. *Org. Lett.* **2017,** *19,* 5505–5508. doi:10.1021/acs.orglett.7b02552
106. Nutan, M. T. H.; Hasan, C. M.; Rashid, M. A. *Fitoterapia* **1999,** *70,* 130–133. doi:10.1016/s0367-326x(98)00021-5
107. Hwang, D.-R.; Uang, B.-J. *Org. Lett.* **2002,** *4,* 463–466. doi:10.1021/ol017229j
108. Kaswan, P.; Porter, A.; Pericherla, K.; Simone, M.; Peters, S.; Kumar, A.; DeBoef, B. *Org. Lett.* **2015,** *17,* 5208–5211. doi:10.1021/acs.orglett.5b02539
109. Mitchell, D.; Cole, K. P.; Pollock, P. M.; Coppert, D. M.; Burkholder, T. P.; Clayton, J. R. *Org. Process Res. Dev.* **2012,** *16,* 70–81. doi:10.1021/op200229j
110. Campbell, A. N.; Cole, K. P.; Martinelli, J. R.; May, S. A.; Mitchell, D.; Pollock, P. M.; Sullivan, K. A. *Org. Process Res. Dev.* **2013,** *17,* 273–281. doi:10.1021/op300344m
111. Alagiri, K.; Kumara, G. S. R.; Prabhu, K. R. *Chem. Commun.* **2011,** *47,* 11787–11789. doi:10.1039/c1cc15050b
112. Jones, K. M.; Karier, P.; Klussmann, M. *ChemCatChem* **2012,** *4,* 51–54. doi:10.1002/cctc.201100324
113. Kaswan, P.; Nandwana, N. K.; DeBoef, B.; Kumar, A. *Adv. Synth. Catal.* **2016,** *358,* 2108–2115. doi:10.1002/adsc.201600225
114. Cheuka, P. M.; Lawrence, N.; Taylor, D.; Wittlin, S.; Chibale, K. *Med. Chem. Commun.* **2018,** *9,* 1733–1745. doi:10.1039/c8md00382c
115. Li, J.; Knochel, P. *Synthesis* **2019,** *51,* 2100–2106. doi:10.1055/s-0037-1611756
116. Ilies, L. *Bull. Chem. Soc. Jpn.* **2021,** *94,* 404–417. doi:10.1246/bcsj.20200349
117. Schwarz, J. L.; Huang, H.-M.; Paulisch, T. O.; Glorius, F. *ACS Catal.* **2020,** *10,* 1621–1627. doi:10.1021/acscatal.9b04222
118. Huang, H.-M.; Bellotti, P.; Daniliuc, C. G.; Glorius, F. *Angew. Chem., Int. Ed.* **2021,** *60,* 2464–2471. doi:10.1002/anie.202011996
119. Schwarz, J. L.; Schäfers, F.; Tlahuext-Aca, A.; Lückemeier, L.; Glorius, F. *J. Am. Chem. Soc.* **2018,** *140,* 12705–12709. doi:10.1021/jacs.8b08052
120. Schäfers, F.; Quach, L.; Schwarz, J. L.; Saladrigas, M.; Daniliuc, C. G.; Glorius, F. *ACS Catal.* **2020,** *10,* 11841–11847. doi:10.1021/acscatal.0c03697
121. Chen, M.; Doba, T.; Sato, T.; Razumkov, H.; Ilies, L.; Shang, R.; Nakamura, E. *J. Am. Chem. Soc.* **2020,** *142,* 4883–4891. doi:10.1021/jacs.0c00127
122. Fulton, B.; Benfield, P. *Drugs* **1996,** *52,* 450–474. doi:10.2165/00003495-199652030-00013
123. Vong, K.; Yamamoto, T.; Chang, T.-c.; Tanaka, K. *Chem. Sci.* **2020,** *11,* 10928–10933. doi:10.1039/d0sc04329j
124. Rong, Z.; Luo, M.; Zeng, X. *Org. Lett.* **2019,** *21,* 6869–6873. doi:10.1021/acs.orglett.9b02504
125. Shi, J.; Liu, J.; Kang, D.; Huang, Y.; Kong, W.; Xiang, Y.; Zhu, X.; Duan, Y.; Huang, Y. *ACS Omega* **2019,** *4,* 6630–6636. doi:10.1021/acsomega.9b00593
126. Hu, Y.; Zhou, B.; Wang, C. *Acc. Chem. Res.* **2018,** *51,* 816–827. doi:10.1021/acs.accounts.8b00028
127. Carney, J. R.; Dillon, B. R.; Thomas, S. P. *Eur. J. Org. Chem.* **2016,** 3912–3929. doi:10.1002/ejoc.201600018
128. Cano, R.; Mackey, K.; McGlacken, G. P. *Catal. Sci. Technol.* **2018,** *8,* 1251–1266. doi:10.1039/c7cy02514a

129. Bruce, M. I.; Iqbal, M. Z.; Stone, F. G. A. *J. Chem. Soc. A* **1970,** 3204–3209. doi:10.1039/j19700003204
130. Paradine, S. M.; Griffin, J. R.; Zhao, J.; Petronico, A. L.; Miller, S. M.; Christina White, M. *Nat. Chem.* **2015,** *7,* 987–994. doi:10.1038/nchem.2366
131. Clark, J. R.; Feng, K.; Sookezian, A.; White, M. C. *Nat. Chem.* **2018,** *10,* 583–591. doi:10.1038/s41557-018-0020-0
132. Xu, R.; Xu, T.; Wang, G. *Cryst. Res. Technol.* **2021,** *56,* 2000117. doi:10.1002/crat.202000117
133. Sun, M.; Xing, F.; Pan, S.; Di, J.; Zeng, S.; Liu, J. *Cent. Eur. J. Biol.* **2013,** *8,* 1230–1240. doi:10.2478/s11535-013-0235-4
134. Yamada, M.; Hirano, S.; Tsuruoka, R.; Takasuga, M.; Uno, K.; Yamaguchi, K.; Yamano, M. *Org. Process Res. Dev.* **2021,** *25,* 327–336. doi:10.1021/acs.oprd.0c00544
135. Barreiro, E. J.; Kümmerle, A. E.; Fraga, C. A. M. *Chem. Rev.* **2011,** *111,* 5215–5246. doi:10.1021/cr200060g
136. Corcoran, E. B.; Schultz, D. M. *Nature* **2020,** *580,* 592–593. doi:10.1038/d41586-020-01167-1
137. Feng, K.; Quevedo, R. E.; Kohrt, J. T.; Oderinde, M. S.; Reilly, U.; White, M. C. *Nature* **2020,** *580,* 621–627. doi:10.1038/s41586-020-2137-8
138. Hoy, S. M. *Drugs* **2013,** *73,* 2077–2091. doi:10.1007/s40265-013-0150-z
139. Zhao, X.; Yoon, D.-O.; Yoo, J.; Park, H.-J. *J. Med. Chem.* **2021,** *64,* 4130–4149. doi:10.1021/acs.jmedchem.1c00031
140. Kaplaneris, N.; Rogge, T.; Yin, R.; Wang, H.; Sirvinskaite, G.; Ackermann, L. *Angew. Chem., Int. Ed.* **2019,** *58,* 3476–3480. doi:10.1002/anie.201812705
141. Yet, L. Biaryls. *Privileged Structures in Drug Discovery: Medicinal Chemistry and Synthesis;* John Wiley & Sons: Chichester, UK, 2018; pp 83–154. doi:10.1002/9781118686263.ch4
142. Liang, Y.-F.; Steinbock, R.; Yang, L.; Ackermann, L. *Angew. Chem., Int. Ed.* **2018,** *57,* 10625–10629. doi:10.1002/anie.201805644
143. Senthilkumar, P.; Long, J.; Swetha, R.; Shruthi, V.; Wang, R.-R.; Preethi, S.; Yogeeswari, P.; Zheng, Y.-T.; Sriram, D. *Nucleosides, Nucleotides Nucleic Acids* **2009,** *28,* 89–102. doi:10.1080/15257770902736442
144. Meyer, T. H.; Samanta, R. C.; Del Vecchio, A.; Ackermann, L. *Chem. Sci.* **2021,** *12,* 2890–2897. doi:10.1039/d0sc05924b
145. Niu, L.; Jiang, C.; Liang, Y.; Liu, D.; Bu, F.; Shi, R.; Chen, H.; Chowdhury, A. D.; Lei, A. *J. Am. Chem. Soc.* **2020,** *142,* 17693–17702. doi:10.1021/jacs.0c08437
146. Lozano-Cruz, T.; Ortega, P.; Batanero, B.; Copa-Patiño, J. L.; Soliveri, J.; de la Mata, F. J.; Gómez, R. *Dalton Trans.* **2015,** *44,* 19294–19304. doi:10.1039/c5dt02230d
147. Dong, J.; Yuan, X.-A.; Yan, Z.; Mu, L.; Ma, J.; Zhu, C.; Xie, J. *Nat. Chem.* **2021,** *13,* 182–190. doi:10.1038/s41557-020-00589-8
148. Hüls, M.; Grootes, P. M.; Nadeau, M.-J. *Radiocarbon* **2011,** *53,* 151–160. doi:10.1017/s0033822200034421
149. Banerjee, A.; Roychoudhury, A. *Ecotoxicol. Environ. Saf.* **2021,** *215,* 112055. doi:10.1016/j.ecoenv.2021.112055
150. Zhang, D.; Jarava-Barrera, C.; Bontemps, S. *ACS Catal.* **2021,** *11,* 4568–4575. doi:10.1021/acscatal.1c00412
151. Liu, J.-B.; Ren, M.; Lai, X.; Qiu, G. *Chem. Commun.* **2021,** *57,* 4259–4262. doi:10.1039/d1cc00870f
152. Zhang, H.; Wang, E.; Geng, S.; Liu, Z.; He, Y.; Peng, Q.; Feng, Z. *Angew. Chem., Int. Ed.* **2021,** *60,* 10211–10218. doi:10.1002/anie.202100049
153. Ferlin, F.; Zangarelli, A.; Lilli, S.; Santoro, S.; Vaccaro, L. *Green Chem.* **2021,** *23,* 490–495. doi:10.1039/d0gc03351k
154. Zhang, Y.; Zhong, D.; Usman, M.; Xue, P.; Liu, W.-B. *Chin. J. Chem.* **2020,** *38,* 1651–1655. doi:10.1002/cjoc.202000299
155. Messinis, A. M.; Finger, L. H.; Hu, L.; Ackermann, L. *J. Am. Chem. Soc.* **2020,** *142,* 13102–13111. doi:10.1021/jacs.0c04837
156. Chen, M. S.; White, M. C. *Science* **2007,** *318,* 783–787. doi:10.1126/science.1148597
157. Rasik, C. M.; Brown, M. K. *Angew. Chem., Int. Ed.* **2014,** *53,* 14522–14526. doi:10.1002/anie.201408055
158. Festa, C.; De Marino, S.; D'Auria, M. V.; Deharo, E.; Gonzalez, G.; Deyssard, C.; Petek, S.; Bifulco, G.; Zampella, A. *Tetrahedron* **2012,** *68,* 10157–10163. doi:10.1016/j.tet.2012.09.106
159. Osberger, T. J.; Rogness, D. C.; Kohrt, J. T.; Stepan, A. F.; White, M. C. *Nature* **2016,** *537,* 214–219. doi:10.1038/nature18941
160. Hung, K.; Condakes, M. L.; Morikawa, T.; Maimone, T. J. *J. Am. Chem. Soc.* **2016,** *138,* 16616–16619. doi:10.1021/jacs.6b11739
161. Pony Yu, R.; Hesk, D.; Rivera, N.; Pelczer, I.; Chirik, P. J. *Nature* **2016,** *529,* 195–199. doi:10.1038/nature16464
162. Hu, P.; Tan, M.; Cheng, L.; Zhao, H.; Feng, R.; Gu, W.-J.; Han, W. *Nat. Commun.* **2019,** *10,* 2425. doi:10.1038/s41467-019-10414-7
163. Hwang, J. Y.; Ji, A. Y.; Lee, S. H.; Kang, E. J. *Org. Lett.* **2020,** *22,* 16–21. doi:10.1021/acs.orglett.9b03542
164. Farooq, S.; Mazhar, A.; Ghouri, A.; Ihsan-Ul-Haq; Ullah, N. *Molecules* **2020,** *25,* 2710. doi:10.3390/molecules25112710
165. Henry, M. C.; Sutherland, A. *Org. Lett.* **2020,** *22,* 2766–2770. doi:10.1021/acs.orglett.0c00754
166. Wang, B.; Zhang, Q.; Luo, J.; Gan, Z.; Jiang, W.; Tang, Q. *Molecules* **2019,** *24,* 2187. doi:10.3390/molecules24112187
167. Das, S. K.; Roy, S.; Khatua, H.; Chattopadhyay, B. *J. Am. Chem. Soc.* **2020,** *142,* 16211–16217. doi:10.1021/jacs.0c07810
168. Suwa, A.; Konishi, Y.; Uruno, Y.; Takai, K.; Nakako, T.; Sakai, M.; Enomoto, T.; Ochi, Y.; Matsuda, H.; Kitamura, A.; Uematsu, Y.; Kiyoshi, A.; Sumiyoshi, T. *Bioorg. Med. Chem. Lett.* **2014,** *24,* 2909–2912. doi:10.1016/j.bmcl.2014.04.083
169. Akrami, H.; Mirjalili, B. F.; Khoobi, M.; Nadri, H.; Moradi, A.; Sakhteman, A.; Emami, S.; Foroumadi, A.; Shafiee, A. *Eur. J. Med. Chem.* **2014,** *84,* 375–381. doi:10.1016/j.ejmech.2014.01.017
170. Lai, Y.-H.; Wu, R.-S.; Huang, J.; Huang, J.-Y.; Xu, D.-Z. *Org. Lett.* **2020,** *22,* 3825–3829. doi:10.1021/acs.orglett.0c01066
171. Llusar, M.; Forés, A.; Badenes, J. A.; Calbo, J.; Tena, M. A.; Monrós, G. *J. Eur. Ceram. Soc.* **2001,** *21,* 1121–1130. doi:10.1016/s0955-2219(00)00295-8
172. Jiang, X.; Ma, Y.; Chen, Y.; Li, Y.; Ma, Q.; Zhang, Z.; Wang, C.; Yang, Y. *Spectrochim. Acta, Part A* **2018,** *190,* 61–67. doi:10.1016/j.saa.2017.08.076
173. Balyts'kyi, A. I.; Kvasnyts'ka, Y. H.; Ivas'kevich, L. M.; Myal'nitsa, H. P. *Mater. Sci. (N. Y., NY, U. S.)* **2018,** *54,* 230–239. doi:10.1007/s11003-018-0178-z
174. Tudoroiu, N.; Zaheeruddin, M.; Tudoroiu, R.-E. *Energies (Basel, Switz.)* **2020,** *13,* 2749. doi:10.3390/en13112749
175. Da Concepción, E.; Fernández, I.; Mascareñas, J. L.; López, F. *Angew. Chem., Int. Ed.* **2021,** *60,* 8182–8188. doi:10.1002/anie.202015202
176. Zada, M.; Guo, L.; Zhang, W.; Ma, Y.; Liang, T.; Sun, W.-H. *Eur. J. Inorg. Chem.* **2021,** 720–733. doi:10.1002/ejic.202001120

177. Piontek, A.; Ochędzan-Siodłak, W.; Bisz, E.; Szostak, M. *ChemCatChem* **2021,** *13,* 202–206. doi:10.1002/cctc.202001347
178. Kadikova, G. N.; D'yakonov, V. A.; Nasretdinov, R. N.; Dzhemileva, L. U.; Dzhemilev, U. M. *Mendeleev Commun.* **2020,** *30,* 318–319. doi:10.1016/j.mencom.2020.05.019
179. Medyouni, R.; Elgabsi, W.; Naouali, O.; Romerosa, A.; Al-Ayed, A. S.; Baklouti, L.; Hamdi, N. *Spectrochim. Acta, Part A* **2016,** *167,* 165–174. doi:10.1016/j.saa.2016.04.045
180. Tokuyasu, T.; Kunikawa, S.; Abe, M.; Masuyama, A.; Nojima, M.; Kim, H.-S.; Begum, K.; Wataya, Y. *J. Org. Chem.* **2003,** *68,* 7361–7367. doi:10.1021/jo030107f
181. Kumon, T.; Wu, J.; Shimada, M.; Yamada, S.; Agou, T.; Fukumoto, H.; Kubota, T.; Hammond, G. B.; Konno, T. *J. Org. Chem.* **2021,** *86,* 5183–5196. doi:10.1021/acs.joc.1c00080
182. Li, M.-H.; Si, X.-J.; Zhang, H.; Yang, D.; Niu, J.-L.; Song, M.-P. *Org. Lett.* **2021,** *23,* 914–919. doi:10.1021/acs.orglett.0c04122
183. Oliveira, J. C. A.; Dhawa, U.; Ackermann, L. *ACS Catal.* **2021,** *11,* 1505–1515. doi:10.1021/acscatal.0c04205
184. Sen, C.; Sarvaiya, B.; Sarkar, S.; Ghosh, S. C. *J. Org. Chem.* **2020,** *85,* 15287–15304. doi:10.1021/acs.joc.0c02120
185. Dethe, D. H.; C B, N.; Bhat, A. A. *J. Org. Chem.* **2020,** *85,* 7565–7575. doi:10.1021/acs.joc.0c00727
186. Lorion, M. M.; Kaplaneris, N.; Son, J.; Kuniyil, R.; Ackermann, L. *Angew. Chem., Int. Ed.* **2019,** *58,* 1684–1688. doi:10.1002/anie.201811668
187. Borthwick, A. D. *Chem. Rev.* **2012,** *112,* 3641–3716. doi:10.1021/cr200398y
188. Friis, S. D.; Johansson, M. J.; Ackermann, L. *Nat. Chem.* **2020,** *12,* 511–519. doi:10.1038/s41557-020-0475-7
189. Calcaterra, N. E.; Barrow, J. C. *ACS Chem. Neurosci.* **2014,** *5,* 253–260. doi:10.1021/cn5000056
190. Guo, Q.; Dong, Y.; Zhang, Y.; Fu, H.; Chen, C.; Wang, L.; Yang, X.; Shen, M.; Yu, J.; Chen, M.; Zhang, J.; Duan, Y. *ACS Appl. Mater. Interfaces* **2021,** *13,* 13990–14003. doi:10.1021/acsami.1c00852
191. Kheirabadi, D.; Safavi, M. R.; Taghvaei, M.; Habibzadeh, M. R.; Honarmand, A. *J. Res. Med. Sci.* **2020,** *25,* 9. doi:10.4103/jrms.jrms_140_19
192. Abida, W.; Patnaik, A.; Campbell, D.; Shapiro, J.; Bryce, A. H.; McDermott, R.; Sautois, B.; Vogelzang, N. J.; Bambury, R. M.; Voog, E.; Zhang, J.; Piulats, J. M.; Ryan, C. J.; Merseburger, A. S.; Daugaard, G.; Heidenreich, A.; Fizazi, K.; Higano, C. S.; Krieger, L. E.; Sternberg, C. N.; Watkins, S. P.; Despain, D.; Simmons, A. D.; Loehr, A.; Dowson, M.; Golsorkhi, T.; Chowdhury, S. *J. Clin. Oncol.* **2020,** *38,* 3763–3772. doi:10.1200/jco.20.01035
193. Boerth, J. A.; Maity, S.; Williams, S. K.; Mercado, B. Q.; Ellman, J. A. *Nat. Catal.* **2018,** *1,* 673–679. doi:10.1038/s41929-018-0123-4
194. Cao, V.; Iehi, A. Y.; Bojaran, M.; Fattahi, M. *Environ. Technol. Innovation* **2020,** *20,* 101103. doi:10.1016/j.eti.2020.101103
195. Westley, J. W.; Benz, W.; Donahue, J.; Evans, R. H., Jr.; Scott, C. G.; Stempel, A.; Berger, J. *J. Antibiot.* **1974,** *27,* 744–753. doi:10.7164/antibiotics.27.744
196. Scamp, R. J.; deRamon, E.; Paulson, E. K.; Miller, S. J.; Ellman, J. A. *Angew. Chem., Int. Ed.* **2020,** *59,* 890–895. doi:10.1002/anie.201911886
197. Ranieri, M. R. M.; Chan, D. C. K.; Yaeger, L. N.; Rudolph, M.; Karabelas-Pittman, S.; Abdo, H.; Chee, J.; Harvey, H.; Nguyen, U.; Burrows, L. L. *Antimicrob. Agents Chemother.* **2019,** *63,* e00472-19. doi:10.1128/aac.00472-19
198. Huang, J.; Ding, J.; Ding, T.-M.; Zhang, S.; Wang, Y.; Sha, F.; Zhang, S.-Y.; Wu, X.-Y.; Li, Q. *Org. Lett.* **2019,** *21,* 7342–7345. doi:10.1021/acs.orglett.9b02632
199. Xavier, S.; Sahu, R. K.; Bontha, S. V.; Mas, V.; Taylor, R. P.; Megyesi, J.; Thielens, N. M.; Portilla, D. *Am. J. Physiol.: Renal Physiol.* **2019,** *317,* F1293–F1304. doi:10.1152/ajprenal.00357.2019
200. Varga, Z.; Saulnier, J.; Hauck, M.; Wallach, J. M.; Fülöp, T., Jr. *Arch. Gerontol. Geriatr.* **1992,** *14,* 273–281. doi:10.1016/0167-4943(92)90027-2
201. Fenton, G.; Newton, C. G.; Wyman, B. M.; Bagge, P.; Dron, D. I.; Riddell, D.; Jones, G. D. *J. Med. Chem.* **1989,** *32,* 265–272. doi:10.1021/jm00121a047
202. Lu, M.-Z.; Ding, X.; Shao, C.; Hu, Z.; Luo, H.; Zhi, S.; Hu, H.; Kan, Y.; Loh, T.-P. *Org. Lett.* **2020,** *22,* 2663–2668. doi:10.1021/acs.orglett.0c00631
203. Altwal, F.; Moon, C.; West, A. R.; Steiner, H. *Cells* **2020,** *9,* 2265. doi:10.3390/cells9102265
204. Kalhor, M.; Dadras, A. *J. Heterocycl. Chem.* **2013,** *50,* 220–224. doi:10.1002/jhet.950
205. Gou, Q.; Tan, X.; Zhang, M.; Ran, M.; Yuan, T.; He, S.; Zhou, L.; Cao, T.; Luo, F. *Org. Lett.* **2020,** *22,* 1966–1971. doi:10.1021/acs.orglett.0c00312
206. Carpio, M. J.; García-Delgado, C.; Marín-Benito, J. M.; Sánchez-Martín, M. J.; Rodríguez-Cruz, M. S. *Agronomy (Basel, Switz.)* **2020,** *10,* 1166. doi:10.3390/agronomy10081166
207. Adisakwattana, S. *Nutrients* **2017,** *9,* 163. doi:10.3390/nu9020163
208. Michigami, K.; Mita, T.; Sato, Y. *J. Am. Chem. Soc.* **2017,** *139,* 6094–6097. doi:10.1021/jacs.7b02775
209. Han, C.; Yu, Z.; Zhang, Y.; Wang, Z.; Zhao, J.; Huang, S.-X.; Ma, Z.; Wen, Z.; Liu, C.; Xiang, W. *J. Agric. Food Chem.* **2021,** *69,* 2108–2117. doi:10.1021/acs.jafc.0c04277
210. Obligacion, J. V.; Bezdek, M. J.; Chirik, P. J. *J. Am. Chem. Soc.* **2017,** *139,* 2825–2832. doi:10.1021/jacs.6b13346
211. Wani, M.; Baheti, A.; Polshettiwar, S.; Nandgude, T.; Shastri, A.; Ozarde, Y. *Int. J. Res. Pharm. Sci. (Madurai, India)* **2020,** *11,* 7293–7300. doi:10.26452/ijrps.v11i4.3868
212. Zhang, G.; Liu, C.; Yi, H.; Meng, Q.; Bian, C.; Chen, H.; Jian, J.-X.; Wu, L.-Z.; Lei, A. *J. Am. Chem. Soc.* **2015,** *137,* 9273–9280. doi:10.1021/jacs.5b05665
213. Mortimer, C. G.; Wells, G.; Crochard, J.-P.; Stone, E. L.; Bradshaw, T. D.; Stevens, M. F. G.; Westwell, A. D. *J. Med. Chem.* **2006,** *49,* 179–185. doi:10.1021/jm050942k
214. Khokra, S.; Arora, K.; Khan, S. A.; Kaushik, P.; Saini, R.; Husain, A. *Iran. J. Pharm. Res.* **2019,** *18,* 1–15. doi:10.22037/ijpr.2019.2384
215. Hruszkewycz, D. P.; Miles, K. C.; Thiel, O. R.; Stahl, S. S. *Chem. Sci.* **2017,** *8,* 1282–1287. doi:10.1039/c6sc03831j
216. Hu, E.; Chen, N.; Bourbeau, M. P.; Harrington, P. E.; Biswas, K.; Kunz, R. K.; Andrews, K. L.; Chmait, S.; Zhao, X.; Davis, C.; Ma, J.; Shi, J.; Lester-Zeiner, D.; Danao, J.; Able, J.; Cueva, M.; Talreja, S.; Kornecook, T.; Chen, H.; Porter, A.; Hungate, R.; Treanor, J.; Allen, J. R. *J. Med. Chem.* **2014,** *57,* 6632–6641. doi:10.1021/jm500713j
217. Li, C.; Cao, Y.-X.; Wang, R.; Wang, Y.-N.; Lan, Q.; Wang, X.-S. *Nat. Commun.* **2018,** *9,* 4951. doi:10.1038/s41467-018-07525-y
218. Wang, Y.; Hedblom, A.; Koerner, S. K.; Li, M.; Jernigan, F. E.; Wegiel, B.; Sun, L. *Bioorg. Med. Chem. Lett.* **2016,** *26,* 5703–5706. doi:10.1016/j.bmcl.2016.10.063

219. Luo, Z.; Sheng, J.; Sun, Y.; Lu, C.; Yan, J.; Liu, A.; Luo, H.-b.; Huang, L.; Li, X. *J. Med. Chem.* **2013,** *56,* 9089–9099. doi:10.1021/jm401047q
220. Li, M.; Wang, J. *Org. Lett.* **2018,** *20,* 6490–6493. doi:10.1021/acs.orglett.8b02812
221. Warawa, E. J.; Migler, B. M.; Ohnmacht, C. J.; Needles, A. L.; Gatos, G. C.; McLaren, F. M.; Nelson, C. L.; Kirkland, K. M. *J. Med. Chem.* **2001,** *44,* 372–389. doi:10.1021/jm000242+
222. Kakkar, S.; Tahlan, S.; Lim, S. M.; Ramasamy, K.; Mani, V.; Shah, S. A. A.; Narasimhan, B. *Chem. Cent. J.* **2018,** *12,* 92. doi:10.1186/s13065-018-0459-5
223. Wang, X.; Chen, Y.; Song, H.; Liu, Y.; Wang, Q. *Org. Lett.* **2020,** *22,* 9331–9336. doi:10.1021/acs.orglett.0c03551
224. Brenet, A.; Hassan-Abdi, R.; Soussi-Yanicostas, N. *Chemosphere* **2021,** *265,* 128781. doi:10.1016/j.chemosphere.2020.128781
225. Ying, J.; Fu, L.-Y.; Zhong, G.; Wu, X.-F. *Org. Lett.* **2019,** *21,* 5694–5698. doi:10.1021/acs.orglett.9b02037
226. Xue, X.; Zhang, Y.; Liu, Z.; Song, M.; Xing, Y.; Xiang, Q.; Wang, Z.; Tu, Z.; Zhou, Y.; Ding, K.; Xu, Y. *J. Med. Chem.* **2016,** *59,* 1565–1579. doi:10.1021/acs.jmedchem.5b01511
227. Trivedi, A.; Mehrotra, A.; Baum, C. E.; Lewis, B.; Basuroy, T.; Blomquist, T.; Trumbly, R.; Filipp, F. V.; Setaluri, V.; de la Serna, I. L. *Epigenet. Chromatin* **2020,** *13,* 14. doi:10.1186/s13072-020-00333-z
228. Feng, Y.; Xiao, S.; Chen, Y.; Jiang, H.; Liu, N.; Luo, C.; Chen, S.; Chen, H. *Eur. J. Med. Chem.* **2018,** *152,* 264–273. doi:10.1016/j.ejmech.2018.04.048
229. Gao, Q.; Lu, J.-M.; Yao, L.; Wang, S.; Ying, J.; Wu, X.-F. *Org. Lett.* **2021,** *23,* 178–182. doi:10.1021/acs.orglett.0c03900
230. Miyashiro, J.; Woods, K. W.; Park, C. H.; Liu, X.; Shi, Y.; Johnson, E. F.; Bouska, J. J.; Olson, A. M.; Luo, Y.; Fry, E. H.; Giranda, V. L.; Penning, T. D. *Bioorg. Med. Chem. Lett.* **2009,** *19,* 4050–4054. doi:10.1016/j.bmcl.2009.06.016
231. Huang, A.; Liu, F.; Zhan, C.; Liu, Y.; Ma, C. *Org. Biomol. Chem.* **2011,** *9,* 7351–7357. doi:10.1039/c1ob05936j
232. Kim, S. J.; Park, H. B.; Lee, J. S.; Jo, N. H.; Yoo, K. H.; Baek, D.; Kang, B.-w.; Cho, J.-H.; Oh, C.-H. *Eur. J. Med. Chem.* **2007,** *42,* 1176–1183. doi:10.1016/j.ejmech.2007.02.001
233. Lu, H.; Li, C.; Jiang, H.; Lizardi, C. L.; Zhang, X. P. *Angew. Chem., Int. Ed.* **2014,** *53,* 7028–7032. doi:10.1002/anie.201400557
234. Mace, N.; Thornton, A. R.; Blakey, S. B. *Angew. Chem., Int. Ed.* **2013,** *52,* 5836–5839. doi:10.1002/anie.201301087
235. Vardanyan, R. S.; Hruby, V. J. Antiviral Drugs. *Synthesis of Essential Drugs;* Elsevier: Amsterdam, Netherlands, 2006; pp 549–557. doi:10.1016/b978-044452166-8/50036-4
236. Lu, H.; Lang, K.; Jiang, H.; Wojtas, L.; Zhang, X. P. *Chem. Sci.* **2016,** *7,* 6934–6939. doi:10.1039/c6sc02231f
237. Zhao, S.; Yuan, J.; Li, Y.-C.; Shi, B.-F. *Chem. Commun.* **2015,** *51,* 12823–12826. doi:10.1039/c5cc05058h
238. Rej, S.; Ano, Y.; Chatani, N. *Chem. Rev.* **2020,** *120,* 1788–1887. doi:10.1021/acs.chemrev.9b00495
239. Lv, N.; Chen, Z.; Liu, Y.; Liu, Z.; Zhang, Y. *Org. Lett.* **2018,** *20,* 5845–5848. doi:10.1021/acs.orglett.8b02526
240. Leenders, R. G. G.; Scheeren, H. W. *Tetrahedron Lett.* **2000,** *41,* 9173–9175. doi:10.1016/s0040-4039(00)01642-7
241. Clarke, Z. Clozapine. *xPharm: The Comprehensive Pharmacology Reference;* Elsevier: Amsterdam, Netherlands, 2007; pp 1–6. doi:10.1016/b978-008055232-3.61501-6
242. Lewis, V. A. Psychopharmacology: Antipsychotic and Antidepressant Drugs. In *Pharmacology and Therapeutics for Dentistry,* 7th ed.; Dowd, F.; Johnson, B.; Mariotti, A., Eds.; Elsevier: Amsterdam, Netherlands, 2017; pp 133–155. doi:10.1016/b978-0-323-39307-2.00010-2
243. Yun, D.; Yoon, S. Y.; Park, S. J.; Park, Y. J. *Int. J. Mol. Sci.* **2021,** *22,* 1653. doi:10.3390/ijms22041653
244. Zhou, S.; Wang, M.; Wang, L.; Chen, K.; Wang, J.; Song, C.; Zhu, J. *Org. Lett.* **2016,** *18,* 5632–5635. doi:10.1021/acs.orglett.6b02870
245. Macdonald, G. J.; Bartolomé, J. M. A Decade of Progress in the Discovery and Development of “atypical” Antipsychotics. *Progress in Medicinal Chemistry;* Elsevier: Amsterdam, Netherlands, 2010; Vol. 49, pp 37–80. doi:10.1016/s0079-6468(10)49002-5
246. Kuwahara, R. T.; Skinner, R. B., III; Skinner, R. B., Jr. *West. J. Med.* **2001,** *175,* 112–114. doi:10.1136/ewjm.175.2.112
247. Ramanujam, A.; Neyhouse, B.; Keogh, R. A.; Muthuvel, M.; Carroll, R. K.; Botte, G. G. *Chem. Eng. J.* **2021,** *411,* 128453. doi:10.1016/j.cej.2021.128453
248. Zhidkov, I. S.; Kukharenko, A. I.; Makarov, A. V.; Savrai, R. A.; Gavrilov, N. V.; Cholakh, S. O.; Kurmaev, E. Z. *Surf. Coat. Technol.* **2020,** *386,* 125492. doi:10.1016/j.surfcoat.2020.125492
249. Ma, X.; Zhang, Y.; Jian, Z. *Polym. Chem.* **2021,** *12,* 1236–1243. doi:10.1039/d0py01689f
250. Yang, W.; Meraz, M.; Fidelis, T. T.; Sun, W.-H. *ChemPhysChem* **2021,** *22,* 585–592. doi:10.1002/cphc.202000959
251. Chen, Y.; Wang, X.; He, X.; An, Q.; Zuo, Z. *J. Am. Chem. Soc.* **2021,** *143,* 4896–4902. doi:10.1021/jacs.1c00618
252. Zhang, J.-W.; Zhang, H.; Ren, T.-Z.; Yuan, Z.-Y.; Bandosz, T. J. *Front. Chem. Sci. Eng.* **2021,** *15,* 279–287. doi:10.1007/s11705-020-1965-2
253. Gómez, M. J.; Lucci, R. O.; Franceschini, E. A.; Lacconi, G. I. *Electrochim. Acta* **2021,** *378,* 138136. doi:10.1016/j.electacta.2021.138136
254. Choudhury, P.; Chattopadhyay, S.; De, G.; Basu, B. *Mater. Adv.* **2021,** *2,* 3042–3050. doi:10.1039/d1ma00143d
255. Campbell, M. W.; Yuan, M.; Polites, V. C.; Gutierrez, O.; Molander, G. A. *J. Am. Chem. Soc.* **2021,** *143,* 3901–3910. doi:10.1021/jacs.0c13077
256. Xu, S.; Chen, H.; Zhou, Z.; Kong, W. *Angew. Chem., Int. Ed.* **2021,** *60,* 7405–7411. doi:10.1002/anie.202014632
257. Xu, P.; Ding, P.-F.; Zhang, M.-Q.; Xia, Y.-S.; Xie, T. *Tetrahedron Lett.* **2021,** *66,* 152825. doi:10.1016/j.tetlet.2021.152825
258. Zhao, T.; Pu, X.; Han, W.; Gao, G. *Org. Lett.* **2021,** *23,* 1199–1203. doi:10.1021/acs.orglett.0c04137
259. Wang, R.-H.; Li, J.-F.; Li, Y.; Qi, S.-L.; Zhang, T.; Luan, Y.-X.; Ye, M. *ACS Catal.* **2021,** *11,* 858–864. doi:10.1021/acscatal.0c04585
260. Loup, J.; Müller, V.; Ghorai, D.; Ackermann, L. *Angew. Chem., Int. Ed.* **2019,** *58,* 1749–1753. doi:10.1002/anie.201813191
261. Zhang, H.; Chen, G.-Y.; Qian, Z.-M.; Li, W.-J.; Li, C.-H.; Hu, Y.-J.; Yang, F.-Q. *Anal. Bioanal. Chem.* **2021,** *413,* 2457–2466. doi:10.1007/s00216-021-03187-w
262. Mohamed, A. R.; El Kerdawy, A. M.; George, R. F.; Georgey, H. H.; Abdel Gawad, N. M. *Bioorg. Chem.* **2021,** *107,* 104569. doi:10.1016/j.bioorg.2020.104569
263. Czaja, R.; Perbandt, M.; Betzel, C.; Hahn, U. *Biochem. Biophys. Res. Commun.* **2005,** *336,* 882–889. doi:10.1016/j.bbrc.2005.08.188
264. Derhamine, S. A.; Krachko, T.; Monteiro, N.; Pilet, G.; Schranck, J.; Tlili, A.; Amgoune, A. *Angew. Chem., Int. Ed.* **2020,** *59,* 18948–18953. doi:10.1002/anie.202006826

265. Ibarra-Lara, L.; Sánchez-Aguilar, M.; Del Valle-Mondragón, L.; Soria-Castro, E.; Cervantes-Pérez, L. G.; Pastelín-Hernández, G.; Sánchez-Mendoza, A. *J. Pharmacol. Sci.* **2020,** *144,* 218–228. doi:10.1016/j.jphs.2020.09.005
266. Sarahian, N.; Mohammadi, M. T.; Darabi, S.; Faghihi, N. *Brain Res.* **2021,** *1758,* 147343. doi:10.1016/j.brainres.2021.147343
267. Joe, C. L.; Doyle, A. G. *Angew. Chem., Int. Ed.* **2016,** *55,* 4040–4043. doi:10.1002/anie.201511438
268. Nielsen, M. K.; Shields, B. J.; Liu, J.; Williams, M. J.; Zacuto, M. J.; Doyle, A. G. *Angew. Chem., Int. Ed.* **2017,** *56,* 7191–7194. doi:10.1002/anie.201702079
269. Miorini, T. J. J.; Raetano, C. G.; Negrisoli, M. M.; Pérez-Hernández, O. *Eur. J. Plant Pathol.* **2021,** *159,* 877–889. doi:10.1007/s10658-021-02212-z
270. Thekkumpurath, A. S.; Girame, R.; Hingmire, S.; Jadhav, M.; Jain, P. *Environ. Sci. Pollut. Res.* **2020,** *27,* 41816–41823. doi:10.1007/s11356-020-10169-5
271. Grillo, M. P.; Hua, F. *Drug Metab. Dispos.* **2003,** *31,* 1429–1436. doi:10.1124/dmd.31.11.1429
272. Cai, Y.; Ye, X.; Liu, S.; Shi, S.-L. *Angew. Chem., Int. Ed.* **2019,** *58,* 13433–13437. doi:10.1002/anie.201907387
273. Fritz, I.; Wagner, P.; Broberg, P.; Einefors, R.; Olsson, H. *Acta Oncol.* **2020,** *59,* 1103–1109. doi:10.1080/0284186x.2020.1769185
274. Muto, K.; Yamaguchi, J.; Itami, K. *J. Am. Chem. Soc.* **2012,** *134,* 169–172. doi:10.1021/ja210249h
275. Xiang, J.; Wang, J.; Wang, M.; Meng, X.; Wu, A. *Tetrahedron* **2014,** *70,* 7470–7475. doi:10.1016/j.tet.2014.08.022
276. Besselièvre, F.; Lebrequier, S.; Mahuteau-Betzer, F.; Piguel, S. *Synthesis* **2009,** 3511–3518. doi:10.1055/s-0029-1216987
277. Rechsteiner, D.; Wettstein, F. E.; Pfeiffer, N.; Hollender, J.; Bucheli, T. D. *Sci. Total Environ.* **2021,** *779,* 146351. doi:10.1016/j.scitotenv.2021.146351
278. Huang, J.; Lu, Y.-J.; Guo, C.; Zuo, S.; Zhou, J.-L.; Wong, W.-L.; Huang, B. *J. Sci. Food Agric.* **2021,** in press. doi:10.1002/jsfa.11162
279. Amaike, K.; Muto, K.; Yamaguchi, J.; Itami, K. *J. Am. Chem. Soc.* **2012,** *134,* 13573–13576. doi:10.1021/ja306062c
280. Swain, S. S.; Paidesetty, S. K.; Padhy, R. N. *Biomed. Pharmacother.* **2017,** *90,* 760–776. doi:10.1016/j.biopha.2017.04.030
281. Muto, K.; Hatakeyama, T.; Yamaguchi, J.; Itami, K. *Chem. Sci.* **2015,** *6,* 6792–6798. doi:10.1039/c5sc02942b
282. Zhang, H.; Lian, Y.; Xie, N.; Cheng, X.; Chen, C.; Xu, H.; Zheng, Y. *Exp. Cell Res.* **2020,** *393,* 112089. doi:10.1016/j.yexcr.2020.112089
283. Okda, T. M.; Abd-Elghaffar, S. K.; Katary, M. A.; Abd-Alhaseeb, M. M. *Biomed. Rep.* **2021,** *14,* 27. doi:10.3892/br.2020.1403
284. Yamamoto, T.; Muto, K.; Komiyama, M.; Canivet, J.; Yamaguchi, J.; Itami, K. *Chem. – Eur. J.* **2011,** *17,* 10113–10122. doi:10.1002/chem.201101091
285. Lockwood, P. A.; Le, V. H.; O'Gorman, M. T.; Patterson, T. A.; Sultan, M. B.; Tankisheva, E.; Wang, Q.; Riley, S. *Clin. Pharmacol. Drug Dev.* **2020,** *9,* 849–854. doi:10.1002/cpdd.789
286. Kim, S. C.; Neogi, T.; Kim, E.; Lii, J.; Desai, R. J. *Arthritis Rheumatol.* **2021,** *73,* 542–543. doi:10.1002/art.41550
287. Giddens, A. C.; Boshoff, H. I. M.; Franzblau, S. G.; Barry, C. E., III; Copp, B. R. *Tetrahedron Lett.* **2005,** *46,* 7355–7357. doi:10.1016/j.tetlet.2005.08.119
288. Nguyen, H. T. T.; Doan, D. N. A.; Truong, T. *J. Mol. Catal. A: Chem.* **2017,** *426,* 141–149. doi:10.1016/j.molcata.2016.11.009
289. Pakulak, A.; Candow, D. G.; Totosy de Zepetnek, J.; Forbes, S. C.; Basta, D. *J. Diet. Suppl.* **2021,** in press. doi:10.1080/19390211.2021.1904085
290. Li, J.; Zhu, S.-R.; Xu, Y.; Lu, X.-C.; Wang, Z.-B.; Liu, L.; Xu, D.-f. *RSC Adv.* **2020,** *10,* 24795–24799. doi:10.1039/d0ra03966g
291. Keri, R. S.; Chand, K.; Budagumpi, S.; Somappa, S. B.; Patil, S. A.; Nagaraja, B. M. *Eur. J. Med. Chem.* **2017,** *138,* 1002–1033. doi:10.1016/j.ejmech.2017.07.038
292. Mohr, Y.; Hisler, G.; Grousset, L.; Roux, Y.; Quadrelli, E. A.; Wisser, F. M.; Canivet, J. *Green Chem.* **2020,** *22,* 3155–3161. doi:10.1039/d0gc00917b
293. Behmaneshfar, A.; Sadrnia, A.; Karimi-Maleha, H. *Chem. Methodol.* **2020,** *4,* 679–694. doi:10.22034/chemm.2020.111201
294. Lu, Q.; Harmalkar, D. S.; Choi, Y.; Lee, K. *Molecules* **2019,** *24,* 3778. doi:10.3390/molecules24203778
295. Zhang, L.; Si, X.; Yang, Y.; Zimmer, M.; Witzel, S.; Sekine, K.; Rudolph, M.; Hashmi, A. S. K. *Angew. Chem., Int. Ed.* **2019,** *58,* 1823–1827. doi:10.1002/anie.201810526
296. Nabergoj, D.; Janeš, D.; Fatur, K.; Glavač, N. K.; Kreft, S. *J. Evol. Biochem. Physiol.* **2020,** *56,* 565–576. doi:10.1134/s0022093020060095
297. Shen, Y.; Gu, Y.; Martin, R. *J. Am. Chem. Soc.* **2018,** *140,* 12200–12209. doi:10.1021/jacs.8b07405
298. Zhang, S.-K.; Struwe, J.; Hu, L.; Ackermann, L. *Angew. Chem., Int. Ed.* **2020,** *59,* 3178–3183. doi:10.1002/anie.201913930
299. Cheng, X.; Lu, H.; Lu, Z. *Nat. Commun.* **2019,** *10,* 3549. doi:10.1038/s41467-019-11392-6
300. Cheltsov, A. V.; Aoyagi, M.; Aleshin, A.; Yu, E. C.-W.; Gilliland, T.; Zhai, D.; Bobkov, A. A.; Reed, J. C.; Liddington, R. C.; Abagyan, R. *J. Med. Chem.* **2010,** *53,* 3899–3906. doi:10.1021/jm901446n
301. Zhu, W.; Wang, J.; Wang, S.; Gu, Z.; Aceña, J. L.; Izawa, K.; Liu, H.; Soloshonok, V. A. *J. Fluorine Chem.* **2014,** *167,* 37–54. doi:10.1016/j.jfluchem.2014.06.026
302. Meucci, E. A.; Nguyen, S. N.; Camasso, N. M.; Chong, E.; Ariafard, A.; Canty, A. J.; Sanford, M. S. *J. Am. Chem. Soc.* **2019,** *141,* 12872–12879. doi:10.1021/jacs.9b06383
303. Li, C.; Cao, Y.-X.; Jin, R.-X.; Bian, K.-J.; Qin, Z.-Y.; Lan, Q.; Wang, X.-S. *Chem. Sci.* **2019,** *10,* 9285–9291. doi:10.1039/c9sc02806d
304. Yang, F.; Koeller, J.; Ackermann, L. *Angew. Chem., Int. Ed.* **2016,** *55,* 4759–4762. doi:10.1002/anie.201512027
305. Qu, G.-R.; Liang, L.; Niu, H.-Y.; Rao, W.-H.; Guo, H.-M.; Fossey, J. S. *Org. Lett.* **2012,** *14,* 4494–4497. doi:10.1021/ol301848v
306. Xu, S.; Wu, G.; Ye, F.; Wang, X.; Li, H.; Zhao, X.; Zhang, Y.; Wang, J. *Angew. Chem., Int. Ed.* **2015,** *54,* 4669–4672. doi:10.1002/anie.201412450
307. Das, D.; Sun, A. X.; Seidel, D. *Angew. Chem., Int. Ed.* **2013,** *52,* 3765–3769. doi:10.1002/anie.201300021
308. Mandal, A.; Selvakumar, J.; Dana, S.; Mukherjee, U.; Baidya, M. *Chem. – Eur. J.* **2018,** *24,* 3448–3454. doi:10.1002/chem.201800337
309. Li, Z.-l.; Sun, K.-k.; Cai, C. *Org. Chem. Front.* **2018,** *5,* 1848–1853. doi:10.1039/c8qo00322j
310. Li, W.; Varenikov, A.; Gandelman, M. *Eur. J. Org. Chem.* **2020,** 3138–3141. doi:10.1002/ejoc.201901929
311. Hua, Y.; Chen, Z.-Y.; Diao, H.; Zhang, L.; Qiu, G.; Gao, X.; Zhou, H. *J. Org. Chem.* **2020,** *85,* 9614–9621. doi:10.1021/acs.joc.0c00936
312. Pacheco-Benichou, A.; Ivendengani, E.; Kostakis, I. K.; Besson, T.; Fruit, C. *Catalysts* **2020,** *11,* 28. doi:10.3390/catal11010028
313. Xie, W.; Heo, J.; Kim, D.; Chang, S. *J. Am. Chem. Soc.* **2020,** *142,* 7487–7496. doi:10.1021/jacs.0c00169
314. Xu, L.-L.; Wang, X.; Ma, B.; Yin, M.-X.; Lin, H.-X.; Dai, H.-X.; Yu, J.-Q. *Chem. Sci.* **2018,** *9,* 5160–5164. doi:10.1039/c8sc01256c

315. Chen, X.; Hao, X.-S.; Goodhue, C. E.; Yu, J.-Q. *J. Am. Chem. Soc.* **2006,** *128,* 6790–6791. doi:10.1021/ja061715q
316. Wang, W.; Pan, C.; Chen, F.; Cheng, J. *Chem. Commun.* **2011,** *47,* 3978–3980. doi:10.1039/c0cc05557c
317. Lu, Y.; Wang, R.; Qiao, X.; Shen, Z. *Synlett* **2011,** 1038–1042. doi:10.1055/s-0030-1259729
318. Mo, S.; Zhu, Y.; Shen, Z. *Org. Biomol. Chem.* **2013,** *11,* 2756–2760. doi:10.1039/c3ob40185e
319. Truong, T.; Klimovica, K.; Daugulis, O. *J. Am. Chem. Soc.* **2013,** *135,* 9342–9345. doi:10.1021/ja4047125
320. Yan, H.; Guo, H.; Zhou, X.; Zuo, Z.; Liu, J.; Zhang, G.; Zhang, S. *Synlett* **2019,** *30,* 1469–1473. doi:10.1055/s-0037-1611847
321. Chen, C.; Hao, Y.; Zhang, T.-Y.; Pan, J.-L.; Ding, J.; Xiang, H.-Y.; Wang, M.; Ding, T.-M.; Duan, A.; Zhang, S.-Y. *Chem. Commun.* **2019,** *55,* 755–758. doi:10.1039/c8cc08708c
322. Zhang, G.; Fan, Q.; Zhao, Y.; Ding, C. *Eur. J. Org. Chem.* **2019,** 5801–5806. doi:10.1002/ejoc.201900947
323. Sahoo, T.; Sarkar, S.; Ghosh, S. C. *Tetrahedron Lett.* **2021,** *67,* 152858. doi:10.1016/j.tetlet.2021.152858
324. Shang, M.; Wang, M.-M.; Saint-Denis, T. G.; Li, M.-H.; Dai, H.-X.; Yu, J.-Q. *Angew. Chem., Int. Ed.* **2017,** *56,* 5317–5321. doi:10.1002/anie.201611287
325. Shang, M.; Shao, Q.; Sun, S.-Z.; Chen, Y.-Q.; Xu, H.; Dai, H.-X.; Yu, J.-Q. *Chem. Sci.* **2017,** *8,* 1469–1473. doi:10.1039/c6sc03383k
326. Lu, W.; Xu, H.; Shen, Z. *Org. Biomol. Chem.* **2017,** *15,* 1261–1267. doi:10.1039/c6ob02582j
327. Wang, F.; Hu, Q.; Shu, C.; Lin, Z.; Min, D.; Shi, T.; Zhang, W. *Org. Lett.* **2017,** *19,* 3636–3639. doi:10.1021/acs.orglett.7b01559
328. Huang, H.; Wu, Y.; Zhang, W.; Feng, C.; Wang, B.-Q.; Cai, W.-F.; Hu, P.; Zhao, K.-Q.; Xiang, S.-K. *J. Org. Chem.* **2017,** *82,* 3094–3101. doi:10.1021/acs.joc.7b00081
329. Roy, S.; Pradhan, S.; Punniyamurthy, T. *Chem. Commun.* **2018,** *54,* 3899–3902. doi:10.1039/c8cc02158a
330. Xiao, Y.; Li, J.; Liu, Y.; Wang, S.; Zhang, H.; Ding, H. *Eur. J. Org. Chem.* **2018,** 3306–3311. doi:10.1002/ejoc.201800104
331. Lai, M.; Zhai, K.; Cheng, C.; Wu, Z.; Zhao, M. *Org. Chem. Front.* **2018,** *5,* 2986–2991. doi:10.1039/c8qo00840j
332. Ge, X.; Cheng, L.; Sun, F.; Liu, X.; Chen, X.; Qian, C.; Zhou, S. *Catal. Commun.* **2019,** *123,* 32–37. doi:10.1016/j.catcom.2019.01.015
333. Wendlandt, A. E.; Suess, A. M.; Stahl, S. S. *Angew. Chem., Int. Ed.* **2011,** *50,* 11062–11087. doi:10.1002/anie.201103945
334. Shang, M.; Sun, S.-Z.; Wang, H.-L.; Wang, M.-M.; Dai, H.-X. *Synthesis* **2016,** *48,* 4381–4399. doi:10.1055/s-0035-1562795
335. Rao, W.-H.; Shi, B.-F. *Org. Chem. Front.* **2016,** *3,* 1028–1047. doi:10.1039/c6qo00156d
336. Li, Z.-K.; Jia, X.-S.; Yin, L. *Synthesis* **2018,** *50,* 4165–4188. doi:10.1055/s-0037-1609932
337. Wu, P.; Huang, W.; Cheng, T.-J.; Lin, H.-X.; Xu, H.; Dai, H.-X. *Org. Lett.* **2020,** *22,* 5051–5056. doi:10.1021/acs.orglett.0c01632
338. Kathiravan, S.; Suriyanarayanan, S.; Nicholls, I. A. *Org. Lett.* **2019,** *21,* 1968–1972. doi:10.1021/acs.orglett.9b00003
339. Kim, H.; Heo, J.; Kim, J.; Baik, M.-H.; Chang, S. *J. Am. Chem. Soc.* **2018,** *140,* 14350–14356. doi:10.1021/jacs.8b08826
340. Liu, D.-Y.; Liu, X.; Gao, Y.; Wang, C.-Q.; Tian, J.-S.; Loh, T.-P. *Org. Lett.* **2020,** *22,* 8978–8983. doi:10.1021/acs.orglett.0c03382
341. Perin, N.; Hok, L.; Beč, A.; Persoons, L.; Vanstreels, E.; Daelemans, D.; Vianello, R.; Hranjec, M. *Eur. J. Med. Chem.* **2021,** *211,* 113003. doi:10.1016/j.ejmech.2020.113003
342. Jin, J.; Wen, Q.; Lu, P.; Wang, Y. *Chem. Commun.* **2012,** *48,* 9933–9935. doi:10.1039/c2cc35046g
343. Chen, Z.-B.; Gao, Q.-Q.; Liu, K.; Zhu, Y.-M. *Synlett* **2019,** *30,* 203–206. doi:10.1055/s-0037-1610680
344. Yan, Y.; Yuan, Y.; Jiao, N. *Org. Chem. Front.* **2014,** *1,* 1176–1179. doi:10.1039/c4qo00205a
345. Gao, D.; Jiao, L. *J. Org. Chem.* **2021,** *86,* 5727–5743. doi:10.1021/acs.joc.1c00209
346. Zając, D.; Honisz, D.; Łapkowski, M.; Sołoducho, J. *Molecules* **2021,** *26,* 1216. doi:10.3390/molecules26051216
347. Nain-Perez, A.; Barbosa, L. C. A.; Araujo, M. H.; Martins, J. P. A.; Takahashi, J. A.; Oliveira, G.; Diniz, R.; Heller, L.; Hoenke, S.; Csuk, R. *ChemistrySelect* **2021,** *6,* 2942–2950. doi:10.1002/slct.202100733
348. Zhao, M.; Yuan, L.-Y.; Guo, D.-L.; Ye, Y.; Da-Wa, Z.-M.; Wang, X.-L.; Ma, F.-W.; Chen, L.; Gu, Y.-C.; Ding, L.-S.; Zhou, Y. *Phytochemistry* **2018,** *148,* 97–103. doi:10.1016/j.phytochem.2018.01.018
349. Lee, S. J.; Makaravage, K. J.; Brooks, A. F.; Scott, P. J. H.; Sanford, M. S. *Angew. Chem., Int. Ed.* **2019,** *58,* 3119–3122. doi:10.1002/anie.201812701
350. Ianni, A.; Iannaccone, M.; Martino, C.; Innosa, D.; Grotta, L.; Bennato, F.; Martino, G. *Int. Dairy J.* **2019,** *94,* 65–71. doi:10.1016/j.idairyj.2019.02.014
351. Shokunbi, O. S.; Adepoju, O. T.; Mojapelo, P. E. L.; Ramaite, I. D. I.; Akinyele, I. O. *J. Food Compos. Anal.* **2019,** *82,* 103245. doi:10.1016/j.jfca.2019.103245
352. Wang, Z.; Gao, J.; Shi, A.; Meng, L.; Guo, Z. *J. Alloys Compd.* **2018,** *735,* 1997–2006. doi:10.1016/j.jallcom.2017.11.385
353. García-Mesa, J. C.; Montoro-Leal, P.; Rodríguez-Moreno, A.; López Guerrero, M. M.; Vereda Alonso, E. I. *Talanta* **2021,** *223,* 121795. doi:10.1016/j.talanta.2020.121795
354. de Azevedo-França, J. A.; Borba-Santos, L. P.; de Almeida Pimentel, G.; Franco, C. H. J.; Souza, C.; de Almeida Celestino, J.; de Menezes, E. F.; dos Santos, N. P.; Vieira, E. G.; Ferreira, A. M. D. C.; de Souza, W.; Rozental, S.; Navarro, M. *J. Inorg. Biochem.* **2021,** *219,* 111401. doi:10.1016/j.jinorgbio.2021.111401
355. Azri, N.; Irmawati, R.; Nda-Umar, U. I.; Saiman, M. I.; Taufiq-Yap, Y. H. *Arabian J. Chem.* **2021,** *14,* 103047. doi:10.1016/j.arabjc.2021.103047
356. de la Cruz-Martínez, F.; Martínez de Sarasa Buchaca, M.; Fernández-Baeza, J.; Sánchez-Barba, L. F.; Rodríguez, A. M.; Castro-Osma, J. A.; Lara-Sánchez, A. *Inorg. Chem.* **2021,** *60,* 5322–5332. doi:10.1021/acs.inorgchem.1c00309
357. Chen, Z.; Nie, X.-D.; Sun, J.-T.; Yang, A.-M.; Wei, B.-G. *Org. Biomol. Chem.* **2021,** *19,* 2492–2501. doi:10.1039/d0ob02603d
358. Węglarz, I.; Michalak, K.; Mlynarski, J. *Adv. Synth. Catal.* **2021,** *363,* 1317–1321. doi:10.1002/adsc.202001043
359. Kulkarni, N. V.; Dash, C.; Jayaratna, N. B.; Ridlen, S. G.; Karbalaei Khani, S.; Das, A.; Kou, X.; Yousufuddin, M.; Cundari, T. R.; Dias, H. V. R. *Inorg. Chem.* **2015,** *54,* 11043–11045. doi:10.1021/acs.inorgchem.5b02134
360. Kalita, B.; Lamar, A. A.; Nicholas, K. M. *Chem. Commun.* **2008,** 4291–4293. doi:10.1039/b805783d
361. Li, L.; Zhou, B.; Wang, Y.-H.; Shu, C.; Pan, Y.-F.; Lu, X.; Ye, L.-W. *Angew. Chem., Int. Ed.* **2015,** *54,* 8245–8249. doi:10.1002/anie.201502553
362. Singh, R.; Kumar, S.; Patil, M. T.; Sun, C.-M.; Salunke, D. B. *Adv. Synth. Catal.* **2020,** *362,* 4027–4077. doi:10.1002/adsc.202000549
363. Yu, J.; Liu, S.-S.; Cui, J.; Hou, X.-S.; Zhang, C. *Org. Lett.* **2012,** *14,* 832–835. doi:10.1021/ol203358f

364. Assiri, M. A.; Ali, T. E.; Ali, M. M.; Yahia, I. S. *Phosphorus, Sulfur Silicon Relat. Elem.* **2018,** *193,* 668–674. doi:10.1080/10426507.2018.1487969

License and Terms

This is an Open Access article under the terms of the Creative Commons Attribution License (https://creativecommons.org/licenses/by/4.0). Please note that the reuse, redistribution and reproduction in particular requires that the author(s) and source are credited and that individual graphics may be subject to special legal provisions.

The license is subject to the *Beilstein Journal of Organic Chemistry* terms and conditions: (https://www.beilstein-journals.org/bjoc/terms)

The definitive version of this article is the electronic one which can be found at:
https://doi.org/10.3762/bjoc.17.126

BEILSTEIN JOURNAL OF ORGANIC CHEMISTRY

Photoredox catalysis in nickel-catalyzed C–H functionalization

Lusina Mantry, Rajaram Maayuri, Vikash Kumar and Parthasarathy Gandeepan[*]

Review

Open Access

Address:
Department of Chemistry, Indian Institute of Technology Tirupati, Tirupati – Renigunta Road, Settipalli Post, Tirupati, Andhra Pradesh 517506, India

Email:
Parthasarathy Gandeepan[*] - pgandeepan@iittp.ac.in

[*] Corresponding author

Keywords:
C–H activation; functionalization; nickel; photocatalysts; photoredox; visible light

Beilstein J. Org. Chem. **2021,** *17,* 2209–2259.
https://doi.org/10.3762/bjoc.17.143

Received: 08 June 2021
Accepted: 18 August 2021
Published: 31 August 2021

This article is part of the thematic issue "Earth-abundant 3d metal catalysis".

Associate Editor: M. Rueping

© 2021 Mantry et al.; licensee Beilstein-Institut.
License and terms: see end of document.

Abstract

Catalytic C–H functionalization has become a powerful strategy in organic synthesis due to the improved atom-, step- and resource economy in comparison with cross-coupling or classical organic functional group transformations. Despite the significant advances in the metal-catalyzed C–H activations, recent developments in the field of metallaphotoredox catalysis enabled C–H functionalizations with unique reaction pathways under mild reaction conditions. Given the relative earth-abundance and cost-effective nature, nickel catalysts for photoredox C–H functionalization have received significant attention. In this review, we highlight the developments in the field of photoredox nickel-catalyzed C–H functionalization reactions with a range of applications until summer 2021.

Introduction

During the last decades, transition-metal-catalyzed transformations have become one of the most reliable and basic tools for designing and manufacturing biologically relevant molecules and functional materials [1-4]. The formation of highly chemo-, regio-, and stereoselective products with excellent yields is the key reason for transition-metal catalysis as a reliable strategy in modern organic synthesis. Palladium-catalyzed cross-coupling reactions such as Mizoroki–Heck [5-8], Suzuki–Miyaura [9-11], Buchwald–Hartwig [12,13], Negishi [14,15], Migita–Stille [16], Sonogashira [17], among others [18-20], significantly changed the design of synthetic routes for modern pharmaceuticals [21,22]. Over the past two decades, nickel has emerged as an attractive alternative to palladium due to its relative earth-abundance, less toxicity, and inexpensiveness.

Despite the fact that the nickel-catalyzed cross-coupling reactions represent a powerful tool in organic synthesis, they generally require prefunctionalized starting materials, which significantly affect the reaction's atom economy and produce inorganic, organometallic salt wastes [23-25]. During the last decade, the oxidative functionalization of inert C–H into carbon–carbon (C–C) and carbon–heteroatom bonds for the construction of complex organic molecules by nickel catalysis significantly improved the atom-, step-, and resource economy by avoiding the substrate prefunctionalizations (Scheme 1) [26-30]. The nickel-catalyzed oxidative C–H functionalization often requires relatively high catalyst loadings, directing groups, high reaction temperatures (100–160 °C), stoichiometric additives, or oxidants such as peroxide or silver salts that can be undesirable for large scale synthesis.

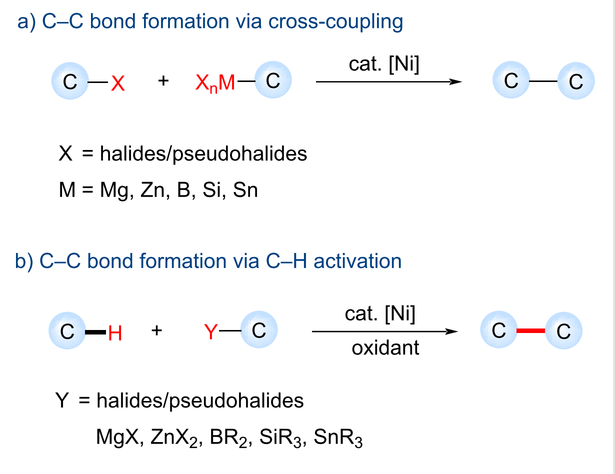
a) C–C bond formation via cross-coupling
C—X + XnM—C
cat. [Ni]
C—C
X = halides/pseudohalides
M = Mg, Zn, B, Si, Sn
b) C–C bond formation via C–H activation
C—H + Y—C
cat. [Ni]
oxidant
C—C
Y = halides/pseudohalides
MgX, ZnX2, BR2, SiR3, SnR3

Scheme 1: Nickel-catalyzed cross-coupling versus C–H activation.

Recently, photoredox dual catalysis has witnessed significant developments, which enables a diverse range of previously inaccessible organic transformations in milder reaction conditions [31-40]. Here, by absorbing visible light, a photocatalyst can function as a single-electron redox mediator through an oxidative or reductive quenching cycle (Figure 1), thereby facilitating redox-neutral transformations in the absence of stoichiometric oxidants/reductants. Given the tendency of nickel to mediate the reactions via Ni(0), Ni(I), Ni(II), and Ni(III) intermediates by both giving and accepting a single electron from a photocatalyst or combined with radical species [41-43], a wide variety of reactions have been discovered. Within a remarkable renaissance of photoredox dual catalysis, nickel/photoredox catalysis has recently been identified as a viable C–H functionalization tool under milder reaction conditions [40,44-47]. In this review, we highlight the developments in C–H activation enabled by nickel photocatalysis.

Review

Arylation

The arylation of C(sp^3)–H bonds constitutes a potential tool for the rapid diversification of simple organic molecules into valuable scaffolds [48-52]. In 2014, Doyle, MacMillan and co-workers demonstrated an inspiring C(sp^3)–H arylation of dimethylaniline (**1a**) with a variety of aryl halides using the photoredox nickel catalysis [53]. Here, the combination of the iridium photocatalyst Ir[dF(CF_3)ppy]$_2$(dtbbpy)PF_6 and the commercially available nickel catalyst $NiCl_2$·glyme were found to be suitable to achieve the transformation in satisfactory yields under visible light irradiation (Scheme 2). The authors hypothesized that the key α-nitrogen carbon-centered radical **5** could be generated via a photoredox-driven *N*-phenyl oxidation and α-C–H deprotonation sequence from dimethylaniline (**1a**) and should intercept with the nickel catalytic cycle to result in the desired products **4**.

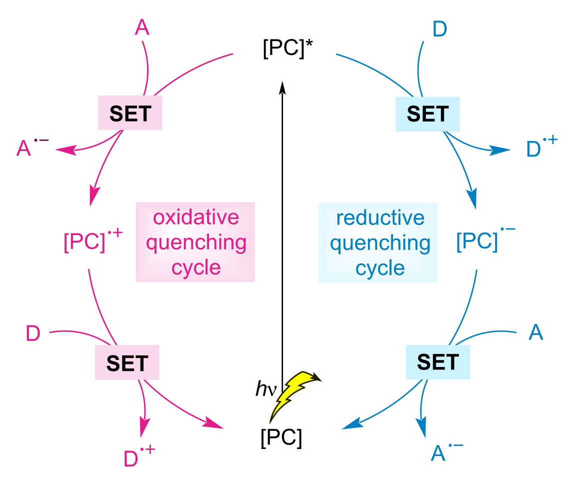

Figure 1: Oxidative and reductive quenching cycles of a photocatalyst. [PC] = photocatalyst, A = acceptor, D = donor.

In another work by the same laboratory, a strategy for the arylation of α-amino C(sp^3)–H bonds in various acyclic and cyclic amine compounds **6** was realized using photoredox-mediated hydrogen atom transfer (HAT) and nickel catalysis [54]. The catalytic system consisting of iridium photocatalyst Ir[dF(CF_3)ppy]$_2$(dtbbpy)PF_6, nickel catalyst $NiBr_2$·$3H_2O$, ligand 4,7-dimethoxy-1,10-phenanthroline (4,7-dOMe-phen), and 3-acetoxyquinuclidine was found to be optimal to afford the desired α-amino C–C coupled products **7** (Scheme 3). It is worth noting that 3-acetoxyquinuclidine serves as both the HAT catalyst and the base in this reaction system. Furthermore, several cyclic and acyclic amine **6** substrates were used as C–H nucleophile coupling partners for (hetero)aryl bromides **3**. Two additional examples for the photoredox nickel-catalyzed arylation of α-oxy C–H bonds of tetrahydrofuran (THF) and oxetane were also shown. Further, the catalytic system also proved compatible for the C–H arylation of the benzylic system.

As shown in Figure 2 [54], the mechanism for the transformation is proposed to involve the generation of nucleophilic α-amino radicals **2-IV** via a photoredox-mediated HAT process. At the same time, the in situ generated nickel(0) species **2-V** by a SET process would undergo oxidative addition into aryl bromide **3**, resulting in the electrophilic nickel(II)–aryl intermedi-

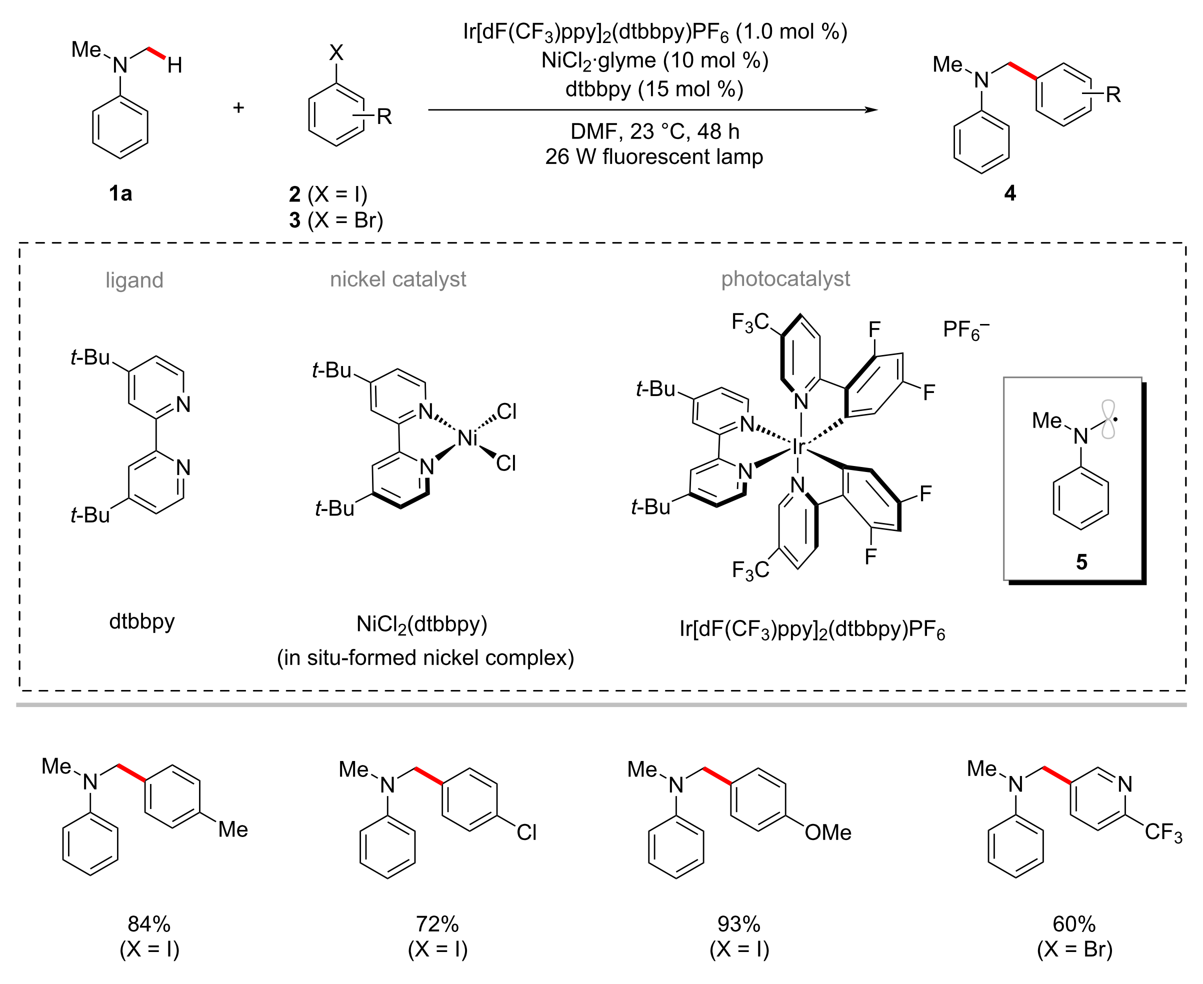
Me
N
H
1a
+
X
R
2 (X = I)
3 (X = Br)
Ir[dF(CF3)ppy]2(dtbbpy)PF6 (1.0 mol %)
NiCl2·glyme (10 mol %)
dtbbpy (15 mol %)
DMF, 23 °C, 48 h
26 W fluorescent lamp
4
ligand
nickel catalyst
photocatalyst
t-Bu
dtbbpy
Ni
Cl
NiCl2(dtbbpy)
(in situ-formed nickel complex)
F3C
F
PF6−
Ir
Ir[dF(CF3)ppy]2(dtbbpy)PF6
5
84%
(X = I)
72%
(X = I)
93%
(X = I)
60%
(X = Br)
OMe
CF3

Scheme 2: Photoredox nickel-catalyzed C(sp^3)–H arylation of dimethylaniline (**1a**).

ate **2-VI**. The rapid coupling of nickel(II) species **2-VI** and radical species **2-IV** forms a nickel(III) intermediate **2-VII**, which undergoes a reductive elimination to afford the desired product **7** and the nickel(I) species **2-VIII**. The SET reduction of **2-VIII** by the iridium(II) species **2-III** regenerates the nickel(0) catalyst **2-V** and the iridium(III) photocatalyst **2-I**.

Subsequently, Ahneman and Doyle reported a related process for the synthesis of a variety of benzylic amines **7** by the arylation of α-amino C(sp^3)–H bonds with aryl iodides **2** involving photoredox nickel catalysis (Scheme 4) [55]. In this protocol, bis(oxazoline) (BiOx) was identified as the suitable ligand instead of the commonly used bipyridyl ligand (vide supra). Notably, the use of the chiral (*S,S*)-Bn-BiOx ligand resulted in a moderate enantioinduction in the C–H arylation product.

The authors proposed a catalytic cycle to account for the photoredox nickel-catalyzed C(sp^3)–H arylation as shown in Figure 3 [55]. Thus, the in situ-generated nickel(0) **3-IV** undergoes an oxidative addition with the aryl iodide **2** to form the nickel(II)–aryl complex **3-V**. The photoredox-generated nucleophilic α-amino radical **3-VIII** readily combines with the nickel(II) species **3-V** to generate nickel(III) intermediate **3-VI**, which results in the cross-coupled product **7** upon reductive elimination. The SET event between the reduced photocatalyst **3-III** and the nickel(0) species **3-IV** regenerates both catalysts simultaneously.

Further studies by the Doyle group established the α-oxy C(sp^3)–H arylation of cyclic and acyclic ethers **9** with aryl chlorides **8** under photoredox nickel catalysis (Scheme 5) [56]. Here, aryl chlorides **8** serve as cross-coupling partners and the chlorine radical source, which rapidly abstracts an α-oxy C(sp^3)–H of the ethers to form the key α-oxyalkyl radical intermediate. Notably, the photocatalytic conditions proved suitable for the benzylic C(sp^3)–H and unactivated alkane cyclohexane C–H arylations. The catalytic cycle is proposed to involve the oxidative addition of nickel(0) **4-IV** into an aryl chloride **8a** to

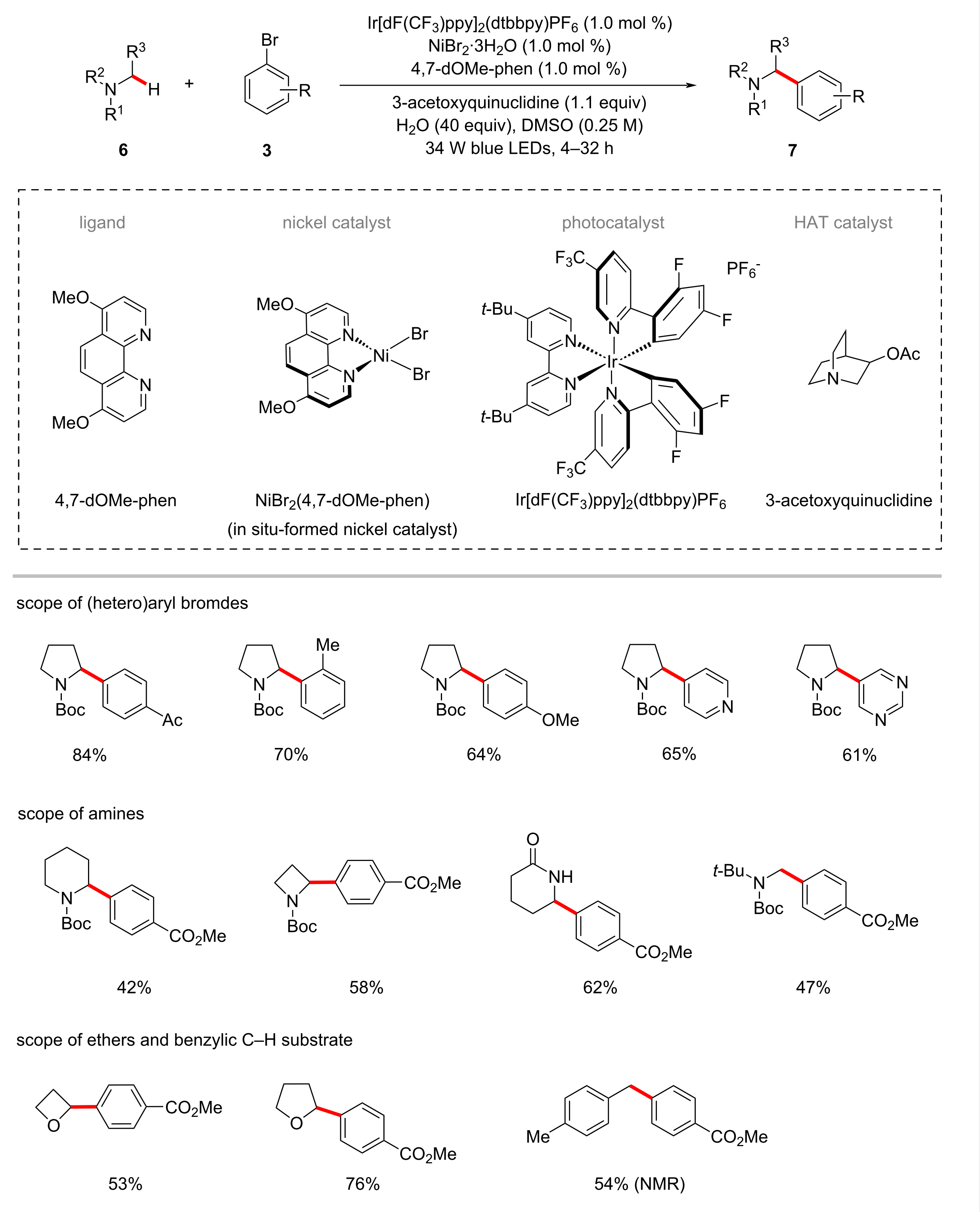
Ir[dF(CF3)ppy]2(dtbbpy)PF6 (1.0 mol %)
NiBr2·3H2O (1.0 mol %)
4,7-dOMe-phen (1.0 mol %)
3-acetoxyquinuclidine (1.1 equiv)
H2O (40 equiv), DMSO (0.25 M)
34 W blue LEDs, 4–32 h
6
3
7
ligand
nickel catalyst
photocatalyst
HAT catalyst
4,7-dOMe-phen
NiBr2(4,7-dOMe-phen)
(in situ-formed nickel catalyst)
Ir[dF(CF3)ppy]2(dtbbpy)PF6
3-acetoxyquinuclidine
scope of (hetero)aryl bromdes
84%
70%
64%
65%
61%
scope of amines
42%
58%
62%
47%
scope of ethers and benzylic C–H substrate
53%
76%
54% (NMR)

Scheme 3: Photoredox nickel-catalyzed arylation of α-amino, α-oxy and benzylic C(sp^3)–H bonds with aryl bromides.

form nickel(II) intermediate **4-V** (Figure 4) [56]. The SET oxidation of **4-V** by the photoexcited iridium(III) photocatalyst **4-II** results in the nickel(III) species **4-VI**. Photolysis of **4-VI** generates a chloride radical, which rapidly abstracts the α-oxy C(sp^3)–H of the ether to provide the alkyl radical species. The alkyl radical rebound to **4-VIII** produces the nickel(III) species **4-IX**, which undergoes reductive elimination to release the desired product **10a**.

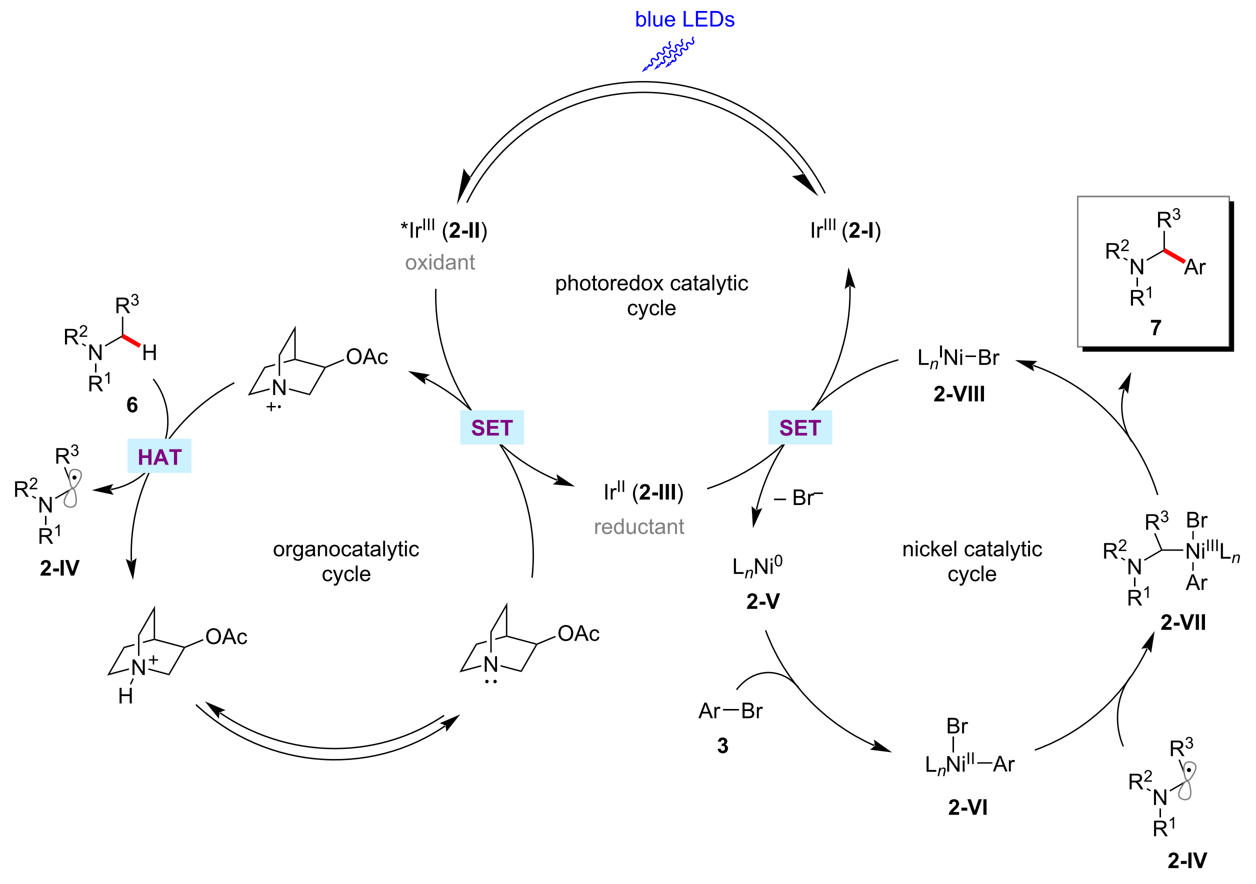
blue LEDs
*Ir^{III} (2-II)
oxidant
Ir^{III} (2-I)
photoredox catalytic cycle
SET
SET
Ir^{II} (2-III)
reductant
HAT
organocatalytic cycle
nickel catalytic cycle
OAc
OAc
OAc
6
2-IV
L_nNi^0
2-V
$L_n{}^INi–Br$
2-VIII
– Br$^−$
Ar–Br
3
L_nNi^{II}–Ar
Br
2-VI
Ni$^{III}L_n$
2-VII
7
2-IV

Figure 2: Proposed catalytic cycle for the photoredox-mediated HAT and nickel catalysis enabled C(sp^3)–H arylation.

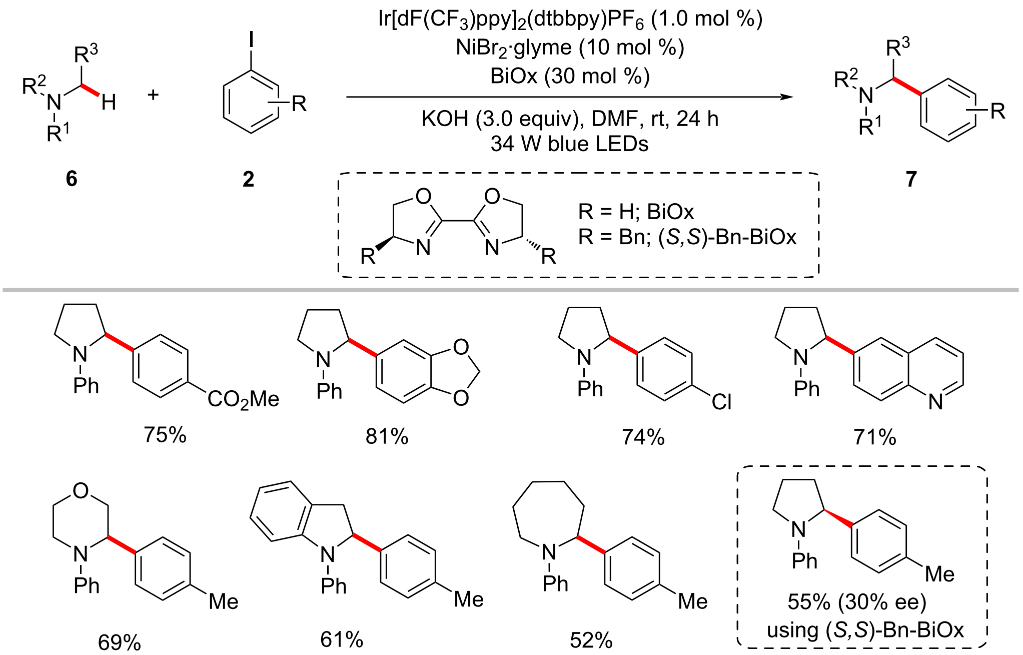
Ir[dF(CF$_3$)ppy]$_2$(dtbbpy)PF$_6$ (1.0 mol %)
NiBr$_2$·glyme (10 mol %)
BiOx (30 mol %)
KOH (3.0 equiv), DMF, rt, 24 h
34 W blue LEDs
6
2
7
R = H; BiOx
R = Bn; (*S*,*S*)-Bn-BiOx
75%
81%
74%
71%
69%
61%
52%
55% (30% ee)
using (*S*,*S*)-Bn-BiOx

Scheme 4: Photoredox arylation of α-amino C(sp^3)–H bonds with aryl iodides.

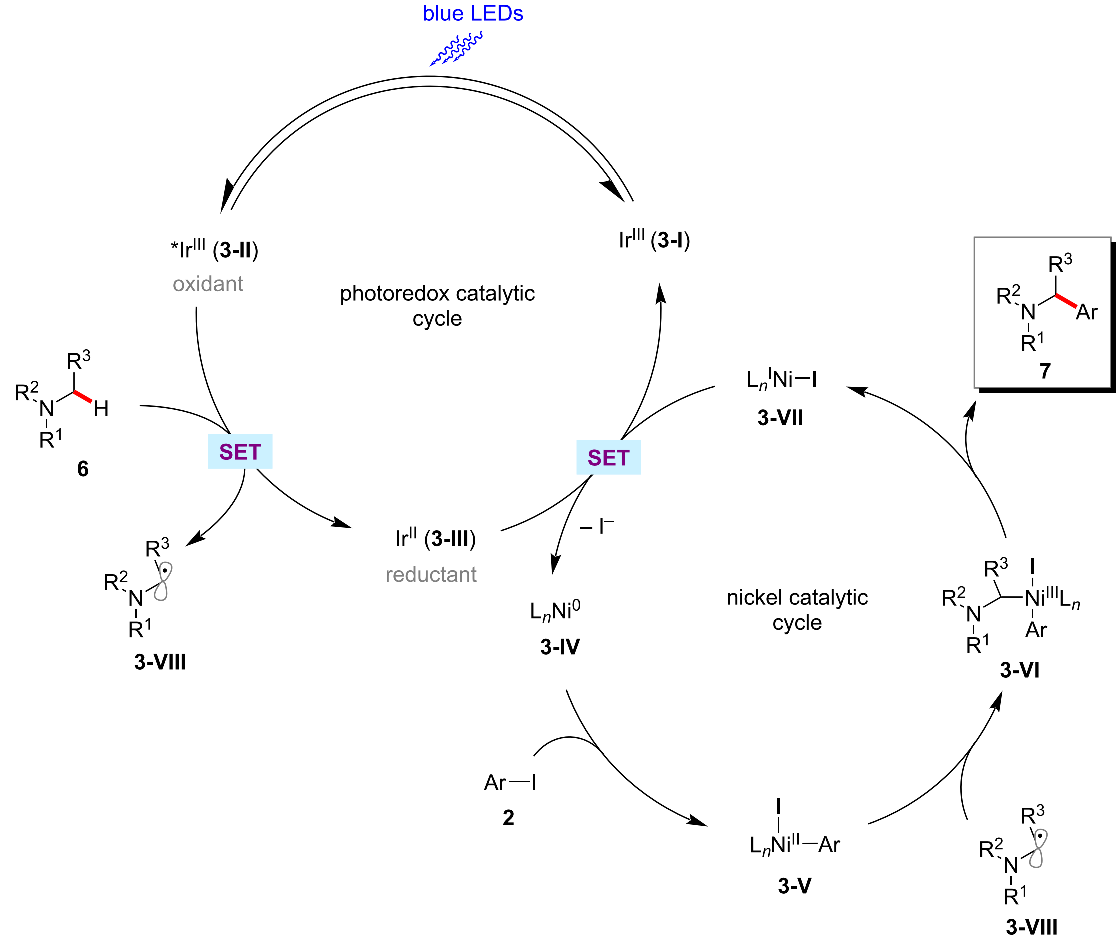
blue LEDs
*Ir^{III} (3-II)
oxidant
Ir^{III} (3-I)
photoredox catalytic cycle
6
SET
3-VIII
Ir^{II} (3-III)
reductant
SET
– I$^-$
L$_n$Ni^I–I
3-VII
7
L$_n$Ni^0
3-IV
nickel catalytic cycle
3-VI
Ar–I
2
L$_n$Ni^{II}–Ar
3-V
3-VIII

Figure 3: Proposed mechanism for photoredox nickel-catalyzed α-amino C–H arylation with aryl iodides.

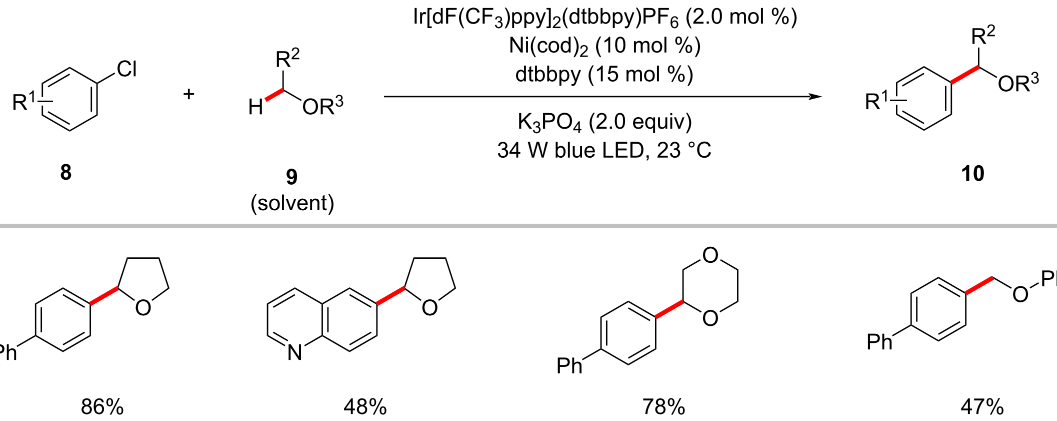
8
9
(solvent)
Ir[dF(CF$_3$)ppy]$_2$(dtbbpy)PF$_6$ (2.0 mol %)
Ni(cod)$_2$ (10 mol %)
dtbbpy (15 mol %)
K$_3$PO$_4$ (2.0 equiv)
34 W blue LED, 23 °C
10
86%
48%
78%
47%

Scheme 5: Nickel-catalyzed α-oxy C(sp^3)–H arylation of cyclic and acyclic ethers.

Concurrently, Molander and co-workers also reported a related nickel-catalyzed arylation of α-heteroatom-substituted or benzylic C(sp^3)–H bonds by aryl bromides **3** at room temperature using an iridium photocatalyst, substoichiometric 4,4′-dimethoxybenzophenone (DMBP) additives, and visible light (Scheme 6) [57]. A variety of cyclic and acyclic ethers **9** reacted with (hetero)aryl bromides **3** under the mild reaction conditions to give the desired products **10** in moderate to good yields, how-

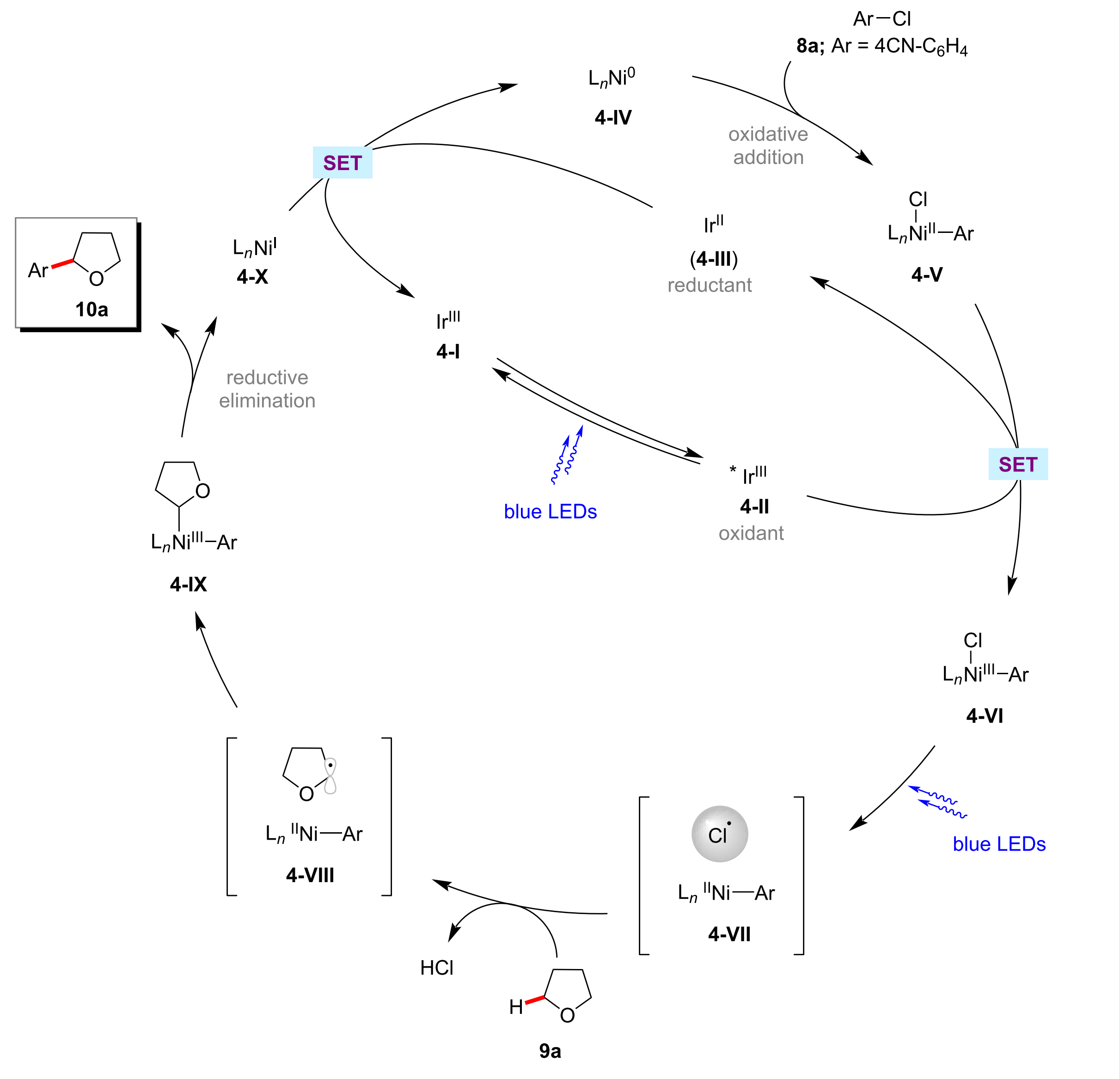
Ar–Cl
8a; Ar = 4CN-C6H4
LnNi0
4-IV
oxidative addition
Cl
LnNiII–Ar
4-V
SET
IrII
(4-III)
reductant
LnNiI
4-X
IrIII
4-I
Ar
O
10a
reductive elimination
blue LEDs
*IrIII
4-II
oxidant
SET
O
LnNiIII–Ar
4-IX
Cl
LnNiIII–Ar
4-VI
blue LEDs
O
LnIINi–Ar
4-VIII
Cl•
LnIINi–Ar
4-VII
HCl
H
O
9a

Figure 4: Proposed catalytic cycle for the C(sp^3)–H arylation of cyclic and acyclic ethers.

ever, with longer reaction times (24–96 h). The authors proposed a catalytic cycle to account for the mode of operation as depicted in Figure 5 [57]. Thus, the in situ-generated nickel(0) complex **5-III** undergoes oxidative addition into aryl bromide **3a** to form nickel(II) complex **5-IV**. The triplet–triplet energy transfer from the excited photocatalyst to the **5-IV** complex resulted in excited **5-V**. Subsequently, the homolysis of the Ni–Br bond in **5-V** followed by a HAT process results in species **5-VI**. The nickel–alkyl–aryl complex **5-VI** undergoes reductive elimination to release the desired product **10a** and regenerates the active nickel(0) catalyst **5-III**.

The synthetic utility of the photoredox nickel-catalyzed C–H arylation was further elaborated to include C–O electrophiles which could be readily derived from phenols, as disclosed by the Yu group [58]. Hence, they reported an arylation protocol for α-amino- and α-oxy C(sp^3)–H bonds with aryl tosylates/triflates **11**. The relatively less expensive ruthenium photocatalyst $Ru(bpy)_3Cl_2{\cdot}6H_2O$ was found to be optimal for primary C(sp^3)–H arylations (Scheme 7a), whereas $Ir[dF(CF_3)ppy]_2(dtbbpy)PF_6$ was the effective photocatalyst for the arylation of secondary C(sp^3)–H bonds (Scheme 7b).

In a subsequent report, Yu and co-workers also realized the arylation of α-amino C(sp^3)–H bonds with aryl tosylates **11** generated in situ from phenols **12** and *p*-toluenesulfonyl chloride (TsCl) [59,60]. The combination of visible-light-photoredox catalysis, hydrogen-atom-transfer catalysis, and

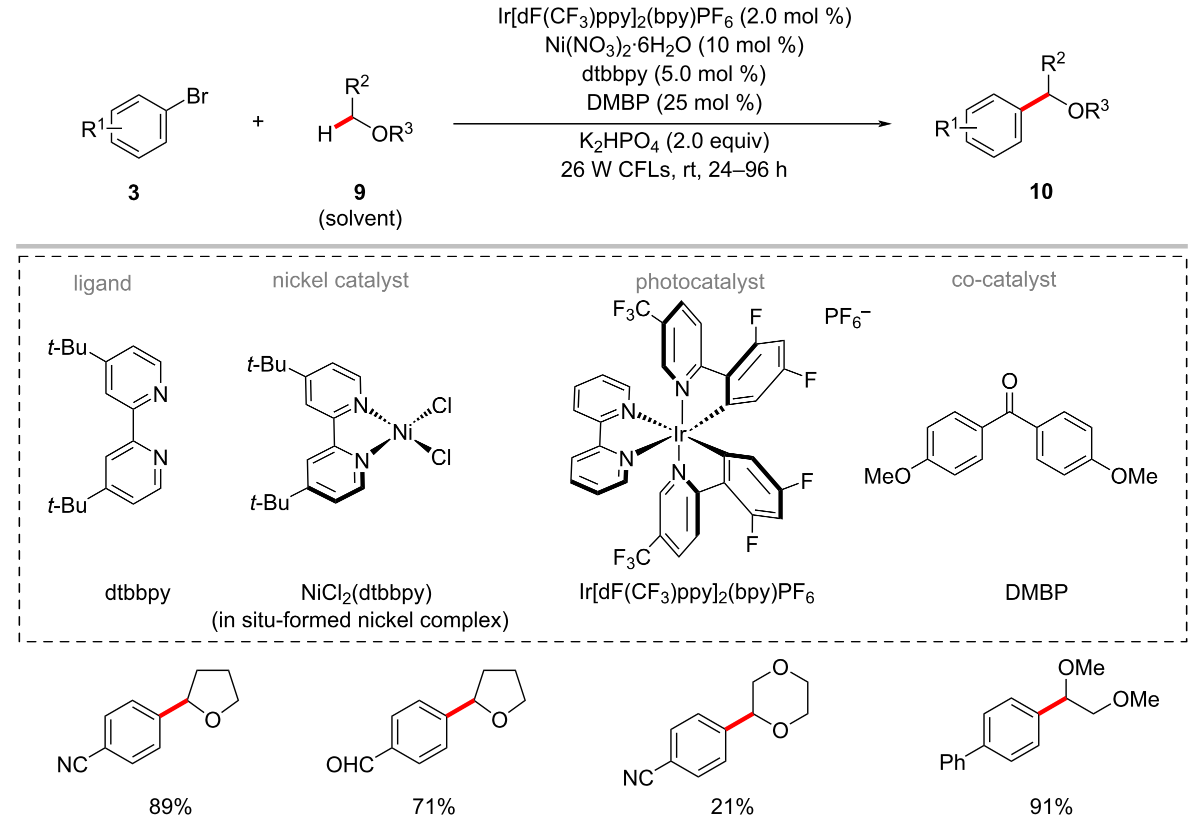

$Ir[dF(CF_3)ppy]_2(bpy)PF_6$ (2.0 mol %)
$Ni(NO_3)_2 \cdot 6H_2O$ (10 mol %)
dtbbpy (5.0 mol %)
DMBP (25 mol %)
K_2HPO_4 (2.0 equiv)
26 W CFLs, rt, 24–96 h
3
9
(solvent)
10
ligand
nickel catalyst
photocatalyst
co-catalyst
dtbbpy
$NiCl_2(dtbbpy)$
(in situ-formed nickel complex)
$Ir[dF(CF_3)ppy]_2(bpy)PF_6$
DMBP
89%
71%
21%
91%

Scheme 6: Photochemical nickel-catalyzed C–H arylation of ethers.

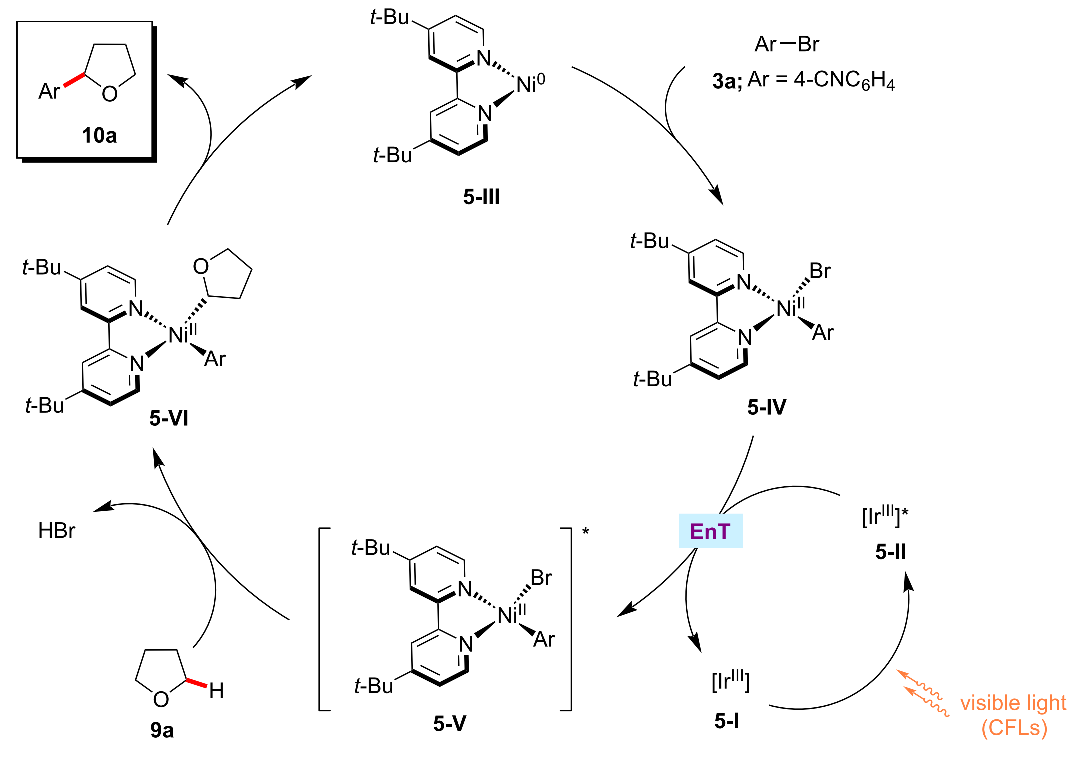

10a
5-III
Ar—Br
3a; Ar = 4-CNC6H4
5-IV
EnT
[IrIII]*
5-II
[IrIII]
5-I
visible light
(CFLs)
5-V
HBr
9a
5-VI

Figure 5: Proposed catalytic cycle for the nickel-catalyzed arylation of ethers with aryl bromides.

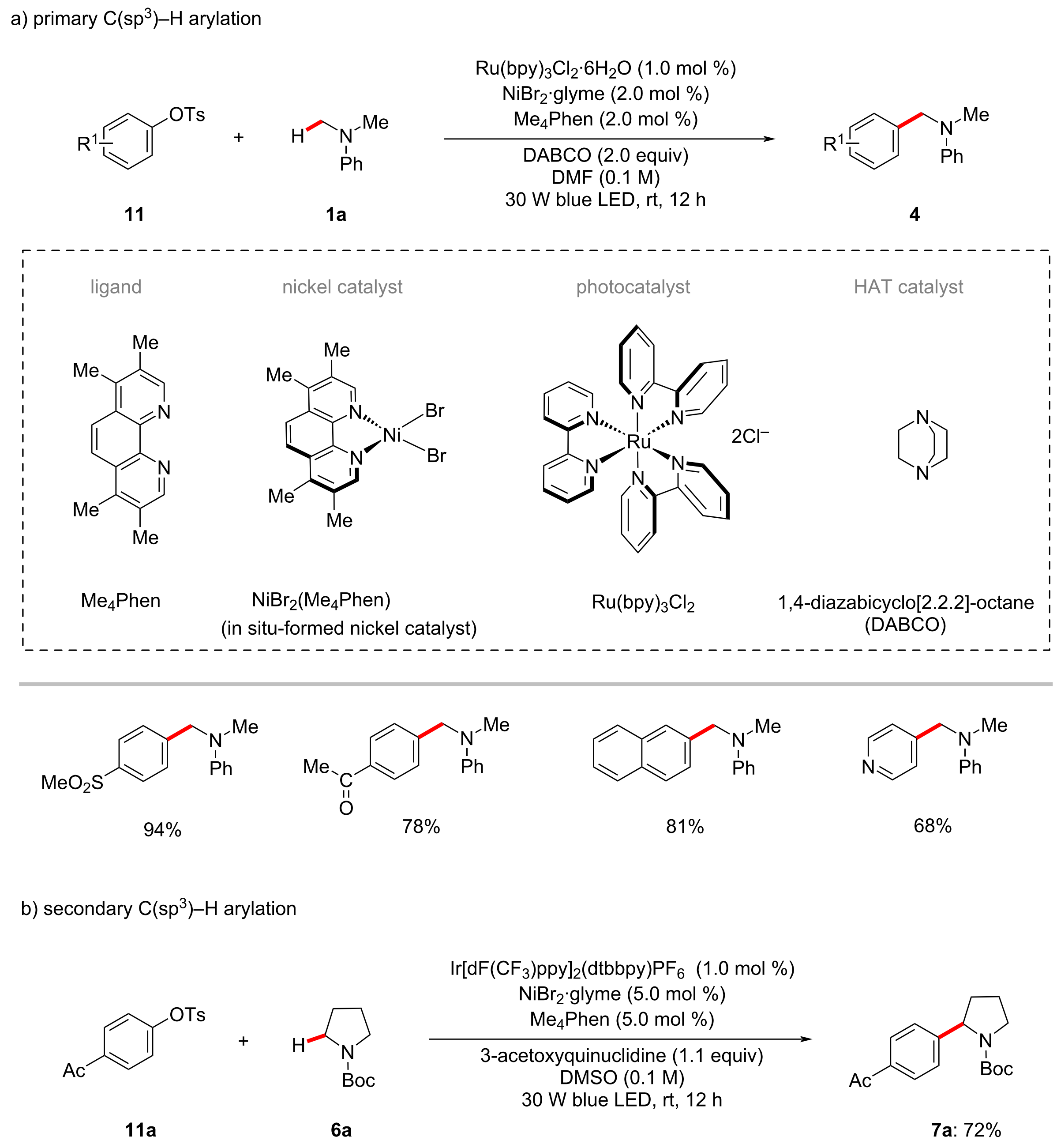
a) primary C(sp^3)–H arylation
Ru(bpy)$_3$Cl$_2$·6H$_2$O (1.0 mol %)
NiBr$_2$·glyme (2.0 mol %)
Me$_4$Phen (2.0 mol %)
DABCO (2.0 equiv)
DMF (0.1 M)
30 W blue LED, rt, 12 h
11
1a
4
ligand
nickel catalyst
photocatalyst
HAT catalyst
Me$_4$Phen
NiBr$_2$(Me$_4$Phen)
(in situ-formed nickel catalyst)
Ru(bpy)$_3$Cl$_2$
1,4-diazabicyclo[2.2.2]-octane
(DABCO)
94%
78%
81%
68%
b) secondary C(sp^3)–H arylation
Ir[dF(CF$_3$)ppy]$_2$(dtbbpy)PF$_6$ (1.0 mol %)
NiBr$_2$·glyme (5.0 mol %)
Me$_4$Phen (5.0 mol %)
3-acetoxyquinuclidine (1.1 equiv)
DMSO (0.1 M)
30 W blue LED, rt, 12 h
11a
6a
7a: 72%

Scheme 7: Nickel-catalyzed α-amino C(sp^3)–H arylation with aryl tosylates.

nickel catalysis enables these protocols at room temperature with ample substrate scope (Scheme 8). Unsymmetrical amine substrates favored arylation at the methylene C–H over methyl C–H with good regioselectivity [59].

In 2017, Doyle utilized the photoredox nickel catalysis approach for the formylation of aryl chlorides **8** through selective 2-functionalization of 1,3-dioxolane (**13**) followed by a mild acidic workup (Scheme 9) [61]. Here, the photocatalyst Ir[dF(CF$_3$)ppy]$_2$(dtbbpy)PF$_6$ and nickel catalyst NiCl$_2$·DME with dtbbpy as ligand, along with K$_3$PO$_4$ as base under irradiation with blue LEDs enabled the regioselective 2-functionalization of 1,3-dioxolane (**13**) with aryl chlorides **8**. It was found that the electron-deficient aryl chlorides resulted in better yields within shorter reaction times over the electron-rich substrates. A possible catalytic cycle was shown to account for the reaction mode, which is similar to that of Figure 4.

The robustness of the photoredox nickel catalysis was further demonstrated by a protocol for the direct arylation of

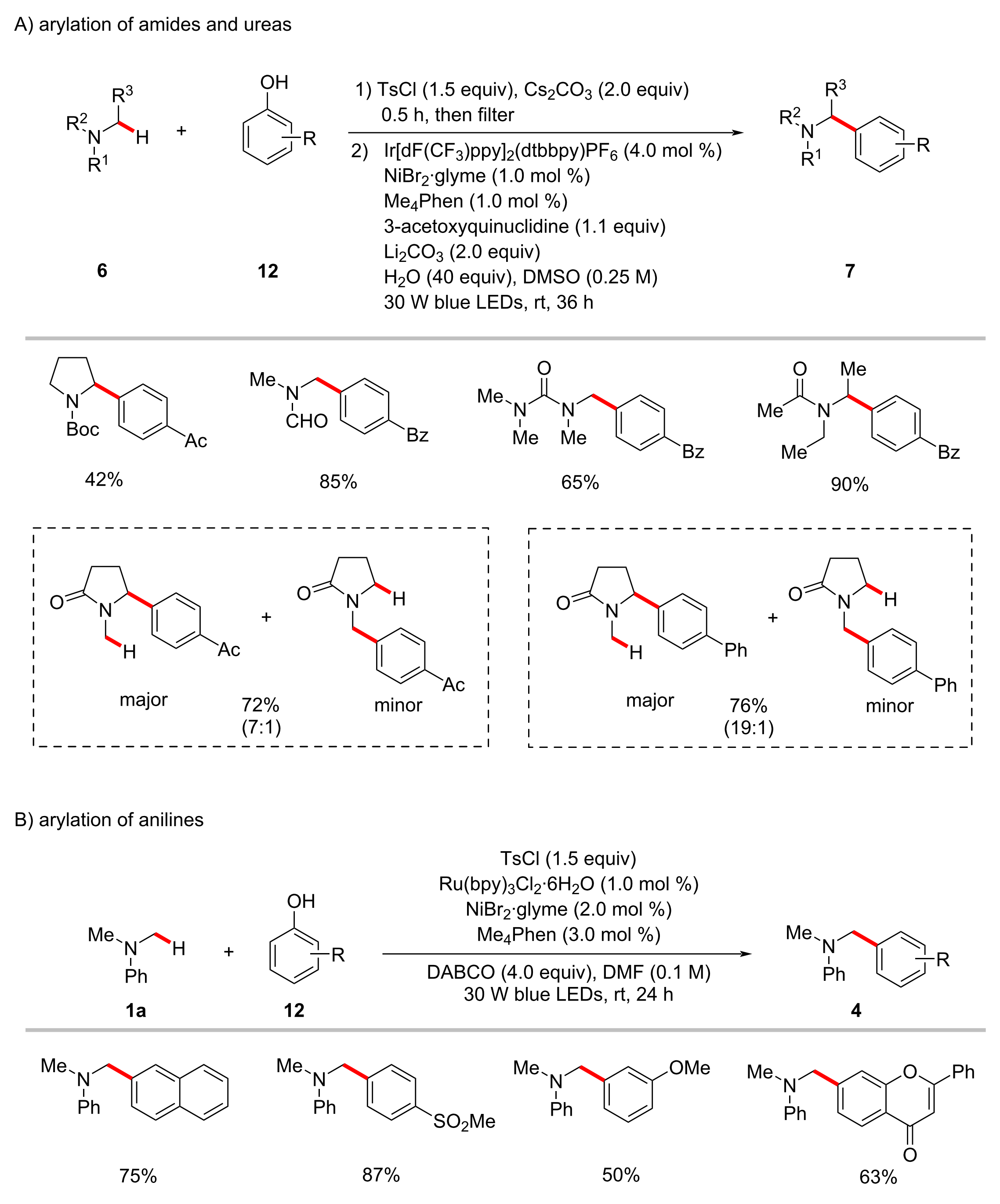
A) arylation of amides and ureas
1) TsCl (1.5 equiv), Cs2CO3 (2.0 equiv)
0.5 h, then filter
2) Ir[dF(CF3)ppy]2(dtbbpy)PF6 (4.0 mol %)
NiBr2·glyme (1.0 mol %)
Me4Phen (1.0 mol %)
3-acetoxyquinuclidine (1.1 equiv)
Li2CO3 (2.0 equiv)
H2O (40 equiv), DMSO (0.25 M)
30 W blue LEDs, rt, 36 h
6
12
7
42%
85%
65%
90%
major
72%
(7:1)
minor
major
76%
(19:1)
minor
B) arylation of anilines
TsCl (1.5 equiv)
Ru(bpy)3Cl2·6H2O (1.0 mol %)
NiBr2·glyme (2.0 mol %)
Me4Phen (3.0 mol %)
DABCO (4.0 equiv), DMF (0.1 M)
30 W blue LEDs, rt, 24 h
1a
12
4
75%
87%
50%
63%

Scheme 8: Arylation of α-amino C(sp^3)–H bonds by in situ generated aryl tosylates from phenols.

inert aliphatic C–H bonds [62]. Thus, MacMillan and co-workers employed tetrabutylammonium decatungstate [$(W_{10}O_{32})^{4-}$·4(Bu_4N^+)] (TBADT) as an efficient HAT photocatalyst to perform the desired C–H abstraction (Scheme 10) [62]. The catalytic reaction required near-ultraviolet light irradiation (Kessil 34 W 390 nm LEDs) and the exclusion of both oxygen and water to the success of the reaction. A variety of cyclic, acyclic, and bicyclic aliphatic systems **16** were arylated in moderate to good yields. This photochemical C–H arylation protocol was also suitable for functionalizing diverse primary and secondary benzylic C–H bonds. The authors proposed a mechanism for this chemo- and regioselective C–H arylation as shown in Figure 6 [62]. The photoexcited decatungstate **6-II** undergoes a HAT process with alkyl substrate **16a** to form singly reduced decatungstate **6-III** and the carbon-centered radical **6-IV**. The active HAT photocatalyst **6-I** is regenerated

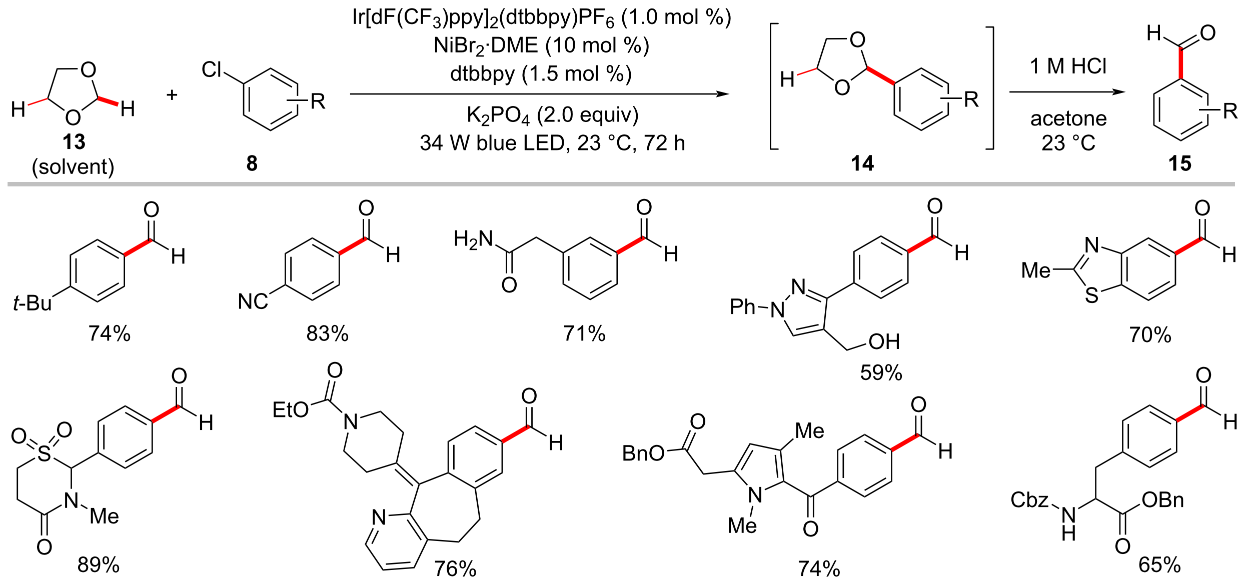
13
(solvent)
8
Ir[dF(CF3)ppy]2(dtbbpy)PF6 (1.0 mol %)
NiBr2·DME (10 mol %)
dtbbpy (1.5 mol %)
K2PO4 (2.0 equiv)
34 W blue LED, 23 °C, 72 h
14
1 M HCl
acetone
23 °C
15
74%
83%
71%
59%
70%
89%
76%
74%
65%

Scheme 9: Formylation of aryl chlorides through redox-neutral 2-functionalization of 1,3-dioxolane (**13**).

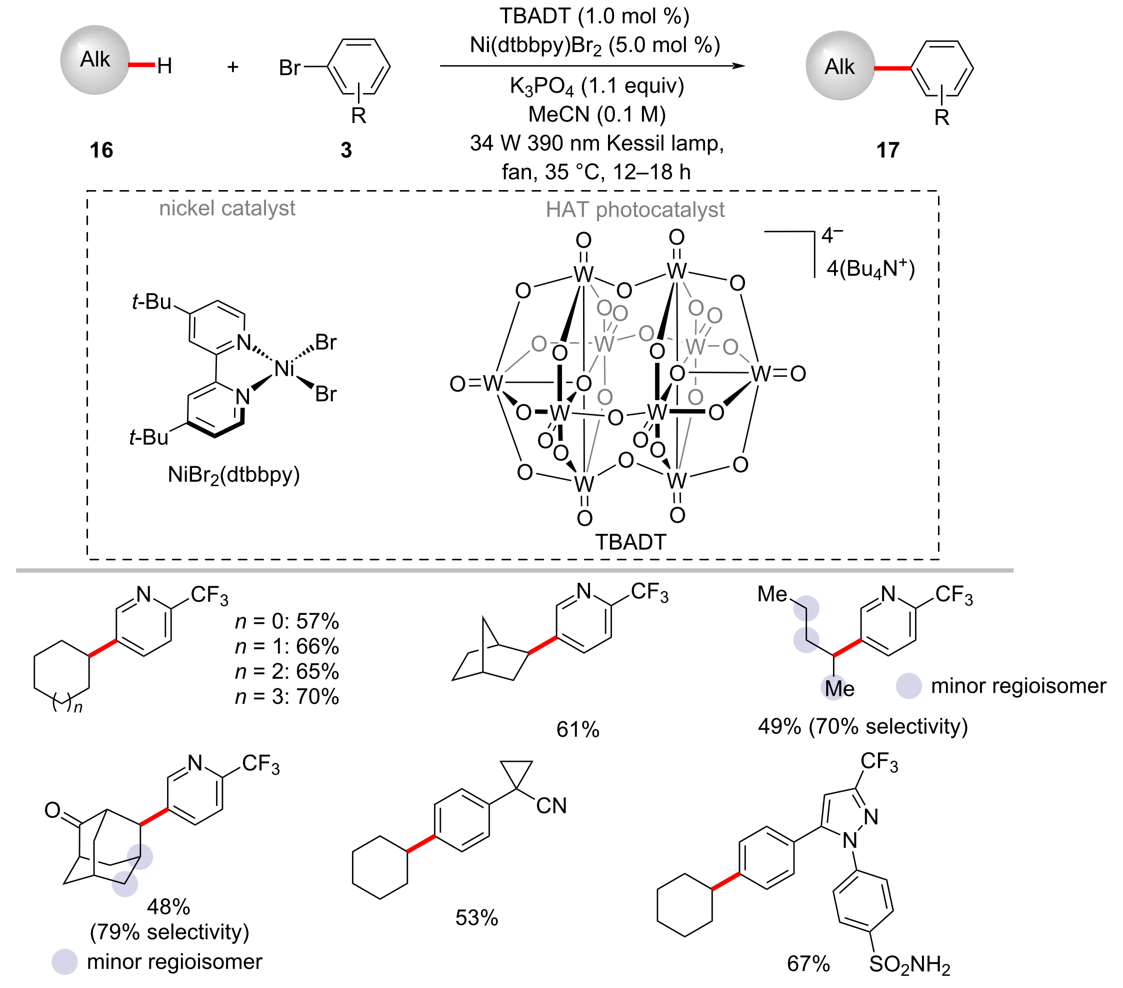
Alk
16
3
TBADT (1.0 mol %)
Ni(dtbbpy)Br2 (5.0 mol %)
K3PO4 (1.1 equiv)
MeCN (0.1 M)
34 W 390 nm Kessil lamp,
fan, 35 °C, 12–18 h
17
nickel catalyst
NiBr2(dtbbpy)
HAT photocatalyst
4−
4(Bu4N+)
TBADT
n = 0: 57%
n = 1: 66%
n = 2: 65%
n = 3: 70%
61%
minor regioisomer
49% (70% selectivity)
48%
(79% selectivity)
minor regioisomer
53%
67%

Scheme 10: Photochemical C(sp^3)–H arylation via a dual polyoxometalate HAT and nickel catalytic manifold.

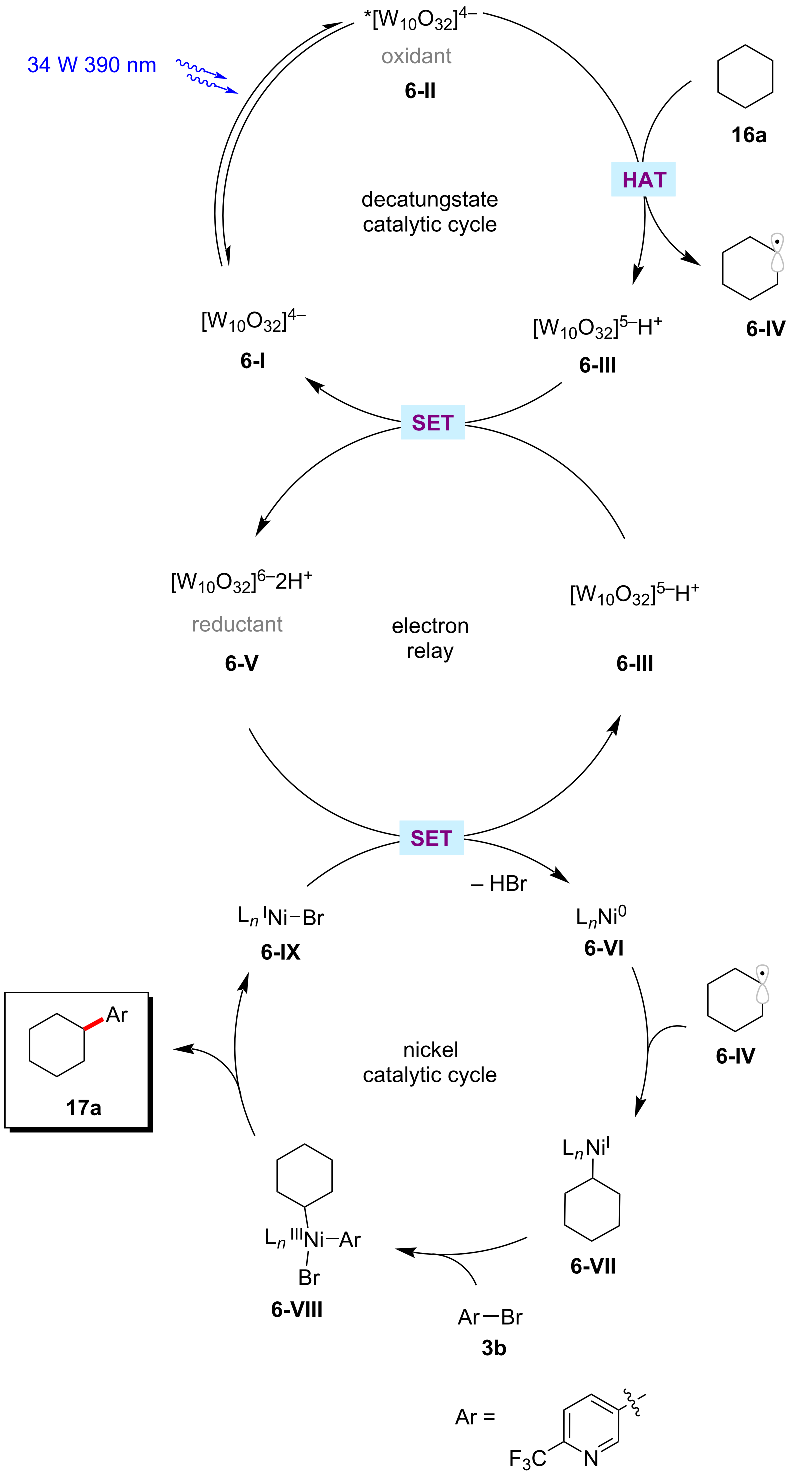

*[W$_{10}$O$_{32}$]$^{4-}$
oxidant
6-II
34 W 390 nm
decatungstate catalytic cycle
HAT
16a
6-IV
[W$_{10}$O$_{32}$]$^{4-}$
6-I
[W$_{10}$O$_{32}$]$^{5-}$H^{+}
6-III
SET
[W$_{10}$O$_{32}$]$^{6-}$2H^{+}
reductant
6-V
electron relay
[W$_{10}$O$_{32}$]$^{5-}$H^{+}
6-III
SET
– HBr
L$_n$^{I}Ni–Br
6-IX
L$_n$Ni^{0}
6-VI
Ar
17a
nickel catalytic cycle
6-IV
L$_n$Ni^{I}
6-VII
L$_n$^{III}Ni–Ar
Br
6-VIII
Ar–Br
3b
Ar =
F$_3$C
N

Figure 6: Proposed mechanism for C(sp^3)–H arylation through dual polyoxometalate HAT and nickel catalytic manifold.

by disproportionation of the singly reduced decatungstate **6-III**. At the same time, a nickel(0) species **6-VI** generated from the nickel(II) pre-catalyst by a SET process, captures the alkyl radical **6-IV** to furnish the nickel(I)–alkyl species **6-VII**. Subsequently, the nickel(I)–alkyl species **6-VII** undergoes oxidative addition into aryl bromide **3b** followed by a reductive elimination to provide the desired cross-coupled product **17a** and nickel(I) bromide complex **6-IX**. The final SET between this nickel(I) bromide species **6-IX** and the doubly reduced polyoxometalate **6-V** regenerates the active nickel(0) catalyst **6-VI** and reduced TBADT **6-I**. The authors also considered an alternative mechanism involving the oxidative addition of the nickel(0) catalyst **6-VI** to aryl bromide **3b**.

The photochemical nickel catalysis is not limited to an α-oxy $C(sp^3)$–H arylation of ethers. MacMillan and co-workers disclosed a method for the selective direct α-arylation of alcohols **18** using photoredox, HAT, and nickel triple catalysts (Scheme 11) [63]. Here, the use of a zinc-based Lewis acid (LA) was found to activate α-hydroxy C–H bonds by forming alkoxide (O–LA) and suppressing the C–O bond formation by inhibiting the formation of a nickel alkoxide species. The authors also claimed that the use of the zinc-based LA also deactivates the other hydridic bonds such as α-amino and α-oxy C–H bonds. Among the tested 24 Lewis acids, the zinc salts ($ZnCl_2$ and $ZnBr_2$) gave the best results. The method's potency was further shown by the synthesis of the drug fluoxetine (**21**) in three steps (Scheme 12) [63]. The transformation was proposed to proceed via a similar mechanism to the one shown in Figure 2.

In 2018, Huang and Rueping devised reaction conditions for the photochemical nickel-catalyzed arylation of allylic $C(sp^3)$–H bonds with aryl bromides **3** in the presence of the organic

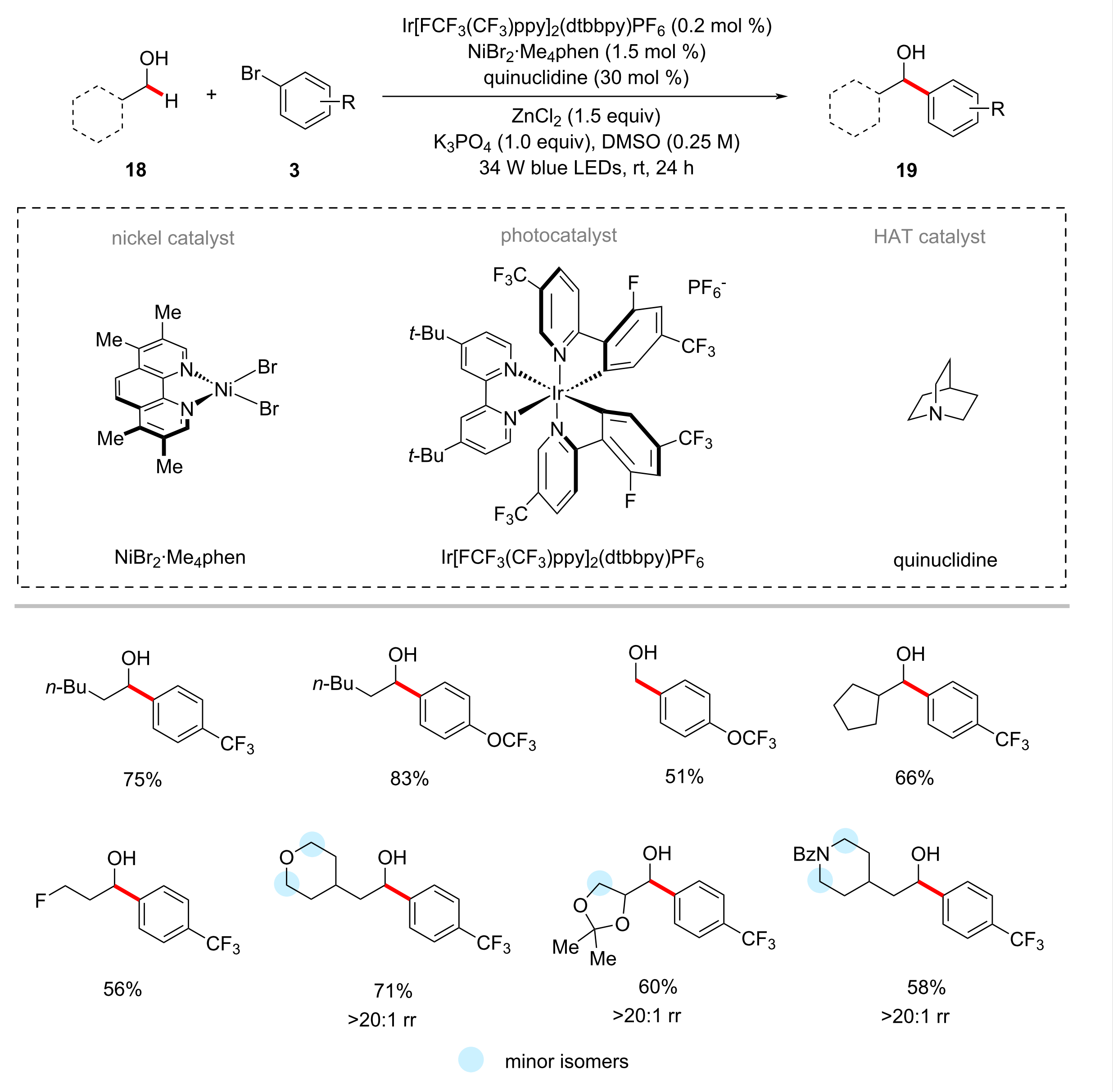
OH
H
Br
R
18
3
Ir[FCF3(CF3)ppy]2(dtbbpy)PF6 (0.2 mol %)
NiBr2·Me4phen (1.5 mol %)
quinuclidine (30 mol %)
ZnCl2 (1.5 equiv)
K3PO4 (1.0 equiv), DMSO (0.25 M)
34 W blue LEDs, rt, 24 h
19
nickel catalyst
photocatalyst
HAT catalyst
Me
Br
Ni
N
PF6-
F3C
F
CF3
t-Bu
Ir
NiBr2·Me4phen
Ir[FCF3(CF3)ppy]2(dtbbpy)PF6
quinuclidine
n-Bu
CF3
75%
OCF3
83%
51%
66%
56%
O
71%
>20:1 rr
Me
60%
>20:1 rr
BzN
58%
>20:1 rr
minor isomers

Scheme 11: Photochemical nickel-catalyzed α-hydroxy C–H arylation.

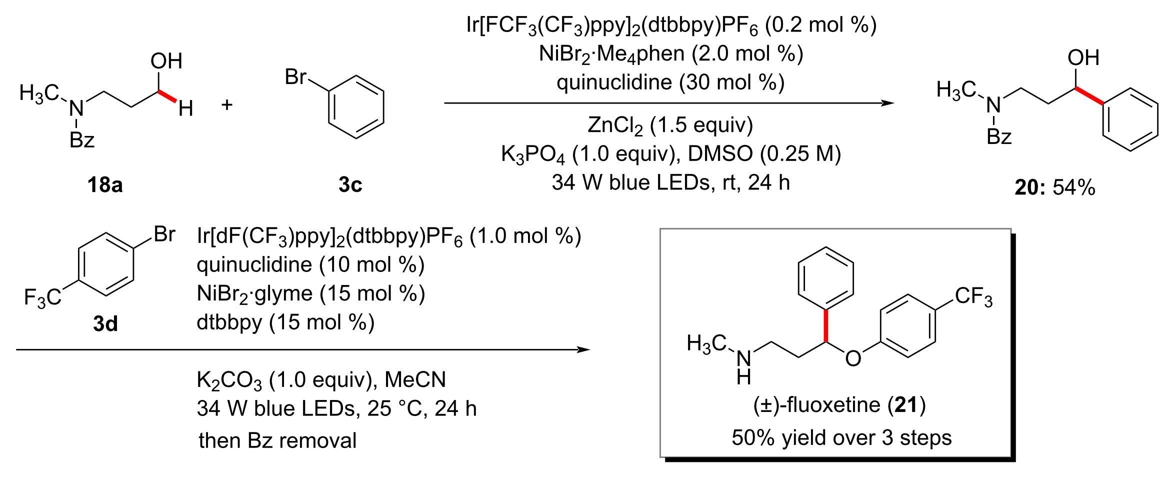
Ir[FCF$_3$(CF$_3$)ppy]$_2$(dtbbpy)PF$_6$ (0.2 mol %)
NiBr$_2$·Me$_4$phen (2.0 mol %)
quinuclidine (30 mol %)
ZnCl$_2$ (1.5 equiv)
K$_3$PO$_4$ (1.0 equiv), DMSO (0.25 M)
34 W blue LEDs, rt, 24 h
18a
3c
20: 54%
3d
Ir[dF(CF$_3$)ppy]$_2$(dtbbpy)PF$_6$ (1.0 mol %)
quinuclidine (10 mol %)
NiBr$_2$·glyme (15 mol %)
dtbbpy (15 mol %)
K$_2$CO$_3$ (1.0 equiv), MeCN
34 W blue LEDs, 25 °C, 24 h
then Bz removal
(±)-fluoxetine (21)
50% yield over 3 steps

Scheme 12: Photochemical synthesis of fluoxetine (**21**).

photocatalyst 9-mesityl-10-methylacridinium perchlorate ([Acr-Mes]$^+$ClO$_4^-$) [64]. The reaction was conveniently achieved at room temperature under blue light irradiation. Moreover, as shown in Scheme 13, electron-deficient aryl bromides were efficient in forming the desired products **23** in optimal yields. In contrast, only trace amounts of cross-coupled products were observed when unsubstituted and electron-rich aryl bromides were used.

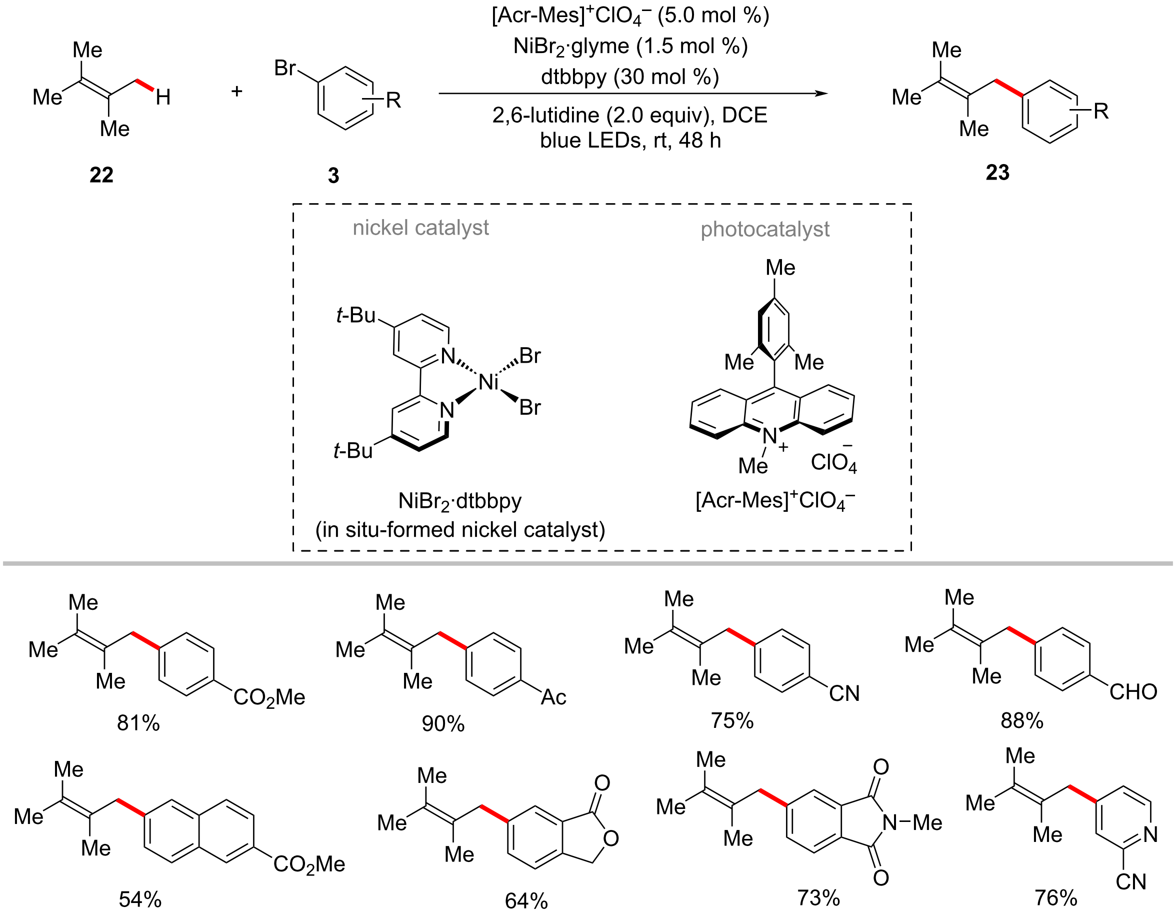
[Acr-Mes]$^+$ClO$_4^-$ (5.0 mol %)
NiBr$_2$·glyme (1.5 mol %)
dtbbpy (30 mol %)
2,6-lutidine (2.0 equiv), DCE
blue LEDs, rt, 48 h
22
3
23
nickel catalyst
photocatalyst
NiBr$_2$·dtbbpy
(in situ-formed nickel catalyst)
[Acr-Mes]$^+$ClO$_4^-$
81%
90%
75%
88%
54%
64%
73%
76%

Scheme 13: Photochemical nickel-catalyzed allylic C(sp^3)–H arylation with aryl bromides.

Based on their experimental results, the authors proposed that a triplet–triplet energy transfer occurs between the nickel(II)–aryl species **7-IV** and the excited acridinium photocatalyst *Mes-Acr-Me$^+$ **7-II** (Figure 7) [64]. Homolysis of the excited nickel(II) species **7-V** results in the formation of a bromine radical, which then readily abstracts the allylic C(sp^3)–H to give the allylic radical species. Thus, the generated allylic radical species rebound to nickel complex and followed by reductive elimination delivers the desired product **23** and the active nickel(0) species **7-III**.

The triplet ketone sensitizers can also be employed in the HAT and SET processes [65]. Thus, Martin and co-workers presented an example of the arylation of α-oxy C(sp^3)–H bonds of ethers **9** with aryl bromides **3** employing synergy between the nickel catalysis and ketone HAT photocatalyst [66]. Here, the catalytic system composed of the ketone photocatalyst (4-methoxyphenyl)(4-(trifluoromethyl)phenyl)methanone (**24**), Ni(acac)$_2$, 5,5'-dimethyl-2,2'-bipyridine (5,5'-diMe-bpy), Na_2CO_3 under visible light (CFL) irradiation was found to be optimal to provide the desired arylated products **17** (Scheme 14). Both electron-deficient and electron-rich aryl bromides proved viable substrates and afforded the products **10/17** in good yields. In addition to a variety of cyclic and acyclic ethers, amines, benzylic and alkane C(sp^3)–H bonds were also arylated under similar reaction conditions with moderate to good yields. Based on their detailed mechanistic studies, the authors proposed a possible catalytic cycle involving a C–H cleavage via a HAT process between the triplet excited ketone photocatalyst **24** and the C(sp^3)–H substrates (Figure 8) [66]. Thus, the formed carbon-centered radical species **8-III** combines with the nickel(II)–aryl intermediate **8-V** to form nickel(III) species **8-VI,** which readily undergoes a reductive elimination to deliver the cross-coupled product **10** and nickel(I) species **8-VII**. The SET process between the ketyl radical **8-II** and the nickel(I) species **8-VII** regenerates the active nickel(0) catalytic species **8-IV** and the ketone photocatalyst **24**.

In a related process, Rueping employed 4,4'-dichlorobenzophenone (**27**) as the HAT photocatalyst along with a nickel catalyst for the direct arylation of benzylic C–H bonds with aryl bromides **3** under visible light irradiation at 35 °C (Scheme 15) [67]. Here, the diaryl ketone photocatalyst played a dual role as hydrogen-atom-transfer (HAT) and electron-transfer agent. This C–H arylation protocol provided the diarylmethane derivatives **26** in moderate to good yields.

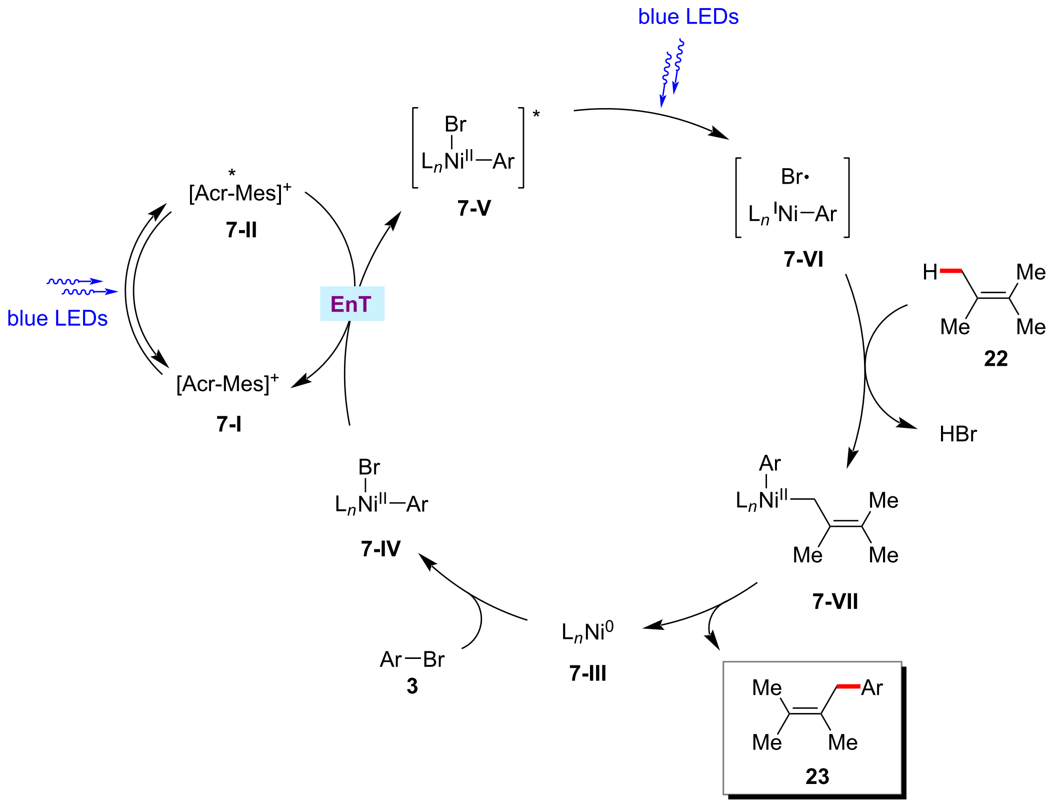

Figure 7: Proposed mechanism for the photochemical nickel-catalyzed allylic C(sp^3)–H arylation with aryl bromides.

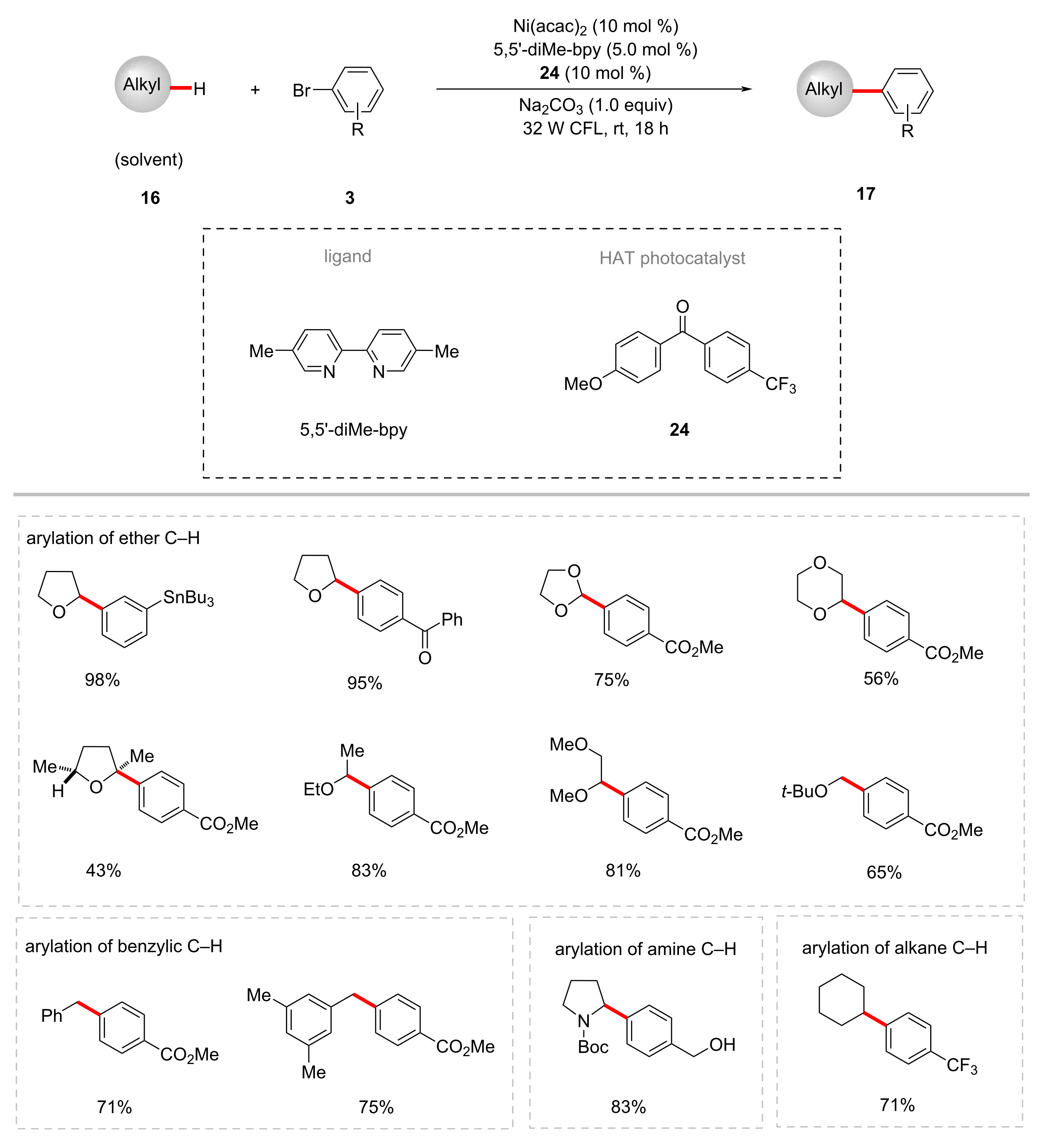
Alkyl–H
+
Br
R
Ni(acac)$_2$ (10 mol %)
5,5'-diMe-bpy (5.0 mol %)
24 (10 mol %)
Na$_2$CO$_3$ (1.0 equiv)
32 W CFL, rt, 18 h
Alkyl
R
(solvent)
16
3
17
ligand
HAT photocatalyst
Me
N
N
Me
5,5'-diMe-bpy
O
MeO
CF$_3$
24
arylation of ether C–H
SnBu$_3$
98%
Ph
95%
CO$_2$Me
75%
CO$_2$Me
56%
Me
Me
H
CO$_2$Me
43%
Me
EtO
CO$_2$Me
83%
MeO
MeO
CO$_2$Me
81%
t-BuO
CO$_2$Me
65%
arylation of benzylic C–H
Ph
CO$_2$Me
71%
Me
Me
CO$_2$Me
75%
arylation of amine C–H
N
Boc
OH
83%
arylation of alkane C–H
CF$_3$
71%

Scheme 14: Photochemical C(sp^3)–H arylation by the synergy of ketone HAT catalysis and nickel catalysis.

In 2019, the Hashmi group discovered the synergistic combination of nickel catalysis and benzaldehyde for the arylation of C(sp^3)–H bonds adjacent to nitrogen or sulfur in amides **6** and thioethers **28**, respectively, under UVA light irradiation [68]. As shown in Scheme 16, both primary and secondary C(sp^3)–H bonds of amides were arylated with moderate to good yields. When both primary and secondary C(sp^3)–H bonds are present in the substrate, regioselectivity favors the secondary position. The catalytic reaction conditions were compatible with the C(sp^3)–H arylation of tetrahydrothiophene (**28a**) as well [68].

The enantioselective C–H functionalization is a valuable method for synthesizing useful organic compounds from simple alkane starting materials [51,69,70]. Recently, Lu and

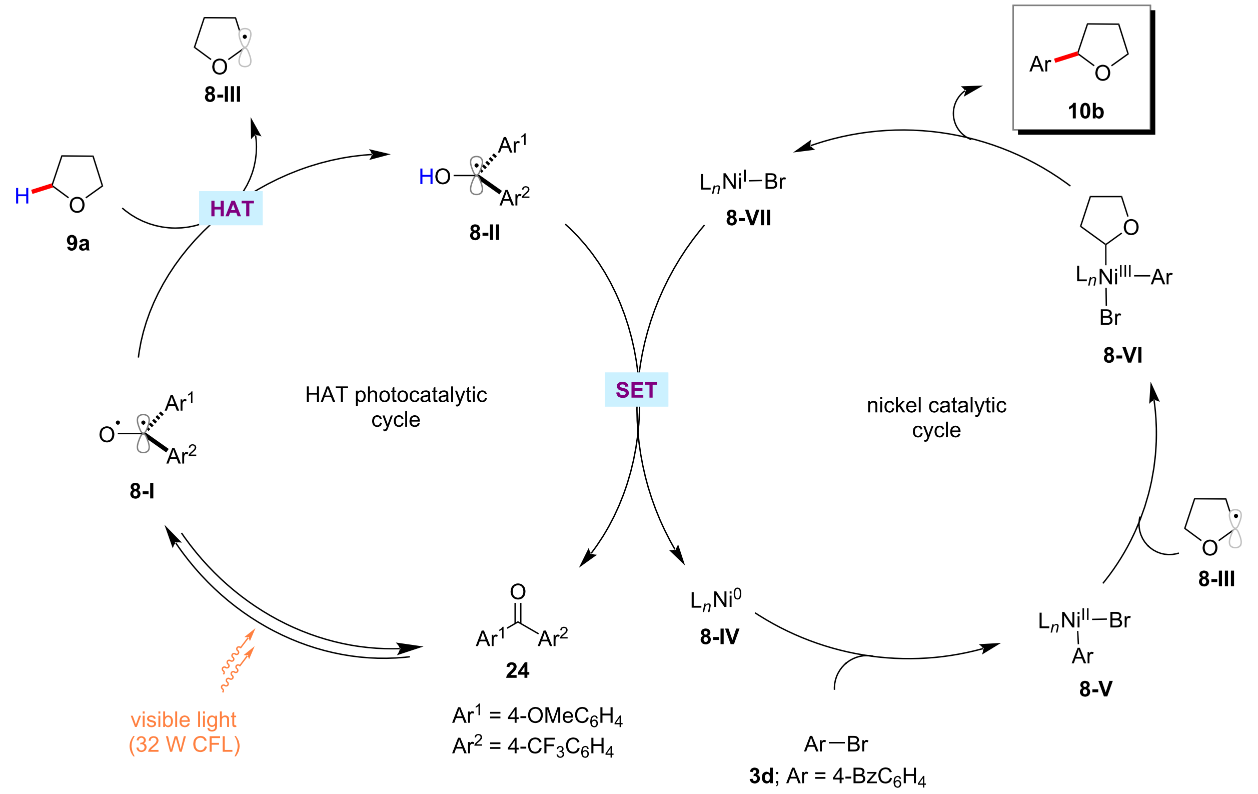
8-III
H
9a
HAT
HO
Ar1
Ar2
8-II
LnNiI–Br
8-VII
Ar
10b
LnNiIII–Ar
Br
8-VI
HAT photocatalytic cycle
SET
nickel catalytic cycle
O•
Ar1
Ar2
8-I
24
Ar1 = 4-OMeC6H4
Ar2 = 4-CF3C6H4
LnNi0
8-IV
LnNiII–Br
Ar
8-V
8-III
Ar–Br
3d; Ar = 4-BzC6H4
visible light
(32 W CFL)

Figure 8: Proposed mechanism for photochemical C(sp^3)–H arylation by the synergy of ketone HAT catalysis and nickel catalysis.

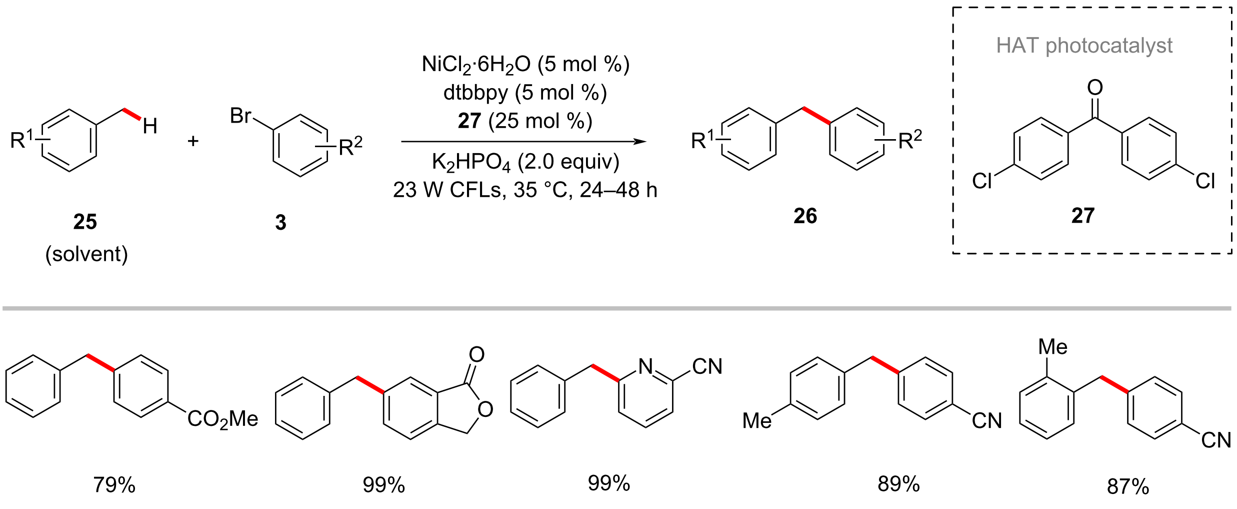
R1
H
25
(solvent)
+
Br
R2
3
NiCl2·6H2O (5 mol %)
dtbbpy (5 mol %)
27 (25 mol %)
K2HPO4 (2.0 equiv)
23 W CFLs, 35 °C, 24–48 h
R1
R2
26
HAT photocatalyst
O
Cl
Cl
27
CO2Me
79%
O
O
99%
N
CN
99%
Me
CN
89%
Me
CN
87%

Scheme 15: Benzophenone- and nickel-catalyzed photoredox benzylic C–H arylation.

co-workers reported an enantioselective benzylic C–H arylation method for synthesizing 1,1-diarylalkanes **26** via a photoredox and nickel dual catalysis (Scheme 17) [71]. The reaction relied on the chiral biimidazoline ligand **30**, which gave the best results among various tested chiral bioxazolines and chiral biimidazoline ligands. Notably, the aryl substituent at the imidazoline nitrogen of the ligands significantly affected the product yields and enantioselectivities. A wide range of aryl

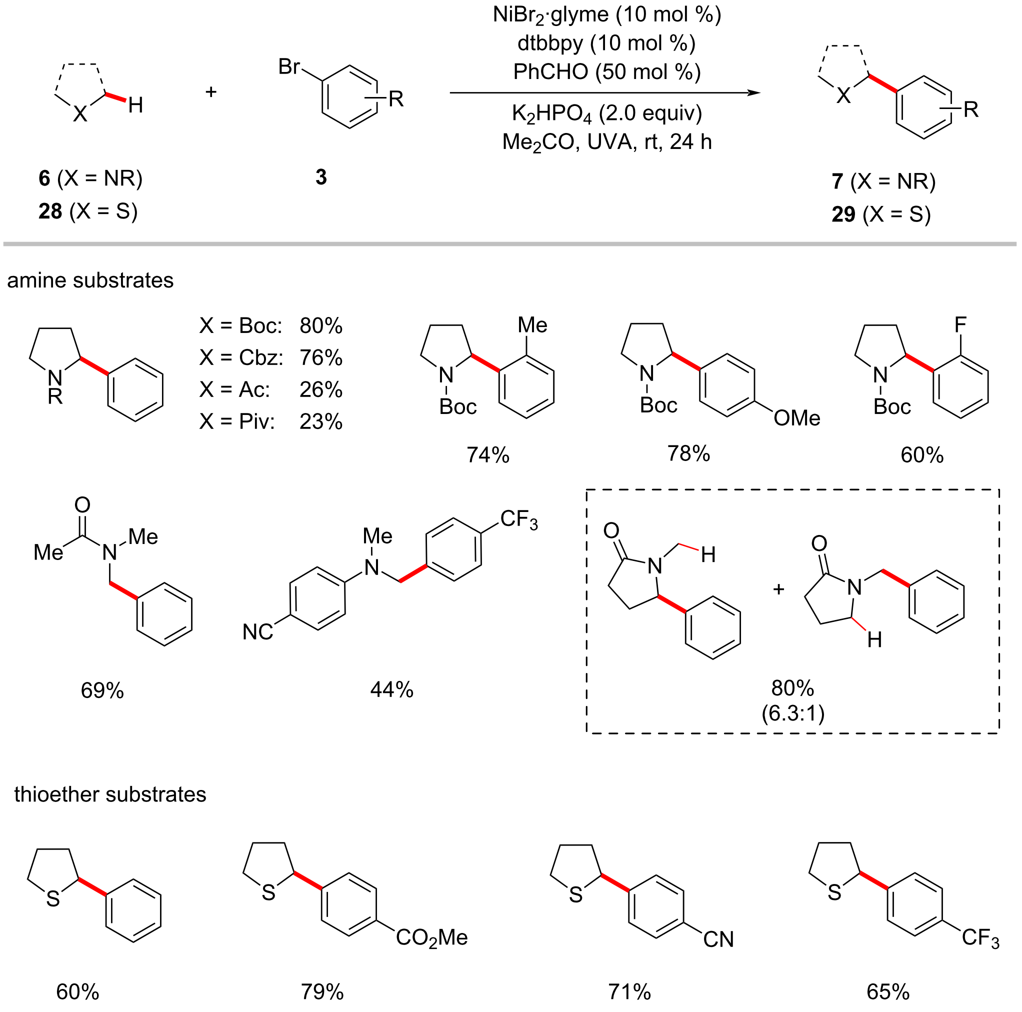

Scheme 16: Benzaldehyde- and nickel-catalyzed photoredox C(sp^3)–H arylation.

bromides **3** were tested with alkylbenzenes **25** under ambient reaction conditions and afforded the desired products **26** in moderate yields and good enantioselectivities. Based on their control experiments and mechanistic studies, it was postulated that a bromine radical might be involved in the HAT process of benzylic C–H bond using DMBP as co-catalyst to deliver benzylic radical species **9-IX** (Figure 9) [71]. The benzylic radical **9-IX** intercepted with the nickel catalytic cycle to result in the desired products **26**.

The photoredox nickel-catalyzed arylation of α-amino C(sp^3)–H bonds are not limited to tertiary amines/amides. Secondary amides could also be arylated, as reported by Montgomery, Martin and co-workers [72]. The authors discovered that the combination of Ir[dF(CF$_3$)ppy]$_2$(dtbbpy)PF$_6$, NiBr$_2$·diglyme, 5,5'-dimethyl-2,2'-bipyridine (5,5'-diMe-bpy), and K$_3$PO$_4$ in dioxane under irradiation of blue LEDs at ambient temperature afforded the desired α-arylation products **32** from secondary amides **31** and (hetero)aryl bromides **3** (Scheme 18) [72]. The method showed a broad substrate scope for both amides and aryl bromides. The authors also realized the enantioselective variant of this protocol using the chiral iPrBiOx ligand under slightly modified reaction conditions (Scheme 19) [72].

Recently, Chu achieved the selective assembly of vinyl and aryl functionalities onto saturated cyclic hydrocarbons via a photoredox nickel-catalyzed sequential C–O decarboxylative vinylation/arylation of cyclic oxalates **33** with terminal alkyne **34** and aryl bromides **3** (Scheme 20) [73]. As to the scope, aryl bromides **3** containing various electron-withdrawing substituents displayed better efficiency over the electron-rich aryl bromides. The authors proposed a plausible catalytic cycle to account for the mode of action of this cascade arylation protocol (Figure 10) [73]. In the photocatalytic cycle, the SET event be-

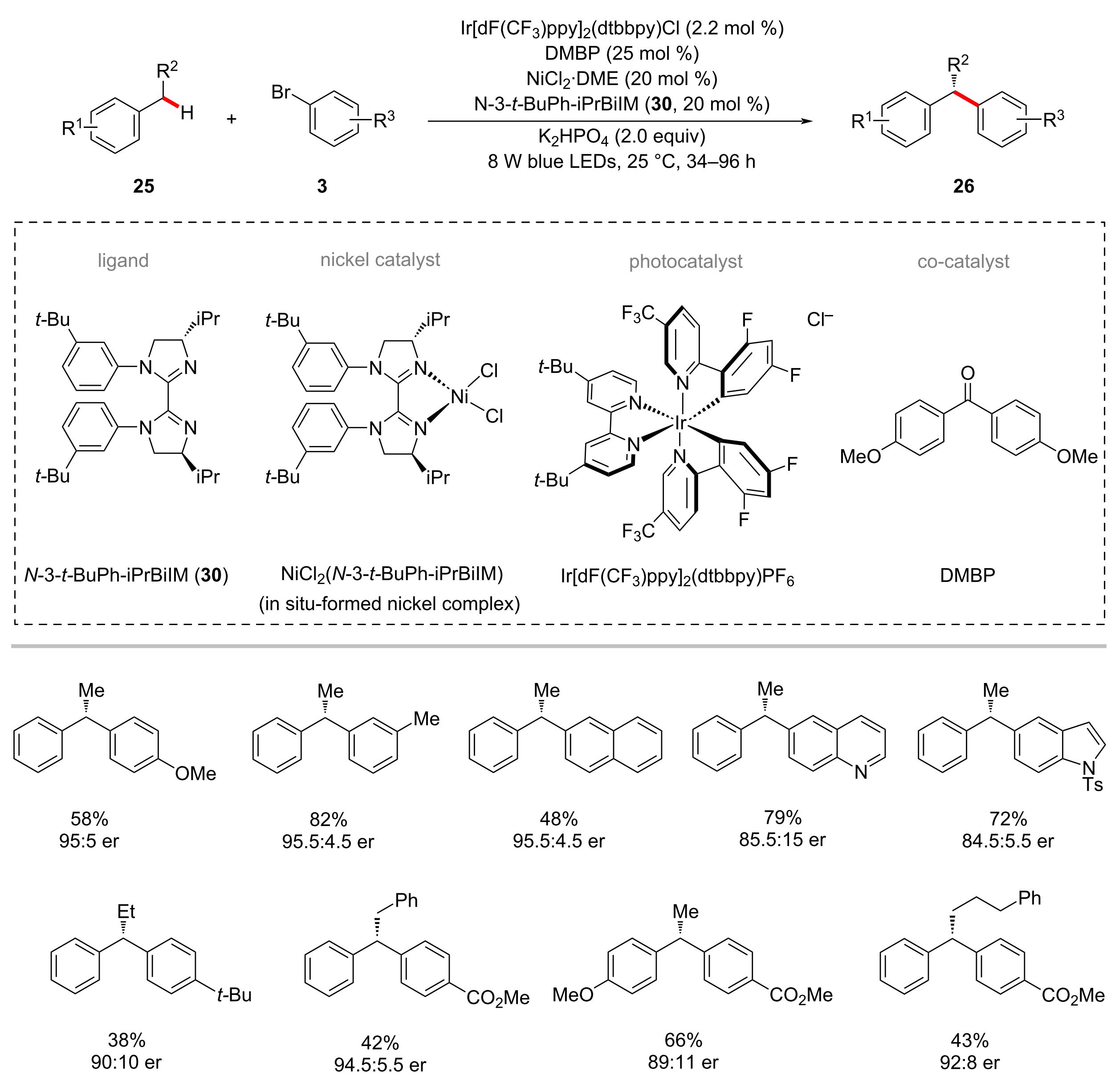

Ir[dF(CF$_3$)ppy]$_2$(dtbbpy)Cl (2.2 mol %)
DMBP (25 mol %)
NiCl$_2$·DME (20 mol %)
N-3-*t*-BuPh-iPrBiIM (**30**, 20 mol %)
K$_2$HPO$_4$ (2.0 equiv)
8 W blue LEDs, 25 °C, 34–96 h
R^1
R^2
H
Br
R^3
25
3
26
ligand
nickel catalyst
photocatalyst
co-catalyst
t-Bu
iPr
N
Ni
Cl
Ir
F$_3$C
F
Cl$^-$
O
MeO
OMe
N-3-*t*-BuPh-iPrBiIM (**30**)
NiCl$_2$(*N*-3-*t*-BuPh-iPrBiIM)
(in situ-formed nickel complex)
Ir[dF(CF$_3$)ppy]$_2$(dtbbpy)PF$_6$
DMBP
Me
Ts
Et
Ph
CO$_2$Me
58%
95:5 er
82%
95.5:4.5 er
48%
95.5:4.5 er
79%
85.5:15 er
72%
84.5:5.5 er
38%
90:10 er
42%
94.5:5.5 er
66%
89:11 er
43%
92:8 er

Scheme 17: Photoredox and nickel-catalyzed enantioselective benzylic C–H arylation.

tween the photoexcited iridium catalyst **10-II** and the substrate oxalate **33** generates a tertiary carbon-centered radical **10-IV** by decarboxylation and the reduced iridium(II) photocatalyst **10-III**. The active iridium(III) photocatalyst **10-I** is regenerated by a SET process between **10-III** and the nickel(I) species **10-X**. The addition of the tertiary radical **10-IV** to the terminal alkyne **34** followed by an intramolecular 1,5-HAT results in a nucleophilic secondary alkyl radical species **10-VI**. Subsequently, the alkyl radical **10-VI** intercepts nickel(0) complex **10-VII** to form a nickel(I)–alkyl intermediate **10-VIII**, which then undergoes oxidative addition to aryl bromide **3** followed by reductive elimination furnishing the desired product **35** and the nickel(I) species **10-X**. The authors noted that the oxidative addition of the nickel(0) species **10-VII** to aryl bromide **3** and subsequent steps to produce nickel(III) intermediate **10-IX** could not be ruled out.

The König group discovered that the arylation of α-amino C(sp^3)–H bonds could be realized with aryl halides using mesoporous graphitic carbon nitride (mpg-CN) [74-76] as a heterogeneous organic semiconductor photocatalyst in combination with nickel catalysis [77]. Here, the catalytic system consisting of NiBr$_2$·glyme, 2,2′-bipyridine, 2,6-lutidine, and mpg-CN under blue light irradiation at ambient temperature was found to

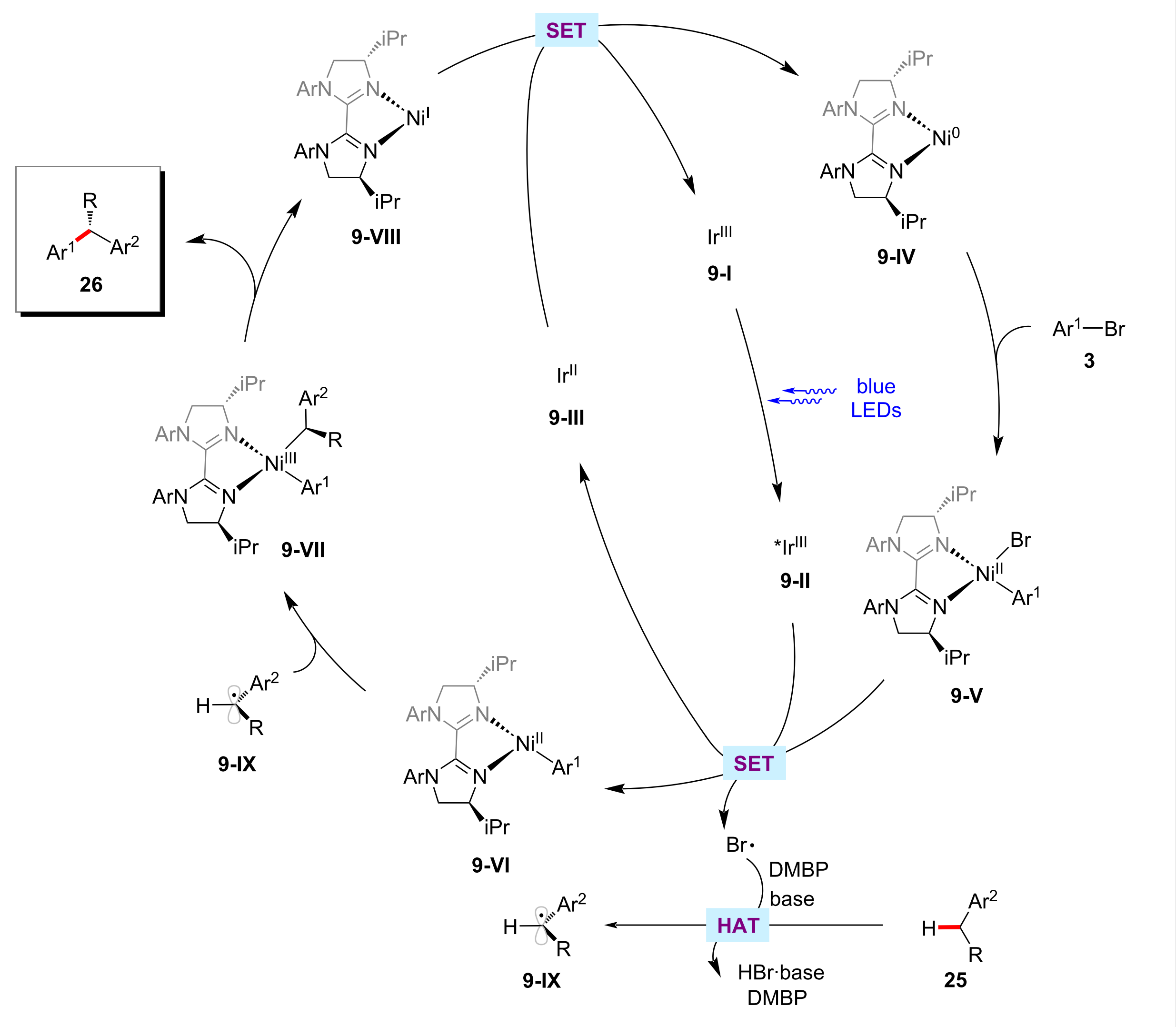
SET
9-VIII
26
9-I
9-IV
Ar1—Br
3
blue LEDs
9-III
9-VII
9-II
9-V
9-IX
9-VI
SET
Br•
DMBP
base
HAT
HBr·base
DMBP
9-IX
25

Figure 9: Proposed mechanism for the photoredox and nickel-catalyzed enantioselective benzylic C–H arylation.

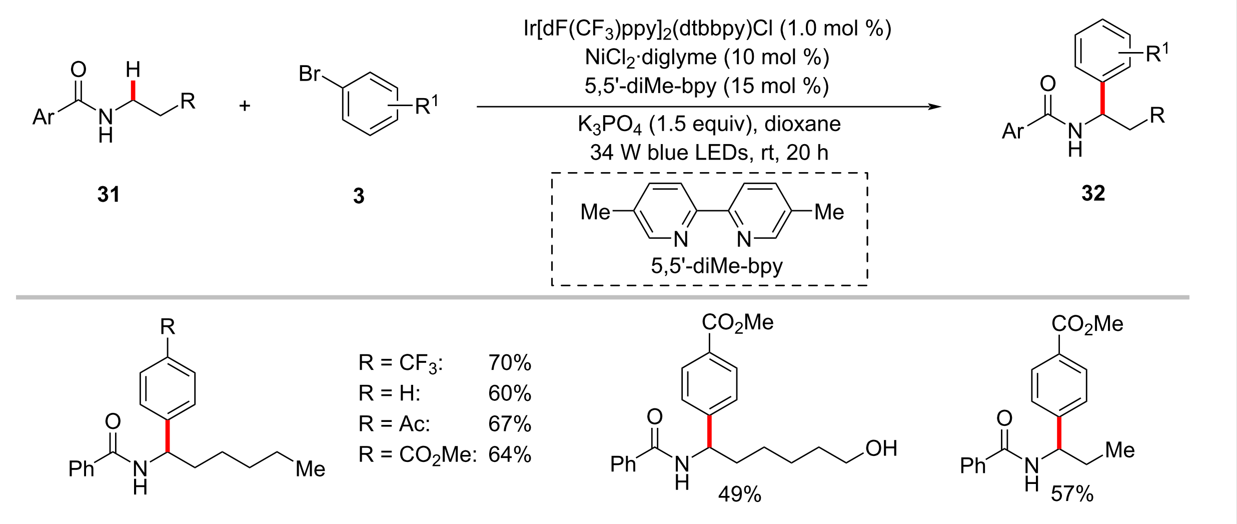
31
3
Ir[dF(CF3)ppy]2(dtbbpy)Cl (1.0 mol %)
NiCl2·diglyme (10 mol %)
5,5'-diMe-bpy (15 mol %)
K3PO4 (1.5 equiv), dioxane
34 W blue LEDs, rt, 20 h
5,5'-diMe-bpy
32
R = CF3: 70%
R = H: 60%
R = Ac: 67%
R = CO2Me: 64%
49%
57%

Scheme 18: Photoredox nickel-catalyzed α-(sp^3)–H arylation of secondary benzamides with aryl bromides.

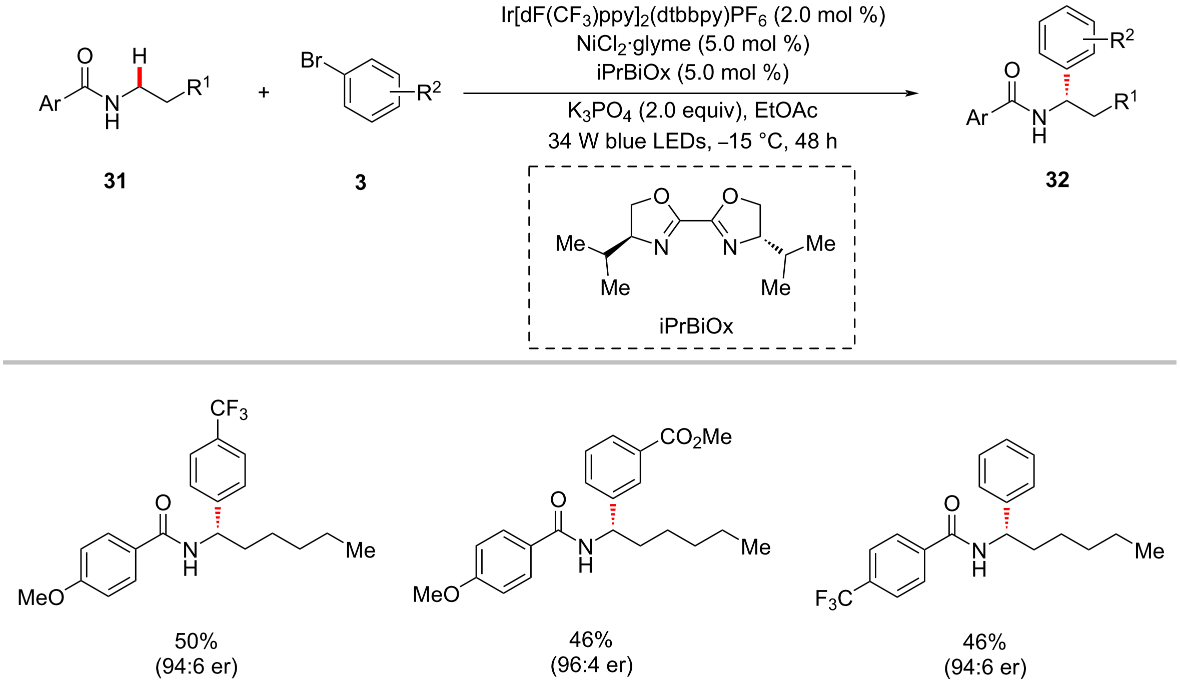
Ir[dF(CF3)ppy]2(dtbbpy)PF6 (2.0 mol %)
NiCl2·glyme (5.0 mol %)
iPrBiOx (5.0 mol %)
K3PO4 (2.0 equiv), EtOAc
34 W blue LEDs, –15 °C, 48 h
31
3
32
iPrBiOx
50%
(94:6 er)
46%
(96:4 er)
46%
(94:6 er)

Scheme 19: Enantioselective sp^3 α-arylation of benzamides.

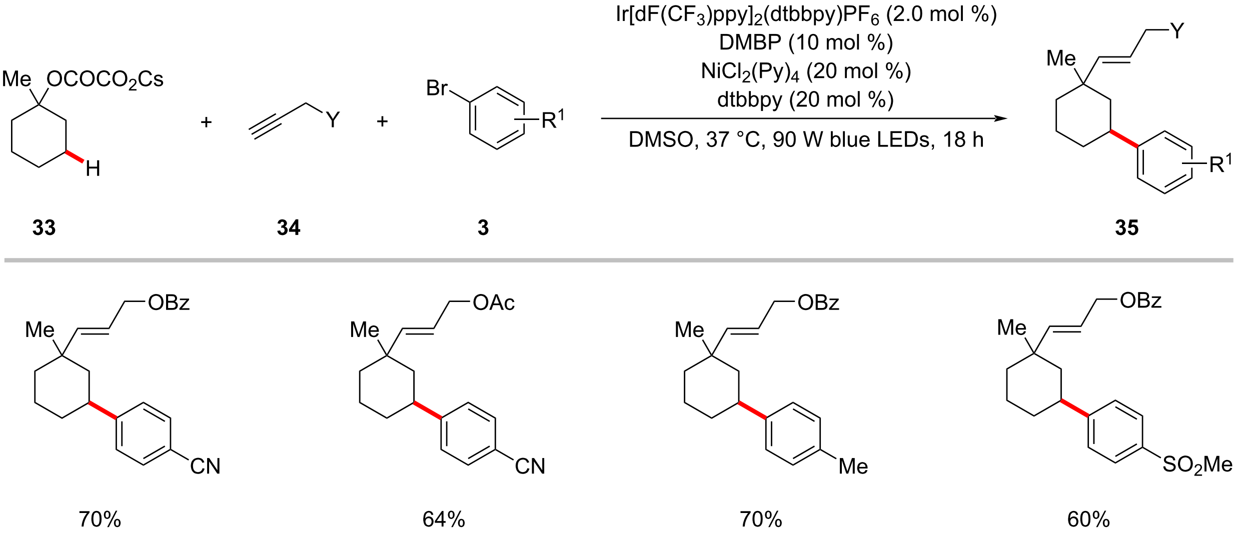
Ir[dF(CF3)ppy]2(dtbbpy)PF6 (2.0 mol %)
DMBP (10 mol %)
NiCl2(Py)4 (20 mol %)
dtbbpy (20 mol %)
DMSO, 37 °C, 90 W blue LEDs, 18 h
33
34
3
35
70%
64%
70%
60%

Scheme 20: Nickel-catalyzed decarboxylative vinylation/C–H arylation of cyclic oxalates.

be optimal to furnish the desired cross-coupled products **37** in satisfactory yields. Furthermore, the method proved applicable to the late-stage diversification of bioactive molecules, pharmaceuticals, and agrochemicals as aryl coupling partners (Scheme 21) [77]. The authors proposed a catalytic cycle that involves an energy-transfer pathway generating an electronically excited nickel complex as a key reactive intermediate (Figure 11).

Photochemical nickel catalysis was used to synthesize 1,1-diarylalkanes **39** from unactivated alkyl bromides **38** and aryl bromides **3** through a reductive migratory cross-coupling

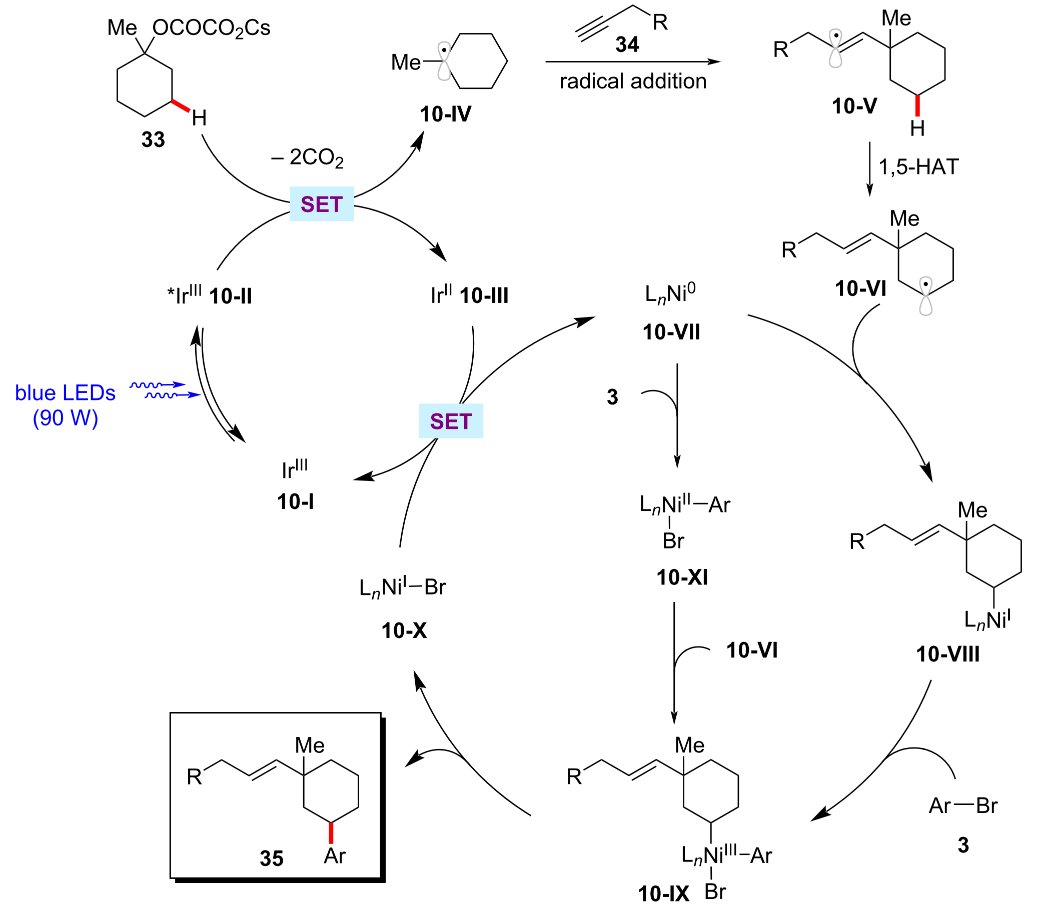
Me OCOCO2Cs
H
33
– 2CO2
SET
Me
10-IV
34
R
radical addition
Me
R
10-V
H
1,5-HAT
Me
R
10-VI
*IrIII 10-II
IrII 10-III
LnNi0
10-VII
blue LEDs
(90 W)
SET
3
IrIII
10-I
LnNiII–Ar
Br
10-XI
Me
R
LnNiI
10-VIII
LnNiI–Br
10-X
10-VI
Me
R
35
Ar
Me
R
LnNiIII–Ar
10-IX
Br
Ar–Br
3

Figure 10: Proposed mechanism for the nickel-catalyzed decarboxylative vinylation/C–H arylation of cyclic oxalates.

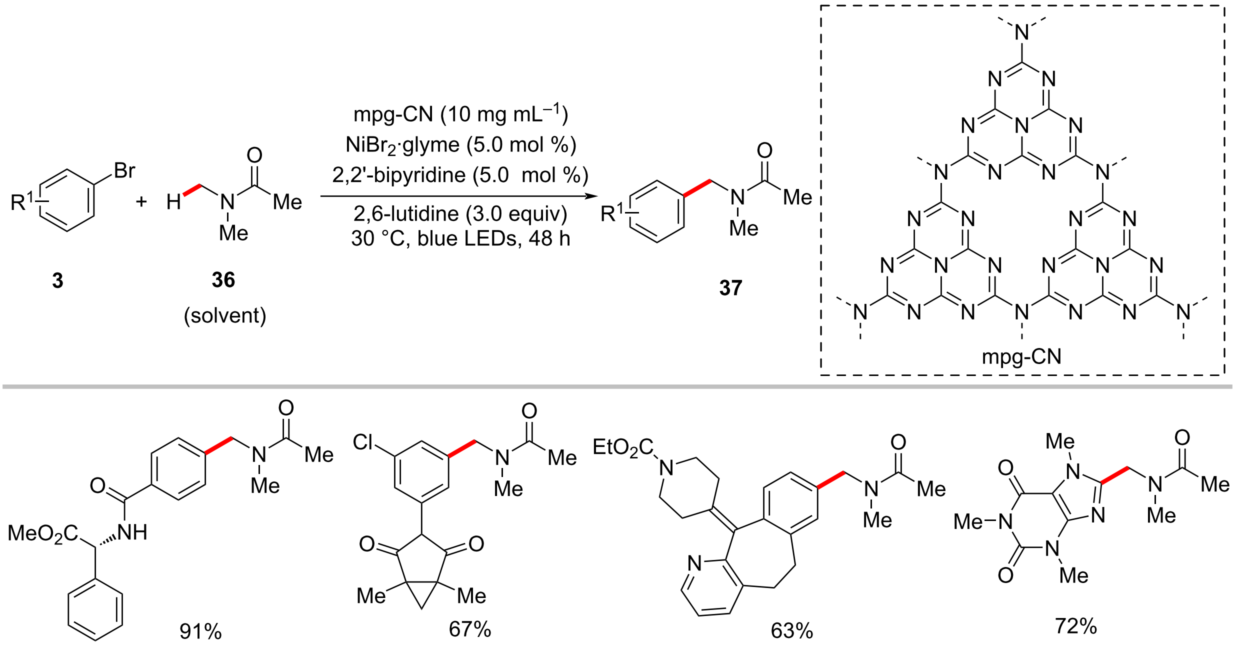
R1
Br
+
H
N
O
Me
Me
3
36
(solvent)
mpg-CN (10 mg mL−1)
NiBr2·glyme (5.0 mol %)
2,2'-bipyridine (5.0 mol %)
2,6-lutidine (3.0 equiv)
30 °C, blue LEDs, 48 h
R1
N
O
Me
Me
37
mpg-CN
O
MeO2C
NH
N
O
Me
Me
91%
Cl
N
O
Me
Me
O
O
Me
Me
67%
EtO2C
N
N
N
O
Me
Me
63%
Me
N
O
N
N
Me–N
N
O
Me
N
O
Me
Me
72%

Scheme 21: C(sp^3)–H arylation of bioactive molecules using mpg-CN photocatalysis and nickel catalysis.

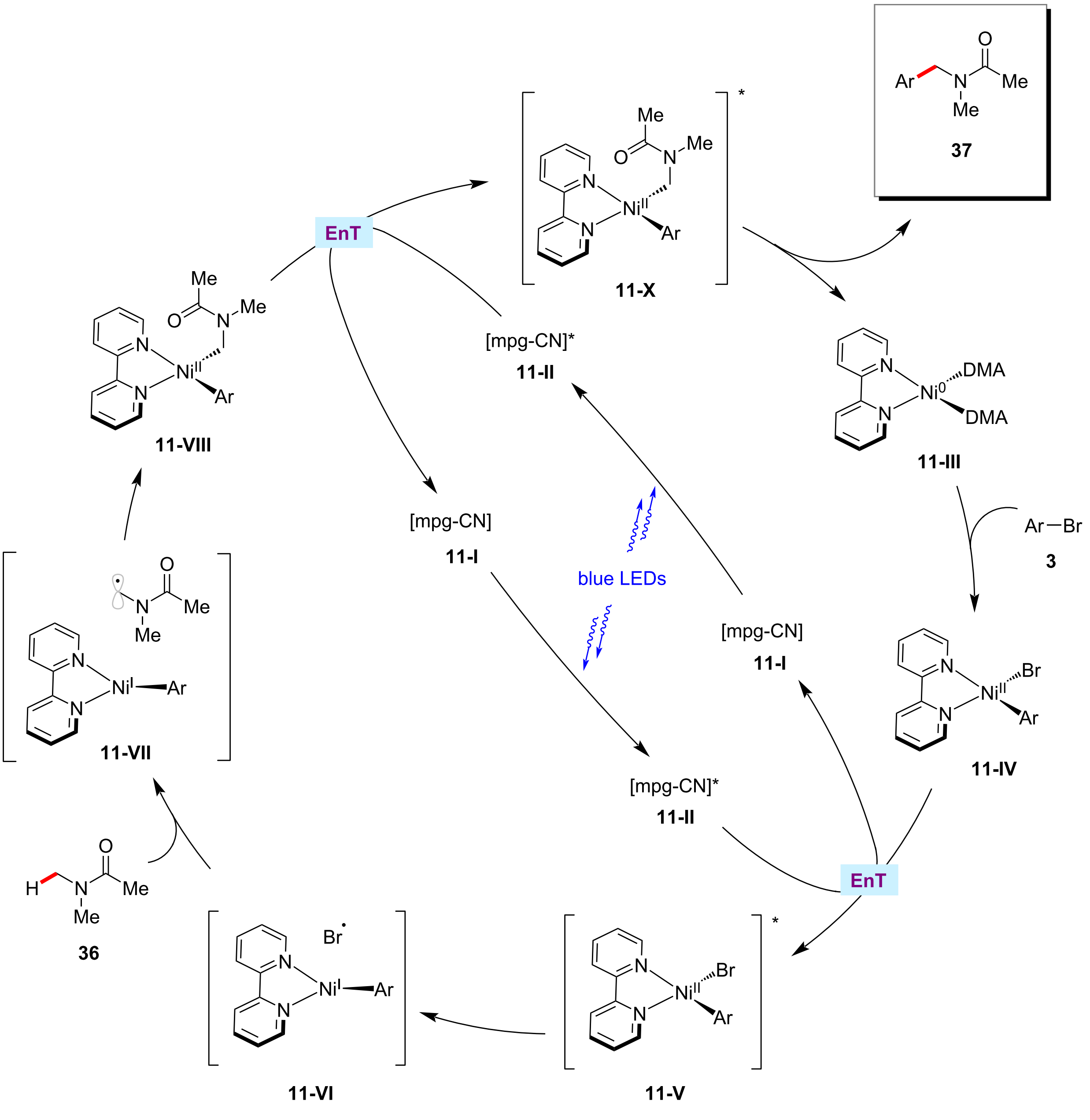

Figure 11: Proposed mechanism for the mpg-CN/nickel photocatalytic C(sp^3)–H arylation.

strategy (Scheme 22) [78]. The use of an iridium-based photocatalyst along with stoichiometric diisopropylamine as the terminal reductant were found to be beneficial to obtain the desired products **39**. Both primary and secondary alkyl bromides **38** proved viable substrates to give the benzylic arylation products **39** with good regioselectivities. The authors proposed a tentative visible-light-driven radical chain mechanistic profile with nickel chain-walking as a key step to rationalize the C–H arylation process [78].

Alkylation

The direct functionalization of C–H bonds in alkyl groups is a fundamental but challenging operation in organic synthesis. While significant advances had been accomplished with (hetero)aromatic C(sp^2)–H alkylations [79-81], examples for C(sp^3)–C(sp^3) couplings through C–H activation are scarce [82-84]. In this context, a synergistic combination of photoredox catalysis and nickel catalysis is also often employed to C(sp^3)–H alkylation transformations. For example, in 2017, MacMillan

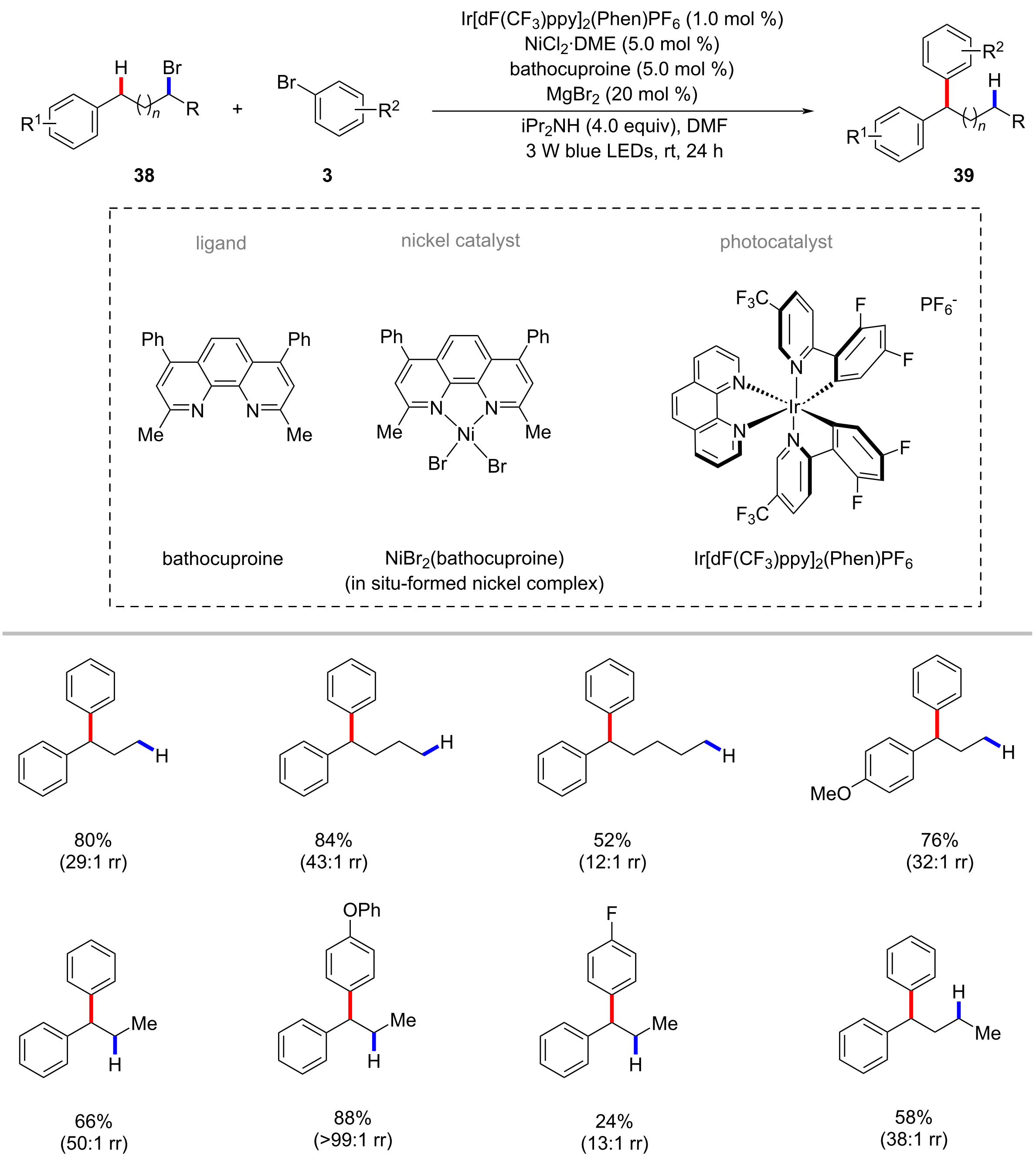
38
3
39
Ir[dF(CF3)ppy]2(Phen)PF6 (1.0 mol %)
NiCl2·DME (5.0 mol %)
bathocuproine (5.0 mol %)
MgBr2 (20 mol %)
iPr2NH (4.0 equiv), DMF
3 W blue LEDs, rt, 24 h
ligand
nickel catalyst
photocatalyst
bathocuproine
NiBr2(bathocuproine)
(in situ-formed nickel complex)
Ir[dF(CF3)ppy]2(Phen)PF6
80% (29:1 rr)
84% (43:1 rr)
52% (12:1 rr)
76% (32:1 rr)
66% (50:1 rr)
88% (>99:1 rr)
24% (13:1 rr)
58% (38:1 rr)

Scheme 22: Nickel-catalyzed synthesis of 1,1-diarylalkanes from alkyl bromides and aryl bromides.

and co-workers reported a selective C(sp^3)–H alkylation protocol via polarity-matched hydrogen atom transfer (HAT) using photoredox and nickel catalysis [85]. This method works through synergistic cooperation of three catalytic cycles of photoredox, nickel, and HAT catalysis (Figure 12). The HAT-metallaphotoredox process selectively alkylates α-C–H of amines **6**, ethers **9**, and sulfides **28** with a variety of alkyl bromides **40** (Scheme 23).

The Hashmi group further developed the photoredox nickel-catalyzed C–H alkylation strategy to use the readily available inexpensive organo-photocatalyst benzaldehyde as the HAT photocatalyst under UVA irradiation [68,86]. Thus, the combination of $NiBr_2$·glyme/dtbbpy, benzaldehyde as both the photosensitizer and hydrogen abstractor, and K_2HPO_4 as a base under irradiation with UVA light enabled the cross-coupling of α-oxy C–H bonds of acyclic/cyclic ethers **9** with alkyl bromides **40**

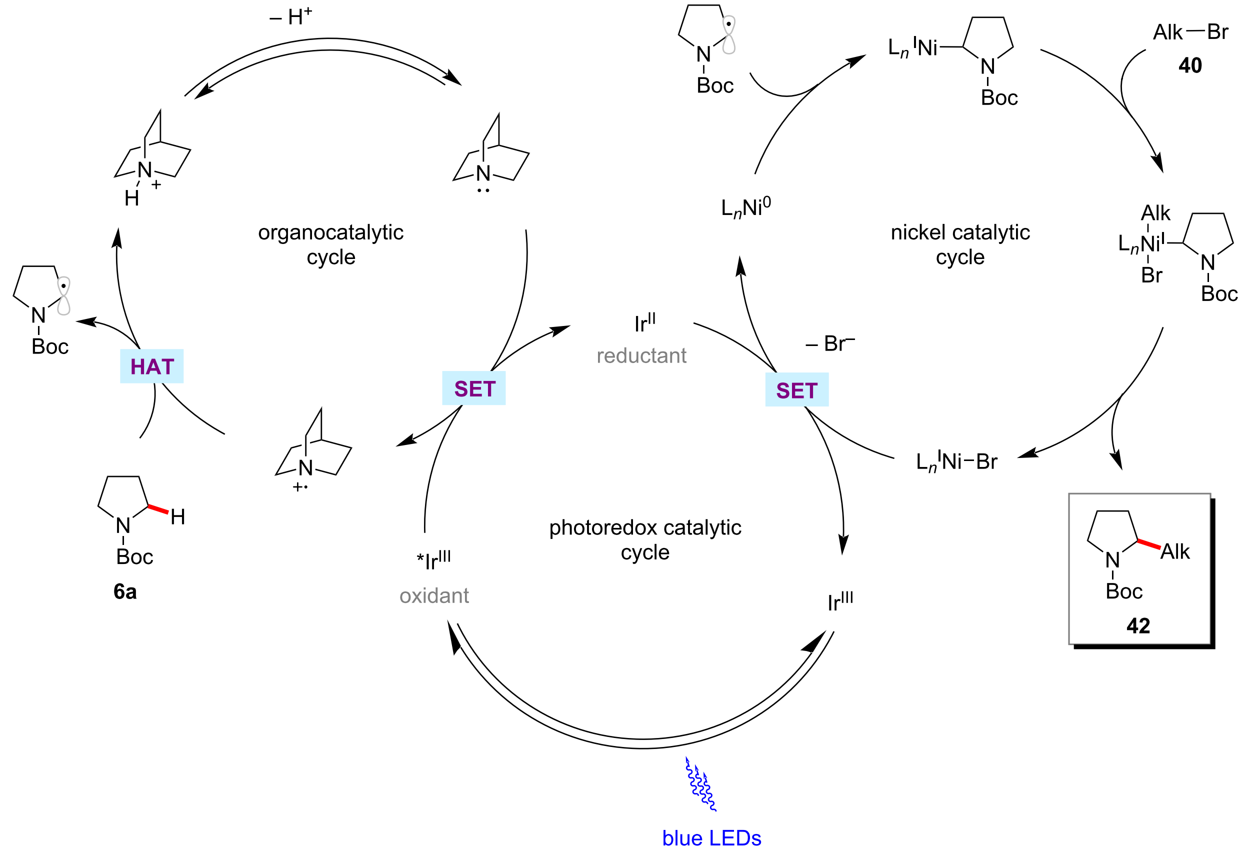

Figure 12: Proposed mechanism for photoredox nickel-catalyzed C(sp^3)–H alkylation via polarity-matched HAT.

(Scheme 24) [86]. The catalytic system was not limited to α-oxy C–H bonds of cyclic ethers, substrates having other heteroatoms such as nitrogen and sulfur that can imbue a hydridic nature of their α-C–H also proved viable under slightly modified reaction conditions, as was reported by Hashmi in 2019 (Scheme 25) [68].

In a recent publication, the group of Martin enabled an intermolecular alkylation of α-amino C–H bonds of benzamides **31** with unactivated alkyl halides **40** [72]. In this transformation, the combination of $NiBr_2$·diglyme/bipyridine in the presence of the iridium photocatalyst $Ir[dF(CF_3)ppy]_2(dtbbpy)PF_6$ under blue light irradiation was found to be appropriate to give optimal results (Scheme 26) [72].

The König group recently disclosed that the organic photocatalyst 1,2,3,5- tetrakis(carbazol-9-yl)-4,6-dicyanobenzene (4-CzIPN) could also be used with nickel catalysis for the alkylation of α-oxy C–H bonds of acyclic/cyclic ethers **9** with alkyl halides **40** (Scheme 27) [87]. The bench stable nickel(II) acetylacetonate can be used as the catalyst along with the dtbbpy ligand. The authors proposed a plausible reaction mechanism to account for the mode of operation as shown in Figure 13 [87]. Here, the halide radical species generated in situ was proposed to mediate the HAT event.

Considering the 'magic methyl' effect in drug candidates [88], there is a strong demand for the direct methylation of C–H bonds because it would provide a convenient access to structures that might not otherwise be available for biological testing [89-91]. Hence, Doyle and co-workers realized an elegant approach for the methylation of (hetero)aryl chlorides **8** using trimethyl orthoformate as a methyl radical source via a nickel/photoredox-catalyzed HAT processes (Scheme 28) [92]. The method was also compatible with other chlorine-containing electrophiles such as acyl chlorides **45** to afford methyl ketones **47** in moderate yields. Based on the detailed mechanistic studies, the authors proposed a catalytic cycle involving the generation of methyl radicals via β-scission of a tertiary radical which in turn was generated from trimethyl orthoformate by a photogenerated chlorine radical-mediated HAT process (Figure 14) [92].

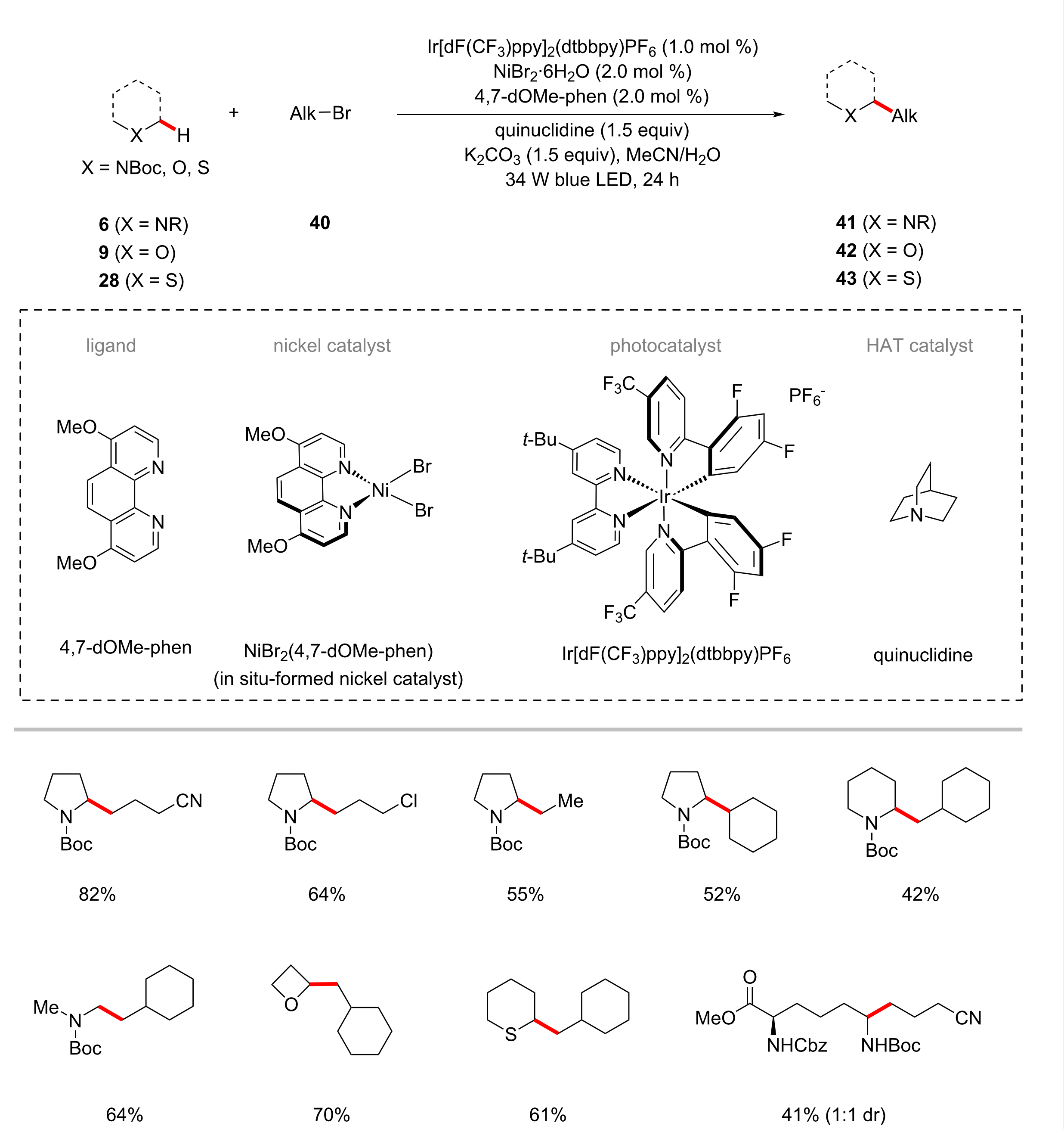
Ir[dF(CF3)ppy]2(dtbbpy)PF6 (1.0 mol %)
NiBr2·6H2O (2.0 mol %)
4,7-dOMe-phen (2.0 mol %)
quinuclidine (1.5 equiv)
K2CO3 (1.5 equiv), MeCN/H2O
34 W blue LED, 24 h
X = NBoc, O, S
Alk–Br
6 (X = NR)
9 (X = O)
28 (X = S)
40
41 (X = NR)
42 (X = O)
43 (X = S)
ligand
nickel catalyst
photocatalyst
HAT catalyst
4,7-dOMe-phen
NiBr2(4,7-dOMe-phen)
(in situ-formed nickel catalyst)
Ir[dF(CF3)ppy]2(dtbbpy)PF6
quinuclidine
82%
64%
55%
52%
42%
64%
70%
61%
41% (1:1 dr)

Scheme 23: Photoredox nickel-catalyzed C(sp^3)–H alkylation via polarity-matched HAT.

Recently, Stahl devised a photoredox nickel-catalyzed methylation of benzylic and α-amino C(sp^3)–H bonds using di-*tert*-butyl peroxide (DTBP) or dicumyl peroxide (DCP) as the methyl source under mild conditions [93]. Based on the substrate structure and peroxide choice, the authors developed four sets of reaction conditions (Scheme 29) [93]. In these reaction conditions, photocatalyst Ir[dF(CF$_3$)ppy]$_2$(dtbbpy)PF$_6$ and nickel catalyst NiCl$_2$·glyme were identified to be optimal and common.

The nickel-catalyzed photoredox-enabled HAT strategy was exploited for the remote functionalization of C(sp^3)–H with alkyl halides as was disclosed by Rovis and co-workers [94]. Thus, a variety of linear amides were alkylated selectively at the δ-methylene position through an intramolecular 1,5-HAT event in synergy with a nickel catalytic cycle. Interestingly, secondary C–H bonds are selectively functionalized in preference over primary C–H, in the case of multiple functionalizable sites were available. The authors examined ample scope of alkyl trifluoro-

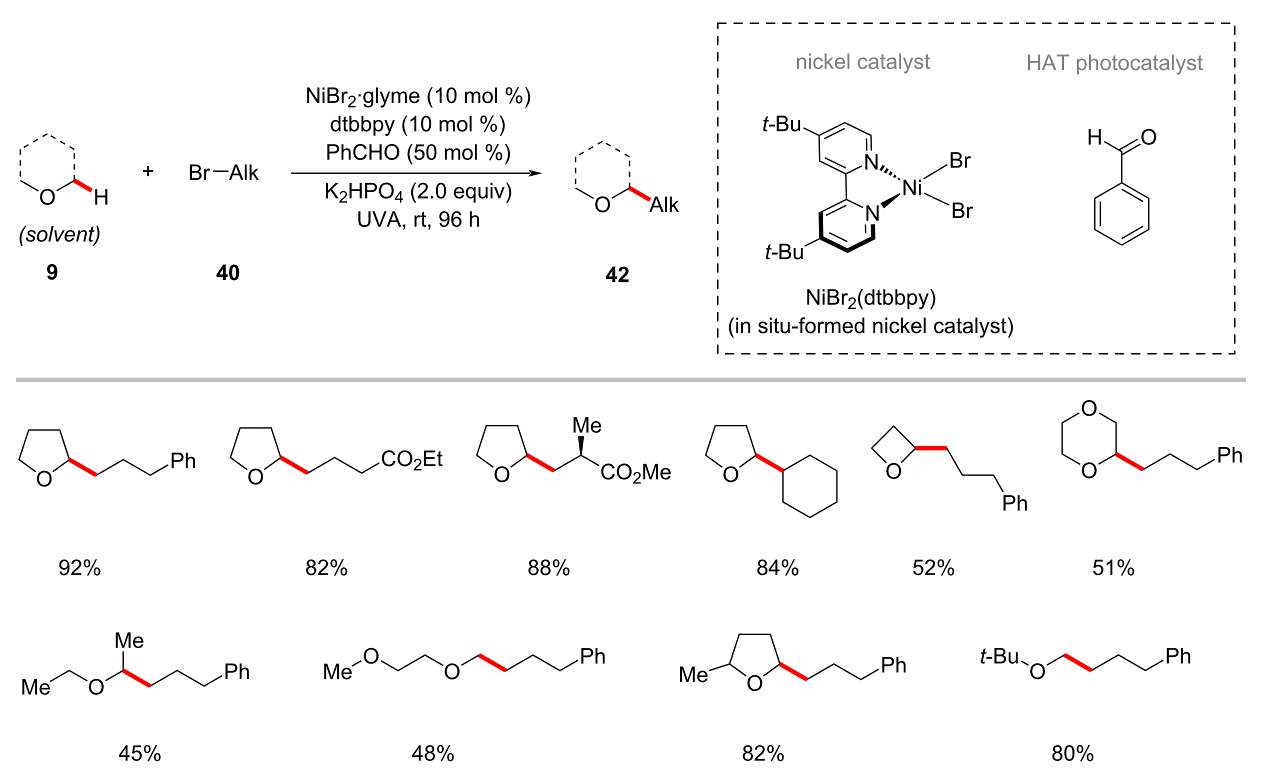
(solvent)
9
40
Br–Alk
NiBr$_2$·glyme (10 mol %)
dtbbpy (10 mol %)
PhCHO (50 mol %)
K$_2$HPO$_4$ (2.0 equiv)
UVA, rt, 96 h
42
Alk
nickel catalyst
HAT photocatalyst
t-Bu
Ni
Br
NiBr$_2$(dtbbpy)
(in situ-formed nickel catalyst)
92%
82%
88%
84%
52%
51%
45%
48%
82%
80%
Ph
CO$_2$Et
CO$_2$Me
Me

Scheme 24: Benzaldehyde- and nickel-catalyzed photoredox C(sp^3)–H alkylation of ethers.

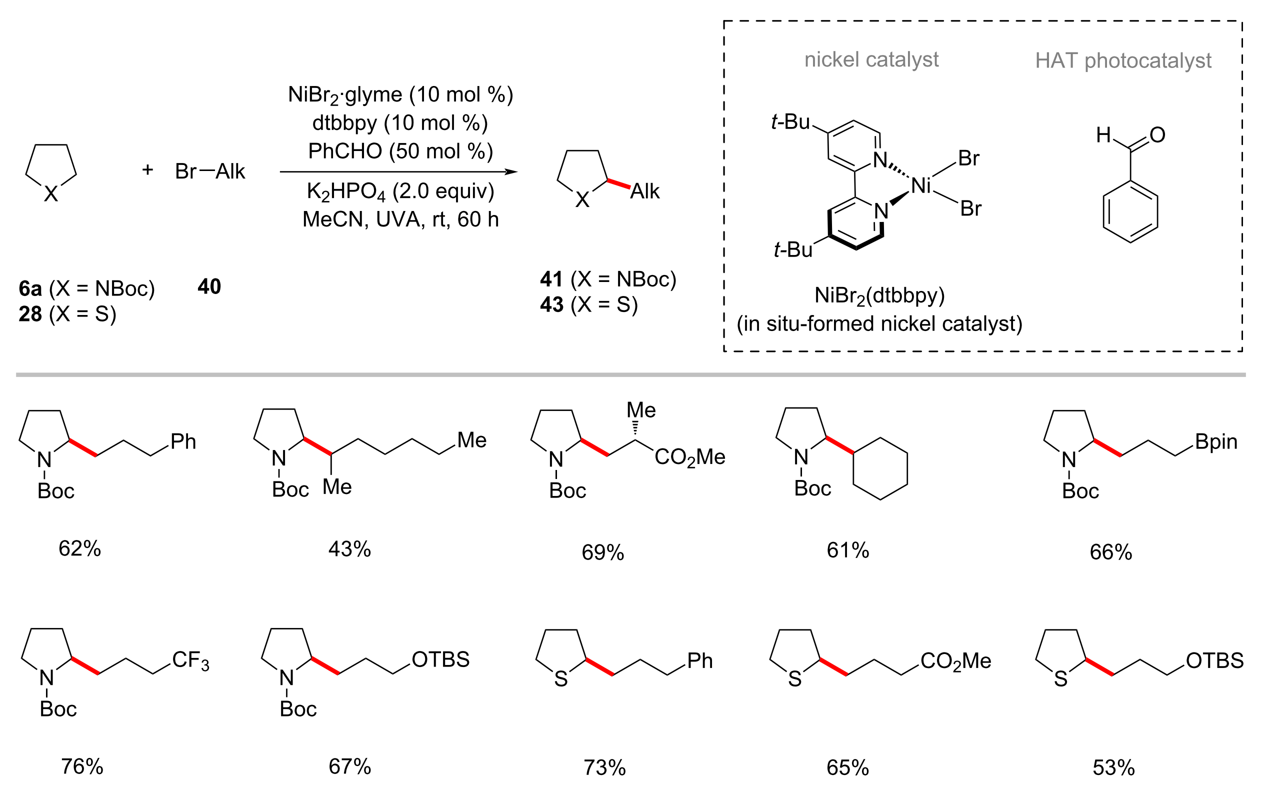
6a (X = NBoc)
28 (X = S)
40
Br–Alk
NiBr$_2$·glyme (10 mol %)
dtbbpy (10 mol %)
PhCHO (50 mol %)
K$_2$HPO$_4$ (2.0 equiv)
MeCN, UVA, rt, 60 h
41 (X = NBoc)
43 (X = S)
Alk
nickel catalyst
HAT photocatalyst
NiBr$_2$(dtbbpy)
(in situ-formed nickel catalyst)
62%
43%
69%
61%
66%
76%
67%
73%
65%
53%
Boc
Bpin
CF$_3$
OTBS

Scheme 25: Benzaldehyde- and nickel-catalyzed photoredox C(sp^3)–H alkylation of amides and thioethers.

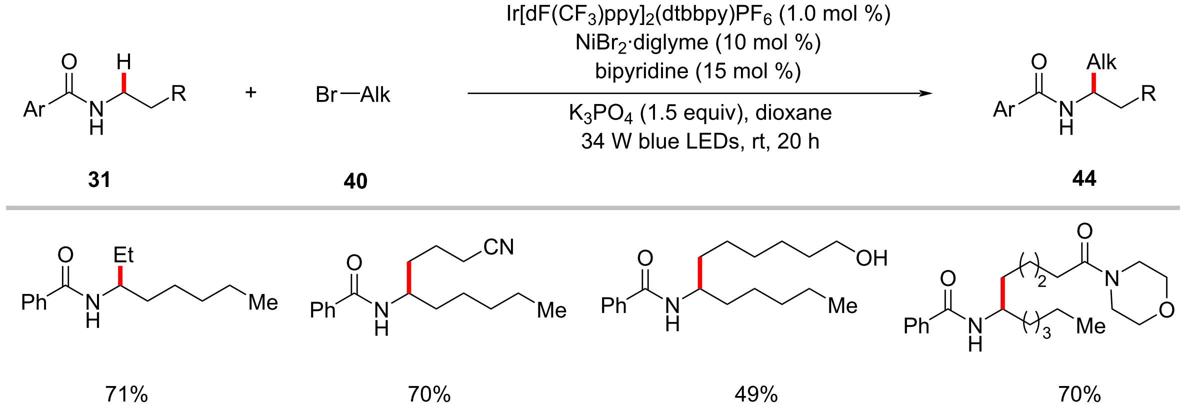
Ir[dF(CF3)ppy]2(dtbbpy)PF6 (1.0 mol %)
NiBr2·diglyme (10 mol %)
bipyridine (15 mol %)
K3PO4 (1.5 equiv), dioxane
34 W blue LEDs, rt, 20 h
31
40
44
Br—Alk
71%
70%
49%
70%

Scheme 26: Photoredox and nickel-catalyzed C(sp^3)–H alkylation of benzamides with alkyl bromides.

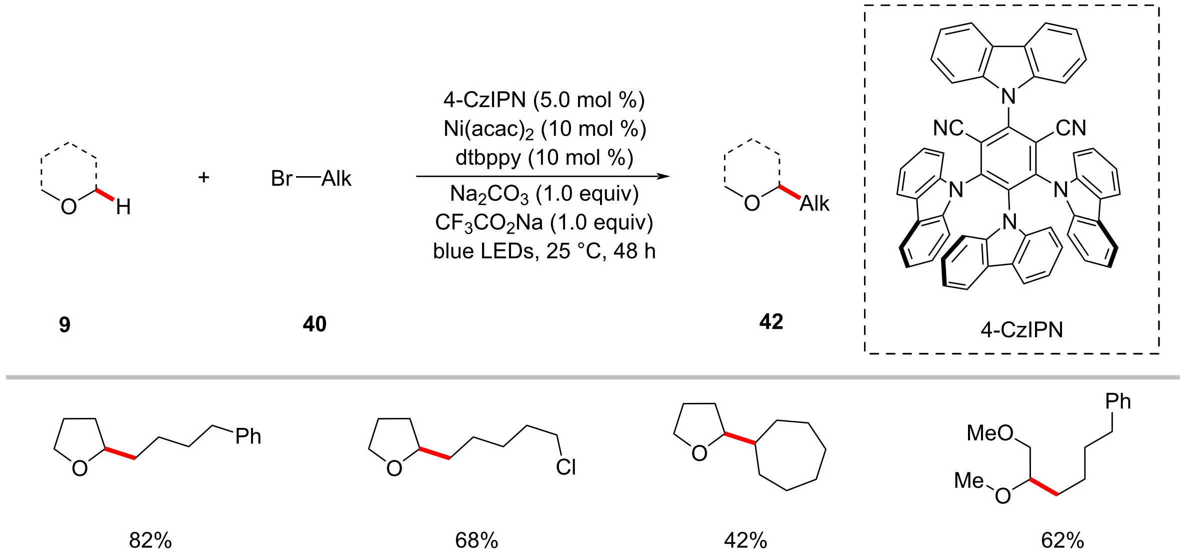
4-CzIPN (5.0 mol %)
Ni(acac)2 (10 mol %)
dtbppy (10 mol %)
Na2CO3 (1.0 equiv)
CF3CO2Na (1.0 equiv)
blue LEDs, 25 °C, 48 h
9
40
42
Br—Alk
4-CzIPN
82%
68%
42%
62%

Scheme 27: CzIPN and nickel-catalyzed C(sp^3)–H alkylation of ethers with alkyl bromides.

acetamides **56** and alkyl bromides **40** to afford the corresponding alkylated products **57** in moderate to good yields (Scheme 30) [94]. As to the modus operandi, the generation of an alkyl radical species through amide directed 1,5-HAT followed by capture of the thus formed alkyl radical by the nickel catalyst was proposed.

Alkenylation

Over the past few decades, outstanding progress has been realized in the direct alkenylation transformation of C(sp^2)–H bonds [95-101]. However, the related C(sp^3)–H alkenylation is much less developed due to lower reactivity, poor regioselectivities and the need of noble metal catalysts [50,102-106]. Recently, Yu and co-workers conveniently achieved the direct alkenylation of α-amino C(sp^3)–H bonds of amines **1** with alkenyl tosylates **58**. The combination of the Ru(bpy)$_3$Cl$_2$·6H$_2$O photocatalyst and NiCl$_2$·glyme as the nickel catalyst enabled this C–H alkenylation protocol using alkenyl C(sp^2)–O electrophiles at ambient reaction temperature under blue light irradiation (Scheme 31) [58]. In general, the method displayed broad substrate scope, good functional group tolerance, and excellent regioselectivities.

In 2017, the Wu group reported a notable C(sp^3)–H functionalization process with internal alkynes by means of photoredox nickel catalysis [107]. Within this study, they showed that

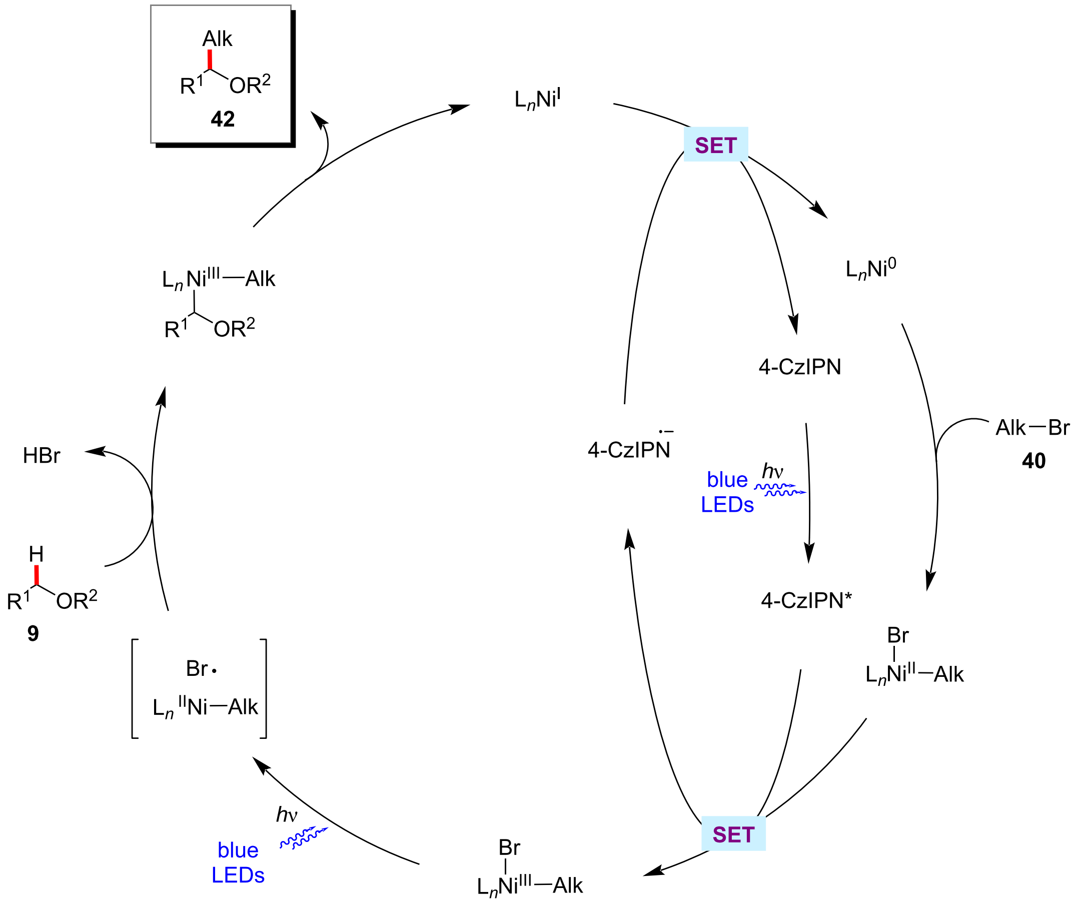
Alk
R1
OR2
42
LnNiI
SET
LnNi0
4-CzIPN
Alk—Br
40
4-CzIPN•−
blue LEDs
hν
4-CzIPN*
Br
LnNiII—Alk
SET
Br
LnNiIII—Alk
hν
blue LEDs
Br•
LnIINi—Alk
HBr
H
R1
OR2
9
LnNiIII—Alk
R1
OR2

Figure 13: Proposed mechanism for the CzIPN and nickel-catalyzed C(sp^3)–H alkylation of ethers.

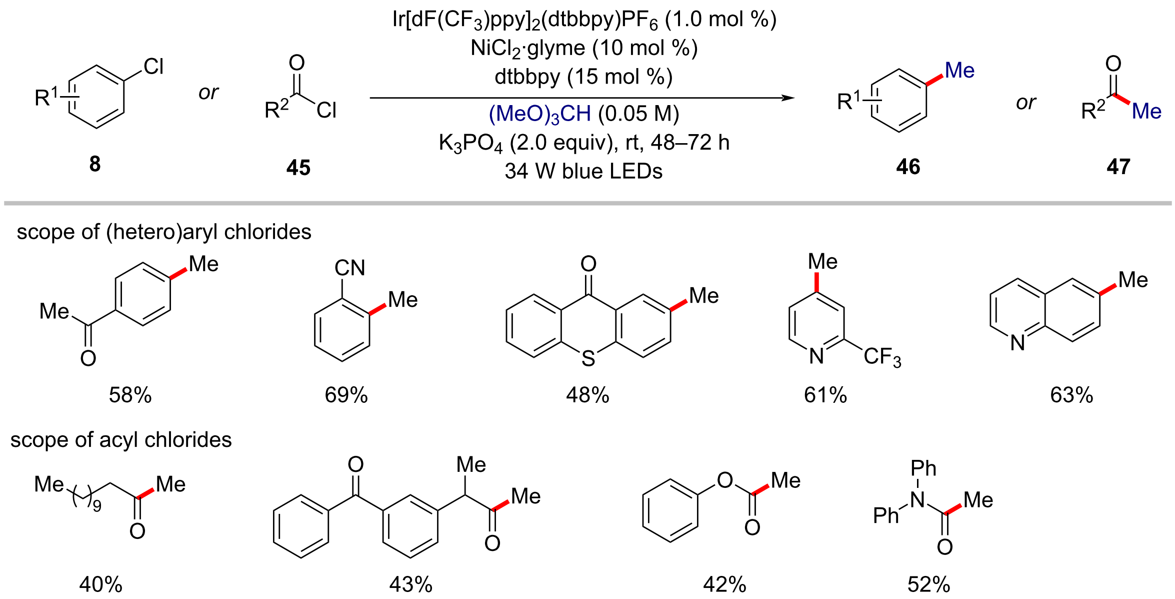
R1
Cl
8
or
O
R2
Cl
45
Ir[dF(CF3)ppy]2(dtbbpy)PF6 (1.0 mol %)
NiCl2·glyme (10 mol %)
dtbbpy (15 mol %)
(MeO)3CH (0.05 M)
K3PO4 (2.0 equiv), rt, 48–72 h
34 W blue LEDs
R1
Me
46
or
O
R2
Me
47
scope of (hetero)aryl chlorides
58%
69%
48%
61%
63%
scope of acyl chlorides
40%
43%
42%
52%

Scheme 28: Nickel/photoredox-catalyzed methylation of (hetero)aryl chlorides and acid chlorides using trimethyl orthoformate.

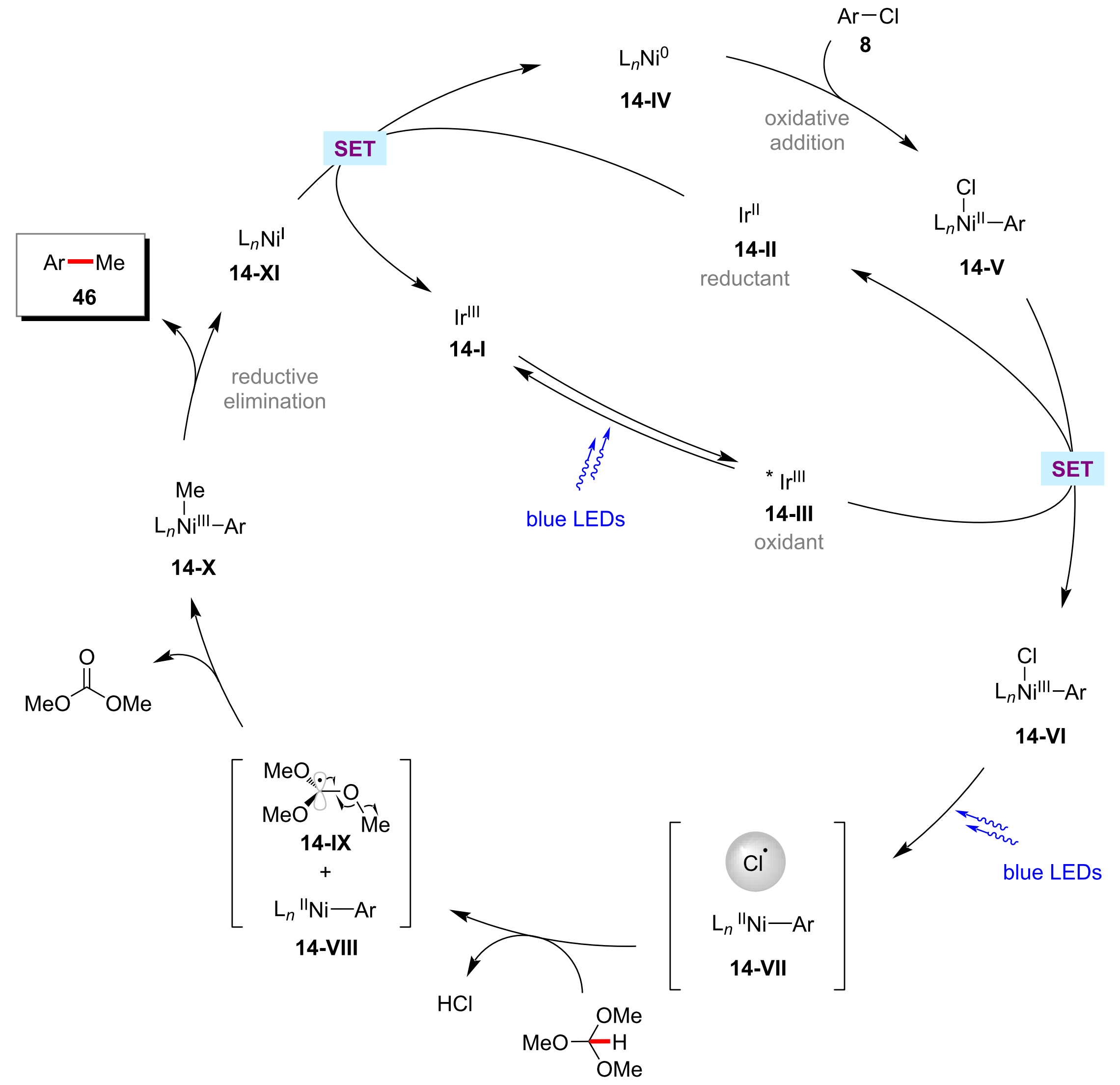
Ar—Cl
8
L_nNi^0
14-IV
oxidative addition
Cl
L_nNi^{II}—Ar
14-V
SET
Ir^{II}
14-II
reductant
L_nNi^I
14-XI
Ar—Me
46
Ir^{III}
14-I
reductive elimination
blue LEDs
* Ir^{III}
14-III
oxidant
SET
Me
L_nNi^{III}–Ar
14-X
Cl
L_nNi^{III}–Ar
14-VI
MeO
OMe
MeO
MeO
O
Me
14-IX
+
L_n ^{II}Ni—Ar
14-VIII
Cl•
L_n ^{II}Ni—Ar
14-VII
blue LEDs
HCl
OMe
MeO
H
OMe

Figure 14: Proposed catalytic cycle for the nickel/photoredox-catalyzed methylation of (hetero)aryl chlorides using trimethyl orthoformate.

the reaction of ethers, or amides with internal alkynes **60** in the presence of the combination of a catalytic amount of Ir[dF(CF$_3$)ppy]$_2$(dtbbpy)PF$_6$, NiCl$_2$, and dtbbpy as ligand at 60 °C under blue LED light irradiation gave alkenylation products **61** in good yields (Scheme 32) [107]. In general, the reaction proceeded with good regioselectivities and excellent *E*/*Z* ratios. Further, the authors also conducted this process in a continuous-flow reactor. The mechanistic studies indicated that a nickel hydride intermediate generated with C(sp^3)–H as the hydride source is involved in this catalytic transformation. The hydronickelation step results in the sterically less hindered vinylnickel intermediate **15-I**, which corresponds to the observed major isomer product (Figure 15).

In a related transformation, Hong realized the exclusively α-selective hydroacylation of ynones, ynoates, and ynamides via photoredox nickel catalysis. Thus, the combination of nickel and iridium catalysts efficiently catalyzed the regioselective α-C(sp^3)–H addition of ethers **9** to triisopropylsilyl (TIPS)-substituted alkynes **62** (Scheme 33) [108]. Notably, among the tested nickel salts, NiCl$_2$·glyme gave superior outcomes than other nickel(II) salts or nickel(0) catalysts, indicating the essential role of chlorine. As to the scope of the reaction, TIPS-protected ynones, ynoates, and ynamides smoothly transformed into the corresponding trisubstituted alkenes **63** in high regio- and stereoselectivities. A possible mechanism was proposed similar to the one shown in Figure 15 to account for the observed high regioselectivity.

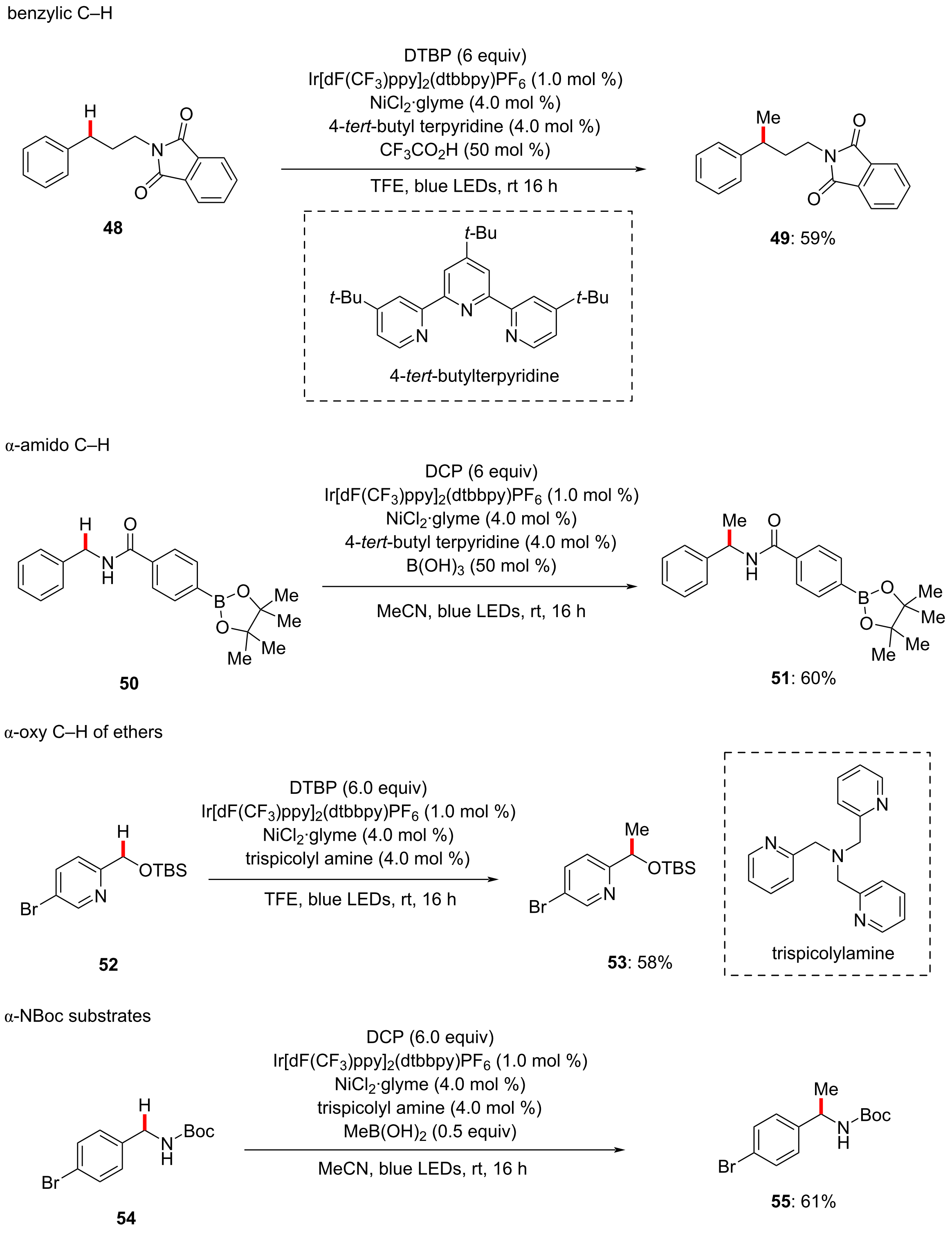
benzylic C–H
DTBP (6 equiv)
Ir[dF(CF3)ppy]2(dtbbpy)PF6 (1.0 mol %)
NiCl2·glyme (4.0 mol %)
4-tert-butyl terpyridine (4.0 mol %)
CF3CO2H (50 mol %)
TFE, blue LEDs, rt 16 h
48
49: 59%
4-tert-butylterpyridine
α-amido C–H
DCP (6 equiv)
Ir[dF(CF3)ppy]2(dtbbpy)PF6 (1.0 mol %)
NiCl2·glyme (4.0 mol %)
4-tert-butyl terpyridine (4.0 mol %)
B(OH)3 (50 mol %)
MeCN, blue LEDs, rt, 16 h
50
51: 60%
α-oxy C–H of ethers
DTBP (6.0 equiv)
Ir[dF(CF3)ppy]2(dtbbpy)PF6 (1.0 mol %)
NiCl2·glyme (4.0 mol %)
trispicolyl amine (4.0 mol %)
TFE, blue LEDs, rt, 16 h
52
53: 58%
trispicolylamine
α-NBoc substrates
DCP (6.0 equiv)
Ir[dF(CF3)ppy]2(dtbbpy)PF6 (1.0 mol %)
NiCl2·glyme (4.0 mol %)
trispicolyl amine (4.0 mol %)
MeB(OH)2 (0.5 equiv)
MeCN, blue LEDs, rt, 16 h
54
55: 61%

Scheme 29: Photochemical nickel-catalyzed C(sp^3)–H methylations.

Allylation

The transition-metal-catalyzed direct allylation of unactivated C–H bonds is considered as the prevalent strategy in organic synthesis. Despite significant advances were accomplished in the allylation of (hetero)aromatic and alkenyl C(sp^2)–H bonds [109], related reactions of C(sp^3)–H are less

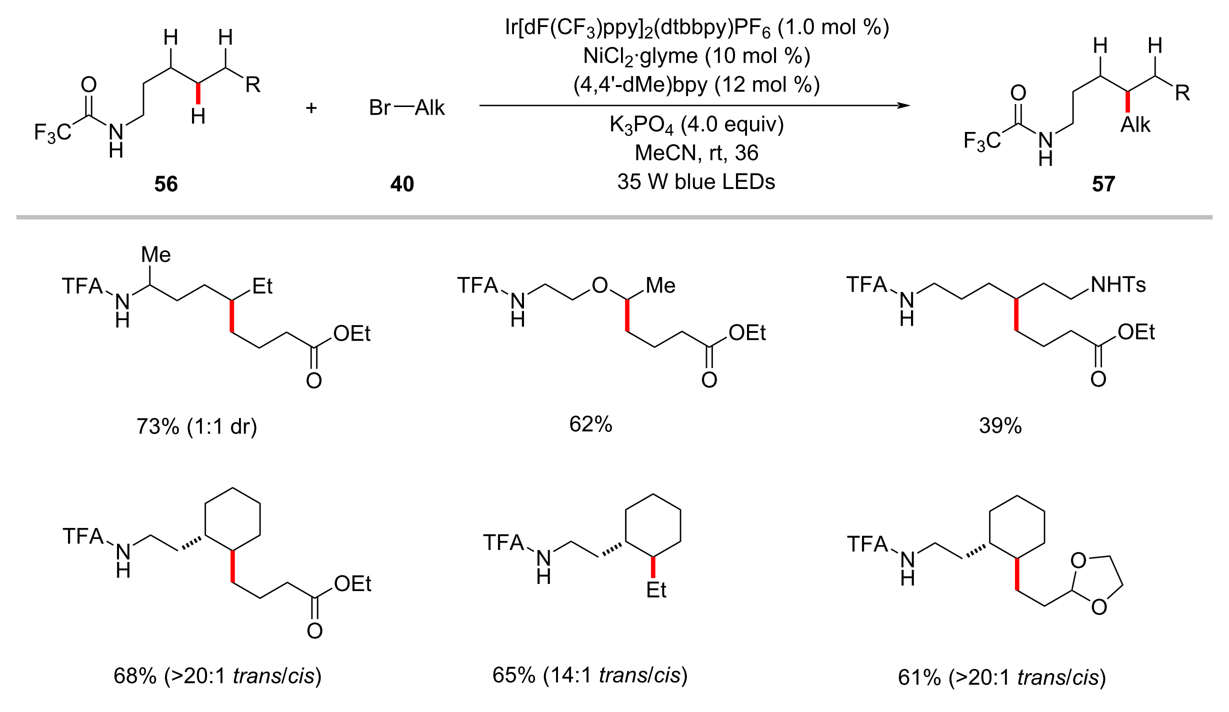
Ir[dF(CF3)ppy]2(dtbbpy)PF6 (1.0 mol %)
NiCl2·glyme (10 mol %)
(4,4'-dMe)bpy (12 mol %)
K3PO4 (4.0 equiv)
MeCN, rt, 36
35 W blue LEDs
56
40
57
Br—Alk
73% (1:1 dr)
62%
39%
68% (>20:1 trans/cis)
65% (14:1 trans/cis)
61% (>20:1 trans/cis)

Scheme 30: Photoredox nickel catalysis-enabled alkylation of unactivated C(sp^3)–H bonds with alkyl bromides.

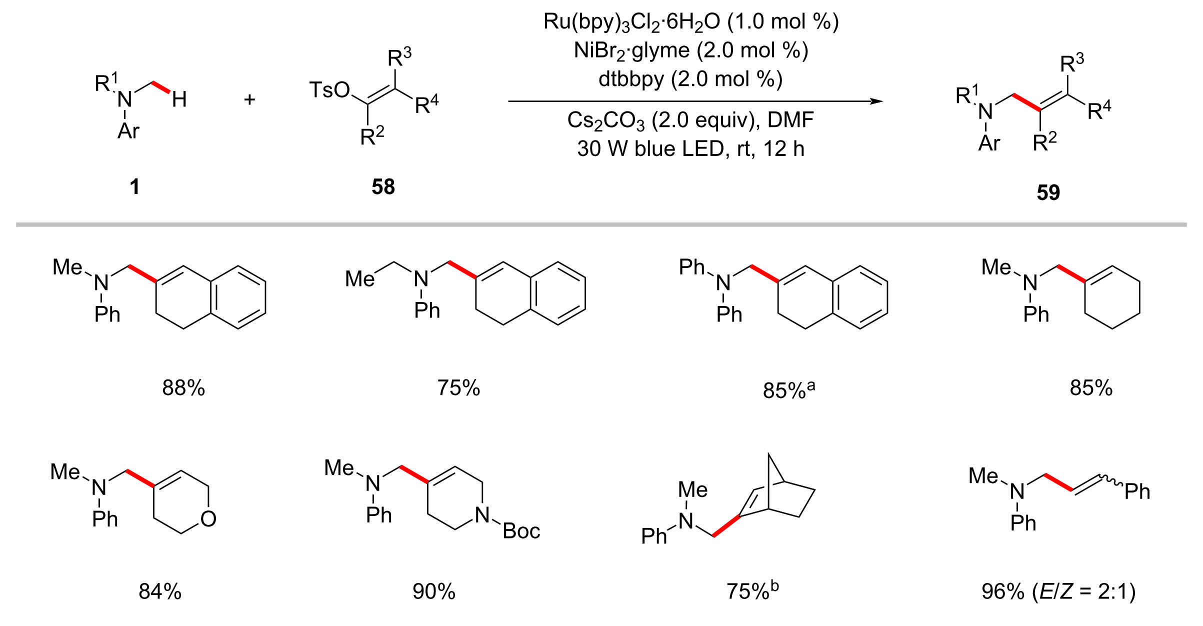
Ru(bpy)3Cl2·6H2O (1.0 mol %)
NiBr2·glyme (2.0 mol %)
dtbbpy (2.0 mol %)
Cs2CO3 (2.0 equiv), DMF
30 W blue LED, rt, 12 h
1
58
59
88%
75%
85%a
85%
84%
90%
75%b
96% (E/Z = 2:1)

^{a}Ir(ppy)$_2$(dtbbpy)(PF$_6$) as photocatalyst.
^{b}triflate was used instead of tosylate.

Scheme 31: Photochemical C(sp^3)–H alkenylation with alkenyl tosylates.

explored [110,111]. In this context, Tambar developed a δ-selective C(sp^3)–H allylation of aliphatic amides **64** using allyl chlorides **65** under visible light photoredox nickel catalysis (Scheme 34) [112]. The optimized reaction conditions exhibited good tolerance to a variety of substitutions on the allyl chloride substrates **65** and the amide

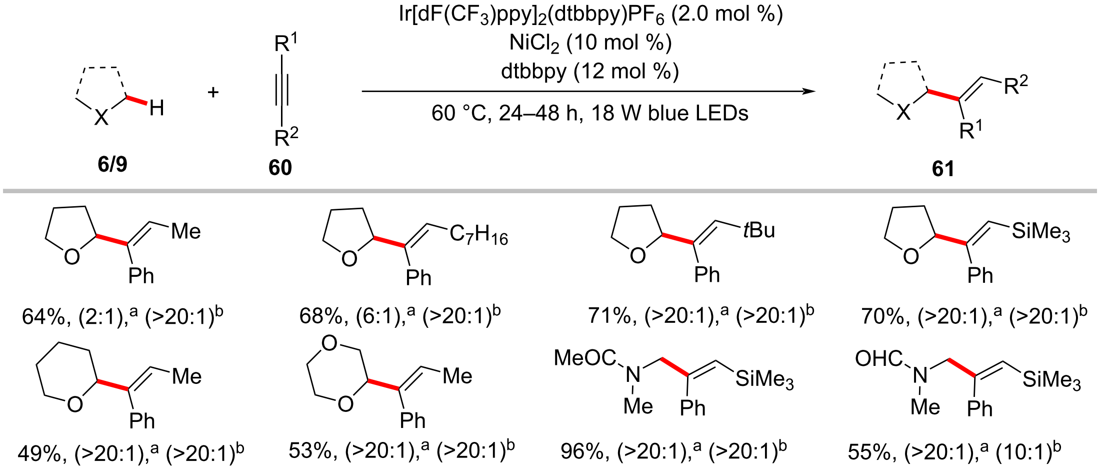
Ir[dF(CF3)ppy]2(dtbbpy)PF6 (2.0 mol %)
NiCl2 (10 mol %)
dtbbpy (12 mol %)
60 °C, 24–48 h, 18 W blue LEDs
X
H
R1
R2
6/9
60
61
Me
Ph
C7H16
tBu
SiMe3
MeOC
OHC
N
O
64%, (2:1),a (>20:1)b
68%, (6:1),a (>20:1)b
71%, (>20:1),a (>20:1)b
70%, (>20:1),a (>20:1)b
49%, (>20:1),a (>20:1)b
53%, (>20:1),a (>20:1)b
96%, (>20:1),a (>20:1)b
55%, (>20:1),a (10:1)b

[a]Ratio of regioisomers, major isomer is shown.

[b]*E/Z* ratio of major regioisomer.

Scheme 32: Photoredox nickel-catalyzed hydroalkylation of internal alkynes.

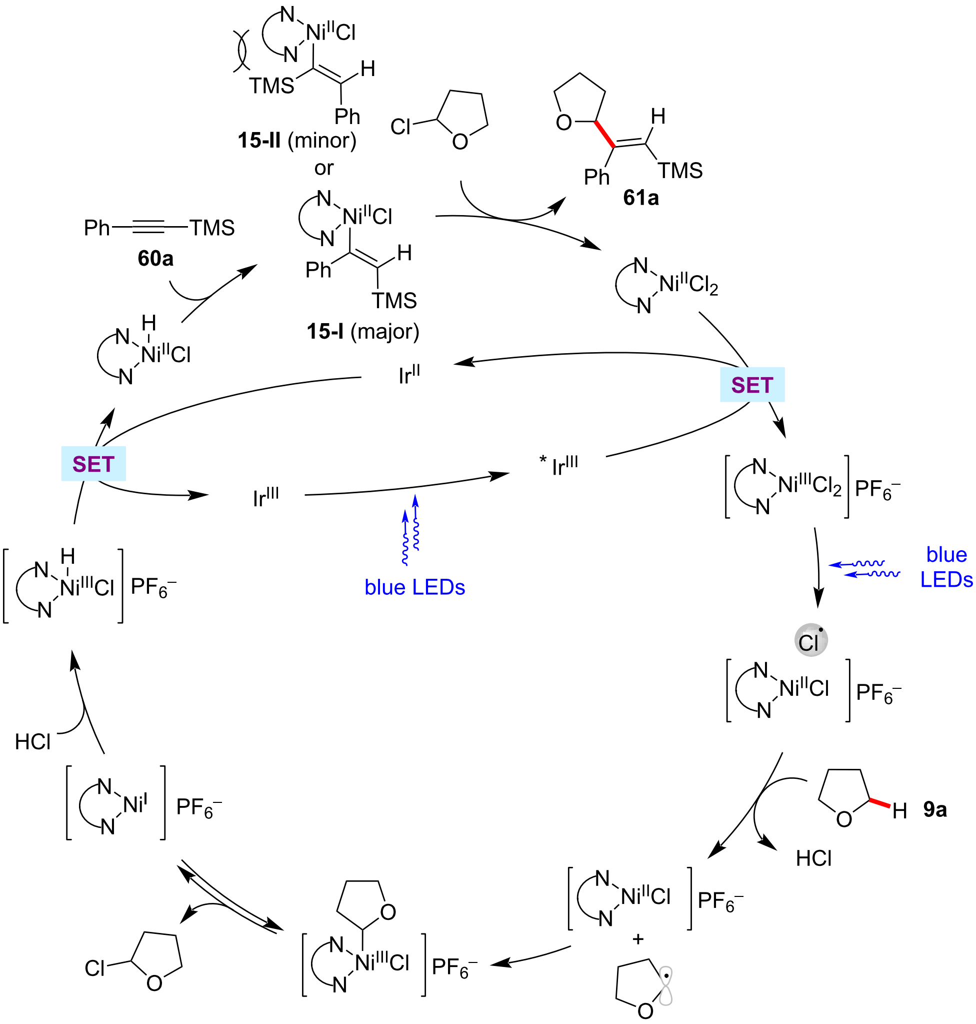
15-II (minor)
or
15-I (major)
TMS
Ph
H
Cl
61a
60a
NiIICl
NiIICl2
SET
IrII
*IrIII
IrIII
blue LEDs
NiIIICl2
PF6−
Cl•
9a
HCl
NiIIICl
NiI

Figure 15: Proposed mechanism for the photoredox nickel-catalyzed hydroalkylation of internal alkynes.

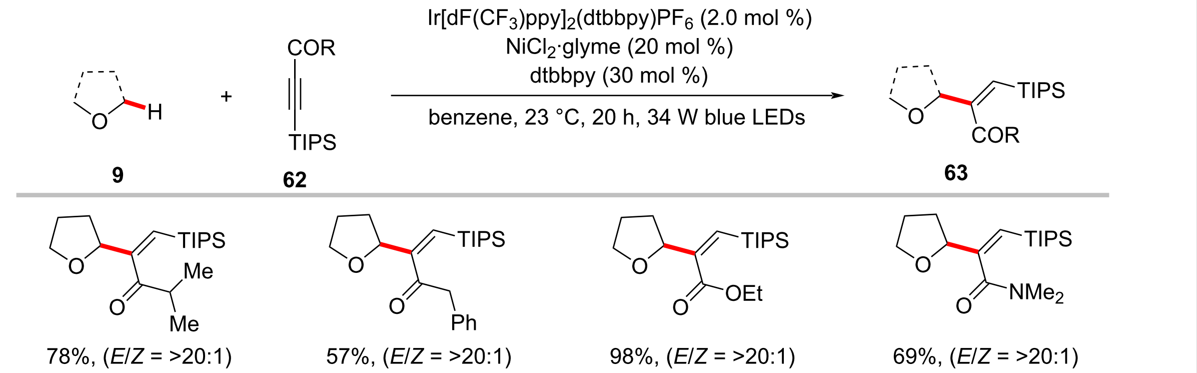
Ir[dF(CF3)ppy]2(dtbbpy)PF6 (2.0 mol %)
NiCl2·glyme (20 mol %)
dtbbpy (30 mol %)
benzene, 23 °C, 20 h, 34 W blue LEDs
COR
TIPS
9
62
63
78%, (E/Z = >20:1)
57%, (E/Z = >20:1)
98%, (E/Z = >20:1)
69%, (E/Z = >20:1)

Scheme 33: Photoredox nickel-catalyzed hydroalkylation of activated alkynes with C(sp^3)–H bonds.

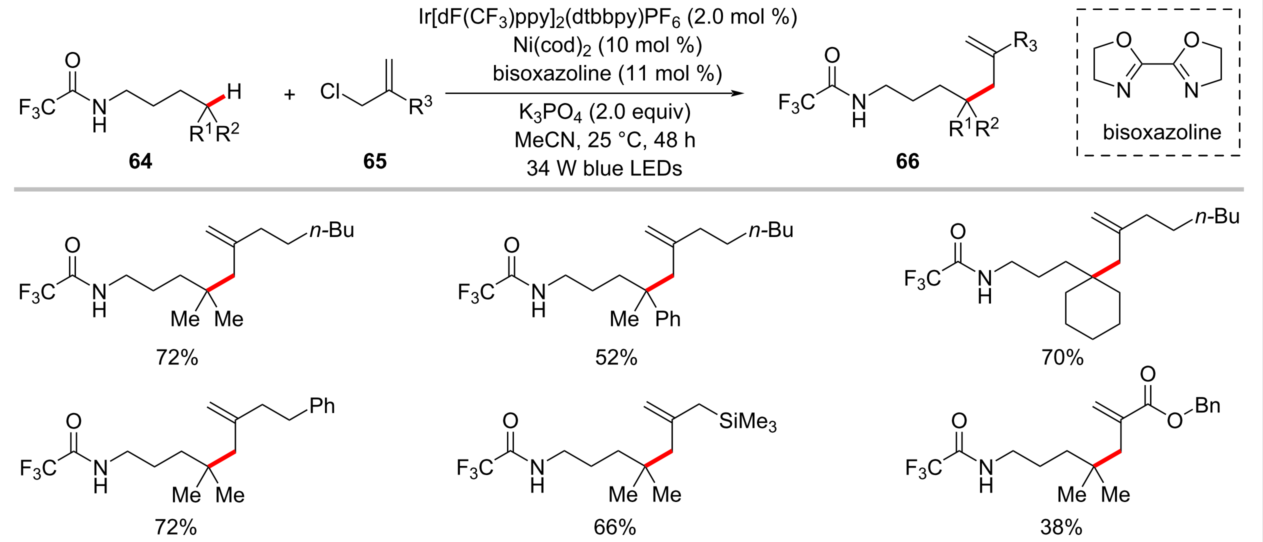
Ir[dF(CF3)ppy]2(dtbbpy)PF6 (2.0 mol %)
Ni(cod)2 (10 mol %)
bisoxazoline (11 mol %)
K3PO4 (2.0 equiv)
MeCN, 25 °C, 48 h
34 W blue LEDs
64
65
66
bisoxazoline
72%
52%
70%
72%
66%
38%

Scheme 34: Allylation of unactivated C(sp^3)–H bonds with allylic chlorides.

substrates **64**. However, the role of the nickel catalyst in this process and the reaction mechanism pathway were not fully established.

The photoredox nickel-catalyzed allylation of α-amino C(sp^3)–H bonds with trifluoromethylated alkenes **68** has been more recently achieved by Martin and co-workers (Scheme 35)

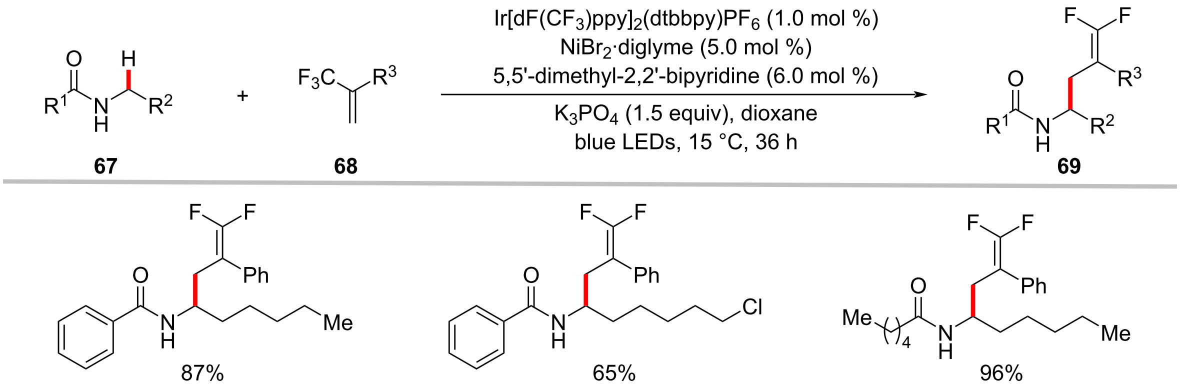
Ir[dF(CF3)ppy]2(dtbbpy)PF6 (1.0 mol %)
NiBr2·diglyme (5.0 mol %)
5,5'-dimethyl-2,2'-bipyridine (6.0 mol %)
K3PO4 (1.5 equiv), dioxane
blue LEDs, 15 °C, 36 h
67
68
69
87%
65%
96%

Scheme 35: Photochemical nickel-catalyzed α-amino C(sp^3)–H allylation of secondary amides with trifluoromethylated alkenes.

[113]. This defluorinative functionalization protocol set the stage for the introduction of *gem*-difluoroalkene motifs into α-amino C(sp^3)–H sites. Interestingly, substrates having a trifluoromethyl group on the amide backbone enabled the functionalization of δ C(sp^3)–H bonds under slightly modified reaction conditions with exclusion of the nickel catalyst (Scheme 36) [113].

Acylation

The ketone motif is an important functional group in pharmaceuticals, agrochemicals, and functional materials [114-117]. Hence continuous efforts devoted to developing a convenient method to introduce keto functional groups onto complex organic molecules. During the last decade, the acylation of hydrocarbons through direct C–H activation has been achieved by means of transition-metal catalysis using various acyl precursors [118,119]. The renaissance of metallaphotoredox catalysis has improved further the C–H acylation procedures by working under mild reaction conditions. Thus, Doyle and Joe reported a mild C–H acylation protocol for the direct functionalization of α-amino C(sp^3)–H bonds of *N*-arylamines **1** with acyl electrophiles such as anhydrides **72** and 2-pyridyl thioester **73** (Scheme 37) [120]. Here, the combination of the iridium photocatalyst, $[Ir(ppy)_2(dtbbpy)]PF_6$ and $Ni(cod)_2$ as the nickel catalyst were found to be optimal to give the desired acylation products **74** in satisfactory yields. Furthermore, a plausible catalytic cycle was proposed to account for the C–H acylation reaction (Figure 16) [120]. A photogenerated α-amino radical **16-IV**

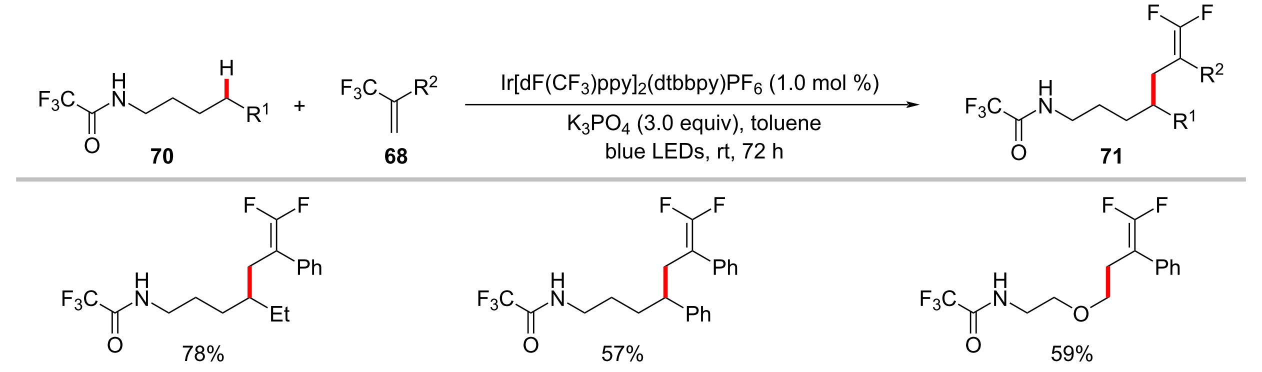
70
68
Ir[dF(CF3)ppy]2(dtbbpy)PF6 (1.0 mol %)
K3PO4 (3.0 equiv), toluene
blue LEDs, rt, 72 h
71
78%
57%
59%

Scheme 36: Photoredox δ C(sp^3)–H allylation of secondary amides with trifluoromethylated alkenes.

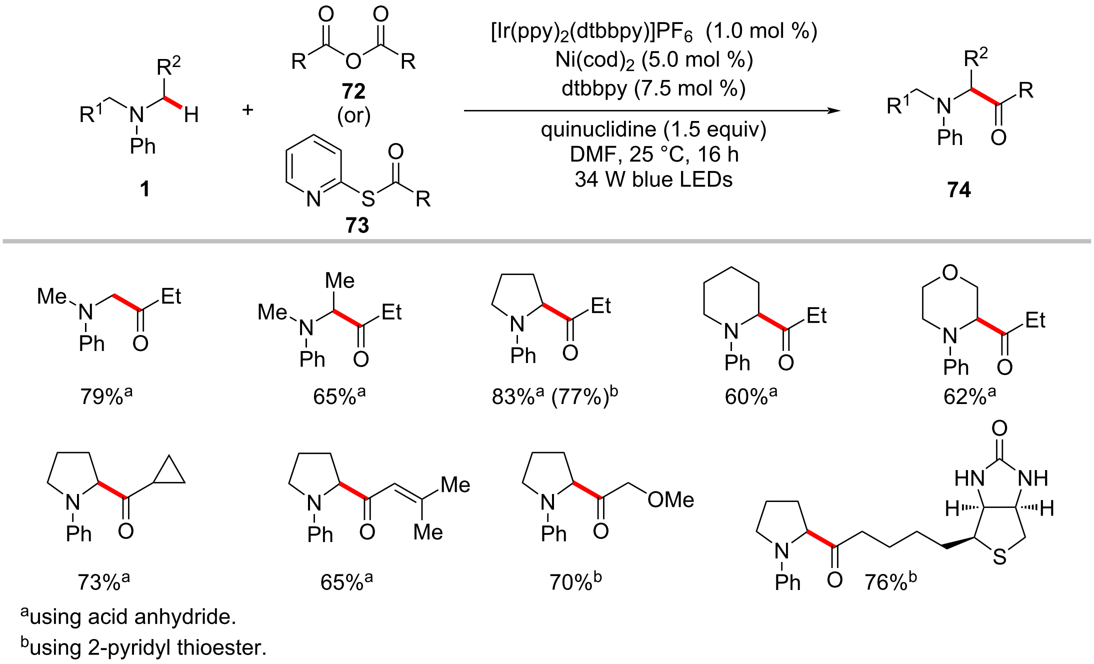
1
72
(or)
73
[Ir(ppy)2(dtbbpy)]PF6 (1.0 mol %)
Ni(cod)2 (5.0 mol %)
dtbbpy (7.5 mol %)
quinuclidine (1.5 equiv)
DMF, 25 °C, 16 h
34 W blue LEDs
74
79%a
65%a
83%a (77%)b
60%a
62%a
73%a
65%a
70%b
76%b
ausing acid anhydride.
busing 2-pyridyl thioester.

Scheme 37: Photoredox nickel-catalyzed acylation of α-amino C(sp^3)–H bonds of *N*-arylamines.

intercepts with the nickel catalytic cycle to generate a key nickel(III) intermediate **16-VII**, which readily undergoes reductive elimination to afford the desired cross-coupled product **74a**.

In 2017, Kamagai and Shibasaki showed that a robust iridium photocatalysis/nickel catalysis enabled the α-C(sp^3)–H acylation of ethers **9** with acid chlorides **45** (Scheme 38) [121]. The optimized catalytic conditions were not limited to acid chlorides as acyl sources, and an acid anhydride proved as viable substrate, albeit in a somewhat lower yield. Based on the mechanistic studies, the authors proposed a catalytic cycle involving a triplet–triplet energy transfer between the excited iridium photocatalyst **17-II** and nickel(II) complex **17-IV** (Figure 17) [121]. The excited nickel(II) complex **17-V** undergoes Ni–Cl bond homolysis followed by a HAT event of the chlorine radical with the ether substrate and subsequent capture of the thus-formed α-oxy C(sp^3) radical by the nickel complex resulting in the nickel(II)(alkyl)acyl complex **17-VI**. Finally, reductive elimination of **17**-**VI** delivered the desired product **75a**.

The nickel-photoredox catalysis was extended to include chloroformates **76** as electrophiles in the C–H functionalization reaction as was reported by the Doyle group (Scheme 39a) [122]. Here, the combination of Ir[dF(CF_3)ppy]$_2$(dtbbpy)PF_6 and Ni(cod)$_2$ enabled this transformation to proceed under blue light irradiation. Notably, addition of stoichiometric quantities of sodium tungstate were found to be beneficial for the formation of the desired cross-coupling products **77**. The authors' investigations suggested that tungstate is acting as a base rather than a photocatalyst. A variety of C–H substrates including unactivated alkanes, amines, and ethers were transformed into ester products **77**. A catalytic cycle was proposed with a chlorine radical involved in the HAT event (Scheme 39b) [122].

The cooperative activity of an iridium photocatalyst and nickel catalyst also enabled the dehydrogenative cross coupling of benzylic and aldehydic C–H bonds (Scheme 40) [123]. Notably, this method proceeds through a unique mechanism (Figure 18) involving five steps: i) anion exchange between the iridium catalyst and nickel catalyst; ii) generation of a bromine radical and nickel(I) species in the photocatalytic cycle; iii) hydrogen atom abstraction events between the bromine radical and toluene as well as aldehyde; iv) product formation in a nickel catalytic cycle; and v) regeneration of nickel(II) species.

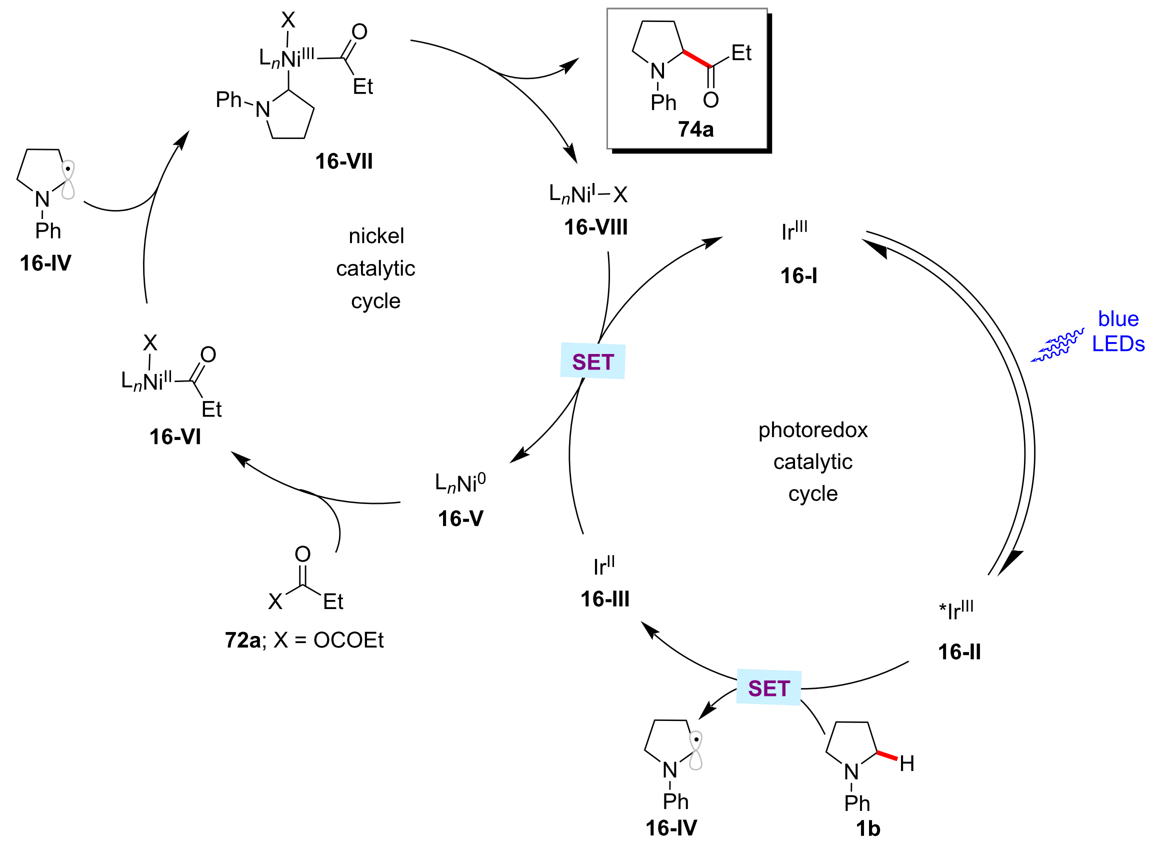

Figure 16: Proposed mechanism for the photoredox nickel-catalyzed acylation of α-amino C(sp^3)–H bonds of *N*-arylamines.

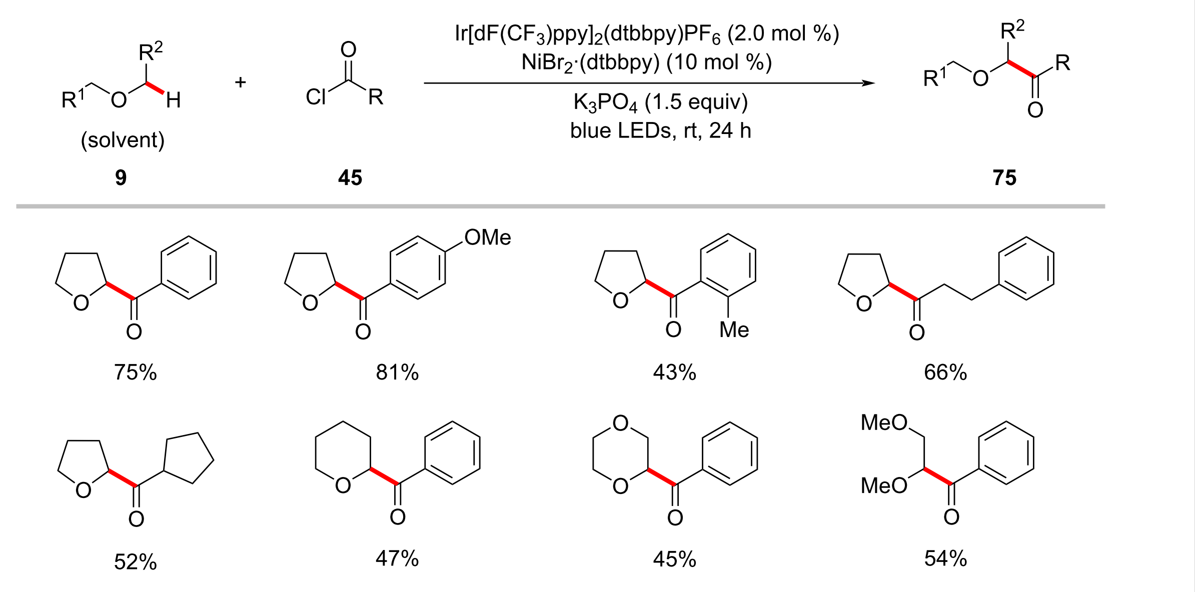
R1 O R2 H
(solvent)
9
+
Cl O R
45
Ir[dF(CF3)ppy]2(dtbbpy)PF6 (2.0 mol %)
NiBr2·(dtbbpy) (10 mol %)
K3PO4 (1.5 equiv)
blue LEDs, rt, 24 h
R1 O R2 R O
75
OMe
Me
75%
81%
43%
66%
MeO
MeO
52%
47%
45%
54%

Scheme 38: Photocatalytic α-acylation of ethers with acid chlorides.

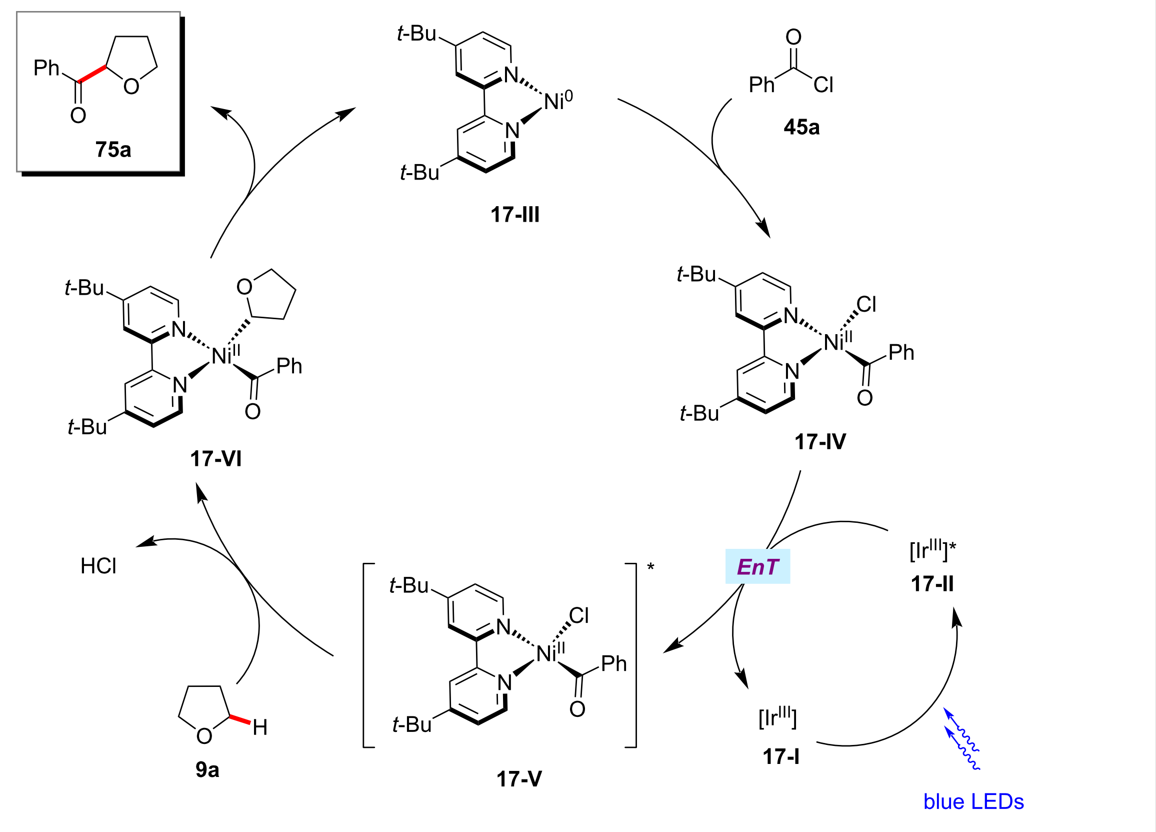
75a
17-III
45a
17-IV
17-VI
EnT
[Ir^{III}]*
17-II
HCl
17-V
[Ir^{III}]
17-I
9a
blue LEDs

Figure 17: Proposed mechanism for the photocatalytic α-acylation of ethers with acid chlorides.

Recently, the group of Huo developed a nickel-catalyzed enantioselective acylation of α-amino C(sp^3)–H bonds with carboxylic acids under visible light irradiation (Scheme 41) [124]. Here, dimethyl dicarbonate (DMDC) was the choice of activator to convert the carboxylic acid to a mixed anhydride in situ. In this protocol, the bisoxazoline-based chiral ligand **83** enabled the synthesis of α-amino ketones in high enantioselectivities under mild reaction conditions. Good yields were ob-

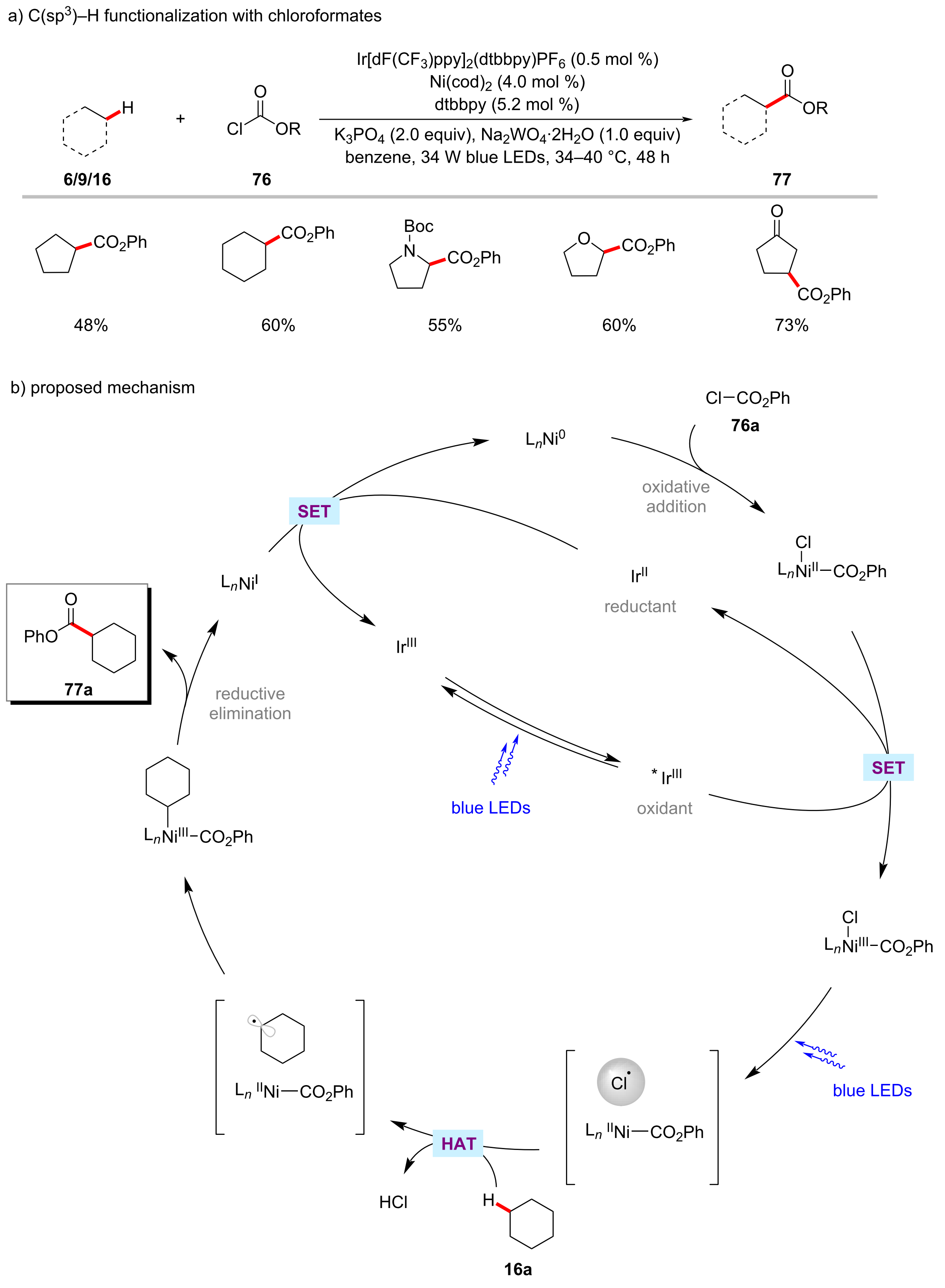
a) C(sp3)–H functionalization with chloroformates
H
+
O
Cl
OR
Ir[dF(CF3)ppy]2(dtbbpy)PF6 (0.5 mol %)
Ni(cod)2 (4.0 mol %)
dtbbpy (5.2 mol %)
K3PO4 (2.0 equiv), Na2WO4·2H2O (1.0 equiv)
benzene, 34 W blue LEDs, 34–40 °C, 48 h
O
OR
6/9/16
76
77
CO2Ph
48%
CO2Ph
60%
Boc
N
CO2Ph
55%
O
CO2Ph
60%
O
CO2Ph
73%
b) proposed mechanism
Cl–CO2Ph
76a
LnNi0
oxidative addition
Cl
LnNiII–CO2Ph
SET
LnNiI
IrII
reductant
IrIII
O
PhO
77a
reductive elimination
blue LEDs
*IrIII
oxidant
SET
LnNiIII–CO2Ph
Cl
LnNiIII–CO2Ph
blue LEDs
Cl•
Ln IINi—CO2Ph
Ln IINi—CO2Ph
HAT
HCl
H
16a

Scheme 39: Photoredox and nickel-catalyzed C(sp^3)–H esterification with chloroformates.

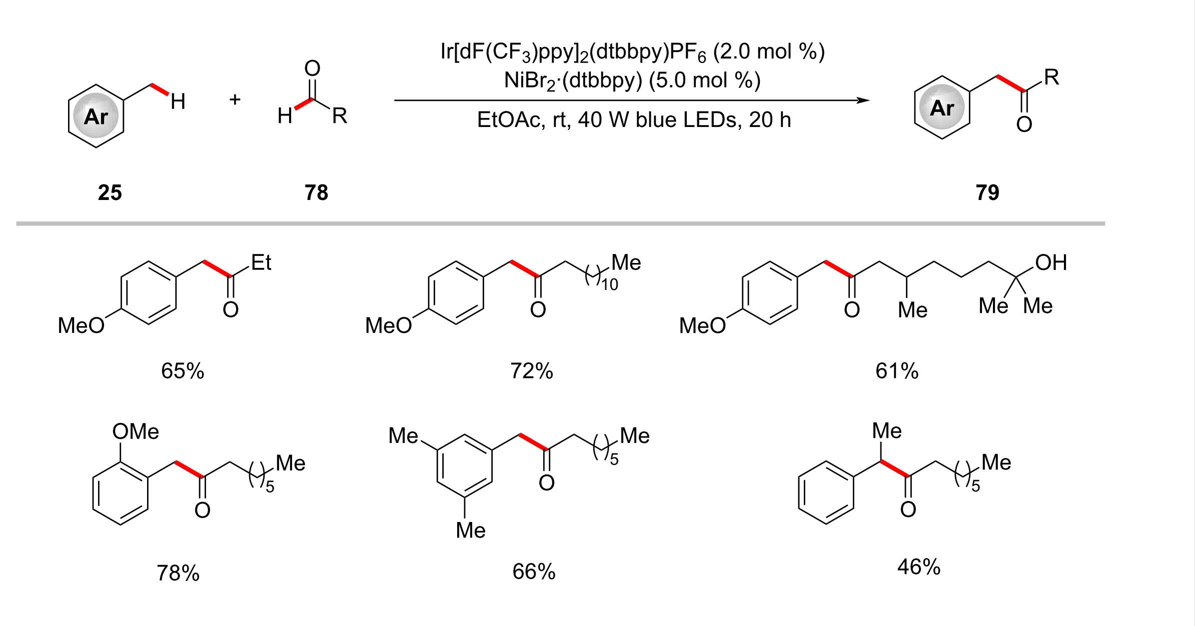

Scheme 40: Photoredox nickel-catalyzed dehydrogenative coupling of benzylic and aldehydic C–H bonds.

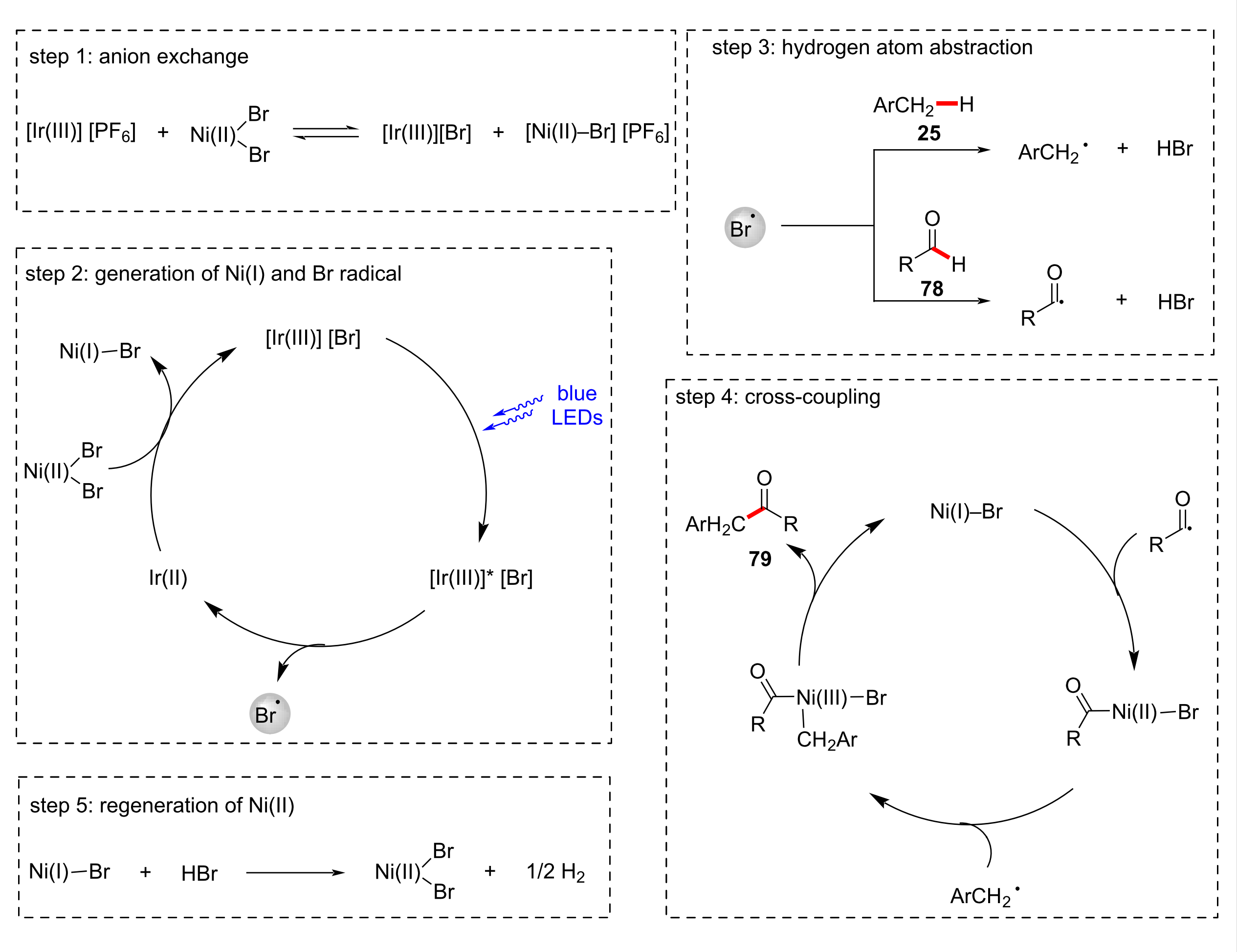

Figure 18: Proposed reaction pathway for the photoredox nickel-catalyzed dehydrogenative coupling of benzylic and aldehydic C–H bonds.

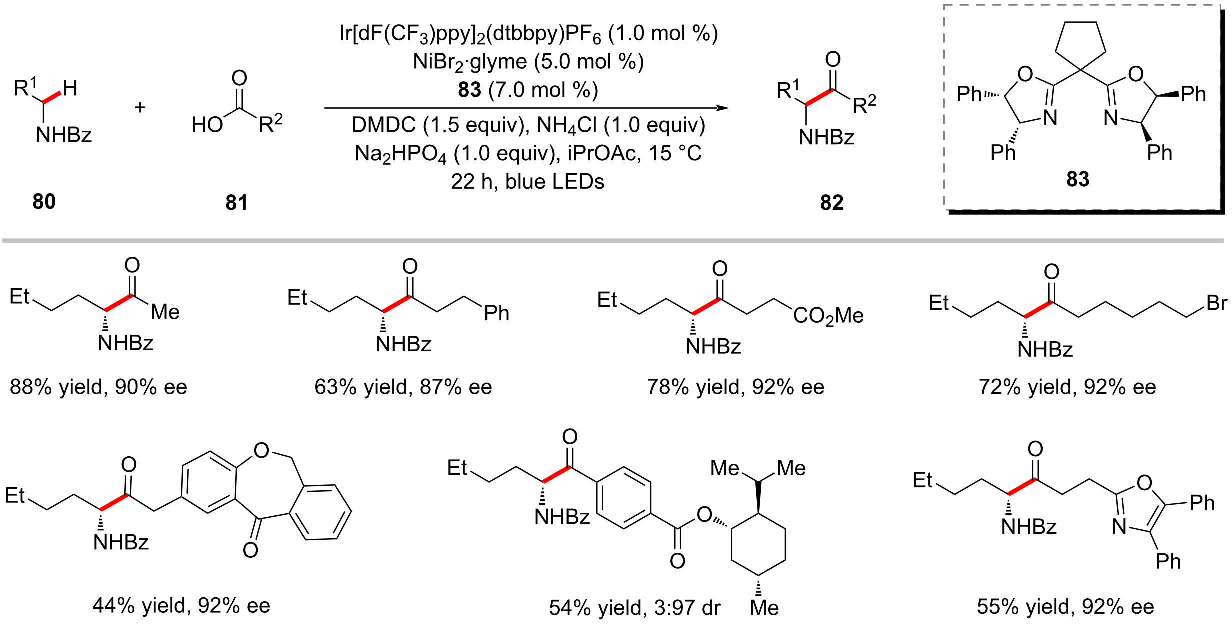

Ir[dF(CF3)ppy]2(dtbbpy)PF6 (1.0 mol %)
NiBr2·glyme (5.0 mol %)
83 (7.0 mol %)
DMDC (1.5 equiv), NH4Cl (1.0 equiv)
Na2HPO4 (1.0 equiv), iPrOAc, 15 °C
22 h, blue LEDs
80
81
82
83
88% yield, 90% ee
63% yield, 87% ee
78% yield, 92% ee
72% yield, 92% ee
44% yield, 92% ee
54% yield, 3:97 dr
55% yield, 92% ee

Scheme 41: Photoredox nickel-catalyzed enantioselective acylation of α-amino C(sp^3)–H bonds with carboxylic acids.

served for carboxylic acid substrates **81** with different steric properties. Similarly, amine substrates **80** with diverse substitution patterns and functional groups were well tolerated to provide the desired products in optimal yields. The proposed mechanism involves the cleavage of the C(sp^3)–H bond by a photo-generated bromine radical to give the carbon-centered alkyl radical, which subsequently engages in the nickel-catalyzed enantioselective acylation.

Amides were also found to be competent acyl surrogates in the photoredox nickel-catalyzed direct C(sp^3)–H acylation reactions as reported by Hong and co-workers (Scheme 42) [125]. Here, the two challenging bonds, the amide C–N and alkane C(sp^3)–H were activated under mild photoredox reaction conditions. Among the various tested amides, *N*-acylsuccinimides **84** were found to be superior acyl surrogates to give the desired products **85** in high yields. Based on the detailed computational

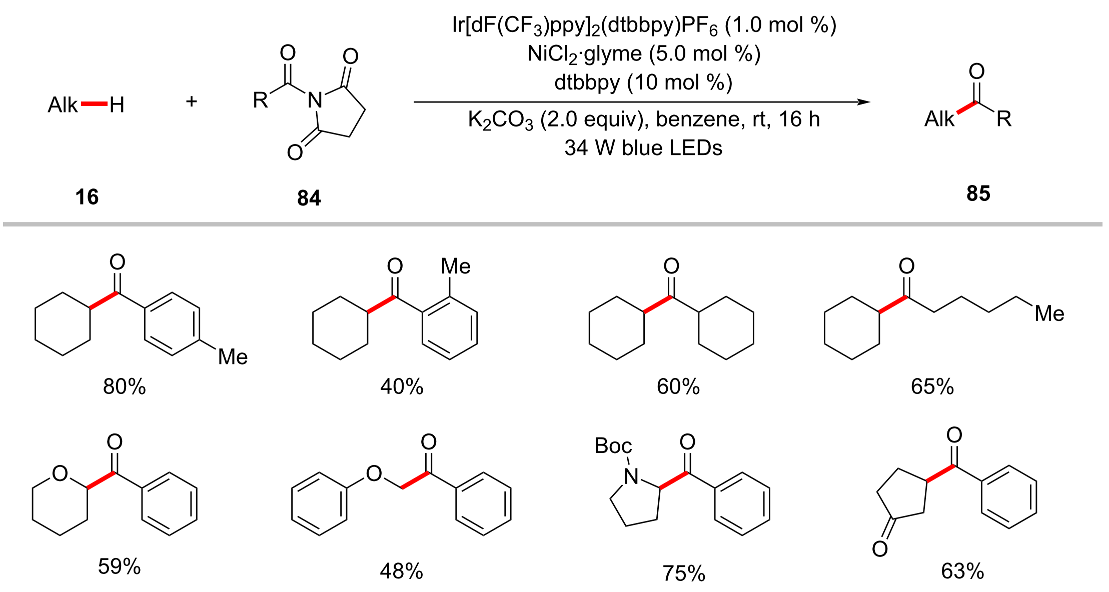

Ir[dF(CF3)ppy]2(dtbbpy)PF6 (1.0 mol %)
NiCl2·glyme (5.0 mol %)
dtbbpy (10 mol %)
K2CO3 (2.0 equiv), benzene, rt, 16 h
34 W blue LEDs
16
84
85
80%
40%
60%
65%
59%
48%
75%
63%

Scheme 42: Nickel-catalyzed C(sp^3)–H acylation with *N*-acylsuccinimides.

and experimental mechanistic studies, the authors proposed a catalytic cycle which involves the C–H cleavage prior to the oxidative addition of *N*-acylsuccinimide (Figure 19) [125].

The acylation of benzylic C–H bonds with acid chlorides **45** by means of photoredox nickel catalysis was demonstrated by Rueping in 2020 (Scheme 43) [126]. Using substituted benzophenone 4-benzoylphenyl acetate as the photocatalyst, a variety of substituted methylbenzenes **25** were transformed into unsymmetrical ketones **79** under visible light irradiation. Both aromatic and aliphatic acid chlorides **45** were well tolerated under the catalytic conditions to offer the ketone products **79**. The authors also showed that acid anhydrides could also be used as viable acylating reagents under the optimized reaction conditions, however, with less efficacy than acid chlorides.

A related process involved the conversion of toluene into 1,2-arylethanone using 4,4'-dichlorobenzophenone (**27**) as the photocatalyst and $NiCl_2$·DME as the nickel catalyst under UVA irradiation (Scheme 44) [127]. Here, *N*-acylsuccinimides **84** were used as the acyl source. Notably, *ortho*-substituted methylbenzenes gave lower yields due to steric effects.

The photoredox nickel-catalyzed C–H acylation was not limited to C(sp^3)–H functionalization. Gu, Yuan and co-workers hence succeeded in preparing 3-acylindoles **88** from indole **86** and α-oxoacids **87** at room temperature by means of iridium photocatalysis and nickel catalysis under blue light irradiation (Scheme 45) [128]. Among the tested several commercially available photocatalysts, Ir[dF(CF_3)ppy]$_2$(dtbbpy)PF_6 was found to provide the desired products in good yields.

Aldehyde C–H functionalization

Inspired by their earlier contributions on HAT-metallaphotoredox-mediated C(sp^3)–H functionalizations [53,54], the MacMillan group reported a photoredox nickel-catalyzed aldehyde C–H arylation, vinylation, or alkylation [129]. The ketone-

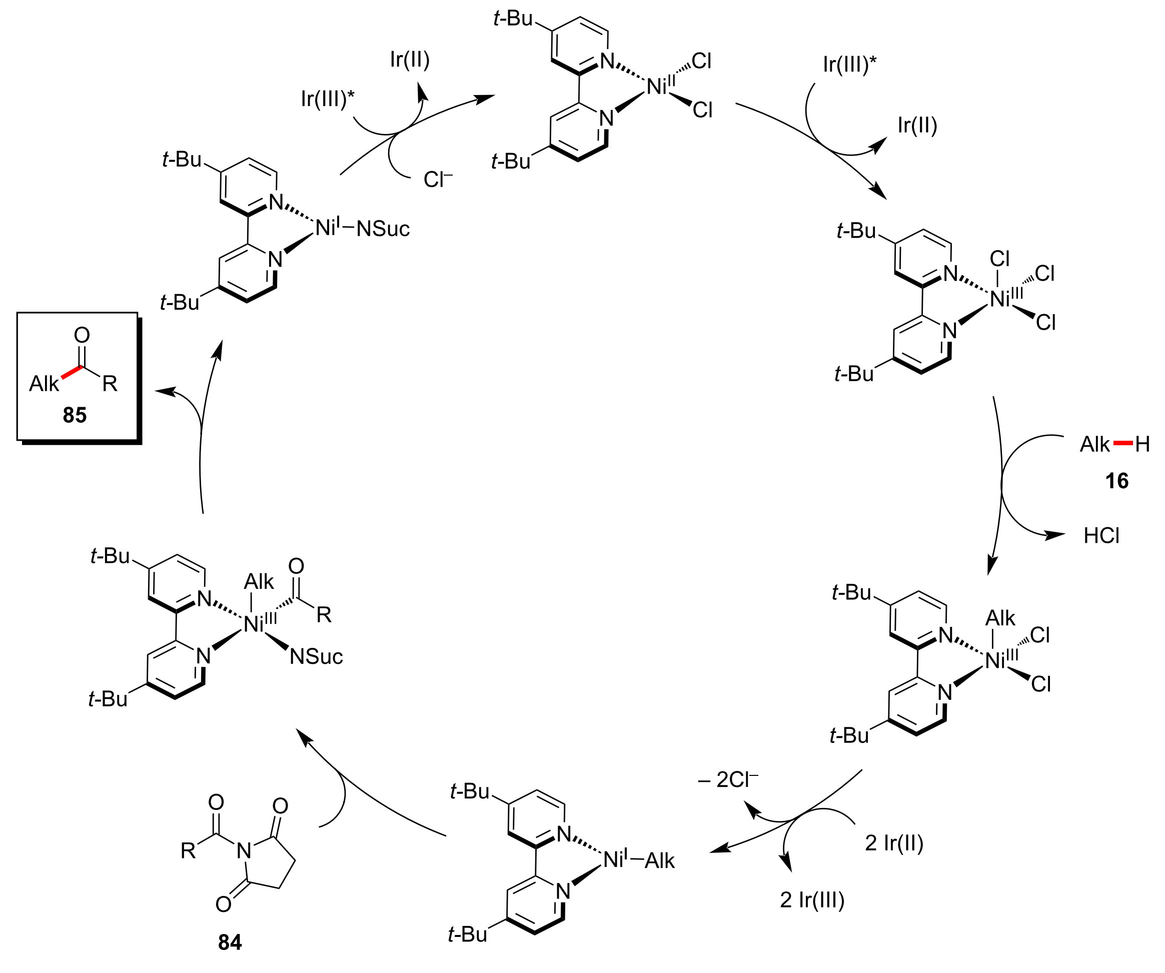

Figure 19: Proposed mechanism for the nickel-catalyzed C(sp^3)–H acylation with *N*-acylsuccinimides.

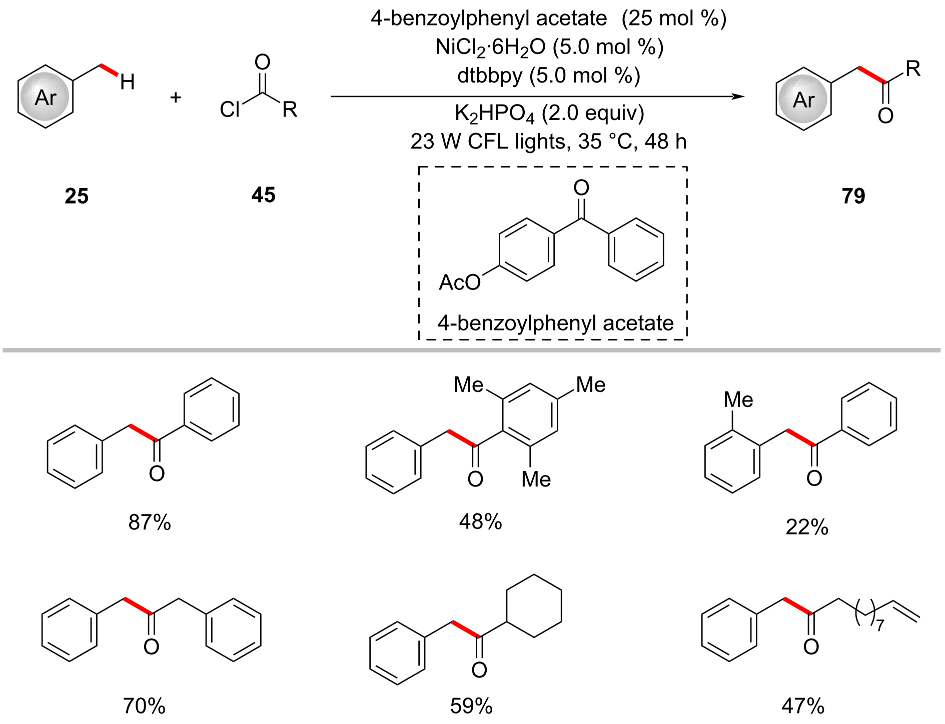
4-benzoylphenyl acetate (25 mol %)
NiCl2·6H2O (5.0 mol %)
dtbbpy (5.0 mol %)
K2HPO4 (2.0 equiv)
23 W CFL lights, 35 °C, 48 h
Ar
H
Cl
R
O
25
45
79
AcO
4-benzoylphenyl acetate
Me
87%
48%
22%
70%
59%
47%
7

Scheme 43: Nickel-catalyzed benzylic C–H functionalization with acid chlorides **45**.

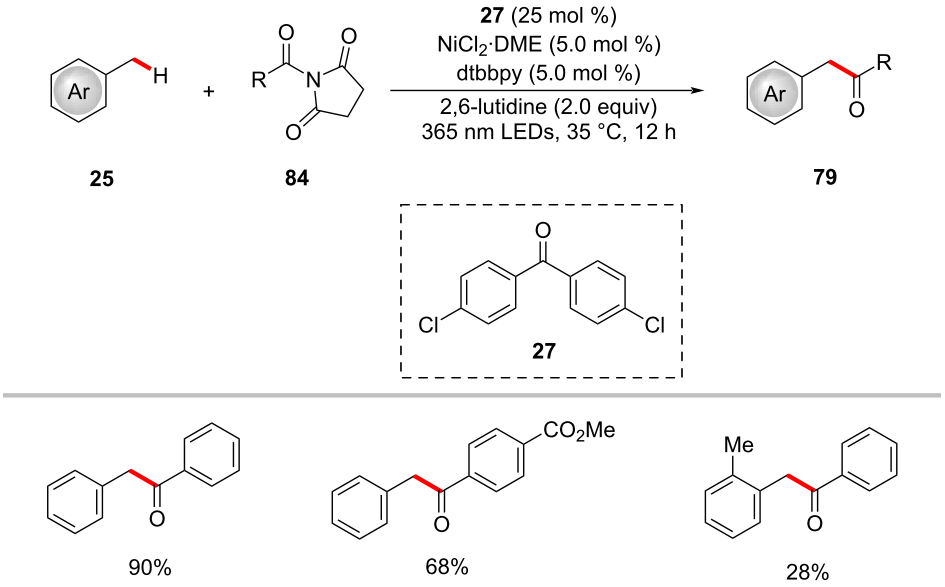
27 (25 mol %)
NiCl2·DME (5.0 mol %)
dtbbpy (5.0 mol %)
2,6-lutidine (2.0 equiv)
365 nm LEDs, 35 °C, 12 h
Ar
H
R
N
O
25
84
79
Cl
27
CO2Me
Me
90%
68%
28%

Scheme 44: Photoredox nickel-catalyzed benzylic C–H acylation with *N*-acylsuccinimides **84**.

forming reaction was conveniently realized by the reaction of aldehydes **89** with aryl, alkenyl, or alkyl bromides in the presence of Ir[dF(CF_3)ppy]$_2$(dtbbpy)PF_6, $NiBr_2$·dtbbpy, quinuclidine, and K_2CO_3 in dioxane under blue light irradiation at ambient reaction temperature (Scheme 46) [129]. Besides aryl bromides, alkenyl and alkyl bromides were found to be viable substrates and showcased the catalytic conditions versatility. Based on their experiments, the authors proposed a working mode for this protocol involving a triple catalysis mechanism (Figure 20) [129]. The synergistic merger of photoredox, nickel,

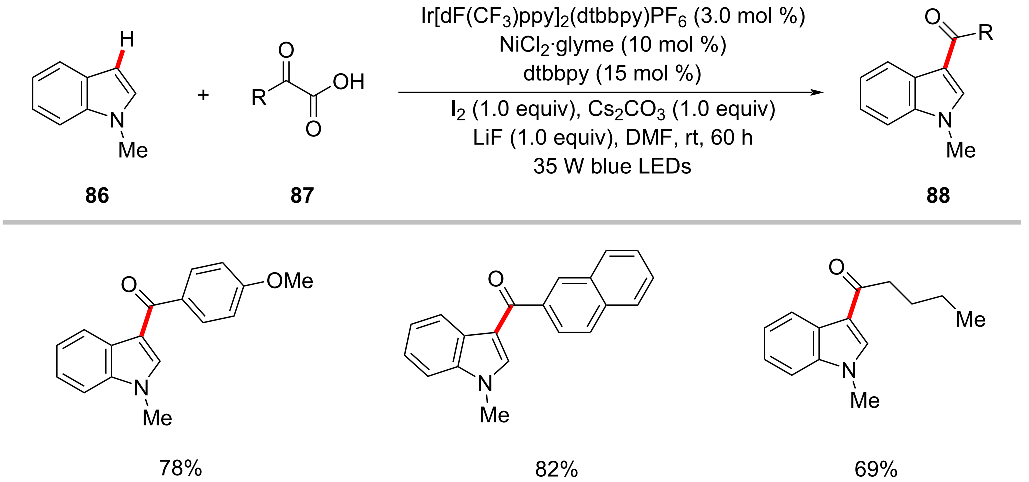
Ir[dF(CF3)ppy]2(dtbbpy)PF6 (3.0 mol %)
NiCl2·glyme (10 mol %)
dtbbpy (15 mol %)
I2 (1.0 equiv), Cs2CO3 (1.0 equiv)
LiF (1.0 equiv), DMF, rt, 60 h
35 W blue LEDs
86
87
88
78%
82%
69%

Scheme 45: Photoredox nickel-catalyzed acylation of indoles **86** with α-oxoacids **87**.

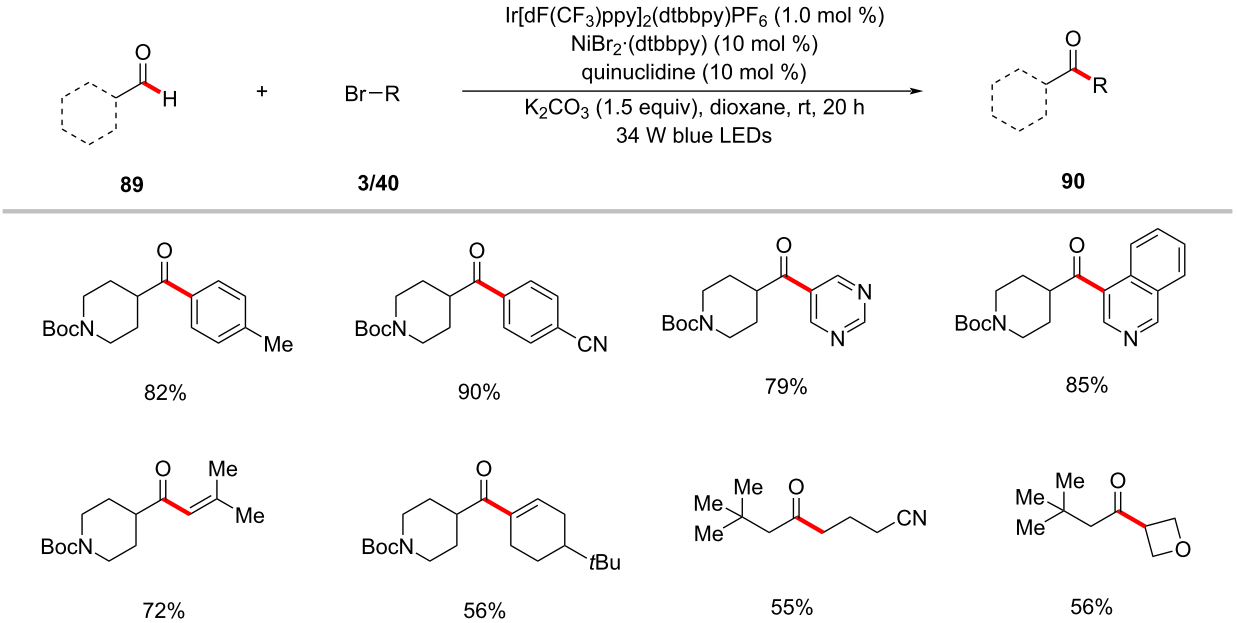
Ir[dF(CF3)ppy]2(dtbbpy)PF6 (1.0 mol %)
NiBr2·(dtbbpy) (10 mol %)
quinuclidine (10 mol %)
K2CO3 (1.5 equiv), dioxane, rt, 20 h
34 W blue LEDs
89
3/40
90
82%
90%
79%
85%
72%
56%
55%
56%

Scheme 46: Nickel-catalyzed aldehyde C–H functionalization.

and HAT catalytic cycles enabled the aldehyde C–H functionalization. Subsequently, a related transformation was also reported by Liu and co-workers [130]. Here, stoichiometric quantities of quinuclidine were used to get optimal results.

Carboxylation

Over the past few decades, significant attention has been devoted to exploit carbon dioxide (CO_2) as the C1 resource [131,132]. In particular, the C–H functionalization with CO_2 is considered an attractive organic synthesis strategy in terms of sustainable aspects [133-135]. In 2019, Murakami and co-workers reported on the photoinduced carboxylation of $C(sp^3)$–H bonds with CO_2 under 1 atm pressure [136]. Here, the authors discovered that the combination of xanthone as the photocatalyst and $NiCl_2·6H_2O$ as the nickel catalyst can efficiently catalyze the transformation of methylarenes **25** into arylacetic acids **91** under UV light irradiation (Scheme 47). Furthermore, the authors also applied this methodology to functionalize unactivated alkanes such as cyclohexane, cyclopentanes, and *n*-pentane. The proposed catalytic cycle is initiated by the absorption of light by xanthone PC **21-I** to get excited (Figure 21) [136]. The excited ketone PC undergoes a HAT

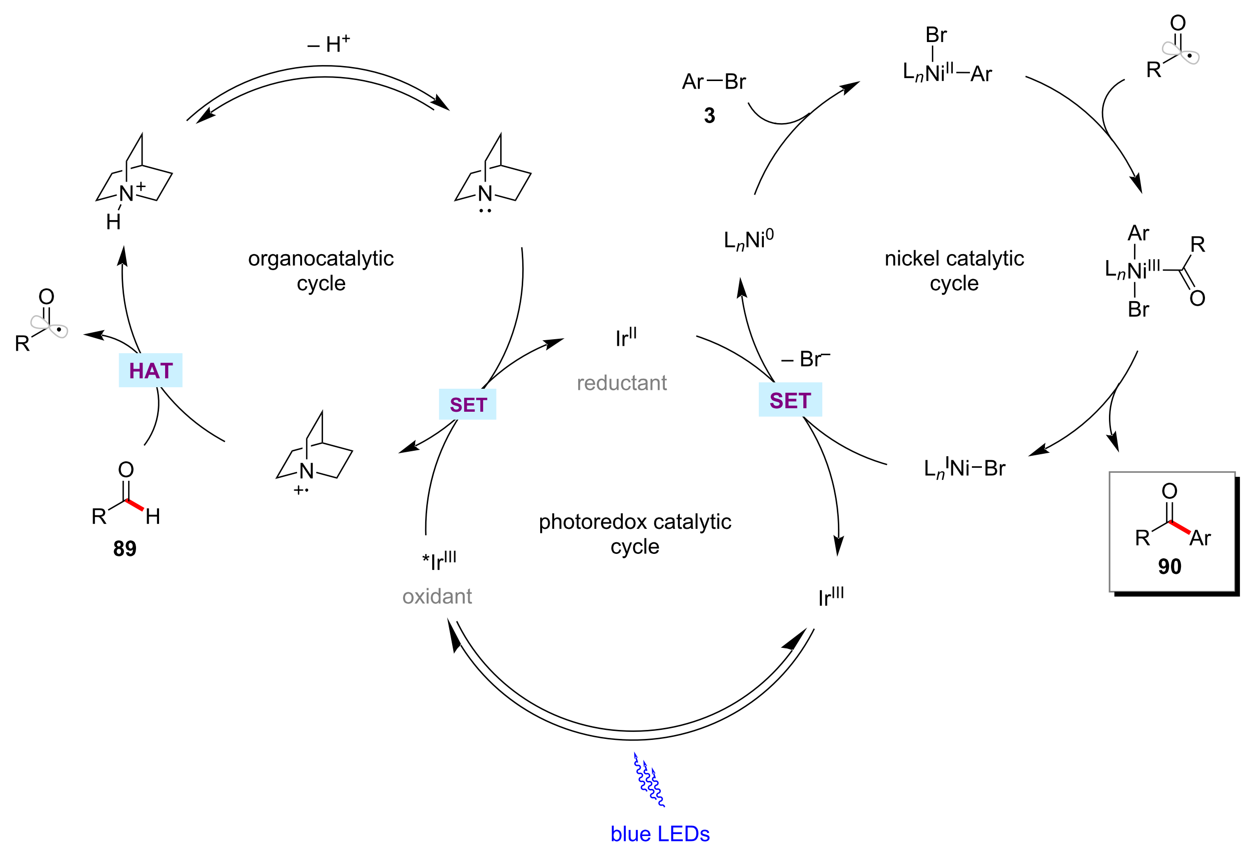
– H+
organocatalytic cycle
HAT
SET
89
Ir^{II}
reductant
*Ir^{III}
oxidant
photoredox catalytic cycle
blue LEDs
Ar–Br
3
L$_n$Ni^0
L$_n$Ni^{II}–Ar
nickel catalytic cycle
– Br−
SET
L$_n$^{I}Ni–Br
Ir^{III}
90

Figure 20: Proposed catalytic cycle for the photoredox nickel-catalyzed aldehyde C–H functionalization.

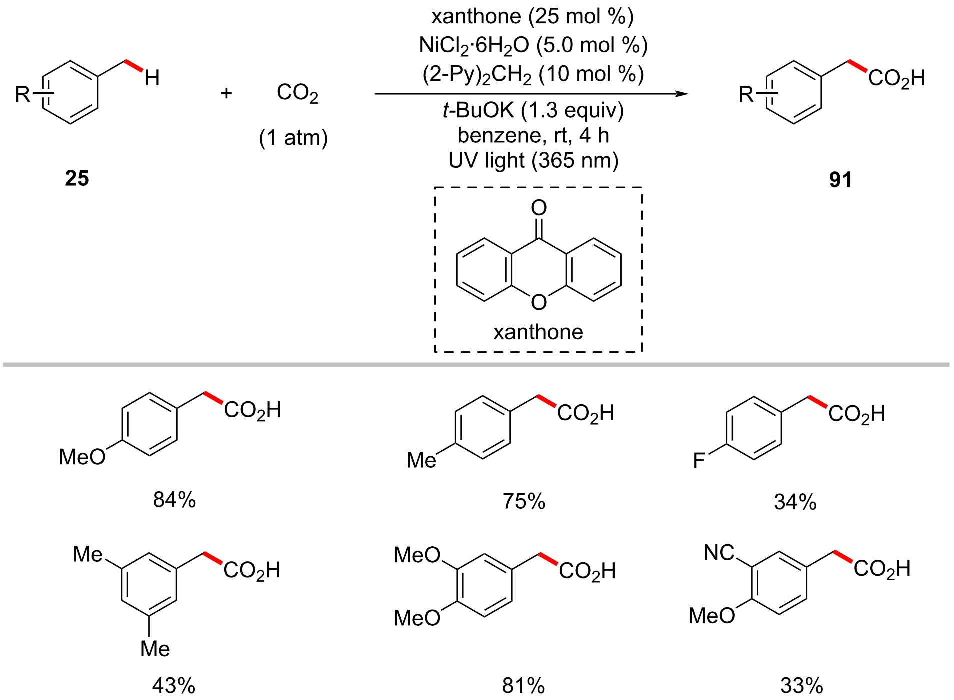
25
CO$_2$
(1 atm)
xanthone (25 mol %)
NiCl$_2$·6H$_2$O (5.0 mol %)
(2-Py)$_2$CH$_2$ (10 mol %)
t-BuOK (1.3 equiv)
benzene, rt, 4 h
UV light (365 nm)
xanthone
91
84%
75%
34%
43%
81%
33%

Scheme 47: Photoredox carboxylation of methylbenzenes with CO_2.

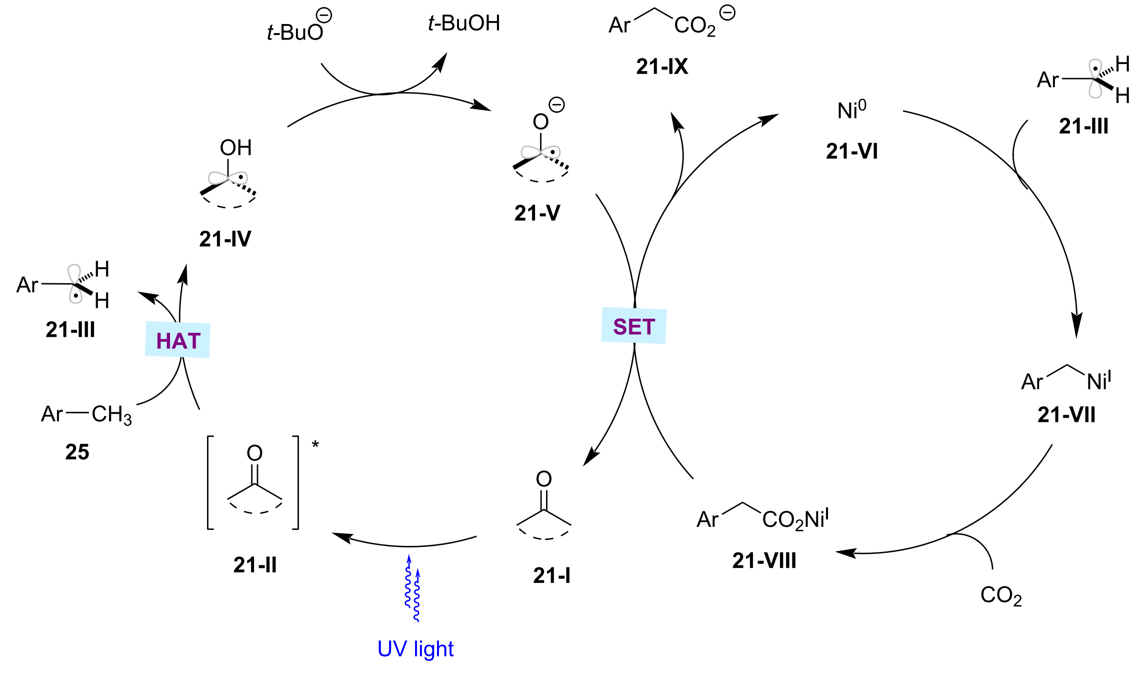

Figure 21: Proposed mechanism for the photoredox carboxylation of methylbenzenes with CO_2.

process with the benzylic C–H substrate to generate a pair of ketyl radical **21-IV** and benzylic radical **21-III**. At the same time, the in situ-generated nickel(0) complex **21-VI** combines with the benzylic radical **21-III**, followed by CO_2 insertion resulting in the nickel(I) carboxylate complex **21-VIII**. The ketyl radical is deprotonated by the base, and then undergoes a SET with nickel(I) carboxylate complex **21-VIII** to regenerate the nickel(0) species **21-VI** and the carboxylate product **21-IX**.

Olefin difunctionalization

Nickel-catalyzed alkene 1,2-difunctionalization is considered as useful method for preparing complex molecules in a single-step reaction [137-139]. In this aspect, the groups by Kong [140] and Molander [141] independently demonstrated photoredox/nickel-catalyzed approaches to olefin difunctionalizations involving $C(sp^3)$–H activation. Thus, Kong devised a synthetic method combining nickel catalysis with tetrabutylammonium decatungstate (TBADT) as photocatalyst for the three component reaction of alkanes **16**, alkenes **92**, and aryl bromides **3** (Scheme 48) [140]. Here, TBADT enables the generation of alkyl radicals from various alkane substrates via a HAT process under near-ultraviolet light irradiation. Both cyclic and linear alkanes were found to be suitable under the reaction conditions. Linear alkanes were preferentially functionalized at the 2-position due to the less steric hindrance. In addition to alkanes, a variety of ethers and amines were also compatible and selectively functionalized at the α-heteroatom positions in moderate to good yields and excellent regioselectivity. Interestingly, ketones and silanes were also found to be compatible to give the desired three-component coupling products. Similarly, the scope of aryl bromides **3** and alkenes **92** were found to be broad. A possible catalytic cycle was proposed to account for the mechanism of the reaction (Figure 22) [140]. Photoexcited decatungstate **22-II** undergoes a HAT process with the $C(sp^3)$–H substrate to form a carbon-centered radical species **22-III** and reduced decatungstate **22-IV**. The thus formed alkyl radical **22-III** adds to the alkene **92** affording the radical adduct **22-VI**, which is intercepted by the nickel(0) species **22-X** to generate alkyl-nickel(I) intermediate **22-VII**. Oxidative addition of the aryl bromide **3** to intermediate **22-VII** results in (alkyl)(aryl)nickel(III) intermediate **22-VIII**, which subsequently undergoes reductive elimination to deliver the desired cross-coupled product **93** and the nickel(I) species **22-IX**. A SET process between **22-IX** and **22-V** regenerates the reduced decatungstate **22-IV** and the active nickel(0) catalyst **22-X**.

In a recent report, Gutierrez and Molander realized the three-component dicarbofunctionalization of alkenes by means of the combination of phororedox HAT catalysis and nickel catalysis [141]. Here, a substituted diaryl ketone, 4-(4-methoxybenzoyl)benzonitrile (**96**) serves as the HAT photocatalyst to activate the $C(sp^3)$–H bonds for olefin functionalization. It was identified that the use of nonpolar, aprotic solvents, such as benzene and α,α,α-trifluorotoluene (TFT) is critical for the formation of the desired products **95**. The scope of the transformation was demonstrated with a variety of activated alkenes **94**, alkyl C–H

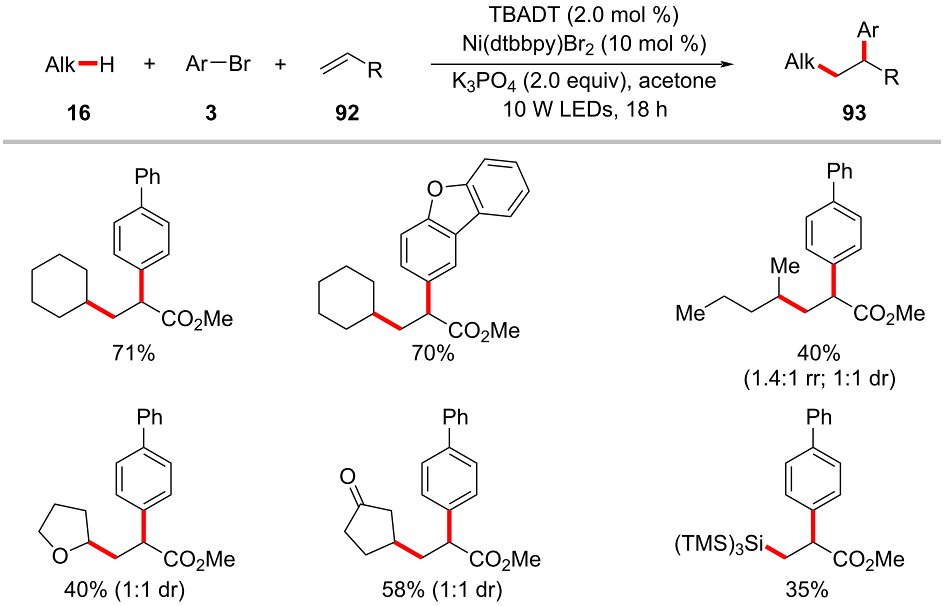
TBADT (2.0 mol %)
Ni(dtbbpy)Br2 (10 mol %)
K3PO4 (2.0 equiv), acetone
10 W LEDs, 18 h
Alk–H 16
Ar–Br 3
92
93
71%
70%
40% (1.4:1 rr; 1:1 dr)
40% (1:1 dr)
58% (1:1 dr)
35%

Scheme 48: Decatungstate photo-HAT and nickel catalysis enabled alkene difunctionalization.

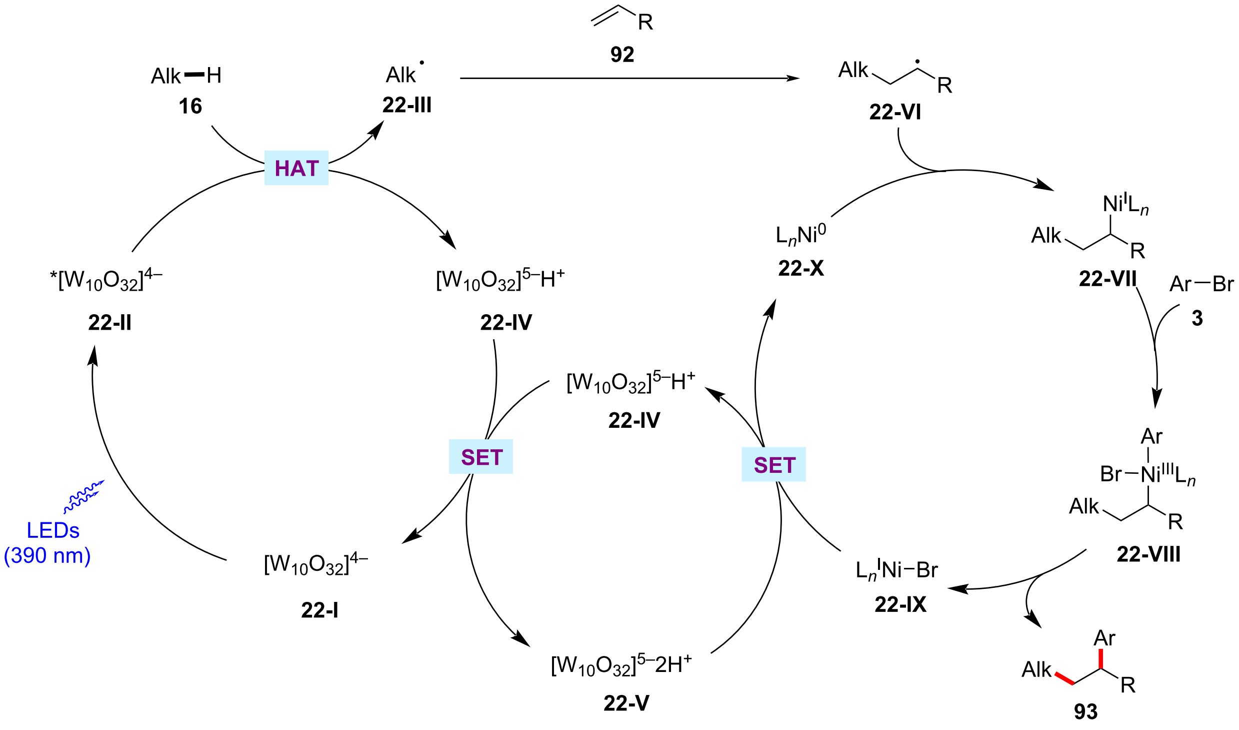
92
Alk–H
16
Alk•
22-III
22-VI
HAT
*[W10O32]4–
22-II
[W10O32]5–H+
22-IV
LnNi0
22-X
NiILn
22-VII
Ar–Br
3
22-IV
SET
SET
LEDs
(390 nm)
[W10O32]4–
22-I
Br–NiIIILn
22-VIII
LnINi–Br
22-IX
[W10O32]5–2H+
22-V
93

Figure 22: Proposed catalytic cycle for the decatungstate photo-HAT and nickel catalysis enabled alkene difunctionalization.

substrates **16**, and aryl bromides **3**. In general, the products were obtained in moderate to good yields and good regioselectivities (Scheme 49) [141]. The detailed experimental and computational studies highlight the involvement of hydrogen bonding assistance during the radical addition to olefine. The proposed reaction mechanism has two synergistic catalytic cycles, namely a photocatalytic cycle and a nickel catalytic cycle (Figure 23). The photoexcitation of the ketone PC **96** results in the triplet-state diradical **23-I**. A HAT process between **23-I** and the alkane substrate generates the desired car-

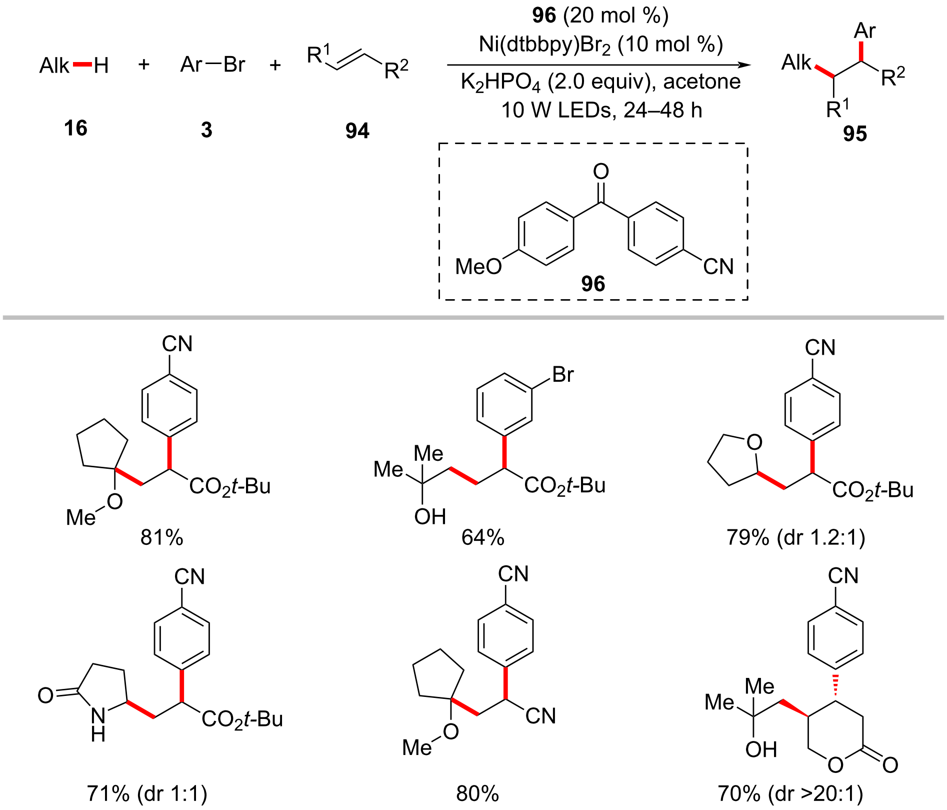
Alk—H
16
Ar—Br
3
94
96 (20 mol %)
Ni(dtbbpy)Br2 (10 mol %)
K2HPO4 (2.0 equiv), acetone
10 W LEDs, 24–48 h
95
MeO
CN
96
81%
64%
79% (dr 1.2:1)
71% (dr 1:1)
80%
70% (dr >20:1)

Scheme 49: Diaryl ketone HAT catalysis and nickel catalysis enabled dicarbofunctionalization of alkenes.

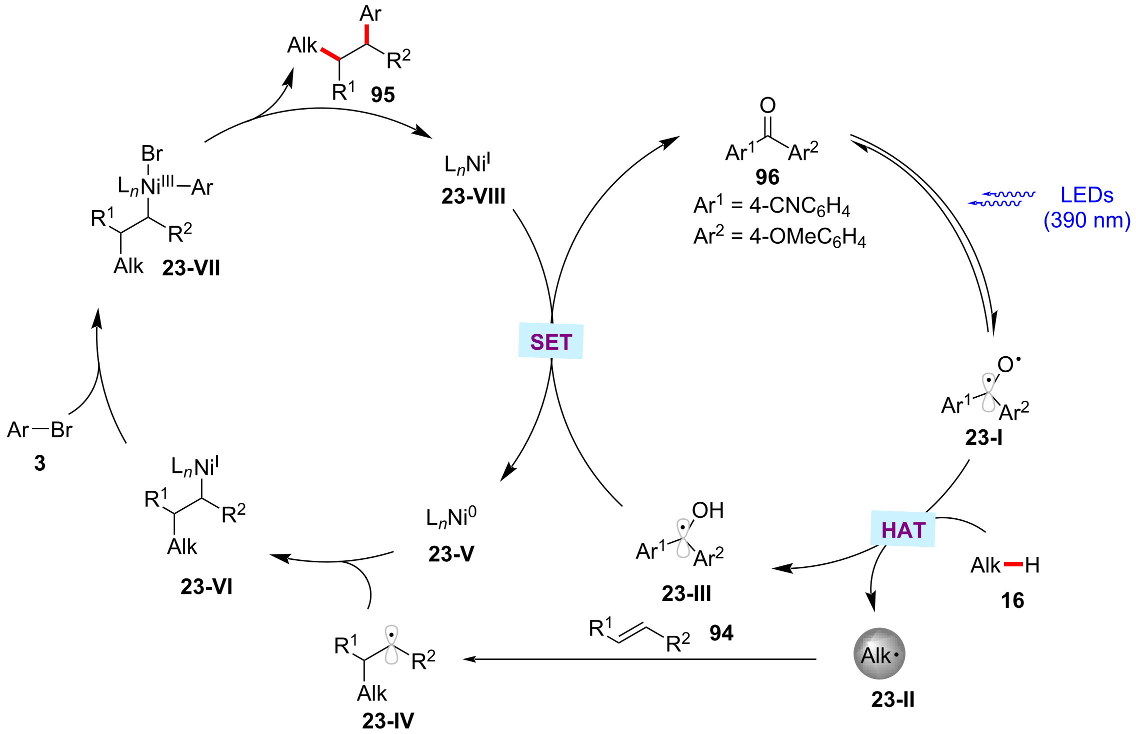
95
LnNiI
23-VIII
LnNiIII—Ar
23-VII
96
Ar1 = 4-CNC6H4
Ar2 = 4-OMeC6H4
LEDs
(390 nm)
SET
23-I
HAT
Alk—H
16
Ar—Br
3
LnNiI
23-VI
LnNi0
23-V
23-III
Alk·
23-II
94
23-IV

Figure 23: Proposed catalytic mechanism for the diaryl ketone HAT catalysis and nickel catalysis enabled dicarbofunctionalization of alkenes.

bon-centered radical **23-II** with concomitant formation of ketyl radical species **23-III**. The thus formed alkyl radical **23-II** undergoes Giese addition to alkene **94** resulting in the radical adduct **23-IV**. The radical adduct **23-IV** is captured by nickel(0) species **23-V** followed by oxidative addition to aryl bromide **3** to give the nickel(III)(alkyl)(aryl) intermediate **23-VII**. Facile C–C-bond forming reductive elimination of **23-VII** delivers the desired product **95** and nickel(I) species **23-VIII**. A SET between **23-VIII** and **23-III** regenerates the active nickel(0) species **23-V** and the ketone PC **96**. Alternatively, the nickel(III) intermediate **23-VII** could also be formed via an oxidative addition of the nickel(0) species **23-V** to aryl bromide **3** followed by the reaction with alkyl radical **23-IV**.

Conclusion

During the last decade, metallaphotoredox catalysis has emerged as an increasingly viable tool in organic synthesis for C–H functionalization. Although significant advances have been achieved with precious palladium catalysts, recently, considerable attention has been devoted to using earth-abundant, less toxic, and cost-effective nickel catalysts. It is clear from the wealth of the different transformations discussed in this review, the merger of photoredox catalysis and nickel catalysis offers a range of new tools for organic synthesis (Scheme 50). The impressive array of transformations involving C(sp^3)–H functionalizations, including arylation, alkylation, alkenylation, allylation, acylation, and carboxylation, highlights their potential utility in organic synthesis. Further, the mild nature of the reaction conditions enables a broad substrate scope, functional group tolerance, and opportunities for late-stage diversification of complex molecules. Despite the significant advances, the photoredox-mediated nickel-catalyzed C–H functionalization is still in its infancy. Thus far, expensive iridium-based complexes are the most common photocatalysts and are essential to achieve satisfactory outcomes; less expensive organic photocatalysts in nickel-catalyzed transformations are less explored. Further, the major challenges of C–H functionalization, including site specificity and functionalization of stronger C–H bonds, remain unexplored. Furthermore, examples of enantioselective C–H functionalizations are scarce and present new opportunities for further exploration. In consideration of the sustainable nature of C–H activation by photoredox nickel catalysis, further exciting developments are expected in this rapidly evolving research area.

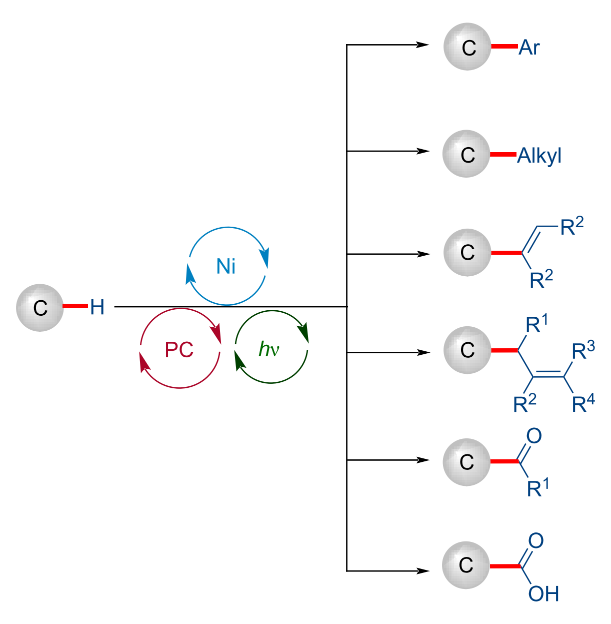

Scheme 50: Overview of photoredox nickel-catalyzed C–H functionalizations.

Funding

We are grateful to the Science and Engineering Research Board (SERB) India (Grant no SRG/2020/000161) and Indian Institute of Technology Tirupati (CHY/21-22/001/NFSG/PGAN) for financial support.

ORCID® iDs

Lusina Mantry - https://orcid.org/0000-0002-6046-753X
Rajaram Maayuri - https://orcid.org/0000-0002-4224-9918
Vikash Kumar - https://orcid.org/0000-0002-2143-0144
Parthasarathy Gandeepan - https://orcid.org/0000-0002-2483-7353

References

1. Boström, J.; Brown, D. G.; Young, R. J.; Keserü, G. M. *Nat. Rev. Drug Discovery* **2018,** *17,* 709–727. doi:10.1038/nrd.2018.116
2. Dreher, S. D. *React. Chem. Eng.* **2019,** *4,* 1530–1535. doi:10.1039/c9re00067d
3. Blakemore, D. C.; Castro, L.; Churcher, I.; Rees, D. C.; Thomas, A. W.; Wilson, D. M.; Wood, A. *Nat. Chem.* **2018,** *10,* 383–394. doi:10.1038/s41557-018-0021-z
4. Hayler, J. D.; Leahy, D. K.; Simmons, E. M. *Organometallics* **2019,** *38,* 36–46. doi:10.1021/acs.organomet.8b00566
5. Johansson Seechurn, C. C. C.; Kitching, M. O.; Colacot, T. J.; Snieckus, V. *Angew. Chem., Int. Ed.* **2012,** *51,* 5062–5085. doi:10.1002/anie.201107017
6. Heck, R. F. *Synlett* **2006,** 2855–2860. doi:10.1055/s-2006-951536
7. Heck, R. F. *Org. React.* **1982,** 345–390. doi:10.1002/0471264180.or027.02
8. Mizoroki, T.; Mori, K.; Ozaki, A. *Bull. Chem. Soc. Jpn.* **1971,** *44,* 581. doi:10.1246/bcsj.44.581
9. Suzuki, A. *Angew. Chem., Int. Ed.* **2011,** *50,* 6722–6737. doi:10.1002/anie.201101379
10. Miyaura, N.; Suzuki, A. *Chem. Rev.* **1995,** *95,* 2457–2483. doi:10.1021/cr00039a007
11. Suzuki, A. *J. Organomet. Chem.* **1999,** *576,* 147–168. doi:10.1016/s0022-328x(98)01055-9

12. Ruiz-Castillo, P.; Buchwald, S. L. *Chem. Rev.* **2016,** *116,* 12564–12649. doi:10.1021/acs.chemrev.6b00512
13. Hartwig, J. F. *Acc. Chem. Res.* **2008,** *41,* 1534–1544. doi:10.1021/ar800098p
14. Negishi, E.-i. *Angew. Chem., Int. Ed.* **2011,** *50,* 6738–6764. doi:10.1002/anie.201101380
15. Negishi, E. *Acc. Chem. Res.* **1982,** *15,* 340–348. doi:10.1021/ar00083a001
16. Stille, J. K. *Angew. Chem., Int. Ed. Engl.* **1986,** *25,* 508–524. doi:10.1002/anie.198605081
17. Sonogashira, K.; Tohda, Y.; Hagihara, N. *Tetrahedron Lett.* **1975,** *16,* 4467–4470. doi:10.1016/s0040-4039(00)91094-3
18. de Meijere, A.; Diederich, F., Eds. *Metal-Catalyzed Cross-Coupling Reactions,* 2nd ed.; Wiley-VCH: Weinheim, Germany, 2004. doi:10.1002/9783527619535
19. Diederich, F.; Stang, P. J., Eds. *Metal-Catalyzed Cross-Coupling Reactions;* Wiley-VCH: Weinheim, Germany, 1998. doi:10.1002/9783527612222
20. Ackermann, L., Ed. *Modern Arylation Methods;* Wiley-VCH: Weinheim, Germany, 2009. doi:10.1002/9783527627325
21. Brown, D. G.; Boström, J. *J. Med. Chem.* **2016,** *59,* 4443–4458. doi:10.1021/acs.jmedchem.5b01409
22. Buskes, M. J.; Blanco, M.-J. *Molecules* **2020,** *25,* 3493. doi:10.3390/molecules25153493
23. Diccianni, J. B.; Diao, T. *Trends Chem.* **2019,** *1,* 830–844. doi:10.1016/j.trechm.2019.08.004
24. Shi, R.; Zhang, Z.; Hu, X. *Acc. Chem. Res.* **2019,** *52,* 1471–1483. doi:10.1021/acs.accounts.9b00118
25. Iwasaki, T.; Kambe, N. *Top. Curr. Chem.* **2016,** *374,* 66. doi:10.1007/s41061-016-0067-6
26. Gandeepan, P.; Müller, T.; Zell, D.; Cera, G.; Warratz, S.; Ackermann, L. *Chem. Rev.* **2019,** *119,* 2192–2452. doi:10.1021/acs.chemrev.8b00507
27. Yamaguchi, J.; Muto, K.; Itami, K. *Top. Curr. Chem.* **2016,** *374,* 55. doi:10.1007/s41061-016-0053-z
28. Castro, L. C. M.; Chatani, N. *Chem. Lett.* **2015,** *44,* 410–421. doi:10.1246/cl.150024
29. Zhang, S.-K.; Samanta, R. C.; Del Vecchio, A.; Ackermann, L. *Chem. – Eur. J.* **2020,** *26,* 10936–10947. doi:10.1002/chem.202001318
30. Tasker, S. Z.; Standley, E. A.; Jamison, T. F. *Nature* **2014,** *509,* 299–309. doi:10.1038/nature13274
31. Fagnoni, M.; Dondi, D.; Ravelli, D.; Albini, A. *Chem. Rev.* **2007,** *107,* 2725–2756. doi:10.1021/cr068352x
32. Narayanam, J. M. R.; Stephenson, C. R. J. *Chem. Soc. Rev.* **2011,** *40,* 102–113. doi:10.1039/b913880n
33. Xuan, J.; Xiao, W.-J. *Angew. Chem., Int. Ed.* **2012,** *51,* 6828–6838. doi:10.1002/anie.201200223
34. Prier, C. K.; Rankic, D. A.; MacMillan, D. W. C. *Chem. Rev.* **2013,** *113,* 5322–5363. doi:10.1021/cr300503r
35. Xi, Y.; Yi, H.; Lei, A. *Org. Biomol. Chem.* **2013,** *11,* 2387–2403. doi:10.1039/c3ob40137e
36. Shaw, M. H.; Twilton, J.; MacMillan, D. W. C. *J. Org. Chem.* **2016,** *81,* 6898–6926. doi:10.1021/acs.joc.6b01449
37. Romero, N. A.; Nicewicz, D. A. *Chem. Rev.* **2016,** *116,* 10075–10166. doi:10.1021/acs.chemrev.6b00057
38. Schultz, D. M.; Yoon, T. P. *Science* **2014,** *343,* 1239176. doi:10.1126/science.1239176
39. Strieth-Kalthoff, F.; James, M. J.; Teders, M.; Pitzer, L.; Glorius, F. *Chem. Soc. Rev.* **2018,** *47,* 7190–7202. doi:10.1039/c8cs00054a
40. Guillemard, L.; Wencel-Delord, J. *Beilstein J. Org. Chem.* **2020,** *16,* 1754–1804. doi:10.3762/bjoc.16.147
41. Milligan, J. A.; Phelan, J. P.; Badir, S. O.; Molander, G. A. *Angew. Chem., Int. Ed.* **2019,** *58,* 6152–6163. doi:10.1002/anie.201809431
42. Cavalcanti, L. N.; Molander, G. A. *Top. Curr. Chem.* **2016,** *374,* 39. doi:10.1007/s41061-016-0037-z
43. Wenger, O. S. *Chem. – Eur. J.* **2021,** *27,* 2270–2278. doi:10.1002/chem.202003974
44. Kariofillis, S. K.; Doyle, A. G. *Acc. Chem. Res.* **2021,** *54,* 988–1000. doi:10.1021/acs.accounts.0c00694
45. Capaldo, L.; Quadri, L. L.; Ravelli, D. *Green Chem.* **2020,** *22,* 3376–3396. doi:10.1039/d0gc01035a
46. Dwivedi, V.; Kalsi, D.; Sundararaju, B. *ChemCatChem* **2019,** *11,* 5160–5187. doi:10.1002/cctc.201900680
47. Twilton, J.; Le, C.; Zhang, P.; Shaw, M. H.; Evans, R. W.; MacMillan, D. W. C. *Nat. Rev. Chem.* **2017,** *1,* 52. doi:10.1038/s41570-017-0052
48. Caplin, M. J.; Foley, D. J. *Chem. Sci.* **2021,** *12,* 4646–4660. doi:10.1039/d1sc00161b
49. Das, J.; Guin, S.; Maiti, D. *Chem. Sci.* **2020,** *11,* 10887–10909. doi:10.1039/d0sc04676k
50. He, C.; Whitehurst, W. G.; Gaunt, M. J. *Chem* **2019,** *5,* 1031–1058. doi:10.1016/j.chempr.2018.12.017
51. Saint-Denis, T. G.; Zhu, R.-Y.; Chen, G.; Wu, Q.-F.; Yu, J.-Q. *Science* **2018,** *359,* eaao4798. doi:10.1126/science.aao4798
52. Baudoin, O. *Chem. Soc. Rev.* **2011,** *40,* 4902–4911. doi:10.1039/c1cs15058h
53. Zuo, Z.; Ahneman, D. T.; Chu, L.; Terrett, J. A.; Doyle, A. G.; MacMillan, D. W. C. *Science* **2014,** *345,* 437–440. doi:10.1126/science.1255525
54. Shaw, M. H.; Shurtleff, V. W.; Terrett, J. A.; Cuthbertson, J. D.; MacMillan, D. W. C. *Science* **2016,** *352,* 1304–1308. doi:10.1126/science.aaf6635
55. Ahneman, D. T.; Doyle, A. G. *Chem. Sci.* **2016,** *7,* 7002–7006. doi:10.1039/c6sc02815b
56. Shields, B. J.; Doyle, A. G. *J. Am. Chem. Soc.* **2016,** *138,* 12719–12722. doi:10.1021/jacs.6b08397
57. Heitz, D. R.; Tellis, J. C.; Molander, G. A. *J. Am. Chem. Soc.* **2016,** *138,* 12715–12718. doi:10.1021/jacs.6b04789
58. Gui, Y.-Y.; Liao, L.-L.; Sun, L.; Zhang, Z.; Ye, J.-H.; Shen, G.; Lu, Z.-P.; Zhou, W.-J.; Yu, D.-G. *Chem. Commun.* **2017,** *53,* 1192–1195. doi:10.1039/c6cc09685a
59. Gui, Y.-Y.; Chen, X.-W.; Zhou, W.-J.; Yu, D.-G. *Synlett* **2017,** *28,* 2581–2586. doi:10.1055/s-0036-1589126
60. Gui, Y.-Y.; Wang, Z.-X.; Zhou, W.-J.; Liao, L.-L.; Song, L.; Yin, Z.-B.; Li, J.; Yu, D.-G. *Asian J. Org. Chem.* **2018,** *7,* 537–541. doi:10.1002/ajoc.201700450
61. Nielsen, M. K.; Shields, B. J.; Liu, J.; Williams, M. J.; Zacuto, M. J.; Doyle, A. G. *Angew. Chem., Int. Ed.* **2017,** *56,* 7191–7194. doi:10.1002/anie.201702079
62. Perry, I. B.; Brewer, T. F.; Sarver, P. J.; Schultz, D. M.; DiRocco, D. A.; MacMillan, D. W. C. *Nature* **2018,** *560,* 70–75. doi:10.1038/s41586-018-0366-x
63. Twilton, J.; Christensen, M.; DiRocco, D. A.; Ruck, R. T.; Davies, I. W.; MacMillan, D. W. C. *Angew. Chem., Int. Ed.* **2018,** *57,* 5369–5373. doi:10.1002/anie.201800749
64. Huang, L.; Rueping, M. *Angew. Chem., Int. Ed.* **2018,** *57,* 10333–10337. doi:10.1002/anie.201805118

65. Zhao, J.; Wu, W.; Sun, J.; Guo, S. *Chem. Soc. Rev.* **2013,** *42,* 5323–5351. doi:10.1039/c3cs35531d
66. Shen, Y.; Gu, Y.; Martin, R. *J. Am. Chem. Soc.* **2018,** *140,* 12200–12209. doi:10.1021/jacs.8b07405
67. Dewanji, A.; Krach, P. E.; Rueping, M. *Angew. Chem., Int. Ed.* **2019,** *58,* 3566–3570. doi:10.1002/anie.201901327
68. Si, X.; Zhang, L.; Hashmi, A. S. K. *Org. Lett.* **2019,** *21,* 6329–6332. doi:10.1021/acs.orglett.9b02226
69. Loup, J.; Dhawa, U.; Pesciaioli, F.; Wencel-Delord, J.; Ackermann, L. *Angew. Chem., Int. Ed.* **2019,** *58,* 12803–12818. doi:10.1002/anie.201904214
70. Woźniak, Ł.; Cramer, N. *Trends Chem.* **2019,** *1,* 471–484. doi:10.1016/j.trechm.2019.03.013
71. Cheng, X.; Lu, H.; Lu, Z. *Nat. Commun.* **2019,** *10,* 3549. doi:10.1038/s41467-019-11392-6
72. Rand, A. W.; Yin, H.; Xu, L.; Giacoboni, J.; Martin-Montero, R.; Romano, C.; Montgomery, J.; Martin, R. *ACS Catal.* **2020,** *10,* 4671–4676. doi:10.1021/acscatal.0c01318
73. Li, H.; Guo, L.; Feng, X.; Huo, L.; Zhu, S.; Chu, L. *Chem. Sci.* **2020,** *11,* 4904–4910. doi:10.1039/d0sc01471k
74. Xiao, J.; Liu, X.; Pan, L.; Shi, C.; Zhang, X.; Zou, J.-J. *ACS Catal.* **2020,** *10,* 12256–12283. doi:10.1021/acscatal.0c03480
75. Mazzanti, S.; Savateev, A. *ChemPlusChem* **2020,** *85,* 2499–2517. doi:10.1002/cplu.202000606
76. Gisbertz, S.; Pieber, B. *ChemPhotoChem* **2020,** *4,* 456–475. doi:10.1002/cptc.202000014
77. Das, S.; Murugesan, K.; Villegas Rodríguez, G. J.; Kaur, J.; Barham, J. P.; Savateev, A.; Antonietti, M.; König, B. *ACS Catal.* **2021,** *11,* 1593–1603. doi:10.1021/acscatal.0c05694
78. Peng, L.; Li, Z.; Yin, G. *Org. Lett.* **2018,** *20,* 1880–1883. doi:10.1021/acs.orglett.8b00413
79. Evano, G.; Theunissen, C. *Angew. Chem., Int. Ed.* **2019,** *58,* 7558–7598. doi:10.1002/anie.201806631
80. Ankade, S. B.; Shabade, A. B.; Soni, V.; Punji, B. *ACS Catal.* **2021,** *11,* 3268–3292. doi:10.1021/acscatal.0c05580
81. Ackermann, L. *Chem. Commun.* **2010,** *46,* 4866–4877. doi:10.1039/c0cc00778a
82. Chen, Z.; Rong, M.-Y.; Nie, J.; Zhu, X.-F.; Shi, B.-F.; Ma, J.-A. *Chem. Soc. Rev.* **2019,** *48,* 4921–4942. doi:10.1039/c9cs00086k
83. Kwiatkowski, M. R.; Alexanian, E. J. *Acc. Chem. Res.* **2019,** *52,* 1134–1144. doi:10.1021/acs.accounts.9b00044
84. Choi, J.; Fu, G. C. *Science* **2017,** *356,* eaaf7230. doi:10.1126/science.aaf7230
85. Le, C.; Liang, Y.; Evans, R. W.; Li, X.; MacMillan, D. W. C. *Nature* **2017,** *547,* 79–83. doi:10.1038/nature22813
86. Zhang, L.; Si, X.; Yang, Y.; Zimmer, M.; Witzel, S.; Sekine, K.; Rudolph, M.; Hashmi, A. S. K. *Angew. Chem., Int. Ed.* **2019,** *58,* 1823–1827. doi:10.1002/anie.201810526
87. Santos, M. S.; Corrêa, A. G.; Paixão, M. W.; König, B. *Adv. Synth. Catal.* **2020,** *362,* 2367–2372. doi:10.1002/adsc.202000167
88. Schönherr, H.; Cernak, T. *Angew. Chem., Int. Ed.* **2013,** *52,* 12256–12267. doi:10.1002/anie.201303207
89. Yan, G.; Borah, A. J.; Wang, L.; Yang, M. *Adv. Synth. Catal.* **2015,** *357,* 1333–1350. doi:10.1002/adsc.201400984
90. Friis, S. D.; Johansson, M. J.; Ackermann, L. *Nat. Chem.* **2020,** *12,* 511–519. doi:10.1038/s41557-020-0475-7
91. Aynetdinova, D.; Callens, M. C.; Hicks, H. B.; Poh, C. Y. X.; Shennan, B. D. A.; Boyd, A. M.; Lim, Z. H.; Leitch, J. A.; Dixon, D. J. *Chem. Soc. Rev.* **2021,** *50,* 5517–5563. doi:10.1039/d0cs00973c
92. Kariofillis, S. K.; Shields, B. J.; Tekle-Smith, M. A.; Zacuto, M. J.; Doyle, A. G. *J. Am. Chem. Soc.* **2020,** *142,* 7683–7689. doi:10.1021/jacs.0c02805
93. Vasilopoulos, A.; Krska, S. W.; Stahl, S. S. *Science* **2021,** *372,* 398–403. doi:10.1126/science.abh2623
94. Thullen, S. M.; Treacy, S. M.; Rovis, T. *J. Am. Chem. Soc.* **2019,** *141,* 14062–14067. doi:10.1021/jacs.9b07014
95. Ali, W.; Prakash, G.; Maiti, D. *Chem. Sci.* **2021,** *12,* 2735–2759. doi:10.1039/d0sc05555g
96. Vivek Kumar, S.; Banerjee, S.; Punniyamurthy, T. *Org. Chem. Front.* **2020,** *7,* 1527–1569. doi:10.1039/d0qo00279h
97. Ma, W.; Gandeepan, P.; Li, J.; Ackermann, L. *Org. Chem. Front.* **2017,** *4,* 1435–1467. doi:10.1039/c7qo00134g
98. Manikandan, R.; Jeganmohan, M. *Chem. Commun.* **2017,** *53,* 8931–8947. doi:10.1039/c7cc03213g
99. Kozhushkov, S. I.; Ackermann, L. *Chem. Sci.* **2013,** *4,* 886–896. doi:10.1039/c2sc21524a
100. Le Bras, J.; Muzart, J. *Chem. Rev.* **2011,** *111,* 1170–1214. doi:10.1021/cr100209d
101. Gandeepan, P.; Ackermann, L. Diastereoselective formation of alkenes through C(sp^2)–H bond activation. In *C–H Activation for Asymmetric Synthesis;* Colobert, F.; Wencel-Delord, J., Eds.; Wiley-VCH: Weinheim, Germany, 2019; pp 239–274. doi:10.1002/9783527810857.ch9
102. Mishra, A. A.; Subhedar, D.; Bhanage, B. M. *Chem. Rec.* **2019,** *19,* 1829–1857. doi:10.1002/tcr.201800093
103. Lim, H. N.; Xing, D.; Dong, G. *Synlett* **2019,** *30,* 674–684. doi:10.1055/s-0037-1610315
104. Gonnard, L.; Guérinot, A.; Cossy, J. *Tetrahedron* **2019,** *75,* 145–163. doi:10.1016/j.tet.2018.11.034
105. Antermite, D.; Bull, J. A. *Synthesis* **2019,** *51,* 3171–3204. doi:10.1055/s-0037-1611822
106. Chu, J. C. K.; Rovis, T. *Angew. Chem., Int. Ed.* **2018,** *57,* 62–101. doi:10.1002/anie.201703743
107. Deng, H.-P.; Fan, X.-Z.; Chen, Z.-H.; Xu, Q.-H.; Wu, J. *J. Am. Chem. Soc.* **2017,** *139,* 13579–13584. doi:10.1021/jacs.7b08158
108. Go, S. Y.; Lee, G. S.; Hong, S. H. *Org. Lett.* **2018,** *20,* 4691–4694. doi:10.1021/acs.orglett.8b02017
109. Mishra, N. K.; Sharma, S.; Park, J.; Han, S.; Kim, I. S. *ACS Catal.* **2017,** *7,* 2821–2847. doi:10.1021/acscatal.7b00159
110. Wu, K.; Wang, L.; Colón-Rodríguez, S.; Flechsig, G.-U.; Wang, T. *Angew. Chem., Int. Ed.* **2019,** *58,* 1774–1778. doi:10.1002/anie.201811004
111. Shu, W.; Genoux, A.; Li, Z.; Nevado, C. *Angew. Chem., Int. Ed.* **2017,** *56,* 10521–10524. doi:10.1002/anie.201704068
112. Xu, B.; Tambar, U. K. *ACS Catal.* **2019,** *9,* 4627–4631. doi:10.1021/acscatal.9b00563
113. Yue, W.-J.; Day, C. S.; Martin, R. *J. Am. Chem. Soc.* **2021,** *143,* 6395–6400. doi:10.1021/jacs.1c03126
114. Rajamalli, P.; Senthilkumar, N.; Gandeepan, P.; Huang, P.-Y.; Huang, M.-J.; Ren-Wu, C.-Z.; Yang, C.-Y.; Chiu, M.-J.; Chu, L.-K.; Lin, H.-W.; Cheng, C.-H. *J. Am. Chem. Soc.* **2016,** *138,* 628–634. doi:10.1021/jacs.5b10950
115. Carroll, F. I.; Blough, B. E.; Abraham, P.; Mills, A. C.; Holleman, J. A.; Wolckenhauer, S. A.; Decker, A. M.; Landavazo, A.; McElroy, K. T.; Navarro, H. A.; Gatch, M. B.; Forster, M. J. *J. Med. Chem.* **2009,** *52,* 6768–6781. doi:10.1021/jm901189z
116. Meltzer, P. C.; Butler, D.; Deschamps, J. R.; Madras, B. K. *J. Med. Chem.* **2006,** *49,* 1420–1432. doi:10.1021/jm050797a

117. Foley, K. F.; Cozzi, N. V. *Drug Dev. Res.* **2003,** *60,* 252–260. doi:10.1002/ddr.10297
118. Penteado, F.; Lopes, E. F.; Alves, D.; Perin, G.; Jacob, R. G.; Lenardão, E. J. *Chem. Rev.* **2019,** *119,* 7113–7278. doi:10.1021/acs.chemrev.8b00782
119. Wu, X.-F. *Chem. – Eur. J.* **2015,** *21,* 12252–12265. doi:10.1002/chem.201501548
120. Joe, C. L.; Doyle, A. G. *Angew. Chem., Int. Ed.* **2016,** *55,* 4040–4043. doi:10.1002/anie.201511438
121. Sun, Z.; Kumagai, N.; Shibasaki, M. *Org. Lett.* **2017,** *19,* 3727–3730. doi:10.1021/acs.orglett.7b01552
122. Ackerman, L. K. G.; Martinez Alvarado, J. I.; Doyle, A. G. *J. Am. Chem. Soc.* **2018,** *140,* 14059–14063. doi:10.1021/jacs.8b09191
123. Kawasaki, T.; Ishida, N.; Murakami, M. *J. Am. Chem. Soc.* **2020,** *142,* 3366–3370. doi:10.1021/jacs.9b13920
124. Shu, X.; Huan, L.; Huang, Q.; Huo, H. *J. Am. Chem. Soc.* **2020,** *142,* 19058–19064. doi:10.1021/jacs.0c10471
125. Lee, G. S.; Won, J.; Choi, S.; Baik, M.-H.; Hong, S. H. *Angew. Chem., Int. Ed.* **2020,** *59,* 16933–16942. doi:10.1002/anie.202004441
126. Krach, P. E.; Dewanji, A.; Yuan, T.; Rueping, M. *Chem. Commun.* **2020,** *56,* 6082–6085. doi:10.1039/d0cc01480j
127. Ren, C.-C.; Wang, T.-Q.; Zhang, Y.; Peng, D.; Liu, X.-Q.; Wu, Q.-A.; Liu, X.-F.; Luo, S.-P. *ChemistrySelect* **2021,** *6,* 2523–2528. doi:10.1002/slct.202100225
128. Gu, L.; Jin, C.; Liu, J.; Zhang, H.; Yuan, M.; Li, G. *Green Chem.* **2016,** *18,* 1201–1205. doi:10.1039/c5gc01931a
129. Zhang, X.; MacMillan, D. W. C. *J. Am. Chem. Soc.* **2017,** *139,* 11353–11356. doi:10.1021/jacs.7b07078
130. Vu, M. D.; Das, M.; Liu, X.-W. *Chem. – Eur. J.* **2017,** *23,* 15899–15902. doi:10.1002/chem.201704224
131. Artz, J.; Müller, T. E.; Thenert, K.; Kleinekorte, J.; Meys, R.; Sternberg, A.; Bardow, A.; Leitner, W. *Chem. Rev.* **2018,** *118,* 434–504. doi:10.1021/acs.chemrev.7b00435
132. Sakakura, T.; Choi, J.-C.; Yasuda, H. *Chem. Rev.* **2007,** *107,* 2365–2387. doi:10.1021/cr068357u
133. Luo, J.; Larrosa, I. *ChemSusChem* **2017,** *10,* 3317–3332. doi:10.1002/cssc.201701058
134. Kleij, A.; Rintjema, J. *Synthesis* **2016,** *48,* 3863–3878. doi:10.1055/s-0035-1562520
135. Yeung, C. S.; Dong, V. M. *Top. Catal.* **2014,** *57,* 1342–1350. doi:10.1007/s11244-014-0301-9
136. Ishida, N.; Masuda, Y.; Imamura, Y.; Yamazaki, K.; Murakami, M. *J. Am. Chem. Soc.* **2019,** *141,* 19611–19615. doi:10.1021/jacs.9b12529
137. Bag, D.; Mahajan, S.; Sawant, S. D. *Adv. Synth. Catal.* **2020,** *362,* 3948–3970. doi:10.1002/adsc.202000630
138. Derosa, J.; Apolinar, O.; Kang, T.; Tran, V. T.; Engle, K. M. *Chem. Sci.* **2020,** *11,* 4287–4296. doi:10.1039/c9sc06006e
139. Qi, X.; Diao, T. *ACS Catal.* **2020,** *10,* 8542–8556. doi:10.1021/acscatal.0c02115
140. Xu, S.; Chen, H.; Zhou, Z.; Kong, W. *Angew. Chem., Int. Ed.* **2021,** *60,* 7405–7411. doi:10.1002/anie.202014632
141. Campbell, M. W.; Yuan, M.; Polites, V. C.; Gutierrez, O.; Molander, G. A. *J. Am. Chem. Soc.* **2021,** *143,* 3901–3910. doi:10.1021/jacs.0c13077

License and Terms

This is an Open Access article under the terms of the Creative Commons Attribution License (https://creativecommons.org/licenses/by/4.0). Please note that the reuse, redistribution and reproduction in particular requires that the author(s) and source are credited and that individual graphics may be subject to special legal provisions.

The license is subject to the *Beilstein Journal of Organic Chemistry* terms and conditions: (https://www.beilstein-journals.org/bjoc/terms)

The definitive version of this article is the electronic one which can be found at:
https://doi.org/10.3762/bjoc.17.143

BEILSTEIN JOURNAL OF ORGANIC CHEMISTRY

Copper-catalyzed monoselective C–H amination of ferrocenes with alkylamines

Zhen-Sheng Jia[1], Qiang Yue[2], Ya Li[*2], Xue-Tao Xu[*1], Kun Zhang[*1]
and Bing-Feng Shi[*2,3,4]

Letter

Open Access

Address:
[1]School of Biotechnology and Health Sciences, Wuyi University, Jiangmen, Guangdong, 529020, China, [2]Department of Chemistry, Zhejiang University, Hangzhou, Zhejiang, 310027, China, [3]Green Catalysis Center and College of Chemistry, Zhengzhou University, Zhengzhou, 450001, China and [4]School of Chemistry and Chemical Engineering, Henan Normal University, Xinxiang, He'nan, 453007, China

Email:
Ya Li* - 11837007@zju.edu.cn; Xue-Tao Xu* - wyuchemxxt@126.com; Kun Zhang* - kzhang@gdut.edu.cn; Bing-Feng Shi* - bfshi@zju.edu.cn

* Corresponding author

Keywords:
amination; C–H activation; copper; ferrocene; mono-selectivity

Beilstein J. Org. Chem. **2021,** *17,* 2488–2495.
https://doi.org/10.3762/bjoc.17.165

Received: 14 August 2021
Accepted: 22 September 2021
Published: 28 September 2021

This article is part of the thematic issue "Earth-abundant 3d metal catalysis".

Associate Editor: L. Ackermann

© 2021 Jia et al.; licensee Beilstein-Institut.
License and terms: see end of document.

Abstract

A copper-catalyzed mono-selective C–H amination of ferrocenes assisted by 8-aminoquinoline is presented here. A range of amines, including bioactive molecules, were successfully installed to the *ortho*-position of ferrocene amides with high efficiency under mild conditions. A range of functionalized ferrocenes were compatible to give the aminated products in moderate to good yields. The gram-scale reaction was smoothly conducted and the directing group could be removed easily under basic conditions.

Introduction

Ferrocene-based compounds have broad applications from asymmetric catalysis to medicinal discovery [1-8]. Therefore, the development of efficient methods to access multifunctional ferrocenes has attracted tremendous attention. Conventionally, functionalized ferrocenes were derived via electrophilic aromatic substitution mediated by strong Lewis acids or direct metalation using strong bases, such as alkyllithium reagents [3,9-12]. However, the above protocols generally proceeded under harsh conditions that led to poor functional group tolerance and generated stoichiometric amounts of waste.

Thus far, the transition-metal-catalyzed C–H functionalization strategy has innovated the way to producing ferrocene derivatives [13-16]. Especially, the 3d transition metals, such as Cu, Co and Ni, have been exploited to convert C–H bonds to various functional groups, attributing to the cost-effective and less toxic properties, which render C–H transformations both economically desirable and environmentally benign (Scheme 1a) [17-22]. Early in 2015, the Ackermann group reported the first example of a low-valent Co-catalyzed C–H alkenylation of 2-pyridinylferrocene [23]. In 2017, the Butenschön group reported the *ortho*-C–H alkylation and arylation of ferrocene derivatives enabled by a combination of Fe or Co catalyst and *N*-containing directing groups, while an excess of Grignard reagents was used [24,25]. Thereafter, they also reported the Cp*Co-catalyzed *ortho*-C–H alkenylation of ferrocenes with alkynes [26] and the mono- and di-selectivity could be controlled by the fine-tuned directing groups. Kumar and co-workers developed a Cu-mediated C–H chalcogenation and sulfonation of ferrocenes [27-29]. The use of a bidentate 1,10-phenathroline ligand was critical to achieve mono-selectivity in the chacogenation reactions [28]. Meanwhile, Co(III)-catalyzed *ortho*-C–H amidation of ferrocene derivatives were also developed by the groups of You [30], Ackermann [31] and Shi [32,33] with 1,4,2-dioxazol-5-ones as versatile amidating reagents. In 2019, the alkynylated ferrocenes were isolated in the formation of alkyne-Cu(I) π-complexes by the Tan group via Cu-mediated C–H alkynylations [34]. Later in 2020, an enantioselective C–H annulation of ferrocenylformamides with alkynes was achieved by the Ye group enabled by Ni-Al bimetallic catalysis and a chiral secondary phosphine oxide (SPO) ligand [35]. Hou et al. also reported the asymmetric C−H alkenylation of quinoline- and pyridine-substituted ferrocenes with alkynes by using an unprecedented half-sandwich Sc catalyst [36]. Very recently, Shi and Zhang demonstrated a Cp*Co-catalyzed *ortho*-C–H allylation of ferrocenes assisted by thioamide using allyl carbonates and vinylcyclopropanes as allylating partners [37]. Meanwhile, Zhang and co-authors also reported the Co-catalyzed C–H alkoxylation of ferrocenes under nearly room temperature [38].

In comparison, despite the direct C–H amination of arenes with alkylamines has emerged as an efficient strategy to prepare substituted anilines [39-49], the application of this environmentally benign, oxidative coupling strategy to the synthesis of valuable *ortho*-amino ferrocene derivatives hasn't been achieved [50], probably ascribing to several challenges. First, unprotected amines are sensitive and unendurable to several oxidants in the presence of transition metals. Second, both amines and the resulting aminated products could coordinate with metal catalysts and cause the deactivation of catalysts. Besides, high reaction temperature could lead to a mixture of byproducts or the decomposition of the ferrocene products. Herein, we described a Cu-catalyzed oxidative C–H/N–H coupling of ferrocenes with free amines to provide mono-aminated ferrocenes exclusively under mild conditions (Scheme 1b). During the preparation of the manuscript of this article, a nice report on Cu-catalyzed C–H amination of ferrocenes directed by 8-aminoquinoline was reported by Fukuzawa and Kanemoto [50]. Notably, our method proceeded under silver-free conditions at relatively lower temperature and in shorter time, providing a complementary alternative to the work of Fukuzawa and Kanemoto.

Results and Discussion

We initiated our study by investigating the C–H amination of ferrocene carboxylic amide **1a** with morpholine (**2a**) using 8-amonoquinoline as directing group [51-56]. The *ortho*-

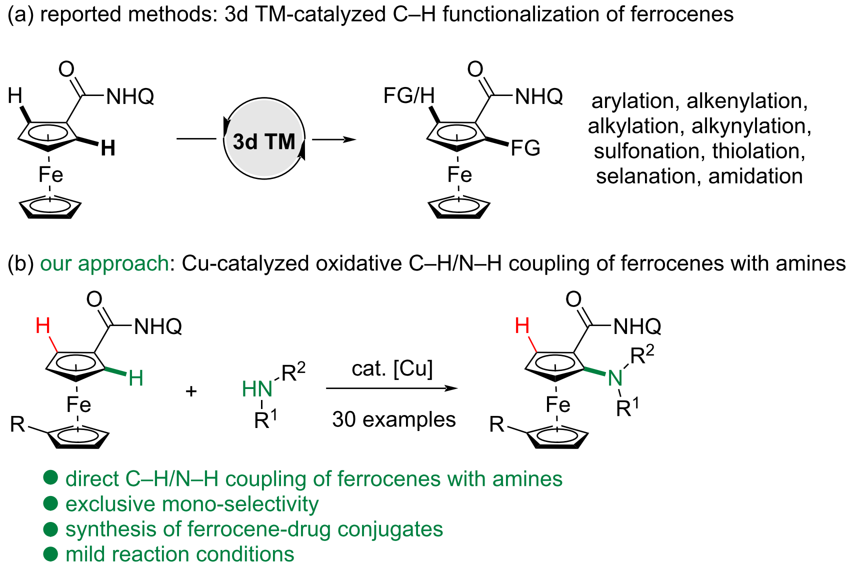
(a) reported methods: 3d TM-catalyzed C–H functionalization of ferrocenes
O
NHQ
H
H
Fe
3d TM
FG/H
O
NHQ
FG
Fe
arylation, alkenylation,
alkylation, alkynylation,
sulfonation, thiolation,
selanation, amidation
(b) our approach: Cu-catalyzed oxidative C–H/N–H coupling of ferrocenes with amines
O
NHQ
H
H
Fe
R
+
HN
R2
R1
cat. [Cu]
30 examples
H
O
NHQ
N
R2
R1
Fe
R
direct C–H/N–H coupling of ferrocenes with amines
exclusive mono-selectivity
synthesis of ferrocene-drug conjugates
mild reaction conditions

Scheme 1: 3d-Transition-metal-catalyzed C–H functionalization to access functionalized ferrocenes.

aminated ferrocenylamide **3a** was isolated in 11% yield in the presence of CuI, *N*-methylmorpholine *N*-oxide (NMO) and K_2CO_3 in DMF (Table 1, entry 1). When the reaction was conducted in MeCN, the yield could be improved to 32% (Table 1, entry 4). Further screening of other oxidants revealed that NMO was the optimal (Table 1, entries 9–11). When the reaction was conducted in neat in the presence of 2-pyridone, **3a** was obtained in 36% yield (Table 1, entry 12). However, significant decomposition of the aminated product **3a** was observed. Consequently, we exclusively evaluated the reaction temperature and time (Table 1, entries 13–16). To our delight, **3a** could be obtained in 80% yield under relatively lower temperature (80 °C) and shorter time (4 hours). To note, this reaction showed excellent mono-selectivity and no diaminated ferrocenylamide was detected. The exclusive monoselectivity is most likely originated from the strong coordination of the amino group, which could form a tridentate copper complex and prevent the second C–H amination [34,50].

Having obtained the optimized reaction conditions, we started to investigate the generality of this C–H amination protocol with regard to modified ferrocenes (Scheme 2). Delightfully, a variety of functional groups tailored to the other cyclopentadienyl (Cp) moieties were well tolerated, furnishing the desired *ortho*-mono-aminating ferrocenes in moderate to good yields. Alkyl substituents on the other Cp ring of ferrocenylamides only showed slightly effects (**3b**–**d**). Notably, the terminal alkenyl group of **3e** was well tolerated during the amination process. Weakly coordinating carbonyl groups were also tolerated and the desired C–H amination occurred selectively at the *ortho* position to the *N*-quinolinyl amides with acceptable yields (**3f**–**l**). Notably, free alcohol was also compatible with this protocol, exclusively giving the mono-aminated product in 73% yield (**3m**) without the observation of any competitive alkoxylation product [38,57,58].

We then explored the scope of multifarious amines. As displayed in Scheme 3, a range of cyclic amines, such as morpholine **4a**,**b**, piperazine **4c**, piperidine **4d**–**j** and thiomorpholine **4l**,**m**, reacted smoothly to give the amination products in 23% to 85% yields. A variety of synthetically useful functionalities, such as ester **4f**, cyano **4g** and ketal **4i**, were well tolerated. Unfortunately, 1,2,3,4-tetrahydroquinoline (**2k**) was proved unreactive under our conditions, probably due to the

Table 1: Optimization of reaction conditions.[a]

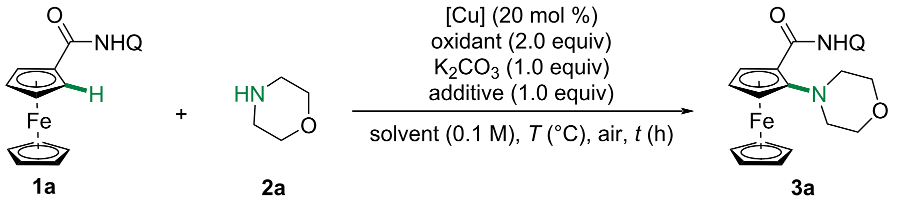

Entry	[Cu]	Solvent	Oxidant	Additive	*T* (°C)	*t* (h)	Yield[b]
1	CuI	DMF	NMO	–	120	12	11%
2	CuI	NMP	NMO	–	120	12	15%
3	CuI	DMSO	NMO	–	120	12	trace
4	CuI	MeCN	NMO	–	120	12	32%
5	$Cu(OAc)_2$	MeCN	NMO	–	120	12	10%
6	CuCN	MeCN	NMO	–	120	12	12%
7	CuCl	MeCN	NMO	–	120	12	18%
8	CuTc	MeCN	NMO	–	120	12	trace
9	CuI	MeCN	TEMPO	–	120	12	23%
10	CuI	MeCN	MnO_2	–	120	12	trace
11[c]	CuI	MeCN	O_2	–	120	12	8%
12[d]	CuI	neat	NMO	2-pyridone	120	12	36%
13[d]	CuI	neat	NMO	2-pyridone	100	12	46%
14[d]	CuI	neat	NMO	2-pyridone	80	12	56%
15[d]	CuI	neat	NMO	2-pyridone	80	6	68%
16[d]	CuI	neat	NMO	2-pyridone	80	4	80%

[a] Reactions conditions: **1a** (0.1 mmol), **2a** (0.3 mmol), [Cu] (20 mol %), oxidant (2.0 equiv), K_2CO_3 (1.0 equiv) and additive (1.0 equiv) in a sealed tube. [b] Isolated yield. [c] Oxygen balloon. [d] 5.0 equiv of morpholine.

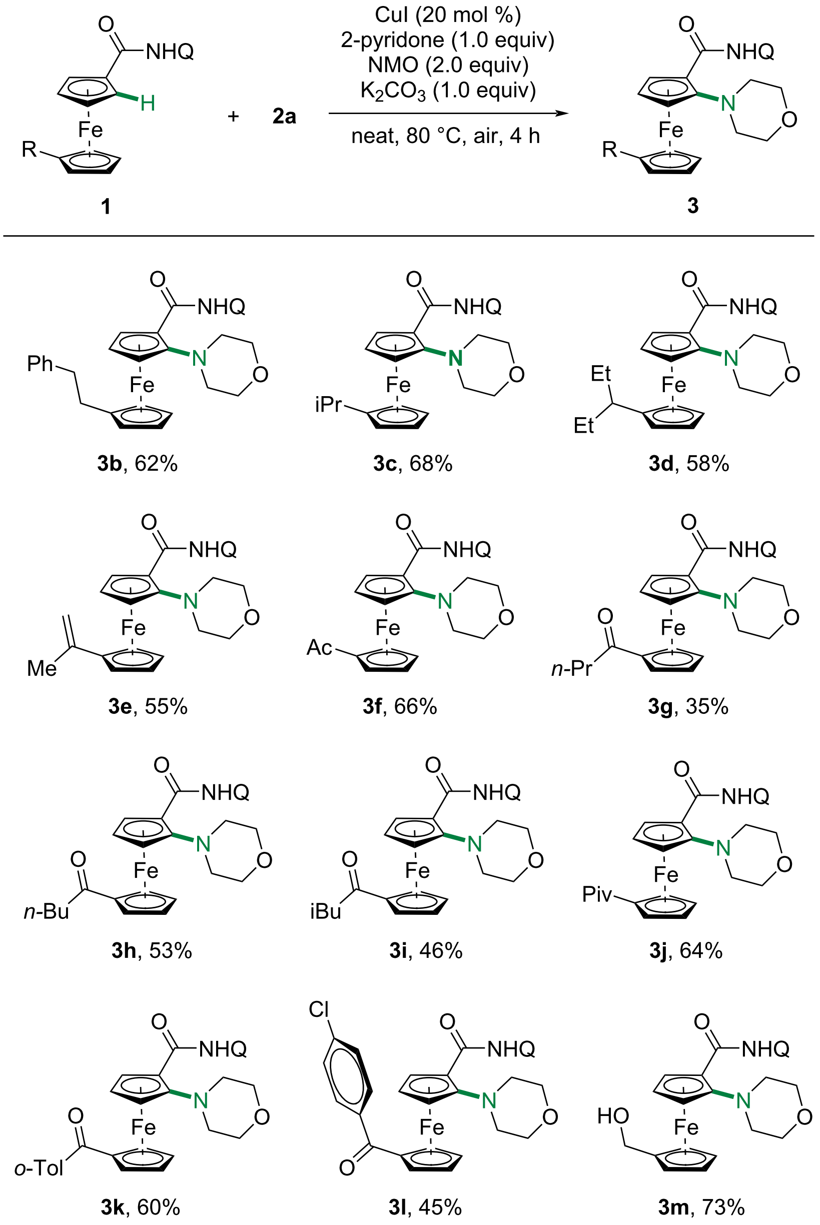
O
NHQ
H
Fe
R
1
+
2a
CuI (20 mol %)
2-pyridone (1.0 equiv)
NMO (2.0 equiv)
K2CO3 (1.0 equiv)
neat, 80 °C, air, 4 h
N
O
3
Ph
iPr
Et
Me
Ac
n-Pr
n-Bu
iBu
Piv
o-Tol
Cl
HO
3b, 62%
3c, 68%
3d, 58%
3e, 55%
3f, 66%
3g, 35%
3h, 53%
3i, 46%
3j, 64%
3k, 60%
3l, 45%
3m, 73%

Scheme 2: Scope of ferrocenes with morpholine.

steric hindrance. Thiomorpholine (**2l**) was compatible with this reaction, albeit with significantly dropped yield (29%), largely due to the poison of copper catalyst by thioether. Acyclic amines were also tested and the amination products were obtained in low yields (**4n**, 18%; **4o**, 15%). Unfortunately, primary amines and anilines were completely inert.

Encouraged by the above results, we further tried to synthesize ferrocene–drug conjugates (Scheme 4a). Three amines used to treat psychosis were subjected to couple with **1a** and the desired conjugates were obtained in good yields (with haloperidol, **4p**, 63%; with buspirone, **4q**, 60%; with perospirone, **4r**, 70%). This protocol was also amendable to gram-scale synthesis, giving **3a** in 50% yield (Scheme 4b, 1.32 g). For synthetic utility, the directing group was conveniently removed by refluxing with KOH in EtOH and the benzyl-protected ester **5** was obtained in 75% yield.

We also conducted several deuteration experiments to shed a preliminary insight into the mechanism. No H/D exchange was observed at the *ortho*-position of **1a** with 3.0 equivalents of CD_3CO_2D under standard conditions (Scheme 5a). Further-

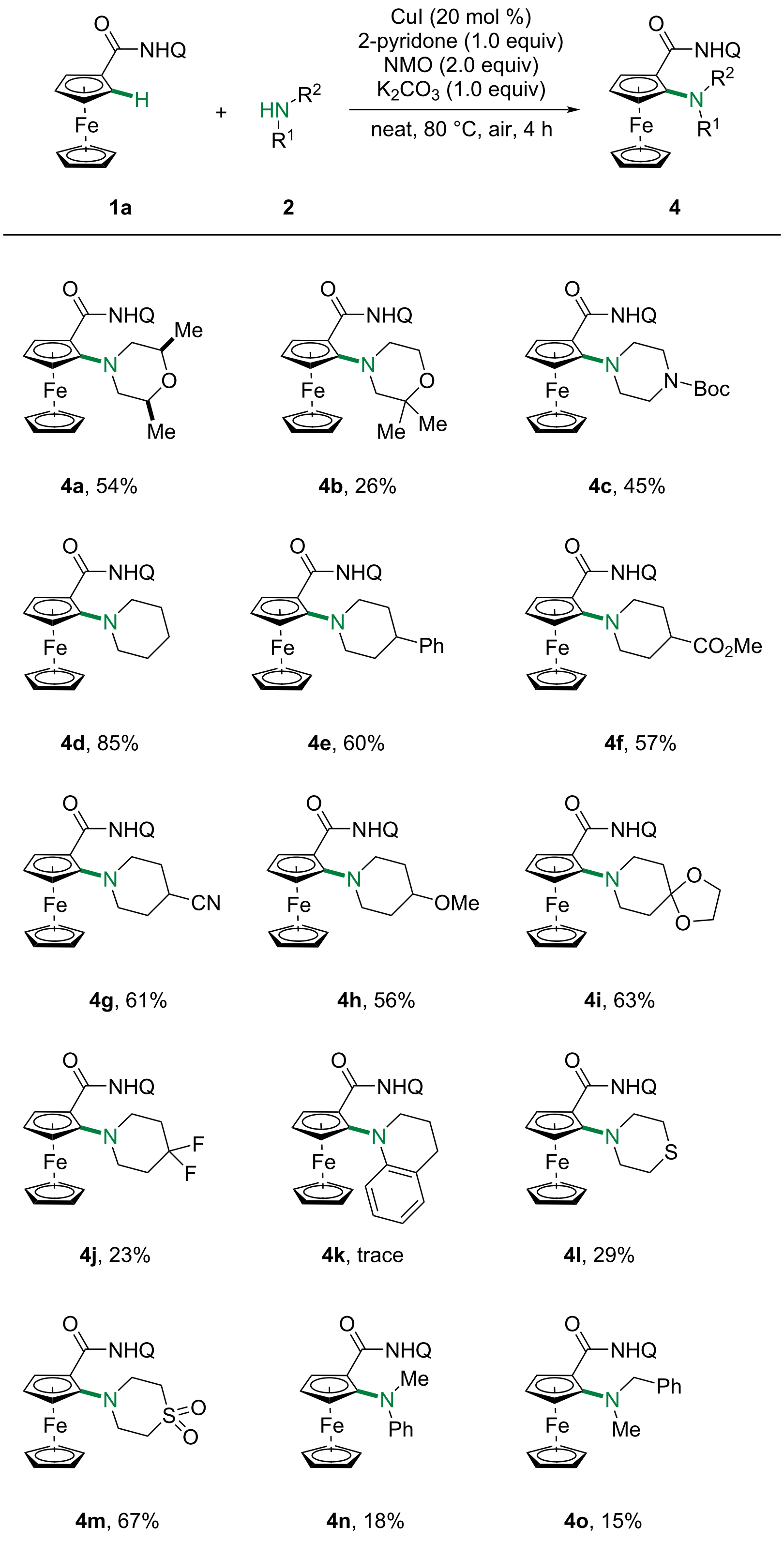
CuI (20 mol %)
2-pyridone (1.0 equiv)
NMO (2.0 equiv)
K2CO3 (1.0 equiv)
neat, 80 °C, air, 4 h
1a
2
4
4a, 54%
4b, 26%
4c, 45%
4d, 85%
4e, 60%
4f, 57%
4g, 61%
4h, 56%
4i, 63%
4j, 23%
4k, trace
4l, 29%
4m, 67%
4n, 18%
4o, 15%

Scheme 3: Scope of various amines with **1a**.

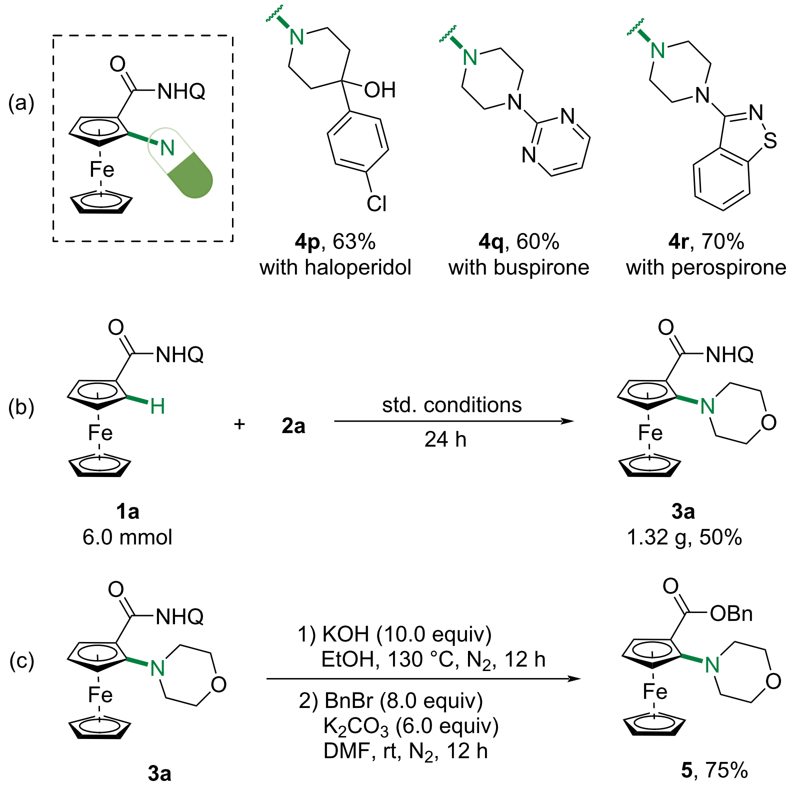
(a)
O
NHQ
N
Fe
N
OH
Cl
4p, 63%
with haloperidol
N
N
N
N
4q, 60%
with buspirone
N
N
N
S
4r, 70%
with perospirone
(b)
O
NHQ
H
Fe
1a
6.0 mmol
+
2a
std. conditions
24 h
O
NHQ
N
O
Fe
3a
1.32 g, 50%
(c)
O
NHQ
N
O
Fe
3a
1) KOH (10.0 equiv)
EtOH, 130 °C, N2, 12 h
2) BnBr (8.0 equiv)
K2CO3 (6.0 equiv)
DMF, rt, N2, 12 h
O
OBn
N
O
Fe
5, 75%

Scheme 4: Synthetic applications.

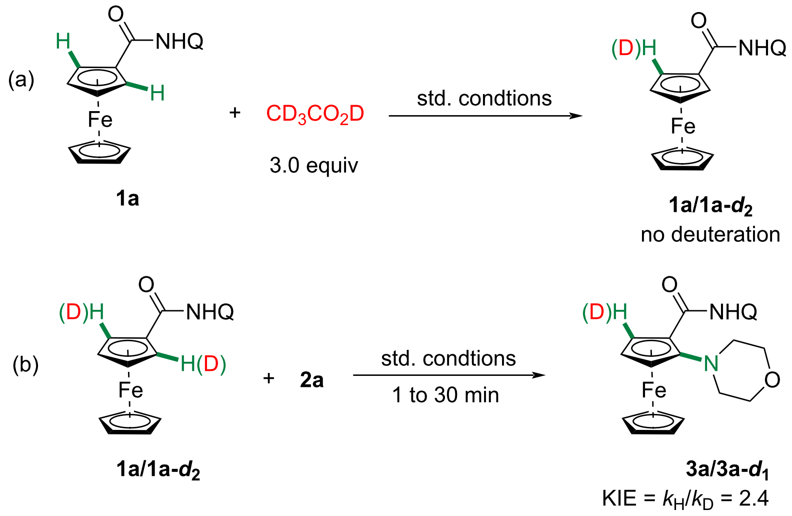
(a)
H
O
NHQ
H
Fe
1a
+
CD3CO2D
3.0 equiv
std. condtions
(D)H
O
NHQ
Fe
1a/1a-d2
no deuteration
(b)
(D)H
O
NHQ
H(D)
Fe
1a/1a-d2
+
2a
std. condtions
1 to 30 min
(D)H
O
NHQ
N
O
Fe
3a/3a-d1
KIE = kH/kD = 2.4

Scheme 5: Mechanistic experiments.

more, a larger value of kinetic isotope effect (KIE = 2.4) was detected (Scheme 5b). These results indicated that the cleavage of C–H bond was most likely involved in the rate-determining step.

Conclusion

To summarize, we have reported a copper-catalyzed direct *ortho*-C–H/N–H coupling reaction of ferrocenes with alkyl amines directed by 8-aminoquinoline. Fruitful mono-aminated ferrocenes were obtained in moderate to good yields and the mild conditions offered the possibility to the preparation of ferrocene–drug conjugates effectively. Mechanistic studies indicated that the C–H activation step was the rate-determining step.

Supporting Information

Supporting Information File 1

Full experimental details, compound characterization, and copies of NMR spectra.
[https://www.beilstein-journals.org/bjoc/content/supplementary/1860-5397-17-165-S1.pdf]

Funding

Financial support from the National Natural Science Foundation of China (21925109 and 21772170), China Postdoctoral Science Foundation (2021M692771), Center of Chemistry for Frontier Technologies of Zhejiang University, and Open Research Fund of School of Chemistry and Chemical Engineering of Henan Normal University is gratefully acknowledged.

ORCID® iDs

Bing-Feng Shi - https://orcid.org/0000-0003-0375-955X

References

1. Hayashi, T.; Togni, A., Eds. *Ferrocenes;* VCH: Weinheim, Germany, 1995.
2. Štěpnička, P., Ed. *Ferrocenes;* John Wiley & Sons: Chichester, UK, 2008.
3. Dai, L.-X.; Hou, X.-L., Eds. *Chiral Ferrocenes in Asymmetric Catalysis;* Wiley-VCH: Weinheim, Germany, 2010. doi:10.1002/9783527628841
4. van Staveren, D. R.; Metzler-Nolte, N. *Chem. Rev.* **2004,** *104,* 5931–5986. doi:10.1021/cr0101510
5. Gómez Arrayás, R.; Adrio, J.; Carretero, J. C. *Angew. Chem., Int. Ed.* **2006,** *45,* 7674–7715. doi:10.1002/anie.200602482
6. Hartinger, C. G.; Dyson, P. J. *Chem. Soc. Rev.* **2009,** *38,* 391–401. doi:10.1039/b707077m
7. Gasser, G.; Ott, I.; Metzler-Nolte, N. *J. Med. Chem.* **2011,** *54,* 3–25. doi:10.1021/jm100020w
8. Toma, Š.; Csizmadiová, J.; Mečiarová, M.; Šebesta, R. *Dalton Trans.* **2014,** *43,* 16557–16579. doi:10.1039/c4dt01784f
9. Tsukazaki, M.; Tinkl, M.; Roglans, A.; Chapell, B. J.; Taylor, N. J.; Snieckus, V. *J. Am. Chem. Soc.* **1996,** *118,* 685–686. doi:10.1021/ja953246q
10. Metallinos, C.; Szillat, H.; Taylor, N. J.; Snieckus, V. *Adv. Synth. Catal.* **2003,** *345,* 370–382. doi:10.1002/adsc.200390042
11. Butt, N. A.; Liu, D.; Zhang, W. *Synlett* **2014,** *25,* 615–630. doi:10.1055/s-0033-1340487
12. Schaarschmidt, D.; Lang, H. *Organometallics* **2013,** *32,* 5668–5704. doi:10.1021/om400564x
13. López, L. A.; López, E. *Dalton Trans.* **2015,** *44,* 10128–10135. doi:10.1039/c5dt01373a
14. Zhu, D.-Y.; Chen, P.; Xia, J.-B. *ChemCatChem* **2016,** *8,* 68–73. doi:10.1002/cctc.201500895
15. Gao, D.-W.; Gu, Q.; Zheng, C.; You, S.-L. *Acc. Chem. Res.* **2017,** *50,* 351–365. doi:10.1021/acs.accounts.6b00573
16. Huang, J.; Gu, Q.; You, S. *Chin. J. Org. Chem.* **2018,** *38,* 51–61. doi:10.6023/cjoc201708030
17. Gandeepan, P.; Müller, T.; Zell, D.; Cera, G.; Warratz, S.; Ackermann, L. *Chem. Rev.* **2019,** *119,* 2192–2452. doi:10.1021/acs.chemrev.8b00507
18. Loup, J.; Dhawa, U.; Pesciaioli, F.; Wencel-Delord, J.; Ackermann, L. *Angew. Chem., Int. Ed.* **2019,** *58,* 12803–12818. doi:10.1002/anie.201904214
19. Woźniak, Ł.; Cramer, N. *Trends Chem.* **2019,** *1,* 471–484. doi:10.1016/j.trechm.2019.03.013
20. Rao, W.-H.; Shi, B.-F. *Org. Chem. Front.* **2016,** *3,* 1028–1047. doi:10.1039/c6qo00156d
21. Liu, J.; Chen, G.; Tan, Z. *Adv. Synth. Catal.* **2016,** *358,* 1174–1194. doi:10.1002/adsc.201600031
22. Liu, Y.-H.; Xia, Y.-N.; Shi, B.-F. *Chin. J. Chem.* **2020,** *38,* 635–662. doi:10.1002/cjoc.201900468
23. Moselage, M.; Sauermann, N.; Richter, S. C.; Ackermann, L. *Angew. Chem., Int. Ed.* **2015,** *54,* 6352–6355. doi:10.1002/anie.201412319
24. Schmiel, D.; Butenschön, H. *Eur. J. Org. Chem.* **2017,** 3041–3048. doi:10.1002/ejoc.201700358
25. Schmiel, D.; Butenschön, H. *Organometallics* **2017,** *36,* 4979–4989. doi:10.1021/acs.organomet.7b00799
26. Schmiel, D.; Gathy, R.; Butenschön, H. *Organometallics* **2018,** *37,* 2095–2110. doi:10.1021/acs.organomet.8b00243
27. Sattar, M.; Shareef, M.; Patidar, K.; Kumar, S. *J. Org. Chem.* **2018,** *83,* 8241–8249. doi:10.1021/acs.joc.8b00974
28. Sattar, M.; Patidar, K.; Thorat, R. A.; Kumar, S. *J. Org. Chem.* **2019,** *84,* 6669–6678. doi:10.1021/acs.joc.9b00311
29. Sattar, M.; Kumar, N.; Yadav, P.; Mandhar, Y.; Kumar, S. *Chem. – Asian J.* **2019,** *14,* 4807–4813. doi:10.1002/asia.201901334
30. Wang, S.-B.; Gu, Q.; You, S.-L. *J. Catal.* **2018,** *361,* 393–397. doi:10.1016/j.jcat.2018.03.007
31. Yetra, S. R.; Shen, Z.; Wang, H.; Ackermann, L. *Beilstein J. Org. Chem.* **2018,** *14,* 1546–1553. doi:10.3762/bjoc.14.131
32. Huang, D.-Y.; Yao, Q.-J.; Zhang, S.; Xu, X.-T.; Zhang, K.; Shi, B.-F. *Org. Lett.* **2019,** *21,* 951–954. doi:10.1021/acs.orglett.8b03938
33. Liu, Y.-H.; Li, P.-X.; Yao, Q.-J.; Zhang, Z.-Z.; Huang, D.-Y.; Le, M. D.; Song, H.; Liu, L.; Shi, B.-F. *Org. Lett.* **2019,** *21,* 1895–1899. doi:10.1021/acs.orglett.9b00511
34. Song, Z.; Yu, Y.; Yu, L.; Liu, D.; Wu, Q.; Xia, Z.; Xiao, Y.; Tan, Z. *Organometallics* **2019,** *38,* 3349–3357. doi:10.1021/acs.organomet.9b00447
35. Chen, H.; Wang, Y.-X.; Luan, Y.-X.; Ye, M. *Angew. Chem., Int. Ed.* **2020,** *59,* 9428–9432. doi:10.1002/anie.202001267
36. Lou, S.-J.; Zhuo, Q.; Nishiura, M.; Luo, G.; Hou, Z. *J. Am. Chem. Soc.* **2021,** *143,* 2470–2476. doi:10.1021/jacs.0c13166
37. Zhang, Z.-Z.; Liao, G.; Chen, H.-M.; Shi, B.-F. *Org. Lett.* **2021,** *23,* 2626–2631. doi:10.1021/acs.orglett.1c00533
38. Zhang, Z.-Z.; Cheng, J.; Yao, Q.-J.; Yue, Q.; Zhou, G. *Adv. Synth. Catal.* **2021,** *363,* 3946–3951. doi:10.1002/adsc.202100423
39. Kim, H.; Chang, S. *ACS Catal.* **2016,** *6,* 2341–2351. doi:10.1021/acscatal.6b00293

40. Tran, L. D.; Roane, J.; Daugulis, O. *Angew. Chem., Int. Ed.* **2013,** *52,* 6043–6046. doi:10.1002/anie.201300135
41. Matsubara, T.; Asako, S.; Ilies, L.; Nakamura, E. *J. Am. Chem. Soc.* **2014,** *136,* 646–649. doi:10.1021/ja412521k
42. Yan, Q.; Chen, Z.; Yu, W.; Yin, H.; Liu, Z.; Zhang, Y. *Org. Lett.* **2015,** *17,* 2482–2485. doi:10.1021/acs.orglett.5b00990
43. Roane, J.; Daugulis, O. *J. Am. Chem. Soc.* **2016,** *138,* 4601–4607. doi:10.1021/jacs.6b01117
44. Yan, Q.; Xiao, T.; Liu, Z.; Zhang, Y. *Adv. Synth. Catal.* **2016,** *358,* 2707–2711. doi:10.1002/adsc.201600282
45. Gao, X.; Wang, P.; Zeng, L.; Tang, S.; Lei, A. *J. Am. Chem. Soc.* **2018,** *140,* 4195–4199. doi:10.1021/jacs.7b13049
46. Zhang, S.-K.; Samanta, R. C.; Sauermann, N.; Ackermann, L. *Chem. – Eur. J.* **2018,** *24,* 19166–19170. doi:10.1002/chem.201805441
47. Kathiravan, S.; Suriyanarayanan, S.; Nicholls, I. A. *Org. Lett.* **2019,** *21,* 1968–1972. doi:10.1021/acs.orglett.9b00003
48. Shang, M.; Shao, Q.; Sun, S.-Z.; Chen, Y.-Q.; Xu, H.; Dai, H.-X.; Yu, J.-Q. *Chem. Sci.* **2017,** *8,* 1469–1473. doi:10.1039/c6sc03383k
49. Wu, P.; Huang, W.; Cheng, T.-J.; Lin, H.-X.; Xu, H.; Dai, H.-X. *Org. Lett.* **2020,** *22,* 5051–5056. doi:10.1021/acs.orglett.0c01632
50. Kanemoto, K.; Horikawa, N.; Hoshino, S.; Tokoro, Y.; Fukuzawa, S.-i. *Org. Lett.* **2021,** *23,* 4966–4970. doi:10.1021/acs.orglett.1c01294
51. Zaitsev, V. G.; Shabashov, D.; Daugulis, O. *J. Am. Chem. Soc.* **2005,** *127,* 13154–13155. doi:10.1021/ja054549f
52. Daugulis, O.; Roane, J.; Tran, L. D. *Acc. Chem. Res.* **2015,** *48,* 1053–1064. doi:10.1021/ar5004626
53. Sambiagio, C.; Schönbauer, D.; Blieck, R.; Dao-Huy, T.; Pototschnig, G.; Schaaf, P.; Wiesinger, T.; Zia, M. F.; Wencel-Delord, J.; Besset, T.; Maes, B. U. W.; Schnürch, M. *Chem. Soc. Rev.* **2018,** *47,* 6603–6743. doi:10.1039/c8cs00201k
54. Zhang, Q.; Shi, B.-F. *Chin. J. Chem.* **2019,** *37,* 647–656. doi:10.1002/cjoc.201900090
55. Rej, S.; Ano, Y.; Chatani, N. *Chem. Rev.* **2020,** *120,* 1788–1887. doi:10.1021/acs.chemrev.9b00495
56. Zhang, Q.; Shi, B.-F. *Acc. Chem. Res.* **2021,** *54,* 2750–2763. doi:10.1021/acs.accounts.1c00168
57. Roane, J.; Daugulis, O. *Org. Lett.* **2013,** *15,* 5842–5845. doi:10.1021/ol402904d
58. Hu, Y.; Wang, M.; Li, P.; Li, H.; Wang, L. *Asian J. Org. Chem.* **2019,** *8,* 171–178. doi:10.1002/ajoc.201800664

License and Terms

This is an Open Access article under the terms of the Creative Commons Attribution License (https://creativecommons.org/licenses/by/4.0). Please note that the reuse, redistribution and reproduction in particular requires that the author(s) and source are credited and that individual graphics may be subject to special legal provisions.

The license is subject to the *Beilstein Journal of Organic Chemistry* terms and conditions: (https://www.beilstein-journals.org/bjoc/terms)

The definitive version of this article is the electronic one which can be found at: https://doi.org/10.3762/bjoc.17.165

BEILSTEIN JOURNAL OF ORGANIC CHEMISTRY

Electrocatalytic C(sp^3)–H/C(sp)–H cross-coupling in continuous flow through TEMPO/copper relay catalysis

Bin Guo and Hai-Chao Xu*

Letter

Open Access

Address:
Key Laboratory of Chemical Biology of Fujian Province and College of Chemistry and Chemical Engineering, Xiamen University, People's Republic of China

Email:
Hai-Chao Xu* - haichao.xu@xmu.edu.cn

* Corresponding author

Keywords:
continuous flow; copper; catalysis; dehydrogenative cross-coupling; electrochemistry

Beilstein J. Org. Chem. **2021,** *17,* 2650–2656.
https://doi.org/10.3762/bjoc.17.178

Received: 31 August 2021
Accepted: 21 October 2021
Published: 28 October 2021

This article is part of the thematic issue "Earth-abundant 3d metal catalysis".

Associate Editor: L. Ackermann

© 2021 Guo and Xu; licensee Beilstein-Institut.
License and terms: see end of document.

Abstract

Electrocatalytic dehydrogenative C(sp^3)–H/C(sp)–H cross-coupling of tetrahydroisoquinolines with terminal alkynes has been achieved in a continuous-flow microreactor through 2,2,6,6-tetramethylpiperidine 1-oxyl (TEMPO)/copper relay catalysis. The reaction is easily scalable and requires low concentration of supporting electrolyte and no external chemical oxidants or ligands, providing straightforward and sustainable access to 2-functionalized tetrahydroisoquinolines.

Introduction

The dehydrogenative cross-coupling of two C–H bonds represents an ideal strategy for the construction of C–C bonds [1,2]. In this context, few methods have been developed for the dehydrogenative cross-coupling of tetrahydroisoquinolines with terminal alkynes because of the prevalence of the tetrahydroisoquinoline moiety in natural products and bioactive molecules [3-10]. These methods proceed through the oxidation of the tetrahydroisoquinoline to an iminium intermediate with various chemical oxidants such as peroxides and DDQ followed by reaction with the copper acetylide species to deliver the 2-substituted tetrahydroisoquinoline product (Scheme 1A). These methods usually require elevated temperatures [3-5], prompting the development of mild conditions by merging photoredox catalysis with copper catalysis (Scheme 1B) [8,9]. Notwithstanding of these outstanding achievements, noble metal-based catalysts and chemical oxidants are employed under these photochemical conditions.

Organic electrochemistry is an ideal tool for promoting dehydrogenative cross-coupling reactions as no external chemical

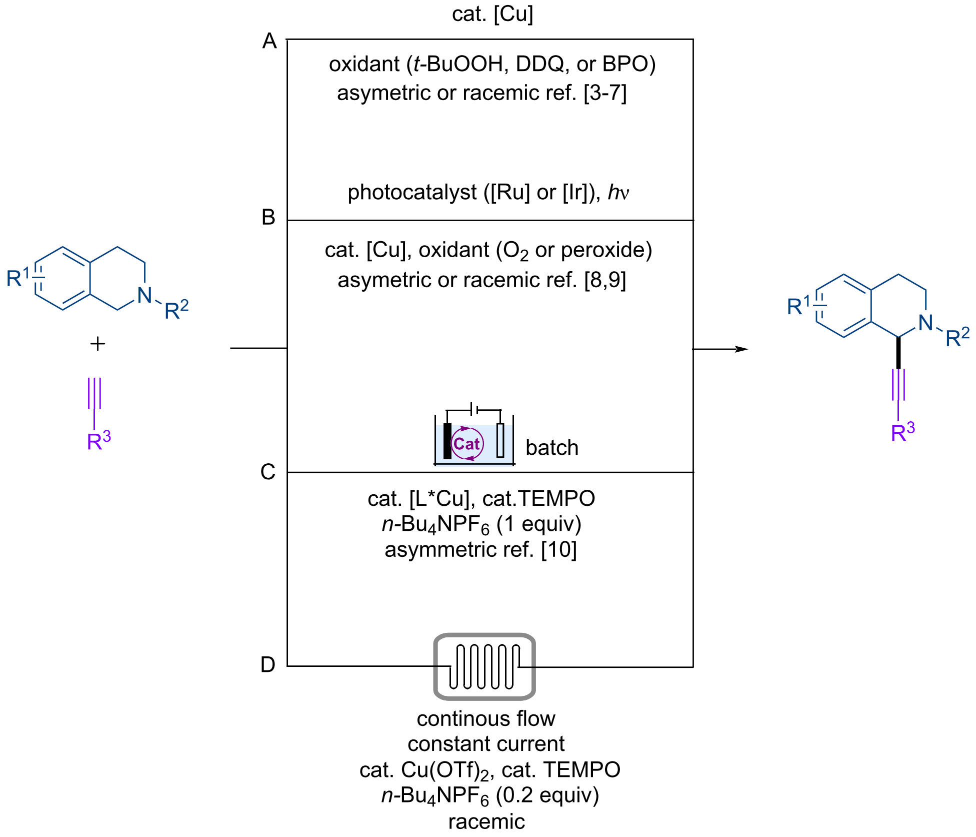
cat. [Cu]
A
oxidant (*t*-BuOOH, DDQ, or BPO)
asymetric or racemic ref. [3-7]
photocatalyst ([Ru] or [Ir]), *h*ν
B
cat. [Cu], oxidant (O_2 or peroxide)
asymetric or racemic ref. [8,9]
Cat
batch
C
cat. [L*Cu], cat.TEMPO
n-Bu_4NPF_6 (1 equiv)
asymmetric ref. [10]
D
continous flow
constant current
cat. $Cu(OTf)_2$, cat. TEMPO
n-Bu_4NPF_6 (0.2 equiv)
racemic
R^1
N
R^2
+
R^3

Scheme 1: C(sp^3)–H alkynylation of tetrahydroisoquinolines. L* = chiral ligand. TEMPO = 2,2,6,6-tetramethylpiperidine 1-oxyl. DDQ = 2,3-dichloro-5,6-dicyano-1,4-benzoquinone. BPO = benzoyl peroxide.

oxidants are needed [11-19]. In this context, Mei and co-workers have reported an elegant TEMPO/[L*Cu] co-catalyzed asymmetric electrochemical dehydrogenative cross-coupling reaction of tetrahydroisoquinolines with terminal alkynes (Scheme 1C) [10]. The chiral ligand was found to be critical for the stereoinduction as well as product formation for these electrochemical reactions that are conducted in batch. Continuous-flow electrochemical microreactors offer several advantages for electrosynthesis and have been employed to reduce the use of supporting electrolyte, facilitate reaction scale-up, and increase reaction efficiency [20-32]. Despite these advantages of continuous-flow electrosynthesis and the intense interests in transition-metal electrocatalysis [33-39], transition-metal electrocatalysis in continuous flow remains underexplored [40]. With our continued interests in transition-metal electrocatalysis [41,42] and continuous-flow electrosynthesis [43-48], we report herein the electrocatalytic dehydrogenative cross-coupling reaction of tetrahydroisoquinolines with terminal alkynes in continuous flow (Scheme 1D). These reactions require low loadings of supporting electrolyte and proceed through Cu/TEMPO relay catalysis without need for additional ligands.

Results and Discussion

The electrosynthesis was conducted in a microreactor equipped with two Pt electrodes as the anode and cathode and operated with a constant current (Table 1). Under the optimized conditions, a solution of tetrahydroisoquinoline **1a** (1 equiv), alkyne **2** (1.5 equiv), $Cu(OTf)_2$ (10 mol %), TEMPO (20 mol %), *n*-Bu_4NPF_6 (0.2 equiv), and TFE (3.5 equiv) in MeCN was passed through the cell at 0.2 mL min^{-1} to give the desired product **3** in 86% yield (Table 1, entry 1). Pleasingly, a good yield of 82% was obtained in the absence of supporting electrolyte (Table 1, entry 2). While product formation was observed without TEMPO (Table 1, entry 3) and TFE (Table 1, entry 4), albeit in low yields, the reaction failed completely without the copper salt (Table 1, entry 5). Other variations also resulted in diminished yield of **3**, such as lowering the loading of $Cu(OTf)_2$ to 5 mol % (Table 1, entry 6), replacing $Cu(OTf)_2$ with other copper salts such as $Cu(acac)_2$ (Table 1, entry 7), $Cu(TFA)_2$, (Table 1, entry 8), $Cu(OAc)_2$ (Table 1, entry 9) and replacing TFE with other protic additives including MeOH (Table 1, entry 10), EtOH (Table 1, entry 11), HFIP (Table 1, entry 12) and H_2O (Table 1, entry 13).

Table 1: Optimization of reaction conditions.[a]

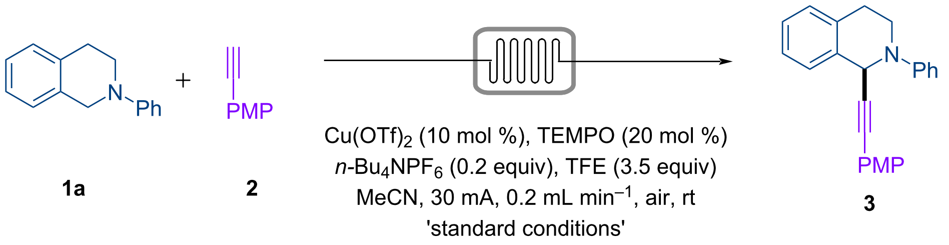
1a
2
PMP
Cu(OTf)2 (10 mol %), TEMPO (20 mol %)
n-Bu4NPF6 (0.2 equiv), TFE (3.5 equiv)
MeCN, 30 mA, 0.2 mL min−1, air, rt
'standard conditions'
3
N
Ph

Entry	Deviation from standard conditions	Yield of **3** (%)
1	none	86[b]
2	no n-Bu_4NPF_6	82
3	no TEMPO	35
4	no TFE	19
5	no $Cu(OTf)_2$	0
6	$Cu(OTf)_2$ (5 mol %)	71
7	$Cu(acac)_2$ instead of $Cu(OTf)_2$	17
8	$Cu(TFA)_2$ instead of $Cu(OTf)_2$	77
9	$Cu(OAc)_2$ instead of $Cu(OTf)_2$	40
10	MeOH instead of TFE	60
11	EtOH instead of TFE	50
12	HFIP instead of TFE	38
13	H_2O instead of TFE	20

[a] Standard conditions: **1a** (0.21 mmol), **2** (0.32 mmol, 1.5 equiv), MeCN (7 mL), Pt anode, Pt cathode, interelectrode distance = 0.25 mm, 3.1 F mol^{-1}. Yield of product **3** is determined by ^1H NMR analysis using 1,3,5-trimethoxybenzene as the internal standard. TFE, 2,2,2-trifluoroethanol. PMP, *p*-methoxyphenyl. HFIP, 1,1,1,3,3,3-hexafluoropropan-2-ol. TEMPO, 2,2,6,6-tetramethylpiperidine 1-oxyl. $Cu(acac)_2$, Copper(II) acetylacetonate. $Cu(TFA)_2$, Copper(II) trifluoroacetate. [b] Isolated yield.

The scope of the continuous-flow electrosynthesis was investigated by varying the substituents of the tetrahydroisoquinoline and the alkyne (Scheme 2). The *N*-phenyl ring of the tetrahydroisoquinoline could be substituted with groups such as OMe (**4**, **5**), Me (**6**), Et (**7**), *t*-Bu (**8**), F (**9**), and Cl (**10**). An *N*-2-naphthalenyl-substituted tetrahydroisoquinoline bearing two OMe groups at 6,7-positions (**11**) also reacted successfully. The alkyne coupling partner also tolerated variation. The reactions were found to be compatible with arylalkynes such as phenylacetylenes bearing at the *para* position a H (**12**), Me (**13**), *t*-Bu (**14**, **16**), or Br (**15**), 2-ethynylpyridine (**17**), alkenylalkynes (**18**), and alkylalkynes (**19**–**21**).

The continuous-flow electrosynthesis is easily scaled up by passing more material through the reactor [43,49]. Hence, repeating the reaction under flow conditions, with a solution containing 0.98 g of tetrahydroisoquinoline **1a** and 1.11 g of alkyne **22** afforded 1.05 g (61%) of product **14** in 13 h (Scheme 3). The productivity could be increased if multiple reactors were employed in parallel [43].

A mechanism for the electrochemical synthesis was proposed based on reported studies (Scheme 4) [3,10]. Anodic oxidation of TEMPO generates the oxoammonium salt $TEMPO^+$ [50,51], which reacts with tetrahydroisoquinoline **23** to generate TEMPOH and iminium ion **24** [52], TEMPOH is oxidized back to $TEMPO^+$ on the anode. On the other hand, **24** is converted to the final product **25** through reaction with copper acetylide **26**, which is generated from Cu^I and the alkyne **27** with the assistance of $CF_3CH_2O^-$. The added Cu^{II} precatalyst is likely reduced at the cathode to produce the requisite Cu^I. The base $CF_3CH_2O^-$ is produced through cathodic reduction of TFE. The addition of TFE to the reactions helps cathodic H_2 evolution and may also stabilize the iminium ion through reversible reaction with this cationic species.

Conclusion

In summary, we have achieved the electrochemical dehydrogenation cross-coupling of tetrahydroisoquinolines with terminal alkynes in continuous flow through Cu/TEMPO relay catalysis.

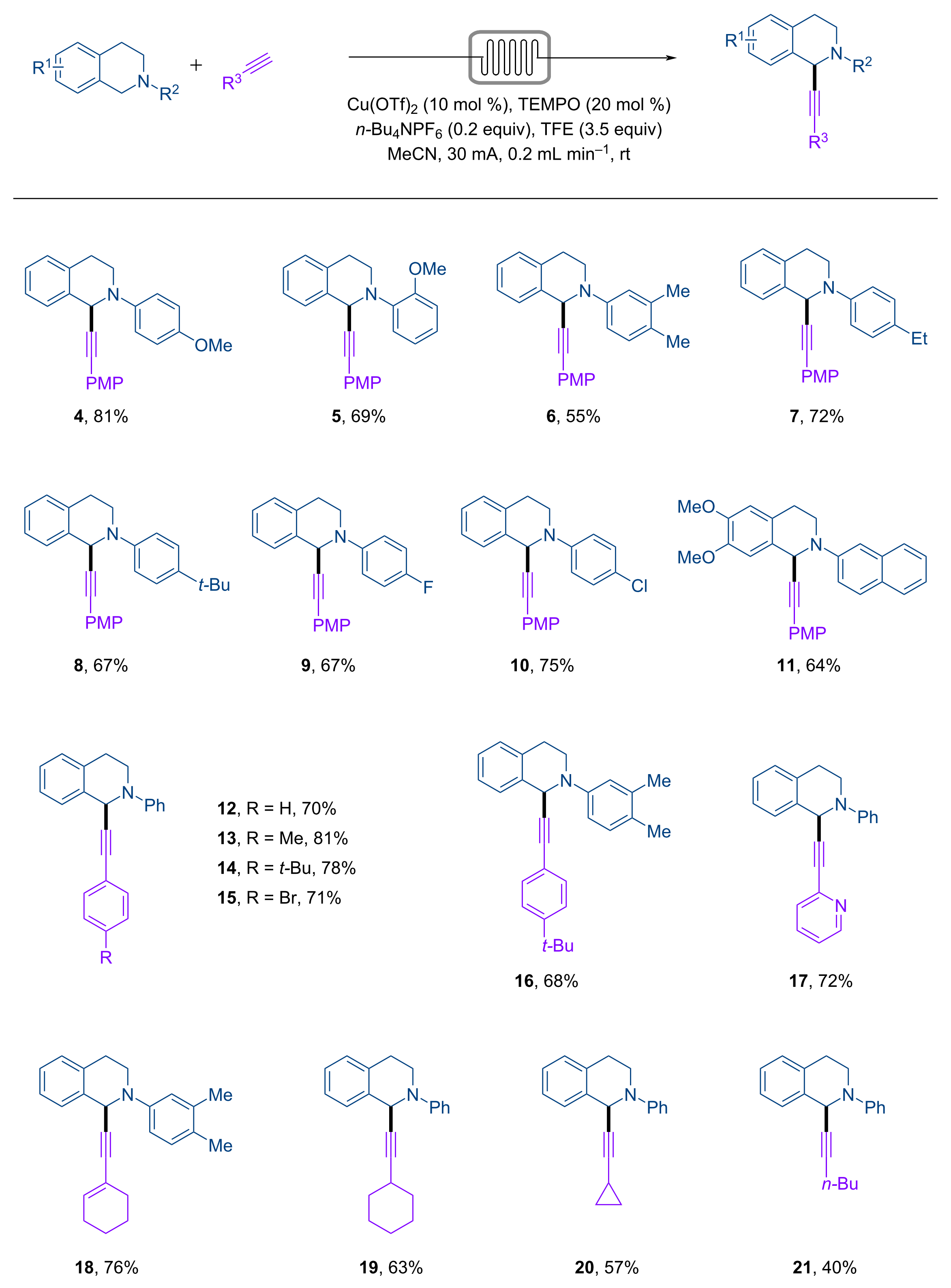
R1
N
R2
+
R3
Cu(OTf)2 (10 mol %), TEMPO (20 mol %)
n-Bu4NPF6 (0.2 equiv), TFE (3.5 equiv)
MeCN, 30 mA, 0.2 mL min−1, rt
R1
N
R2
R3
N
OMe
PMP
4, 81%
OMe
N
PMP
5, 69%
N
Me
Me
PMP
6, 55%
N
Et
PMP
7, 72%
N
t-Bu
PMP
8, 67%
N
F
PMP
9, 67%
N
Cl
PMP
10, 75%
MeO
MeO
N
PMP
11, 64%
N
Ph
R
12, R = H, 70%
13, R = Me, 81%
14, R = t-Bu, 78%
15, R = Br, 71%
N
Me
Me
t-Bu
16, 68%
N
Ph
N
17, 72%
N
Me
Me
18, 76%
N
Ph
19, 63%
N
Ph
20, 57%
N
Ph
n-Bu
21, 40%

Scheme 2: Substrate scope. Reaction conditions: Pt anode, Pt cathode, interelectrode distance 0.25 mm, **1** (0.03 M, 0.21 mmol), **2** (0.045 M, 1.5 equiv), $Cu(OTf)_2$ (10 mol %), TEMPO (20 mol %), $n\text{-}Bu_4NPF_6$ (20 mol %), TFE (3.5 equiv), MeCN (7 mL), I = 30 mA, flow rate = 0.20 mL min^{-1}, rt. Isolated yields are reported.

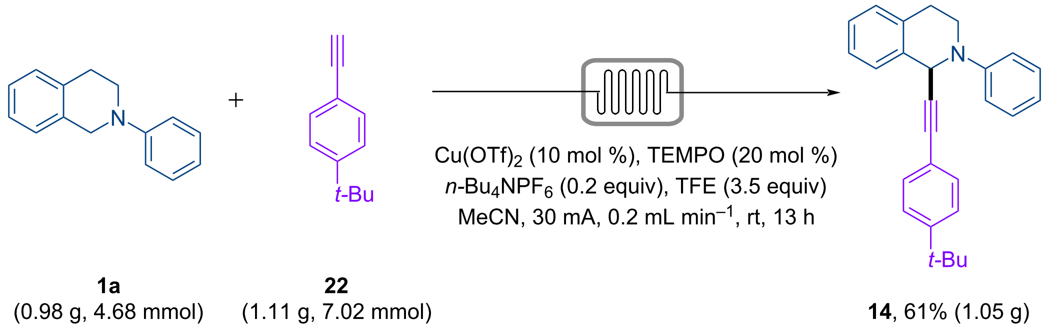
+
t-Bu
Cu(OTf)$_2$ (10 mol %), TEMPO (20 mol %)
n-Bu$_4$NPF$_6$ (0.2 equiv), TFE (3.5 equiv)
MeCN, 30 mA, 0.2 mL min^{-1}, rt, 13 h
N
t-Bu
1a
(0.98 g, 4.68 mmol)
22
(1.11 g, 7.02 mmol)
14, 61% (1.05 g)

Scheme 3: Reaction scale-up.

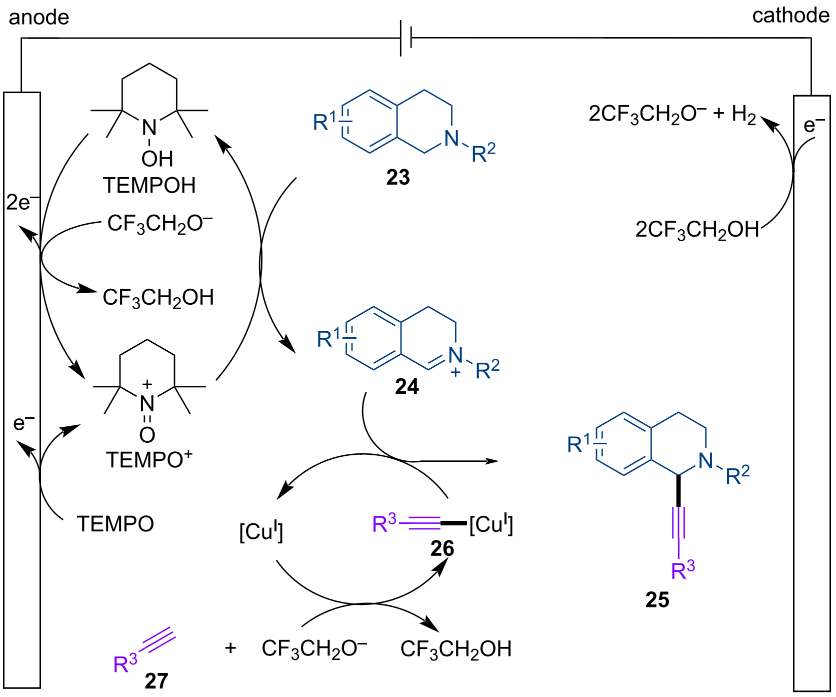
anode
cathode
N
OH
TEMPOH
2e$^-$
CF$_3$CH$_2$O$^-$
CF$_3$CH$_2$OH
+
N
O
TEMPO$^+$
e$^-$
TEMPO
R^1
N
R^2
23
R^1
N
+
R^2
24
[Cu^I]
R^3
[Cu^I]
26
R^3
27
+
CF$_3$CH$_2$O$^-$
CF$_3$CH$_2$OH
2CF$_3$CH$_2$O$^-$ + H$_2$
e$^-$
2CF$_3$CH$_2$OH
R^1
N
R^2
R^3
25

Scheme 4: Proposed mechanism.

This work demonstrates that continuous-flow electrochemical microreactors can be a viable tool for developing efficient transition-metal electrocatalysis.

Supporting Information

Supporting Information File 1

General procedure, characterization data for electrolysis products and NMR spectra.
[https://www.beilstein-journals.org/bjoc/content/supplementary/1860-5397-17-178-S1.pdf]

Funding

Financial support of this research from NSFC (21971213) and the Fundamental Research Funds for the Central Universities is acknowledged.

ORCID® iDs

Bin Guo - https://orcid.org/0000-0003-2080-5087
Hai-Chao Xu - https://orcid.org/0000-0002-3008-5143

References

1. Li, C.-J. *Acc. Chem. Res.* **2009,** *42,* 335–344. doi:10.1021/ar800164n
2. Wang, H.; Gao, X.; Lv, Z.; Abdelilah, T.; Lei, A. *Chem. Rev.* **2019,** *119,* 6769–6787. doi:10.1021/acs.chemrev.9b00045

3. Li, Z.; Li, C.-J. *J. Am. Chem. Soc.* **2004,** *126,* 11810–11811. doi:10.1021/ja0460763
4. Li, Z.; Li, C.-J. *Org. Lett.* **2004,** *6,* 4997–4999. doi:10.1021/ol047814v
5. Li, Z.; MacLeod, P. D.; Li, C.-J. *Tetrahedron: Asymmetry* **2006,** *17,* 590–597. doi:10.1016/j.tetasy.2006.02.007
6. Su, W.; Yu, J.; Li, Z.; Jiang, Z. *J. Org. Chem.* **2011,** *76,* 9144–9150. doi:10.1021/jo2015533
7. Yu, J.; Li, Z.; Jia, K.; Jiang, Z.; Liu, M.; Su, W. *Tetrahedron Lett.* **2013,** *54,* 2006–2009. doi:10.1016/j.tetlet.2013.02.007
8. Rueping, M.; Koenigs, R. M.; Poscharny, K.; Fabry, D. C.; Leonori, D.; Vila, C. *Chem. – Eur. J.* **2012,** *18,* 5170–5174. doi:10.1002/chem.201200050
9. Perepichka, I.; Kundu, S.; Hearne, Z.; Li, C.-J. *Org. Biomol. Chem.* **2015,** *13,* 447–451. doi:10.1039/c4ob02138j
10. Gao, P.-S.; Weng, X.-J.; Wang, Z.-H.; Zheng, C.; Sun, B.; Chen, Z.-H.; You, S.-L.; Mei, T.-S. *Angew. Chem., Int. Ed.* **2020,** *59,* 15254–15259. doi:10.1002/anie.202005099
11. Yuan, Y.; Lei, A. *Acc. Chem. Res.* **2019,** *52,* 3309–3324. doi:10.1021/acs.accounts.9b00512
12. Yan, M.; Kawamata, Y.; Baran, P. S. *Chem. Rev.* **2017,** *117,* 13230–13319. doi:10.1021/acs.chemrev.7b00397
13. Moeller, K. D. *Chem. Rev.* **2018,** *118,* 4817–4833. doi:10.1021/acs.chemrev.7b00656
14. Röckl, J. L.; Pollok, D.; Franke, R.; Waldvogel, S. R. *Acc. Chem. Res.* **2020,** *53,* 45–61. doi:10.1021/acs.accounts.9b00511
15. Xiong, P.; Xu, H.-C. *Acc. Chem. Res.* **2019,** *52,* 3339–3350. doi:10.1021/acs.accounts.9b00472
16. Chen, N.; Xu, H.-C. *Green Synth. Catal.* **2021,** *2,* 165–178. doi:10.1016/j.gresc.2021.03.002
17. Jiang, Y.; Xu, K.; Zeng, C. *Chem. Rev.* **2018,** *118,* 4485–4540. doi:10.1021/acs.chemrev.7b00271
18. Shi, S.-H.; Liang, Y.; Jiao, N. *Chem. Rev.* **2021,** *121,* 485–505. doi:10.1021/acs.chemrev.0c00335
19. Ye, Z.; Zhang, F. *Chin. J. Chem.* **2019,** *37,* 513–528. doi:10.1002/cjoc.201900049
20. Elsherbini, M.; Wirth, T. *Acc. Chem. Res.* **2019,** *52,* 3287–3296. doi:10.1021/acs.accounts.9b00497
21. Noël, T.; Cao, Y.; Laudadio, G. *Acc. Chem. Res.* **2019,** *52,* 2858–2869. doi:10.1021/acs.accounts.9b00412
22. Atobe, M.; Tateno, H.; Matsumura, Y. *Chem. Rev.* **2018,** *118,* 4541–4572. doi:10.1021/acs.chemrev.7b00353
23. Pletcher, D.; Green, R. A.; Brown, R. C. D. *Chem. Rev.* **2018,** *118,* 4573–4591. doi:10.1021/acs.chemrev.7b00360
24. Laudadio, G.; Bartolomeu, A. d. A.; Verwijlen, L. M. H. M.; Cao, Y.; de Oliveira, K. T.; Noël, T. *J. Am. Chem. Soc.* **2019,** *141,* 11832–11836. doi:10.1021/jacs.9b06126
25. Laudadio, G.; Barmpoutsis, E.; Schotten, C.; Struik, L.; Govaerts, S.; Browne, D. L.; Noël, T. *J. Am. Chem. Soc.* **2019,** *141,* 5664–5668. doi:10.1021/jacs.9b02266
26. Amri, N.; Wirth, T. *Synthesis* **2020,** *52,* 1751–1761. doi:10.1055/s-0039-1690868
27. Folgueiras-Amador, A. A.; Qian, X.-Y.; Xu, H.-C.; Wirth, T. *Chem. – Eur. J.* **2018,** *24,* 487–491. doi:10.1002/chem.201705016
28. Watts, K.; Gattrell, W.; Wirth, T. *Beilstein J. Org. Chem.* **2011,** *7,* 1108–1114. doi:10.3762/bjoc.7.127
29. Folgueiras-Amador, A. A.; Philipps, K.; Guilbaud, S.; Poelakker, J.; Wirth, T. *Angew. Chem., Int. Ed.* **2017,** *56,* 15446–15450. doi:10.1002/anie.201709717
30. Hielscher, M. M.; Gleede, B.; Waldvogel, S. R. *Electrochim. Acta* **2021,** *368,* 137420. doi:10.1016/j.electacta.2020.137420
31. Lin, X.; Fang, Z.; Zeng, C.; Zhu, C.; Pang, X.; Liu, C.; He, W.; Duan, J.; Qin, N.; Guo, K. *Chem. – Eur. J.* **2020,** *26,* 13738–13742. doi:10.1002/chem.202001766
32. Mo, Y.; Lu, Z.; Rughoobur, G.; Patil, P.; Gershenfeld, N.; Akinwande, A. I.; Buchwald, S. L.; Jensen, K. F. *Science* **2020,** *368,* 1352–1357. doi:10.1126/science.aba3823
33. Qiu, Y.; Zhu, C.; Stangier, M.; Struwe, J.; Ackermann, L. *CCS Chem.* **2021,** *3,* 1529–1552. doi:10.31635/ccschem.020.202000365
34. Ackermann, L. *Acc. Chem. Res.* **2020,** *53,* 84–104. doi:10.1021/acs.accounts.9b00510
35. Meyer, T. H.; Finger, L. H.; Gandeepan, P.; Ackermann, L. *Trends Chem.* **2019,** *1,* 63–76. doi:10.1016/j.trechm.2019.01.011
36. Gandeepan, P.; Finger, L. H.; Meyer, T. H.; Ackermann, L. *Chem. Soc. Rev.* **2020,** *49,* 4254–4272. doi:10.1039/d0cs00149j
37. Ma, C.; Fang, P.; Liu, Z.-R.; Xu, S.-S.; Xu, K.; Cheng, X.; Lei, A.; Xu, H.-C.; Zeng, C.; Mei, T.-S. *Sci. Bull.* **2021,** in press. doi:10.1016/j.scib.2021.07.011
38. Jiao, K.-J.; Xing, Y.-K.; Yang, Q.-L.; Qiu, H.; Mei, T.-S. *Acc. Chem. Res.* **2020,** *53,* 300–310. doi:10.1021/acs.accounts.9b00603
39. Yang, Q.-L.; Fang, P.; Mei, T.-S. *Chin. J. Chem.* **2018,** *36,* 338–352. doi:10.1002/cjoc.201700740
40. Kong, W.-J.; Finger, L. H.; Messinis, A. M.; Kuniyil, R.; Oliveira, J. C. A.; Ackermann, L. *J. Am. Chem. Soc.* **2019,** *141,* 17198–17206. doi:10.1021/jacs.9b07763
41. Xu, F.; Li, Y.-J.; Huang, C.; Xu, H.-C. *ACS Catal.* **2018,** *8,* 3820–3824. doi:10.1021/acscatal.8b00373
42. Wu, Z.-J.; Su, F.; Lin, W.; Song, J.; Wen, T.-B.; Zhang, H.-J.; Xu, H.-C. *Angew. Chem., Int. Ed.* **2019,** *58,* 16770–16774. doi:10.1002/anie.201909951
43. Huang, C.; Li, Z.-Y.; Song, J.; Xu, H.-C. *Angew. Chem., Int. Ed.* **2021,** *60,* 11237–11241. doi:10.1002/anie.202101835
44. Yan, H.; Song, J.; Zhu, S.; Xu, H.-C. *CCS Chem.* **2021,** *3,* 317–325. doi:10.31635/ccschem.021.202000743
45. Yan, H.; Zhu, S.; Xu, H.-C. *Org. Process Res. Dev.* **2021,** in press. doi:10.1021/acs.oprd.1c00038
46. Huang, C.; Xu, H.-C. *Sci. China: Chem.* **2019,** *62,* 1501–1503. doi:10.1007/s11426-019-9554-1
47. Huang, C.; Qian, X.-Y.; Xu, H.-C. *Angew. Chem., Int. Ed.* **2019,** *58,* 6650–6653. doi:10.1002/anie.201901610
48. Xu, F.; Qian, X.-Y.; Li, Y.-J.; Xu, H.-C. *Org. Lett.* **2017,** *19,* 6332–6335. doi:10.1021/acs.orglett.7b03152
49. Dong, Z.; Wen, Z.; Zhao, F.; Kuhn, S.; Noël, T. *Chem. Eng. Sci.: X* **2021,** *10,* 100097. doi:10.1016/j.cesx.2021.100097
50. Nutting, J. E.; Rafiee, M.; Stahl, S. S. *Chem. Rev.* **2018,** *118,* 4834–4885. doi:10.1021/acs.chemrev.7b00763
51. Xu, F.; Zhu, L.; Zhu, S.; Yan, X.; Xu, H.-C. *Chem. – Eur. J.* **2014,** *20,* 12740–12744. doi:10.1002/chem.201404078
52. Wang, F.; Stahl, S. S. *Acc. Chem. Res.* **2020,** *53,* 561–574. doi:10.1021/acs.accounts.9b00544

License and Terms

This is an Open Access article under the terms of the Creative Commons Attribution License (https://creativecommons.org/licenses/by/4.0). Please note that the reuse, redistribution and reproduction in particular requires that the author(s) and source are credited and that individual graphics may be subject to special legal provisions.

The license is subject to the *Beilstein Journal of Organic Chemistry* terms and conditions: (https://www.beilstein-journals.org/bjoc/terms)

The definitive version of this article is the electronic one which can be found at:
https://doi.org/10.3762/bjoc.17.178

BEILSTEIN JOURNAL OF ORGANIC CHEMISTRY

Iron-catalyzed domino coupling reactions of π-systems

Austin Pounder and William Tam*

Review

Open Access

Address:
Guelph-Waterloo Centre for Graduate Work in Chemistry and Biochemistry, Department of Chemistry, University of Guelph, Guelph, Ontario, N1G 2W1, Canada

Email:
William Tam* - wtam@uoguelph.ca

* Corresponding author

Keywords:
cascade; catalysis; coupling; earth-abundant; iron

Beilstein J. Org. Chem. **2021,** *17,* 2848–2893.
https://doi.org/10.3762/bjoc.17.196

Received: 22 September 2021
Accepted: 24 November 2021
Published: 07 December 2021

This article is part of the thematic issue "Earth-abundant 3d metal catalysis".

Associate Editor: L. Ackermann

© 2021 Pounder and Tam; licensee Beilstein-Institut.
License and terms: see end of document.

Abstract

The development of environmentally benign, inexpensive, and earth-abundant metal catalysts is desirable from both an ecological and economic standpoint. Certainly, in the past couple decades, iron has become a key player in the development of sustainable coupling chemistry and has become an indispensable tool in organic synthesis. Over the last ten years, organic chemistry has witnessed substantial improvements in efficient synthesis because of domino reactions. These protocols are more atom-economic, produce less waste, and demand less time compared to a classical stepwise reaction. Although iron-catalyzed domino reactions require a mindset that differs from the more routine noble-metal, homogenous iron catalysis they bear the chance to enable coupling reactions that rival that of noble-metal-catalysis. This review provides an overview of iron-catalyzed domino coupling reactions of π-systems. The classifications and reactivity paradigms examined should assist readers and provide guidance for the design of novel domino reactions.

Introduction

Over the past couple decades, the use of transition-metal-catalyzed cross-coupling reactions have become a staple within the organic chemist's arsenal of carbon–carbon and carbon–heteroatom bond-forming reactions. Catalysis, as a synthetic tool, is widely employed to accomplish transformations to produce many various pharmaceuticals, polymeric materials, and fine chemicals [1-8]. Catalysis is one of the fundamental pillars of green chemistry, the design of chemical products and processes that reduce or eliminate the use and generation of hazardous substances, as well as increase the atom economy of the reaction [9]. Among the transition-metal (TM) catalysts often used, the late transition metals like rhodium [10-14], palladium [15-19], nickel [20-23], and iridium [24-27] have taken center stage when it comes to the development of synthetic methodology. Although these late TMs have contributed enormously to the various fields of organic, inorganic, and organometallic chemistry, growing concerns regarding their economic and ecological impacts have risen. This has prompted interest into the use of cheap, benign, and readily available first-row TMs [28-34].

A prominent earth abundant TM bringing a renaissance to the idea of green catalysis is iron. Notably, iron is the most earth-abundant d-block element. Moreover, it is found iron is less expensive by several magnitudes compared to other late TM catalysts (Figure 1) [35].

Although the first Fe-catalyzed homo-coupling of aryl Grignard species was reported in 1941 by Kharasch and Fields [36], it wasn't until 1971 Kochi and Tamura demonstrated the first Fe-catalyzed cross-coupling reaction between Grignard reagents and vinyl halides [37]. As of late, the development of Fe-catalyzed cross-coupling methodology and mechanistic rationales have burgeoned [38]. Today, the rate of growth within the field of iron catalysis is much greater than that compared to the more studied late TMs [39-43].

Besides the more recognized concept of TM cross-coupling reactions revolving around an organic electrophile bearing a leaving group and an organometallic nucleophile, there is another large area of cross-coupling reactions that have been under significant development over the past 10 years. First achieved by Li and co-workers in 2007 [44], cross-dehydrogenative-coupling (CDC) reactions offer a highly atom economic approach to carbon–carbon (C–C) and carbon–heteroatom (C–X) bond formation via C–H activation [45,46]. Generally speaking, C–C bond forming reactions can be classified into three types (Scheme 1): the reaction of a compound bearing functional group (X), coupling with another compound bearing functional group (Y), producing a new C–C bond through the formation of X–Y (Scheme 1a). Secondly, the reaction of a C–H compound with a C–X functionalized compound

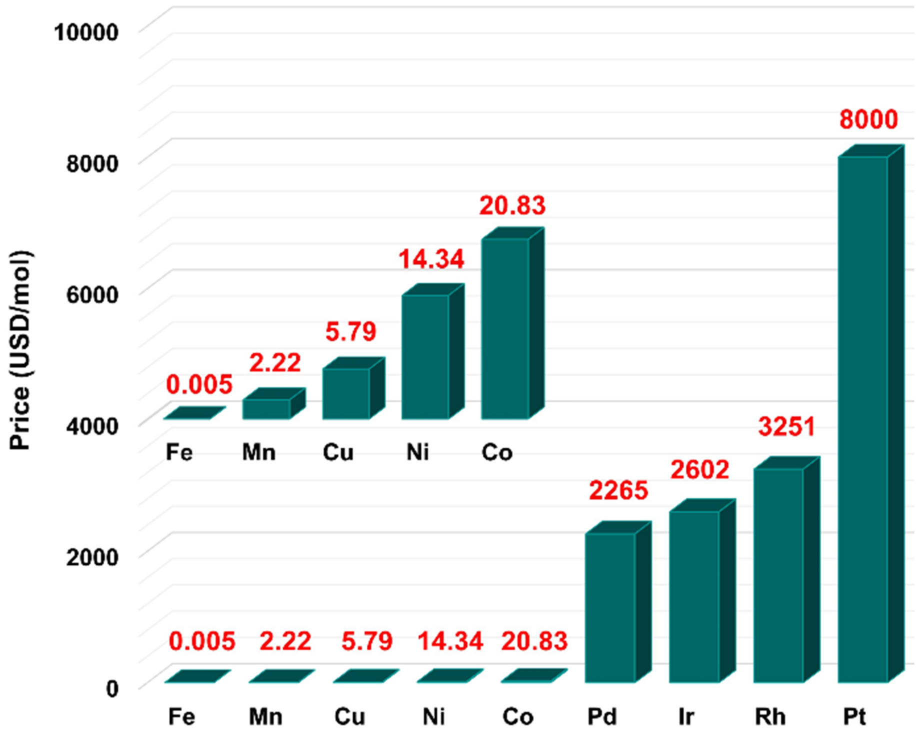

Figure 1: Price comparison among iron and other transition metals used in catalysis.

$$\text{(a)}\quad \text{C–X} + \text{C'–Y} \xrightarrow{[\text{M}]} \text{C–C'} + \text{XY}$$

$$\text{(b)}\quad \text{C–H} + \text{C'–Y} \xrightarrow{[\text{M}]} \text{C–C'} + \text{HY}$$

$$\text{(c)}\quad \text{C–H} + \text{C'–H} \xrightarrow{[\text{M}]} \text{C–C'} + \text{H}_2$$

Scheme 1: Typical modes of C–C bond formation.

(Scheme 1b). Lastly, the reaction between two C–H compounds to form a C–C bond, formally eliminating H_2, hence the dehydrogenative reference (Scheme 1c). As this coupling reaction does not require functionalization prior to coupling, it shortens the synthetic route, and lowers the production of byproducts.

Iron catalysis offers an attractive, and sustainable, approach to the aforementioned economic and ecological concerns. In the same vein, cascade reactions are important tools to meet such challenges currently facing synthetic chemists and have received considerable attention as of late. Introduced by Tietze, cascade reactions are sequences of transformations where subsequent transformations occur only in virtue of functionality formed in previous steps [47]. This process repeats until a product stable under the reaction conditions is formed and the reaction terminates. Compared to the late TMs, iron can possess a wide array of oxidation states, ranging from 2− to 6+, allowing for iron catalysis to be utilized and perform several different types of reactions. As such, a closer look at Fe-catalyzed cascade reactions reveals several distinct features. One possible method for the initiation of a multistep reaction is through the generation of an organoiron species. This can occur by the oxidative insertion of a low-valent iron into a C–X bond (Scheme 2). Evidently, iron in low oxidation states may operate as an iron-centered nucleophile, and catalyze reactions involving oxidative addition, transmetallation, and reductive elimination processes. On the other hand, iron may act as a Lewis acid, activating carbon–carbon multiple bonds via π-binding or heteroatoms via σ-complexes. This can either generate the organoiron complex after nucleophilic attack or produce a carbocation which will react further. However, reactions catalyzed by the Lewis-acidic character of iron salts are beyond the scope of this review. Iron also has the ability to transfer one or two electrons to a substrate. This opens the possibility for radical reactions via a single electron transfer (SET). Once initiated, the reaction will propagate, which typically involves the insertion of a π-system (carbometallation of alkenes/alkynes) in the case of organoiron species (Scheme 2). Alternatively, the generated radical species may undergo radical addition to alkenes, alkynes, or aromatic arenes. The final step is the termination of the reaction through the trapping of the reactive intermediate. Organoiron complexes have been shown to undergo electrophilic trapping with external species or proceed through cross-coupling eventually undergoing reductive elimination. Radical addition will typically conclude with the reductive addition or difunctionalization of the π-system; however, it has been demonstrated the radical intermediate can go through a SET oxidation/elimination to recover the initiating π-functionality.

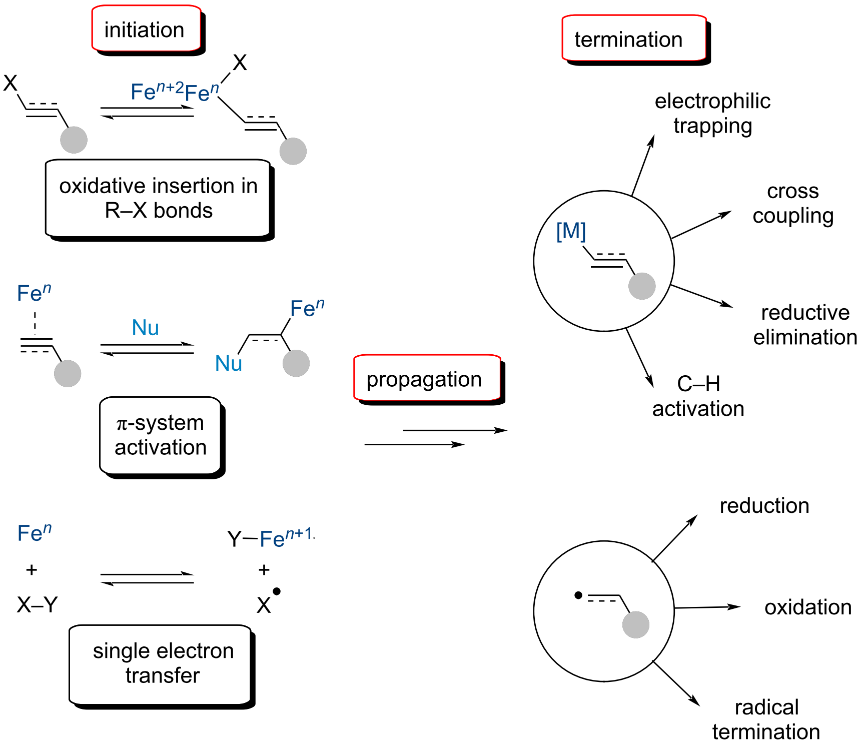

Scheme 2: The components of an iron-catalyzed domino reaction.

In this review, Fe-catalyzed domino coupling reactions involving π-systems will be discussed. Recent methods in the pursuit for efficient and economical carbon–carbon and carbon–heteroatom bond-forming reactions, such as cross-coupling, CDC, and oxidative coupling/difunctionalizations, will be summarized. The review is categorized by reaction type, and the type of bonds being formed. For reasons of clarity, newly formed bonds are sketched in red, with newly formed cyclic structures being highlighted.

Review

Iron-catalyzed cross-coupling

Metal-catalyzed cross-coupling reactions have become a staple for carbon–carbon bond formation. The late TMs that have dominated the field of cross-coupling reactions have largely been relegated to coupling partners containing either sp^2- or sp-hybridized carbons. Excellent progress has been made demonstrating reactions involving sp^3-hybridized substrates, as well as systems bearing β-hydrogens, operate efficiently under certain Fe-catalyzed conditions constituting serious competition for the established late TM-catalyzed systems. For more information, covering non-sequential Fe-catalyzed cross coupling reactions, we direct the interested readers to the several excellent reviews that described the chemistry therein [48-51].

The area of iron-catalyzed cross-coupling reactions of alkyl halides began in 2004 when Nakamura first reported the TMEDA-mediated Fe-catalyzed cross-coupling reaction between secondary bromides with aryl Grignard reagents [52]. Since then, several reports of alkyl halide cross-coupling reactions have been reported [53]. In 2015, Kang and co-workers described a $FeCl_2$-catalyzed tandem cyclization/cross-coupling reaction of alkyl iodides **1** with aryl Grignard reagents **2** to give arylmethyl-substituted pyrrolidines and tetrahydrofurans **3** in poor to excellent yield (Scheme 3) [54].

The concept of alkyl halide tandem cross-coupling reactions was first introduced by Fürstner in 2004 who disclosed specific iodoalkanes with pendant olefins undergo cyclization prior to the anticipated cross-coupling with Grignard reagents [55]. This has since been recognized by a number of other reports, indicating a SET process [56-58]. The authors investigated the effect of alkenyl substitution on the reaction to better understand mechanistic details. On inspection of the results, it is clear the radical cyclization pathway precedes the cross-coupling pathway. Moreover, no dehalogenation or β-hydride elimination byproducts were detected which supports the absence of an initial oxidative addition between the alkyl iodide and the active Fe catalyst. The possibility of a radical process rather than ionic cross-coupling is supported by the tandem cyclization/cyclopropyl ring-opening reaction, similar to previous reports [59]. The authors proposed a plausible catalytic cycle based on a series of mechanistic studies (Scheme 3). First, $FeCl_2$ will react with the aryl Grignard reagent to form an aryliron complex **8** which can undergo a SET with the iodoalkane to yield the radical substrate **9**. A 5-*exo-dig* cyclization will produce the pyrrolidinyl methyl radical **10** which may add to the iron center to form the Fe(III) complex **11**. Reductive elimination would give rise to the final product, and transmetallation with a Grignard reagent regenerates the active Fe species. Alternatively, release of the aryl radical via *ipso*-attack of the alkyl radical generating the cross-coupled product cannot be ruled out [57,60].

In 2020, Gutierrez and co-workers developed a Fe-catalyzed intra- and intermolecular difunctionalization of vinyl cyclopropanes **14** with alkyl bromides **13** and aryl Grignard reagents **2** (Scheme 4) [61]. Using sterically hindered tertiary alkyl bromides, the authors were able to favor intermolecular radical addition of the generated alkyl radical **17** to the vinylcyclopropane, outcompeting radical rebound to an aryl Fe species. The incipient radical can then undergo ring-opening of the cyclopropane **18**. Work by Fürstner [62] and Plietker [63] showed iron catalysts were able to ring-open vinylcyclopropanes for monocarbofunctionalization terminating in protonation; however, Gutierrez demonstrated the resultant radical could undergo Fe-catalyzed cross-coupling reactions. The authors noted the reaction was tolerable of both electron-donating and withdrawing groups on all three components of the reaction affording products in good yield; however, the reaction produced geometric isomers, consistently favoring the *E* isomer. The authors applied their methodology towards an asymmetric variant using a chiral diphosphine ligand. Preliminary results demonstrated the chiral iron species moderately controlled the enantioselectivity of the aryl Grignard cross-coupling. This work provided a proof-of-concept towards the use of vinylcyclopropanes as useful 1,5-synthons in asymmetric Fe-catalyzed cross-coupling reactions. Although poor enantioinduction was observed, several Fe-catalyzed non-sequential cross-coupling protocols have been established with yields and enantioselectivity rivaling Pd-catalyzed reactions [64,65]. Mechanistically, these reactions differ by not including a π-system which allows for propagation of reaction.

In the same year, the Gutierrez Lab reported the first three-component 1,2-dicarbofunctionalzation of alkenes **21** (Scheme 5) [66]. The authors noted π-systems bearing O- and S-heteroatoms had little to no compatibility with the transformation as well as sterically hindered Grignard reagents **2**. Similar to their previous report, primary and secondary alkyl halides were prone to undergoing direct cross-coupling rather than radical addition across the π-system. Consistent with the proposed

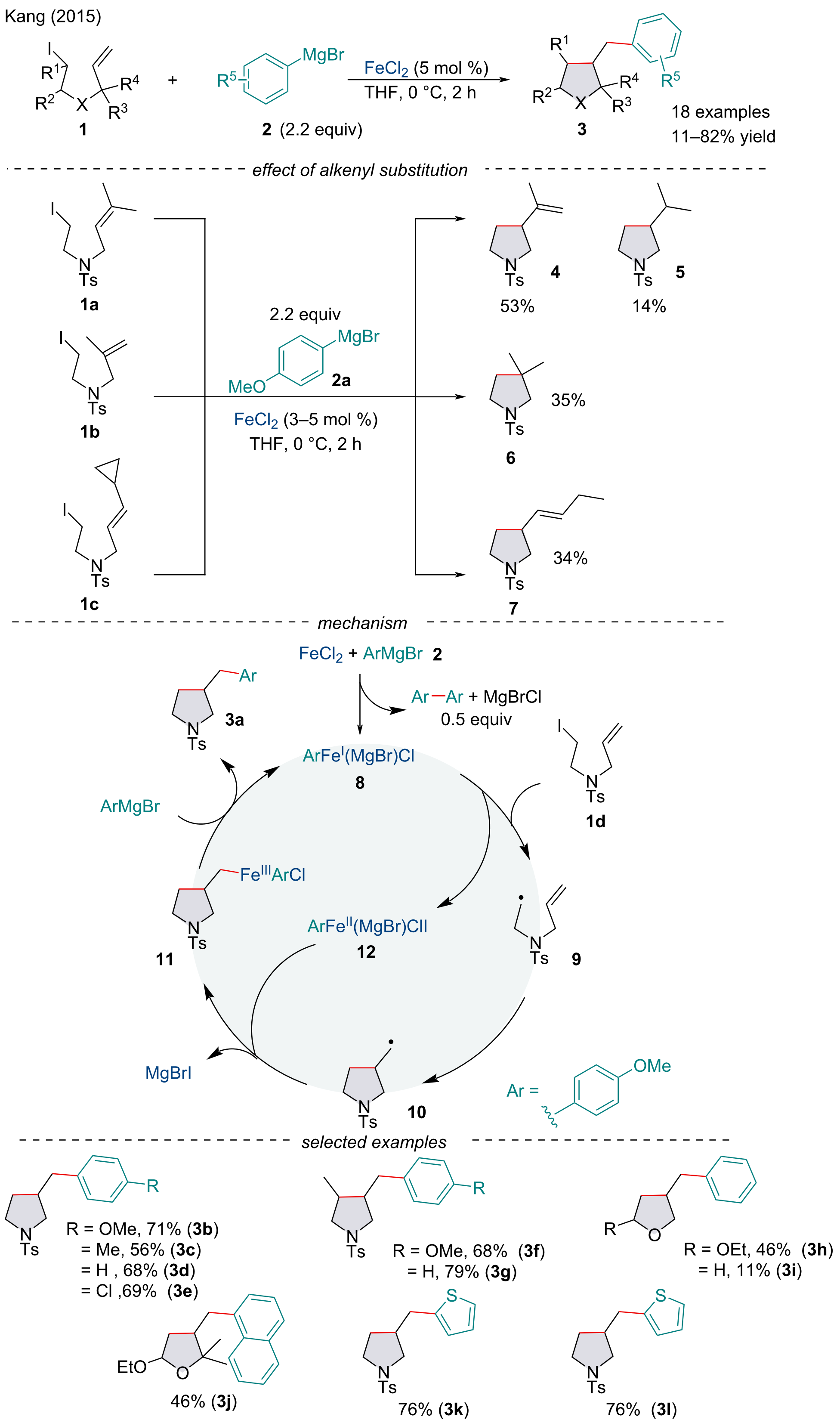
Kang (2015)
1
2 (2.2 equiv)
FeCl2 (5 mol %)
THF, 0 °C, 2 h
3
18 examples
11–82% yield
effect of alkenyl substitution
1a
1b
1c
2.2 equiv
2a
FeCl2 (3–5 mol %)
THF, 0 °C, 2 h
4
53%
5
14%
35%
6
34%
7
mechanism
FeCl2 + ArMgBr 2
Ar—Ar + MgBrCl
0.5 equiv
ArFeI(MgBr)Cl
8
1d
9
10
ArFeII(MgBr)ClI
12
11
3a
ArMgBr
MgBrI
Ar =
selected examples
R = OMe, 71% (3b)
= Me, 56% (3c)
= H , 68% (3d)
= Cl ,69% (3e)
R = OMe, 68% (3f)
= H, 79% (3g)
R = OEt, 46% (3h)
= H, 11% (3i)
46% (3j)
76% (3k)
76% (3l)

Scheme 3: Iron-catalyzed tandem cyclization and cross-coupling reactions of iodoalkanes **1** with aryl Grignard reagents **2**.

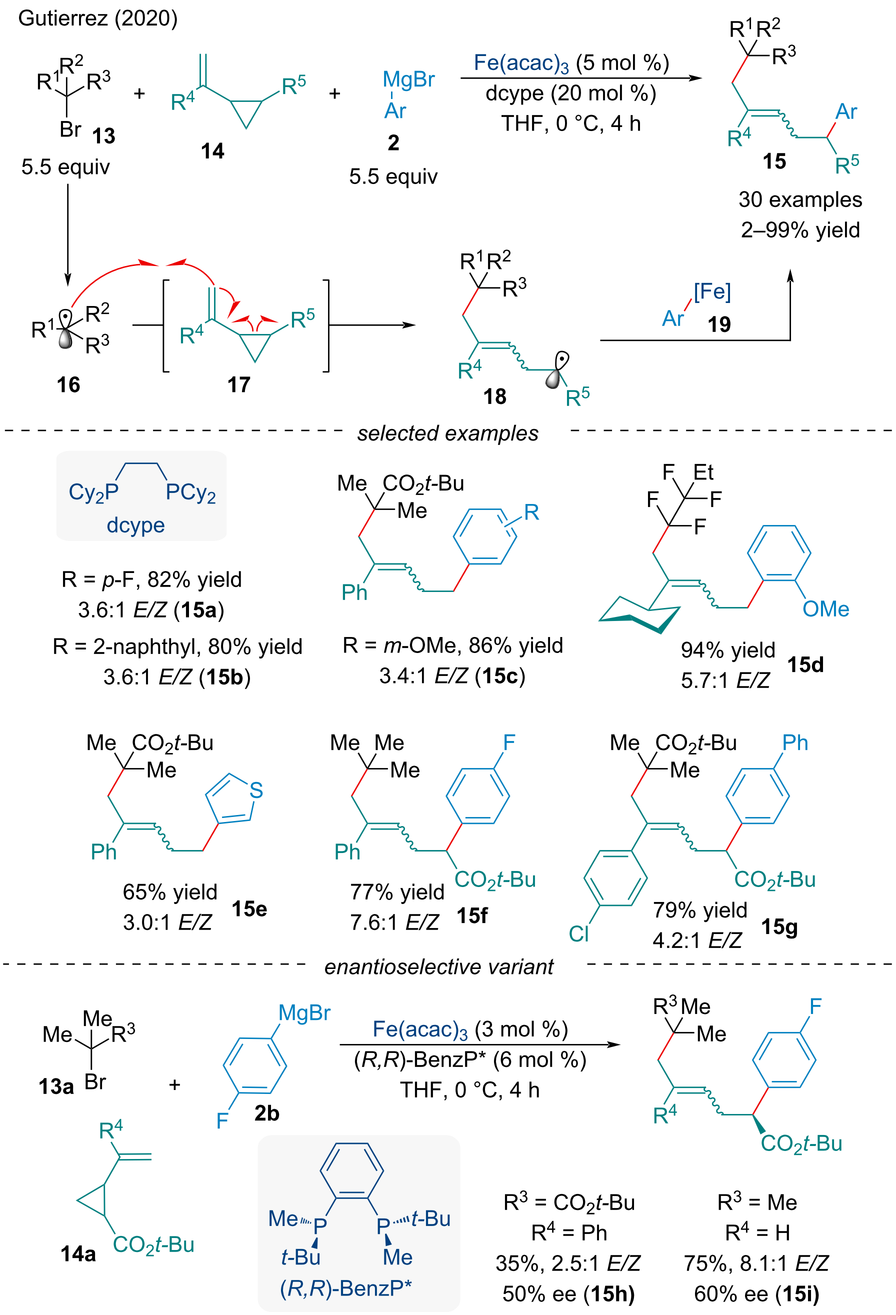
Gutierrez (2020)
13
5.5 equiv
14
MgBr
Ar
2
5.5 equiv
Fe(acac)3 (5 mol %)
dcype (20 mol %)
THF, 0 °C, 4 h
15
30 examples
2–99% yield
16
17
18
[Fe]
Ar
19
selected examples
Cy2P PCy2
dcype
R = p-F, 82% yield
3.6:1 E/Z (15a)
R = 2-naphthyl, 80% yield
3.6:1 E/Z (15b)
R = m-OMe, 86% yield
3.4:1 E/Z (15c)
94% yield
5.7:1 E/Z
15d
65% yield
3.0:1 E/Z
15e
77% yield
7.6:1 E/Z
15f
79% yield
4.2:1 E/Z
15g
enantioselective variant
13a
2b
14a
Fe(acac)3 (3 mol %)
(R,R)-BenzP* (6 mol %)
THF, 0 °C, 4 h
(R,R)-BenzP*
R3 = CO2t-Bu
R4 = Ph
35%, 2.5:1 E/Z
50% ee (15h)
R3 = Me
R4 = H
75%, 8.1:1 E/Z
60% ee (15i)

Scheme 4: Three component iron-catalyzed dicarbofunctionalization of vinyl cyclopropanes **14**.

mechanism, perfluorinated *n*-alkyl radicals performed well, suggesting ease of Giese addition is crucial [67]. The group expanded the reaction to include 1,6-dienes **24** leading to **25** via the formation of three C–C bonds through a radical cyclization/arylation cascade, like that reported by Kang et al. (Scheme 3).

The authors hypothesized the alkyl halide could react with aryl iron species **27** to form the alkyl radical **28** (Scheme 5). Regioselective Giese addition to the π-system **21** would generate the transient 2° alkyl radical **29**. Due to the high energetic barrier associated with direct cross-coupling between sterically hindered 3° alkyl radicals and aryliron complexes, it is assumed the persistent aryliron species is stable enough to be selectively trapped by the less sterically demanding 2° alkyl radical **29**. Reductive elimination would form the difunctionalized product and transmetallation with an aryl Grignard reagent regenerates the active Fe species **26**, restarting the catalytic cycle. As driving Giese addition is paramount, this method is currently

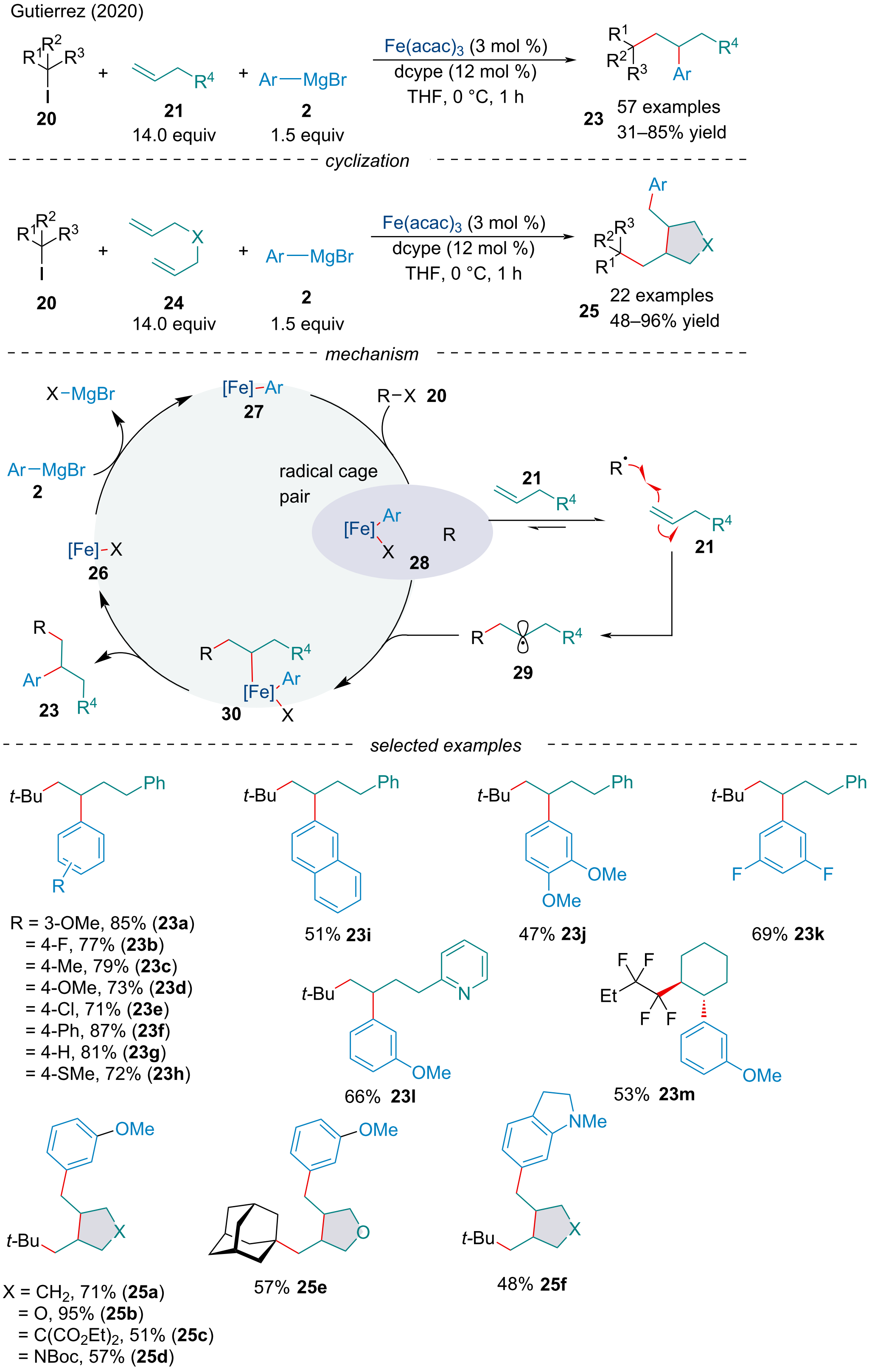
Gutierrez (2020)
20
21
14.0 equiv
2
1.5 equiv
Fe(acac)3 (3 mol %)
dcype (12 mol %)
THF, 0 °C, 1 h
23
57 examples
31–85% yield
cyclization
24
25
22 examples
48–96% yield
mechanism
[Fe]–Ar
27
R–X 20
X–MgBr
Ar–MgBr
2
radical cage pair
28
[Fe]–X
26
29
30
23
selected examples
R = 3-OMe, 85% (23a)
= 4-F, 77% (23b)
= 4-Me, 79% (23c)
= 4-OMe, 73% (23d)
= 4-Cl, 71% (23e)
= 4-Ph, 87% (23f)
= 4-H, 81% (23g)
= 4-SMe, 72% (23h)
51% 23i
47% 23j
69% 23k
66% 23l
53% 23m
X = CH2, 71% (25a)
= O, 95% (25b)
= C(CO2Et)2, 51% (25c)
= NBoc, 57% (25d)
57% 25e
48% 25f

Scheme 5: Three-component iron-catalyzed dicarbofunctionalization of alkenes **21**.

limited to the use of a large excess of olefins; however, activated alkenes could circumvent this requirement.

In 2016, the Deng group studied a novel double carbomagnesiation of unsymmetrical internal alkynes **31** with alkyl Grignard reagents **32** producing 1,3-dienylmagnesium reagents **33** with high regio- and stereoselectivity (Scheme 6) [68]. A major problem with the carbomagnesiation of internal alkynes bearing no heteroatoms is the relatively harsh conditions required producing poor selectivity in some cases [69,70]. The strong σ-donating nature of the IEt_2Me_2NHC ligand and its appropriate steric properties are thought to be crucial to the success of the reaction [71]. The authors showed the in situ-formed 1,3-dienylmagnesium species **33** can also be trapped by a variety of electrophiles, demonstrating the synthetic utility of the reaction.

In 2016, Fürstner and Echeverria demonstrated a mechanistically distinct protocol for the synthesis of 1,3-dienes **36** (Scheme 7) [72]. Compared to previous Fe-catalyzed carbomagnesiation reactions (Scheme 6) where carbometallation occurs in a concerted *syn*-manner this protocol, instead, is initiated by the oxidative cyclization of the 1,6-enyne **35** followed by reductive elimination of the carbon nucleophile **38**. Interestingly, this reaction proceeds via the cleavage of heteroelements and activated C–C bonds prior to reductive elimination of the metallacyclic ate-complex, resulting in the net formation of two new C–C bonds. Noteworthy, this methodology demonstrated a wide substrate scope, namely reacting smoothly with all-carbon backboned substrates **36c**, as well as being applicable to esters and tosylamides, proving it to be a powerful protocol for the synthesis of stereocontrolled tetrasubstituted alkenes.

In 2017, Sweeney and co-workers established a Heck/Kumada cross-coupling cascade to construct nitrogen and oxygen-containing *cis*-heterospirocycles **40** in high yield and diastereoselectivity with inexpensive $Fe(acac)_3$ as the precatalyst (Scheme 8) [73]. Interestingly, this protocol was applicable to substrates bearing classically sensitive functionalities like esters and aryl chlorides. Exposure of the iron catalyst to one equivalent of aryl Grignard reagent **2b** in the absence of the halide substrate afforded the bimetallic Fe(II) complex $FeBr_2[Mg(acac)_2](THF)_2$. Using $FeBr_2[Mg(acac)_2](THF)_2$ in place of $Fe(acac)_3$ in the arylative spirocyclization reaction delivered product **40a** in comparable yield, suggesting an initial

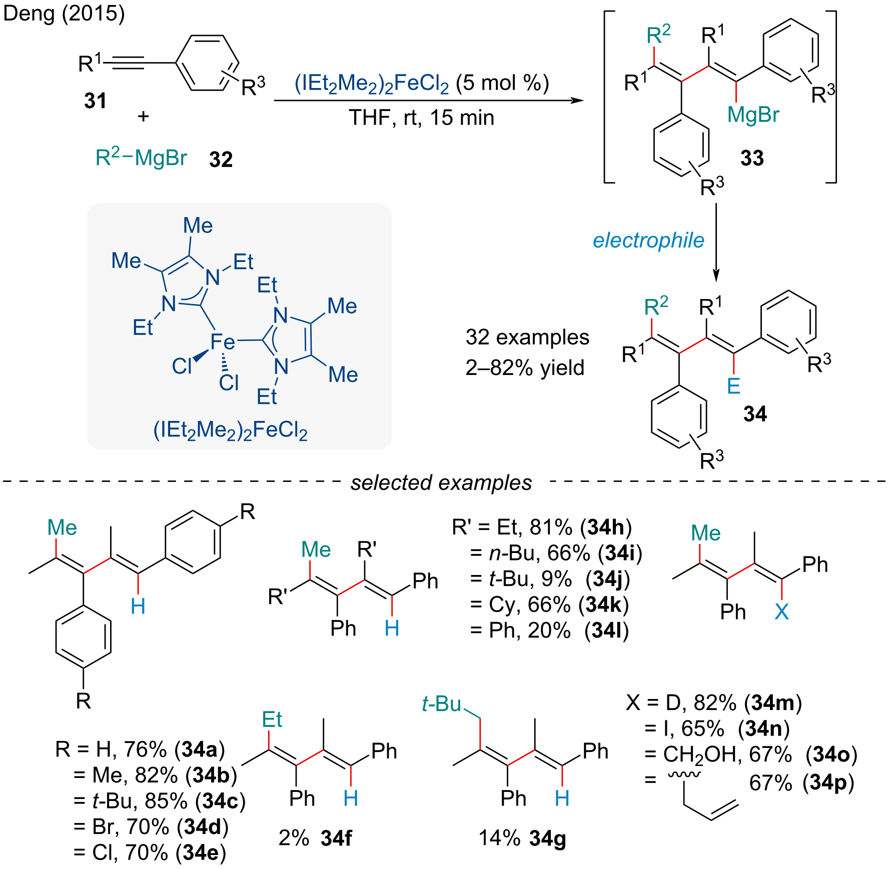

Scheme 6: Double carbomagnesiation of internal alkynes **31** with alkyl Grignard reagents **32**.

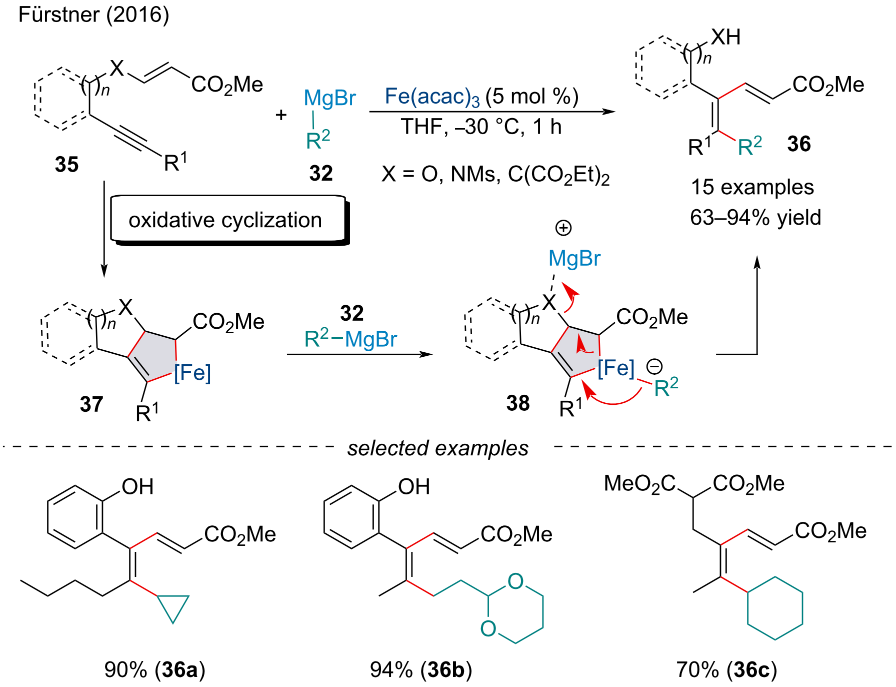

Scheme 7: Iron-catalyzed cycloisomerization/cross-coupling of enyne derivatives **35** with alkyl Grignard reagents **32**.

in situ reduction of the Fe(III) precatalyst occurs in the early stages of the catalytic cycle.

Although the mechanisms of Fe-catalyzed cross-coupling reactions are often complex [74,75] (Scheme 8), the authors believe this reaction likely proceeds with the σ-aryliron intermediate **42** cyclizing to give the η^1-allyliron species **45**. Isomerization of **45** would deliver the less-hindered isomer **48** (path i). The stereochemical outcome can be rationalized by the steric interactions of the iron residue and the C–H bond of the aromatic ring in **47**. Capturing of the iron complex by the Grignard reagent **2**, followed by reductive elimination would deliver the observed product **40**. Alternatively, the iron species **45** may undergo direct *anti*-attack by the Grignard reagent (path ii) [76]. One final possibility is the reaction proceeds via a radical mechanism (path iii) [77], although use of radical inhibitors had little impact on the success of the reaction. It seems unlikely a radical pathway is involved in the reaction mechanism; however, it cannot be categorically excluded.

In 2021, the Koh group demonstrated the first three-component alkenylboration of alkenes **50** (Scheme 9) [78]. The authors noted the described methodology regioselectively installs both the boryl functionality and olefin across both activated and unactivated π-systems **50**; however, the later required the use of (dppe)$FeBr_2$ in DMF to deliver products in appreciable yield. Alkenyl fluoride, chloride, and bromide substrates **51**/**52** were found to be amenable to the reaction although with varying degrees of success, likely due to the competing base-promoted 1,2-elimination. With the cyclopropylidene-functionalized substrates **50a**, ring-cleavage led to trisubstituted (*E*)-alkenylboronates **55**, acting as a 1,5-synthon, similar to Gutierrez‘s vinylcyclopropanes (Scheme 4) [66]. Based on mechanistic investigations, Koh proposed the catalytically active iron-boryl species **57** is generated through the ligand exchange of **56** with B_2pin_2 which can undergo borylmetallation across the alkene in a *syn*-fashion **58**. Side-on coordination of the haloalkene’s π-bond can trigger a *syn*-carbometallation **59**. A base-mediated 1,2- elimination will deliver the alkenylboration product as well as regenerate **56**. The methodology was applied towards the synthesis of (±)-imperanene.

Iron-catalyzed cross dehydrogenative coupling

Transition-metal-catalyzed carbon–carbon (C–C) or carbon–heteroatom (C–X) bond formation involving two different C–H bonds or one C–H and one X–H bond is formally known as cross dehydrogenative coupling (CDC) and is quite attractive to synthetic organic chemists [79]. Such coupling eliminates the need for prefunctionalization of the substrate, thus making synthetic schemes shorter and more efficient improving the atom and step-economy of the reaction. Other than

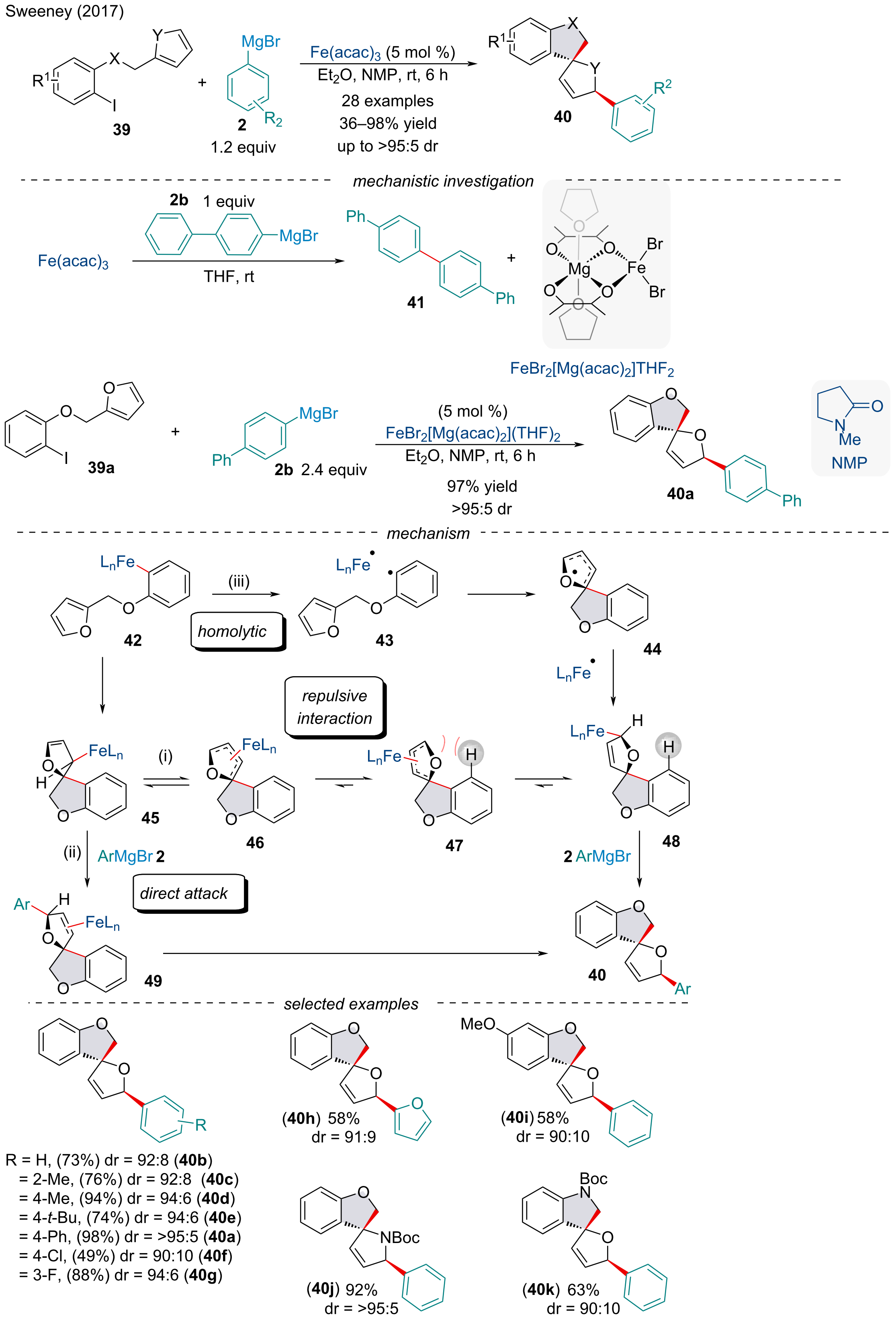
Sweeney (2017)
39
2
1.2 equiv
Fe(acac)3 (5 mol %)
Et2O, NMP, rt, 6 h
28 examples
36–98% yield
up to >95:5 dr
40
mechanistic investigation
2b 1 equiv
Fe(acac)3
THF, rt
41
FeBr2[Mg(acac)2]THF2
39a
2b 2.4 equiv
(5 mol %)
FeBr2[Mg(acac)2](THF)2
Et2O, NMP, rt, 6 h
97% yield
>95:5 dr
40a
NMP
mechanism
42
(iii)
homolytic
43
44
repulsive interaction
45
(i)
46
47
48
(ii) ArMgBr 2
direct attack
49
2 ArMgBr
40
selected examples
R = H, (73%) dr = 92:8 (40b)
= 2-Me, (76%) dr = 92:8 (40c)
= 4-Me, (94%) dr = 94:6 (40d)
= 4-t-Bu, (74%) dr = 94:6 (40e)
= 4-Ph, (98%) dr = >95:5 (40a)
= 4-Cl, (49%) dr = 90:10 (40f)
= 3-F, (88%) dr = 94:6 (40g)
(40h) 58% dr = 91:9
(40i) 58% dr = 90:10
(40j) 92% dr = >95:5
(40k) 63% dr = 90:10

Scheme 8: Iron-catalyzed spirocyclization/cross-coupling cascade.

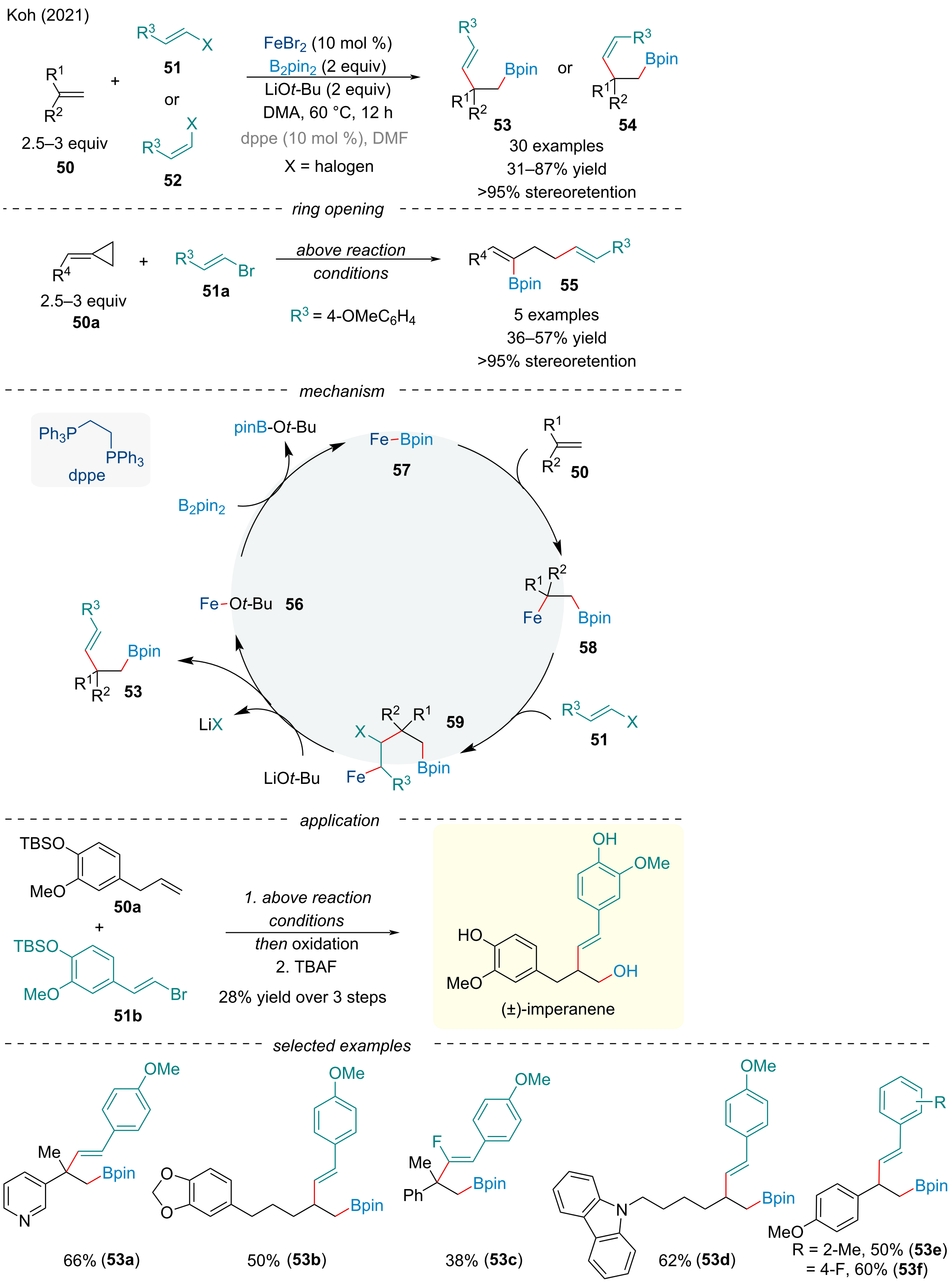
Koh (2021)
R1
R2
2.5–3 equiv
50
R3
X
51
or
X
R3
52
FeBr2 (10 mol %)
B2pin2 (2 equiv)
LiOt-Bu (2 equiv)
DMA, 60 °C, 12 h
dppe (10 mol %), DMF
X = halogen
R3
Bpin
R1
R2
53
or
R3
Bpin
R1
R2
54
30 examples
31–87% yield
>95% stereoretention
ring opening
R4
2.5–3 equiv
50a
R3
Br
51a
above reaction
conditions
R3 = 4-OMeC6H4
R4
Bpin
55
R3
5 examples
36–57% yield
>95% stereoretention
mechanism
Ph3P
PPh3
dppe
pinB-Ot-Bu
Fe–Bpin
57
B2pin2
R1
R2
50
Fe–Ot-Bu 56
R1 R2
Fe
Bpin
58
R3
Bpin
R1
R2
53
LiX
R3
X
51
R2 R1
X
59
Fe
R3
Bpin
LiOt-Bu
application
TBSO
MeO
50a
+
TBSO
MeO
Br
51b
1. above reaction
conditions
then oxidation
2. TBAF
28% yield over 3 steps
OH
OMe
HO
MeO
OH
(±)-imperanene
selected examples
OMe
Me
Bpin
N
66% (53a)
OMe
O
O
Bpin
50% (53b)
OMe
F
Me
Ph
Bpin
38% (53c)
OMe
N
Bpin
62% (53d)
R
Bpin
MeO
R = 2-Me, 50% (53e)
= 4-F, 60% (53f)

Scheme 9: Iron-catalyzed alkenylboration of alkenes **50**.

the clear economic benefits CDC offers, it's also a facile method for the coupling of sp^3 C–H species. However, the CDC reaction is not without its challenges, mainly due to the poor reactivity of C–H bonds; thus, chemists have devised protocols to activate different types of C–H bonds for the formation of C–C and C–X bonds. We classified the different CDC cascade reactions into two different sections: strictly carbon CDC reactions and heteroatomic CDC reactions.

Iron-catalyzed carbon–carbon cross dehydrogenative coupling

In 2013, Li and co-workers reported the FeCl$_3$-catalyzed arylalkylation of activated alkenes **60** for the synthesis of oxindoles **62** (Scheme 10) [80]. Mechanistic studies, including kinetic isotope effects and radical trapping, suggested a radical mechanism. The hydroperoxide, in the presence of an iron catalyst, abstracts the hydrogen atom alpha to the heteroatom. The alkyl radical may attack the acrylamide; subsequent intramolecular radical cyclization with the aryl ring would give the oxindole scaffold. Hydrogen abstraction would regenerate the reduced iron catalyst and produce the final product. Two years later, Zhou and co-workers expanded the reaction for the synthesis of substituted isoquinoline-1,3(2*H*,4*H*)-dione derivatives **64** (Scheme 10) [81]. Both laboratories observed similar trends in reactivity and came to the same mechanistic conclusions. Mechanistically, sequential and nonsequential CDC reactions are nearly identical. Typically, a CDC reaction is initiated through iron-mediated oxidation processes. In the case of a sp^3

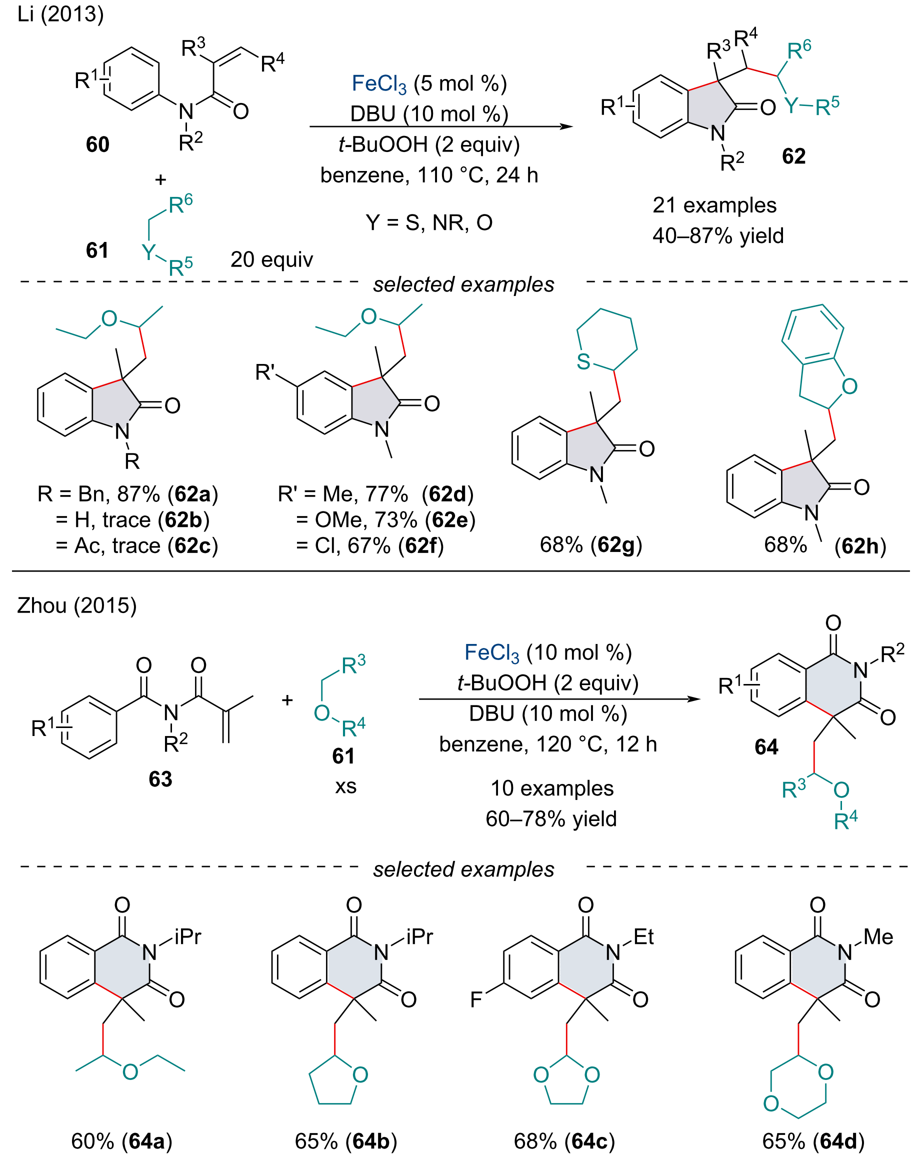
Li (2013)
R1
R3
R4
N
O
R2
60
+
R6
Y
R5
61
20 equiv
FeCl3 (5 mol %)
DBU (10 mol %)
t-BuOOH (2 equiv)
benzene, 110 °C, 24 h
Y = S, NR, O
R3 R4
R6
R1
O
Y–R5
N
R2
62
21 examples
40–87% yield
selected examples
R = Bn, 87% (62a)
= H, trace (62b)
= Ac, trace (62c)
R' = Me, 77% (62d)
= OMe, 73% (62e)
= Cl, 67% (62f)
68% (62g)
68% (62h)
Zhou (2015)
R1
O
O
N
R2
63
+
R3
O
R4
61
xs
FeCl3 (10 mol %)
t-BuOOH (2 equiv)
DBU (10 mol %)
benzene, 120 °C, 12 h
10 examples
60–78% yield
64
R2
selected examples
iPr
Et
Me
F
60% (64a)
65% (64b)
68% (64c)
65% (64d)

Scheme 10: *N*-Alkyl–*N*-aryl acrylamide **60** CDC cyclization with C(sp^3)–H bonds adjacent to a heteroatom.

C–H species, an alkyl radical can be generated. This is where sequential and nonsequential CDC reactions diverge. In the case of a nonsequential CDC reaction, the alkyl radical will directly attack an electrophilic species [79]. On the other hand, sequential CDC reactions involve propagation reactions. These propagation steps typically involve a radical addition across a two-carbon fragment, generating a new carbon-based radical species. There is no limit to the number of propagation sites a coupling partner can have; however, controlling the chronology of the radical additions can be difficult. Once the intermediate has expended all propagation sites it is terminated, typically through the generation of a new radical species.

The Zhu group followed up on this work by disclosing the use of acetonitrile as the radical precursor for the cyanomethylation/arylation of arylacrylamides to access oxindoles [82]. Despite the small scope of aliphatic nitriles explored, the reaction further demonstrated the synthetic potential of C(sp^3)–H species within CDC methodology.

In 2013, the Li group established a carbonyl-arylation of *N*-arylacrylamides **60** with alkyl and aryl aldehydes **65** (Scheme 11) [83]. Like Li's report in 2013 (Scheme 10) [80], the reaction begins with a radical addition to the acrylamide **60** followed by subsequent radical cyclization with the aryl ring. A few substituent effects were noted, namely *ortho*-substituents on the aryl ring were detrimental to the reaction. Moreover, terminal alkenes preformed poorer than their 1,1-disubstituted counterparts, perhaps due to the generation of the more stable 3° radical intermediate. In the following year, Song and Li reported a reaction shortcut for the carbonyl-arylation of *N*-arylacrylamides **60** through the *in-situ* oxidation of alcohols **67** (Scheme 11) [84]. Under the optimized reaction conditions, both primary and secondary alcohols are oxidized to the corresponding aldehyde/ketone, so the chronology of the addition remains unclear whether the reaction proceeds exclusively via an alkyl radical followed by subsequent oxidation, an acyl radical, or a combination of both. Further, slight modifications of the reaction conditions have allowed for the synthesis of

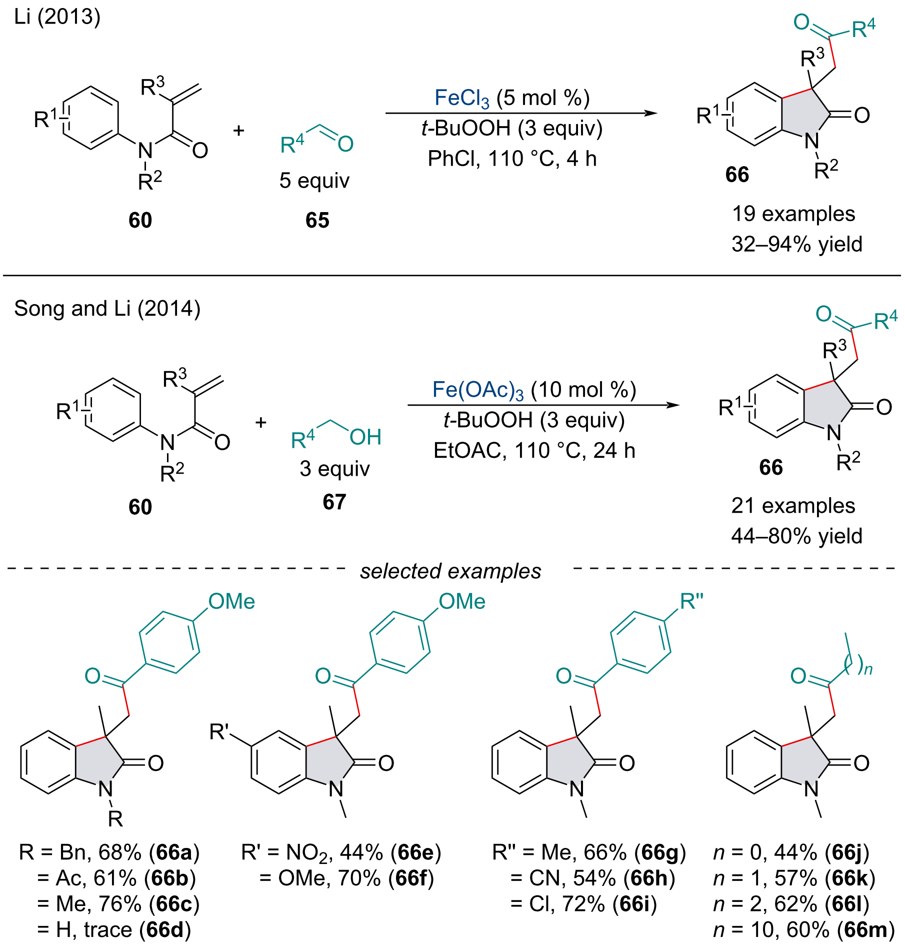
Li (2013)
R1
R3
N
R2
O
60
+
R4
O
5 equiv
65
FeCl3 (5 mol %)
t-BuOOH (3 equiv)
PhCl, 110 °C, 4 h
O
R4
R3
R1
O
N
R2
66
19 examples
32–94% yield
Song and Li (2014)
R1
R3
N
R2
O
60
+
R4
OH
3 equiv
67
Fe(OAc)3 (10 mol %)
t-BuOOH (3 equiv)
EtOAC, 110 °C, 24 h
O
R4
R3
R1
O
N
R2
66
21 examples
44–80% yield
selected examples
OMe
O
O
N
R
OMe
O
R'
O
N
R''
O
O
N
O
n
O
N
R = Bn, 68% (66a)
= Ac, 61% (66b)
= Me, 76% (66c)
= H, trace (66d)
R' = NO2, 44% (66e)
= OMe, 70% (66f)
R'' = Me, 66% (66g)
= CN, 54% (66h)
= Cl, 72% (66i)
n = 0, 44% (66j)
n = 1, 57% (66k)
n = 2, 62% (66l)
n = 10, 60% (66m)

Scheme 11: 1,2-Carboacylation of activated alkenes **60** with aldehydes **65** and alcohols **67**.

indolines and dihydropyran frameworks through tandem carbonylarylation and carbamoylarylation reactions of olefins [85,86].

In 2016, Li and co-workers investigated the dicarbonylation of alkenes **68** (Scheme 12) [87]. It was noted both EWGs and EDGs on the phenyl ring were amenable to the reaction; however, the yield was dramatically reduced with electron-deficient *N*-substituents. Substitution of the alcohol partner was well-tolerated though sterically demanding functionality lowered its reactivity. On the basis of the experimental results, the authors proposed a catalytic cycle (Scheme 12). First, the hydroperoxide, in the presence of an Fe(II) species, generates an Fe(III) intermediate and the alkoxy radical which can oxidize the incoming alcohol **67** to an aldehyde **70**. Another equivalent of hydroxy radical, either generated under thermal conditions or through the Fe redox cycle, can abstract the aldehydic hydrogen to form the acyl radical **71**. Subsequent radical addition to the alkene **68** to form **72** followed by cyclization with the nitrile affords the iminyl radical **73** which can abstract a hydrogen atom to form the more stable imine **74**. Hydrolysis of the imine affords the final product **69**. In 2020, Sun and Liu reported the iminyl cyclization could also be achieved with DMSO as a methyl-radical precursor [88].

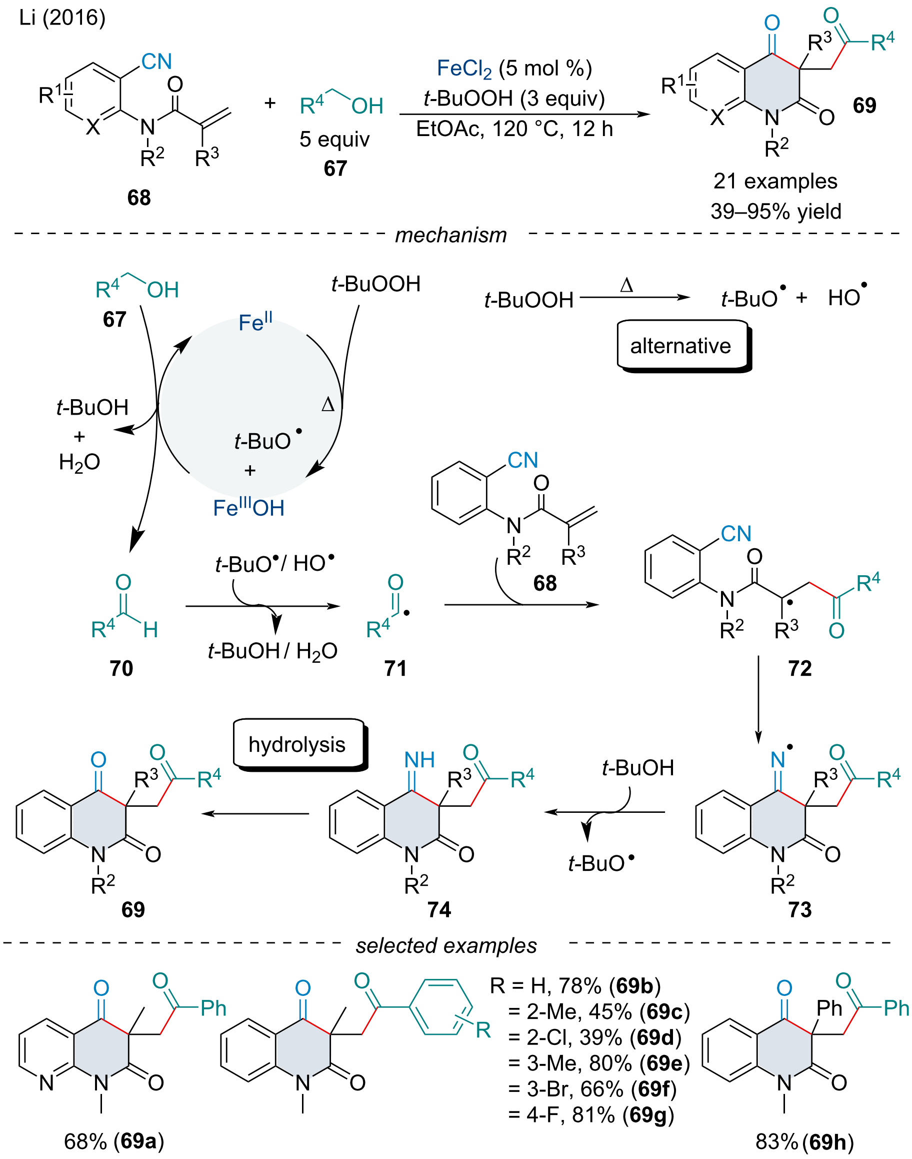
Li (2016)
CN
O
R1
X
N
R2
R3
68
+
R4
OH
5 equiv
67
FeCl2 (5 mol %)
t-BuOOH (3 equiv)
EtOAc, 120 °C, 12 h
69
21 examples
39–95% yield
mechanism
t-BuOOH
FeII
Δ
t-BuO•
+
FeIIIOH
t-BuOH
+
H2O
t-BuOOH
Δ
t-BuO• + HO•
alternative
70
t-BuO•/ HO•
t-BuOH / H2O
71
68
72
73
t-BuOH
t-BuO•
74
hydrolysis
NH
69
selected examples
Ph
68% (69a)
R = H, 78% (69b)
= 2-Me, 45% (69c)
= 2-Cl, 39% (69d)
= 3-Me, 80% (69e)
= 3-Br, 66% (69f)
= 4-F, 81% (69g)
83% (69h)

Scheme 12: Iron-catalyzed dicarbonylation of activated alkenes **68** with alcohols **67**.

In 2017, the Zhu group developed an Fe(acac)$_3$-catalyzed cyanoalkylative dearomatization of *N*-phenylcinnamamides **75** for the synthesis of 1-azaspiro[4.5]decanes **77** (Scheme 13) [89]. The reaction was amenable to both EWGs and EDGs; however, substitution at the *ortho*-position of the cinnamamide lowered the product yield. Mechanistic experiments suggest the reaction proceeds through a radical reaction. Moreover, kinetic isotope studies revealed the cleavage of the C(sp^3)–H bond may be involved in the rate-determining step of this transformation. Mechanistically, prototypical homolysis of the peroxide in the presence of the Fe(II) catalyst will generate the alkyl radical **78** formed via hydrogen abstraction. The intermediate **78** may regioselectively attack the α-position of the carbonyl **75a**. A thermodynamically controlled 5-*exo* cyclization with the aryl ring **79** would afford the spirocyclic intermediate **80**. The authors theorize the >20:1 diastereoselectivity of the reaction arises from the steric interaction between the aromatic and cyano groups. The oxidation of species **80** would reduce the Fe catalyst back to its reduced form, while a *tert*-butyl alkoxide can furnish the final product through acid-base catalysis.

In 2019, Li and co-workers investigated a three-component dialkylation of alkenes **82** with common alkanes **83** and 1,3-dicarbonyl compounds **84** via synergistic photoredox/iron catalysis (Scheme 14) [90]. This protocol parallels Li's seminal report in 2007 [44]; however, under these reaction conditions, the reactive radical was propagated across an alkene before termination with the activated methylene unit. Notably, the reaction did not proceed in the dark or in the absence of the photosensitizer at 30 °C; further, the reaction generated the desired product in lower yield at 120 °C. The scope was broad and tolerated a wide array of 1,3-keto esters and 1,3-diketones, as well as both benzylic and aliphatic C(sp^3)–H compounds.

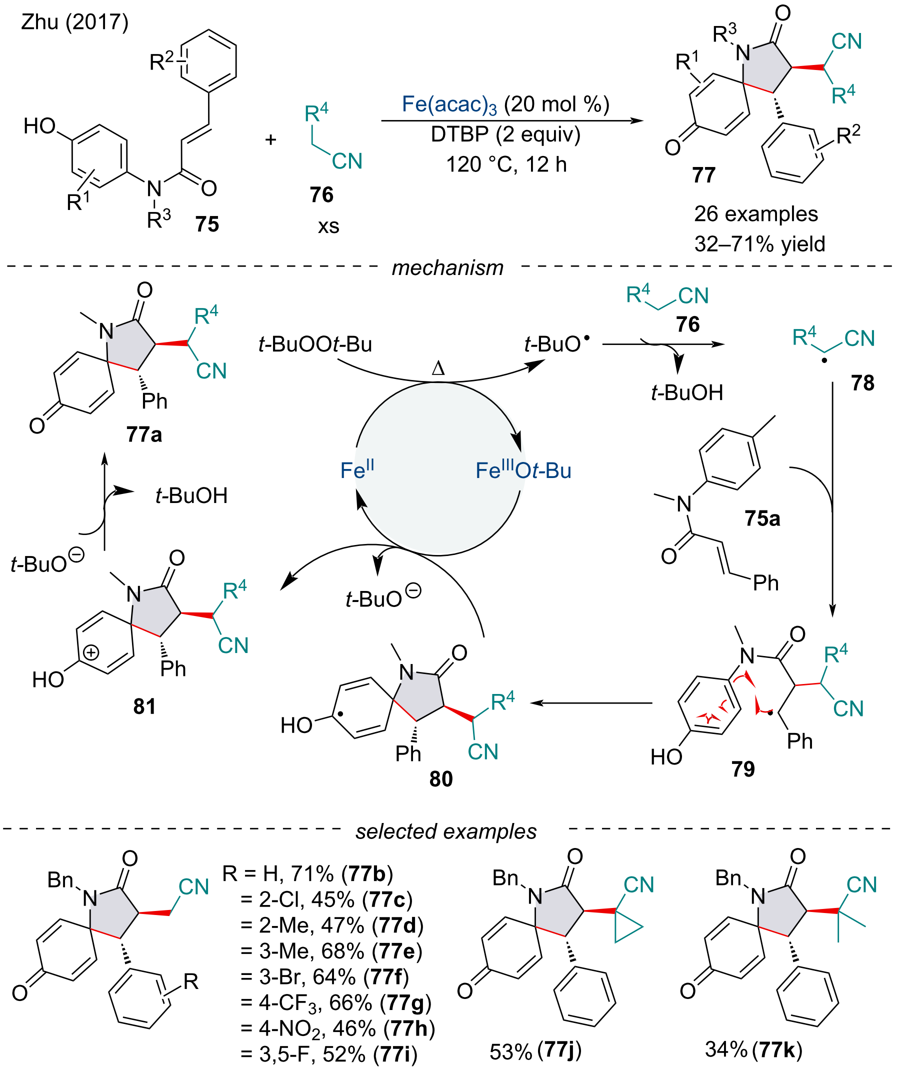
Zhu (2017)
HO
R1
R2
N
R3
O
75
+
R4
CN
76
xs
Fe(acac)3 (20 mol %)
DTBP (2 equiv)
120 °C, 12 h
R3
N
O
CN
R4
R1
O
R2
77
26 examples
32–71% yield
mechanism
77a
t-BuOOt-Bu
Δ
t-BuO•
76
t-BuOH
78
FeII
FeIIIOt-Bu
t-BuOH
t-BuO⊖
81
t-BuO⊖
75a
Ph
80
79
HO
selected examples
Bn
R = H, 71% (77b)
= 2-Cl, 45% (77c)
= 2-Me, 47% (77d)
= 3-Me, 68% (77e)
= 3-Br, 64% (77f)
= 4-CF3, 66% (77g)
= 4-NO2, 46% (77h)
= 3,5-F, 52% (77i)
53% (77j)
34% (77k)

Scheme 13: Iron-catalyzed cyanoalkylation/radical dearomatization of acrylamides **75**.

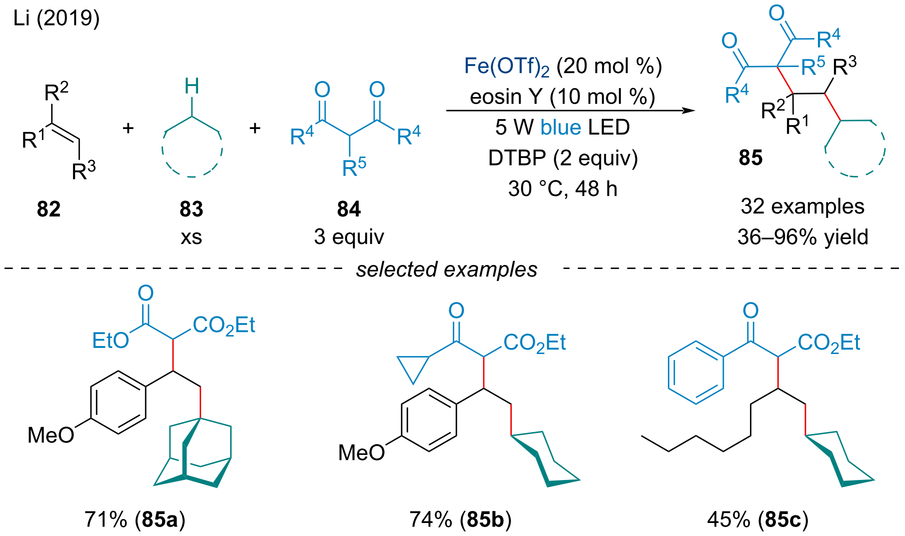
Li (2019)
82
83
xs
84
3 equiv
Fe(OTf)2 (20 mol %)
eosin Y (10 mol %)
5 W blue LED
DTBP (2 equiv)
30 °C, 48 h
85
32 examples
36–96% yield
selected examples
71% (85a)
74% (85b)
45% (85c)

Scheme 14: Synergistic photoredox/iron-catalyzed 1,2-dialkylation of alkenes **82** with common alkanes **83** and 1,3-dicarbonyl compounds **84**.

Iron-catalyzed heteroatomic cross dehydrogenative coupling

In 2013, Lei and Pappo independently reported an $FeCl_3$-catalyzed oxidative coupling/cyclization cascade of phenol derivatives **86** and alkenes **87** (Scheme 15) [91,92]. Similar trends were reported by both groups namely electron-rich phenols, as well as those bearing halogen substituents, were suitable substrates under these reaction conditions. In Lei's report, the reaction shuts down in the presence of TEMPO and in the absence of DDQ; thus, the formation of a phenoxy radical was proposed.

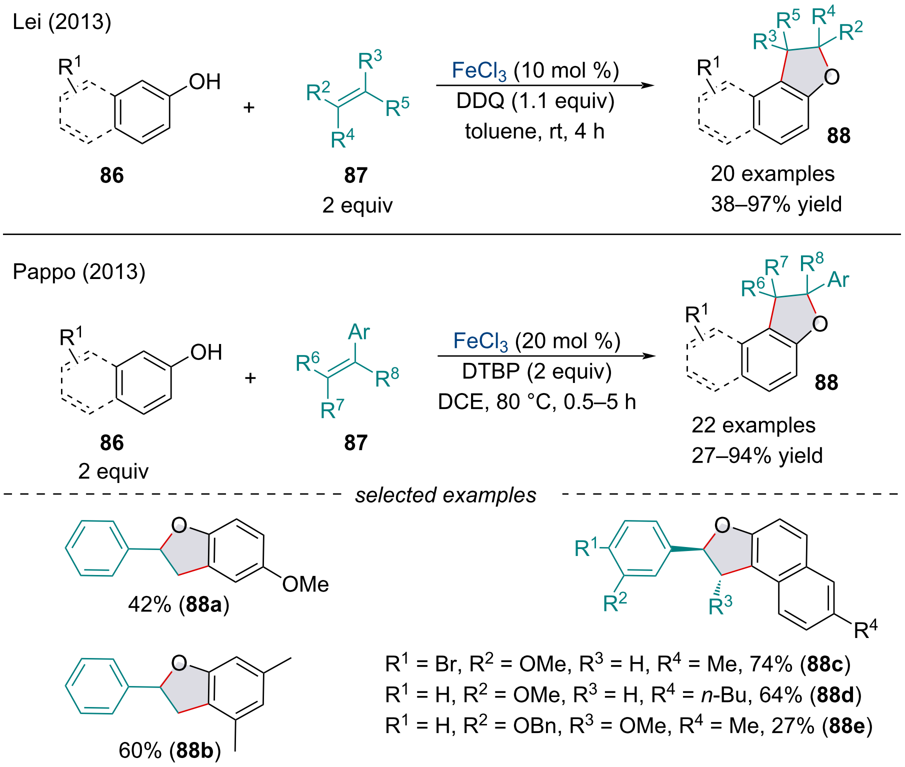
Lei (2013)
86
87
2 equiv
FeCl3 (10 mol %)
DDQ (1.1 equiv)
toluene, rt, 4 h
88
20 examples
38–97% yield
Pappo (2013)
86
2 equiv
87
FeCl3 (20 mol %)
DTBP (2 equiv)
DCE, 80 °C, 0.5–5 h
88
22 examples
27–94% yield
selected examples
42% (88a)
60% (88b)

R^1 = Br, R^2 = OMe, R^3 = H, R^4 = Me, 74% (**88c**)
R^1 = H, R^2 = OMe, R^3 = H, R^4 = *n*-Bu, 64% (**88d**)
R^1 = H, R^2 = OBn, R^3 = OMe, R^4 = Me, 27% (**88e**)

Scheme 15: Iron-catalyzed oxidative coupling/cyclization of phenol derivatives **86** and alkenes **87**.

In 2018, Zhong and co-workers reported a similar approach towards the assembly of 2,2-disubstituted indolines from *N*-sulfonylanilines and substituted styrene derivatives [93].

In 2014, the Jiao group investigated the carbosulfonation of alkenes **60** for the synthesis of oxindoles **90** through sequential C–S/C–C-bond formation (Scheme 16) [94]. Interestingly, the protocol used air as the oxidant, avoiding the use of stoichiometric oxidants like previous radical cyclization cascades. Generally, substrates with an electron-withdrawing group afforded the product in greater yield. The reaction proceeds through the formation of a sulfonyl radical under aerobic conditions. Tandem attack on the alkenyl π-system with the sulfonyl radical followed by radical cyclization with the aryl ring constructs the substituted oxindoles **90**.

In 2017, Song and Li reported an oxidative spriocyclization of *N*-arylpropiolamides **91** with silanes **92** for the synthesis of 3-silylspiro[4,5]trienones **93** in good yield (Scheme 17) [95]. Compared to previously reported inter-/intramolecular CDC cascades, the authors were able to capture the post-cyclization aryl radical with the peroxide initiator rather than simply termi-

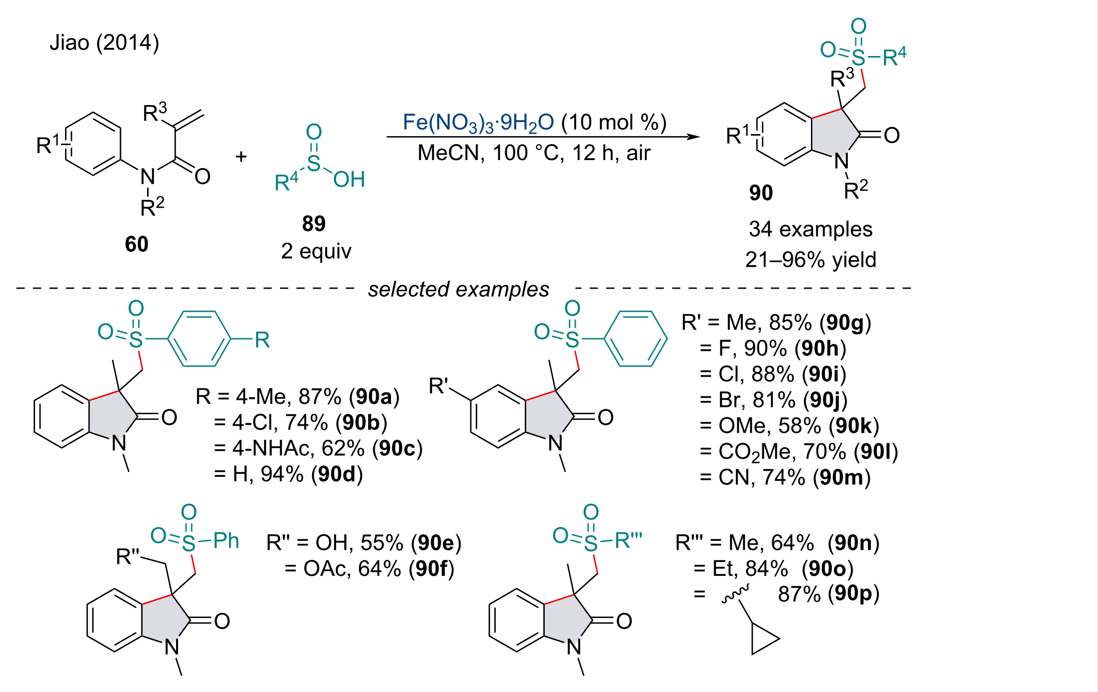
Jiao (2014)
R1
R3
N
O
R2
60
+
O
S
R4
OH
89
2 equiv
Fe(NO3)3·9H2O (10 mol %)
MeCN, 100 °C, 12 h, air
O
O=S–R4
R3
R1
N
O
R2
90
34 examples
21–96% yield
selected examples
O=S
R
O
N
R = 4-Me, 87% (90a)
= 4-Cl, 74% (90b)
= 4-NHAc, 62% (90c)
= H, 94% (90d)
R'
R' = Me, 85% (90g)
= F, 90% (90h)
= Cl, 88% (90i)
= Br, 81% (90j)
= OMe, 58% (90k)
= CO2Me, 70% (90l)
= CN, 74% (90m)
O=S–Ph
R''
R'' = OH, 55% (90e)
= OAc, 64% (90f)
O=S–R'''
R''' = Me, 64% (90n)
= Et, 84% (90o)
= 87% (90p)

Scheme 16: Iron-catalyzed carbosulfonylation of activated alkenes **60**.

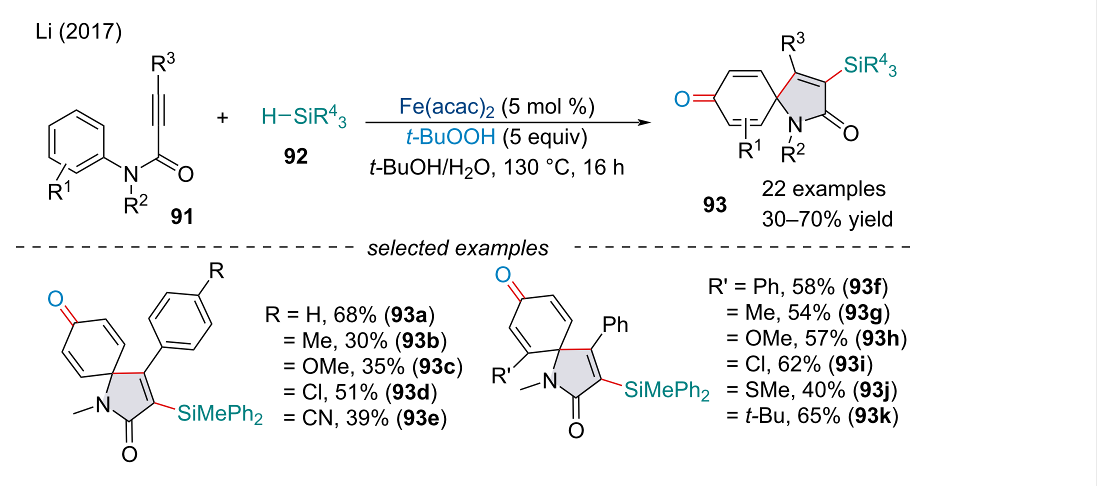
Li (2017)
R3
R1
N
O
R2
91
+
H–SiR4 3
92
Fe(acac)2 (5 mol %)
t-BuOOH (5 equiv)
t-BuOH/H2O, 130 °C, 16 h
R3
SiR4 3
O
N
R1
R2
O
93
22 examples
30–70% yield
selected examples
R
O
N
SiMePh2
O
R = H, 68% (93a)
= Me, 30% (93b)
= OMe, 35% (93c)
= Cl, 51% (93d)
= CN, 39% (93e)
O
Ph
R'
N
SiMePh2
O
R' = Ph, 58% (93f)
= Me, 54% (93g)
= OMe, 57% (93h)
= Cl, 62% (93i)
= SMe, 40% (93j)
= t-Bu, 65% (93k)

Scheme 17: Iron-catalyzed oxidative spirocyclization of *N*-arylpropiolamides **91** with silanes **92** and *tert*-butyl hydroperoxide.

nating the reaction with protonation. In terms of the scope of the reaction, substrates bearing an electron-rich functionality were less reactive than substrates with electron-deficient groups. Isotopic labeling revealed the oxygen functionality installed came from the peroxide initiator rather than the water present, suggesting the water plays another role in the reaction, potentially as a promoter of the catalyst.

In 2020, Li and co-workers investigated a carbosilylation cascade for the synthesis of various silylated dihydroisoquinolinones and 1,3-isoquinolinediones **95** (Scheme 18) [96]. The scope of the reaction was broad and could tolerate a variety of electron-donating and electron-withdrawing groups, though bulky silanes **92** afforded the products in reduced yield. The reaction proceeds through the formation of a silicon-centered radical generated via a Fe redox cycle (vide supra). Sequential attack on the alkenyl π-system followed by radical cyclization with the aryl ring constructs the 6-membered heterocyclic framework.

In 2015, the Li group investigated the radical addition/cyclization of olefinic malonate and β-diketone compounds **96** with aldehydes **97** (Scheme 19) [97]. The reaction was feasible with ketones; however, lower product yields were observed. The efficiency of the reaction seems to be dependent on the deprotonation of the α-position of the olefinic malonate species. The authors noted decarbonylated products were obtained when cyclohexane carboxaldehyde and pivaldehyde were applied, consistent with the stability of the generated acyl radicals [98]. Concurrently, Guo and co-workers reported a similar approach towards the synthesis of dihydrofurans **101** through the sequential radical addition/cyclization of inactivated $C(sp^3)$–H bonds **100** with olefinic dicarbonyl species **99** (Scheme 19) [99]. Both accounts found the reaction was shut down in the presence of radical scavengers. Both laboratories suggested the mechanism, wherein, after *tert*-butoxyl radical production, hydrogen abstraction can generate the appropriate radical species. Subsequent radical addition to the π-system followed by a 5-*endo*-trig radical cyclization would afford the furan framework. Following Fe-catalyzed oxidation, the resulting oxonium cation can be deprotonated to afford the final dihydrofuran. Further, this inter-/intramolecular radical addition/cyclization methodology has been applied for the synthesis of various substituted dihydropyrans [100,101] and dihydrofurans [102].

In 2019, the Li group studied the selective activation of the α-$C(sp^3)$–H of ketones and esters **103** for the tandem addition/cyclization of *o*-vinylanilides **102** (Scheme 20) [103]. Through a series of mechanistic experiments, it was noted the cleavage of the $C(sp^3)$–H bond may be involved in the rate-determining step of this transformation, as well as free radicals being involved in the reaction mechanism.

In 2017, Luo and Li described a three-component Ag-mediated Fe-catalyzed 1,2-carboamination of alkenes **82** using alkyl nitriles **76** and amines **105** for the synthesis of γ-amino alkyl nitriles **106** (Scheme 21) [104]. The use of Ag_2CO_3 as a SET oxidant was shown to be key for the success of the reaction, as typical organic oxidants, like peroxides, displayed low activity. No clear trend was observed for the difference in efficiency between the Fe catalysts used. It was noted the use of the Fe catalyst wasn't necessary to promote the reaction, but the yield of the cascade was significantly increased upon loading. The scope of the π-systems was limited to alkenes conjugated to electron-

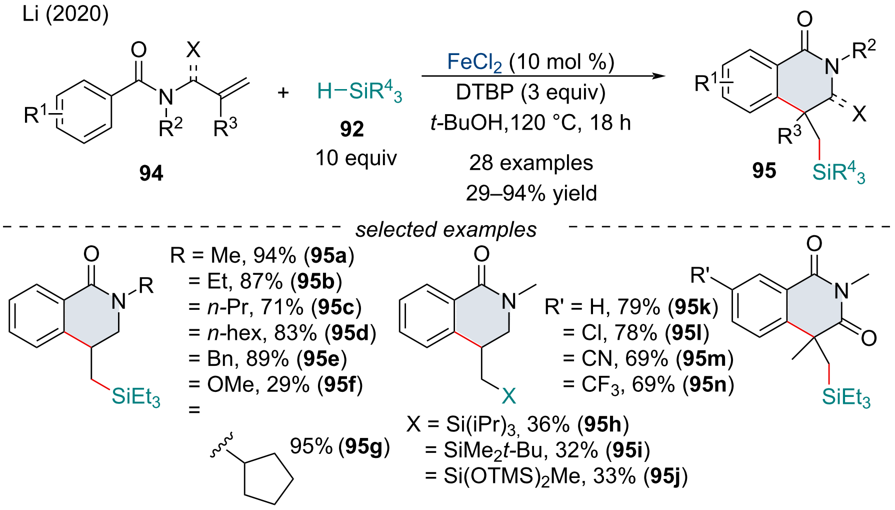

Scheme 18: Iron-catalyzed free radical cascade difunctionalization of unsaturated benzamides **94** with silanes **92**.

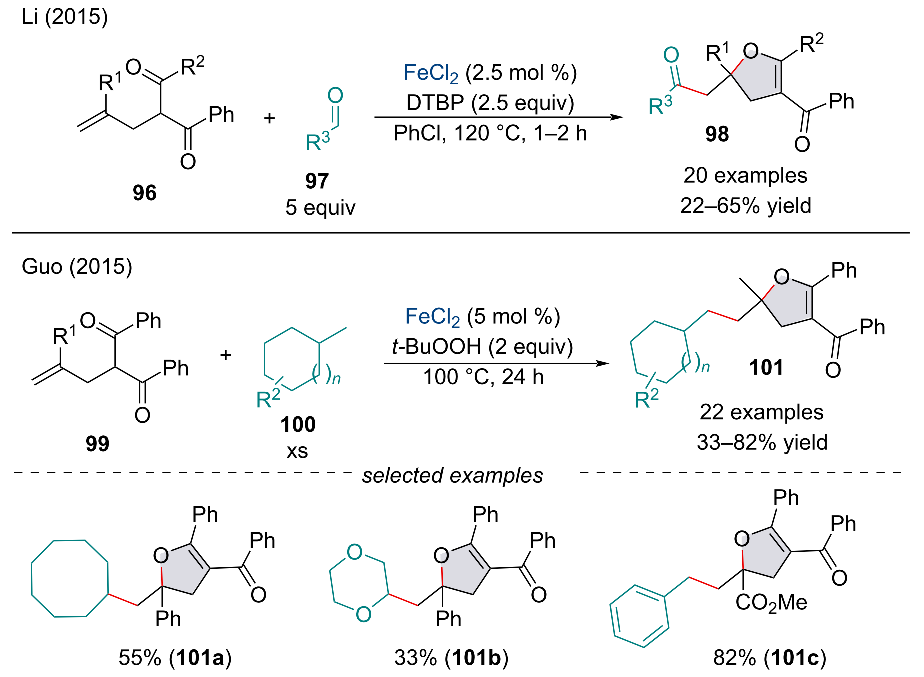
Li (2015)
96
97
5 equiv
FeCl2 (2.5 mol %)
DTBP (2.5 equiv)
PhCl, 120 °C, 1–2 h
98
20 examples
22–65% yield
Guo (2015)
99
100
xs
FeCl2 (5 mol %)
t-BuOOH (2 equiv)
100 °C, 24 h
101
22 examples
33–82% yield
selected examples
55% (101a)
33% (101b)
82% (101c)

Scheme 19: Iron-catalyzed cyclization of olefinic dicarbonyl compounds **97** and **100** with C(sp^3)–H bonds.

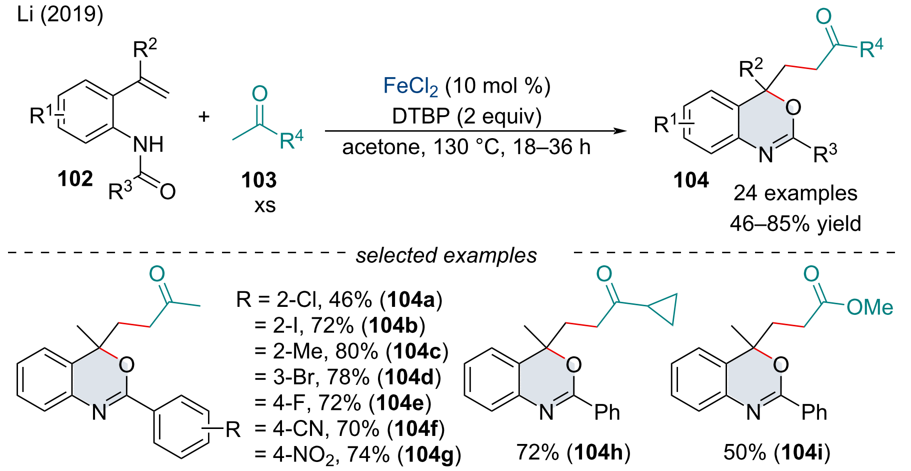
Li (2019)
102
103
xs
FeCl2 (10 mol %)
DTBP (2 equiv)
acetone, 130 °C, 18–36 h
104
24 examples
46–85% yield
selected examples
R = 2-Cl, 46% (104a)
= 2-I, 72% (104b)
= 2-Me, 80% (104c)
= 3-Br, 78% (104d)
= 4-F, 72% (104e)
= 4-CN, 70% (104f)
= 4-NO2, 74% (104g)
72% (104h)
50% (104i)

Scheme 20: Radical difunctionalization of *o*-vinylanilides **102** with ketones and esters **103**.

rich aryl species. Various nitrogen nucleophiles including primary/secondary amines and sulfonamides were compatible with the nucleophilic capture process. In the proposed mechanism, the α-hydrogen of the alkyl nitrile is deprotonated to form an organosilver species which undergoes SET oxidation with Ag(I) to afford the alkyl radical. Next, the α-cyanocarbon radical can add across the styrene derivative generating a benzylic radical which can be oxidized by Ag(I) to afford the corresponding benzylic cation. Nucleophilic trapping with an amine will produce the final product.

In the same year, Song and co-workers reported a dehydrogenative 1,2-difunctionalization of conjugated alkenes **107** with silanes **92** and various nucleophiles **108** (Scheme 22) [105]. This protocol offers an expedient approach to 1-amino-2-silylalkanes, a classically difficult framework to synthesize, typically requiring harsh reaction conditions, multistep synthetic routes, or the use of expensive silicon reagents [106]. Moreover, the methodology was extended to the carbosilylation of olefins with carbon nucleophiles **108** including indoles, pyrroles, and 1,3-dicarbonyls. The scope of the reaction was broad and could

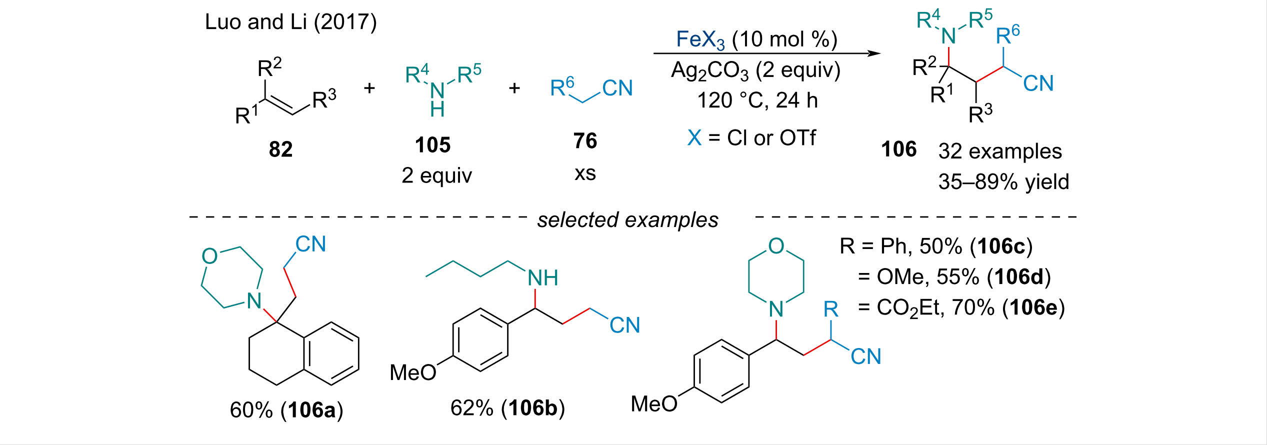
Luo and Li (2017)
82
105
2 equiv
76
xs
FeX3 (10 mol %)
Ag2CO3 (2 equiv)
120 °C, 24 h
X = Cl or OTf
106
32 examples
35–89% yield
selected examples
60% (106a)
62% (106b)
R = Ph, 50% (106c)
= OMe, 55% (106d)
= CO2Et, 70% (106e)

Scheme 21: Dehydrogenative 1,2-carboamination of alkenes **82** with alkyl nitriles **76** and amines **105**.

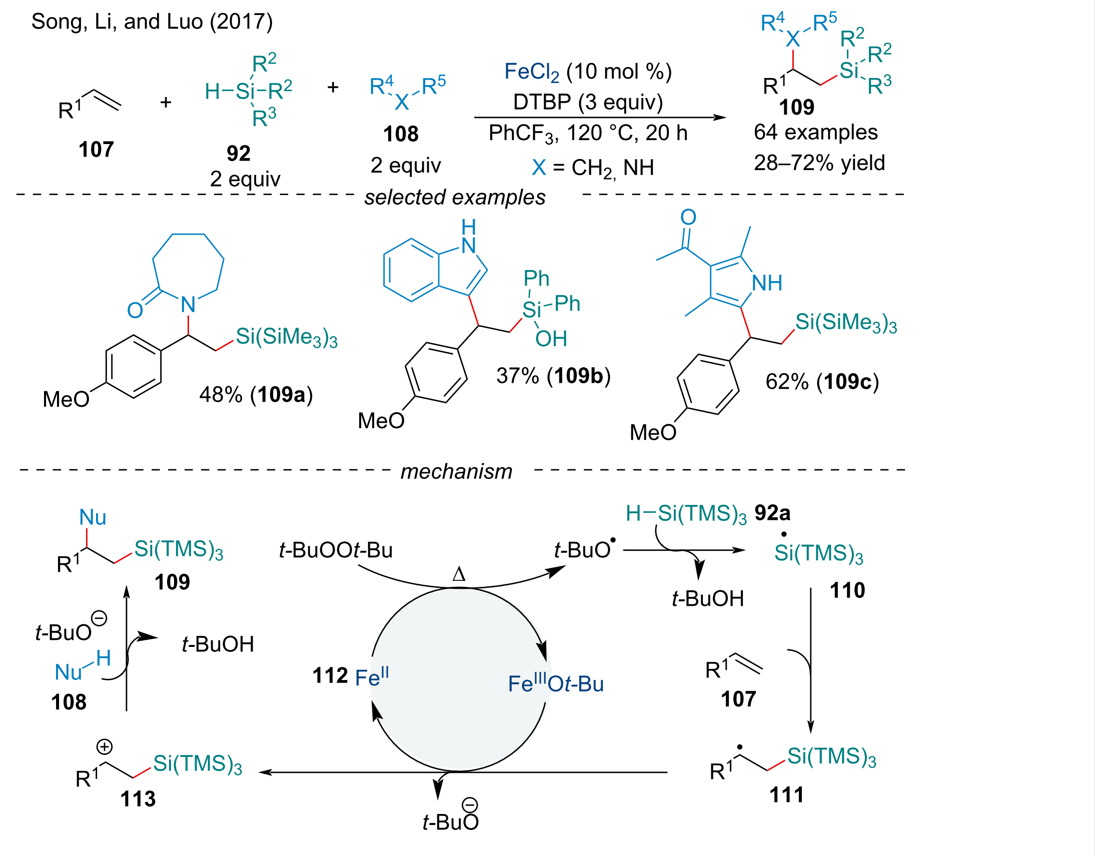
Song, Li, and Luo (2017)
107
92
2 equiv
108
2 equiv
FeCl2 (10 mol %)
DTBP (3 equiv)
PhCF3, 120 °C, 20 h
X = CH2, NH
109
64 examples
28–72% yield
selected examples
48% (109a)
37% (109b)
62% (109c)
mechanism
t-BuOOt-Bu
Δ
t-BuO•
H–Si(TMS)3 92a
t-BuOH
•Si(TMS)3
110
107
111
112 FeII
FeIIIOt-Bu
t-BuO⊖
113
t-BuO⊖
Nu–H
108
t-BuOH
109

Scheme 22: Iron-catalyzed intermolecular 1,2-difunctionalization of conjugated alkenes **107** with silanes **92** and nucleophiles **108**.

tolerate a variety of functional groups; however, electron-deficient alkenes afforded the products in slightly diminished yield. After the prototypical homolysis of the peroxide in the presence of the Fe(II) catalyst, a silicon-centered radical **110** is formed via hydrogen abstraction. The addition of radical **110** across the alkene generates the alkyl radical intermediate **111**. Oxidation of **111** by Fe(III)O*t*-Bu delivers the alkyl cation **113**. Nucleophilic trapping of the carbocation provides the final product. In 2018, the Li group continued to explore Fe-catalyzed silylation cascade chemistry. Their protocol investigated the silylperoxidation of activated alkenes in good yield [107].

In 2019, Yang and co-workers described a four-component radical dual difunctionalization and ordered assembly of two chemically distinct alkenes **114**/**115**, aldehyde **65**, and *tert*-butyl peroxide (Scheme 23) [108]. In order to selectively couple one alkene to another, without the formation of oligomers, the authors utilized the different electronic properties of the alkenes to control the chronology of the additions. The rate of addition of the acyl radical to an electro-deficient alkene is about three times greater than that of a styrene derivative [109,110]. The electrophilic radical, adjacent to an EWG, will favor the subsequent addition to the styrene derivative selectively to afford a metastable benzyl radical [111] which is captured by $BuOO^•$ via a radical termination process.

Iron-catalyzed oxidative addition/coupling and functionalization

Carbofunctionalization

Moving forward, the Fe-catalyzed carbofunctionalization of alkenes will be discussed as a method for the formation of multiple bonds in a single step. Mechanistically, Fe-catalyzed oxidative addition and functionalization reactions proceed similarly to cross dehydrogenative couplings (vide supra); however, these reactions will result in byproducts other than the formal elimination of H_2. This section is categorized by the initiating step and the types of bonds being formed.

Denitrogenative C–C/C–C coupling

In 2014, Yu's and Du's groups independently described the arylcarbonylation of alkenes for the synthesis of oxindoles **118** from *N*-alkyl,*N*-arylacrylamides **60** and carbazates **117** (Scheme 24) [112,113]. Both protocols utilized a catalytic loading of $FeCl_2·4H_2O$ mediated by *tert*-butyl hydroperoxide.

The scopes of both reactions were broad and tolerated a variety of functional groups; however, both groups noted unsubstituted terminal alkenes and *N*-arylacrylamides **60** with a free N–H did not undergo this transformation. Interestingly, Du's protocol tolerated substrates with a free carbinol moiety. On the other hand, Yu reported the same substrate failed to produce any product owing it to oxidative instability, yet more must be at play. Since 2014, modifying the reaction conditions has allowed for several different difunctionalization reactions of alkenes through the denitrogenative radical generation of carbazates. The subsequent radical has been shown to undergo coupling with oxygen sources like peroxides [114,115] and air [116].

In 2020, Qian and Cheng investigated the cascade cyclization of dienes **119** with alkyl carbazates **117** for the synthesis of fused nitrogen heterocyclic compounds **120** (Scheme 25) [117]. Diene substrates possessing EDGs reacted smoothly under the optimized conditions while their electron-deficient counterparts delivered the products in diminished yields. This transformation was sensitive to steric hindrance, as *ortho*-substituted aryl species and bulky alkyl carbazates failed to react under these reaction conditions. Based on control experiments, the authors proposed a tentative catalytic cycle. Initially, in the presence of an Fe(II) species and $S_2O_8^{2-}$, a cascade of SET reactions between the alkylcarbazate and the Fe catalyst will lead to the formation of the alkoxycarbonyl **125**. Regioselective addition of the radical across the electron-neutral olefin will generate the radical intermediate **126**, followed by the 6-*endo* radical cyclization with the activated alkene **127**. Ring closing with the *ortho*-carbon of the aryl ring generates aryl radical **128** which

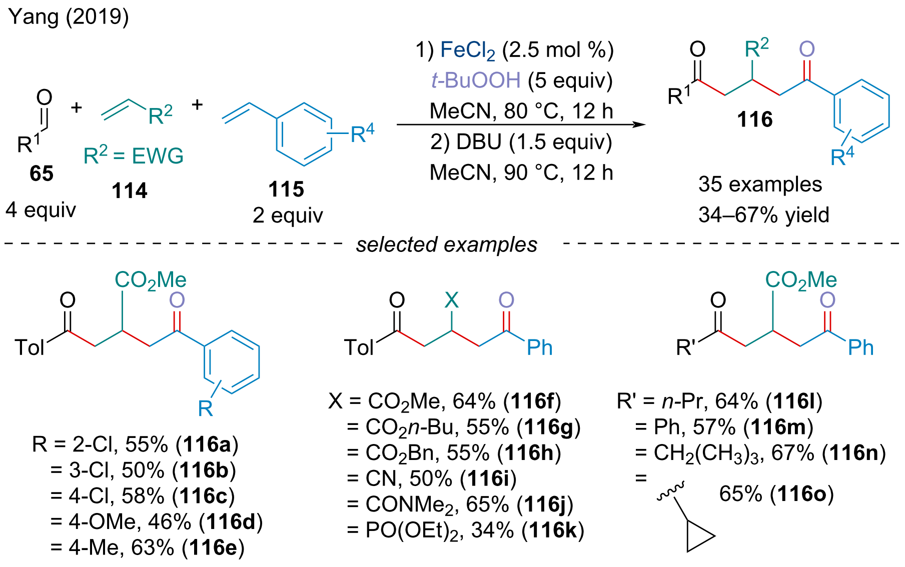

Scheme 23: Four-component radical difunctionalization of chemically distinct alkenes **114**/**115** with aldehydes **65** and *tert*-butyl hydroperoxide.

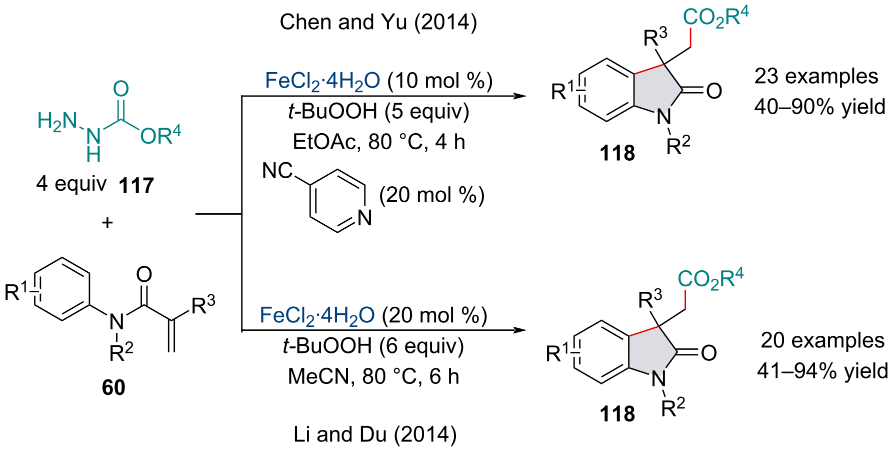

Scheme 24: Iron-catalyzed carbocarbonylation of activated alkenes **60** with carbazates **117**.

was confirmed not to be the rate-determining step by kinetic isotope effect studies. Subsequently, **128** is oxidized by $S_2O_8^{2-}$ and deprotonated to form the desired product **120**.

Homolytic-cleavage-initiated C–C/C–C coupling

In 2018, Du and co-workers explored the decarboxylative radical addition/cyclization of *tert*-butyl peresters **129** and *N*-arylacrylamides **60** for the synthesis of oxindoles **130** (Scheme 26) [118]. The scope of the reaction was broad and tolerated a variety of functional groups with neither EDGs nor EWGs altering the reactivity of the acrylamide. Once synthesized, the authors demonstrated the oxindoles could be transformed into fused indoline–heterocycle frameworks in good yield, an attractive scaffold found in many biologically active compounds [119].

In the same year, the Du group investigated the $FeCl_2·4H_2O$ decarboxylative radical alkylative cyclization of cinnamamides **131**/**134** as an expedient approach towards dihydroquinolinone **133** and pyrrolo[1,2-*a*]indole **135** analogues in good yield and excellent diastereoselectivity (Scheme 27) [120]. In terms of the dihydroquinolinones **133**, acrylamide starting materials **131** containing EWGs or EDGs all proceeded well, producing the cyclized products with excellent diastereoselectivity. Likewise, the scope of peresters investigated was broad and well received; however, a lower reactivity was observed for sterically demanding alkyl groups. Overall, when the protocol was applied towards the synthesis of pyrrolo[1,2-*a*]indoles **135**, product yields were slightly diminished; however, the scope was equally as broad and tolerated most functional groups. Sterically demanding peresters were shown to react poorly with the indole starting material **134**, with tertiary peresters failing to react. The mechanism begins with an outer-sphere SET from Fe(II) to perester **132** leading to the O–O bond cleavage, generating the reactive alkyl radical **136**, Fe(III), CO_2, and *t*-BuO$^-$. Addition of **136** across the alkene **131a** generates radical intermediate **137**. Subsequently, intramolecular cyclization of **137** generates radical intermediate **138** which then successively undergoes a SET of Fe(III) and deprotonation by *t*-BuO$^-$ to give the annulated product **133a** and regenerates the Fe(II) active catalyst.

In 2014, the Loh group reported an $FeCl_2$-catalyzed carbochloromethylation of activated alkenes **60** (Scheme 28) [121]. The reaction was amenable to a range of commercially available chlorinated methane units **139**; however, CH_2Cl_2 and CCl_4 (**139a**) performed the best and delivered the oxindole products **140** in good to excellent yield. The authors noted the use of the diaryliodonium salt Ph_2IOTf was critical, with no reaction being observed in its absence. In 2020, Li and Shen reported a similar transformation for the synthesis of chloro-containing oxindoles **141** (Scheme 28) [122]. Interestingly, the authors reported the reaction was able to operate in the absence of any external oxidants under an inert atmosphere. Although not investigated, Loh's transformation most likely begins with the generation of an aryl radical from the reduction of the diaryliodonium salt with Fe(II) which subsequently abstracts a hydrogen from CH_2Cl_2 to generate an alkyl radical. Perchlorinated species **139a**, like the substrates investigated by Li and Shen, most likely undergo thermal homolytic bond cleavage and do not rely on a radical initiator.

In 2016, Shi and co-workers investigated the trifluoromethylation cascade of acrylamide-tethered alkylidenecyclopropanes **142** for the synthesis of polycyclic benzazepine derivatives **144** (Scheme 29) [123]. The authors noted electron-withdrawing

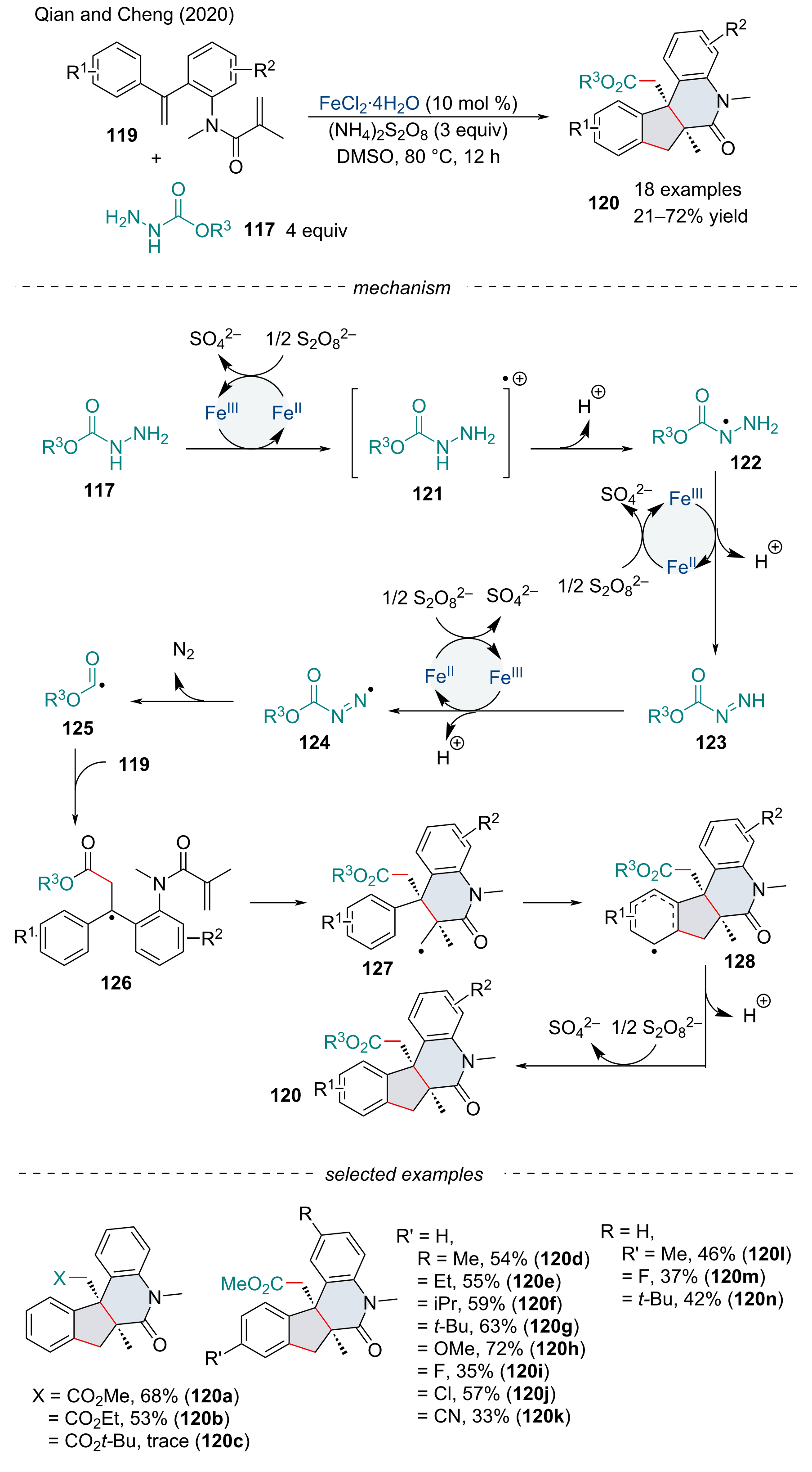
Qian and Cheng (2020)
R1
R2
119
+
N
O
H2N
N
H
O
OR3
117 4 equiv
FeCl2·4H2O (10 mol %)
(NH4)2S2O8 (3 equiv)
DMSO, 80 °C, 12 h
R3O2C
R1
R2
N
O
120
18 examples
21–72% yield
mechanism
SO4 2–
1/2 S2O8 2–
FeIII
FeII
117
121
H⊕
122
123
124
125
N2
119
126
127
128
120
H⊕
selected examples
X = CO2Me, 68% (120a)
= CO2Et, 53% (120b)
= CO2t-Bu, trace (120c)
MeO2C
R
R'
R' = H,
R = Me, 54% (120d)
= Et, 55% (120e)
= iPr, 59% (120f)
= t-Bu, 63% (120g)
= OMe, 72% (120h)
= F, 35% (120i)
= Cl, 57% (120j)
= CN, 33% (120k)
R = H,
R' = Me, 46% (120l)
= F, 37% (120m)
= t-Bu, 42% (120n)

Scheme 25: Iron-catalyzed radical 6-*endo* cyclization of dienes **119** with carbazates **117**.

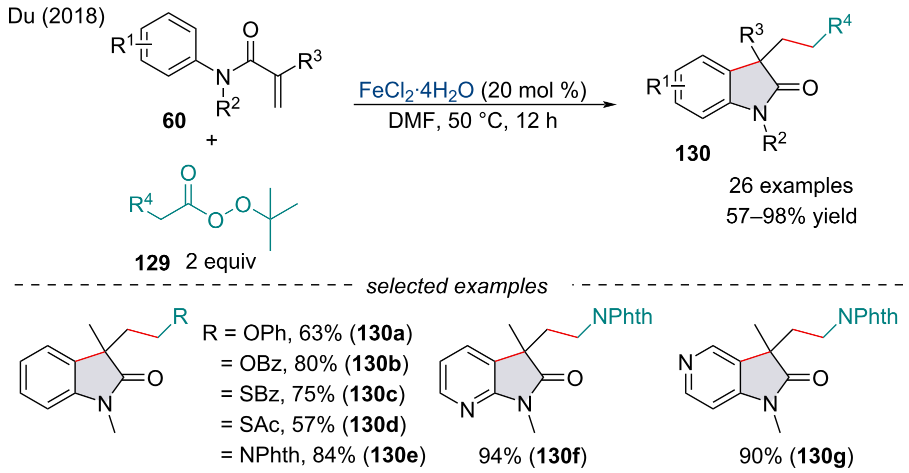
Du (2018)
R1
O
R3
N
R2
60
+
FeCl2·4H2O (20 mol %)
DMF, 50 °C, 12 h
R3
R4
R1
O
N
R2
130
26 examples
57–98% yield
O
R4
O
O
129 2 equiv
selected examples
R
O
N
R = OPh, 63% (130a)
= OBz, 80% (130b)
= SBz, 75% (130c)
= SAc, 57% (130d)
= NPhth, 84% (130e)
NPhth
O
N
N
94% (130f)
NPhth
N
O
N
90% (130g)

Scheme 26: Iron-catalyzed decarboxylative synthesis of functionalized oxindoles **130** with *tert*-butyl peresters **129**.

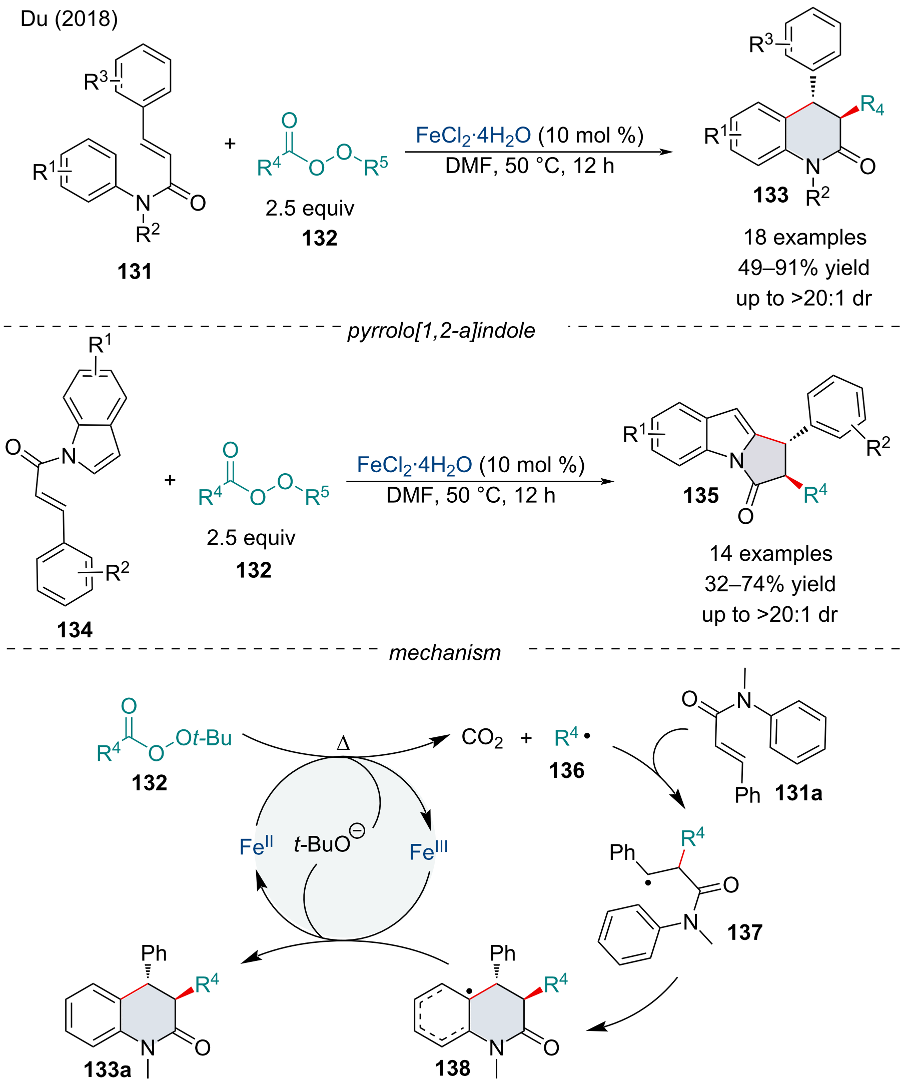
Du (2018)
R3
R1
N
O
R2
131
+
O
R4
O
O
R5
2.5 equiv
132
FeCl2·4H2O (10 mol %)
DMF, 50 °C, 12 h
R3
R4
R1
N
O
133
R2
18 examples
49–91% yield
up to >20:1 dr
pyrrolo[1,2-a]indole
R1
O
N
R2
134
+
O
R4
O
O
R5
2.5 equiv
132
FeCl2·4H2O (10 mol %)
DMF, 50 °C, 12 h
R1
R2
N
R4
O
135
14 examples
32–74% yield
up to >20:1 dr
mechanism
O
R4
O
Ot-Bu
132
Δ
CO2
+
R4 •
136
O
N
Ph
131a
FeII
t-BuO⊖
FeIII
Ph
R4
O
N
137
Ph
R4
N
O
133a
Ph
R4
N
O
138

Scheme 27: Iron-catalyzed decarboxylative alkylation/cyclization of cinnamamides **131**/**134**.

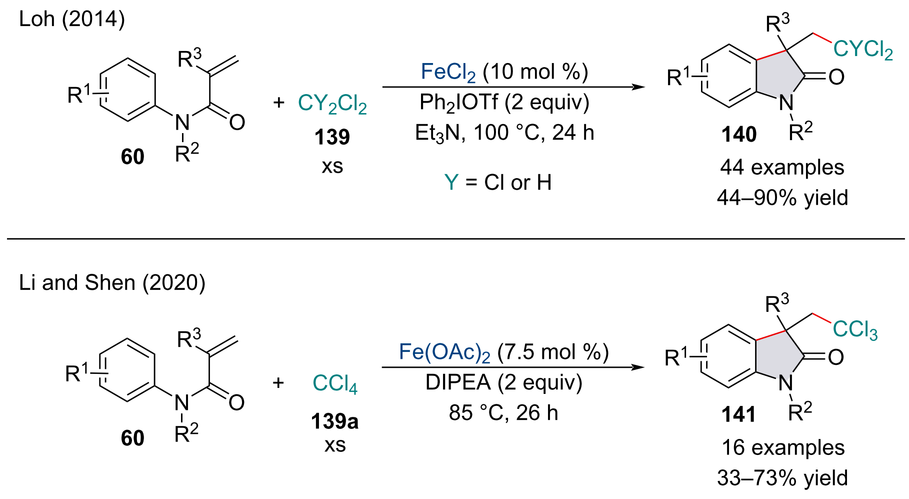
Loh (2014)
R1
R3
N
R2
O
60
+ CY_2Cl_2
139
xs
$FeCl_2$ (10 mol %)
Ph_2IOTf (2 equiv)
Et_3N, 100 °C, 24 h
Y = Cl or H
R1
R3
$CYCl_2$
O
N
R2
140
44 examples
44–90% yield
Li and Shen (2020)
R1
R3
N
R2
O
60
+ CCl_4
139a
xs
$Fe(OAc)_2$ (7.5 mol %)
DIPEA (2 equiv)
85 °C, 26 h
R1
R3
CCl_3
O
N
R2
141
16 examples
33–73% yield

Scheme 28: Iron-catalyzed carbochloromethylation of activated alkenes **60**.

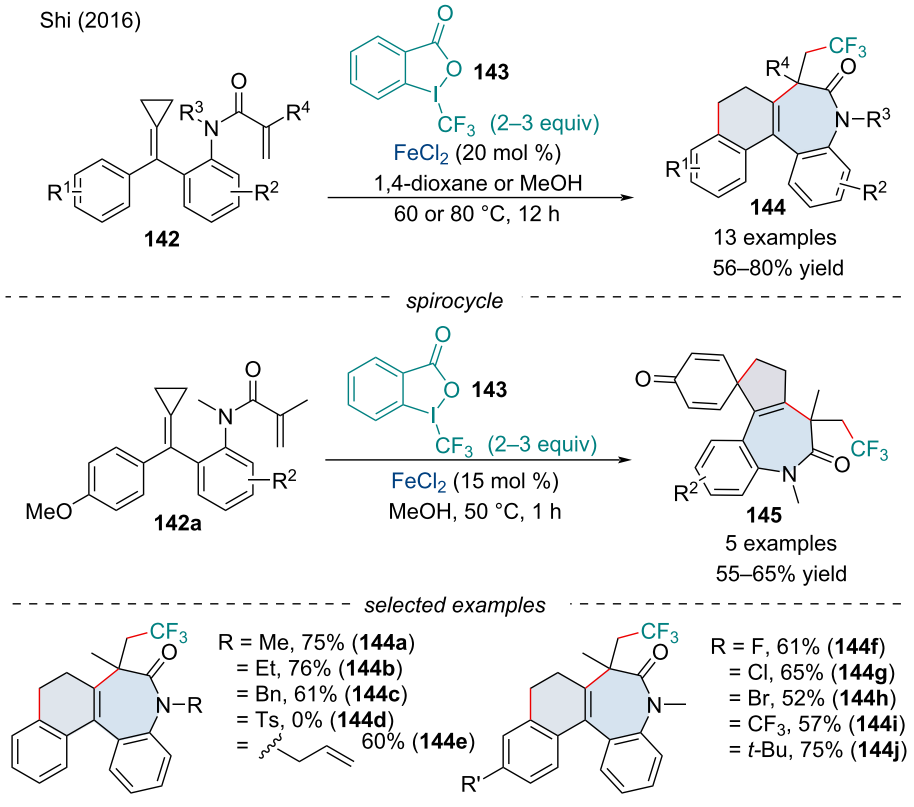
Shi (2016)
O
O
I
CF_3
143
(2–3 equiv)
$FeCl_2$ (20 mol %)
1,4-dioxane or MeOH
60 or 80 °C, 12 h
R1
R3
N
O
R4
R2
142
R4
CF_3
O
N–R3
R1
R2
144
13 examples
56–80% yield
spirocycle
MeO
N
O
R2
142a
143
(2–3 equiv)
$FeCl_2$ (15 mol %)
MeOH, 50 °C, 1 h
O
CF_3
O
N
R2
145
5 examples
55–65% yield
selected examples
CF_3
O
N–R
R = Me, 75% (144a)
= Et, 76% (144b)
= Bn, 61% (144c)
= Ts, 0% (144d)
= 60% (144e)
CF_3
O
N—
R'
R = F, 61% (144f)
= Cl, 65% (144g)
= Br, 52% (144h)
= CF_3, 57% (144i)
= t-Bu, 75% (144j)

Scheme 29: Iron-catalyzed trifluoromethylation of dienes **142**.

substituents were detrimental to the efficacy of the reaction with electron-withdrawing *N*-substituents failing to react. When a methoxy group was installed at the *para*-position of the aryl ring, a spirocyclic product **145** was formed via a radical cyclization/dearomatization process. Mechanistic investigations revealed the reaction operates through a radical pathway.

In 2017, the Li group described a Ag-mediated, Fe-catalyzed alkylarylation of styrene derivatives **115** with α-carbonyl alkyl bromides **147** and indole derivatives **146** (Scheme 30) [124]. Although the reaction operated in the absence of the iron catalyst, its use is crucial for high yielding reactions. Preliminary mechanistic studies suggest the reaction proceeds through a

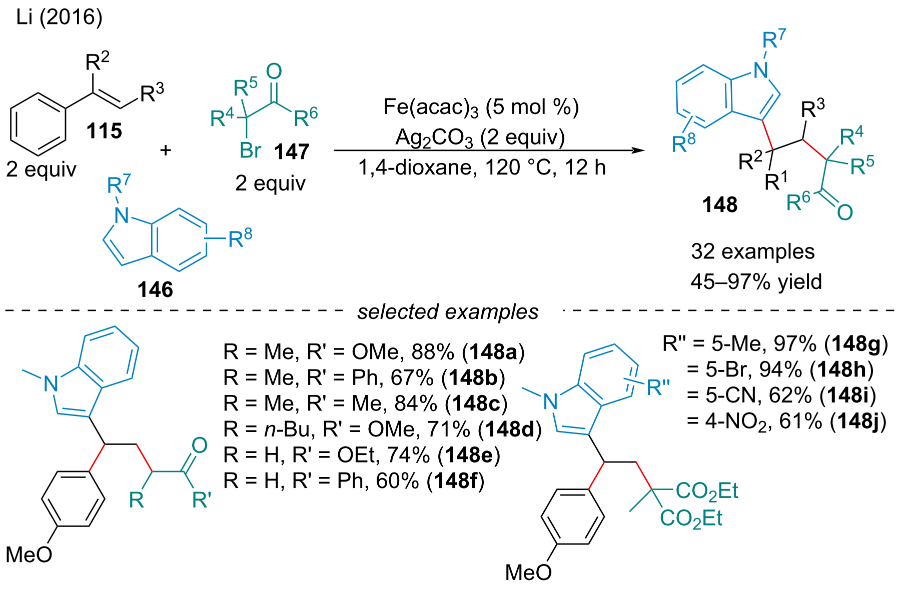
Li (2016)
2 equiv
115
147
2 equiv
146
Fe(acac)$_3$ (5 mol %)
Ag$_2$CO$_3$ (2 equiv)
1,4-dioxane, 120 °C, 12 h
148
32 examples
45–97% yield
selected examples
R = Me, R' = OMe, 88% (**148a**)
R = Me, R' = Ph, 67% (**148b**)
R = Me, R' = Me, 84% (**148c**)
R = *n*-Bu, R' = OMe, 71% (**148d**)
R = H, R' = OEt, 74% (**148e**)
R = H, R' = Ph, 60% (**148f**)
R'' = 5-Me, 97% (**148g**)
= 5-Br, 94% (**148h**)
= 5-CN, 62% (**148i**)
= 4-NO$_2$, 61% (**148j**)
MeO
CO$_2$Et
CO$_2$Et

Scheme 30: Iron-catalyzed, silver-mediated arylalkylation of conjugated alkenes **115**.

radical addition of the carbon-centered alkyl radical across the alkene to afford the benzylic radical. Oxidation of the corresponding radical affords the benzylic carbocation which is attacked by the indole nucleophile. The authors applied the reaction methodology to pyrrole as a substrate; however, only one example was given in a 50% yield. Further examining of other potential arenes capable of undergoing electrophilic aromatic substitution would expand the applicability of the reaction.

Carboazidation

In 2018, Yang investigated the three-component carboazidation of styrene derivatives **115** with alkanes **101**/**139b** and trimethylsilyl azide for the synthesis of chain extended azides **149** and γ-azido chloroalkanes **150** in good yield (Scheme 31) [125]. The electronic nature of the alkene had no clear effect on the reactivity of the system; however, no product was detected when unactivated alkenes like when cyclohexene was used. This strategy was also explored using chloroalkanes to form di- and trichlorinated products **150**. Despite previous reports demonstrating dichloromethane **139b** in the presence of peroxide [126] and iron salts [127] form 1,1,1- and 1,1,1,3-substituted chloroalkanes, under the authors' optimized reaction conditions only the carboazidation product was observed. In the same year, the Xu laboratory demonstrated Togni's reagent could be employed for the synthesis of γ-azido fluoroalkanes [128].

In 2019, Chu and co-workers demonstrated the three-component carboazidation of alkenes with chloroalkanes and trimethylsilyl azide could be solvent-tuned [129]. In neat CH_2Cl_2, the reaction produced the expected β-trichloromethyl alkyl azide; however, the reaction was chemoselective for diazidation when *tert*-butanol was used as co-solvent. The authors hypothesized the presence of the alcohol suppresses the polar-unmatched HAT process from forming $CHCl_2$ radicals [130].

In 2019, the Bao group demonstrated alkyl iodides **20** were suitable radical precursors for the carboazidation reaction (Scheme 32) [131]. Additionally, the authors demonstrated the carboazidation of alkynes **160**, a challenging reaction which has only had success under copper catalysis [132]. Electron-rich alkyl iodides did not produce the desired product with only perfluorinated and ester-containing alkyl iodides **20** working well. Despite the limited applicability of nucleophiles, the reaction was extremely fast, typically finishing in under 10 minutes. To show the synthetic utility of their reaction, the authors studied the one-pot conversion of the vinyl azides to 2*H*-azirines **161**. The carboazidation reaction for the aryl alkynes was completed in a comparable amount of time. A myriad of different functionalized π-systems was tolerated by the reaction, demonstrating its applicability in late-stage functionalization. The Bao group has since demonstrated many other carbon-centered radicals were amenable in the carboazidation reaction of alkenes including diacylperoxides [133] and aldehydes [134].

In 2021, the Bao group followed up on their previous work and developed an asymmetric carboazidation of styrene derivatives **115** (Scheme 33) [135]. The authors propose the enantioselectivity originates from the diastereoisomeric azido group transfer

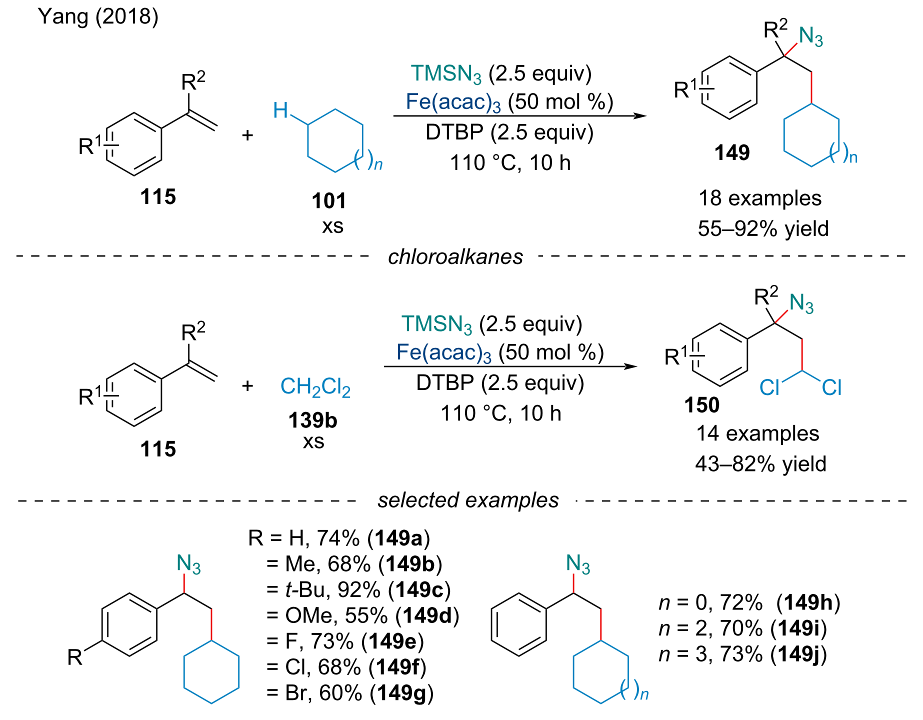
Yang (2018)
115
101
xs
TMSN3 (2.5 equiv)
Fe(acac)3 (50 mol %)
DTBP (2.5 equiv)
110 °C, 10 h
149
18 examples
55–92% yield
chloroalkanes
CH2Cl2
139b
xs
150
14 examples
43–82% yield
selected examples
R = H, 74% (149a)
= Me, 68% (149b)
= t-Bu, 92% (149c)
= OMe, 55% (149d)
= F, 73% (149e)
= Cl, 68% (149f)
= Br, 60% (149g)
n = 0, 72% (149h)
n = 2, 70% (149i)
n = 3, 73% (149j)

Scheme 31: Iron-catalyzed three-component carboazidation of conjugated alkenes **115** with alkanes **101**/**139b** and trimethylsilyl azide.

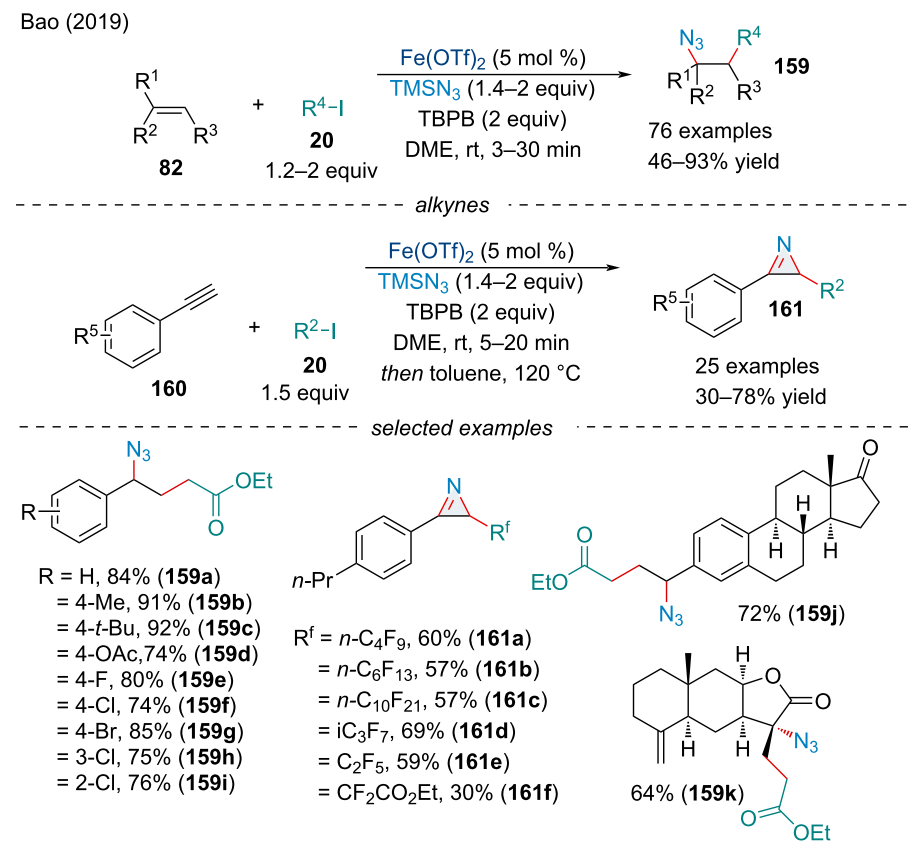
Bao (2019)
82
R4–I
20
1.2–2 equiv
Fe(OTf)2 (5 mol %)
TMSN3 (1.4–2 equiv)
TBPB (2 equiv)
DME, rt, 3–30 min
159
76 examples
46–93% yield
alkynes
160
R2–I
20
1.5 equiv
Fe(OTf)2 (5 mol %)
TMSN3 (1.4–2 equiv)
TBPB (2 equiv)
DME, rt, 5–20 min
then toluene, 120 °C
161
25 examples
30–78% yield
selected examples
R = H, 84% (159a)
= 4-Me, 91% (159b)
= 4-t-Bu, 92% (159c)
= 4-OAc,74% (159d)
= 4-F, 80% (159e)
= 4-Cl, 74% (159f)
= 4-Br, 85% (159g)
= 3-Cl, 75% (159h)
= 2-Cl, 76% (159i)
Rf = n-C4F9, 60% (161a)
= n-C6F13, 57% (161b)
= n-C10F21, 57% (161c)
= iC3F7, 69% (161d)
= C2F5, 59% (161e)
= CF2CO2Et, 30% (161f)
72% (159j)
64% (159k)

Scheme 32: Iron-catalyzed carboazidation of alkenes **82** and alkynes **160** with iodoalkanes **20** and trimethylsilyl azide.

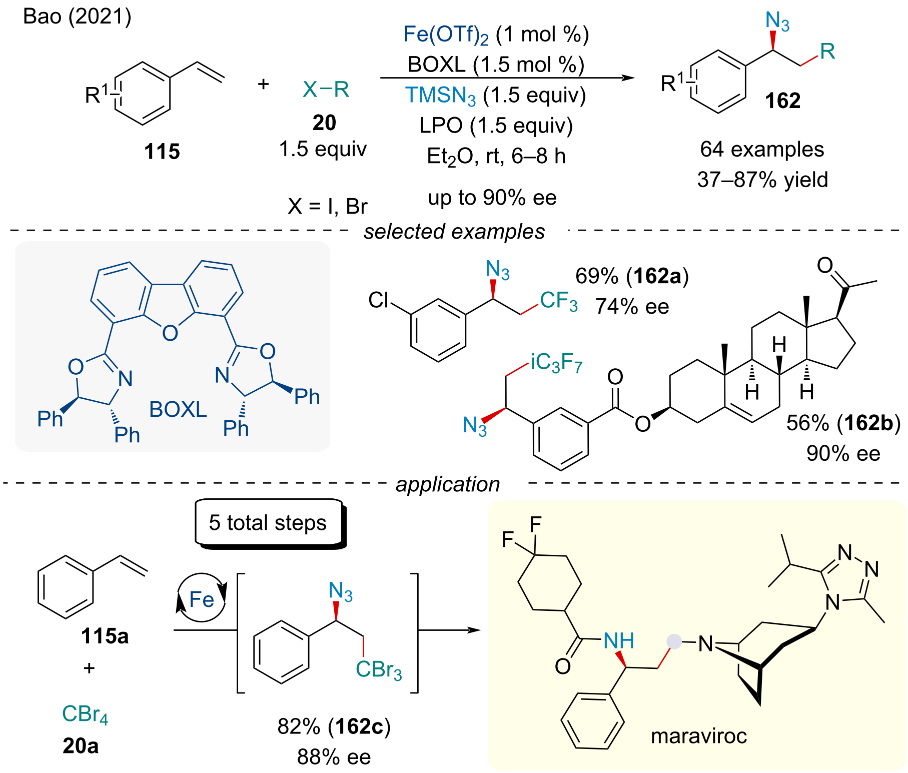

Scheme 33: Iron-catalyzed asymmetric carboazidation of styrene derivatives **115**.

from the Fe(III) center to the benzylic radical. Not only did the described methodology produce enantiopure products in up to 90% ee, the reactivity and applicability outperformed the racemic variant. Application of this methodology was applied towards the total synthesis of maraviroc, an anti-HIV drug, which was synthesized in 5 steps starting from styrene (**115a**) and CBr_4 (**20a**).

Carboamination

In 2017, the Bao group investigated the carboamination of activated alkenes **115** with alkyl diacyl peroxides **163** and acetonitrile (Scheme 34) [136]. Their efficient protocol featured a broad substrate scope, including diversely functionalized styrene derivatives, various alkyl diacyl peroxides, and a few different nitrile solvents which provided the desired carboamination product **164**. By using methyl cinnamate derivatives, the reactions were highly diastereoselective for the formation of 1,2-*anti* carboamination products. Notably, the Ritter reaction was found to be the origin of diastereoselectivity on the basis of a density functional theory (DFT) mechanistic study. The authors proposed a radical-polar crossover mechanism. First, a SET from Fe(II) to the alkyl diacyl peroxide generates the alkyl acyloxy radical which decarboxylates to afford the alkyl radical **165**. Addition of the radical across the alkene affords the benzylic radical **166** which is oxidized by Fe(III) to a carbocation species **167**. Subsequent attack by the nitrile affords the nitrilium ion **168** which upon hydrolysis gives the final product **164**.

Oxime esters and ethers represent a widely used starting material for the generation of nitrogen-containing heterocycles. Due to the breadth of reactions viable from iminyl radicals, generating through the homolytic cleavage of the N–O bond, a number of Fe-catalyzed domino reactions have been investigated.

In 2018, Okamoto and Ohe reported an iminoarylation of γ,δ-unsaturated oxime esters **165** with arenes **166** (Scheme 35) [137]. The reaction most likely involves an iminyl radical which undergoes a 5-*exo-trig* cyclization with the alkene to form the alkyl radical intermediate. Homolytic aromatic substitution (HAS) with the arene will afford the final functionalized product. Interestingly, electron-poor, electron-rich, and heteroarenes were all well-tolerated; however, monosubstituted aryl rings suffered from low regioselectivity which is in accordance with HAS-type reactions [138].

In 2020, the Wu group expanded on the radical cyclization chemistry of γ,δ-unsaturated oxime esters, describing a

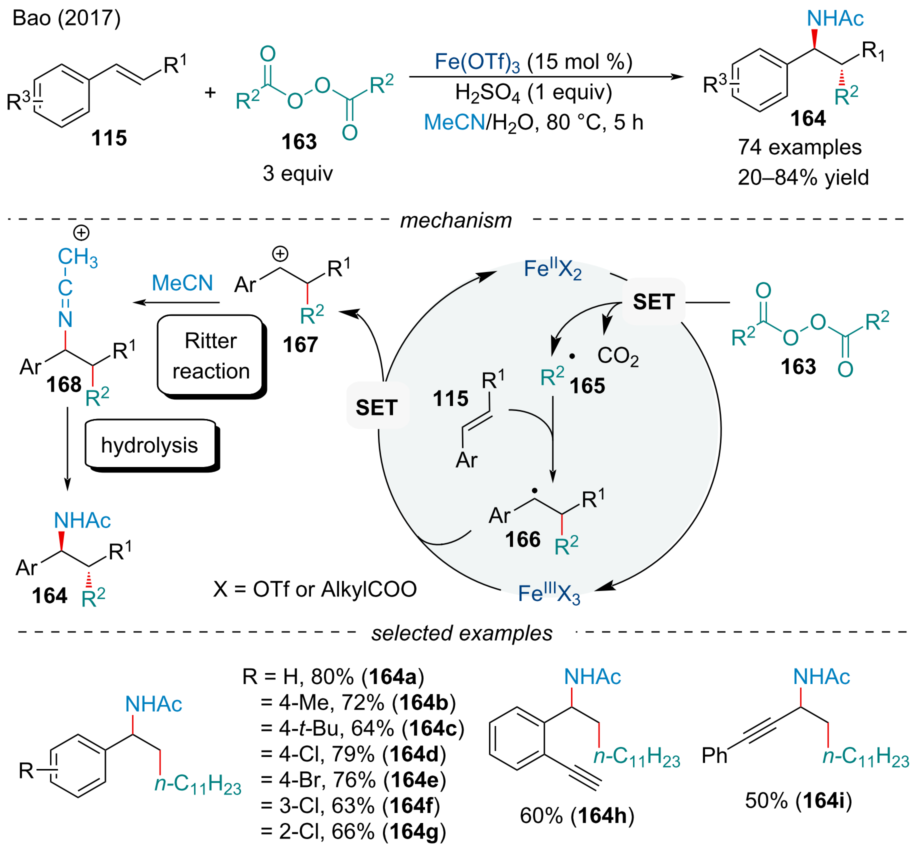
Bao (2017)
115
+
163
3 equiv
Fe(OTf)3 (15 mol %)
H2SO4 (1 equiv)
MeCN/H2O, 80 °C, 5 h
NHAc
164
74 examples
20–84% yield
mechanism
MeCN
Ritter reaction
167
168
hydrolysis
164
FeIIX2
SET
CO2
165
115
166
FeIIIX3
163
X = OTf or AlkylCOO
selected examples
R = H, 80% (164a)
= 4-Me, 72% (164b)
= 4-t-Bu, 64% (164c)
= 4-Cl, 79% (164d)
= 4-Br, 76% (164e)
= 3-Cl, 63% (164f)
= 2-Cl, 66% (164g)
60% (164h)
50% (164i)

Scheme 34: Iron-catalyzed carboamination of conjugated alkenes **115** with alkyl diacyl peroxides **163** and acetonitrile.

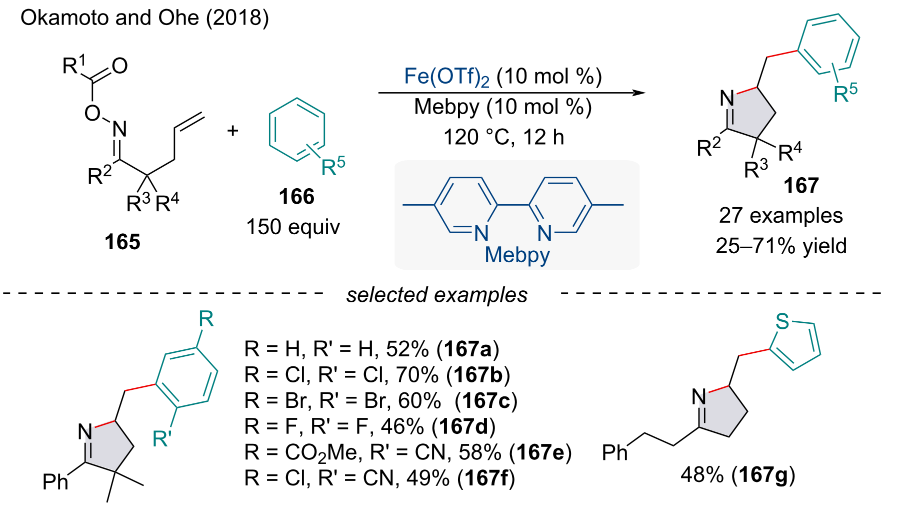
Okamoto and Ohe (2018)
165
+
166
150 equiv
Fe(OTf)2 (10 mol %)
Mebpy (10 mol %)
120 °C, 12 h
Mebpy
167
27 examples
25–71% yield
selected examples
R = H, R' = H, 52% (167a)
R = Cl, R' = Cl, 70% (167b)
R = Br, R' = Br, 60% (167c)
R = F, R' = F, 46% (167d)
R = CO2Me, R' = CN, 58% (167e)
R = Cl, R' = CN, 49% (167f)
48% (167g)

Scheme 35: Iron-catalyzed carboamination using oxime esters **165** and arenes **166**.

carbonylative cyclization with amine nucleophiles [139]. Following an iminyl radical-mediated intramolecular 1,5-cyclization, the subsequent alkyl radical could propagate across carbon monoxide, eventually terminating with an alkyl or aryl amine. In the following year, the Li group described an interesting radical cyclization of β,γ-unsaturated oximes using iron(III) nitrate at a 50% catalytic loading in which the catalyst also acted as a source of nitrate ions for the reaction [140]. Upon oxidation of the alkyl radical, the Fe(III) species is reduced to Fe(II) releasing a nitrate anion which attacks the now electrophilic carbocation for a net iminyl-nitrooxylation reaction [140].

In 2020, Wei and co-workers studied an iminyl radical-triggered 1,5-hydrogen atom transfer (HAT) and [5 + 2] annulation processes for the synthesis of azepine derivatives **170** (Scheme 36) [141]. The reaction was tolerable of both electron-donating and electron-withdrawing substituents on the oxime; however, the reaction required highly activated alkenes to proceed. 1,2-Disubstituted alkenes were tolerated and were diastereoselective for the *anti*-addition product. When maleimides **171** were used as the 2-carbon coupling partner, a [5 + 1] annulation was observed generating spiro succinimidetetrahydropyridine derivatives **172**. To understand the chemoselectivity of the reaction, the authors performed a DFT mechanistic study. After the iminyl radical is generated it will undergo a 1,5-HAT to form the more stable alkyl radical which will add across the alkene. In the case of activated alkenes, the species will undergo a 7-*exo-trig* cyclization. On the other hand, it is energetically more favorable for the maleimide species to sequentially undergo a 1,4-HAT, 1,4-HAT, 1,6-HAT and intramolecular cyclization to form the 6-membered ring. Further, by applying different coupling partners, both bi- [142] and tricyclic [143] fused heterocyclic frameworks have been synthesized through iminyl radical cascade cyclization and annulation reactions.

Carbooxygenation

In 2017, the Bao group reported the first decarboxylative alkyl etherification of alkenes **108** with alcohols **67** and aliphatic acids **173** (Scheme 37) [144]. Through a DCC-mediated dehydrogenative condensation with hydroperoxides, carboxylic acids could generate alkyl diacyl peroxides and peresters in situ. Decarboxylation followed by radical addition across the alkene **108** would generate a succeeding alkyl radical. Oxidation of the alkyl radical would form the corresponding carbocation which could be captured by oxygen nucleophiles **67** to afford the carboetherification product.

In 2020, Iwasaki and Nishihara investigated the inter-/intramolecular alkylative cyclization of carboxylic acid and alcohol-tethered alkenes **175** (Scheme 38) [145]. Control experiments determined the reaction involved a radical process. The proposed mechanism comprised a conventional generation of the alkyl radical through a SET which subsequently adds across the alkene. Compared to Guo's and Li's seminal reports (Scheme 19), the authors propose the intramolecular cyclization proceeds via the nucleophilic attack of a brominated or cationic benzylic position rather than a radical cyclization. In 2021, Tang and Zhang demonstrated a similar radical annula-

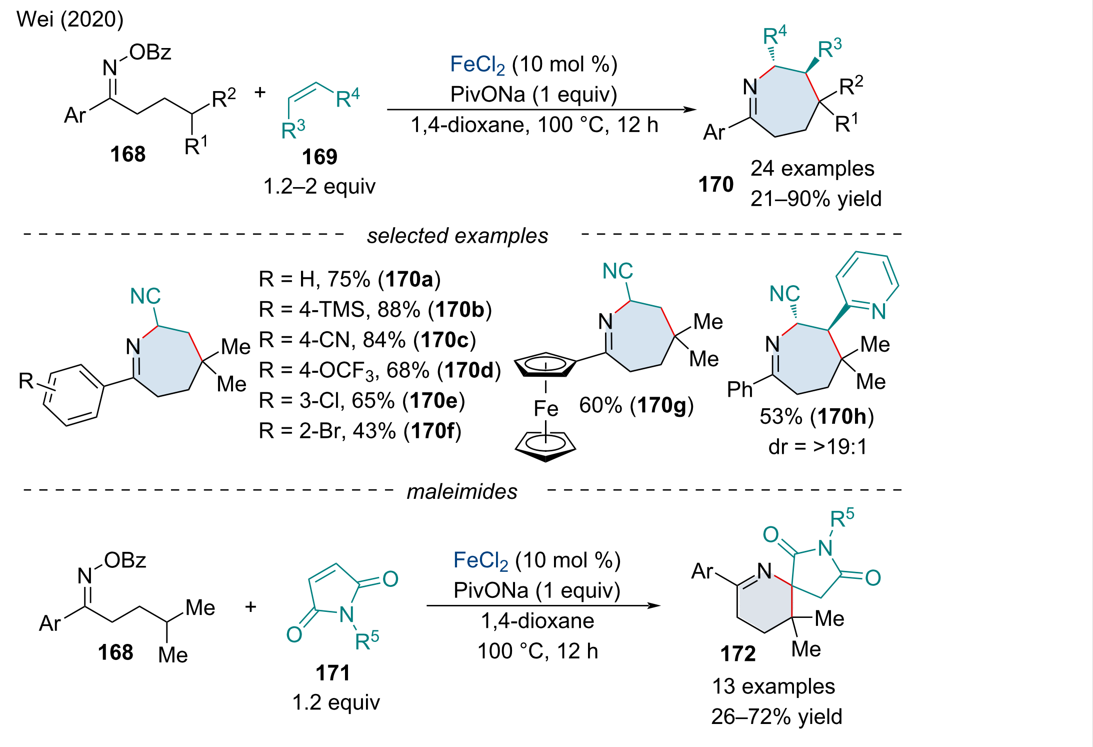
Wei (2020)
N OBz
Ar
R2
R1
168
+
R3
R4
169
1.2–2 equiv
FeCl2 (10 mol %)
PivONa (1 equiv)
1,4-dioxane, 100 °C, 12 h
R4
R3
N
R2
R1
Ar
170
24 examples
21–90% yield
selected examples
NC
R
Me
Me
R = H, 75% (170a)
R = 4-TMS, 88% (170b)
R = 4-CN, 84% (170c)
R = 4-OCF3, 68% (170d)
R = 3-Cl, 65% (170e)
R = 2-Br, 43% (170f)
NC
Me
Me
Fe
60% (170g)
NC
N
Me
Me
Ph
53% (170h)
dr = >19:1
maleimides
N OBz
Ar
Me
Me
168
+
O
N
R5
O
171
1.2 equiv
FeCl2 (10 mol %)
PivONa (1 equiv)
1,4-dioxane
100 °C, 12 h
R5
O
N
O
Ar
N
Me
Me
172
13 examples
26–72% yield

Scheme 36: Iron-catalyzed iminyl radical-triggered [5 + 2] and [5 + 1] annulation reactions with oxime esters **168** and alkenes **169**.

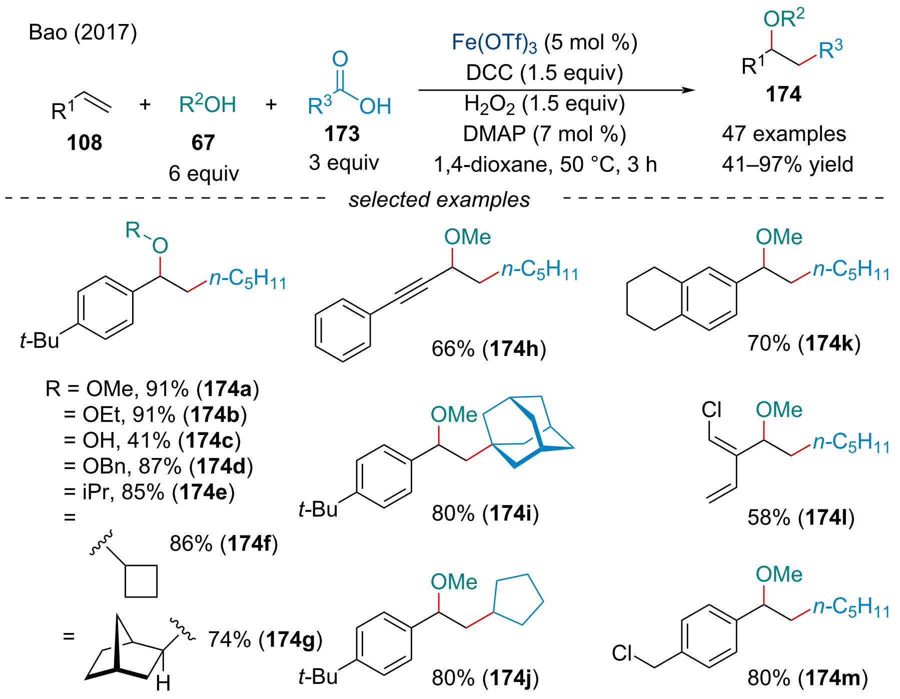
Bao (2017)
108
67
6 equiv
173
3 equiv
Fe(OTf)3 (5 mol %)
DCC (1.5 equiv)
H2O2 (1.5 equiv)
DMAP (7 mol %)
1,4-dioxane, 50 °C, 3 h
174
47 examples
41–97% yield
selected examples
R = OMe, 91% (174a)
= OEt, 91% (174b)
= OH, 41% (174c)
= OBn, 87% (174d)
= iPr, 85% (174e)
86% (174f)
74% (174g)
66% (174h)
70% (174k)
80% (174i)
58% (174l)
80% (174j)
80% (174m)

Scheme 37: Iron-catalyzed decarboxylative alkyl etherification of alkenes **108** with alcohols **67** and aliphatic acids **173**.

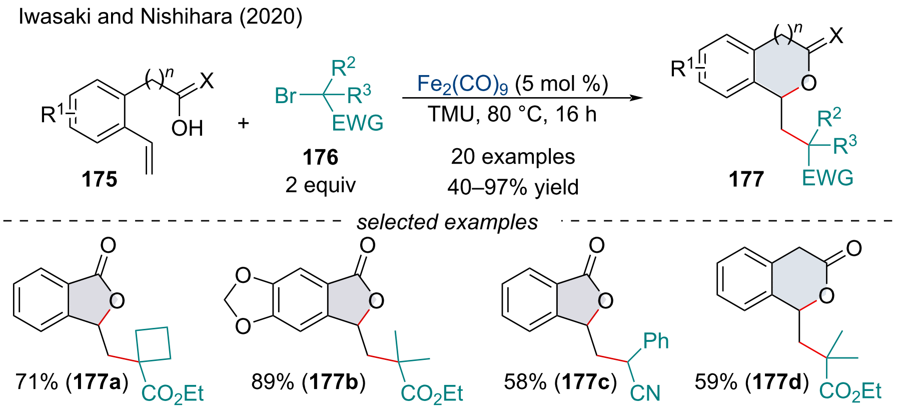
Iwasaki and Nishihara (2020)
175
176
2 equiv
Fe2(CO)9 (5 mol %)
TMU, 80 °C, 16 h
20 examples
40–97% yield
177
selected examples
71% (177a)
89% (177b)
58% (177c)
59% (177d)

Scheme 38: Iron-catalyzed inter-/intramolecular alkylative cyclization of carboxylic acid and alcohol-tethered alkenes **175**.

tion of unsaturated carboxylic acids with disulfides for the synthesis of γ-lactones [146].

In 2020, Cai and co-workers reported a three-component intermolecular trifluoromethyl-esterification of activated alkenes **115** with NaOTf and aryl carboxylic acids **178** (Scheme 39) [147]. Notably, the use of NaOTf as a CF_3 source, compared to pre-prepared trifluoromethylating agents like Togni's reagent, is ideal because of its stability, low toxicity, and cost [148]. In terms of scope, the electronic nature of the benzoic acid had no effect on the reaction. On the other hand, only electron-rich styrene derivatives were found to work well in the reaction, with unactivated and aliphatic alkenes having little to no reactivity.

Carbohalogenation

In 2009, Liu's group established benzyl halides can be added across aryl alkynes for the synthesis of alkenyl halides [149]. Similarly, the addition of perfluoroiodides **181** across π-systems **180** was reported by Hu in 2014 (Scheme 40) [150]. Carboiodination of terminal alkynes was stereoselective for the formation of the *E*-isomer **181**. Compared the Liu's report, this reaction

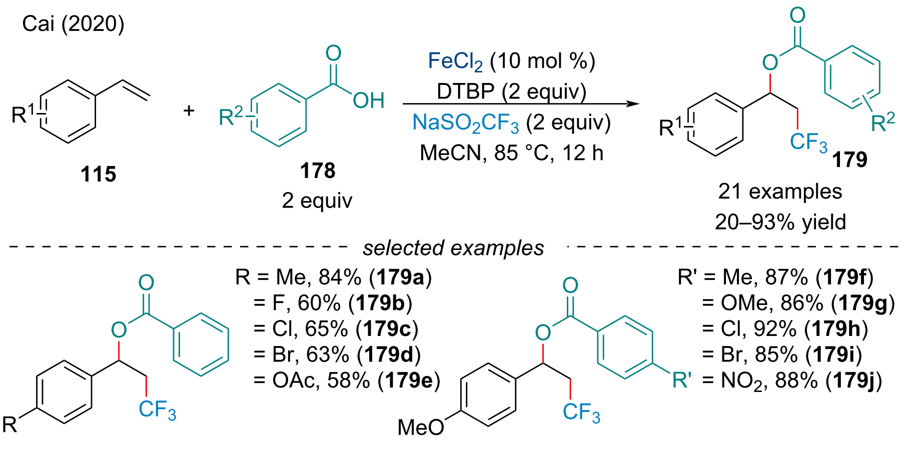
Cai (2020)
R1
115
+
R2
O
OH
178
2 equiv
FeCl2 (10 mol %)
DTBP (2 equiv)
NaSO2CF3 (2 equiv)
MeCN, 85 °C, 12 h
O
O
R1
CF3
R2
179
21 examples
20–93% yield
selected examples
O
O
R
CF3
R = Me, 84% (179a)
= F, 60% (179b)
= Cl, 65% (179c)
= Br, 63% (179d)
= OAc, 58% (179e)
O
O
MeO
CF3
R'
R' = Me, 87% (179f)
= OMe, 86% (179g)
= Cl, 92% (179h)
= Br, 85% (179i)
= NO2, 88% (179j)

Scheme 39: Iron-catalyzed intermolecular trifluoromethyl-acyloxylation of styrene derivatives **115**.

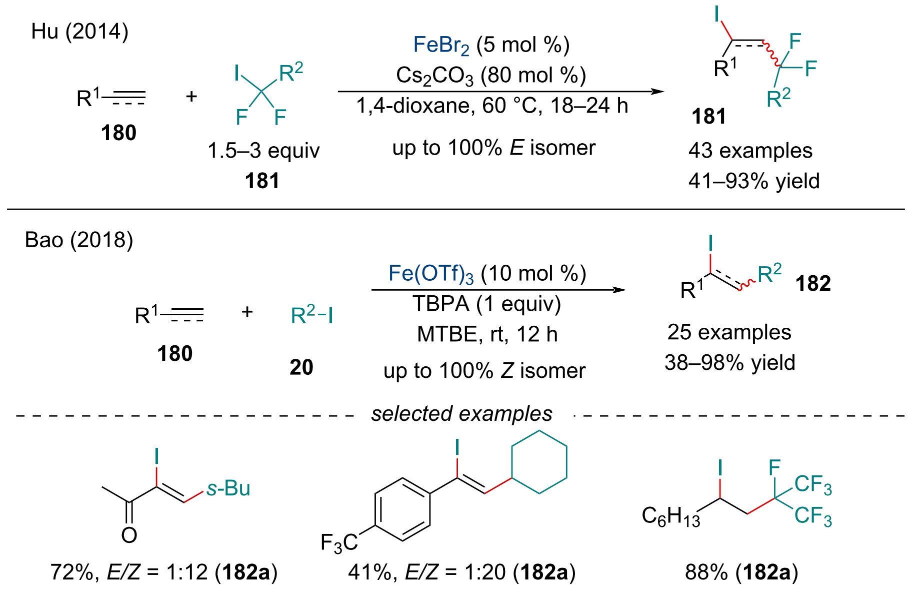
Hu (2014)
R1
180
+
I
R2
F
F
1.5–3 equiv
181
FeBr2 (5 mol %)
Cs2CO3 (80 mol %)
1,4-dioxane, 60 °C, 18–24 h
up to 100% E isomer
I
F
F
R1
R2
181
43 examples
41–93% yield
Bao (2018)
R1
180
+
R2–I
20
Fe(OTf)3 (10 mol %)
TBPA (1 equiv)
MTBE, rt, 12 h
up to 100% Z isomer
I
R1
R2
182
25 examples
38–98% yield
selected examples
I
s-Bu
O
72%, E/Z = 1:12 (182a)
I
F3C
41%, E/Z = 1:20 (182a)
I
F
CF3
CF3
C6H13
88% (182a)

Scheme 40: Iron-catalyzed carboiodination of terminal alkenes and alkynes **180**.

was applicable to both aliphatic alkenes and alkynes. To show the applicability of this transformation, the authors performed a series of cross-coupling reactions, demonstrating the neighboring perfluoroalkyl groups did not impede the reaction. In 2018, Bao and co-workers expanded on the carboiodination reaction (Scheme 40) [151]. Their method allowed for the general alkyl chains, as well as ester and cyano moieties, to be added across the alkene. Both aryl and aliphatic alkenes and alkynes **180** were found to work well in the transformation. Interestingly, alkyl iodides **20** provided the corresponding vinyl iodide with overall *anti* addition. When the iodo-substrate was equipped with an electron-withdrawing group, up to 100% of the *syn* product **182** was observed.

In 2018, the Xia laboratory reported a Cu/Fe-cocatalyzed cascade perfluoroalkylation/cyclization of 1,6-enynes **183**/**185** for the synthesis of fluoroalkylated pyrrolidines and benzofurans **184**/**186** (Scheme 41) [152]. When either catalyst was used on its own, the reaction had little to no success, demonstrating the necessity for tandem catalysis. When terminal alkynes **185** were used, the transformation was terminated by an iodine transfer process rather than hydrogen abstraction to furnish vinyl iodides **186**. When tetrasubstituted vinyl iodides were synthesized and exposed to the reaction conditions, a deiodination occurred, suggesting the vinyl iodide may be an intermediate in the mechanism. The authors propose sequential addition of the alkyl radical across the alkene followed by the alkyne

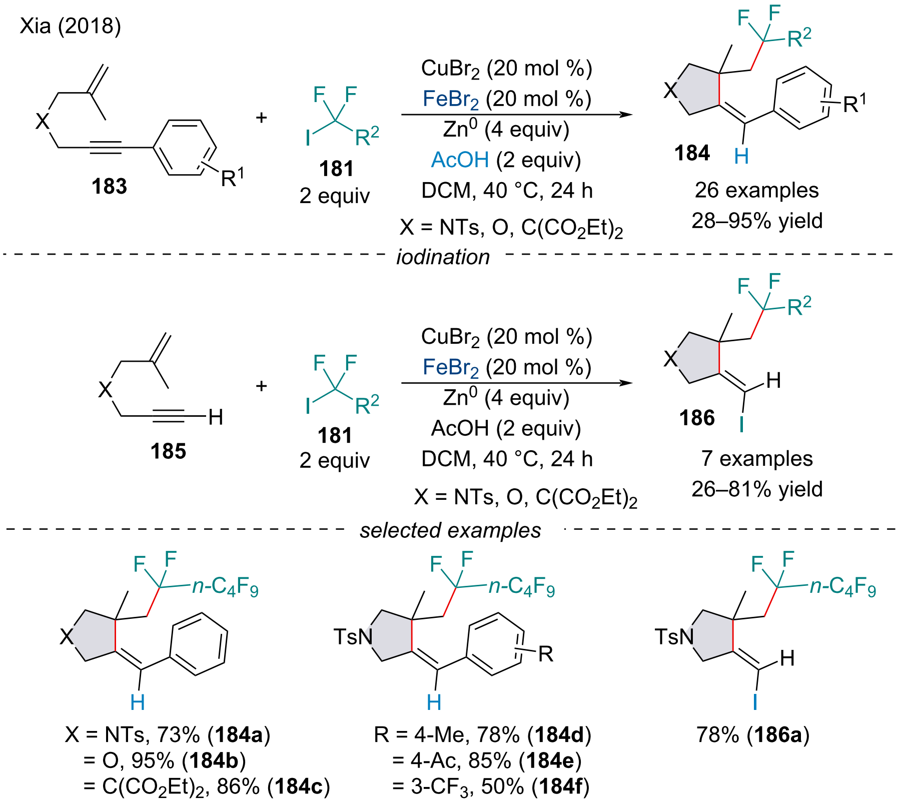

Scheme 41: Copper/iron-cocatalyzed cascade perfluoroalkylation/cyclization of 1,6-enynes **183**/**185**.

produces the cyclization intermediate. This intermediate may undergo halogen abstraction to form the vinylic iodide. If an internal alkyne is used, the iodide may undergo oxidative addition followed by reduction and protonation. Alternatively, the internal alkyne-cyclized intermediate may simply proceed through a vinylic metallic species which is reduced by zinc metal and protonated.

Carbosilylation

In 2017, the Nakamura group demonstrated the carbosilylation of alkynes **187** (Scheme 42) [153]. The protocol allowed for the use of various alkyl halides as electrophiles. Interestingly, both *syn-* and *anti*-selective carbosilylation could be achieved by altering the reaction conditions and employing different silylboranes. The authors hypothesized the oxygen functionality on the silylborane coordinates with the iron center to form a more stable, chelated *Z*-alkenyliron species. Trialkylsilanes were incompatible with the reaction, suggesting a Lewis-acidic silyl center is preferred in the reaction pathway; hence, the necessity for at least one phenyl substituent.

Carbosulfinylation

In 2019, the Cai laboratory demonstrated the first difluoroalkylative–thiolation of alkenes **82** by Fe-facilitated visible-light photoredox catalysis (Scheme 43) [154]. During optimization, the authors noted both the photocatalyst and iron salt critically affected the efficacy of the reaction. When no photocatalyst was present the reaction failed entirely, and only a trace amount of desired product was obtained in the absence of the iron salt. Consistent with many Fe-catalyzed difunctionalization reactions, only activated alkenes were tolerated in the reaction, with aliphatic olefins having reduced reactivity. Both electron-rich and deficient thiophenols **190** were shown to react smoothly under the reaction conditions; however, future work should be done examining the applicability of the reaction with aliphatic thiol coupling partners. In the same year, Cai and co-workers elaborated on their previous study to explore the potential of amines as coupling partners in the three-component difluoroalkylamination of alkenes mediated by photoredox and iron cooperative catalysis [155]. Similar reactivity trends were observed for the alkene component of the reaction; however, electron-deficient arylamines were found to be unreactive.

Hetero-difunctionalization

In recent years, many advances in two and three-component hetero-difunctionalization reactions have been made, offering a powerful method for increasing molecular complexity in organic synthesis. Recent accounts have demonstrated Fe-cata-

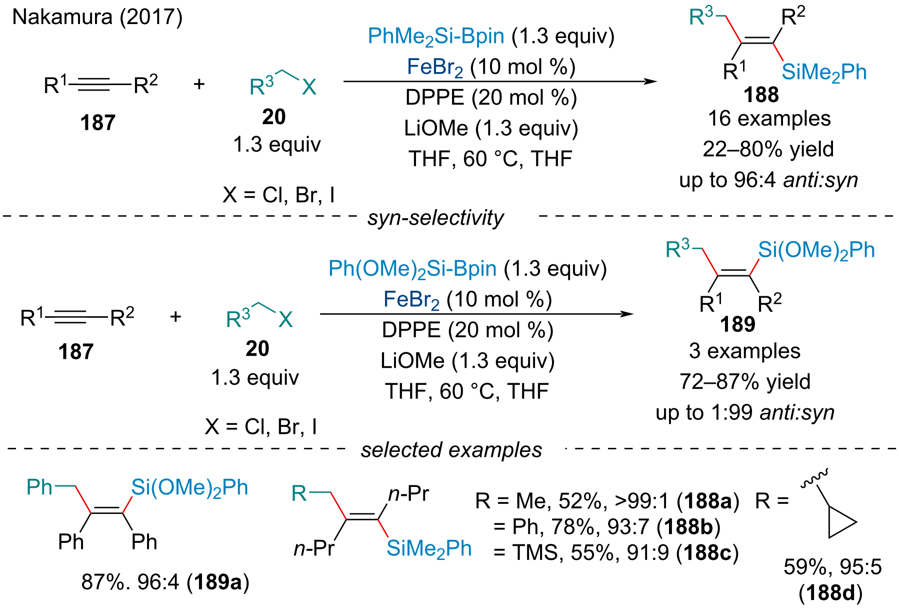
Nakamura (2017)
R1—≡—R2
187
+
R3⌒X
20
1.3 equiv
X = Cl, Br, I
PhMe2Si-Bpin (1.3 equiv)
FeBr2 (10 mol %)
DPPE (20 mol %)
LiOMe (1.3 equiv)
THF, 60 °C, THF
R3
R2
R1
SiMe2Ph
188
16 examples
22–80% yield
up to 96:4 anti:syn
syn-selectivity
Ph(OMe)2Si-Bpin (1.3 equiv)
FeBr2 (10 mol %)
DPPE (20 mol %)
LiOMe (1.3 equiv)
THF, 60 °C, THF
Si(OMe)2Ph
189
3 examples
72–87% yield
up to 1:99 anti:syn
selected examples
Ph
Si(OMe)2Ph
Ph
Ph
87%. 96:4 (189a)
R
n-Pr
n-Pr
SiMe2Ph
R = Me, 52%, >99:1 (188a)
= Ph, 78%, 93:7 (188b)
= TMS, 55%, 91:9 (188c)
R =
59%, 95:5
(188d)

Scheme 42: Iron-catalyzed stereoselective carbosilylation of internal alkynes **187**.

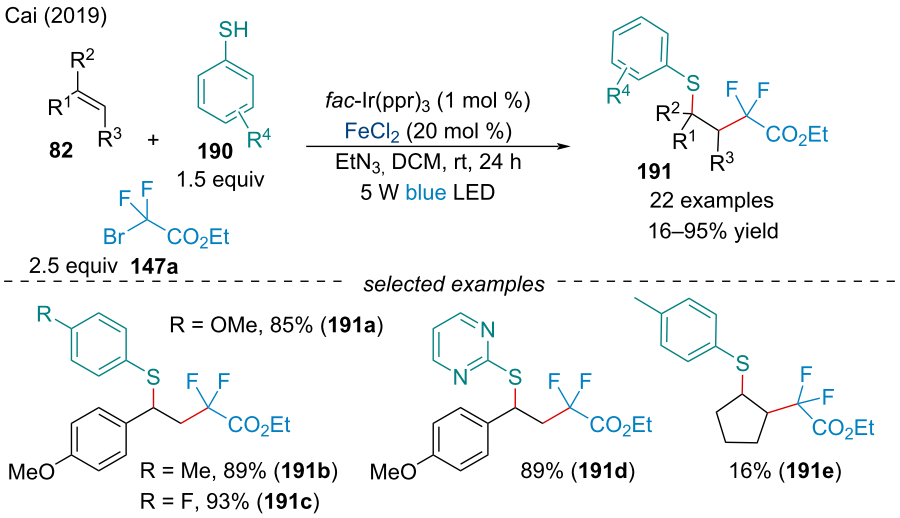
Cai (2019)
R2
R1
R3
82
+
SH
R4
190
1.5 equiv
F
F
Br
CO2Et
2.5 equiv 147a
fac-Ir(ppr)3 (1 mol %)
FeCl2 (20 mol %)
EtN3, DCM, rt, 24 h
5 W blue LED
R4
S
F F
R2
R1
R3
CO2Et
191
22 examples
16–95% yield
selected examples
R
R = OMe, 85% (191a)
S
F F
CO2Et
MeO
R = Me, 89% (191b)
R = F, 93% (191c)
N
N
S
F F
CO2Et
MeO
89% (191d)
S
F
F
CO2Et
16% (191e)

Scheme 43: Synergistic photoredox/iron catalyzed difluoroalkylation–thiolation of alkenes **82**.

lyzed cascade reactions can promote the incorporation of several heteroatoms across π-systems, quickly assembling multiple carbon–heteroatom bonds in a single reaction.

Aminoazidation

The synthesis of undifferentiated vicinal diamines and diazides has been described by Xu and co-workers as powerful tool for accessing symmetrical difunctionalized compounds; these reactions suffer where two chemically distinct amino groups need to be orthogonally synthesized [156]. In 2020, the Morandi group developed an Fe(OTf)$_2$-catalyzed aminoazidation of alkenes **82** for the synthesis of unprotected primary 2-azidoamines **193** (Scheme 44) [157]. The catalytic process demonstrated a considerable scope, with good yields, and with cyclic alkenes, good diastereoselectivity. Further, the mild conditions allowed for superior functional group tolerance. Its potential for early- and late-stage functionalization is highlighted with the artemether derivative **193c** where the highly oxidized cage structure and

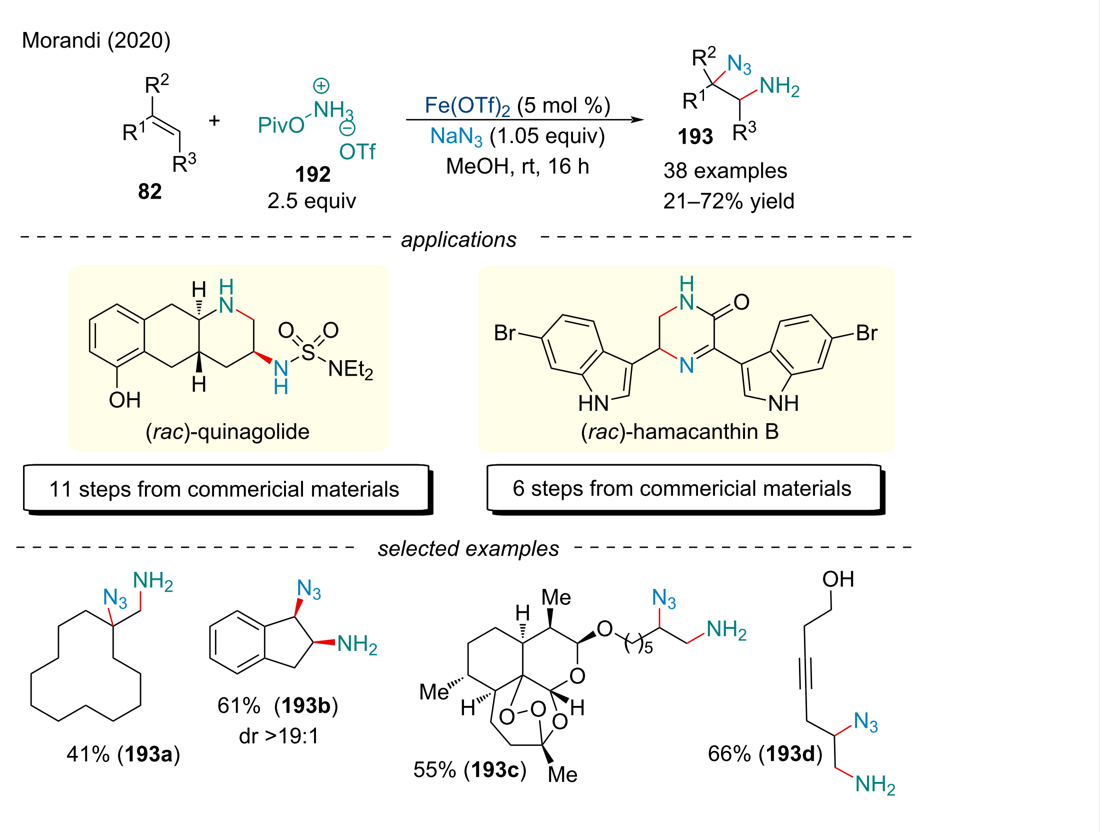
Morandi (2020)
R2
R1
R3
82
+
PivO
NH3
OTf
192
2.5 equiv
Fe(OTf)2 (5 mol %)
NaN3 (1.05 equiv)
MeOH, rt, 16 h
R2
N3
NH2
R1
193
R3
38 examples
21–72% yield
applications
(rac)-quinagolide
11 steps from commericial materials
(rac)-hamacanthin B
6 steps from commericial materials
selected examples
41% (193a)
61% (193b)
dr >19:1
55% (193c)
66% (193d)

Scheme 44: Iron-catalyzed three-component aminoazidation of alkenes **82**.

the sensitive peroxo group were left intact. Application of this methodology to the total synthesis of (±)-hamacanthin B and (±)-quinagolide further demonstrated the broad synthetic potential.

Efforts to expand the scope of aminoazidation reactions were met with success in 2021, when a report from the Bao group described a method for accessing chiral organo azides [158]. Using a chiral BOX ligand, the authors demonstrated a large scope with excellent yields (up to 98%) and enantioselectivity (up to 96% ee). Unlike Morandi's report (Scheme 44) [157], the authors only included styrene derivatives in the scope of potential alkenes. Adaptation of the reaction conditions also allowed for the synthesis of enantioenriched diazido products [158].

In 2020, Berhal and Prestate demonstrated a tandem intra/intermolecular aminoazidation of unactivated alkenes **194** for the synthesis of a variety of heterocyclic scaffolds **195** (Scheme 45) [159]. Although yields of up to 90% were achieved, yields were typically moderated at best. Despite the low yield, the protocol offered a more economically and ecologically sustainable method for the production of azido-containing imidazolidinone, oxazolidinone, and pyrrolidinones which avoided highly shock and friction sensitive reagents.

Oxyazidation

In 2017, Gillaizeau and co-workers investigated the intermolecular oxyazidation of enamides **196** using azidobenziodoxolone derivatives **197** (Scheme 46) [160]. Both cyclic and acyclic enamides were amenable to the reaction and were compatible with a variety of functional groups. Interestingly, the reaction was mild enough to afford difunctionalized products in the presence of alkynes **198a**,**b** which could be converted into tricyclic triazine derivatives **199a/199b** via a thermal Huisgen 1,3-dipolar cycloaddition in quantitative yield.

Aminooxygenation

In 2016, the Morandi group reported the aminohydroxylation of alkenes **82** for the synthesis of unprotected amino alcohols **200** in good yield (Scheme 47) [161]. Their account relied on the use of $PivONH_3OTf$ **192** as an easily accessible aminating reagent. Various functionalized styrene derivatives afforded the corresponding product in good yield; however, strongly electron-withdrawing groups were detrimental to the reaction. Further, under the optimized reaction conditions, most unactivated alkenes had little to no reactivity. The method could be extended to other oxygen nucleophiles for access to amino ethers; however, the scope of applicable alcohols was low. Application of this protocol allowed for the rapid synthesis of

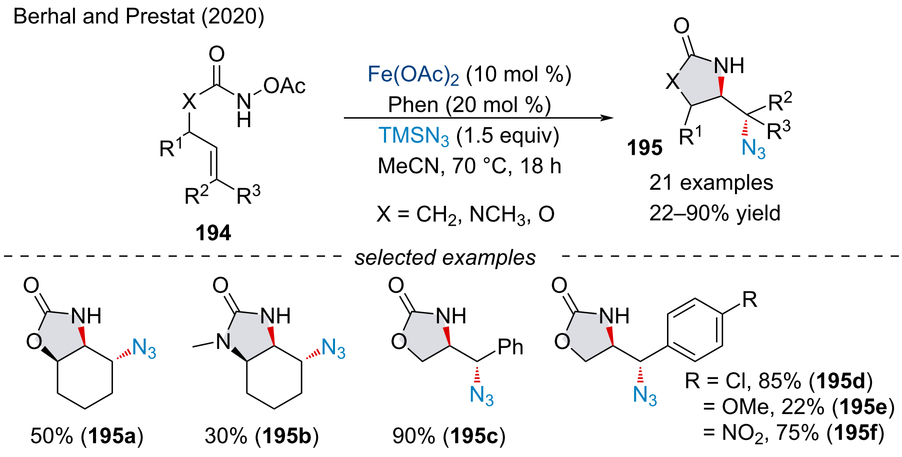
Berhal and Prestat (2020)
194
Fe(OAc)2 (10 mol %)
Phen (20 mol %)
TMSN3 (1.5 equiv)
MeCN, 70 °C, 18 h
X = CH2, NCH3, O
195
21 examples
22–90% yield
selected examples
50% (195a)
30% (195b)
90% (195c)
R = Cl, 85% (195d)
= OMe, 22% (195e)
= NO2, 75% (195f)

Scheme 45: Iron-catalyzed intra-/intermolecular aminoazidation of alkenes **194**.

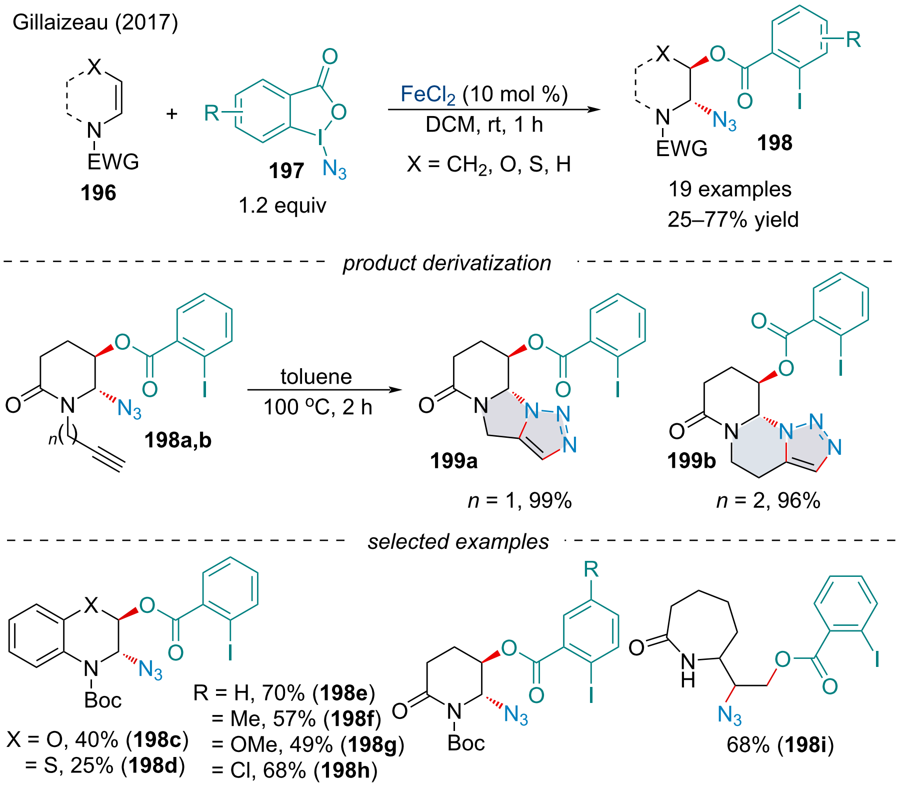
Gillaizeau (2017)
196
197
1.2 equiv
FeCl2 (10 mol %)
DCM, rt, 1 h
X = CH2, O, S, H
198
19 examples
25–77% yield
product derivatization
198a,b
toluene
100 °C, 2 h
199a
n = 1, 99%
199b
n = 2, 96%
selected examples
X = O, 40% (198c)
= S, 25% (198d)
R = H, 70% (198e)
= Me, 57% (198f)
= OMe, 49% (198g)
= Cl, 68% (198h)
68% (198i)

Scheme 46: Stereoselective iron-catalyzed oxyazidation of enamides **196** using hypervalent iodine reagents **197**.

aegoline-*O*-methyl ether and phenylephrine in good yield. Through a series of mechanistic studies, the authors propose two potential pathways. First, the iron catalyst will react with the hydroxylamine salt to form either an Fe(IV) nitrene complex **203** or an Fe(III) aminyl species **206**. The Fe(IV) nitrene can add across the alkene **82** to form a protonated aziridine **204** which is opened by intermolecular nucleophilic attack by the oxygen nucleophile. Alternatively, the Fe(III) aminyl species adds across the alkene **82** to form the radical intermediate **207**. Oxidization by a SET forms the carbocation **208** which is captured by the oxygen nucleophile.

Efforts to expand the scope of aminohydroxylation reactions were met with success in 2019, when a report from the Arnold

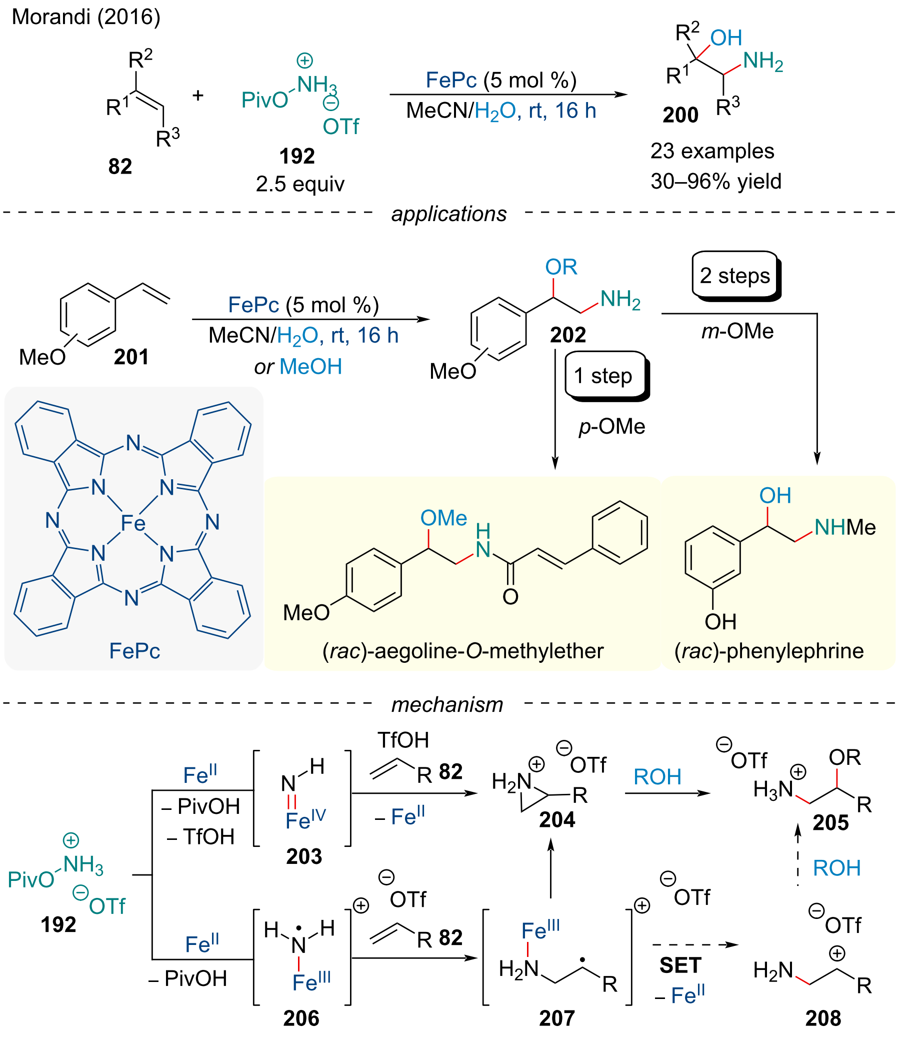
Morandi (2016)
82
192
2.5 equiv
FePc (5 mol %)
MeCN/H2O, rt, 16 h
200
23 examples
30–96% yield
applications
201
FePc (5 mol %)
MeCN/H2O, rt, 16 h
or MeOH
202
2 steps
m-OMe
1 step
p-OMe
FePc
(rac)-aegoline-O-methylether
(rac)-phenylephrine
mechanism
192
Fe^II
– PivOH
– TfOH
203
TfOH
R 82
– Fe^II
204
ROH
205
ROH
Fe^II
– PivOH
206
R 82
207
SET
– Fe^II
208

Scheme 47: Iron-catalyzed aminooxygenation for the synthesis of unprotected amino alcohols **200**.

group described a method for accessing enantioenriched amino alcohols [162]. Using an engineered hemoprotein biocatalyst based on a thermostable cytochrome c. Not only could the engineered protein deliver the product in good yield and excellent enantioselectivity (up to 90% ee), but the protocol also boasts turnover numbers up to 2500. Similar to Morandi's account [161], the reaction's efficacy drops significantly when electron-deficient or unactivated alkenes were examined.

Aminohalogenation

In 2014, the Xu group investigated a diastereoselective Fe-catalyzed aminofluorination of alkenes **209** to produce cyclic carbamates **211** (Scheme 48) [163]. During optimization, both aminofluorinated and aminohydroxylated [164,165] products were observed; however, the use of carboxylate trapping reagent XtalFluor-E® suppressed the competing aminohydroxylation process. Noteworthy, both *E* and *Z* isomers of the olefin starting material **209** led to the same major diastereomer. Based on the observed stereoconvergence, the reaction likely occurs in a stepwise fashion. Based on a mechanistic investigation, the authors propose a working mechanism. First, the Fe complex will reductively cleave the N–O bond to generate Fe-nitrenoid complex **212**. In the presence of a fluoride source, an anion metathesis converts the nitrenoids to difluoride **213**. Subsequent stepwise cycloamination generates carbon-centered radical intermediate **214** which is in fast equilibrium with **215**. Rotation of the σ-bond at this step could potentially explain the observed stereoconvergence.

In the following year, the same group explored the diastereoselective intramolecular Fe-catalyzed aminochlorination of alkenes **209** (Scheme 49) [166]. Initially, the authors developed a racemic reaction employing $Fe(NTf)_2$ and phenanthroline with tetrabutylammonium chloride (TEAC). In contrast to the

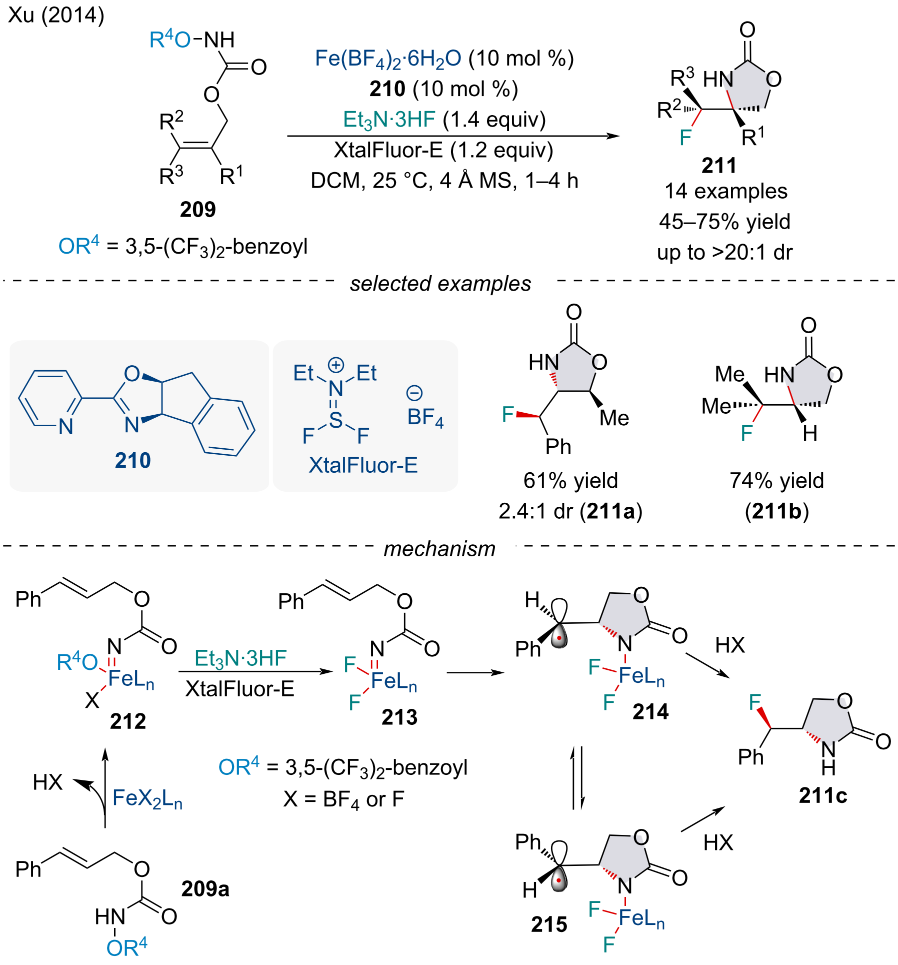
Xu (2014)
R^4O-NH
209
OR^4 = 3,5-$(CF_3)_2$-benzoyl
$Fe(BF_4)_2 \cdot 6H_2O$ (10 mol %)
210 (10 mol %)
$Et_3N \cdot 3HF$ (1.4 equiv)
XtalFluor-E (1.2 equiv)
DCM, 25 °C, 4 Å MS, 1–4 h
211
14 examples
45–75% yield
up to >20:1 dr
selected examples
210
XtalFluor-E
61% yield
2.4:1 dr (211a)
74% yield
(211b)
mechanism
212
$Et_3N \cdot 3HF$
XtalFluor-E
213
214
215
HX
211c
FeX_2L_n
209a
OR^4 = 3,5-$(CF_3)_2$-benzoyl
X = BF_4 or F

Scheme 48: Iron-catalyzed intramolecular aminofluorination of alkenes **209**.

work of Bach [167], the corresponding acyl azide failed to react under the reactions conditions and was fully recovered. Expanding the single enantioselective aminofluorination reaction reported in 2014 [163], Xu and co-workers developed an asymmetric Fe-catalyzed aminochlorination of alkenes **209** through the use of a bisoxazole ligand [166]. The reaction regioselectively led to a range of chiral products in moderate to good yields (45–84%) combined with moderate to high enantioselectivities (54–92% ee). In the same year, the authors applied the enantiomeric catalyst to promote the asymmetric intramolecular aminobromination of alkenes **209** with tetraethylammonium bromide (TEAB) [168].

In 2016, the Xu group continued to investigate Fe-catalyzed aminohalogenation reactions of alkenes **82** (Scheme 50) [169]. Using $Et_3NH \cdot 3HF$ as the fluoride source, the authors reported the first intermolecular aminofluorination of alkenes. Similar to their 2014 report [163], the use of XtalFluor-E® as a carboxylate trapping agent was key to the success of the reaction. Various unfunctionalized alkenes, were amenable to the reaction allowing for the production of a wide range of vicinal fluorocarbamates **220** in high regioselectivity [169]. Later, the authors developed an enantioselective Fe-catalyzed intermolecular aminofluorination reaction of indene [169]. A series of acyloxyl carbamates and chiral PyBOX ligands were screened with the *anti*-2-amino fluoride being delivered in poor to good ee. Compared to the racemic variant, the yield and diastereoselectivity of the reaction was slightly diminished.

In 2018, the Morandi group continued studying the Fe-catalyzed amination reactions. The group reported the addition of NaCl enabled the formation of 2-chloroalkylamine products **221** in good yields and excellent *anti*-Markovnikov selectivity (Scheme 51) [170]. In 2020, the scope of this aminochlorination reaction was expanded to include both primary and secondary amines **222**/**224** [171]. Impressively, both methods proceeded under exceedingly mild conditions with excellent functional group tolerance using stable and inexpensive

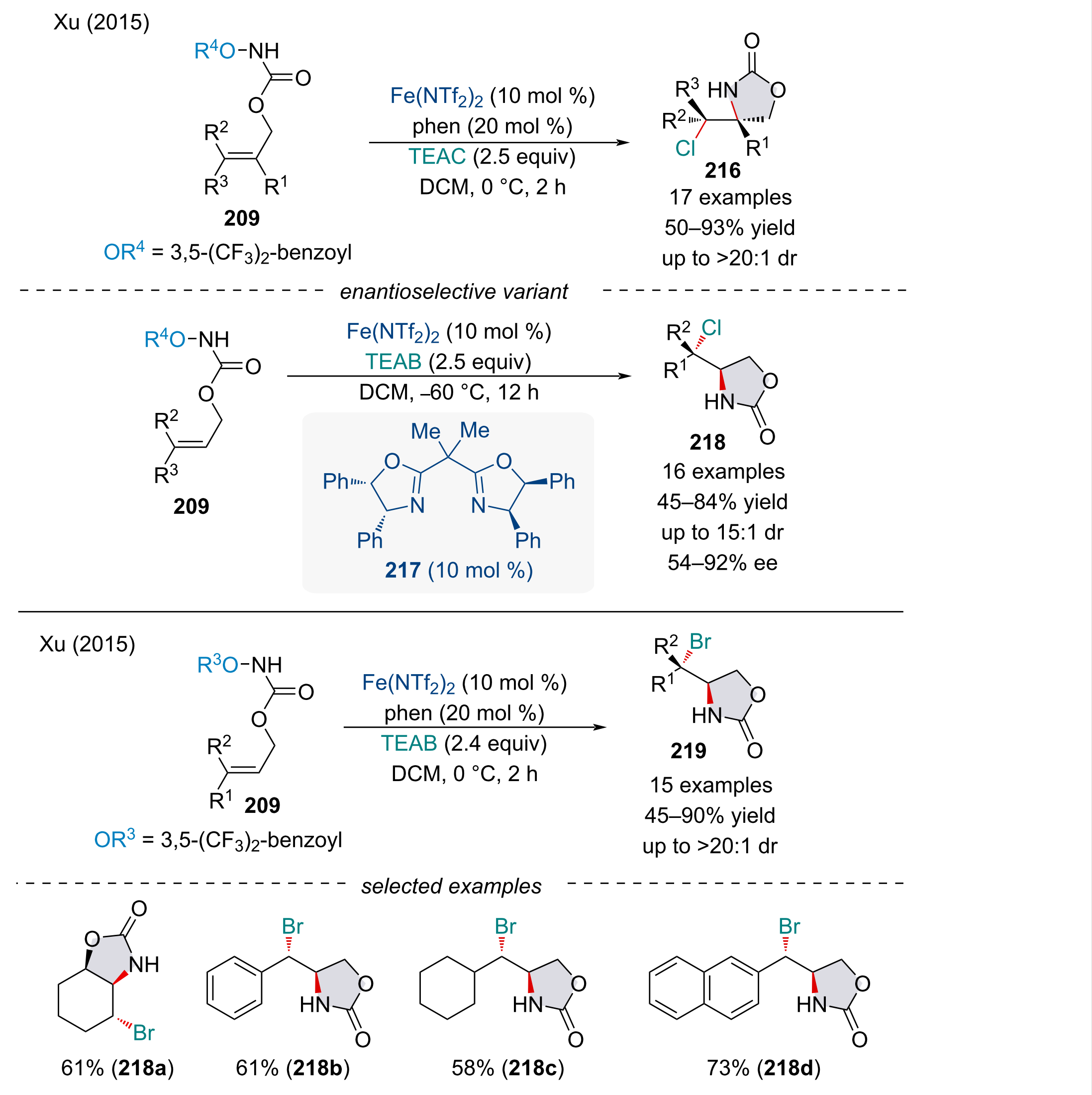
Xu (2015)
R⁴O-NH
O
R²
R³
R¹
209
OR⁴ = 3,5-(CF₃)₂-benzoyl
Fe(NTf₂)₂ (10 mol %)
phen (20 mol %)
TEAC (2.5 equiv)
DCM, 0 °C, 2 h
R³ HN
Cl
216
17 examples
50–93% yield
up to >20:1 dr
enantioselective variant
Fe(NTf₂)₂ (10 mol %)
TEAB (2.5 equiv)
DCM, –60 °C, 12 h
Me Me
Ph
N
217 (10 mol %)
R² Cl
R¹
HN
218
16 examples
45–84% yield
up to 15:1 dr
54–92% ee
Xu (2015)
R³O-NH
209
OR³ = 3,5-(CF₃)₂-benzoyl
Fe(NTf₂)₂ (10 mol %)
phen (20 mol %)
TEAB (2.4 equiv)
DCM, 0 °C, 2 h
R² Br
219
15 examples
45–90% yield
up to >20:1 dr
selected examples
NH
Br
61% (218a)
61% (218b)
58% (218c)
73% (218d)

Scheme 49: Iron-catalyzed intramolecular aminochlorination and aminobromination of alkenes **209**.

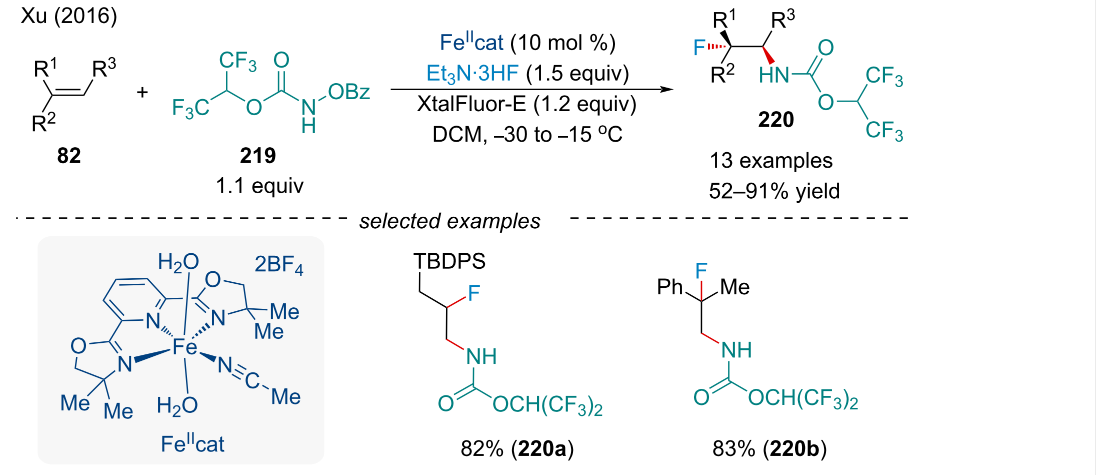
Xu (2016)
R¹ R³
R²
82
+
CF₃ O
F₃C
N
H
OBz
219
1.1 equiv
Fe^II cat (10 mol %)
Et₃N·3HF (1.5 equiv)
XtalFluor-E (1.2 equiv)
DCM, –30 to –15 °C
F
HN
CF₃
220
13 examples
52–91% yield
selected examples
H₂O
2BF₄
N
Fe
Me
H₂O
Fe^II cat
TBDPS
NH
OCH(CF₃)₂
82% (220a)
Ph Me
83% (220b)

Scheme 50: Iron-catalyzed intermolecular aminofluorination of alkenes **82**.

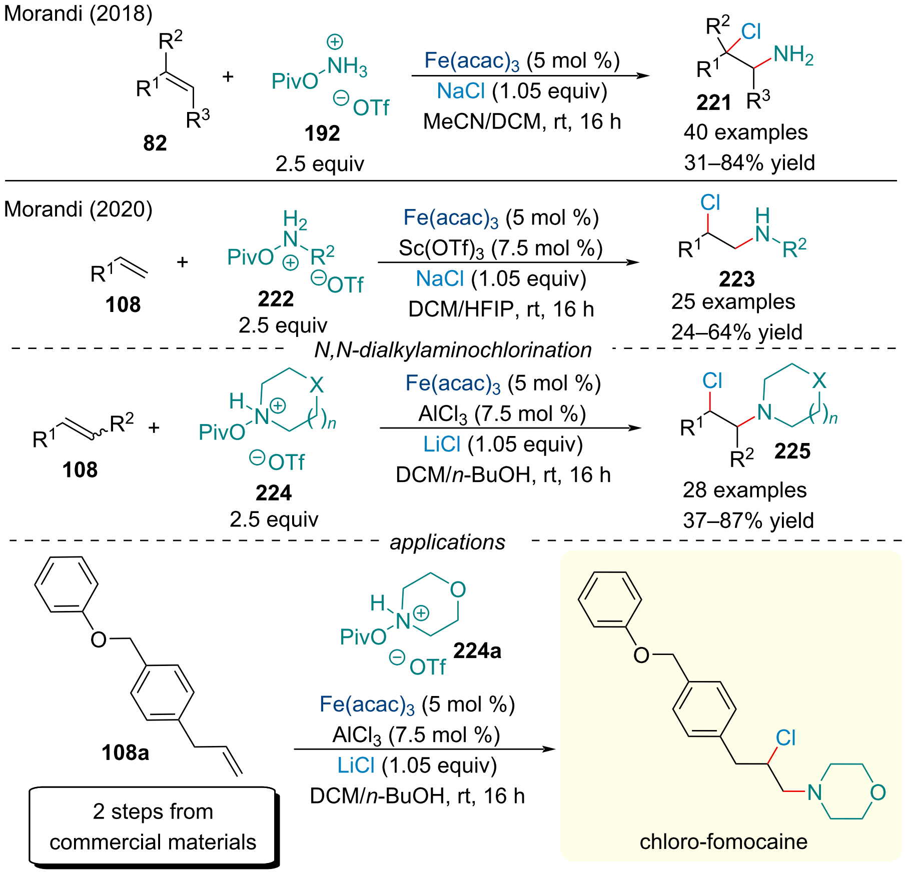
Morandi (2018)
82
192
2.5 equiv
Fe(acac)3 (5 mol %)
NaCl (1.05 equiv)
MeCN/DCM, rt, 16 h
221
40 examples
31–84% yield
Morandi (2020)
108
222
2.5 equiv
Fe(acac)3 (5 mol %)
Sc(OTf)3 (7.5 mol %)
NaCl (1.05 equiv)
DCM/HFIP, rt, 16 h
223
25 examples
24–64% yield
N,N-dialkylaminochlorination
108
224
2.5 equiv
Fe(acac)3 (5 mol %)
AlCl3 (7.5 mol %)
LiCl (1.05 equiv)
DCM/n-BuOH, rt, 16 h
225
28 examples
37–87% yield
applications
108a
2 steps from commercial materials
224a
Fe(acac)3 (5 mol %)
AlCl3 (7.5 mol %)
LiCl (1.05 equiv)
DCM/n-BuOH, rt, 16 h
chloro-fomocaine

Scheme 51: Iron-catalyzed aminochlorination of alkenes **82**.

aminochlorinating reagents, applicable for late-stage functionalization. In contrast to their previous report, the reactions displayed broad reactivity and worked well for unactivated internal alkenes. To illustrate the versatility of this protocol, the authors synthesized a chlorinated fomocaine analog in three steps.

Phosphinoylazidation

In 2021, the Bao group described the phosphinoylazidation of alkenes **108** under mild conditions with diarylphosphine oxides **226** and TMSN$_3$ (Scheme 52) [172]. Through a DFT investigation, the authors noted the azido transfer from PcFe(III)N$_3$ to a benzylic cation has an activation energy of 4.8 kcal/mol. This

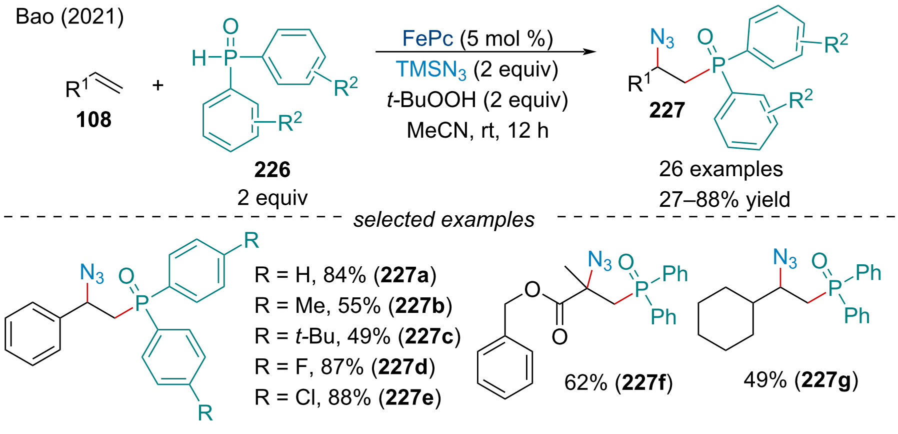
Bao (2021)
108
226
2 equiv
FePc (5 mol %)
TMSN3 (2 equiv)
t-BuOOH (2 equiv)
MeCN, rt, 12 h
227
26 examples
27–88% yield
selected examples
R = H, 84% (227a)
R = Me, 55% (227b)
R = t-Bu, 49% (227c)
R = F, 87% (227d)
R = Cl, 88% (227e)
62% (227f)
49% (227g)

Scheme 52: Iron-catalyzed phosphinoylazidation of alkenes **108**.

barrier is remarkably low compared to similar reactions using other earth abundant metals like copper [173] and manganese [174] which have barriers ranging 7.0–10.7 kcal/mol. In terms of scope, only diarylphosphine oxide derivatives were found to be applicable, with dialkylphosphine oxide and phosphonate compounds failing to produce the desired product. Unactivated alkenes were tolerated but less fruitful, most likely due to the instability of the carbocationic intermediate.

Aminoselenation

In 2020, Yang and Xia explored the visible-light enabled, $FeBr_3$-catalyzed aminoselenation of alkenes **82** with amines **105** and diselenides **228** under an air atmosphere (Scheme 53) [175]. Excellent functional group tolerance was observed while scoping the reaction out. Primary anilines bearing electron-withdrawing groups typically provided the difunctionalized products in a greater yield compared to electron-rich or second-

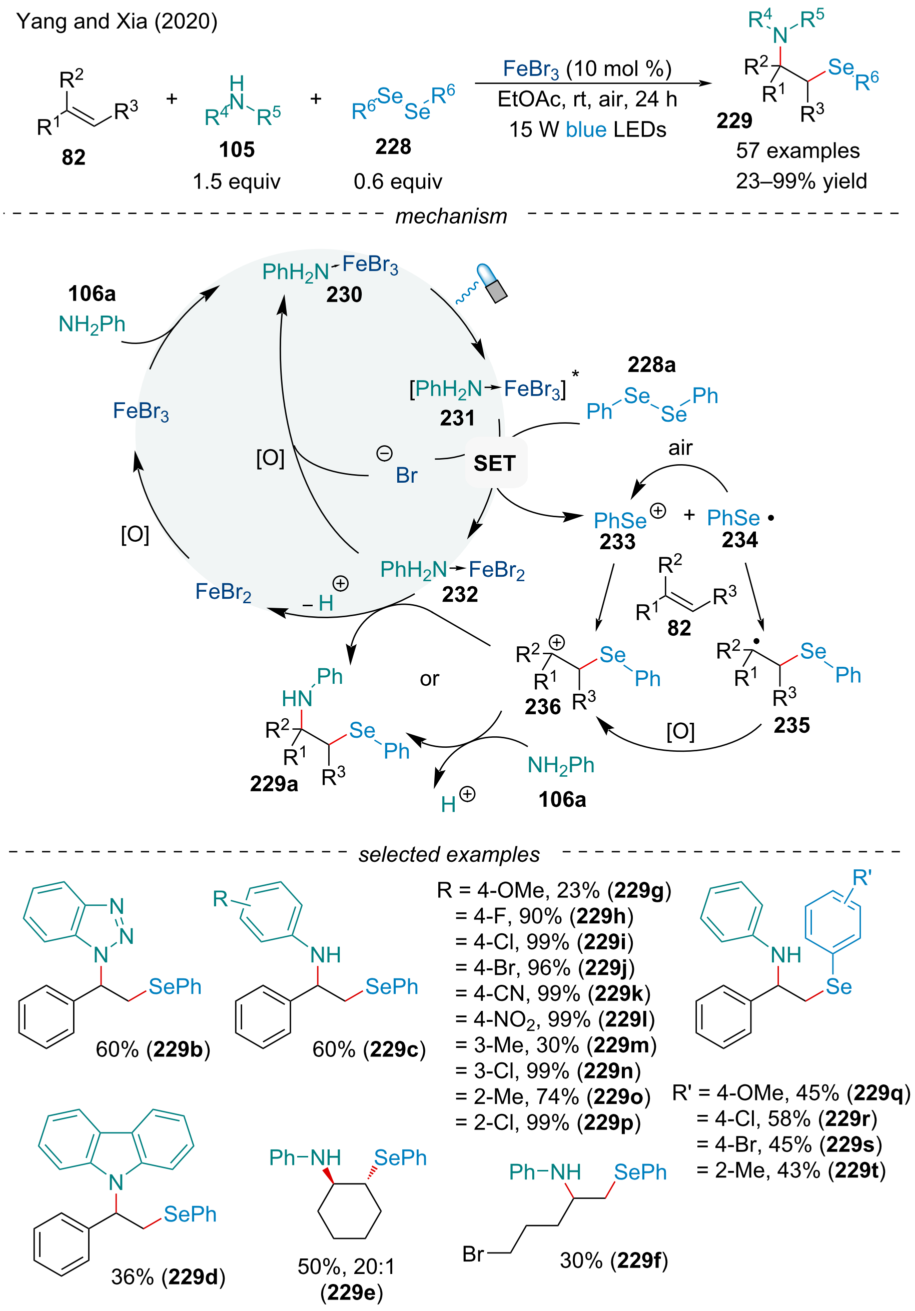

Yang and Xia (2020)
82
105
1.5 equiv
228
0.6 equiv
FeBr3 (10 mol %)
EtOAc, rt, air, 24 h
15 W blue LEDs
229
57 examples
23–99% yield
mechanism
106a
NH2Ph
PhH2N-FeBr3
230
[PhH2N→FeBr3]*
231
228a
FeBr3
[O]
Br
SET
air
PhSe⊕
233
PhSe•
234
[O]
FeBr2
– H⊕
PhH2N→FeBr2
232
82
or
236
235
229a
[O]
NH2Ph
106a
H⊕
selected examples
60% (229b)
60% (229c)
R = 4-OMe, 23% (229g)
= 4-F, 90% (229h)
= 4-Cl, 99% (229i)
= 4-Br, 96% (229j)
= 4-CN, 99% (229k)
= 4-NO2, 99% (229l)
= 3-Me, 30% (229m)
= 3-Cl, 99% (229n)
= 2-Me, 74% (229o)
= 2-Cl, 99% (229p)
R' = 4-OMe, 45% (229q)
= 4-Cl, 58% (229r)
= 4-Br, 45% (229s)
= 2-Me, 43% (229t)
36% (229d)
50%, 20:1
(229e)
30% (229f)

Scheme 53: Synergistic photoredox/iron-catalyzed three-component aminoselenation of trisubstituted alkenes **82**.

ary anilines. Due to the lack of photo-absorption, aliphatic amines failed to react. Aliphatic diselenides worked, but showed low reactivity compared to aromatic diselenides. Based on mechanistic observations, the initial step is presumed to be the interaction of the amine with the Fe(III) to generate $[FeBr_3 \cdot NH_2Ph]$ **230** which can be photo-excited to reach the excited state **231**. The latter reacts through a SET oxidation with diselenide **228a** generating one equivalent of $PhSe^+$ (**233**) and $PhSe^\bullet$ (**234**). Addition of the two selenium species **233/234** across the alkene followed by oxidation produces the benzylic carbocation **236** which undergoes reaction with the nucleophilic amine to yield the final product.

Conclusion

This review summarized Fe-catalyzed domino coupling reactions of π-systems and illustrated the major breakthroughs in the field. Considerable developments have been accomplished in the field of iron catalysis providing non-toxic, inexpensive, and overall greener alternatives to precious metal catalysis. Despite the prevalence of precious metals in the field of catalysis, iron has proven a competitive rival for its reactivity in a variety of coupling reactions. Among them, significant progress has been made in cross-coupling reactions, proving competent with various electrophiles and organometallic reagents. Likewise, cross-dehydrogenative-coupling has offered a sustainable variant to traditional coupling reactions, with highly selective and fruitful coupling reactions being developed. Oxidative coupling and functionalization reactions have widely been used in rapidly increase molecular complexity for the addition of many different carbon and heteroatom functionalities.

Further work in this field will undoubtedly continue to expand the scope of potential coupling partners within Fe-catalyzed domino reactions. As with the majority of domino methodology, reactions are generally extremely substrate-dependent and rarely lead to the discovery of novel broad-scope reactivity; however, connecting known reactivity paradigms and reagents to substrates with varying propagation sites will lead to the development of novel complex scaffolds. Adoption of this methodology in total synthesis will further demonstrate the utility of these protocols and continue to advance the field's scope and applicability. To date, a great deal of Fe-catalyzed multifunctionalization reactions employ styrene derivatives, or other activated π-systems, placing limitations on its relevance. Expanding the scope to include less reactive alkenes is necessary to see further advancements in this field. Although great progress has been made in the development of asymmetric variants, there is still significant room for improvement. The use of novel chiral ligands, or the use of chiral auxiliaries, could improve the scope of enantioselective cross-coupling and cross-dehydrogenative-coupling reactions.

While selectivity within multicomponent domino reactions is a challenging task, recent achievements have provided straightforward protocols for the construction and complex molecules through the generation of multiple carbon–carbon and carbon–heteroatom bonds in a single step. Increasing the selectivity and expanding the applicable substrate scope of Fe-catalyzed domino reactions is imminent. Future advancements of such methodology will make Fe-catalyzed domino reactions a mainstay in the organic chemist's toolbox.

Funding

This work was supported by a Discovery Grants (WT) from the Natural Sciences and Engineering Research Council (NSERC) of Canada. AP also acknowledges NSERC for financial support through the PGS-D Scholarship.

ORCID® iDs

William Tam - https://orcid.org/0000-0002-1375-881X

References

1. Sarhan, A. A. O.; Bolm, C. *Chem. Soc. Rev.* **2009,** *38,* 2730–2744. doi:10.1039/b906026j
2. Hayler, J. D.; Leahy, D. K.; Simmons, E. M. *Organometallics* **2019,** *38,* 36–46. doi:10.1021/acs.organomet.8b00566
3. Kirchhoff, M. M. *Resour., Conserv. Recycl.* **2005,** *44,* 237–243. doi:10.1016/j.resconrec.2005.01.003
4. Busacca, C. A.; Fandrick, D. R.; Song, J. J.; Senanayake, C. H. *Adv. Synth. Catal.* **2011,** *353,* 1825–1864. doi:10.1002/adsc.201100488
5. Gensch, T.; Hopkinson, M. N.; Glorius, F.; Wencel-Delord, J. *Chem. Soc. Rev.* **2016,** *45,* 2900–2936. doi:10.1039/c6cs00075d
6. Haibach, M. C.; Ickes, A. R.; Wilders, A. M.; Shekhar, S. *Org. Process Res. Dev.* **2020,** *24,* 2428–2444. doi:10.1021/acs.oprd.0c00367
7. Singer, R. A.; Monfette, S.; Bernhardson, D. J.; Tcyrulnikov, S.; Hansen, E. C. *Org. Process Res. Dev.* **2020,** *24,* 909–915. doi:10.1021/acs.oprd.0c00104
8. Buono, F.; Nguyen, T.; Qu, B.; Wu, H.; Haddad, N. *Org. Process Res. Dev.* **2021,** *25,* 1471–1495. doi:10.1021/acs.oprd.1c00053
9. Anastas, P. T.; Kirchhoff, M. M.; Williamson, T. C. *Appl. Catal., A* **2001,** *221,* 3–13. doi:10.1016/s0926-860x(01)00793-1
10. Li, S.-S.; Qin, L.; Dong, L. *Org. Biomol. Chem.* **2016,** *14,* 4554–4570. doi:10.1039/c6ob00209a
11. Song, G.; Wang, F.; Li, X. *Chem. Soc. Rev.* **2012,** *41,* 3651–3678. doi:10.1039/c2cs15281a
12. Ye, B.; Cramer, N. *Acc. Chem. Res.* **2015,** *48,* 1308–1318. doi:10.1021/acs.accounts.5b00092
13. Colby, D. A.; Bergman, R. G.; Ellman, J. A. *Chem. Rev.* **2010,** *110,* 624–655. doi:10.1021/cr900005n
14. Piou, T.; Rovis, T. *Acc. Chem. Res.* **2018,** *51,* 170–180. doi:10.1021/acs.accounts.7b00444
15. Biffis, A.; Centomo, P.; Del Zotto, A.; Zecca, M. *Chem. Rev.* **2018,** *118,* 2249–2295. doi:10.1021/acs.chemrev.7b00443
16. Selander, N.; Szabó, K. J. *Chem. Rev.* **2011,** *111,* 2048–2076. doi:10.1021/cr1002112

17. McCarthy, S.; Braddock, D. C.; Wilton-Ely, J. D. E. T. *Coord. Chem. Rev.* **2021,** *442,* 213925. doi:10.1016/j.ccr.2021.213925
18. Muñiz, K. *Angew. Chem., Int. Ed.* **2009,** *48,* 9412–9423. doi:10.1002/anie.200903671
19. Ye, J.; Lautens, M. *Nat. Chem.* **2015,** *7,* 863–870. doi:10.1038/nchem.2372
20. Ananikov, V. P. *ACS Catal.* **2015,** *5,* 1964–1971. doi:10.1021/acscatal.5b00072
21. Tasker, S. Z.; Standley, E. A.; Jamison, T. F. *Nature* **2014,** *509,* 299–309. doi:10.1038/nature13274
22. Clevenger, A. L.; Stolley, R. M.; Aderibigbe, J.; Louie, J. *Chem. Rev.* **2020,** *120,* 6124–6196. doi:10.1021/acs.chemrev.9b00682
23. Marchese, A. D.; Adrianov, T.; Lautens, M. *Angew. Chem., Int. Ed.* **2021,** *60,* 16750–16762. doi:10.1002/anie.202101324
24. Iglesias, M.; Oro, L. A. *Chem. Soc. Rev.* **2018,** *47,* 2772–2808. doi:10.1039/c7cs00743d
25. Tosatti, P.; Nelson, A.; Marsden, S. P. *Org. Biomol. Chem.* **2012,** *10,* 3147–3163. doi:10.1039/c2ob07086c
26. Cheng, Q.; Tu, H.-F.; Zheng, C.; Qu, J.-P.; Helmchen, G.; You, S.-L. *Chem. Rev.* **2019,** *119,* 1855–1969. doi:10.1021/acs.chemrev.8b00506
27. Nagamoto, M.; Nishimura, T. *ACS Catal.* **2017,** *7,* 833–847. doi:10.1021/acscatal.6b02495
28. Fukuzumi, S.; Lee, Y.-M.; Nam, W. *Coord. Chem. Rev.* **2018,** *355,* 54–73. doi:10.1016/j.ccr.2017.07.014
29. Hunter, B. M.; Gray, H. B.; Müller, A. M. *Chem. Rev.* **2016,** *116,* 14120–14136. doi:10.1021/acs.chemrev.6b00398
30. Gandeepan, P.; Müller, T.; Zell, D.; Cera, G.; Warratz, S.; Ackermann, L. *Chem. Rev.* **2019,** *119,* 2192–2452. doi:10.1021/acs.chemrev.8b00507
31. Irrgang, T.; Kempe, R. *Chem. Rev.* **2019,** *119,* 2524–2549. doi:10.1021/acs.chemrev.8b00306
32. Cheng, L.-J.; Mankad, N. P. *Chem. Soc. Rev.* **2020,** *49,* 8036–8064. doi:10.1039/d0cs00316f
33. Li, Y.-Y.; Yu, S.-L.; Shen, W.-Y.; Gao, J.-X. *Acc. Chem. Res.* **2015,** *48,* 2587–2598. doi:10.1021/acs.accounts.5b00043
34. Su, B.; Cao, Z.-C.; Shi, Z.-J. *Acc. Chem. Res.* **2015,** *48,* 886–896. doi:10.1021/ar500345f
35. Zell, T.; Langer, R. *Phys. Sci. Rev.* **2018,** *4,* 20170009. doi:10.1515/psr-2017-0009
36. Kharasch, M. S.; Fields, E. K. *J. Am. Chem. Soc.* **1941,** *63,* 2316–2320. doi:10.1021/ja01854a006
37. Tamura, M.; Kochi, J. K. *J. Am. Chem. Soc.* **1971,** *93,* 1487–1489. doi:10.1021/ja00735a030
38. Neidig, M. L.; Carpenter, S. H.; Curran, D. J.; DeMuth, J. C.; Fleischauer, V. E.; Iannuzzi, T. E.; Neate, P. G. N.; Sears, J. D.; Wolford, N. J. *Acc. Chem. Res.* **2019,** *52,* 140–150. doi:10.1021/acs.accounts.8b00519
39. Fürstner, A. *ACS Cent. Sci.* **2016,** *2,* 778–789. doi:10.1021/acscentsci.6b00272
40. Rana, S.; Biswas, J. P.; Paul, S.; Paik, A.; Maiti, D. *Chem. Soc. Rev.* **2021,** *50,* 243–472. doi:10.1039/d0cs00688b
41. Shi, W.; Liu, C.; Lei, A. *Chem. Soc. Rev.* **2011,** *40,* 2761–2776. doi:10.1039/c0cs00125b
42. Shang, R.; Ilies, L.; Nakamura, E. *Chem. Rev.* **2017,** *117,* 9086–9139. doi:10.1021/acs.chemrev.6b00772
43. Bauer, I.; Knölker, H.-J. *Chem. Rev.* **2015,** *115,* 3170–3387. doi:10.1021/cr500425u
44. Li, Z.; Cao, L.; Li, C.-J. *Angew. Chem., Int. Ed.* **2007,** *46,* 6505–6507. doi:10.1002/anie.200701782
45. Girard, S. A.; Knauber, T.; Li, C.-J. *Angew. Chem., Int. Ed.* **2014,** *53,* 74–100. doi:10.1002/anie.201304268
46. Peng, K.; Dong, Z.-B. *Adv. Synth. Catal.* **2021,** *363,* 1185–1201. doi:10.1002/adsc.202001358
47. Tietze, L. F. *Chem. Rev.* **1996,** *96,* 115–136. doi:10.1021/cr950027e
48. Piontek, A.; Bisz, E.; Szostak, M. *Angew. Chem., Int. Ed.* **2018,** *57,* 11116–11128. doi:10.1002/anie.201800364
49. Czaplik, W. M.; Mayer, M.; Cvengros, J.; von Wangelin, A. J. *ChemSusChem* **2009,** *2,* 396–417. doi:10.1002/cssc.200900055
50. Mako, T. L.; Byers, J. A. *Inorg. Chem. Front.* **2016,** *3,* 766–790. doi:10.1039/c5qi00295h
51. Kuzmina, O. M.; Steib, A. K.; Moyeux, A.; Chaiez, G.; Knochel, P. *Synthesis* **2015,** *47,* 1696–1705. doi:10.1055/s-0034-1380195
52. Nakamura, M.; Matsuo, K.; Ito, S.; Nakamura, E. *J. Am. Chem. Soc.* **2004,** *126,* 3686–3687. doi:10.1021/ja049744t
53. Sherry, B. D.; Fürstner, A. *Acc. Chem. Res.* **2008,** *41,* 1500–1511. doi:10.1021/ar800039x
54. Kim, J. G.; Son, Y. H.; Seo, J. W.; Kang, E. J. *Eur. J. Org. Chem.* **2015,** 1781–1789. doi:10.1002/ejoc.201403511
55. Martin, R.; Fürstner, A. *Angew. Chem., Int. Ed.* **2004,** *43,* 3955–3957. doi:10.1002/anie.200460504
56. Liu, L.; Lee, W.; Zhou, J.; Bandyopadhyay, S.; Gutierrez, O. *Tetrahedron* **2019,** *75,* 129–136. doi:10.1016/j.tet.2018.11.043
57. Hatakeyama, T.; Kondo, Y.; Fujiwara, Y.-i.; Takaya, H.; Ito, S.; Nakamura, E.; Nakamura, M. *Chem. Commun.* **2009,** 1216–1218. doi:10.1039/b820879d
58. Bedford, R. B.; Betham, M.; Bruce, D. W.; Davis, S. A.; Frost, R. M.; Hird, M. *Chem. Commun.* **2006,** 1398–1400. doi:10.1039/b601014h
59. Bedford, R. B.; Betham, M.; Bruce, D. W.; Danopoulos, A. A.; Frost, R. M.; Hird, M. *J. Org. Chem.* **2006,** *71,* 1104–1110. doi:10.1021/jo052250+
60. Ghorai, S. K.; Jin, M.; Hatakeyama, T.; Nakamura, M. *Org. Lett.* **2012,** *14,* 1066–1069. doi:10.1021/ol2031729
61. Liu, L.; Lee, W.; Yuan, M.; Acha, C.; Geherty, M. B.; Williams, B.; Gutierrez, O. *Chem. Sci.* **2020,** *11,* 3146–3151. doi:10.1039/d0sc00467g
62. Sherry, B. D.; Fürstner, A. *Chem. Commun.* **2009,** 7116–7118. doi:10.1039/b918818e
63. Dieskau, A. P.; Holzwarth, M. S.; Plietker, B. *J. Am. Chem. Soc.* **2012,** *134,* 5048–5051. doi:10.1021/ja300294a
64. Jin, M.; Adak, L.; Nakamura, M. *J. Am. Chem. Soc.* **2015,** *137,* 7128–7134. doi:10.1021/jacs.5b02277
65. Tyrol, C. C.; Yone, N. S.; Gallin, C. F.; Byers, J. A. *Chem. Commun.* **2020,** *56,* 14661–14664. doi:10.1039/d0cc05003b
66. Liu, L.; Lee, W.; Youshaw, C. R.; Yuan, M.; Geherty, M. B.; Zavalij, P. Y.; Gutierrez, O. *Chem. Sci.* **2020,** *11,* 8301–8305. doi:10.1039/d0sc02127j
67. Avila, D. V.; Ingold, K. U.; Lusztyk, J.; Dolbier, W. R.; Pan, H. Q. *J. Am. Chem. Soc.* **1993,** *115,* 1577–1579. doi:10.1021/ja00057a054
68. Liu, Y.; Wang, L.; Deng, L. *J. Am. Chem. Soc.* **2016,** *138,* 112–115. doi:10.1021/jacs.5b12522
69. Fürstner, A.; Méndez, M. *Angew. Chem., Int. Ed.* **2003,** *42,* 5355–5357. doi:10.1002/anie.200352441
70. Zhang, D.; Ready, J. M. *J. Am. Chem. Soc.* **2006,** *128,* 15050–15051. doi:10.1021/ja0647708
71. Wang, X.; Zhang, J.; Wang, L.; Deng, L. *Organometallics* **2015,** *34,* 2775–2782. doi:10.1021/acs.organomet.5b00028

72. Echeverria, P.-G.; Fürstner, A. *Angew. Chem., Int. Ed.* **2016,** *55,* 11188–11192. doi:10.1002/anie.201604531
73. Adams, K.; Ball, A. K.; Birkett, J.; Brown, L.; Chappell, B.; Gill, D. M.; Lo, P. K. T.; Patmore, N. J.; Rice, C. R.; Ryan, J.; Raubo, P.; Sweeney, J. B. *Nat. Chem.* **2017,** *9,* 396–401. doi:10.1038/nchem.2670
74. Cassani, C.; Bergonzini, G.; Wallentin, C.-J. *ACS Catal.* **2016,** *6,* 1640–1648. doi:10.1021/acscatal.5b02441
75. Bedford, R. B. *Acc. Chem. Res.* **2015,** *48,* 1485–1493. doi:10.1021/acs.accounts.5b00042
76. Sekine, M.; Ilies, L.; Nakamura, E. *Org. Lett.* **2013,** *15,* 714–717. doi:10.1021/ol400056z
77. Ekomié, A.; Lefèvre, G.; Fensterbank, L.; Lacôte, E.; Malacria, M.; Ollivier, C.; Jutand, A. *Angew. Chem., Int. Ed.* **2012,** *51,* 6942–6946. doi:10.1002/anie.201200589
78. Yu, X.; Zheng, H.; Zhao, H.; Lee, B. C.; Koh, M. J. *Angew. Chem., Int. Ed.* **2021,** *60,* 2104–2109. doi:10.1002/anie.202012607
79. Li, C.-J. *Acc. Chem. Res.* **2009,** *42,* 335–344. doi:10.1021/ar800164n
80. Wei, W.-T.; Zhou, M.-B.; Fan, J.-H.; Liu, W.; Song, R.-J.; Liu, Y.; Hu, M.; Xie, P.; Li, J.-H. *Angew. Chem., Int. Ed.* **2013,** *52,* 3638–3641. doi:10.1002/anie.201210029
81. Zhang, M.; Xie, P.; Zhao, W.; Niu, B.; Wu, W.; Bian, Z.; Pittman, C. U., Jr.; Zhou, A. *J. Org. Chem.* **2015,** *80,* 4176–4183. doi:10.1021/acs.joc.5b00158
82. Pan, C.; Zhang, H.; Zhu, C. *Org. Biomol. Chem.* **2015,** *13,* 361–364. doi:10.1039/c4ob02172j
83. Jia, F.; Liu, K.; Xi, H.; Lu, S.; Li, Z. *Tetrahedron Lett.* **2013,** *54,* 6337–6340. doi:10.1016/j.tetlet.2013.09.048
84. Ouyang, X.-H.; Song, R.-J.; Li, J.-H. *Eur. J. Org. Chem.* **2014,** 3395–3401. doi:10.1002/ejoc.201400043
85. Correia, V. G.; Abreu, J. C.; Barata, C. A. E.; Andrade, L. H. *Org. Lett.* **2017,** *19,* 1060–1063. doi:10.1021/acs.orglett.7b00078
86. Lv, L.; Qi, L.; Guo, Q.; Shen, B.; Li, Z. *J. Org. Chem.* **2015,** *80,* 12562–12571. doi:10.1021/acs.joc.5b02457
87. Wang, S.-S.; Fu, H.; Wang, G.; Sun, M.; Li, Y.-M. *RSC Adv.* **2016,** *6,* 52391–52394. doi:10.1039/c6ra08976c
88. Sun, H.; Jiang, Y.; Lu, M.-K.; Li, Y.-Y.; Li, L.; Liu, J.-K. *Synlett* **2020,** *31,* 2049–2053. doi:10.1055/s-0039-1691574
89. Zhang, H.; Zhu, C. *Org. Chem. Front.* **2017,** *4,* 1272–1275. doi:10.1039/c7qo00157f
90. Ouyang, X.-H.; Li, Y.; Song, R.-J.; Hu, M.; Luo, S.; Li, J.-H. *Sci. Adv.* **2019,** *5,* aav9839. doi:10.1126/sciadv.aav9839
91. Kshirsagar, U. A.; Regev, C.; Parnes, R.; Pappo, D. *Org. Lett.* **2013,** *15,* 3174–3177. doi:10.1021/ol401532a
92. Huang, Z.; Jin, L.; Feng, Y.; Peng, P.; Yi, H.; Lei, A. *Angew. Chem., Int. Ed.* **2013,** *52,* 7151–7155. doi:10.1002/anie.201210023
93. Ni, Y.; Yu, Q.; Liu, Q.; Zuo, H.; Yu, H.-B.; Wei, W.-J.; Liao, R.-Z.; Zhong, F. *Org. Lett.* **2018,** *20,* 1404–1408. doi:10.1021/acs.orglett.8b00176
94. Shen, T.; Yuan, Y.; Song, S.; Jiao, N. *Chem. Commun.* **2014,** *50,* 4115–4118. doi:10.1039/c4cc00401a
95. Wu, L.-J.; Tan, F.-L.; Li, M.; Song, R.-J.; Li, J.-H. *Org. Chem. Front.* **2017,** *4,* 350–353. doi:10.1039/c6qo00691d
96. Ge, Y.; Tian, Y.; Wu, J.; Yan, Q.; Zheng, L.; Ren, Y.; Zhao, J.; Li, Z. *Chem. Commun.* **2020,** *56,* 12656–12659. doi:10.1039/d0cc05213b
97. Lv, L.; Lu, S.; Guo, Q.; Shen, B.; Li, Z. *J. Org. Chem.* **2015,** *80,* 698–704. doi:10.1021/jo502535k
98. Chatgilialoglu, C.; Crich, D.; Komatsu, M.; Ryu, I. *Chem. Rev.* **1999,** *99,* 1991–2070. doi:10.1021/cr9601425
99. Guo, L.-N.; Wang, S.; Duan, X.-H.; Zhou, S.-L. *Chem. Commun.* **2015,** *51,* 4803–4806. doi:10.1039/c5cc00426h
100. Lv, L.; Li, Z. *Chin. J. Chem.* **2017,** *35,* 303–306. doi:10.1002/cjoc.201600721
101. Lv, L.; Xi, H.; Bai, X.; Li, Z. *Org. Lett.* **2015,** *17,* 4324–4327. doi:10.1021/acs.orglett.5b02138
102. Kang, Q.-Q.; Meng, Y.-N.; Zhang, J.-H.; Li, L.; Ge, G.-P.; Zheng, H.; Liu, H.; Wei, W.-T. *New J. Chem.* **2021,** *45,* 13639–13643. doi:10.1039/d1nj02378k
103. Tian, Y.; Ge, Y.; Zheng, L.; Yan, Q.; Ren, Y.; Wang, Z.; Zhang, K.; Wang, Z.; Zhao, J.; Li, Z. *Asian J. Org. Chem.* **2019,** *8,* 2188–2191. doi:10.1002/ajoc.201900591
104. Liu, Y.-Y.; Yang, X.-H.; Song, R.-J.; Luo, S.; Li, J.-H. *Nat. Commun.* **2017,** *8,* 14720. doi:10.1038/ncomms14720
105. Yang, Y.; Song, R.-J.; Ouyang, X.-H.; Wang, C.-Y.; Li, J.-H.; Luo, S. *Angew. Chem., Int. Ed.* **2017,** *56,* 7916–7919. doi:10.1002/anie.201702349
106. Zhang, X.; Fang, J.; Cai, C.; Lu, G. *Chin. Chem. Lett.* **2021,** *32,* 1280–1292. doi:10.1016/j.cclet.2020.09.058
107. Lu, S.; Tian, T.; Xu, R.; Li, Z. *Tetrahedron Lett.* **2018,** *59,* 2604–2606. doi:10.1016/j.tetlet.2018.05.072
108. Wu, C.-S.; Liu, R.-X.; Ma, D.-Y.; Luo, C.-P.; Yang, L. *Org. Lett.* **2019,** *21,* 6117–6121. doi:10.1021/acs.orglett.9b02264
109. Lee, E.; Hur, C. U.; Rhee, Y. H.; Park, Y. C.; Kim, S. Y. *J. Chem. Soc., Chem. Commun.* **1993,** 1466–1468. doi:10.1039/c39930001466
110. Citterio, A.; Arnoldi, A.; Minisci, F. *J. Org. Chem.* **1979,** *44,* 2674–2682. doi:10.1021/jo01329a017
111. Wu, C.-S.; Li, R.; Wang, Q.-Q.; Yang, L. *Green Chem.* **2019,** *21,* 269–274. doi:10.1039/c8gc02834f
112. Wang, G.; Wang, S.; Wang, J.; Chen, S.-Y.; Yu, X.-Q. *Tetrahedron* **2014,** *70,* 3466–3470. doi:10.1016/j.tet.2014.03.062
113. Xu, X.; Tang, Y.; Li, X.; Hong, G.; Fang, M.; Du, X. *J. Org. Chem.* **2014,** *79,* 446–451. doi:10.1021/jo402529r
114. Zong, Z.; Lu, S.; Wang, W.; Li, Z. *Tetrahedron Lett.* **2015,** *56,* 6719–6721. doi:10.1016/j.tetlet.2015.10.052
115. Tang, Y.; Li, M.; Huang, H.; Wang, F.; Hu, X.; Zhang, X. *Synlett* **2021,** *32,* 1219–1222. doi:10.1055/a-1469-5742
116. Taniguchi, T.; Sugiura, Y.; Zaimoku, H.; Ishibashi, H. *Angew. Chem., Int. Ed.* **2010,** *49,* 10154–10157. doi:10.1002/anie.201005574
117. Qiao, S.; Qian, P.-C.; Chen, F.; Cheng, J. *Org. Biomol. Chem.* **2020,** *18,* 7086–7089. doi:10.1039/d0ob01438a
118. Cui, Z.; Du, D.-M. *Adv. Synth. Catal.* **2018,** *360,* 93–99. doi:10.1002/adsc.201700976
119. Zeeli, S.; Weill, T.; Finkin-Groner, E.; Bejar, C.; Melamed, M.; Furman, S.; Zhenin, M.; Nudelman, A.; Weinstock, M. *J. Med. Chem.* **2018,** *61,* 4004–4019. doi:10.1021/acs.jmedchem.8b00001
120. Cui, Z.; Du, D.-M. *J. Org. Chem.* **2018,** *83,* 5149–5159. doi:10.1021/acs.joc.8b00511
121. Lu, M.-Z.; Loh, T.-P. *Org. Lett.* **2014,** *16,* 4698–4701. doi:10.1021/ol502411c
122. Li, D.; Shen, X. *Tetrahedron Lett.* **2020,** *61,* 152316. doi:10.1016/j.tetlet.2020.152316
123. Yu, L.-Z.; Xu, Q.; Tang, X.-Y.; Shi, M. *ACS Catal.* **2016,** *6,* 526–531. doi:10.1021/acscatal.5b02400

124. Ouyang, X.-H.; Song, R.-J.; Hu, M.; Yang, Y.; Li, J.-H. *Angew. Chem., Int. Ed.* **2016,** *55,* 3187–3191. doi:10.1002/anie.201511624
125. Li, W.-Y.; Wu, C.-S.; Wang, Z.; Luo, Y. *Chem. Commun.* **2018,** *54,* 11013–11016. doi:10.1039/c8cc05090b
Correction: Li, W.-Y.; Wu, C.-S.; Wang, Z.; Yang, L. *Chem. Commun.* **2018,** *54,* 11973. doi:10.1039/C8CC90435A
126. Kharasch, M. S.; Jensen, E. V.; Urry, W. H. *J. Am. Chem. Soc.* **1946,** *68,* 154–155. doi:10.1021/ja01205a521
127. Asscher, M.; Vofsi, D. *J. Chem. Soc.* **1963,** 1887–1896. doi:10.1039/jr9630001887
128. Zhu, C.-L.; Wang, C.; Qin, Q.-X.; Yruegas, S.; Martin, C. D.; Xu, H. *ACS Catal.* **2018,** *8,* 5032–5037. doi:10.1021/acscatal.8b01253
129. Xu, L.; Chen, J.; Chu, L. *Org. Chem. Front.* **2019,** *6,* 512–516. doi:10.1039/c8qo01142g
130. Roberts, B. P. *Chem. Soc. Rev.* **1999,** *28,* 25–35. doi:10.1039/a804291h
131. Xiong, H.; Ramkumar, N.; Chiou, M.-F.; Jian, W.; Li, Y.; Su, J.-H.; Zhang, X.; Bao, H. *Nat. Commun.* **2019,** *10,* 122. doi:10.1038/s41467-018-07985-2
132. Wang, F.; Zhu, N.; Chen, P.; Ye, J.; Liu, G. *Angew. Chem., Int. Ed.* **2015,** *54,* 9356–9360. doi:10.1002/anie.201503412
133. Wei, R.; Xiong, H.; Ye, C.; Li, Y.; Bao, H. *Org. Lett.* **2020,** *22,* 3195–3199. doi:10.1021/acs.orglett.0c00969
134. Ge, L.; Li, Y.; Bao, H. *Org. Lett.* **2019,** *21,* 256–260. doi:10.1021/acs.orglett.8b03688
135. Ge, L.; Zhou, H.; Chiou, M.-F.; Jiang, H.; Jian, W.; Ye, C.; Li, X.; Zhu, X.; Xiong, H.; Li, Y.; Song, L.; Zhang, X.; Bao, H. *Nat. Catal.* **2021,** *4,* 28–35. doi:10.1038/s41929-020-00551-4
136. Qian, B.; Chen, S.; Wang, T.; Zhang, X.; Bao, H. *J. Am. Chem. Soc.* **2017,** *139,* 13076–13082. doi:10.1021/jacs.7b06590
137. Shimbayashi, T.; Okamoto, K.; Ohe, K. *Chem. – Asian J.* **2018,** *13,* 395–399. doi:10.1002/asia.201701634
138. Uchiyama, N.; Shirakawa, E.; Nishikawa, R.; Hayashi, T. *Chem. Commun.* **2011,** *47,* 11671–11673. doi:10.1039/c1cc14694g
139. Zhang, Y.; Wu, X.-F. *Chem. Commun.* **2020,** *56,* 14605–14608. doi:10.1039/d0cc06671k
140. Yu, W.; Wang, P.-L.; Xu, K.; Li, H. *Asian J. Org. Chem.* **2021,** *10,* 831–837. doi:10.1002/ajoc.202100040
141. Liang, W.; Jiang, K.; Du, F.; Yang, J.; Shuai, L.; Ouyang, Q.; Chen, Y.-C.; Wei, Y. *Angew. Chem., Int. Ed.* **2020,** *59,* 19222–19228. doi:10.1002/anie.202007825
142. Shimbayashi, T.; Nakamoto, D.; Okamoto, K.; Ohe, K. *Org. Lett.* **2018,** *20,* 3044–3048. doi:10.1021/acs.orglett.8b01073
143. Du, F.; Li, S.-J.; Jiang, K.; Zeng, R.; Pan, X.-C.; Lan, Y.; Chen, Y.-C.; Wei, Y. *Angew. Chem., Int. Ed.* **2020,** *59,* 23755–23762. doi:10.1002/anie.202010752
144. Jian, W.; Ge, L.; Jiao, Y.; Qian, B.; Bao, H. *Angew. Chem., Int. Ed.* **2017,** *56,* 3650–3654. doi:10.1002/anie.201612365
145. Iwasaki, M.; Kazao, Y.; Ishida, T.; Nishihara, Y. *Org. Lett.* **2020,** *22,* 7343–7347. doi:10.1021/acs.orglett.0c02671
146. Cheng, F.; Wang, L.-L.; Mao, Y.-H.; Dong, Y.-X.; Liu, B.; Zhu, G.-F.; Yang, Y.-Y.; Guo, B.; Tang, L.; Zhang, J.-Q. *J. Org. Chem.* **2021,** *86,* 8620–8629. doi:10.1021/acs.joc.1c00284
147. Xu, R.; Cai, C. *Org. Chem. Front.* **2020,** *7,* 318–323. doi:10.1039/c9qo01342c
148. Langlois, B. R.; Laurent, E.; Roidot, N. *Tetrahedron Lett.* **1991,** *32,* 7525–7528. doi:10.1016/0040-4039(91)80524-a
149. Liu, Z.; Wang, J.; Zhao, Y.; Zhou, B. *Adv. Synth. Catal.* **2009,** *351,* 371–374. doi:10.1002/adsc.200800708
150. Xu, T.; Cheung, C. W.; Hu, X. *Angew. Chem., Int. Ed.* **2014,** *53,* 4910–4914. doi:10.1002/anie.201402511
151. Deng, W.; Li, Y.; Li, Y.-G.; Bao, H. *Synthesis* **2018,** *50,* 2974–2980. doi:10.1055/s-0037-1609448
152. Xia, X.-F.; Yu, J.; Wang, D. *Adv. Synth. Catal.* **2018,** *360,* 562–567. doi:10.1002/adsc.201701258
153. Iwamoto, T.; Nishikori, T.; Nakagawa, N.; Takaya, H.; Nakamura, M. *Angew. Chem., Int. Ed.* **2017,** *56,* 13298–13301. doi:10.1002/anie.201706333
154. Xu, R.; Cai, C. *Chem. Commun.* **2019,** *55,* 4383–4386. doi:10.1039/c9cc00730j
155. Xu, R.; Cai, C. *Org. Biomol. Chem.* **2019,** *17,* 8541–8545. doi:10.1039/c9ob01815h
156. Yuan, Y.-A.; Lu, D.-F.; Chen, Y.-R.; Xu, H. *Angew. Chem., Int. Ed.* **2016,** *55,* 534–538. doi:10.1002/anie.201507550
157. Makai, S.; Falk, E.; Morandi, B. *J. Am. Chem. Soc.* **2020,** *142,* 21548–21555. doi:10.1021/jacs.0c11025
158. Lv, D.; Sun, Q.; Zhou, H.; Ge, L.; Qu, Y.; Li, T.; Ma, X.; Li, Y.; Bao, H. *Angew. Chem., Int. Ed.* **2021,** *60,* 12455–12460. doi:10.1002/anie.202017175
159. Fayssal, S. A.; Giungi, A.; Berhal, F.; Prestat, G. *Org. Process Res. Dev.* **2020,** *24,* 695–703. doi:10.1021/acs.oprd.9b00400
160. Bertho, S.; Rey-Rodriguez, R.; Colas, C.; Retailleau, P.; Gillaizeau, I. *Chem. – Eur. J.* **2017,** *23,* 17674–17677. doi:10.1002/chem.201704499
161. Legnani, L.; Morandi, B. *Angew. Chem., Int. Ed.* **2016,** *55,* 2248–2251. doi:10.1002/anie.201507630
162. Cho, I.; Prier, C. K.; Jia, Z.-J.; Zhang, R. K.; Görbe, T.; Arnold, F. H. *Angew. Chem., Int. Ed.* **2019,** *58,* 3138–3142. doi:10.1002/anie.201812968
163. Lu, D.-F.; Liu, G.-S.; Zhu, C.-L.; Yuan, B.; Xu, H. *Org. Lett.* **2014,** *16,* 2912–2915. doi:10.1021/ol501051p
164. Liu, G.-S.; Zhang, Y.-Q.; Yuan, Y.-A.; Xu, H. *J. Am. Chem. Soc.* **2013,** *135,* 3343–3346. doi:10.1021/ja311923z
165. Lu, D.-F.; Zhu, C.-L.; Jia, Z.-X.; Xu, H. *J. Am. Chem. Soc.* **2014,** *136,* 13186–13189. doi:10.1021/ja508057u
166. Zhu, C.-L.; Tian, J.-S.; Gu, Z.-Y.; Xing, G.-W.; Xu, H. *Chem. Sci.* **2015,** *6,* 3044–3050. doi:10.1039/c5sc00221d
167. Bach, T.; Schlummer, B.; Harms, K. *Synlett* **2000,** 1330–1332. doi:10.1055/s-2000-7129
168. Tian, J.-S.; Zhu, C.-L.; Chen, Y.-R.; Xu, H. *Synthesis* **2015,** *47,* 1709–1715. doi:10.1055/s-0034-1378719
169. Lu, D.-F.; Zhu, C.-L.; Sears, J. D.; Xu, H. *J. Am. Chem. Soc.* **2016,** *138,* 11360–11367. doi:10.1021/jacs.6b07221
170. Legnani, L.; Prina-Cerai, G.; Delcaillau, T.; Willems, S.; Morandi, B. *Science* **2018,** *362,* 434–439. doi:10.1126/science.aat3863
171. Falk, E.; Makai, S.; Delcaillau, T.; Gürtler, L.; Morandi, B. *Angew. Chem., Int. Ed.* **2020,** *59,* 21064–21071. doi:10.1002/anie.202008247
172. Ma, X.; Chiou, M.-F.; Ge, L.; Li, X.; Li, Y.; Wu, L.; Bao, H. *Chin. J. Catal.* **2021,** *42,* 1634–1640. doi:10.1016/s1872-2067(21)63847-0
173. Wu, L.; Zhang, Z.; Wu, D.; Wang, F.; Chen, P.; Lin, Z.; Liu, G. *Angew. Chem., Int. Ed.* **2021,** *60,* 6997–7001. doi:10.1002/anie.202015083
174. Huang, X.; Bergsten, T. M.; Groves, J. T. *J. Am. Chem. Soc.* **2015,** *137,* 5300–5303. doi:10.1021/jacs.5b01983
175. Huang, B.; Li, Y.; Yang, C.; Xia, W. *Green Chem.* **2020,** *22,* 2804–2809. doi:10.1039/c9gc04163j

License and Terms

This is an open access article licensed under the terms of the Beilstein-Institut Open Access License Agreement (https://www.beilstein-journals.org/bjoc/terms), which is identical to the Creative Commons Attribution 4.0 International License (https://creativecommons.org/licenses/by/4.0). The reuse of material under this license requires that the author(s), source and license are credited. Third-party material in this article could be subject to other licenses (typically indicated in the credit line), and in this case, users are required to obtain permission from the license holder to reuse the material.

The definitive version of this article is the electronic one which can be found at:
https://doi.org/10.3762/bjoc.17.196